Neural Plasticity

Stress Induced Glial Changes in Neurological Disorders

Lead Guest Editor: Fushun Wang
Guest Editors: Hajime Hirase, Alexei Verkhratsky, and Jason H. Huang

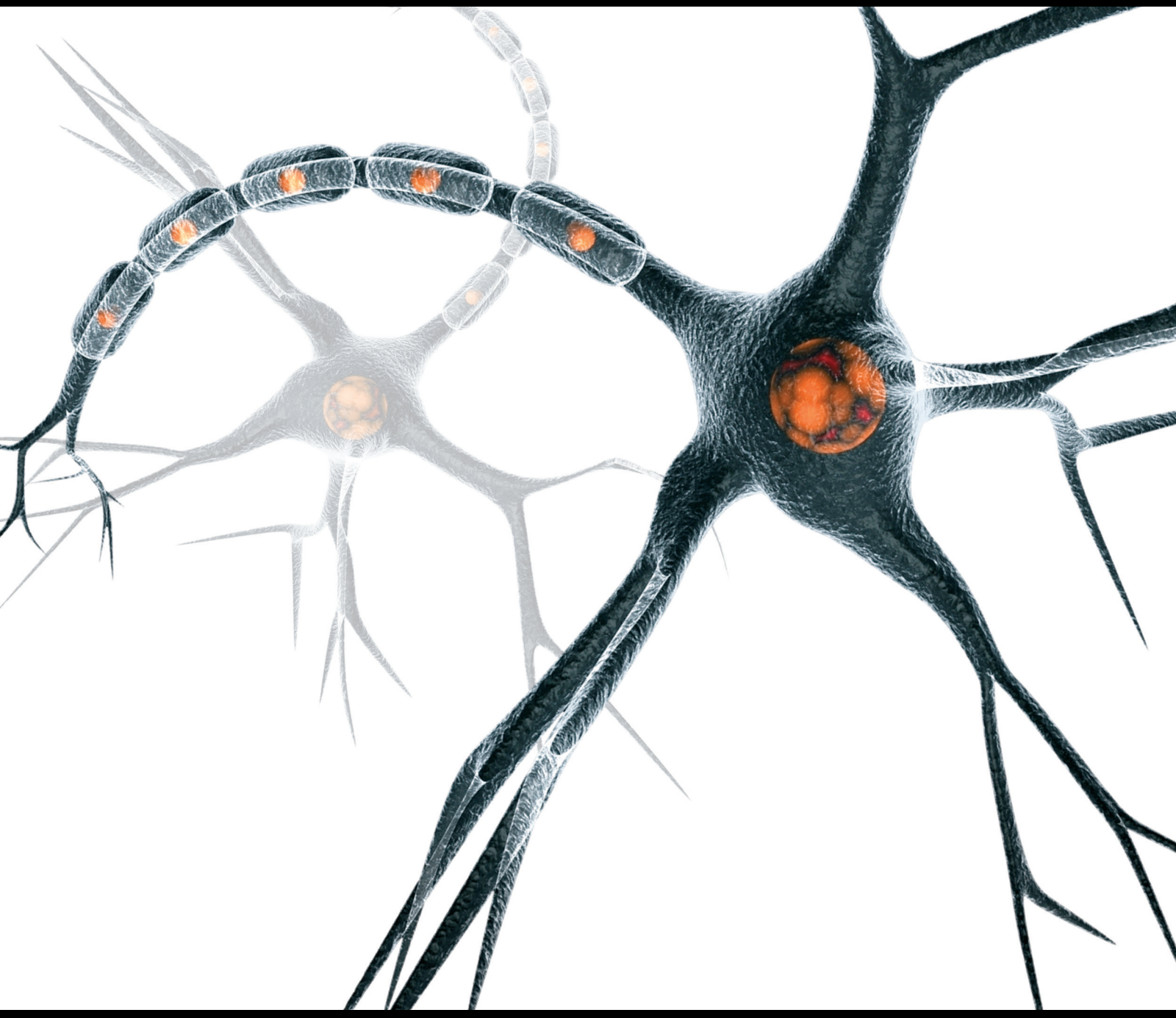

Stress Induced Glial Changes in Neurological Disorders

Neural Plasticity

Stress Induced Glial Changes in Neurological Disorders

Lead Guest Editor: Fushun Wang
Guest Editors: Hajime Hirase, Alexei Verkhratsky, and Jason H. Huang

Contents

Hindawi
Neural Plasticity
Volume 2021, Article ID 8851066, 13 pages
https://doi.org/10.1155/2021/8851066

Review Article

Negative and Positive Bias for Emotional Faces: Evidence from the Attention and Working Memory Paradigms

Qianru Xu,[1,2] **Chaoxiong Ye**,[1,2] **Simeng Gu**,[1,3] **Zhonghua Hu**,[1] **Yi Lei**,[1] **Xueyan Li**,[4] **Lihui Huang**,[5] **and Qiang Liu**[1]

[1]*Institute of Brain and Psychological Sciences, Sichuan Normal University, Chengdu, China*
[2]*Department of Psychology, University of Jyvaskyla, Jyväskylä, Finland*
[3]*Department of Medical Psychology, Jiangsu University Medical School, Zhenjiang, China*
[4]*School of Foreign Languages, Dalian University of Technology, Dalian, China*
[5]*Faculty of Education, Sichuan Normal University, Chengdu, China*

Correspondence should be addressed to Chaoxiong Ye; cxye1988@163.com

Received 10 May 2020; Revised 23 August 2020; Accepted 13 May 2021; Published 28 May 2021

Academic Editor: Yasuo Terao

Visual attention and visual working memory (VWM) are two major cognitive functions in humans, and they have much in common. A growing body of research has investigated the effect of emotional information on visual attention and VWM. Interestingly, contradictory findings have supported both a negative bias and a positive bias toward emotional faces (e.g., angry faces or happy faces) in the attention and VWM fields. We found that the classical paradigms—that is, the visual search paradigm in attention and the change detection paradigm in VWM—are considerably similar. The settings of these paradigms could therefore be responsible for the contradictory results. In this paper, we compare previous controversial results from behavioral and neuroscience studies using these two paradigms. We suggest three possible contributing factors that have significant impacts on the contradictory conclusions regarding different emotional bias effects; these factors are stimulus choice, experimental setting, and cognitive process. We also propose new research directions and guidelines for future studies.

1. Introduction

In the processing of visual information, attention and memory are two cognitive processes that play pivotal roles in human life, and they are extremely important aspects of psychology and cognitive neuroscience research. Previously, however, these two topics have been studied separately; for example, memory studies have not tended to explore the effect of selective attention on memory encoding, while attention studies have often neglected the consequence of past experience [1]. In recent years, a growing body of research has begun to explicitly link visual attention to visual working memory (VWM, which could also be called "visual short-term memory," VSTM). These studies have reached a broad consensus that attention and VWM are intimately linked [2–4]. This consensus is unsurprising, given that the definitions of "attention" and "VWM" already overlap significantly.

As defined by Olivers et al. [2], visual attention describes a process during which individuals select relevant information and ignore irrelevant information. By contrast, VWM describes the process during which individuals temporarily retain relevant information and suppress irrelevant information. In addition to the similarity of their definitions, the visual attention and VWM processes may have many overlapping mechanisms, such as the activation of many similar brain regions (e.g., the supplementary motor area and frontal eye fields, the lateral prefrontal cortex, the anterior cingulate, the superior and inferior parietal cortex, and the occipital area) and a similar capacity limitation (for about four units or chunks), as well as similar control processes (for a review, see [3]). Therefore,

exploring the relationship between visual attention and VWM is highly significant for obtaining a better understanding of basic human cognition [5–11].

Emotional processing, another major cognitive function for humans, has attracted considerable interest in both the visual attention and VWM fields. Regarding visual attention, many studies have examined attentional bias toward emotional stimuli, which can be further divided into negative bias and positive bias (for negative bias, see [12–15]; for positive bias, see [16–18]; for reviews, see [19, 20]). (The phenomenon of negative and positive bias has been studied extensively using a variety of emotional materials, such as faces, scenes, and words [19, 21]. However, we mainly focus in this paper on previous studies that have used emotional faces for the following reasons. First, humans are experts in assessing faces [22]. Compared to other stimuli, faces more easily attract visual attention, and they are more likely to be stored in the human VWM than other complex stimuli [23]. Second, the same facial identity can reflect different types of emotions with little physical difference between the emotions, while other emotional stimulus materials (e.g., different emotional scenes) differ greatly in physical features between emotions [24]. Finally, due to the short history of researching VWM as such [25, 26], the study of the emotional bias effect on VWM began only decades ago, mostly using emotional faces as materials [27–29].) "Negative bias" refers to the processing advantage of negative stimuli (e.g., angry, fearful, sad, or disgusted faces) over positive stimuli (i.e., happy faces); conversely, a "positive bias" refers to the preference for positive stimuli (i.e., happy faces) in emotional processing [19, 21]. Interestingly, VWM studies have revealed a similar phenomenon, finding both negative and positive advantages to VWM performance (for negative bias, see [27, 28, 30, 31]; for positive bias, see [32–34]). These controversial results are derived mainly from two kinds of paradigms, namely, the *visual search paradigm* in visual attention studies and the *change detection paradigm* in VWM studies. Some previous review papers have discussed the contradictory findings of previous visual attention studies (e.g., [19, 20, 35–37]). However, to our knowledge, no studies have yet combined the findings of visual attention studies with those of VWM studies to discuss the possible factors that have contributed to their contradictory outcomes. Therefore, in this paper, we conduct a literature review on previous studies that have investigated the different emotional bias effects in (a) visual attention studies using the visual search paradigm and (b) VWM studies using the change detection paradigm. Our purposes in conducting this work are to list the distinct behavioral and neural levels of evidence, to discuss the possible reasons behind the existing controversial results, and to provide new guidelines and suggestions for future emotional bias studies.

2. Controversial Results in Different Expressions

2.1. Behavior and Neural Evidence with Different Emotional Faces in the Visual Search Paradigm

2.1.1. Negative Bias. With their use of a visual search paradigm, Hansen and Hansen [12] first found an attentional bias toward angry faces presented as black-and-white photographs, with the bias reflected in a shorter response time (RT) and a lower error rate for angry faces versus happy and neutral faces (see Figure 1 for an illustration of the stimulus conditions; see Supplementary Materials for more detailed introduction of this paradigm and frequently used behavioral and neural indexes). However, this result soon met with challenges from other studies because of the extraneous dark areas in Hansen and Hansen's black-and-white stimuli [38]. Nevertheless, even with better control of the stimuli, some follow-up studies still found an attentional bias toward angry faces (e.g., [15, 39, 40]). In addition to angry faces, fearful faces (commonly referred to as "threatening faces"—together with angry faces) have been suggested to have a similar automatic attention capture as angry faces [39]. Indeed, a fearful face seems even easier to detect than an angry face [41]. The attentional bias toward angry and fearful faces, taken together, has been called the "threat superiority effect." This threatening bias is more widely validated by schematic face studies (e.g., [13, 42, 43]) than by studies using photographs of real faces. However, some studies have suggested that the attentional bias toward threatening faces in schematic experiments was actually an attentional bias to sad faces because the participants were more likely to label the corresponding stimulus material as "sad faces" [13].

In addition to behavioral studies, studies using other techniques have also supported the threat superiority effect. Using the eye tracking technique—which allows for relatively direct and continuous measurement of overt visual attention—a previous study using schematic faces found that, in the context of neutral faces, participants took a longer time and more fixations to fixate on the emotional face target if it was a positive face versus a negative face [44]. Another study using photographs found that participants fixated on more distractors before first fixating on a happy face target compared to an angry face target [45]. The use of electroencephalogram (EEG) technology in previous studies confirmed that angry face targets induced earlier and greater N2pc (N2-posterior-contralateral) than did happy face targets [46]. An enhanced contralateral delay activity (CDA) (also known as sustained posterior contralateral negativity [SPCN]) then indicated that angry faces might involve more subsequent processing than was required for happy faces. Moreover, lateralized early posterior negativity (EPN) showed that angry faces already induced greater negativity than happy faces at 160 ms, indicating early threat-relevant information processing.

2.1.2. Positive Bias. Although early research found evidence supporting the bias toward happy faces, this phenomenon has not received sufficient attention. Most studies tended to regard it as a perceptual confounder rather than an emotional factor (see, e.g., [16]). However, further accumulation of relevant evidence [17, 18, 47–49] has renewed interest in this phenomenon. For example, Becker et al. [18] used photographs and realistic computer-graphic faces to control all the confounding variables that have arisen in previous attentional bias studies, and they found no support for efficiently detecting angry faces; however, they did find a robust positive bias effect across seven experiments. They suggested that the

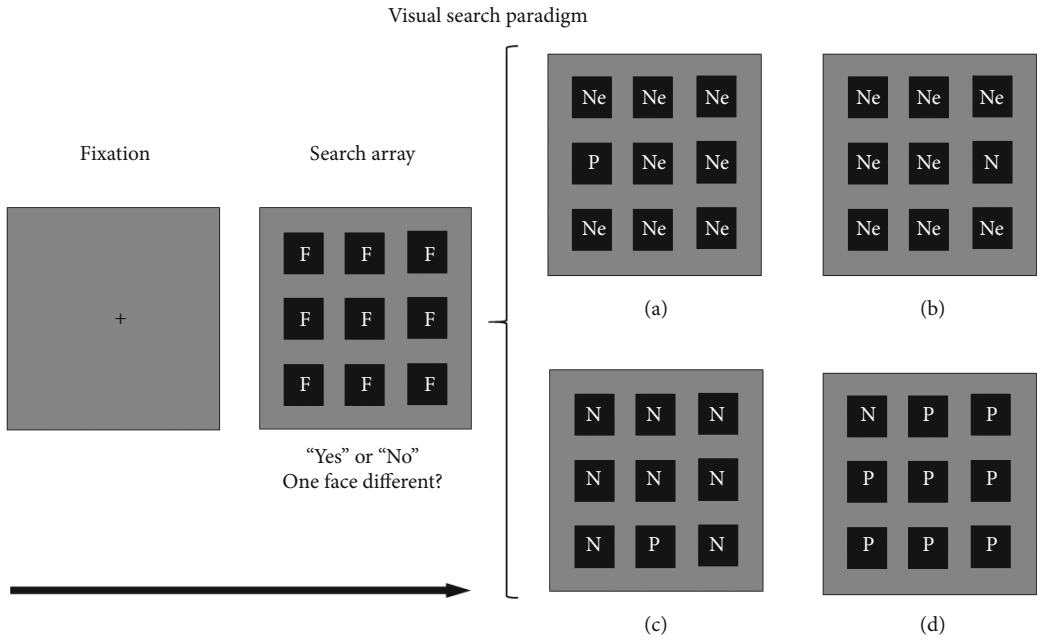

Figure 1: Illustration of a visual search paradigm. Participants needed to detect whether one face differed from the other faces. The letter F denotes a face in the search array. Usually, in half of the trials, all faces show the same expression, while in the other half of the trials, one face shows a different expression from the other faces. The trials containing different kinds of expressions (as presented in panels (a)–(d)) have usually occurred in four versions: (a) one positive face with a neutral face background (P: positive face; Ne: neutral face); (b) one negative face with a neutral face background (N: negative face; Ne: neutral face); (c) one positive face with a negative background (P: positive face; N: negative face); (d) one negative face with a positive background (N: negative face; P: positive face). Note that the set size in each search array can differ across studies. Negative face: angry, fearful, sad, or disgusted expression face; positive face: happy expression face; neutral face: neutral expression face.

positive bias in their studies could not be attributed to low-level visual confounders [18]. Unlike the negative bias, which yielded a robust effect with schematic stimuli, little evidence supported the positive bias with schematic faces [19]. Only one study showed a positive bias when the distractors were changed to a heterogeneous (i.e., using different identities in the search array) background instead of a homogenous (i.e., using the same identity in the search array) background [50].

Similarly, several other neuroscience studies have supported the positive bias. For example, studies using the eye-tracking technique have provided evidence for an attentional bias toward happy faces. Calvo et al. [48], in their study, showed that happy targets were detected faster than any other expressions (e.g., surprised, disgusted, fearful, angry, or sad). Conversely, and in contrast to previous studies [44, 45], angry faces were detected more slowly and less accurately than were happy, surprised, disgusted, and fearful faces [48]. However, compared to studies on the search advantage of angry faces, fewer EEG studies have supported a bias toward happy faces, which only indirect evidence has implied. For example, one study [51] suggested that the widely used stimuli in previous studies (e.g., happy and angry faces) are not equal in biological relevance to observers. Therefore, the authors used baby faces as positive stimuli and compared the results with angry adult faces (as negative stimuli) in an attention task. Their results indicated that positive and negative stimuli induced similar modulations in P1 amplitude and with corresponding topography and source localization, suggesting that both positive and negative stimuli have similar advantages in capturing attention at the neural level [51].

2.2. Behavior and Neuroscience Evidence with Different Emotional Faces in the Change Detection Paradigm

2.2.1. Negative Bias. Using the change detection paradigm (see Figure 2 for an illustration of the stimulus conditions; see Supplementary Materials for more detailed introduction of this paradigm and frequently used behavioral and neural indexes), Jackson et al. [27] first examined how expression and identity interact with one another (face identity was task relevant while expression was task irrelevant). Their results consistently showed enhanced VWM performance with different set sizes, durations, and face sets. With schematic faces, other researchers limited the cognitive resources by manipulating the encoding time and set size, and they found better memory performance for angry faces with short exposure time (150 ms) and a large set size of stimuli (five items) [52]. Similarly, researchers found that participants could better maintain fearful faces in VWM than they could retain neutral faces [30, 53]. Research has also shown enhanced VWM storage for fearful faces compared to neutral faces [30, 54].

The use of EEG confirmed that threatening faces (both fearful and angry faces) showed an enhanced N170 response and higher theta power compared to both positive faces (very happy and somewhat happy faces) and neutral faces, both at the encoding stage and at the early maintenance interval after

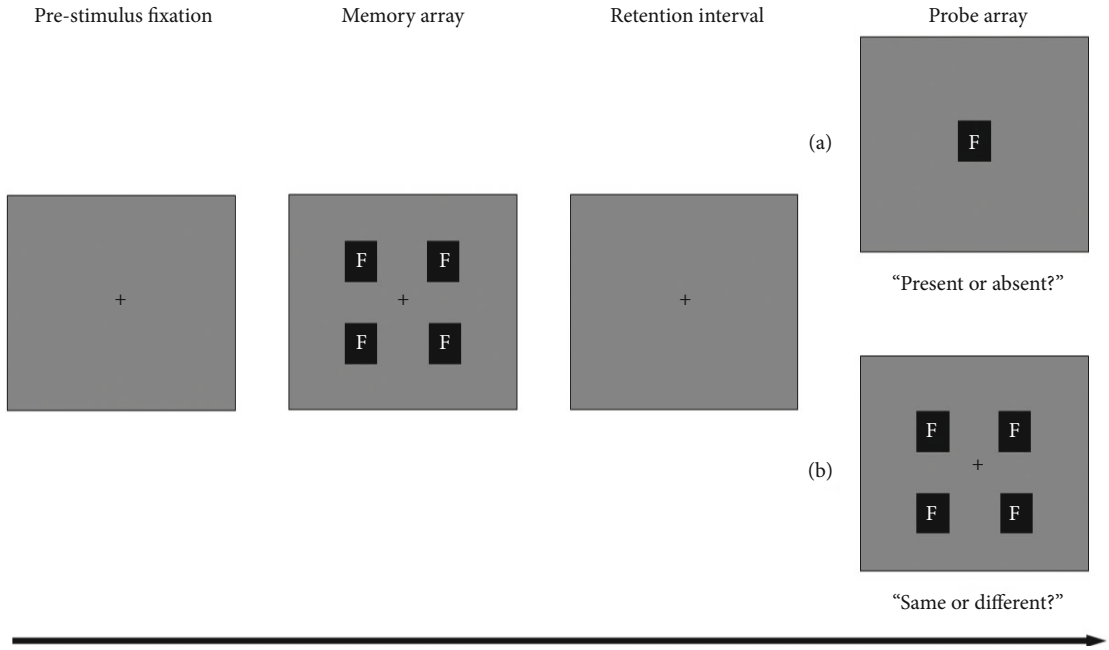

Figure 2: Two versions of the change detection paradigm. Participants need to detect (a) whether the single probe is present or absent in the memory array or (b) whether the probe array is identical to the memory array or one of the faces has changed. The letter F denotes a face, which can be emotional (positive or negative) or neutral in different studies. Note that the set size in the search array can differ across studies. Negative face: angry, fearful, sad, or disgusted expression face; positive face: happy expression face; neutral face: neutral expression face.

the memory array disappeared [55]. Sessa et al. [30] found that fearful faces showed an enhanced CDA compared to neutral faces, which suggested an increased maintenance for a fearful face in VWM than for a neutral face. With a similar experimental setting as their own study, Jackson et al. [28] found the results of functional magnetic resonance imaging (fMRI) supported a benefit of angry faces in the change detection paradigm. Compared to happy and neutral faces, angry faces significantly enhanced blood oxygen level-dependent responses—particularly in three areas of the right hemisphere: the prefrontal cortex, the superior temporal sulcus, and the globus pallidus internus [28].

2.2.2. Positive Bias. Although initial studies have generally reported a negative bias in VWM, the happy face benefit (or threatening face cost) has appeared in recent studies [32–34, 53, 56]. One study that used photographs [53] found superior memory sensitivity for fearful faces but also for happy faces compared to neutral faces. Interestingly, by manipulating memory array and encoding time, Curby et al. [34] found worse VWM performance for fearful faces than for neutral and happy faces, which suggested a fearful face cost in VWM compared to happy and neutral faces. The addition of location information to the change detection paradigm also revealed that the relocation accuracy for happy faces was significantly enhanced compared to angry faces [33]. Studies using schematic faces have also found that, although no memory differences occurred between different emotional faces (approach-oriented positive faces versus avoid-oriented negative faces), high-capacity participants tended to maintain more positive (e.g., happy) than negative (e.g., sad/angry) faces, and this was reflected in a significant correlation between affective bias and the participants' VWM capacity [32].

However, as with the attention studies, the positive advantage in VWM has found less support from neuroscientific evidence. Compared to happy faces, sad faces tend to significantly attenuate facial identity recognition, a finding supported by the exhibited components of N170, N250, P3b, vertex positive potential, and late positive potential [57]. This finding can be partially verified by the overall emotional advantage effect. For example, using the EEG technique, researchers examined the event-related potential (ERP) components of P1, N170, P3b, and N250r in a VWM task [58]. Their results showed that none of these ERP components were modulated by emotional faces during the encoding stage. During maintenance, a decreased early P3b and increased N250r for emotional faces were observed when compared to neutral faces, but no difference in ERP components was apparent between positive and negative faces.

Overall, the development processes and evidence patterns of the change detection paradigm and visual search paradigm are quite similar. The findings of a negative bias have a relatively longer history and greater support from empirical research using cognitive neuroscience techniques. By contrast, the findings of a positive bias have mostly resulted from recent behavioral studies with better control over the potential confounding variables. However, scant neuroscience evidence has supported the positive bias for either the attentional or the VWM studies.

3. Possible Contributing Factors for Emotional Bias

The findings above show that both attention and VWM studies have revealed some controversial results regarding emotional bias. Some studies have discussed and listed several potential contributors for the emotional bias in attention (e.g., [19, 20, 35, 36]). However, to the best of our knowledge, no study has summarized the positive and negative face advantages in VWM. Therefore, we have summarized and listed these advantages in Supplementary Table 1 (including 20 papers with 36 experiments), especially regarding the adoption of the change detection paradigm [27, 28, 30–34, 52, 53, 55–65]. Based on the table summarized by previous studies on visual attention (see [18] for a summary of the visual search paradigm; see [19] for more general methods) and our table for VWM (see Supplementary Material Table 1), we found some common factors responsible for the contradictions in these two areas—especially for studies using the visual search and change detection paradigms. Below, we discuss these possible contributing factors separately, using three aspects: stimulus choice, experimental setting, and cognitive process.

3.1. Differences in Stimulus Choice. In both visual search and change detection paradigm, the experimental materials used for different studies often differ. Previous controversial results could therefore simply reflect the different choices in stimulus materials.

3.1.1. Schematic Faces versus Real Faces. Both photographs of real faces and schematic faces are widely used stimuli in the visual search and change detection paradigms. However, a more consistent negative bias occurs with schematic faces, while photographs of real faces show more evidence of a positive bias for visual attention (for reviews, see [19, 37]). Thus, the choice of stimulus (schematic or real faces) used in an experiment is crucial. Similarly, in the field of VWM, as we mentioned in the previous section, different studies using different stimuli have yielded different results.

For visual attention, a schematic face undoubtedly allows for better control of physical features than can be achieved with photographs. However, the representative expressions of a schematic face are limited, and they lack ecological validity. Thus, schematic faces have been criticized for presenting differences in the perceived configuration of the stimulus itself, rather than reflecting a direct response to emotions [66–68]. For example, some researchers have emphasized that the attentional bias toward angry faces in the visual search paradigm using schematic faces resulted from perceptual grouping, in which participants perceived happy faces as a group more easily than angry faces; therefore, angry faces were more salient when happy faces served as distractors [68]. Photographs of real faces are more ecologically valid; however, the results differ significantly for visual search studies. Previous studies have even found different results based on individual differences and different stimulus sets as the materials in the visual search paradigm [69]. Moreover, when using photographs, various settings of the eyes and mouth may be potential influencing factors. For example, emotional bias can be obtained from the eye characteristics alone (for bias toward angry faces, see [70]; for bias toward happy faces, see [18]). Whether the teeth are exposed also leads to different results as well [71]. However, these factors undeniably also serve as the major composition of the expression per se; thus, one cannot entirely attribute this controversy to perceptual differences, especially for photographs.

Similarly, in the change detection paradigm, the results for schematic faces have also tended to favor either a negative bias or an overall affective bias, which may also relate to problems that we mentioned earlier in attention studies. Different studies using photographs have used various sets of stimulus materials (see Supplementary Table 1). For example, the series of experiments by Jackson et al. [27] used the Ekman set [72] and the Karolinska Directed Emotional Faces (KDEF) database [73], while the materials used by Curby et al. [34] were a collection of four stimulus databases (the NimStim database [74], the KDEF database [73], the CVL Face Database [75], and the Radboud Faces Database [76]). These variations in stimulus materials from different studies complicate any direct comparison of the two effects. Besides, the stimuli used in previous studies did not rule out the effect of some subtle issues that we mentioned above, such as potential influences from the eyes or mouth regions. Although we cannot conclude that different results are due to the use of different stimuli (e.g., the study by Jackson et al. [27] validated an angry face advantage in both image databases), neither can we completely reject the possibility that different memory advantages are irrelevant to the choice of stimulus material.

3.1.2. Stimulus Arousal. "Stimulus arousal" refers to the intensity of metabolic and neural activations of the independent or coactive appetitive or aversive system [77]. Arousal, combined with emotional valence and dominance, has been suggested as a universal, three-dimensional conceptualization of the emotional stimuli [78] in which arousal and valence are culture-free, accounting for major proportion variance in emotional judgment [79, 80]. Reasonably, then, a fair comparison of different expressions requires similar fundamental parameters used in different stimuli. We have found controversial results in previous studies using faces with different emotional valences (i.e., negative and positive biases). Thus, we suggest that stimulus arousal may, in part, be considered responsible for these past results.

A recent meta-analysis of attention studies found a larger negative bias effect for high-arousal scenic or verbal emotional stimuli than for low-arousal stimuli [21]. Although this meta-analysis did not include the factor of face stimuli, other studies have suggested that the degree of arousal also affects the processing of different expressions [81]. For example, in the study by Lundqvist et al. [81], the authors reanalyzed their previous studies (e.g., [16, 82, 83]) and found that the degree of arousal from a picture was highly correlated with the participants' response as the direction of their corresponding superiority effect. At the same time, the researchers asked the participants to rescore the degree of arousal to the photographic stimuli widely used in the visual

search research, and they predicted attentional bias based on the arousal score collected from the original stimulus set. The predicted result ultimately fit well with previous studies [81]. Thus, these findings suggest that the contradiction between negative and positive bias in the visual search paradigm is based on the degree of arousal in response to picture stimulation.

No VWM studies have directly investigated the effect of emotional arousal on memory bias toward positive or negative faces. However, although lacking a direct comparison to emotional arousal between happy and angry faces, one study found that different intensities of angry expressions evoked different CDA amplitudes [61]. Specifically, full expressions had a higher amplitude than both subtle (intermediate intensity angry face, morphed from the continuum between neutral and intense angry face) and neutral expressions, while neutral faces had a higher amplitude than subtle expressions, suggesting that different intensities of emotional faces may affect VWM [61]. Studies have also suggested a reduced overall working memory performance when people need to memorize several high-arousal stimuli simultaneously [84]. Taken together, these results indicate that arousal could at least partly affect VWM performance. However, not all previous studies have measured and controlled for a stimulus's arousal level (see Supplementary Table 1; e.g., [55, 56]), and variations exist in the definition of arousal across different studies, i.e., some studies used intensity as their index (e.g., [34]) while others used arousal (e.g., [58]).

In brief, the choice of stimulus material, as well as stimulus arousal, affects the results of both the visual search and the change detection paradigms. However, some studies have used similar materials and obtained different results (e.g., both used schematic faces or photographs but obtained different results), suggesting that differences in stimulus material choices are not the only reason for the inconsistent results. Thus, differences in experimental settings can also account for some variance in results. We further discuss this issue below.

3.2. Differences in Experimental Settings. The visual search and change detection are different paradigms; however, several aspects in the experimental settings are similar and affect the experimental results for both paradigms. We next discuss the possible experimental settings that may affect the results of the emotional bias from three main perspectives.

3.2.1. Visual Display Size and Corresponding Time. In both the visual search and change detection paradigms, the visual display set size is an essential index concerning behavioral results, such as the search slope (the function of RT and display set size) in the visual search paradigm and number of VWM representations in the change detection paradigm. Thus, both the display set size and the amount of time given to participants to process the task matter.

Previous attention studies have shown that varying the time settings can lead to differences in the composition of an individual's attention [85]. Using an attention task, researchers have found that a probed stimulus presentation time of 100 ms accompanies an attentional bias toward negative stimuli (such as angry faces in an angry–neutral stimuli pair and neutral faces in a neutral–happy stimuli pair), and this trend was reversed when the presentation time was extended to 500 ms [86]. Although this hypothesis may not explain all the previous studies on the visual search paradigm, the time setting seems to affect the results of emotional bias. For example, in studies supporting a negative bias, participants have usually needed to respond in a limited time [15, 42]. However, in studies supporting a positive bias, participants have usually not had specific time limits for their responses. These trials ended when participants pressed a button (e.g., [16, 17]) or when the interval time was much longer than participants needed (e.g., 10 s in [18] or 30 s in [71]).

VWM studies have found more direct evidence supporting the effect of display size and corresponding time. For example, one study found that high perceptual processing competition (e.g., 150 ms exposure time for encoding) revealed an emotional face advantage (i.e., both happy and angry faces had an advantage over neutral faces). By contrast, an angry face advantage emerged when the competition between stimuli was further increased by increasing the stimulus set size [52]. Furthermore, with the same set size of five, a previous study found a VWM performance cost for fearful faces compared to neutral faces, but only with a longer encoding duration (4,000 ms), as it showed no differences with a shorter encoding duration (1,000 ms [34]: Experiment 1 and Experiment 2). Consistently, the advantage of happy faces compared to angry and fearful faces has also been extractable from a long encoding time condition (4,000 ms [34]: Experiment 4a). These results suggest that the emotional bias in VWM may be affected by the set size and stimulus exposure time of memory array. However, we should note that as the processing time of a single stimulus reduces or extends, the VWM representations might risk being confounded with representations of perception or long-term memory.

3.2.2. The Manner of Stimulus Presentation. The visual search is a very context-dependent process; therefore, discussions of targets should not be isolated from those of background stimuli. This concept is also true for the process of the change detection paradigm in which multiple stimuli are usually presented simultaneously, rather than sequentially. Consequently, differences in the manner of the stimulus presentation for the target and the distractor or background stimuli may also contribute to variations in the results on emotional bias.

For example, the presentation of happy and angry faces in the same visual search array could result in different processing speeds for distractors instead of targets [13, 87]. This hypothesis is mainly applicable to situations where opposite emotions are used as the distractors. For example, one study set a homogenous condition in which all stimuli were presented with the same emotional face. The authors found that participants responded more slowly to all-negative faces than to all-positive and neutral faces [13]. From this point of view, the faster processing of angry target stimuli can be explained by the faster processing of happy distractor stimuli, whereas the slower perception of happy target stimuli can be explained by the degree to which negative faces cause attentional difficulties in attention disengagement from the distractors. Thus, the different setting in distractors may ultimately result in processing differences for both types of target stimuli. In addition, the use

of heterogeneous or homogenous identities as a background can also lead to different results. For example, while previous schematic faces had yielded more consistent results for a negative bias, a positive bias emerged when a heterogeneous background was used [50]. However, this phenomenon does not fully explain the results obtained with photographs because some studies with a heterogeneous background showed a positive bias [16, 18], while others showed a negative bias [40, 45].

The effect of the manner of presentation may be generalized to the findings of VWM studies. Previous studies can be roughly divided into two kinds of settings in terms of stimulus presentation, namely, different identities with the same expression [27, 28] and the same identity with a different expression [52, 56]. Although these settings do not appear to directly cause different results, differences in stimulus presentation have occurred across studies despite the use of a similar experimental paradigm. In addition, the change detection paradigm typically involves two stimulus arrays, a "memory array" and a "probe array." The patterns of both arrays affect the experimental results, and the results may also be influenced by the visual search process itself—either at the memory array or the probe array. Besides memory maintenance, memory filtering is another essential aspect of studying VWM. The manipulation of fearful and neutral faces as targets or distractors in a change detection task has revealed in previous studies that—in general—fearful faces are more challenging to filter than are neutral faces, thereby reflecting a larger CDA amplitude in the fearful-distractor-with-neutral-target condition [54]. Follow-up behavioral and fMRI studies found similar result patterns [88, 89]. Ye et al. [90], who used the CDA component, found that participants with high VWM capacity were able to filter all the facial distractors from VWM, regardless of their expression, while low-capacity participants failed to filter the neutral and angry faces but efficiently filtered happy faces. In addition, a follow-up study used a similar paradigm and found that participants in the personal relative deprivation group failed to filter out neutral or angry facial distractors but succeeded in filtering out happy facial distractors from VWM [91]. All these studies suggest that the expression types of stimuli modulate both storage and distractor filtering in VWM. From this point of view, the use of the same or different emotional faces in a memory array could also lead to different results.

3.2.3. Differing Demands in Experiments. Another important aspect in experimental settings relates to the observers. We human beings, as subjective animals with our own thoughts, may also be indirectly affected by how experimenters provide instructions and by our own understanding of an experiment. As Supplementary Table 1 shows, although the paradigm remains basically the same, the participants' task can be further divided (e.g., detect whether identity is present or absent, detect whether identity is the same or different, detect whether the expression is the same or different, and detect whether the probe is the same or different). Therefore, the demands placed by the experiment and the participants' own strategies in understanding the task instructions could partially affect the results of emotional bias.

Previous studies using a visual search have suggested employing a fixed target to avoid the discrepancies caused by different strategies across participants. That is, the specific target would be given an emotion (e.g., happy face) at the beginning of the task, and the participants were then asked to constantly search for this target emotion across trials [35]. Although this type of control reduces the variation in subjects' own search strategies, we argue that it also makes the search task more difficult to distinguish from the recognition task. Unlike the controversial results on the visual search, which require a rapid but less in-depth process, expression recognition studies have more consistently supported positive bias [37]. Most of the previous visual search studies supporting negative bias also did not specify the target stimulus before conducting their experiments with participants [12, 13, 43]. On the contrary, studies in favor of positive bias have often asked participants to find target stimuli for specific emotions (i.e., they used a fixed target [16, 18, 47]). These results also raise concerns that some of the positive bias findings might be confounded with the interference of face recognition.

A similar impact from experiment instruction can also occur in VWM studies using the change detection paradigm. For example, the information that participants were required to remember has differed across studies (see column 8 in Supplementary Table 1). Some studies have regarded emotional information as a form of task-independent information [27, 28, 30, 34], while others have regarded the expression as task-related information [31, 32, 52]. Although this setup difference may not directly explain the observed discrepancy, a deeper processing of emotional information seems to be more likely to trigger positive bias. For example, in a relocated task [33], or when a longer encoding time was provided [34], the happy face advantage emerged in VWM.

These results suggest that different experimental settings may involve different cognitive resources. Therefore, by moving beyond these methodological challenges, a more likely explanation for the conflicting results of previous studies is that negative bias and positive bias act at different cognitive stages.

3.3. Different Stages in the Cognitive Process. In both the visual search and the change detection paradigms, the participants must finish several cognitive processes to accomplish their whole task. In attention research, the process of the visual search paradigm has, conventionally, contained at least two distinct but interrelated stages: the preattentive stage and the attentive or postattentive stage. The preattentive stage occurs before the attentional selection of a target stimulus. In this stage, the process does not require attentional allocation to the stimulus, whereas the attentive or postattentive process involves the direct focus on a target stimulus [92]. Calvo et al. [48], who used eye movement techniques, proposed a third stage of visual search for emotional faces called "decision efficiency." The decision efficiency stage occurs immediately before decision-making, as the varying decision times between fixing the gaze on the target stimulus and making a choice have shown for different emotional faces

[48]. For VWM studies, the change detection paradigm process comprises four stages: the encoding stage, the consolidation stage, the maintenance stage, and the retrieval stage [93]. The encoding stage in VWM overlaps with the processes in attention research, during which, perception representations are created and then consolidated into VWM representations during the consolidation stage. After the stimulus disappears, the participants need to "maintain" VWM representations and then "retrieve" them in subsequent tasks to complete the whole cognitive process of VWM. In addition, the VWM consolidation comprises two different stages [94–96]. In the early consolidation stage, individuals automatically create low-precision representations. Subsequently, in the late consolidation stage, individuals can voluntarily create high-precision representations.

For visual search studies, one possibility is that an automatic bias toward negative emotions exists in the early preattentive stage, whereas the positive bias is revealed in the later recognition and/or decision-making stages. Consistent with this point of view, the use of an emotion classification task combined with the EEG technique has revealed that N170, in the early stage, showed a higher response to negative faces—such as angry, fearful, and sad faces. By contrast, happy faces tended to correlate with facilitation in categorization (reflected by P3b) and decision-making (reflected by a slow positive wave in the later stage) [97]. LeDoux [98] concluded from animal model studies that the fear response could comprise two pathways. In the subcortical pathway, information is sent rapidly and directly to the amygdala. By contrast, in the cortical path, information is sent to the cortex for subsequent analysis before reaching the amygdala. Therefore, the subcortical pathway activates the amygdala in advance and enables a ready state for fearful information. Thus, once information on the cortical path is transmitted to the amygdala, the individual can respond immediately. Therefore, the amygdala can combine limited information for a rough but rapid assessment of threat stimulation at the early stage. This first stage of quick evaluation is likely the neural mechanism that produces the superiority effect of threat stimuli (angry and fearful faces). However, other emotional information (i.e., a happy face) may reach the cortical path with more comprehensive processing. Studies have confirmed that although happy faces can also activate the amygdala, the effect is mainly observed at the later stimulus presentation time [99]. On the contrary, Becker and Rheem [36] have an opposite view and suggest that threatening faces are privileged at a later stage because of the difficulty of attention disengagement. For either order, however, future studies will need to separate the different stages, as this may help to shed light on the real reasons for the discrepancies in previous results.

Similarly, for VWM studies, although memory usually requires more in-depth processing of task-related information, different emotional information could also affect VWM at different processing stages. For example, different expressions did not show any effect at the encoding stage, but emotional faces (both angry and happy) showed a greater resource allocation at the maintenance stage [58]. Information with different emotional valences also influences VWM via different neural bases [100]. More importantly, previous studies have not been able to dissociate attention from VWM. Therefore, whether attention or VWM is responsible for this discrepancy is difficult to discern.

In conclusion, after controlling for the effects of stimulus materials and experimental procedures, further delineation of different cognitive processing stages may be an effective way to resolve previous conflicts.

4. Summary and Prospects

In this paper, we have mainly considered studies on attention and VWM using different emotional faces, and we have proposed three possible factors that could explain the mixed results of the previous studies. A recent study by Becker and Rheem [36] listed five necessary points of guidance for future researchers who use the visual search paradigm to study expressions. (Extracted from the conclusion of Searching for a Face in the Crowd: Pitfalls and Unexplored Possibilities ([36], p. 635). "(a) Vary the crowd size so that search slopes can be assessed. (b) Account for the speed with which distractors are rejected by considering the target-absent search rates or ensure that all of the distractor arrays are equivalent. (c) Ensure that participants are processing the stimulus signal of interest rather than low-level features that are correlated with this signal. (d) Vary the distractors and targets in ways that keep participants from learning to use any low-level features to complete the task. (e) Jitter the positions of the items in the crowds so that textural gestalts cannot be exploited.") In addition to their guidance, we offer several other suggestions for addressing the problems common to both the visual search paradigm and the change detection paradigm. We first discuss the limitations and recommendations of the existing paradigms related to the visual search and change detection paradigms in order to minimize discrepancies. We then propose some possible directions for future research.

4.1. The Choice of Emotional Stimuli. Above all, in studies of change detection and visual search, researchers need to be more careful in the selection of stimulus materials, especially regarding the control of low-level physical features and stimuli's arousal. The degree of arousal resulting from the stimulus itself should be defined (e.g., distinguish between arousal and intensity) and evaluated comprehensively. Collecting the participants' own arousal evaluations for each experimental stimulus within the study is also important since arousal as such is subjective. We offer three other suggestions for the selection of emotional stimuli.

First, future research should pay more attention to the selection of photographs and schematic faces. Therefore, more advanced technology for further control of facial expression—for example, using computer-generated techniques to create human-like pictures [101]—is needed in future work. The application of dynamic facial expressions, as well as body expressions, also offers possible directions for future exploration [40, 102, 103].

First, future research should pay more attention to the selection of photographs and schematic faces in terms of physical features. Therefore, more advanced technology or

accurate way for further control of physical features—for example, using computer-generated techniques to create human-like pictures [101]—is needed in future work. In addition, the application of dynamic facial expressions, as well as body expressions, also offers possible directions that future research should explore [18, 102, 103].

Second, both attention and VWM studies have considered the use of neutral faces as a baseline setting for comparison with emotional faces. However, neutral faces are more likely to be perceived as negative than positive [19]. This tendency may lead to imbalance in a search array or the encoding stage of a memory array. The use of fearful and angry faces for the threat effect should also be interpreted with caution. Although fearful and angry faces have usually been classified into the same category as threatening faces by previous studies (e.g., [13, 42, 43]), they actually contain different information. The threat source of anger is basically the face per se, while fear serves as a reminder of the threat in the viewer's environment [34, 104]. Therefore, future studies should discuss fearful and angry faces separately, rather than simply categorizing both of them as threatening stimuli.

Third, since emotional faces (e.g., angry faces) are already a source of emotional information per se, another question that future studies should address is whether the currently available results are due to emotional states triggered by expression stimuli. The answer to this question may be negative, mainly because emotional induction usually takes time and needs to remain relatively stable. In typical visual search and change detection paradigms, different emotional faces (positive and negative) often randomly appear in the same trial or in adjacent trials, which can create difficulty for the participants to form a stable emotional state. Thus, emotional states should not be the main cause of the previous controversial studies. However, this suggestion does not negate the effects of emotional states on an individual's processing of attentional or memory tasks. Indeed, previous studies have shown that emotional states or mental illnesses (e.g., depression, anxiety, and worry) can affect attention and VWM [64, 65, 88, 105–109]. However, knowledge is currently limited regarding the influence of emotional states on the results of the visual search or change detection paradigms that use emotional face stimuli. This area should therefore be explored further in future research.

4.2. Standardization of the Experimental Setting. Based on our summary, the experimental settings for both paradigms evidently require further standardization. For example, when testing different visual matrix sizes, future studies should also consider the timing of the stimulus presentation and explore the effects of different combinations of stimulus set sizes and times for both paradigms. The experimental instructions should also be carefully controlled to prevent the involvement of unnecessary cognitive processes.

Most previous studies have used the visual search paradigm and change detection paradigm to investigate emotional face processing in attention and VWM; however, some other paradigms can investigate similar topics in these fields. For example, in the field of attention, the dot-probe paradigm [86], rapid serial visual presentation task (RSVP) [110], and visual crowding paradigm [111] can also explore attentional bias to emotional faces. Similar contradictory results have also been found for emotional bias in studies using the RSVP paradigm (for negative bias, see [112]; for positive bias, see [113]). Some studies have even suggested that VWM and the attentional blink observed in the RSVP paradigm might share the same neural processing and storage capacity mechanisms [52, 114]. In the VWM field, the N-back task [115] is also an appropriate paradigm for testing emotional bias. A growing body of research has used N-back tasks or other tasks to explore the potential differential impact of emotional faces versus neutral faces (for a review, see [116]). Thus, future research should examine whether paradigm types modulate emotional bias in attention and VWM. Likewise, many of the issues mentioned in this paper (e.g., selection of stimulus materials) are applicable to other attention or VWM studies.

4.3. Controlling and Tracking Cognitive Processes. Future studies also need to explore the causes of the positive and negative biases underlying different cognitive processes. This exploration will require that future studies define and divide the different processing stages in corresponding paradigms. Future studies can succeed in this regard by combining traditional behavioral indicators with other neuroscience techniques. Specifically, they can combine different ERP indicators (e.g., N2pc in visual attention studies and CDA in VWM studies) or combine EEG with eye movements to generate fixation-based ERPs [117].

In VWM studies, both attention and memory play vital roles; therefore, different emotional advantages may already exist in the attention process rather than in the memory process. This makes determining whether attention or memory processes caused the mixed results from VWM studies in emotional advantages rather difficult. Future studies can try to separate the attention-related process from the VWM-related process when exploring emotional face advantages in VWM. Alternatively, future studies could include attention and VWM in the same context (e.g., using similar stimuli and experimental settings) and examine the associations between visual attention and VWM. For example, previous study showed a high correlation between the reciprocals of VWM capacity and the visual search slope with line-drawing objects [118]. Therefore, a joint study of these two paradigms could be a feasible alternative to better study the role that attention serves in the emotional bias of VWM.

5. Conclusion

This review of the literature supports the view that the mixed results from previous studies could have been arisen due to differences in stimuli, experimental settings, and processing stages at the neural level. The empirical research and the theoretical background indicate that both negative and positive biases are likely. However, if we eliminate the influence of the stimulus materials and experimental settings, a more likely explanation would be that both biases occur but in different cognitive stages. Researchers should adapt more comparable and well-designed paradigms to provide new evidence of positive and negative bias for emotional faces in

future studies. A combination of neuroscience techniques and advanced data analysis should be also applied to this field to provide a better understanding of the mechanism behind the advantage effect of different expressions. We believe that the adoption of these suggestions will help to settle the controversy of positive/negative emotional bias in visual attention and VWM.

Conflicts of Interest

There is no interest conflict among the authors.

Authors' Contributions

QX and CY developed the concept of the review. QX wrote the first draft of the manuscript. CY supervised the review and assisted in paper revision. QL, SG, LY, HZ, XL and LH provided critical revisions. All authors read and approved the submitted version.

Acknowledgments

This work was supported by grants from the National Natural Science Foundation of China (No. 31700948 and No. 31970989) and from the Academy of Finland (No. 333649 to CY). All the authors had full independence from the funding sources. We would like to thank Dr. Wenbo Luo, Dr. Weiqi He, Dr. Piia Astikainen, and Dr. Jarmo Hämäläinen for their insightful comments especially regarding the attentional part and Dr. Weizhen Xie for the valuable discussion.

Supplementary Materials

Supplementary Material 1 summarizes the paradigms and measures used in visual search and change detection paradigm. Supplementary Table 1 lists the key setups and results in previous VWM studies, especially on the adoption of the change detection paradigm. *(Supplementary materials)*

References

[1] M. M. Chun and N. B. Turk-Browne, "Interactions between attention and memory," *Current Opinion in Neurobiology*, vol. 17, no. 2, pp. 177–184, 2007.

[2] C. N. L. Olivers, F. Meijer, and J. Theeuwes, "Feature-based memory-driven attentional capture: visual working memory content affects visual attention," *Journal of Experimental Psychology. Human Perception and Performance*, vol. 32, no. 5, pp. 1243–1265, 2006.

[3] C. N. L. Olivers, "Interactions between visual working memory and visual attention," *Frontiers in Bioscience*, vol. 13, no. 13, pp. 1182–1191, 2008.

[4] K. Oberauer, "Working memory and attention – a conceptual analysis and review," *Journal of Cognition*, vol. 2, no. 1, 2019.

[5] A. S. Souza and K. Oberauer, "In search of the focus of attention in working memory: 13 years of the retro-cue effect, attention, perception," *Attention, Perception, & Psychophysics*, vol. 78, no. 7, pp. 1839–1860, 2016.

[6] C. Ye, Q. Xu, X. Liu et al., "Individual differences in working memory capacity are unrelated to the magnitudes of retrocue benefits," *Scientific Reports*, vol. 11, pp. 1–11, 2021.

[7] C. Ye, Z. Hu, T. Ristaniemi, M. Gendron, and Q. Liu, "Retro-dimension-cue benefit in visual working memory," *Scientific Reports*, vol. 6, no. 1, pp. 1–13, 2016.

[8] J. Lu, L. Tian, J. Zhang, J. Wang, C. Ye, and Q. Liu, "Strategic inhibition of distractors with visual working memory contents after involuntary attention capture," *Scientific Reports*, vol. 7, no. 1, pp. 1–9, 2017.

[9] Y. Zhang, C. Ye, D. Roberson, G. Zhao, C. Xue, and Q. Liu, "The bilateral field advantage effect in memory precision," *The Quarterly Journal of Experimental Psychology*, vol. 71, no. 3, pp. 749–758, 2018.

[10] T. Liang, X. Chen, C. Ye, J. Zhang, and Q. Liu, "Electrophysiological evidence supports the role of sustained visuospatial attention in maintaining visual WM contents," *International Journal of Psychophysiology*, vol. 146, pp. 54–62, 2019.

[11] K. Fukuda and E. K. Vogel, "Human variation in overriding attentional capture," *The Journal of Neuroscience*, vol. 29, no. 27, pp. 8726–8733, 2009.

[12] C. H. Hansen and R. D. Hansen, "Finding the face in the crowd: an anger superiority effect," *Journal of Personality and Social Psychology*, vol. 54, no. 6, pp. 917–924, 1988.

[13] E. Fox, V. Lester, R. Russo, R. J. Bowles, A. Pichler, and K. Dutton, "Facial expressions of emotion: are angry faces detected more efficiently?," *Cogn. Emot.*, vol. 14, no. 1, pp. 61–92, 2000.

[14] G. Horstmann and A. Bauland, "Search asymmetries with real faces: testing the anger-superiority effect," *Emotion*, vol. 6, no. 2, pp. 193–207, 2006.

[15] A. E. Pinkham, M. Griffin, R. Baron, N. J. Sasson, and R. C. Gur, "The face in the crowd effect: anger superiority when using real faces and multiple identities," *Emotion*, vol. 10, no. 1, pp. 141–146, 2010.

[16] P. Juth, D. Lundqvist, A. Karlsson, A. Ohman, and A. Öhman, "Looking for foes and friends: perceptual and emotional factors when finding a face in the crowd," *Emotion*, vol. 5, no. 4, pp. 379–395, 2005.

[17] M. Williams, S. Moss, J. Bradshaw, and J. Mattingley, "Look at me, I'm smiling: visual search for threatening and non-threatening facial expressions," *Visual Cognition*, vol. 12, no. 1, pp. 29–50, 2005.

[18] D. V. Becker, U. S. Anderson, C. R. Mortensen, S. L. Neufeld, and R. Neel, "The face in the crowd effect unconfounded: happy faces, not angry faces, are more efficiently detected in single- and multiple-target visual search tasks," *Journal of Experimental Psychology. General*, vol. 140, no. 4, pp. 637–659, 2011.

[19] C. Kauschke, D. Bahn, M. Vesker, and G. Schwarzer, "The role of emotional valence for the processing of facial and verbal stimuli—positivity or negativity bias?," *Frontiers in Psychology*, vol. 10, pp. 1–15, 2019.

[20] Q. Xu, W. He, C. Ye, and W. Luo, "Attentional bias processing mechanism of emotional faces: anger and happiness superiority effects," *Sheng Li Xue Bao*, vol. 71, pp. 86–94, 2019.

[21] J. Yuan, Y. Tian, X. Huang, H. Fan, and X. Wei, "Emotional bias varies with stimulus type, arousal and task setting: meta-analytic evidences," *Neuroscience and Biobehavioral Reviews*, vol. 107, pp. 461–472, 2019.

[22] I. Gauthier, P. Skudlarski, J. C. Gore, and A. W. Anderson, "Expertise for cars and birds recruits brain areas involved in face recognition," *Nature Neuroscience*, vol. 3, pp. 191–197, 2002.

[23] K. M. Curby and I. Gauthier, "A visual short-term memory advantage for faces," *Psychonomic Bulletin & Review*, vol. 14, no. 4, pp. 620–628, 2007.

[24] D. Sabatinelli, E. E. Fortune, Q. Li et al., "Emotional perception: meta-analyses of face and natural scene processing," *NeuroImage*, vol. 54, no. 3, pp. 2524–2533, 2011.

[25] S. J. Luck and E. K. Vogel, "The capacity of visual working memory for scenes," *Nature*, vol. 390, no. 10, pp. 279–281, 2018.

[26] S. J. Luck and E. K. Vogel, "Visual working memory capacity: from psychophysics and neurobiology to individual differences," *Trends in Cognitive Sciences*, vol. 17, no. 8, pp. 391–400, 2013.

[27] M. C. Jackson, C. Y. Wu, D. E. J. Linden, and J. E. Raymond, "Enhanced visual short-term memory for angry faces," *Journal of Experimental Psychology. Human Perception and Performance*, vol. 35, no. 2, pp. 363–374, 2009.

[28] M. C. Jackson, C. Wolf, S. J. Johnston, J. E. Raymond, and D. E. J. Linden, "Neural correlates of enhanced visual short-term memory for angry faces: an fMRI study," *PLoS ONE*, vol. 3, no. 10, p. e3536, 2008.

[29] F. Gambarota and P. Sessa, "Visual working memory for faces and facial expressions as a useful "tool" for understanding social and affective cognition," *Frontiers in Psychology*, vol. 10, pp. 1–7, 2019.

[30] P. Sessa, R. Luria, A. Gotler, P. Jolicœur, and R. Dell'acqua, "Interhemispheric ERP asymmetries over inferior parietal cortex reveal differential visual working memory maintenance for fearful versus neutral facial identities," *Psychophysiology*, vol. 48, no. 2, pp. 187–197, 2011.

[31] D. V. Becker, C. R. Mortensen, U. S. Anderson, and T. Sasaki, "Out of sight but not out of mind: memory scanning is attuned to threatening faces," *Evolutionary Psychology*, vol. 12, no. 5, pp. 147470491401200–147470491401912, 2014.

[32] W. Xie, H. Li, X. Ying et al., "Affective bias in visual working memory is associated with capacity," *Cogn. Emot.*, vol. 31, no. 7, pp. 1345–1360, 2017.

[33] S. Spotorno, M. Evans, and M. C. Jackson, "Remembering who was where: a happy expression advantage for face identity-location binding in working memory," *Journal of Experimental Psychology. Learning, Memory, and Cognition*, vol. 44, no. 9, pp. 1365–1383, 2018.

[34] K. M. Curby, S. D. Smith, D. Moerel, and A. Dyson, "The cost of facing fear: visual working memory is impaired for faces expressing fear," *British Journal of Psychology*, vol. 110, no. 2, pp. 428–448, 2019.

[35] A. Frischen, J. D. Eastwood, and D. Smilek, "Visual search for faces with emotional expressions," *Psychological Bulletin*, vol. 134, no. 5, pp. 662–676, 2008.

[36] D. V. Becker and H. Rheem, "Searching for a face in the crowd: Pitfalls and unexplored possibilities," *Attention, Perception, & Psychophysics*, vol. 82, no. 2, pp. 626–636, 2020.

[37] L. Nummenmaa and M. G. Calvo, "Dissociation between recognition and detection advantage for facial expressions: a meta-analysis," *Emotion*, vol. 15, no. 2, pp. 243–256, 2015.

[38] D. G. Purcell, A. L. Stewart, and R. B. Skov, "It takes a confounded face to pop out of a crowd," *Perception*, vol. 25, no. 9, pp. 1091–1108, 1996.

[39] V. Lobue, "More than just another face in the crowd: superior detection of threatening facial expressions in children and adults," *Developmental Science*, vol. 12, no. 2, pp. 305–313, 2009.

[40] F. Ceccarini and C. Caudek, "Anger superiority effect: the importance of dynamic emotional facial expressions," *Visual Cognition*, vol. 21, no. 4, pp. 498–540, 2013.

[41] A. Taylor and J. Barton, "The detection of fearful and angry expressions in visual search," *Journal of Vision*, vol. 15, no. 12, pp. 1354–1354, 2015.

[42] A. Öhman, D. Lundqvist, and F. Esteves, "The face in the crowd revisited: a threat advantage with schematic stimuli," *Journal of Personality and Social Psychology*, vol. 80, no. 3, pp. 381–396, 2001.

[43] G. Horstmann, "Visual search for schematic affective faces: stability and variability of search slopes with different instances," *Cognition & Emotion*, vol. 23, no. 2, pp. 355–379, 2009.

[44] M. G. Reynolds, J. D. Eastwood, M. Partanen, A. Frischen, and D. Smilek, "Monitoring eye movements while searching for affective faces," *Visual Cognition*, vol. 17, no. 3, pp. 318–333, 2009.

[45] J. R. Shasteen, N. J. Sasson, and A. E. Pinkham, "Eye tracking the face in the crowd task: why are angry faces found more quickly?," *PLoS ONE*, vol. 9, no. 4, p. e93914, 2014.

[46] T. Feldmann-Wüstefeld, M. Schmidt-Daffy, and A. Schubö, "Neural evidence for the threat detection advantage: differential attention allocation to angry and happy faces," *Psychophysiology*, vol. 48, no. 5, pp. 697–707, 2011.

[47] M. G. Calvo and L. Nummenmaa, "Detection of emotional faces: salient physical features guide effective visual search," *Journal of Experimental Psychology. General*, vol. 137, no. 3, pp. 471–494, 2008.

[48] M. G. Calvo, L. Nummenmaa, and P. Avero, "Visual search of emotional faces eye-movement assessment of component processes," *Experimental Psychology*, vol. 55, no. 6, pp. 359–370, 2008.

[49] M. G. Calvo and H. Marrero, "Visual search of emotional faces: the role of affective content and featural distinctiveness," *Cognition & Emotion*, vol. 23, no. 4, pp. 782–806, 2009.

[50] B. M. Craig, S. I. Becker, and O. V. Lipp, "Different faces in the crowd: a happiness superiority effect for schematic faces in heterogeneous backgrounds," *Emotion*, vol. 14, pp. 794–803, 2014.

[51] T. Brosch, D. Sander, G. Pourtois, and K. R. Scherer, "Beyond fear," *Psychological Science*, vol. 19, no. 4, pp. 362–370, 2008.

[52] L. Simione, L. Calabrese, F. S. Marucci, M. O. Belardinelli, A. Raffone, and F. A. Maratos, "Emotion based attentional priority for storage in visual short-term memory," *PLoS One*, vol. 9, no. 5, p. e95261, 2014.

[53] H. J. Lee and Y. S. Cho, "Memory facilitation for emotional faces: visual working memory trade-offs resulting from attentional preference for emotional facial expressions," *Memory and Cognition*, vol. 47, no. 6, pp. 1231–1243, 2019.

[54] D. M. Stout, A. J. Shackman, and C. L. Larson, "Failure to filter: anxious individuals show inefficient gating of threat from working memory," *Frontiers in Human Neuroscience*, vol. 7, pp. 1–10, 2013.

[55] C. A. Brenner, S. P. Rumak, A. M. N. Burns, and P. D. Kieffaber, "The role of encoding and attention in facial emotion

memory: an EEG investigation," *International Journal of Psychophysiology*, vol. 93, no. 3, pp. 398–410, 2014.

[56] D. Švegar, I. Kardum, and M. Polič, "Happy face superiority effect in change detection paradigm," *Psihologijske teme*, vol. 22, pp. 249–269, 2013.

[57] M. Liu, L. Zhou, X. Wang, and B. Ye, "Sad expressions during encoding attenuate recognition of facial identity in visual working memory: behavioural and electrophysiological evidence," *Cognition and Emotion*, vol. 34, no. 6, pp. 1271–1283, 2020.

[58] S. J. E. Langeslag, H. M. Morgan, M. C. Jackson, D. E. J. Linden, and J. W. Van Strien, "Electrophysiological correlates of improved short-term memory for emotional faces," *Neuropsychologia*, vol. 47, no. 3, pp. 887–896, 2009.

[59] M. C. Jackson, D. E. J. Linden, and J. E. Raymond, ""Distracters" do not always distract: visual working memory for angry faces is enhanced by incidental emotional words," *Frontiers in Psychology*, vol. 3, pp. 1–9, 2012.

[60] M. C. Jackson, D. E. J. Linden, and J. E. Raymond, "Angry expressions strengthen the encoding and maintenance of face identity representations in visual working memory," *Cogn. Emot.*, vol. 28, no. 2, pp. 278–297, 2014.

[61] P. Sessa, A. S. Lomoriello, and R. Luria, "Neural measures of the causal role of observers' facial mimicry on visual working memory for facial expressions," *Social Cognitive and Affective Neuroscience*, vol. 13, no. 12, pp. 1281–1291, 2018.

[62] S. C. Linden, M. C. Jackson, L. Subramanian, D. Healy, and D. E. J. Linden, "Sad benefit in face working memory: an emotional bias of melancholic depression," *Journal of Affective Disorders*, vol. 135, no. 1-3, pp. 251–257, 2011.

[63] P. M. J. Thomas, M. C. Jackson, and J. E. Raymond, "A threatening face in the crowd: effects of emotional singletons on visual working memory," *Journal of Experimental Psychology. Human Perception and Performance*, vol. 40, no. 1, pp. 253–263, 2014.

[64] T. Maran, P. Sachse, and M. Furtner, "From specificity to sensitivity: affective states modulate visual working memory for emotional expressive faces," *Frontiers in Psychology*, vol. 6, pp. 1–16, 2015.

[65] L. Zhou, M. Liu, B. Ye, X. Wang, and Q. Liu, "Sad expressions during encoding enhance facial identity recognition in visual working memory in depression: behavioural and electrophysiological evidence," *Journal of Affective Disorders*, vol. 279, pp. 630–639, 2021.

[66] D. G. Purcell and A. L. Stewart, "Still another confounded face in the crowd," *Attention, Perception, & Psychophysics*, vol. 72, no. 8, pp. 2115–2127, 2010.

[67] K. M. Mak-Fan, W. F. Thompson, and R. E. A. Green, "Visual search for schematic emotional faces risks perceptual confound," *Cognition & Emotion*, vol. 25, no. 4, pp. 573–584, 2011.

[68] S. I. Becker, G. Horstmann, and R. W. Remington, "Perceptual grouping, not emotion, accounts for search asymmetries with schematic faces," *Journal of Experimental Psychology. Human Perception and Performance*, vol. 37, no. 6, pp. 1739–1757, 2011.

[69] R. A. Savage, S. I. Becker, and O. V. Lipp, "Visual search for emotional expressions: effect of stimulus set on anger and happiness superiority," *Cogn. Emot.*, vol. 30, no. 4, pp. 713–730, 2016.

[70] E. Fox and L. Damjanovic, "The eyes are sufficient to produce a threat superiority effect," *Emotion*, vol. 6, no. 3, pp. 534–539, 2006.

[71] G. Horstmann, O. V. Lipp, and S. I. Becker, "Of toothy grins and angry snarls–Open mouth displays contribute to efficiency gains in search for emotional faces," *Journal of Vision*, vol. 12, no. 5, pp. 7–7, 2012.

[72] P. Ekman and W. V. Friesen, "Measuring facial movement," *Environmental Psychology and Nonverbal Behavior*, vol. 1, no. 1, pp. 56–75, 1976.

[73] D. Lundqvist, A. Flykt, and A. Öhman, "The Karolinska directed emotional faces (KDEF)," in *CD ROM from Department of Clinical Neuroscience, Psychology section*, Karolinska Institutet, 1998.

[74] N. Tottenham, J. W. Tanaka, A. C. Leon et al., "The NimStim set of facial expressions: Judgments from untrained research participants," *Psychiatry Research*, vol. 168, no. 3, pp. 242–249, 2009.

[75] F. Solina, P. Peer, B. Batagelj, S. Juvan, and J. Kovač, *Color-based face detection in the "15 seconds of fame" art installation*, Proceedings of Mirage INRIA Rocquencourt, France, 2003, http://web.mit.edu/emeyers/www/face_databases.html.

[76] O. Langner, R. Dotsch, G. Bijlstra, D. H. J. Wigboldus, S. T. Hawk, and A. D. Van Knippenberg, "Presentation and validation of the Radboud Faces Database," *Cognition & Emotion*, vol. 24, no. 8, pp. 1377–1388, 2010.

[77] P. J. Lang, M. M. Bradley, and B. N. Cuthbert, "Emotion, motivation, and anxiety: brain mechanisms and psychophysiology," *Biological Psychiatry*, vol. 44, no. 12, pp. 1248–1263, 1998.

[78] J. A. Russell, "Culture and the categorization of emotions," *Psychological Bulletin*, vol. 110, no. 3, pp. 426–450, 1991.

[79] J. A. Russell, "A circumplex model of affect," *Journal of Personality and Social Psychology*, vol. 39, no. 6, pp. 1161–1178, 1980.

[80] J. A. Russell, "Is there universal recognition of emotion from facial expression? A review of the cross-cultural studies," *Psychological Bulletin*, vol. 115, no. 1, pp. 102–141, 1994.

[81] D. Lundqvist, P. Juth, and A. Öhman, "Using facial emotional stimuli in visual search experiments: the arousal factor explains contradictory results," *Cognition and Emotion*, vol. 28, no. 6, pp. 1012–1029, 2014.

[82] A. Öhman, P. Juth, and D. Lundqvist, "Finding the face in a crowd: relationships between distractor redundancy, target emotion, and target gender," *Cognition & Emotion*, vol. 24, no. 7, pp. 1216–1228, 2010.

[83] T. B. Lonsdorf, P. Juth, C. Rohde, M. Schalling, and A. Ohman, "Attention biases and habituation of attention biases are associated with 5-HTTLPR and COMTval158met," *Cognitive, Affective, & Behavioral Neuroscience*, vol. 14, no. 1, pp. 354–363, 2014.

[84] M. Mather and M. R. Sutherland, "Arousal-biased competition in perception and memory," *Perspectives on Psychological Science*, vol. 6, no. 2, pp. 114–133, 2011.

[85] E. Fox, R. Russo, and K. Dutton, "Attentional bias for threat: evidence for delayed disengagement from emotional faces," *Cogn. Emot.*, vol. 16, no. 3, pp. 355–379, 2002.

[86] R. M. Cooper and S. R. H. Langton, "Attentional bias to angry faces using the dot-probe task? It depends when you look for it," *Behaviour Research and Therapy*, vol. 44, no. 9, pp. 1321–1329, 2006.

[87] G. Horstmann, I. Scharlau, and U. Ansorge, "More efficient rejection of happy than of angry face distractors in visual search," *Psychonomic Bulletin & Review*, vol. 13, no. 6, pp. 1067–1073, 2006.

[88] D. M. Stout, A. J. Shackman, J. S. Johnson, and C. L. Larson, "Confocal imaging–guided laser ablation of basal cell carcinomas: an ex vivo study," *Journal of Investigative Dermatology*, vol. 135, no. 2, pp. 612–615, 2015.

[89] D. M. Stout, A. J. Shackman, W. S. Pedersen, T. A. Miskovich, and C. L. Larson, "Neural circuitry governing anxious individuals' mis-allocation of working memory to threat," *Scientific Reports*, vol. 7, no. 1, 2017.

[90] C. Ye, Q. Xu, Q. Liu et al., "The impact of visual working memory capacity on the filtering efficiency of emotional face distractors," *Biological Psychology*, vol. 138, pp. 63–72, 2018.

[91] L. Zhang, L. Qiao, M. Xu et al., "Personal relative deprivation impairs ability to filter out threat-related distractors from visual working memory," *International Journal of Psychophysiology*, vol. 162, pp. 86–94, 2021.

[92] D. Smilek, A. Frischen, M. G. Reynolds, C. Gerritsen, and J. D. Eastwood, "What influences visual search efficiency? Disentangling contributions of preattentive and postattentive processes," *Perception & Psychophysics*, vol. 69, no. 7, pp. 1105–1116, 2007.

[93] C. Ye, "Visual working memory resource allocation mechanism in consolidation and maintenance phase," *Jyväskylä studies in computing*, vol. 280, 2018.

[94] C. Ye, Z. Hu, H. Li, T. Ristaniemi, Q. Liu, and T. Liu, "A two-phase model of resource allocation in visual working memory," *Journal of Experimental Psychology. Learning, Memory, and Cognition*, vol. 43, no. 10, pp. 1557–1566, 2017.

[95] C. Ye, H. J. Sun, Q. Xu, T. Liang, Y. Zhang, and Q. Liu, "Working memory capacity affects trade-off between quality and quantity only when stimulus exposure duration is sufficient: evidence for the two-phase model," *Scientific Reports*, vol. 9, no. 1, 2019.

[96] C. Ye, T. Liang, Y. Zhang, Q. Xu, Y. Zhu, and Q. Liu, "The two-stage process in visual working memory consolidation," *Scientific Reports*, vol. 10, no. 1, pp. 1–11, 2020.

[97] M. G. Calvo and D. Beltrán, "Recognition advantage of happy faces: tracing the neurocognitive processes," *Neuropsychologia*, vol. 51, no. 11, pp. 2051–2061, 2013.

[98] J. LeDoux, "Chapter 26 Emotional networks and motor control: a fearful view," *Progress in Brain Research*, vol. 107, pp. 437–446, 1996.

[99] L. H. Somerville, H. Kim, T. Johnstone, A. L. Alexander, and P. J. Whalen, "Human amygdala responses during presentation of happy and neutral faces: correlations with state anxiety," *Biological Psychiatry*, vol. 55, no. 9, pp. 897–903, 2004.

[100] M. Osaka, K. Yaoi, T. Minamoto, and N. Osaka, "When do negative and positive emotions modulate working memory performance?," *Scientific Reports*, vol. 3, no. 1, pp. 1–8, 2013.

[101] J. Spencer-Smith, H. Wild, Å. H. Innes-Ker et al., "Making faces: creating three-dimensional parameterized models of facial expression," *Behavior Research Methods, Instruments, & Computers*, vol. 33, no. 2, pp. 115–123, 2001.

[102] T. Gilbert, R. Martin, and M. Coulson, "Attentional biases using the body in the crowd task: are angry body postures detected more rapidly?," *Cogn. Emot.*, vol. 25, no. 4, pp. 700–708, 2011.

[103] E. G. Krumhuber, A. Kappas, and A. S. R. Manstead, "Effects of dynamic aspects of facial expressions: a review," *Emotion Review*, vol. 5, no. 1, pp. 41–46, 2013.

[104] F. C. Davis, L. H. Somerville, E. J. Ruberry, A. B. L. Berry, L. M. Shin, and P. J. Whalen, "A tale of two negatives: Differential memory modulation by threat-related facial expressions," *Emotion*, vol. 11, no. 3, pp. 647–655, 2011.

[105] Y. Bar-Haim, D. Lamy, L. Pergamin, M. J. Bakermans-Kranenburg, and M. H. van IJzendoorn, "Threat-related attentional bias in anxious and nonanxious individuals: a meta-analytic study," *Psychological Bulletin*, vol. 133, no. 1, pp. 1–24, 2007.

[106] Q. Xu, E. M. Ruohonen, C. Ye et al., "Automatic processing of changes in facial emotions in dysphoria: a magnetoencephalography study," *Frontiers in Human Neuroscience*, vol. 12, p. 186, 2018.

[107] E. M. Ruohonen, V. Alhainen, and P. Astikainen, "Event-related potentials to task-irrelevant sad faces as a state marker of depression," *Biological Psychology*, vol. 149, p. 107806, 2020.

[108] F. Long, C. Ye, Z. Li, Y. Tian, and Q. Liu, "Negative emotional state modulates visual working memory in the late consolidation phase," *Cognition and Emotion*, vol. 34, no. 8, pp. 1646–1663, 2020.

[109] E. H. Ronold, J. Joormann, and Å. Hammar, "Facing recovery: Emotional bias in working memory, rumination, relapse, and recurrence of major depression; an experimental paradigm conducted five years after first episode of major depression," *Applied Neuropsychology: Adult*, vol. 27, no. 4, pp. 299–310, 2020.

[110] W. Luo, W. Feng, W. He, N. Wang, and Y. Luo, "Three stages of facial expression processing: ERP study with rapid serial visual presentation," *NeuroImage*, vol. 49, no. 2, pp. 1857–1867, 2010.

[111] M. Gong and L. J. Smart, "The anger superiority effect revisited: a visual crowding task," *Cognition and Emotion*, vol. 35, no. 2, pp. 214–224, 2021.

[112] F. A. Maratos, K. Mogg, and B. P. Bradley, "Identification of angry faces in the attentional blink," *Cognition & Emotion*, vol. 22, no. 7, pp. 1340–1352, 2008.

[113] S. Miyazawa and S. Iwasaki, "Do happy faces capture attention? The happiness superiority effect in attentional blink," *Emotion*, vol. 10, no. 5, pp. 712–716, 2010.

[114] L. Simione, A. Raffone, G. Wolters et al., "ViSA: a neurodynamic model for visuo-spatial working memory, attentional blink, and conscious access," *Psychological Review*, vol. 119, no. 4, pp. 745–769, 2012.

[115] E. A. Kensinger and S. Corkin, "Effect of negative emotional content on working memory and long-term memory," *Emotion*, vol. 3, no. 4, pp. 378–393, 2003.

[116] S. Schweizer, A. B. Satpute, S. Atzil et al., "The impact of affective information on working memory: a pair of meta-analytic reviews of behavioral and neuroimaging evidence," *Psychological Bulletin*, vol. 145, no. 6, pp. 566–609, 2019.

[117] L. Kulke, "Neural mechanisms of overt attention shifts to emotional faces," *Neuroscience*, vol. 418, pp. 59–68, 2019.

[118] G. A. Alvarez and P. Cavanagh, "The capacity of visual short-term memory is set both by visual information load and by number of objects," *Psychological Science*, vol. 15, no. 2, pp. 106–111, 2004.

Hindawi
Neural Plasticity
Volume 2021, Article ID 8874296, 21 pages
https://doi.org/10.1155/2021/8874296

Research Article

Synergistic Network Pharmacology for Traditional Chinese Medicine Liangxue Tongyu Formula in Acute Intracerebral Hemorrhagic Stroke

Yang Chen,[1,2] Ju Dong,[1] Dongqing Yang,[1] Qin Qian,[1] Pengcheng Wang,[1] Xiaojuan Yang,[1] Wei Li,[1] Guochun Li,[1] Xu Shen,[2] and Fushun Wang[3]

[1]*Department of Public Health of Nanjing University of Chinese Medicine, 210023 Nanjing, Jiangsu Province, China*
[2]*State Key Laboratory Cultivation Base for TCM Quality and Efficacy, Nanjing University of Chinese Medicine, 210023 Nanjing, Jiangsu Province, China*
[3]*Institute of Brain and Psychology, Sichuan Normal University, 610060 Chengdu, Sichuan Province, China*

Correspondence should be addressed to Guochun Li; liguochuncn@126.com, Xu Shen; xshen@njucm.edu.cn, and Fushun Wang; 13814541138@163.com

Received 12 May 2020; Revised 22 June 2020; Accepted 5 February 2021; Published 27 February 2021

Academic Editor: J. Michael Wyss

Background. Nowadays, acute intracerebral hemorrhage stroke (AICH) still causes higher mortality. Liangxue Tongyu Formula (LXTYF), originating from a traditional Chinese medicine (TCM) prescription, is widely used as auxiliary treatment for AICH. *Objective*. To dig into the multicomponent, multitarget, and multipathway mechanism of LXTYF on treating AICH via network pharmacology and RNA-seq. *Methods*. Network pharmacology analysis was used by ingredient collection, target exploration and prediction, network construction, and Gene Ontology (GO) and KEGG analysis, with the Cytoscape software and ClusterProfiler package in R. The RNA-seq data of the AICH-rats were analyzed for differential expression and functional enrichments. Herb-Compound-Target-Pathway (H-C-T-P) network was shown to clarify the mechanism of LXTYF for AICH. *Results*. 76 active ingredients (quercetin, Alanine, kaempferol, etc.) of LXTYF and 376 putative targets to alleviate AICH (PTGS2, PTGS1, ESR1, etc.) were successfully identified. The protein-protein interaction (PPI) network indicated the important role of STAT3. The functional enrichment of GO and KEGG pathway showed that LXTYF is most likely to influence MAPK and PI3K-Akt signaling pathways for AICH treatment. From the RNA-seq of AICH-rats, 583 differential mRNAs were identified and 14 of them were consistent with the putative targets of LXTYF for AICH treatment. The KEGG pathway enrichment also implied that the MAPK signaling pathway was the most correlated one among all the related signaling pathways. Many important targets with expression changes of LXTYF for AICH treatment and their related pathways are great markers of antioxidation, anti-inflammatory, antiapoptosis, and lowering blood pressure, which indicated that LXTYF may play mutiroles in the mechanisms for AICH treatment. *Conclusion*. The LXTYF attenuates AICH partially by antioxidation, anti-inflammatory, and antiapoptosis and lowers blood pressure roles through regulating the targets involved MAPK, calcium, apoptosis, and TNF signaling pathway, which provide notable clues for further experimental validation.

1. Introduction

Nowadays, stroke is still a major threat to people's health. Statistics from the World Health Organization show that 15 million people suffer the disease worldwide each year [1]. Less frequently than ischemic strokes, intracerebral hemorrhage (ICH) makes up 10%-20% of all strokes. But a higher fatality rate is caused in the acute phase of intracerebral hemorrhage (AICH), up to 40%-54% [2, 3]. ICH leads to stroke damage when a troubled brain blood vessel bursts, blood leaks, and the brain is loss of oxygen and blood. Deep brain and nerve damage is made due to the dead blood clot cells and released toxins. High blood pressure is the most common cause of ICH [4]. Various forms

of surgical decompression are in widespread use to treat this kind of stroke, but the effect remains controversial. Unfortunately, there is still no proven (in phase 3 trials) beneficial medical treatment for AICH [5, 6].

In the last two thousand years, traditional Chinese medicines (TCMs) have been applied in treating various kinds of diseases in China, including stroke [7, 8]. Compared with Western medical treatment for AICH, TCMs have fewer adverse effects and holistic and systematic influence on more pharmacological activities and efficacies. Currently, an important challenge is to discover proven therapeutic medication for AICH. Buyang Huanwu Decoction, Fufang Danshen Injection, Xueshuantong Injection, and Liangxue Tongyu Formula are of the most common use for ICH herbal patent injections [9]. Among them, Liangxue Tongyu Formula (LXTYF) is a good prescription beneficial for ameliorating AICH, created by Chinese Medical Master Zhongying Zhou, who has 70 years of medical experience in China. It comprises six botanical medicinal materials like *Rheum palmatum* L. (Dahuang, DaH), *Rehmannia glutinosa* Libosch. (Dihuang, DiH), *Panax notoginseng* (Burk.) F.H.Chen (Sanqi, SQ), *Paeonia lactiflora* Pall. (Chishao, CS), *Paeonia suffruticosa* Andr (Mudanpi, MDP), and *Acori Tatarinowii* Schott (Shichangpu, SCP) and two animal medicines like *Bubali Cornu* (Shuiniujiao, SNJ), *Pheretima aspergillum* (E. Perrier) (Dilong, DL). This formula was adapted from Xijiao Dihuang Decoction, an ancient TCM classical prescriptions reserved in one of the classic works of ancient Chinese medicine called Essential Recipes for Emergent Use Worth A Thousand Gold, and only replaced *Rhinoceri Asiatici Cornu* (rhinoceros horn) with SNJ for the similar medicinal effects and compliance with animal protection and regulations [10]. According to previous research, LXTYF may improve symptoms of AICH, attenuate nerve injury, and remove blood stasis of patients, as well as ameliorate brain edemas in AICH rats [11, 12]. For Ma's 96 AICH patients and Guo's 168 AICH patients in treatment group, LXTYF combined with Western medicine treatment was reported to have a better therapeutic effect than Western medication only [12, 13]. It attenuated symptoms of AICH, promoted the absorption of intracerebral hematoma, improved the recovery of consciousness, and reduced the nerve damage of patients, thus improving the prognosis and reduced the disability rate [12, 13]. Li's previous work has indicated that LXTYF had great pharmacology efficacy on AICH by in vivo and in vitro experiment [14].

In our research, network pharmacology method is applied to predict active components, targets, and pathways of LXTYF to alleviate AICH. TCMs provide multiple components, targets, and pathways, also with similar characteristics with systems biology and network pharmacology. This indicates that we can use the approach of the network pharmacology to deeply investigate the mechanisms of TCMs to alleviate AICH [15]. Further, pivotal human genes and pathways were verified after the conversion of rat transcriptomics RNA-seq data (Figure 1). Especially, in the animal experiment, the commonly used AICH model of spontaneous hypertension rats (SHRs) induced by collagenase was made, and LXTYF administration was then conducted for RNA-seq.

This study is aimed at digging into the system pharmacological mechanism of Liangxue Tongyu Formula (LXTYF) on treating intracerebral hemorrhage via network pharmacology method and RNA sequencing data and providing notable clues for further experimental validation.

2. Materials and Methods

2.1. Herb Formulation Ingredients Collection. The chemical ingredients of six botanical medicinal materials in LXTYF were obtained from Traditional Chinese Medicine Systems Pharmacology Database and Analysis Platform (TCMSP) (http://lsp. http://nwu.edu.cn/tcmsp.php) [16]. TCMSP is a distinctive platform for TCM pharmacology, able to provide herbal information, ADME data for the screening process and related targets of each chemical ingredient. The chemical ingredients of the other two animal medicines in LXTYF were derived from BATMAN-TCM (https://bionet.ncpsb.org/batman-tcm) [17]. BATMAN-TCM is the first online Bioinformatics Analysis Tool for the Molecular mechanism of TCM, which can provide the active ingredients and ranked target prediction of animal medicines for analysis.

2.2. Active Ingredients Screening. The active ingredients from herbs of LXTYF were filtered by OB and DL. OB represents the relative amount of a drug absorbed into the blood circulation, and DL is used to describe pharmaceutical properties of compounds [18, 19]. Based on literature and suggestions in TCMSP, $OB \geq 30\%$ and $DL \geq 0.18$ were selected as a screening threshold [20–22]. Ingredients that meet the above rules will be preserved for further analysis. Moreover, several active ingredients of Dihuang, Sanqi, and Shichangpu with important pharmacological effects were added into the compound database for analysis based on the literature about chemical composition and the Chinese Pharmacopoeia 2015.

2.3. Active Ingredient-Associated Target Prediction. TCMSP and BATMAN-TCM databases are integrated to collect known targets of active ingredients in LXTYF. The target names were obtained from the TCMSP and then converted into Uniprot ID in the "Retrieve/ID Mapping" tool of Uniprot (Universal Protein Resource) database (http://www.uniprot.org/), which is specialized for protein information [23]. To analyze those active components that have unknown target proteins, the following databases were used. PubChem is the world's largest collection of chemical information, in which name, molecular formula, structure, physical properties, and so on can be found [24]. Open Babel toolkit is a toolbox transforming multiple chemical file formats [25, 26]. With the help of these two databases, SMILES formats of those active components were converted. SwissTargetPrediction is a web-based tool used to predict the most possible targets for small molecules. The target predictions are achieved through reverse screening based on the similarity principle [27]. The top 15 potential targets of each active component were predicted from the SwissTargetPrediction database.

2.4. ICH-Associated Target Prediction. Different genes linked to ICH were collected from three existing resources with Medical Subject Heading (MeSH) "Cerebral Hemorrhage".

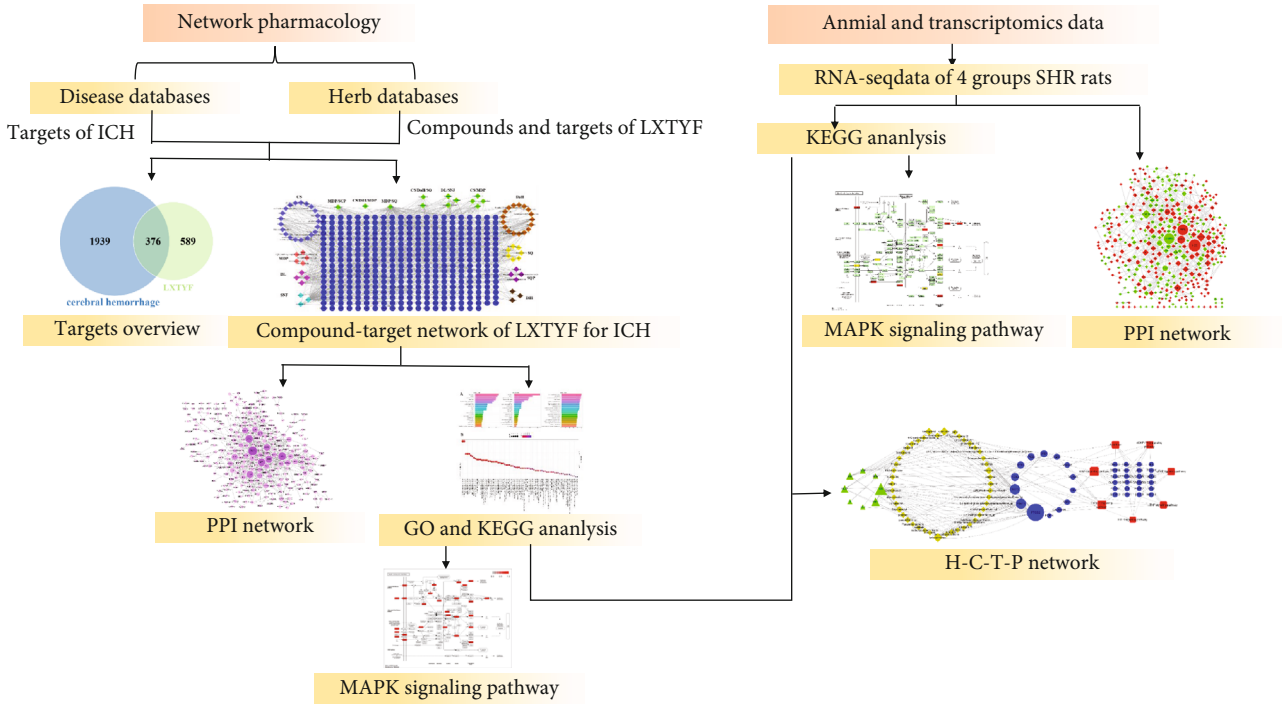

Figure 1: Outline of the study. Network pharmacology method and transcriptomics data were applied to explore the LXTYF effect on AICH.

(1) GAD (http://geneticassociationdb.nih.gov/), a public genetic association database serving for human genetic diseases based on integrated datas of more than 5000 published studies [28]. (2) Genecards (https://www.genecards.org/), an automatically mined database of human genes and a very wide range of resources for gene-centric information in the human genome [29, 30]. (3) DisGeNET (http://www.disgenet.org/web/DisGeNET), which integrates data from animal models, GWAS catalogues, expertly curated repositories, and the scientific literature, constructing a comprehensive platform studying human disease-associated genes and variants [31].

2.5. Network Construction and Key Nodes Analysis. Putative targets of LXTYF for the treatment of AICH were obtained based on the interaction data between active ingredient-associated targets and ICH-associated targets, and Cytoscape software (Version 3.2.1) was utilized to visualize the network for AICH-associated-active ingredients and targets. Degree and betweenness centrality are important topological parameters of networks and were calculated in Cytoscape to measure the topological importance of target and compound nodes [32–34]. The nodes were identified as key targets and key chemical ingredients according to the "Degree" and "Betweenness Centrality" values, which were larger than the average degree and average betweenness centrality of all nodes in the network.

2.6. PPI Network Construction. Proteins are rare to achieve specific functions alone and tend to form macromolecular complexes by interaction in a single cell to complete biological functions [34]. So, it is necessary to analyze the interactions in the proteins-proteins interaction (PPI) network. STRING 11.0 (https://string-db.org/) is a database with integrated data from several active interaction sources such as text mining, experiments, databases, and coexpression. It uploads gene datasets as input and visualizes them in a network for the next analysis [35]. In this study, STRING was used to analyze the interactions between targets (cut – off critical level of high interaction score confidence = 0.95) of LXTYF for AICH.

2.7. Gene Ontology and Pathway Enrichment. The ClusterProfiler package installed in R offers the *groupGO* method to classify genes [36]. There are three aspects associated with GO terms as follows: cellular components (CC), molecular functions (MF), and biological processes (BP). Also, by hypergeometric distribution, *enrichKEGG* function is provided to proceed with enrichment test for KEGG pathways. *p .adjust values* are also estimated to prevent a high false discovery rate (FDR). Pathways that the p.adjust ≤ 0.05 were reserved to analyze.

2.8. Animals and Reagents. Eight crude herbs of LXTYF were purchased from Tongrentang Chinese Medicine Company (Since 1669). Spontaneous hypertension rats (SHRs) were purchased from Beijing Vital River Laboratory Animal Technology Co., Ltd., and animal license number was SCXK (Beijing) 2016-0006. Collagenase type VII was purchased from Sigma-Aldrich (St Louis, MO, USA). Brain stereotaxic instruments and electric drills were bought from Yuyan Instruments Co., Ltd. (Shanghai, China). TJ-1A microinjection pump was purchased from Lange Constant Flow Pump Co., Ltd. (Baoding, China). Microneedle was purchased from Gaoge Industry & Trade Co., Ltd. (Shanghai, China). Chloral hydrate and penicillin were bought from Sinopharm

Chemical Reagent Co., Ltd. (Shanghai, China). TRIzol® Reagent and TBS380 Picogreen were purchased from Invitrogen (Carlsbad, CA, USA). Magnetic frame Ribo-Zero Magnetic kit was bought from EpiCentre (USA). TruSeqTM Stranded Total RNA Library Prep Kit, UNG enzyme, HiSeq 4000 PE Cluster Kit, and HiSeq 4000 SBS Kit (300cycles) were purchased from Illumina (San Diego, CA, USA). Certified Low Range Ultra Agarose was purchased from Bio-Rad (Hercules, CA, USA).

2.9. LXTYF Preparation and Animal Administration. LXTYF consisted of *Cornu Bubali* (SNJ), *Rheum palmatum* L. (DaH), *Rehmannia glutinosa* Libosch. (DiH), *Panax notoginseng* (Burk.) F.H.Chen (SQ), *Radix paeoniae rubra* (CS), Moutan Cortex (MDP), *Pheretima aspergillum* (DL), and *Acori Tatarinowii Rhizoma* (SCP). The crude herbs mixed in the weight ratio of 30 : 10 : 20 : 5 : 15 : 10 : 10 : 10 and extracted by means of reflux in ethanol and water for 3 hours. LXTYF decoction was prepared with 8 : 1 water/oil.

All procedures concerning animals in this study were approved by the ethics committee of Nanjing University of Chinese Medicine. Spontaneous hypertension rats (SHRs) were randomly assigned into cages and adapted for experiment environment in the SPF-room for one week, with food and water regularly and temperature at 20-25°C. 20 male SHR rats (230-260 g) were divided into four groups randomly for modeling and experiments: control group (CG), control group with LXTYF treatment (CGT), ICH-model group (MG), and AICH model with LXTYF-treatment group (MGT), with 5 SHR rats in each group. Rats in CG and MG were given physiological saline, while CGT and MGT rats received intragastric administration of LXTYF decoction for 5 days. 12 h-fasting-rats in MG and MGT were made AICH models by using 0.12 U collagenase of 2 μl and brain stereotaxic instrument. According to our previous study, the middle dose of 11.55 g/kg of LXTYF has the best efficiency on survival time and rate for rats with AICH. So, all the dosage of the following administration was 11.55 g/kg. After 24 hours of modeling, rats were sacrificed by decapitation, and brain tissue of the rat was quickly obtained from where the microinjector was inserted. The specimens of brain tissues were frozen in liquid nitrogen and stored in -80°C refrigerator for RNA-seq.

2.10. Sequencing for Differentially Expressed mRNA. The specimens of brain tissues were obtained from the rats (4 groups with 3 replicates). Total RNA was extracted from brain tissue specimens and tested for its concentration and purity. 5 μg of rat total RNA was started, and the concentration was ≥250 ng/ml. OD260/280 was between 1.8 and 2.2. After removing the rRNA, indexed libraries were prepared from purified RNA with TruSeqTM Stranded Total RNA Library Prep Kit (Illumina) according to the manufacturer's instructions. Randomly interrupted with metal ions, 2000 bp mRNA fragments were obtained. The first strand cDNA synthesis was performed according to the mRNA fragments as described in the Illumina kit. The second strand cDNA synthesis was modified by exchanging dTTP with dUTP. After adding end repair mix to double-stranded cDNA, blunt ends were performed, and A bases were added to attach the Y-shaped adapters. The UNG enzyme digested the second-strand cDNA, and the library only contained the first-strand cDNA. Bridge PCR amplification was performed on cBot, and 2 ∗ 150 bp sequencing was performed on Illumina Hiseq. Further details can be found in the references [37, 38].

2.11. Verification of Related mRNAs and Pathways. With the thresholds of ≥2-fold and the p value of ≤0.05 via edgeR (the Empirical Analysis of Digital Gene Expression in R, v3.2.4) software, differentially expressed mRNAs were identified especially the MGT and MG. Rat genes were converted into human genes based on homology mapping through the Biomart package in R. Compared with the putative targets that LXTYF treats for AICH, PPI network of verified genes and other genes was constructed in STRING and Cytoscape software.

KEGG orthology-based annotation system (KOBAS) is a web server for annotation and identification of enriched pathways and diseases [39]. In our research, enrichment analysis of the differentially expressed mRNAs was performed using KOBAS 3.0 (http://kobas.cbi.pku.edu.cn/anno_iden.php). In the KEGG database, Fisher's exact test was used as a statistical method, and Benjamini and Hochberg was used as an FDR correction method. Enriched pathways that p value ≦ 0.05 were identified compared with former pathway enrichment prediction.

2.12. Herb-Compound-Target-Pathway(H-C-T-P) Network Construction. Compared the pathways enriched by the network pharmacology method with those enriched by RNA-seq data, the common and most likely pathways are obtained. Differentially expressed genes related to common pathways are achieved from the RNA-seq data. The verified gene-related compounds and herbs are found from the collected network pharmacology datas, connections among them were shown in the Herb-Compound-Target-Pathway(H-C-T-P) network and visualized in Cytoscape software.

3. Results

3.1. Active Ingredients of LXTYF. A total of 517 compounds of 8 herbs in LXTYF were collected from TCMSP and BATMAN-TCM database after removing duplicate items, including 119 compounds from CS, 92 compounds from DaH, 76 compounds from DiH, 119 compounds from SQ, 55 compounds from MDP, 105 compounds from SCP, 6 compounds from SNJ, and 8 compounds from DL (S1 Table).

Considering the drug formation of the compound and metabolism after being absorbed into the human body, 81 active ingredients of LXTYF filtered by OB and DL were screened out from the 517 compounds with ADME parameters as shown in Table 1. Specifically, there were 30 active ingredients in CS, 19 active ingredients in DaH, 12 active ingredients in MDP, 12 active ingredients in SQ, 7 active ingredients in DL, 6 active ingredients in SNJ, 5 active ingredients in DiH, and 5 active ingredients in SCP. Among them,

Table 1: Description of ADME parameters of LXTYF active ingredients.

Herb	Mol ID	Molecule name	MW	OB (%)	DL
CS	MOL001002	Ellagic acid	302.2	43.06	0.43
CS	MOL001918	Paeoniflorgenone	318.35	87.59	0.37
CS	MOL001924	Paeoniflorin	480.51	53.87	0.79
CS	MOL002714	Baicalein	270.25	33.52	0.21
CS	MOL002776	Baicalin	446.39	40.12	0.75
CS	MOL002883	Ethyl oleate (NF)	310.58	32.4	0.19
CS	MOL004355	Spinasterol	412.77	42.98	0.76
CS	MOL005043	Campest-5-en-3beta-ol	400.76	37.58	0.71
CS	MOL006992	(2R,3R)-4-methoxyl-distylin	318.3	59.98	0.3
CS	MOL006999	Stigmast-7-en-3-ol	414.79	37.42	0.75
CS	MOL001921	Lactiflorin	462.49	49.12	0.8
CS	MOL006990	(1S,2S,4R)-trans-2-hydroxy-1,8-cineole-B-D-glucopyranoside	332.44	30.25	0.27
CS	MOL006994	1-O-beta-d-glucopyranosyl-8-o-benzoylpaeonisuffrone_qt	302.35	36.01	0.3
CS	MOL006996	1-O-beta-d-glucopyranosylpaeonisuffrone_qt	332.38	65.08	0.35
CS	MOL007004	Albiflorin	480.51	30.25	0.77
CS	MOL007005	Albiflorin_qt	318.35	48.7	0.33
CS	MOL007008	4-Ethyl-paeoniflorin_qt	332.38	56.87	0.44
CS	MOL007012	4-O-methyl-paeoniflorin_qt	332.38	56.7	0.43
CS	MOL007014	8-Debenzoylpaeonidanin	390.43	31.74	0.45
CS	MOL007016	Paeoniflorigenone	318.35	65.33	0.37
CS	MOL007018	9-Ethyl-neo-paeoniaflorin A_qt	334.4	64.42	0.3
CS	MOL007022	Evofolin B	318.35	64.74	0.22
CS	MOL007025	Isobenzoylpaeoniflorin	584.62	31.14	0.54
DaH	MOL000096	(-)-Catechin	290.29	49.68	0.24
DaH	MOL000471	Aloe-emodin	270.25	83.38	0.24
DaH	MOL000554	Gallic acid-3-O-(6′-O-galloyl)-glucoside	484.4	30.25	0.67
DaH	MOL002235	EUPATIN	360.34	50.8	0.41
DaH	MOL002259	Physciondiglucoside	608.6	41.65	0.63
DaH	MOL002268	Rhein	284.23	47.07	0.28
DaH	MOL002280	Torachrysone-8-O-beta-D-(6′-oxayl)-glucoside	480.46	43.02	0.74
DaH	MOL002281	Toralactone	272.27	46.46	0.24
DaH	MOL002297	Daucosterol_qt	386.73	35.89	0.7
DaH	MOL002251	Mutatochrome	552.96	48.64	0.61
DaH	MOL002260	Procyanidin B-5,3′-O-gallate	730.67	31.99	0.32
DaH	MOL002276	Sennoside E_qt	524.5	50.69	0.61
DaH	MOL002288	Emodin-1-O-beta-D-glucopyranoside	432.41	44.81	0.8
DaH	MOL002293	Sennoside D_qt	524.5	61.06	0.61
DaH	MOL002303	Palmidin A	510.52	32.45	0.65
DaH	MOL000472	Emodin*	270.25	24.4	0.24
DaH	MOL001729	Crysophanol*	254.25	18.64	0.21
DaH	MOL000476	Physcion*	284.28	22.29	0.27
DiH	MOL002819	Catalpol*	362.37	5.07	0.44
DiH	MOL003333	Acteoside*	624.65	2.94	0.62
DiH	MOL000732	Stachyose*	666.66	3.25	0.59
MDP	MOL000211	Mairin	456.78	55.38	0.78
MDP	MOL007374	5-[[5-(4-Methoxyphenyl)-2-furyl]`methylene]barbituric acid	312.3	43.44	0.3
MDP	MOL007369	4-O-methylpaeoniflorin_qt	332.38	67.24	0.43

Table 1: Continued.

Herb	Mol ID	Molecule name	MW	OB (%)	DL
MDP	MOL007382	Mudanpioside-h_qt 2	336.37	42.36	0.37
MDP	MOL007384	Paeonidanin_qt	330.41	65.31	0.35
SQ	MOL001494	Mandenol	308.56	42	0.19
SQ	MOL001792	DFV	256.27	32.76	0.18
SQ	MOL002879	Diop	390.62	43.59	0.39
SQ	MOL005344	Ginsenoside rh2	622.98	36.32	0.56
SQ	MOL007475	Ginsenoside f2	785.14	36.43	0.25
SQ	MOL007476	Ginsenoside rb1*	1,109.46	6.29	0.04
SQ	MOL005338	Ginsenoside Re*	947.3	4.27	0.12
SQ	MOL005341	Sanchinoside C1*	801.14	10.04	0.28
SQ	MOL007487	Notoginsenoside r1*	933.27	5.43	0.13
SCP	MOL001944	Marmesin	246.28	50.28	0.18
SCP	MOL003542	8-Isopentenyl-kaempferol	354.38	38.04	0.39
SCP	MOL003576	(1R,3aS,4R,6aS)-1,4-bis(3,4-dimethoxyphenyl)-1,3,3a,4,6,6a-hexahydrofuro[4,3-c]furan	386.48	52.35	0.62
SCP	MOL003578	Cycloartenol	426.8	38.69	0.78
MDP/SQ	MOL000098	Quercetin	302.25	46.43	0.28
CS/DaH/SQ	MOL000358	Beta-sitosterol	414.79	36.91	0.75
CS/DiH/MDP	MOL000359	Sitosterol	414.79	36.91	0.75
MDP/SCP	MOL000422	Kaempferol	286.25	41.88	0.24
CS/DiH/SQ	MOL000449	Stigmasterol	412.77	43.83	0.76
CS/MDP	MOL000492	(+)-Catechin	290.29	54.83	0.24
CS/MDP	MOL000874	Paeonol*	166.19	28.79	0.04
CS/MDP	MOL001925	Paeoniflorin_qt	318.35	68.18	0.4
CS/MDP	MOL007003	Benzoyl paeoniflorin	584.62	31.14	0.54
DL	——	Xanthine	——	——	——
DL	——	Guanosine	——	——	——
DL	——	Xanthinin	——	——	——
DL	——	Hyrcanoside	——	——	——
SNJ	——	Arginine	——	——	——
SNJ	——	Aspartic acid	——	——	——
SNJ	——	Alanine	——	——	——
DL/SNJ	——	4-Guanidino-1-butanol	——	——	——
DL/SNJ	——	Cholesterol	——	——	——
DL/SNJ	——	Guanidine	——	——	——

"*" means the active ingredients retrieved by literature mining that cannot fit the earlier screening criteria but with important pharmacological effects. "——" means the active ingredients collected from the BAT-MAN database with no ADME parameters. SNJ: *Cornu Bubali*; DaH: *Rheum palmatum* L.; DiH: *Rehmannia glutinosa* Libosch.; SQ: *Panax notoginseng* (Burk.) F.H.Chen; CS: *Radix paeoniae rubra*; MDP: Moutan Cortex; DL: *Pheretima aspergillum*; SCP: *Acori Tatarinowii Rhizoma*.

beta-sitosterol, sitosterol, and stigmasterol are shared by three herbs. Quercetin, kaempferol, (+)-catechin, paeonol, paeoniflorin_qt, benzoyl paeoniflorin, 4-guanidino-1-butanol, cholesterol, and guanidine are common active ingredients of two herbs.

3.2. Putative Targets of LXTYF for the Treatment of AICH and Network Construction. On the basis of the 81 active ingredients of LXTYF above, 965 targets were collected from two databases with no duplicate values. Among them, 874 targets of the active ingredients were obtained from the TCMSP (S2 Table), and 149 targets of those active components that have unknown target protein were predicted from the SwissTargetPrediction database (S3 Table). From the GAD, Genecards, and DisGeNET database, 2315 targets relating to ICH were collected (S4 Table). After overlapping the 2315 targets with former 965 targets, 376 targets of LXTYF for treating AICH were obtained as shown in Figure 2(a). At the help of Cytoscape, a putative component-target network composed of 452 nodes and 890

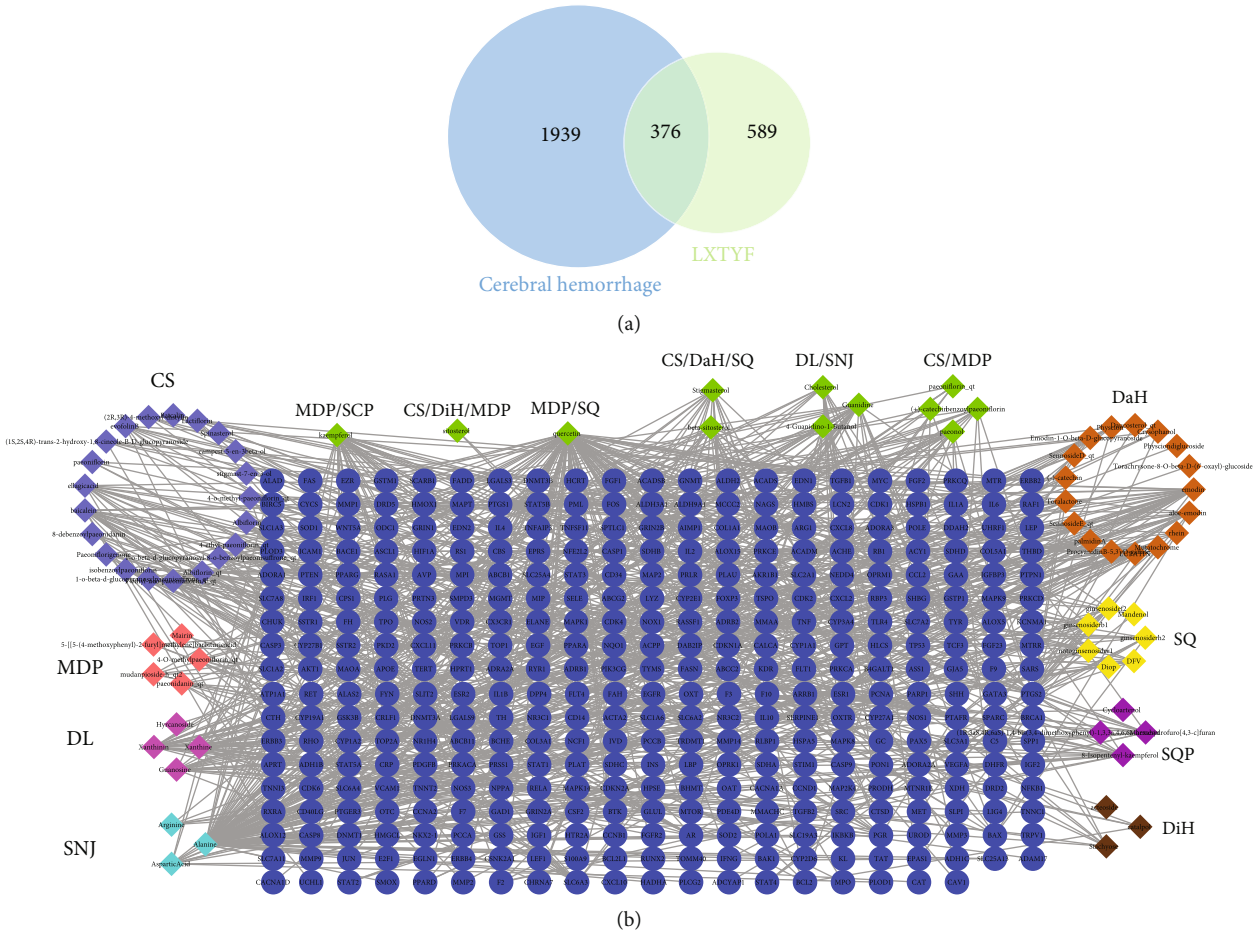

Figure 2: Network construction. (a) Veen diagram describing targets distribution of LXTYF and ICH. (b) The network of Putative Component-Target. Blue ellipses refer to 376 targets of LXTYF for AICH treatment. Different color triangles represent 76 active components in LXTYF. In particular, green triangles stand for common compounds of three and two herbs.

edges were constructed based on 376 targets and the corresponding 76 components as Figure 2(b).

3.3. Network Analysis and Key Nodes Screening. Topological analysis is an effective approach to evaluate the above-mentioned component-target network based on the degree and betweenness centrality parameters (S5 Table for details). The following are the obtained results of the network topological analysis: network heterogeneity (2.144), network density (0.009), and shortest paths (202052, 99%). In the component-target network, the first three targets are PTGS2 (degree = 24), PTGS1 (degree = 21), and ESR1 (degree = 17). The first three components are quercetin (degree = 112), alanine (degree = 104), and kaempferol (degree = 39), which are, respectively, from MDP/SQ, SNJ, and MDP/SCP.

From an in-depth analysis of the complete network above, key components and targets with imporant biological functions can be identified. The nodes (compound and target) whose degrees and betweeness centralities are both larger than the average ones were identified as key targets and chemical ingredients. The average degree of the nodes is 3.938, and 122 nodes are larger than this number. The average betweenness centrality of nodes is 0.006549 and 85 nodes are larger than it. In general, 74 key nodes (35 key components from 76 components and 39 key targets from 376 targets) were obtained, which was shown in Table 2. They were extracted and the connections of the key-compound-target network were displayed in S1 Fig. The first 3 key targets are PTGS2, PTGS1, and AR, and the first 3 key components are quercetin, kaempferol, and emodin, which may all have a great effect on AICH treatment.

3.4. PPI Network Construction. For analysis of the proteins-proteins interaction network of LXTYF for AICH, STRING 11.0 was used to analyze the targets of LXTYF (Results in S6 Table). Apart from the targets independent of the network and the confidence level of interaction score less than 0.95, 275 related targets (from 376 targets) and 850 interactions were included in the network visualized by Cytoscape in Figure 3. The importance of key proteins was then evaluated in light of the degree of the nodes exported from the STRING database. It is clear that the STAT3 (degree = 45) is much larger than other nodes in the network (Avg.numbers of neighbors = 6.182), followed by TP53, AKT1, SRC, JUN, TNF, and MAPK1 (degree values larger than 30). The topological parameters of the PPI network are shown in S7 Table.

Table 2: Key nodes of component-target network.

Herb	Node	Degree	Betweenness centrality
MDP/SQ	Quercetin	112	0.36958975
SNJ	Alanine	104	0.41797809
MDP/SCP	Kaempferol	39	0.06875802
DaH	Emodin	29	0.04544646
DL/SNJ	Guanidine	27	0.08907938
DL	Xanthinin	25	0.08396791
DL	Xanthine	24	0.08789741
CS	Baicalein	23	0.02318204
CS/MDP	Paeonol	20	0.02429964
CS/DaH/SQ	Beta-sitosterol	20	0.02791937
DL	Guanosine	19	0.06005265
SCP	8-Isopentenyl-kaempferol	18	0.02608771
DaH	Aloe-emodin	18	0.01960079
CS/DaH/SQ	Stigmasterol	18	0.03894191
DL/SNJ	Cholesterol	16	0.05001097
CS	Ellagicacid	15	0.01790131
SNJ	Aspartic acid	13	0.03120851
SCP	Marmesin	13	0.0165369
DL/SNJ	4-Guanidino-1-butanol	12	0.03705792
DaH	EUPATIN	12	0.01168363
CS/MDP	Benzoylpaeoniflorin	12	0.01694236
CS	Albiflorin_qt	12	0.0149345
SQ	Ginsenoside rb1	11	0.01531869
SQ	Ginsenoside rh2	10	0.01552107
CS	1-O-beta-d-glucopyranosyl-8-o-benzoylpaeonisuffrone_qt	10	0.00756521
CS	Evofolin B	10	0.01443392
SQ	Notoginsenoside r1	9	0.00950678
SQ	Ginsenoside f2	9	0.0087669
DaH	Mutatochrome	9	0.0191967
DaH	Procyanidin B-5,3′-O-gallate	9	0.02300249
CS	Albiflorin	9	0.00983057
DiH	Stachyose	8	0.00668771
DaH	Palmidin A	6	0.010557
CS	8-Debenzoylpaeonidanin	4	1.33*E*-02
CS	Paeoniflorin	4	0.00892285
Target	PTGS2	24	0.03392333
Target	PTGS1	21	0.0243207
Target	ESR1	17	0.04743098
Target	MAPT	15	0.02405041
Target	PRKACA	15	0.0125587
Target	AR	14	0.0546651
Target	PTAFR	14	0.01000789
Target	PGR	13	0.04286906
Target	SLC6A2	13	0.01380599
Target	SLC6A3	12	0.00778408
Target	ADRB2	9	0.06270829
Target	BAX	8	0.01594706
Target	ESR2	8	0.01052083
Target	F10	8	0.0115522
Target	PRKCA	8	0.07827366
Target	RXRA	8	0.01249876
Target	TOP2A	8	0.01135885
Target	CDK2	7	0.00778363
Target	F7	7	0.00821191
Target	TNF	7	0.01279629
Target	F2	6	0.00701019
Target	IL1B	6	0.06205608
Target	NOS2	6	0.01729864
Target	PRKCD	6	0.00681975
Target	VEGFA	6	0.01754771
Target	AKR1B1	5	0.02396875
Target	JUN	5	0.02537208
Target	MMP9	5	0.00770693
Target	NOS3	5	0.02534139
Target	NR3C2	5	0.0069026
Target	STAT1	5	0.01728485
Target	ADORA1	4	0.04165433
Target	ADRA2A	4	0.01897542
Target	CYP1A1	4	0.01430838
Target	GSTP1	4	0.02559893
Target	HIF1A	4	0.02506214
Target	PPARD	4	0.02353186
Target	TGFB1	4	1.03*E*-02
Target	VDR	4	8.61*E*-03

3.5. Gene Ontology and Pathway Enrichment for Putative Targets. For further study about the putative targets of LXTYF on AICH action, Clusterprofiler package in R was used for analysis due to its higher classification and enrichment accuracy, as well as the visualization module for the results [36]. 376 targets above were applied to run the package for gene classification and KEGG enrichment analysis (FDR ≤ 0.05). Figure 4(a) depicted the top 20 GO terms of biological processes (BP), molecular functions (MF), and cellular components (CC), respectively. Results covered that 376 targets of LXTYF for treatment on AICH in BP were mainly associated with positive regulation of the cellular process, signal transduction, and cellular macromolecule metabolic process. In the aspect of MF, the targets mainly participated in the process of protein binding, ion binding, and cyclic compound binding. Obviously, the cellular components mainly occur in the cytoplasm, intracellular organelle, and nucleus.

Figure 4(b) showed 72 enriched KEGG pathways identified using the Clusterprofiler package. The top 5 enriched

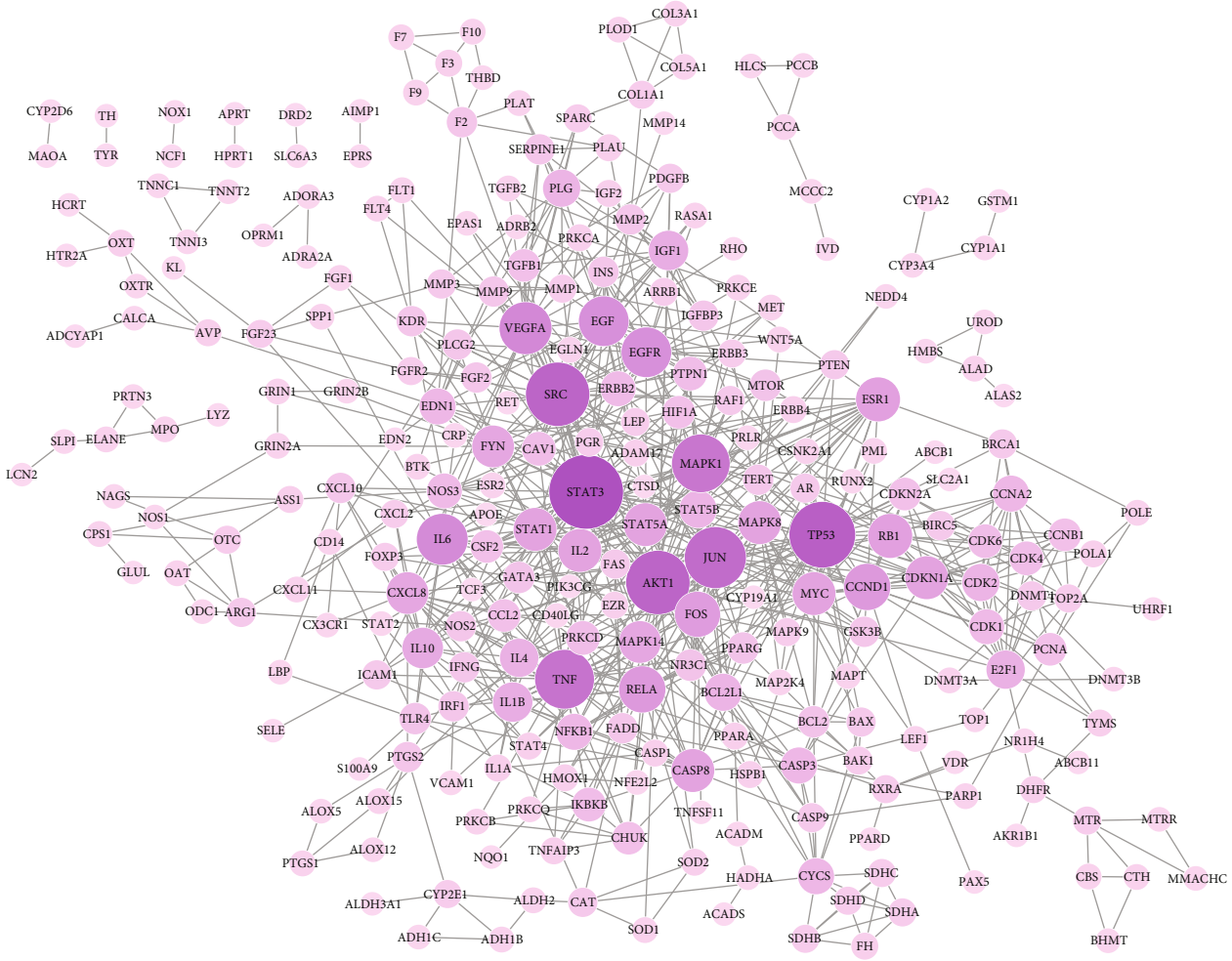

Figure 3: PPI network of LXTYF targets for treating intracerebral hemorrhage (larger degree of the target node with larger and deeper color).

pathways were MAPK signaling pathway, PI3K-Akt signaling pathway, TNF signaling pathway, cAMP signaling pathway, and Ras signaling pathway, with 49,49,33,33, and 33 genes, respectively. See S8 Table for results of putative targets for KEGG pathway enrichment analysis. The most highly enriched pathways related to LXTYF for AICH were the MAPK signaling pathway and the PI3K-Akt signaling pathway. MAPK signaling pathway was shown in Figure 5.

3.6. Identification of Mutually Expressed mRNAs. With a fold-change cutoff of 2 ($p \leq 0.05$), the analysis of differently expressed genes among four groups from the RNA-seq data was shown in Table 3 (3 duplicate values in each group). 766 differentially expressed genes between MG (AICH group) and CG (Control group) showed AICH-induced pathological changes in the SHR rats. Also, 583 differentially expressed mRNAs were identified between MGT and MG, with 308 upregulated mRNAs and 275 downregulated mRNAs. Detailed information for genes is displayed in S9 Table. The 583 rat genes were converted into human genes based on homology mapping using Biomart package in R. Removing the duplicate values, 519 human genes were obtained. Compared with the putative 376 targets that LXTYF for AICH, 14 genes were verified as follows: PTEN, CTH, PTGS2, PTAFR, FOS, NOS1, NOS2, PGR, MMP3, PON1, NEDD4, ACADSB, KL, and CASP3. The interaction network between 14 genes and other 403 genes was shown in Figure 6 at the help of the STRING database (cut off of confidence = 0.4) and Cytoscape. Obviously, FOS, CASP3, and PTEN played an important role among them. Many important targets with expression changes, especially the 14 verified genes and the important gene nodes in the PPI network, are great markers of antioxidation, anti-inflammatory, antiapoptosis, and lowering blood pressure, which indicated that LXTYF may play mutiroles in the mechanisms for AICH treatment.

3.7. KEGG Pathway Analysis of the mRNAs. In total, 519 differentially expressed mRNAs were submitted to KOBAS. The 33 enriched pathways that p value ≤ 0.05 were shown in Table 4. Expression changes of the genes and their related pathways of LXTYF for AICH treatment, such as the MAPK signaling pathway, calcium signaling pathway, Apoptosis, TNF signaling pathway, cGMP-PKG signaling pathway, cAMP signaling pathway, and HIF-1 signaling pathway, are involved in the biological processes of the antioxidation,

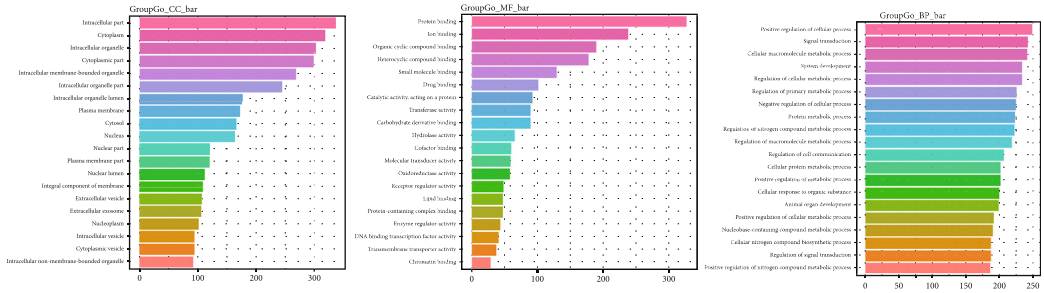

(a)

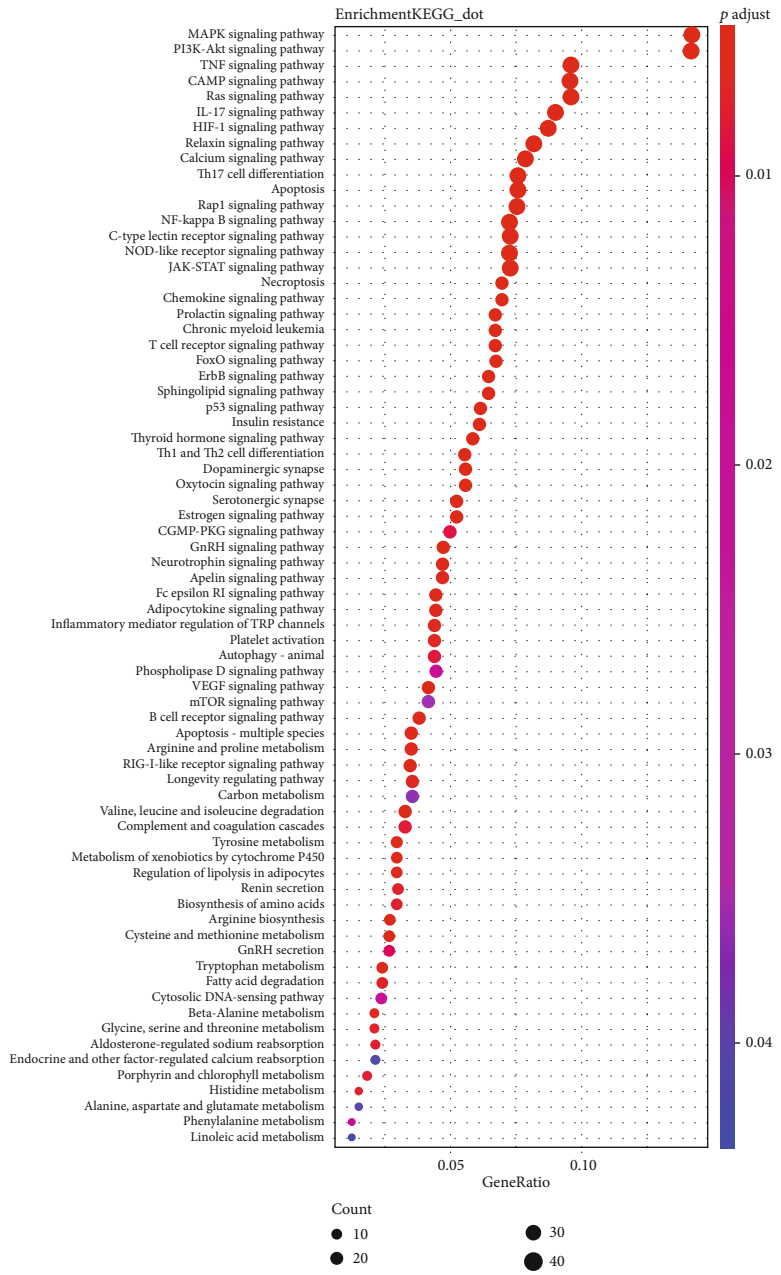

(b)

Figure 4: Enrichment analysis. (a) *groupGO* function for go ontology of 376 targets. The horizontal axis describes the number of genes and the vertical axis describes the GO terms. (b) *enrichKEGG* function for KEGG pathway enrichment analysis of 345 targets. The horizontal axis denotes generatio, and the vertical axis represents KEGG pathway terms. The size of the spot indicates the gene numbers enriched in each pathway and color indicates FDR value.

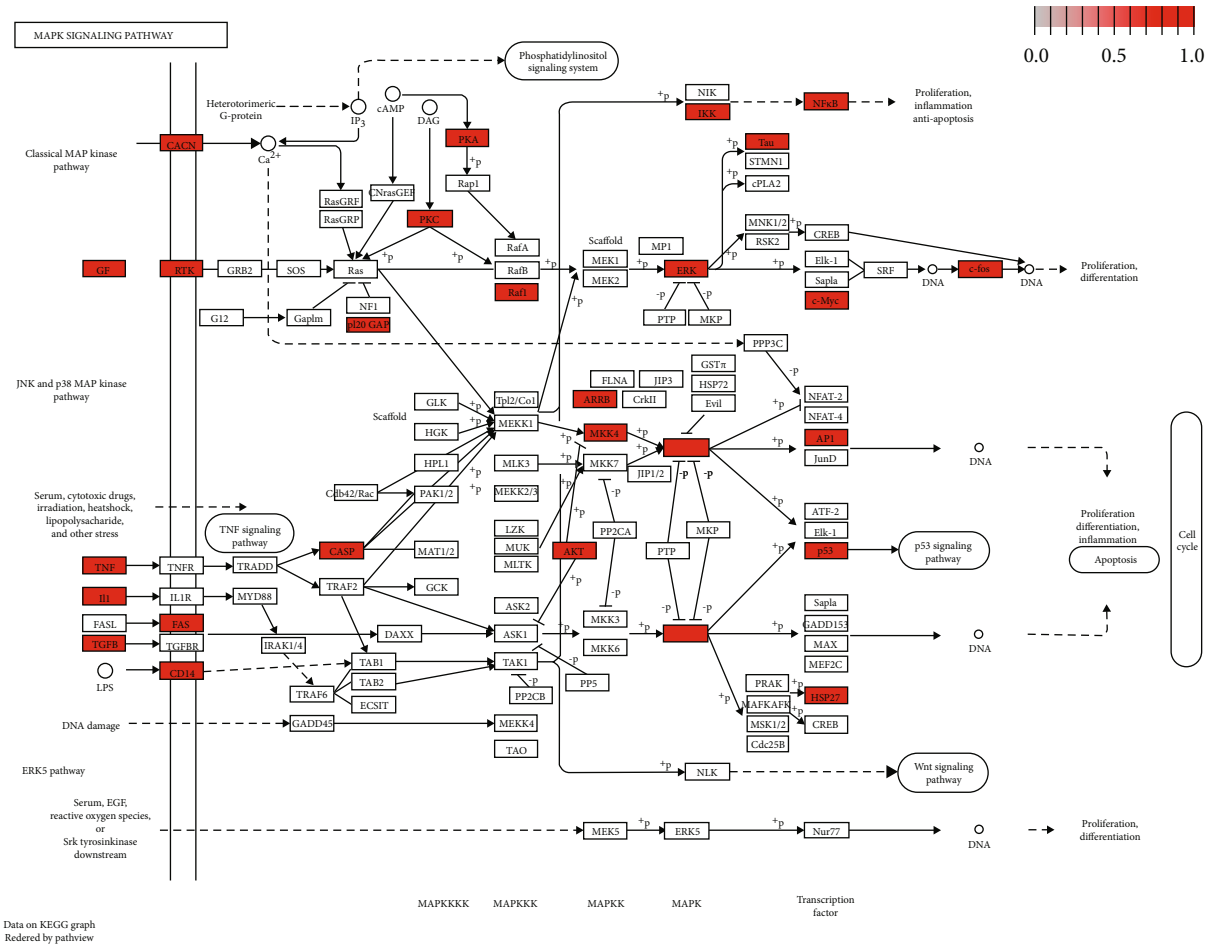

Figure 5: MAPK signaling pathways related to LXTYF for AICH. KEGG ID=hsa04010, enriched with 49 genes.

Table 3: Number of genes expressed in each group of RNA-seq data.

Group	Total genes	Differently expressed genes	Upregulated genes	Downregulated genes
CGT vs. CG	29049	613	324	289
MG vs. CG	29049	766	314	452
MGT vs. MG	29049	583	308	275

CG: control group; CGT: the control group with LXTYF treatment; MG: ICH-model group; MGT: AICH model with LXTYF-treatment group.

anti-inflammatory, antiapoptosis, and lowering blood pressure.

Obviously, most pathways are metabolic pathways, and the analysis identified MAPK signaling pathway as the most correlated signaling pathway, which is consistent with the prediction of the former related pathways of LXTYF intervention on AICH. At the help of the KEGG mapper function in the KEGG database, 11 genes were enriched in the MAPK signaling pathway in Figure 7 as follows: GADD45G, DUSP1, FOS, NR4A11, IL1RAP, MEF2C, NLK, SRF, CASP3, CACNA1H, and TAOK2.

3.8. Herb-Compound-Target-Pathway(H-C-T-P) Network Construction. In view of the mapping results between putative 72 pathways enriched by network pharmacology and 33 pathways and genes enriched in RNA-seq, 7 most common possible pathways were obtained. 38 differently expressed genes related to 7 pathways were achieved in RNA-seq data. Relevant 46 compounds and 8 herbs of the verified 14 genes were achieved from the data collected by network pharmacology. Network connections of the Herb-Compound-Target-Pathway (H-C-T-P) verified in RNA-seq were shown in Figure 8 and Table S10. In this network, nodes of degree among 10~33 which have great topological importance were as follows: CS and DaH in Herb, beta-sitosterol and quercetin in compound, PTAFR and CASP3 in Target, MAPK signaling pathway, and calcium signaling pathway in pathway. Details of connections among the 8 important nodes were shown in Table 5.

The results visually clarify the mechanisms of the multicomponent, multitarget, and multipathway of LXTYF on the treatment of AICH. Further studies can be made and

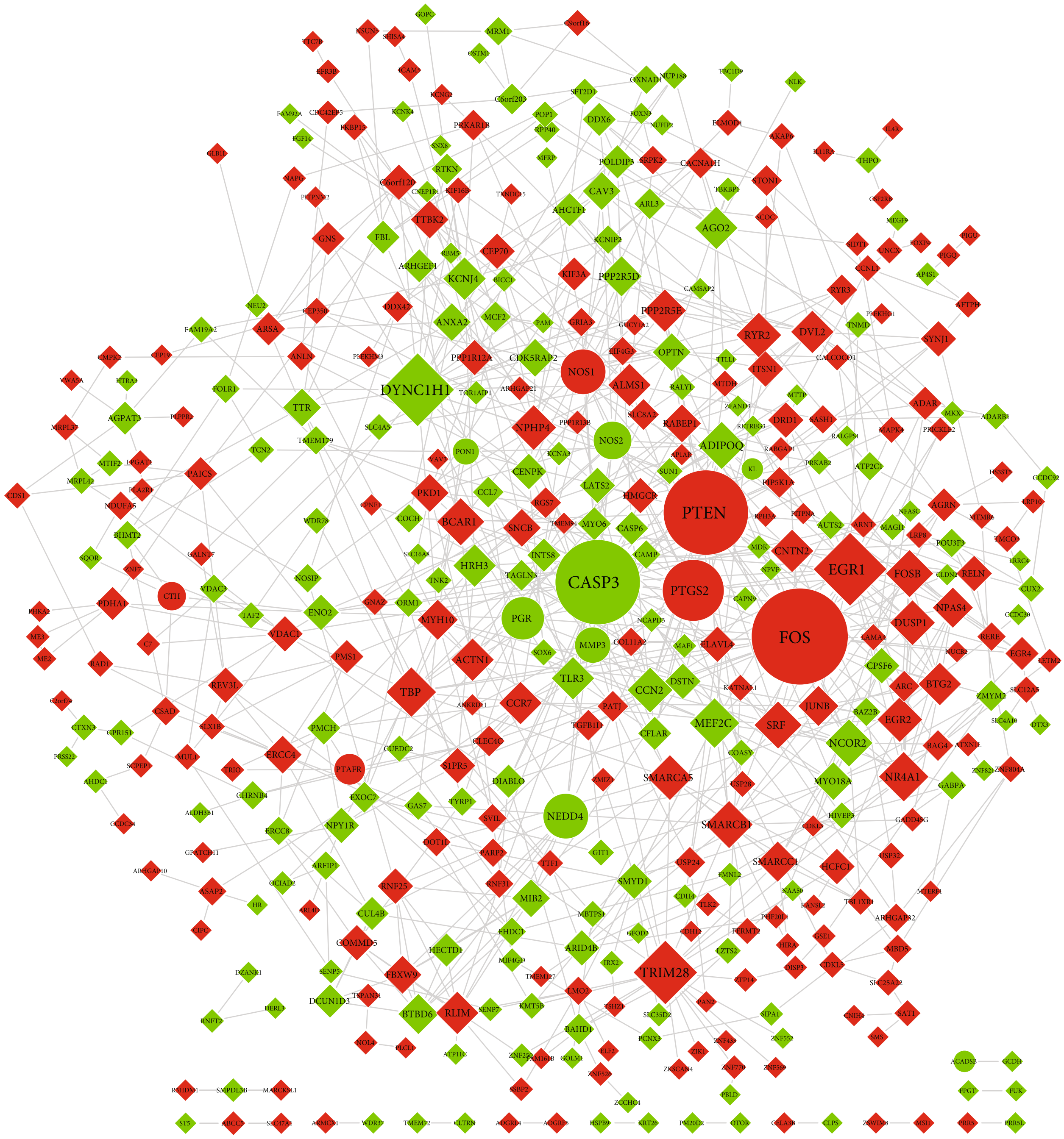

Figure 6: PPI network of identified genes and other differentially expressed genes from the RNA-seq. Compared with the MG, green shapes represent downregulated mRNAs, and red shapes represent upregulated mRNAs in MGT. Ellipses represent the verified genes treated by LXTYF for AICH, and diamonds represent other genes differentially expressed. A larger degree of the target nodes with larger shapes.

deeply investigate mechanisms upon the connections among the H-C-T-P network of LXTYF to treat AICH in our study.

4. Discussion

TCM has been developed and applied in China for more than 2000 years to prevent and treat diseases. To explore active ingredients, predict the targets, and reveal compounds action and drug-gene-disease associations in depth, TCM network pharmacology approach was constructed through “network target, multicomponents” mode [40]. The method is of predictable and systematic features. However, systematically investigating the scientific foundation of TCM formula for diseases at the molecular level is still a great challenge [40]. On the other hand, the development of modern molecular biology and genomic technologies, together with more advances in omics data and computational methods, can help to investigate complex biological pathways and mechanisms of medicines from molecular and cellular levels [41]. Li’s previous study in our group showed LXTYF inhibited apoptosis

Table 4: KOBAS pathway enrichment results of 583 differentially expressed mRNAs.

Pathway name	ID	Input number	Background number	p value	Corrected p value
Metabolic pathways	hsa01100	37	1243	4.87E-06	0.000776
MAPK signaling pathway	hsa04010	11	255	0.000719	0.022949
Calcium signaling pathway	hsa04020	11	180	4.07E-05	0.004326
Oxytocin signaling pathway	hsa04921	9	158	0.00033	0.014855
Regulation of actin cytoskeleton	hsa04810	9	215	0.002595	0.063668
Endocytosis	hsa04144	9	260	0.008413	0.107348
Apoptosis	hsa04210	8	140	0.000686	0.022949
Focal adhesion	hsa04510	8	203	0.006202	0.104136
Neuroactive ligand-receptor interaction	hsa04080	8	278	0.032413	0.198843
Circadian entrainment	hsa04713	7	95	0.000356	0.014855
TNF signaling pathway	hsa04668	7	110	0.000812	0.02355
cGMP-PKG signaling pathway	hsa04022	7	167	0.007476	0.106674
cAMP signaling pathway	hsa04024	7	199	0.017613	0.156542
Tight junction	hsa04530	6	139	0.011322	0.124199
RNA degradation	hsa03018	5	77	0.004147	0.094488
Phosphatidylinositol signaling system	hsa04070	5	98	0.010704	0.121948
Leukocyte transendothelial migration	hsa04670	5	118	0.02151	0.171545
AMPK signaling pathway	hsa04152	5	125	0.026528	0.188053
Dopaminergic synapse	hsa04728	5	130	0.030533	0.1948
Cell adhesion molecules (CAMs)	hsa04514	5	146	0.045802	0.231919
Arginine and proline metabolism	hsa00330	4	50	0.005113	0.10411
Lysine degradation	hsa00310	4	52	0.005821	0.10411
Inositol phosphate metabolism	hsa00562	4	71	0.015938	0.154071
mRNA surveillance pathway	hsa03015	4	92	0.035408	0.200721
Fc gamma R-mediated phagocytosis	hsa04666	4	93	0.036571	0.201138
HIF-1 signaling pathway	hsa04066	4	103	0.049393	0.242404
Pyruvate metabolism	hsa00620	3	40	0.017749	0.156542
Cysteine and methionine metabolism	hsa00270	3	45	0.023739	0.180305
Nucleotide excision repair	hsa03420	3	47	0.026404	0.188053
Notch signaling pathway	hsa04330	3	48	0.027794	0.18808
Fanconi anemia pathway	hsa03460	3	55	0.038589	0.206572
Arginine biosynthesis	hsa00220	2	21	0.034827	0.200721
Glycosylphosphatidylinositol(GPI)-anchor biosynthesis	hsa00563	2	25	0.046729	0.232917

and promoted proliferation in PC12 cells damaged by L-glutamate. Also, a decrease in levels of functional proteins in SHRs such as TNF-a, IL-1, D2D, S-100B, and NSE after LXTYF administration showed LXTYF exerted great pharmacology effect related to anti-inflammatory, anticoagulation, and blood vessel protection activity [14]. Huang's study also showed the cooling-blood and activating-blood effects of LXTYF and its parts via decreases in rectal temperature, blood viscosity, and plasma viscosity of SD rats [42]. In a rat model induced by intrastriatal autologous blood injection, LXTYF significantly ameliorated brain edema after AICH by upregulating metalloproteinase-1 (TIMP-1) and inhibiting metalloproteinase-9 (MMP-9) expression [11].

Network pharmacology and transcriptomics data were applied in this study to understand the underlying different mechanisms and actions of LXTYF for AICH treatment. We successfully identified 76 active ingredients (quercetin, alanine, kaempferol, and so on) of LXTYF and 376 putative targets to alleviate AICH (PTGS2, PTGS1, ESR1, and so on). PPI network indicated the important role of STAT3 in the proteins-proteins interaction. Gene Ontology and KEGG pathway enrichment analysis indicated that LXTYF is most likely to influence the MAPK signaling pathway and PI3K-Akt signaling pathway. From the RNA-seq data of AICH-rats, 583 differentially expressed mRNAs were identified, and 14 of them were consistent with the putative targets of LXTYF treatment of AICH. KEGG pathway enrichment results showed that the MAPK signaling pathway was the most correlated one among the pathways.

4.1. Ingredients and Targets of LXTYF for AICH. Ingredient-target-pathway analysis on herb prescriptions is helpful to uncover the complicated mechanisms underlying diseases and the therapy. Network pharmacology is an effective method

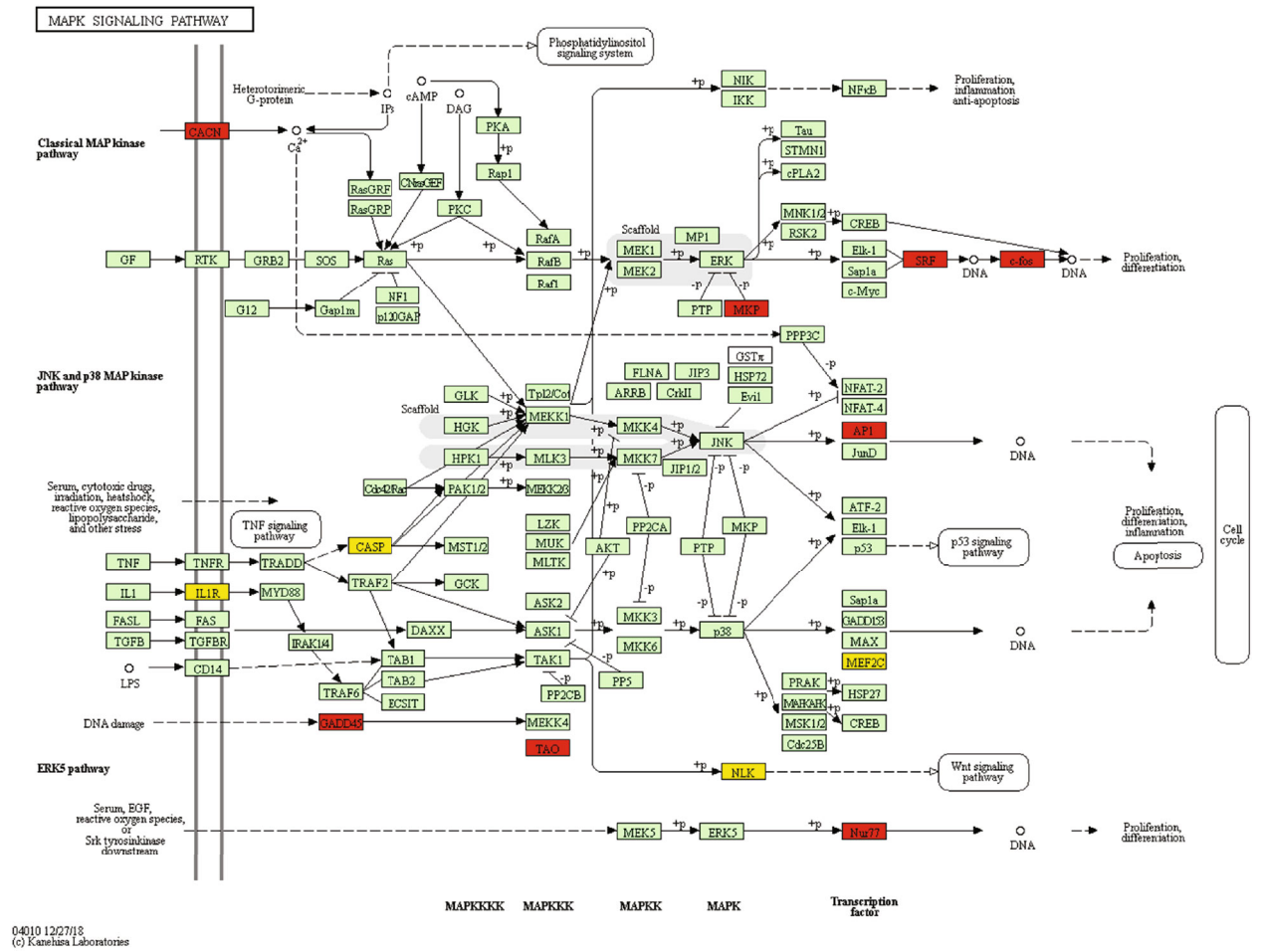

Figure 7: The most correlated MAPK signaling pathway enriched in KEGG mapper. All green boxes represent targets of MAPK signaling pathway in human. 8 red boxes (GADD45(GADD45G), MKP (DUSP1), c-fos (FOS), AP1 (FOS), Nur77(NR4A11), SRF, CACN (CACNA1H), and TAO(TAOK2)) represent upregulated targets. 4 yellow boxes (IL1R(IL1RAP), MEF2C, NLK, and CASP(CASP3)) represent downregulated targets.

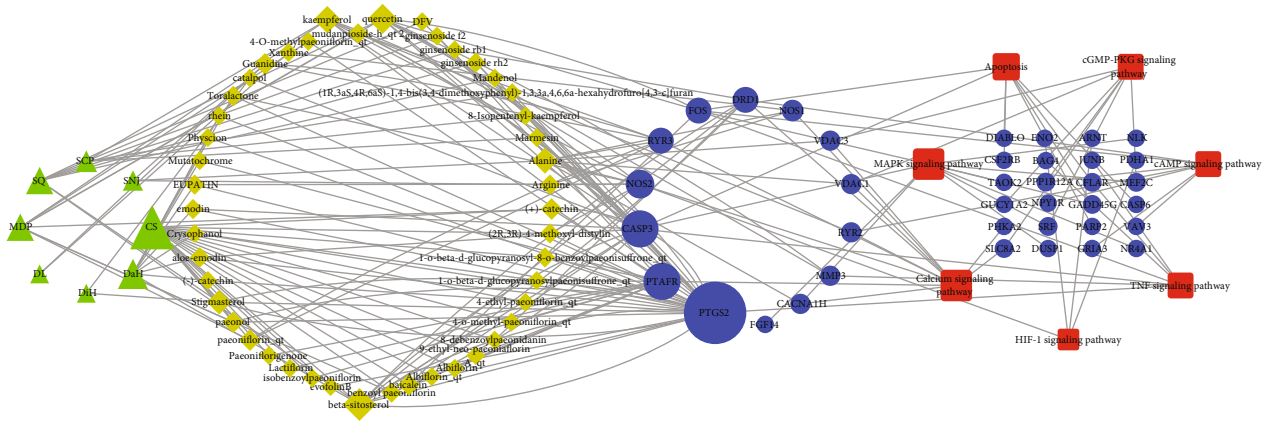

Figure 8: Herb-Compound-Target-Pathway(H-C-T-P) verified network related to the treatment of LXTYF for AICH in RNA-seq. Green triangles represent 8 herbs, yellow diamonds represent 46 compounds, blue ellipses represent 38 targets, and red round rectangles represent 7 pathways. A larger degree of the target nodes with larger shapes.

to deeply investigate the mechanisms of TCMs to treat AICH through muti-ingredients and mutitargets. In this study, 76 active ingredients and 376 targets of LXTYF for treating AICH were obtained at the help of 2315 ICH targets, the deeper results than the 34 active ingredients, 146 targets, and the 1436 ICH targets in our former study [14].

Table 5: Details of connections of important nodes in the H-C-T-P network.

Connections	Node 1	Node 2
Herb-Cpmpound	CS	(+)-Catechin, (2R,3R)-4-methoxyl-distylin, 1-o-beta-d-glucopyranosyl-8-o-benzoylpaeonisuffrone_qt, 1-o-beta-d-glucopyranosylpaeonisuffrone_qt, baicalein, benzoylpaeoniflorin, beta-sitosterol, evofolin B, isobenzoylpaeoniflorin, lactiflorin, paeoniflorigenone, paeoniflorin_qt, paeonol, 4-ethyl-paeoniflorin_qt, 4-o-methyl-paeoniflorin_qt, 8-debenzoylpaeonidanin, 9-ethyl-neo-paeoniaflorinA_qt, albiflorin, albiflorin_qt, stigmasterol
Herb-Cpmpound	DaH	(-)-Catechin, aloe-emodin, beta-sitosterol, crysophanol, emodin, EUPATIN, mutatochrome, physcion, rhein, toralactone
Compound-target	1-O-beta-d-glucopyranosyl-8-o-benzoylpaeonisuffrone_qt, 1-o-beta-d-glucopyranosylpaeonisuffrone_qt, 4-ethyl-paeoniflorin_qt, 4-O-methylpaeoniflorin_qt, 4-o-methyl-paeoniflorin_qt, 9-ethyl-neo-paeoniaflorinA_qt, albiflorin, albiflorin_qt, benzoylpaeoniflorin, ginsenosidef2, isobenzoylpaeoniflorin, lactiflorin, mutatochrome, paeoniflorigenone	PTAFR
Compound-target	Aloe-emodin, baicalein, beta-sitosterol, catalpol, emodin, ginsenosiderh2, kaempferol, quercetin	CASP3
Target-pathway	CACNA1H, CASP3, DUSP1, FGF14, FOS, GADD45G, MEF2C, NLK, NR4A1, SRF, TAOK2	MAPK signaling pathway
Target-pathway	CACNA1H, PTAFR, DRD1, NOS1, NOS2, PHKA2, RYR2, RYR3, SLC8A2, VDAC1, VDAC3	Calcium signaling pathway

The active ingredients involved in eight herbs were screened by OB and DL values, which represent the vast majority of the ingredients absorbed into the blood circulation and pharmaceutical properties of compounds in the prescription, and form a relatively complete chemical component library. To some extent, they can reflect the pharmacodynamic ingredients of LXTYF that may play a role in the clinical medication. Results of the active component-target network of LXTYF to treat AICH showed that most components affected multiple targets. Quercetin, alanine, and kaempferol from MDP/SQ, SNJ, and MDP/SCP acted on 112, 104, and 39 targets, respectively. They are of high OB and DL values and regulated most targets for AICH treatment, also with anti-inflammatory, antioxidant, and antiapoptotic properties. The findings were consistent with previous studies as follows. Alanine was reported to have antioxidant and procoagulant efficacy [10, 43]. D-alanine D-leucine enkephalin (DADLE) has anti-inflammatory, antioxidant, neuroregenerative, and antiapoptotic properties [44]. Quercetin can promote neuronal and behavioral recovery by its antioxidant activity and restraining inflammatory response and apoptosis in a rat model of ICH [45, 46]. Kaempferol can effectively prevent nitrosative-oxidative stress after ischemia/reperfusion via the mechanism of inhibiting the nitrotyrosines and preventing apoptosis by degrading caspase-9 activity and poly-(ADP-ribose) polymerase in model rats [47]. On the other hand, kaempferol glycosides suppress brain injury and inflammation by inhibiting the activation of NF-κB and STAT3 in stroke rats [48]. So, quercetin, alanine, and kaempferol might reasonably be regarded as crucial active compounds of LXTYF to treat AICH.

Numerous constituents make up the complexed TCM system, and combinations of them play a role in the treatment of diseases. From the H-C-T-P network, the compounds of animal herbs like xanthine and guanidine in DL and guanidine, arginine and alanine in SNJ play vital role in the putative mechanisms of LXTYF to treat AICH. SNJ has been a good substitute for *Rhinoceri Asiatici Cornu* (a highly endangered species) since the 1970s because it is abundant, has low price and with similar inorganic, amino acid constituents, and comparable pharmacological properties [10]. Thus, it is favorable to keep the balance between legislation and apparent indispensability of *Rhinoceri Asiatici Cornu* in TCM. The research and discovery of the active ingredients in this study will contribute to find alternative medicines of endangered animals to better protect animals and treat diseases.

Via evaluating topological paramters, among all the putative targets of LXTYF associated with AICH, PTGS2, Bax, TNF, JUN, IL1B, and NOS2 are examples of relatively important targets which are involved in MAPK, PI3K-Akt, TNF, and apoptosis signaling pathways, while RNA-seq analysis showed that the LXTYF administration significantly regulated 583 gene transcriptions in AICH rat models. Combined with putative targets in network pharmacology, a total of 14 genes were verified. PTEN, CTH, PTGS2, PTAFR, FOS, and NOS1 are six upregulated genes, and NOS2, PGR, MMP3, PON1, NEDD4, ACADSB, KL, and

CASP3 are eight downregulated genes. Especially CTH, PTAFR, PGR, PON1, NEDD4, ACADSB, and KL are 7 new genes compared with our previous study [49]. And PPI network of them showed that FOS, PTEN, and CASP3 were core genes playing important roles among the differently expressed genes.

PTGS2 and PTGS1 (Prostaglandin G/H synthase, PTGS) are genes that code for the COX-2 and COX-1(COX enzymes, cyclooxygenase) proteins, respectively [50]. COX enzyme is a key therapeutic target, and its inhibitors such as NSAIDs are widely used in clinical treatment for inflammation, pain, fever, and son on [50]. But inhibition of COX-2 conveys a definite risk of myocardial infraction and stroke due to thrombosis and hypertensive effects [51]. Therefore, upregulation of the PTGS2 gene indicates that LXTYF may reduce the risk of blood pressure elevation, which is conducive to antihypertensive therapy in the early stage of an intracerebral hemorrhage.

Phosphatase and tensin homolog deleted on chromosome 10 (PTEN) is a tumor suppressor, a proapoptotic gene mainly via inactivation of PI3K/AKT signaling pathway, and *PTEN* conditional knockouts have become a potentially approach targeting cancer and obesity treatment [52]. But in stroke treatment, PTEN is a double-edged sword [53]. The previous study showed that PTEN was upregulated in AICH stage, and its inhibition has been reported to be neuroprotective against ischemic stroke in experimental models [53, 54]. While it has been demonstrated that PTEN deletion can lead to cognitive impairment and PTEN loss in neurons and astrocytes is, respectively, unfavorable to long-term functional recovery, exacerbates damage, enhances astrogliosis, and induces inflammation [53]. So, upregulation of PTEN in our study may show that LXTYF treatment has no harm on cognition function and play roles on neuronal-damage recovery after AICH.

Nitric oxide synthases (NOS), with 3 isoforms called neuronal NOS (nNOS/NOS1), inducible NOS (iNOS/-NOS2), and endothelial NOS (eNOS/NOS3), form NO and play dual roles of damage and protection in ICH [55]. NO formed via NOS1 and NOS3 gives rises to vasodilatation, hypotension, inhibitions of platelet aggregation, and adhesion, and as an antioxidant, it exerts other beneficial actions. NOS1 has great significance in controlling salt-water balance, and blood pressure, especially the long-term blockade of NOS1 by 7-NI, a specific inhibitor of NOS, leads to hypertension in rats [55], while NO through NOS2 during inflammation increases oxidative and nitrative stress, causing neurodegeneration and enhancement of apoptosis [56]. Selective NOS2 inhibitors that exhibit neuroprotective properties can be candidate treatments for acute ischemic stroke [57]. So, LXTYF may play function of vasodilatation and antihypertension via upregulation of NOS1 and supress oxidative stress and apoptosis via downregulation of NOS2 to treat AICH.

FOS is one of the components of AP1, the inducer of cell proliferation. It can activate nerve growth factor and has gene repair activities after neuronal death in the stroke model. Knockdown of c-fos enhances necrosis significantly [58]. But serving as an immediate-early gene, its role of expression is complex and has neurotoxic and neuroprotective effects. Especially its neuroprotective effect is mainly on gene repair activities after neuronal death, with intact c-fos transcript playing roles in the necrosis core and oxidative DNA lesions [58]. So, upregulated changes of FOS in RNA-seq showed that LXTYF may have neuroprotective effect and attenuated oxidative DNA lesions and necrosis after AICH, similar to 7-nitroindazole (7-NI). 7-NI is a specific inhibitor of NOS and can increasec-fos mRNA levels and attenuate oxidative DNA lesions, nitric oxide, and necrosis after stroke [58]. But several previous reports showed that upregulation of c-Fos after AICH leads to neuronal apoptosis, and FOS is regarded to be neurotoxic. So, role of FOS in AICH also needs further study.

Caspase 3, a member of caspases family involved in cell death, has been recognized as a crucial mediator of neuronal apoptosis [59]. Stroke is usually of great neuronal cell death and serum caspase-3 concentrations rise in rat models and AICH patients [59–61]. Downregulation of Caspase 3 after administration in this study shows that LXTYF may treat AICH via apoptosis inhibition.

4.2. Pathway Analysis of LXTYF for AICH Treatment. Multicomponent, multitarget, and multipathway are general features of TCMs, and LXTYF has therapeutic effects by making contributions to several pathways. In this present work, putative targets were enriched significantly in 72 KEGG pathways, and the two most important enriched pathways were the MAPK signaling pathway and PI3K-Akt signaling pathway. Our previous study has verified that LXTYF inhibited the apoptosis to treat AICH based on the PI3K-AKT pathway on the level of transcription and protein [14]. Meanwhile, MAPK (mitogen-activated protein kinase) signaling pathway is the most important enriched and verified pathway in our RNA-seq analysis, which plays roles in modulating oxidative stress, inflammatory action, and cell death [62]. It can response to extracellular stimuli, then sequential phosphorylation of kinase cascades MAPKK kinases (MAPKKKs), MAPK kinases (MAPKKs), dual phosphorylation of the tripeptide motif (Thr-X-Tyr), and MAPK were activated, thus transmitting signals to the nucleus [63]. MAPK family consists of four subfamilies: extracellular signal-regulated kinase 1/2 (ERK1/2), p38 kinase, c-Jun amino terminal kinase (JNK), and ERK5. It has been viewed as a potential therapeutic target for stroke and hemorrhagic cerebral vascular disease [64]. Studies have found that the balance of MAPK activities determines cell fate. ERK is activated by various growth factors and shows benefits to cell growth and cellular survival. In contrast, p38 and JNK are activated by stress conditions, leading to inflammation and apoptosis via various mechanisms [65]. Some preclinical researches proved that MAPK inhibition (MAPKi) can dramatically increase the efficacy of immunotherapy, especially in cancer types [66]. Proinflammatory cytokines (interleukin-1beta (IL-1β), tumor necrosis factor-alpha (TNF-α)) and transforming growth factor-beta (TGF-β) activate p38 MAPK, and its specific inhibitors were used as the treatment of peripheral inflammatory diseases [64]. It is known that p38s and ERK5 can trigger phosphorylation of MEF2c and

then increase c-Jun expression [67, 68], which is distinct among several diseases like brain ischemia, injury, cell death, neuro-inflammatory, and neurodegenerative disease [69]. MEF2C, a member of the myocyte-enhancer factor 2 (MEF2) group of transcription factors, was verfied to be downregulated. Thus, it is reasonable to speculate that p38 MAPK was inhibited; phosphorylation of MEF2C and c-jun mRNA transcription was decreased to prevent inflammatory response and apoptosis for treatment of AICH after LXTYF administration [70, 71]. Proteins of the Fos and Jun families can form homodimers or heterodimers called AP-1 (activating protein-1) to mediate transcriptional activation and DNA binding activity on target genes, involved in apoptotic functions and cell proliferation [66, 72]. Most time c-Fos is a necessary inducer of cell proliferation during the cell cycle phases in growing cells [67]. FOS and FOSB, verified to upregulated, are possible to play the proliferative role and induce compensatory cell proliferation via JNK and ERK pathways for the treatment of AICH after LXTYF administration. Dual-specificity protein phosphatase (DUSP) is an antiapoptotic phosphatase, which can dephosphorylate and inactivates the downstream effectors such as JNK, p38, and ERK [65, 73]. Downregulation of DUSP1 and increase of JNK phosphorylation were observed in the IR injury of the heart. Reproduction of DUSP1 can not only reduce the cellular death and shows the protective effects but also limit inflammatory responses upon LPS stimulation [65, 73, 74]. So, upregulation of DUSP1 shows that LXTYF may have a decrease in MAPKs phosphorylation and inactivates JNK and p38 pathways, suppressing inflammation and apoptosis to treat AICH.

Moreover, the other pathways such as the calcium signaling pathway, apoptosis, TNF signaling pathway, cGMP-PKG signaling pathway, cAMP signaling pathway, and HIF-1 signaling pathway are the common signaling pathways of differentially expressed genes and putative targets in LXTYF. The calcium signaling pathway generates Ca^{2+} signals to regulate physiological processes [75]. Research progress shows that low blood calcium leads to increased hematoma volume and poor prognosis of AICH, and calcium intake in the diet can lower the risk of stroke by about 24% [76]. Blood calcium on reducing stroke is mainly from several mechanisms such as inhibition of fat synthesis, lowering of blood pressure, and stability of blood glucose [76]. Activation of the apoptosis pathway is known to contribute to neuronal loss and become the core problem in the pathogenesis of stroke [77]. Bcl-2 family proteins and caspase proteins regulate neuronal apoptosis via mitochondria and ER. What is more, oxidative and nitrosative stress after stroke injury will lead to apoptotic cell death [77]. DIABLO (direct IAP-binding protein with low pI) is released from mitochondria into the cytosol, interacts with multiple IAPs, and removes IAP-mediated inhibition of caspases [78]. So, when it comes to the downregulation of DIABLO, Caspase-3, and Caspase-6 in RNA-seq data, it is reasonable to speculate the mechanism that LXTYF can help to decrease mRNA expression of DIABLO, then reduced inhibition of IAPs and promoted inhibition of caspase-3 and caspase-6. The TNF signaling pathway plays pleiotropic roles in the CNS [79]. Tumor necrosis factors (TNF) consists of soluble TNF (solTNF) and transmembrane TNF (tmTNF), which has a preference for TNF receptor 1 (TNFR1) and TNF receptor 2 (TNFR2), respectively [79]. Observations have suggested that in acute stroke and reduce injury, solTNF action can be inhibited by intraventricular infusion of the TNFR1 decoy receptor, but in the aspect of hippocampal repair and neurogenesis after ischemic injury, tmTNF action through TNFR2 is crucial [79]. Therefore, the adverse effects of anti-TNF therapies in the CNS may be reduced by selectively supressing TNFR1-mediated signaling while sparing TNFR2 activation [79]. BAG4/SODD is an antiapoptotic protein and identified as a silencer of death domain that can bind to TNFR1. High levels of SODD/BAG-4 protect against TNFa-induced cell death. So, elevation of BAG-4 indicates the control of LXTYF on the TNF signaling pathway.

4.3. Limitations of the Research. Compared to the previous two papers published in Frontiers in Pharmacology and Journal of Ethnopharmacology, all studies used reasonable models and reliable validation data to detect the network effect of LXTYF to treat AICH and verified some components, targets, and pathways [14, 78]. But our current work is different in the following aspects. We think that comprehensive ingredients in the prescription, the method with low false positive for pathway enrichment, and detailed differential mRNA expression can more systematically and efficiently validate the network pharmacology effects. Results in our study can supplement the mechanisms of LXTYF on AICH in a more systematic and comprehensive way. We collected compounds of all 8 herbs; more ICH targets and PPI network were analyzed in detail. A more structured and detailed network pharmacology approach via packages in R was also applied in our study. Also, compared with the predictive network and RNA-seq analysis results, new genes and new pathways (14 genes and MAPK signaling pathway) were verified and enriched. In the future, more targets and pathways will be explored deeply, conformed, and fully depict the pharmacology mechanism of TCM on AICH.

There are still some limitations to our study. The insufficient research on medicine composition of this prescription, especially the animal herbs, cannot completely dig into all the effective components. Further progress of chemical component separation technology is in great need to fully clarify all chemical components in the prescription. Also, results of PPI network prediction showed that STAT3 may play an important role of the bridge to connect other proteins among the pharmacological actions, but it did not verify in RNA-seq and needs to investigate in the next future. More subsequent experiments on differently expressed mRNA and enriched pathways are necessary to be investigated deeply. Moreover, it is common to see that some genes have dual effects and play opposite roles in different physical conditions, especially some are unsure and need further study. Critical insight for targets and pathways are necessary for mutual promotion between pharmacological research and physiological/pathology research.

5. Conclusion

Taken together, network pharmacology method and enrichment analysis in R were applied in our study to identify the 76 active components and 376 putative targets of LXTYF alleviating AICH. Compared with RNA-seq results of AICH rat models and enrichment analysis, we found that LXTYF attenuates AICH partially by regulating the targets involved MAPK, calcium, apoptosis, and TNF signaling pathway and plays antioxidation, anti-inflammatory, antiapoptosis and lowers blood pressure roles in the treatment mechanisms.

Data Availability

The chemical ingredients of six botanical medicinal materials in LXTYF were obtained from Traditional Chinese Medicine Systems Pharmacology Database and Analysis Platform (TCMSP) (http://lsp.nwu.edu.cn/tcmsp.php) The chemical ingredients of the other two animal medicines in LXTYF were derived from BATMAN-TCM (http://bionet.ncpsb.org/batman-tcm). Different genes linked to ICH were collected from three existing resources with Medical Subject Heading (MeSH) "Cerebral Hemorrhage": (1) GAD (https://geneticassociationdb.nih.gov/), (2) Genecards (https://www.genecards.org/), and (3) DisGeNET (http://www.disgenet.org/web/DisGeNET).

Conflicts of Interest

The authors declare that there is no conflict of interest regarding the publication of this article.

Authors' Contributions

YC designed the study, performed the network pharmacological analysis and RNA-seq data analysis, and wrote the manuscript. JD analyzed the data and reviewed the manuscript. DY performed the quality control of statistical analysis. QQ, PW, XY, and WL performed the animal experiments. GL also designed the study, with XS and FW revised the manuscript as corresponding authors. All authors read and approved the final manuscript. Yang Chen and Ju Dong are first authors.

Acknowledgments

This work was supported by three grants from the Natural Science Foundation of Jiangsu Province of China (Grant no.: BK20161575), National Natural Science Foundation of China (Grant no.: 81373512), and the Priority Academic Program Development of Jiangsu Higher Education Institutions (integration of Chinese and western medicine). Funding body provided the funds, and funds were used to afford the cost of the rats and RNA sequencing of samples in companies.

Supplementary Materials

S1 Table. 517 compounds of 8 herbs in LXTYF collected from TCMSP and BATMAN-TCM database. S2 Table. 874 targets of the active ingredients obtained from the TCMSP. S3 Table. 149 targets of active components predicted from the SwissTargetPrediction database. S4 Table. 2315 targets relating to ICH collected from GAD, Genecards, and DisGeNET database. S5 Table. Topological parameters of component-target network. S6 Table. Proteins-proteins interaction information of LXTYF targets for AICH in STRING 11.0. S7 Table. Topological parameters of the PPI network. S8 Table. Results of putative targets for KEGG pathway enrichment analysis. S9 Table. Detailed information of 583 differentially expressed mRNAs identified between MGT and MG. S10 Table. Details of the Herb-Compound-Target-Pathway(H-C-T-P) network connection verified in RNA-seq. *(Supplementary Materials)*

References

[1] R. Rodrigo, R. Fernandez-Gajardo, R. Gutierrez et al., "Oxidative stress and pathophysiology of ischemic stroke: novel therapeutic opportunities," *CNS & Neurological Disorders Drug Targets*, vol. 12, no. 5, pp. 698–714, 2013.

[2] T. Emiru, E. M. Bershad, N. D. Zantek et al., "Intracerebral hemorrhage," *Clinical and Applied Thrombosis/Hemostasis*, vol. 19, no. 6, pp. 652–662, 2013.

[3] A. Fahlström, L. Tobieson, H. N. Redebrandt et al., "Differences in neurosurgical treatment of intracerebral haemorrhage: a nation-wide observational study of 578 consecutive patients," *Acta Neurochirurgica*, vol. 161, no. 5, pp. 955–965, 2019.

[4] A. I. Qureshi, S. Tuhrim, J. P. Broderick, H. H. Batjer, H. Hondo, and D. F. Hanley, "Spontaneous intracerebral hemorrhage," *The New England Journal of Medicine*, vol. 344, no. 19, pp. 1450–1460, 2001.

[5] C. Cordonnier, A. Demchuk, W. Ziai, and C. S. Anderson, "Intracerebral haemorrhage: current approaches to acute management," *Lancet*, vol. 392, no. 10154, pp. 1257–1268, 2018.

[6] R. F. Keep, Y. Hua, and G. Xi, "Intracerebral haemorrhage: mechanisms of injury and therapeutic targets," *Lancet Neurology*, vol. 11, no. 8, pp. 720–731, 2012.

[7] J. C. Chen, "The effects of acupuncture and traditional Chinese medicines on apoptosis of brain tissue in a rat intracerebral hemorrhage model," *Physiology & Behavior*, vol. 151, pp. 421–425, 2015.

[8] Y. Wang, Y. C. Fan, C. L. Xie, and G. Q. Zheng, "History of post-stroke epilepsy in ancient China," *Journal of Neurology*, vol. 258, no. 8, pp. 1555–1558, 2011.

[9] H. Q. Li, J. J. Wei, W. Xia et al., "Promoting blood circulation for removing blood stasis therapy for acute intracerebral hemorrhage: a systematic review and meta-analysis," *Acta Pharmacologica Sinica*, vol. 36, no. 6, pp. 659–675, 2015.

[10] R. Liu, Q. Huang, J. Shan et al., "Metabolomics of the antipyretic effects of Bubali Cornu (water buffalo horn) in rats," *PLoS One*, vol. 11, no. 7, article e0158478, 2016.

[11] C. Y. He, J. H. Huang, W. J. Wang et al., "Effects of Liangxue Tongyu Formula on brain edema and expressions of matrix metalloproteinase-9 and tissue inhibitor of metalloproteinase-1 in rats with intracerebral hemorrhage," *Journal of Chinese Integrative Medicine*, vol. 8, no. 4, pp. 347–351, 2010.

[12] W. F. Guo, L. K. Zhang, M. H. Wu et al., "Liangxue Tongyu Fang for treating acuter-phase cerebral hemorrhage in 168 cases," *Journal of Beijing University of Traditional Chinese Medicine*, vol. 35, no. 9, pp. 603–616, 2012.

[13] M. A. Hui-Min, W. F. Guo, Y. Yuan, H. X. Zhang, and L. I. Jian-Xiang, "Treatment with Liangxuetongyu Formula in 96 patients with syndrome of stasis-heat obstructing orifices of acute cerebral hemorrhage," *Journal of Beijing University of Traditional Chinese Medicine*, vol. 34, no. 5, pp. 348–352, 2011.

[14] X. Li, X. Huang, Y. Tang et al., "Assessing the pharmacological and therapeutic efficacy of traditional Chinese medicine Liangxue Tongyu prescription for intracerebral hemorrhagic stroke in neurological disease models," *Frontiers in Pharmacology*, vol. 9, p. 1169, 2018.

[15] G. Bai, Y. Y. Hou, M. Jiang, and J. Gao, "integrated systems biology and chemical biology approach to exploring mechanisms of traditional Chinese medicines," *Chinese Herbal Medicines*, vol. 8, no. 2, pp. 99–106, 2016.

[16] J. Ru, P. Li, J. Wang et al., "TCMSP: a database of systems pharmacology for drug discovery from herbal medicines," *Journal of Cheminformatics*, vol. 6, no. 1, p. 13, 2014.

[17] Z. Liu, F. Guo, Y. Wang et al., "BATMAN-TCM: a bioinformatics analysis tool for molecular mechanism of traditional Chinese medicine," *Scientific Reports*, vol. 6, no. 1, p. 21146, 2016.

[18] W. Tao, X. Xu, X. Wang et al., "Network pharmacology-based prediction of the active ingredients and potential targets of Chinese herbal _Radix Curcumae_ formula for application to cardiovascular disease," *Journal of Ethnopharmacology*, vol. 145, no. 1, pp. 1–10, 2013.

[19] X. Xu, W. Zhang, C. Huang et al., "A novel chemometric method for the prediction of human oral bioavailability," *International Journal of Molecular Sciences*, vol. 13, no. 6, pp. 6964–6982, 2012.

[20] S. J. Yue, J. Liu, W. W. Feng et al., "System pharmacology-based dissection of the synergistic mechanism of Huangqi and Huanglian for diabetes mellitus," *Frontiers in Pharmacology*, vol. 8, p. 694, 2017.

[21] Y. Yao, X. Zhang, Z. Wang et al., "Deciphering the combination principles of Traditional Chinese Medicine from a systems pharmacology perspective based on Ma-huang Decoction," *Journal of Ethnopharmacology*, vol. 150, no. 2, pp. 619–638, 2013.

[22] X. X. Xu, J. P. Bi, L. Ping, P. Li, and F. Li, "A network pharmacology approach to determine the synergetic mechanisms of herb couple for treating rheumatic arthritis," *Drug Design, Development and Therapy*, vol. Volume 12, pp. 967–979, 2018.

[23] S. Pundir, M. J. Martin, C. O'Donovan, and The UniProt Consortium, "UniProt tools," *Current Protocols in Bioinformatics*, vol. 53, no. 1, pp. 1.29.1–1.29.15, 2016.

[24] S. Kim, J. Chen, T. Cheng et al., "PubChem 2019 update: improved access to chemical data," *Nucleic Acids Research*, vol. 47, no. D1, pp. D1102–D1109, 2019.

[25] C. Wang, Q. Ren, X. T. Chen et al., "System pharmacology-based strategy to decode the synergistic mechanism of Zhizhu Wan for functional dyspepsia," *Frontiers in Pharmacology*, vol. 9, p. 841, 2018.

[26] N. M. O'Boyle, M. Banck, C. A. James, C. Morley, T. Vandermeersch, and G. R. Hutchison, "Open Babel: an open chemical toolbox," *Journal of Cheminformatics*, vol. 3, no. 1, p. 33, 2011.

[27] A. Daina, O. Michielin, and V. Zoete, "SwissTargetPrediction: updated data and new features for efficient prediction of protein targets of small molecules," *Nucleic Acids Research*, vol. 47, no. W1, pp. W357–W364, 2019.

[28] K. G. Becker, K. C. Barnes, T. J. Bright, and S. A. Wang, "The genetic association database," *Nature Genetics*, vol. 36, no. 5, pp. 431-432, 2004.

[29] M. Shklar, L. Strichman-Almashanu, O. Shmueli, M. Shmoish, M. Safran, and D. Lancet, "GeneTide–Terra incognita discovery endeavor: a new transcriptome focused member of the GeneCards/GeneNote suite of databases," *Nucleic Acids Research*, vol. 33, no. Database issue, pp. D556–D561, 2005.

[30] M. Safran, I. Dalah, J. Alexander et al., "GeneCards version 3: the human gene integrator," *Database*, vol. 2010, p. baq020, 2010.

[31] J. Piñero, A. Bravo, N. Queralt-Rosinach et al., "DisGeNET: a comprehensive platform integrating information on human disease-associated genes and variants," *Nucleic Acids Research*, vol. 45, no. D1, pp. D833–D839, 2017.

[32] F. F. Cai, Y. Q. Bian, R. Wu et al., "Yinchenhao decoction suppresses rat liver fibrosis involved in an apoptosis regulation mechanism based on network pharmacology and transcriptomic analysis," *Biomedicine & Pharmacotherapy*, vol. 114, p. 108863, 2019.

[33] S. H. Shi, Y. P. Cai, X. J. Cai et al., "A network pharmacology approach to understanding the mechanisms of action of traditional medicine: Bushenhuoxue formula for treatment of chronic kidney disease," *PLoS One*, vol. 9, no. 3, article e89123, 2014.

[34] G. Chen, C. Huang, Y. Liu et al., "A network pharmacology approach to uncover the potential mechanism of Yinchensini decoction," *Evidence-based Complementary and Alternative Medicine*, vol. 2018, 14 pages, 2018.

[35] D. Szklarczyk, A. L. Gable, D. Lyon et al., "STRING v11: protein-protein association networks with increased coverage, supporting functional discovery in genome-wide experimental datasets," *Nucleic Acids Research*, vol. 47, no. D1, pp. D607–D613, 2019.

[36] G. Yu, L. G. Wang, Y. Han, and Q. Y. He, "clusterProfiler: an R package for comparing biological themes among gene clusters," *Omics : a journal of integrative biology.*, vol. 16, no. 5, pp. 284–287, 2012.

[37] G. Cimmino, R. Tarallo, G. Nassa et al., "Activating stimuli induce platelet microRNA modulation and proteome reorganisation," *Thrombosis and Haemostasis*, vol. 114, no. 7, pp. 96–108, 2017.

[38] M. Sultan, S. Dökel, V. Amstislavskiy et al., "A simple strand-specific RNA-Seq library preparation protocol combining the Illumina TruSeq RNA and the dUTP methods," *Biochemical and Biophysical Research Communications*, vol. 422, no. 4, pp. 643–646, 2012.

[39] C. Xie, X. Mao, J. Huang et al., "KOBAS 2.0: a web server for annotation and identification of enriched pathways and diseases," *Nucleic Acids Research*, vol. 39, suppl_2, pp. W316–W322, 2011.

[40] S. Li and B. Zhang, "Traditional Chinese medicine network pharmacology: theory, methodology and application," *Chinese Journal of Natural Medicines*, vol. 11, no. 2, pp. 110–120, 2013.

[41] B. Boezio, K. Audouze, P. Ducrot, and O. Taboureau, "Network-based approaches in pharmacology," *Molecular Informatics*, vol. 36, no. 10, 2017.

[42] X. Huang, G. C. Li, L. Yin, Z. H. Zhang, Y. X. Liang, and H. B. Chen, "The effective parts of liangxue tongyu prescription on cooling-blood and activating-blood and analysis of chemical constituents by HPLC-MS and GC-MS," *Acta Pharmaceutica Sinica*, vol. 50, no. 1, pp. 86–93, 2015.

[43] R. Liu, J. A. Duan, W. U. Hao, P. Liu, E. X. Shang, and D. W. Qian, "Analysis and identification of water soluble components of water buffalo horn," *Acta Pharmaceutica Sinica*, vol. 50, no. 5, pp. 594–598, 2015.

[44] M. G. Liska, M. G. Crowley, J. P. Tuazon, and C. V. Borlongan, "Neuroprotective and neuroregenerative potential of pharmacologically-induced hypothermia with D-alanine D-leucine enkephalin in brain injury," *Neural Regeneration Research*, vol. 13, no. 12, pp. 2029–2037, 2018.

[45] Y. Zhang, B. Yi, J. Ma et al., "Quercetin promotes neuronal and behavioral recovery by suppressing inflammatory response and apoptosis in a rat model of intracerebral hemorrhage," *Neurochemical Research*, vol. 40, no. 1, pp. 195–203, 2015.

[46] A. R. Galho, M. F. Cordeiro, S. A. Ribeiro et al., "Protective role of free and quercetin-loaded nanoemulsion against damage induced by intracerebral haemorrhage in rats," *Nanotechnology*, vol. 27, no. 17, p. 175101, 2016.

[47] C. López-Sánchez, F. J. Martín-Romero, F. Sun et al., "Blood micromolar concentrations of kaempferol afford protection against ischemia/reperfusion-induced damage in rat brain," *Brain Research*, vol. 1182, no. 1, pp. 123–137, 2007.

[48] L. Yu, C. Chen, L. F. Wang et al., "Neuroprotective effect of kaempferol glycosides against brain injury and neuroinflammation by inhibiting the activation of NF-κB and STAT3 in transient focal stroke," *PLoS One*, vol. 8, no. 2, article e55839, 2013.

[49] Q. Guo, S. Yang, D. Yang et al., "Differential mRNA expression combined with network pharmacology reveals network effects of Liangxue Tongyu Prescription for acute intracerebral hemorrhagic rats," *Journal of Ethnopharmacology*, vol. 246, p. 112231, 2020.

[50] J. A. G. Agúndez, M. Blanca, J. A. Cornejo-García, and E. García-Martín, "Pharmacogenomics of cyclooxygenases," *Pharmacogenomics*, vol. 16, no. 5, pp. 501–522, 2015.

[51] T. Grosser, S. Fries, and G. A. FitzGerald, "Biological basis for the cardiovascular consequences of COX-2 inhibition: therapeutic challenges and opportunities," *The Journal of Clinical Investigation*, vol. 116, no. 1, pp. 4–15, 2006.

[52] C. A. Worby and J. E. Dixon, "PTEN," *Annual Review of Biochemistry*, vol. 83, no. 1, pp. 641–669, 2014.

[53] W. Li, R. Huang, Z. Chen, L. J. Yan, J. W. Simpkins, and S. H. Yang, "PTEN degradation after ischemic stroke: a double-edged sword," *Neuroscience*, vol. 274, pp. 153–161, 2014.

[54] K. Zhou, Q. Zhong, Y. C. Wang et al., "Regulatory T cells ameliorate intracerebral hemorrhage-induced inflammatory injury by modulating microglia/macrophage polarization through the IL-10/GSK3β/PTEN axis," *Journal of Cerebral Blood Flow and Metabolism*, vol. 37, no. 3, pp. 967–979, 2017.

[55] X. Wang, K. Chandrashekar, L. Wang et al., "Inhibition of nitric oxide synthase 1 induces salt-sensitive hypertension in nitric oxide synthase 1α knockout and wild-type mice," *Hypertension*, vol. 67, no. 4, pp. 792–799, 2016.

[56] N. Toda, K. Ayajiki, and T. Okamura, "Cerebral blood flow regulation by nitric oxide: recent advances," *Pharmacological Reviews*, vol. 61, no. 1, pp. 62–97, 2009.

[57] M. Willmot, C. Gibson, L. Gray, S. Murphy, and P. Bath, "Nitric oxide synthase inhibitors in experimental ischemic stroke and their effects on infarct size and cerebral blood flow: a systematic review," *Free Radical Biology & Medicine*, vol. 39, no. 3, pp. 412–425, 2005.

[58] P. K. Liu, "Ischemia-reperfusion-related repair deficit after oxidative stress: implications of faulty transcripts in neuronal sensitivity after brain injury," *Journal of Biomedical Science*, vol. 10, no. 1, pp. 4–13, 2003.

[59] M. D'Amelio, V. Cavallucci, and F. Cecconi, "Neuronal caspase-3 signaling: not only cell death," *Cell Death and Differentiation*, vol. 17, no. 7, pp. 1104–1114, 2010.

[60] Z. Yanling, C. Kangning, S. Shuqin, and W. Ying, "Relationship between apoptosis and expression of caspase-3 after cerebral hemorrhage," *Journal of the Fourth Military Medical University*, vol. 25, no. 1, pp. 23–26, 2004.

[61] D. B. Sun, M. J. Xu, Q. M. Chen, and H. T. Hu, "Significant elevation of serum caspase-3 levels in patients with intracerebral hemorrhage," *Clinica Chimica Acta*, vol. 471, pp. 62–67, 2017.

[62] M. Chen, L. Lai, X. Li et al., "Baicalein attenuates neurological deficits and preserves blood-brain barrier integrity in a rat model of intracerebral hemorrhage," *Neurochemical Research*, vol. 41, no. 11, pp. 3095–3102, 2016.

[63] A. Bhinge, S. C. Namboori, X. Zhang, A. M. J. Vandongen, and L. W. Stanton, "Genetic correction of SOD1 mutant iPSCs reveals ERK and JNK activated AP1 as a driver of neurodegeneration in amyotrophic lateral sclerosis," *Stem Cell Reports.*, vol. 8, no. 4, pp. 856–869, 2017.

[64] J. Sun and G. Nan, "The mitogen-activated protein kinase (MAPK) signaling pathway as a discovery target in stroke," *Journal of Molecular Neuroscience*, vol. 59, no. 1, pp. 90–98, 2016.

[65] Q. Jin, R. Li, N. Hu et al., "DUSP1 alleviates cardiac ischemia/reperfusion injury by suppressing the Mff- required mitochondrial fission and Bnip3-related mitophagy via the JNK pathways," *Redox Biology*, vol. 14, pp. 576–587, 2018.

[66] V. Atsaves, V. Leventaki, G. Z. Rassidakis, and F. X. Claret, "AP-1 transcription factors as regulators of immune responses in cancer," *Cancers*, vol. 11, no. 7, p. 1037, 2019.

[67] E. Shaulian and M. Karin, "AP-1 in cell proliferation and survival," *Oncogene*, vol. 20, no. 19, pp. 2390–2400, 2001.

[68] X. Wei, W. Sun, R. Fan et al., "MEF2C regulates c-Jun but not TNF-α gene expression in stimulated mast cells," *European Journal of Immunology*, vol. 33, no. 10, pp. 2903–2909, 2003.

[69] G. Raivich, "C-Jun expression, activation and function in neural cell death, inflammation and repair," *Journal of Neurochemistry*, vol. 107, no. 4, pp. 898–906, 2008.

[70] J. Han, Y. Jiang, Z. Li, V. V. Kravchenko, and R. J. Ulevitch, "Activation of the transcription factor MEF2C by the MAP kinase p38 in inflammation," *Nature*, vol. 386, no. 6622, pp. 296–299, 1997.

[71] S. H. Yang, A. Galanis, and A. D. Sharrocks, "Targeting of p38 mitogen-activated protein kinases to MEF2 transcription factors," *Molecular and Cellular Biology*, vol. 19, no. 6, pp. 4028–4038, 1999.

[72] H. H. Wang, H. L. Hsieh, C. Y. Wu, C. C. Sun, and C. M. Yang, "Oxidized low-density lipoprotein induces matrix metalloproteinase-9 expression via a p42/p44 and JNK-dependent AP-1 pathway in brain astrocytes," *Glia*, vol. 57, no. 1, pp. 24–38, 2009.

[73] M. Hammer, J. Mages, H. Dietrich et al., "Dual specificity phosphatase 1 (DUSP1) regulates a subset of LPS-induced genes and protects mice from lethal endotoxin shock," *The Journal of Experimental Medicine*, vol. 203, no. 1, pp. 15–20, 2006.

[74] D. M. Taylor, R. Moser, E. Regulier et al., "MAP kinase phosphatase 1 (MKP-1/DUSP1) is neuroprotective in Huntington's disease via additive effects of JNK and p38 inhibition," *The Journal of Neuroscience*, vol. 33, no. 6, pp. 2313–2325, 2013.

[75] M. J. Berridge, "The inositol trisphosphate/calcium signaling pathway in health and disease," *Physiological Reviews*, vol. 96, no. 4, pp. 1261–1296, 2016.

[76] J. Liu, H. Yang, and B. Yu, "The correlation between blood calcium level, hematoma volume, stroke severity and prognosis in patients with acute cerebral hemorrhage," *European Review for Medical and Pharmacological Sciences*, vol. 20, no. 19, pp. 4119–4123, 2016.

[77] E. Sekerdag, I. Solaroglu, and Y. Gursoy-Ozdemir, "Cell death mechanisms in stroke and novel molecular and cellular treatment options," *Current Neuropharmacology*, vol. 16, no. 9, pp. 1396–1415, 2018.

[78] Y. Shi, "Mechanisms of caspase activation and inhibition during apoptosis," *Molecular Cell*, vol. 9, no. 3, pp. 459–470, 2002.

[79] M. K. McCoy and M. G. Tansey, "TNF signaling inhibition in the CNS: implications for normal brain function and neurodegenerative disease," *Journal of Neuroinflammation*, vol. 5, no. 1, p. 45, 2008.

Hindawi
Neural Plasticity
Volume 2021, Article ID 8825698, 10 pages
https://doi.org/10.1155/2021/8825698

Research Article

Neuroprotective Effects of ZiBuPiYin Recipe on db/db Mice via PI3K-Akt Signaling Pathway by Activating Grb2

Wei-ming Ren,[1] Ze-bin Weng,[1] Xin Li,[2,3] and Li-bin Zhan[1]

[1]*School of Traditional Chinese Medicine & School of Integrated Chinese and Western Medicine, Nanjing University of Chinese Medicine, Nanjing 210023, China*
[2]*Nanjing Hospital of Chinese Medicine Affiliated to Nanjing University of Chinese Medicine, Nanjing 210023, China*
[3]*Dalian Medical University, Dalian, Liaoning 116044, China*

Correspondence should be addressed to Li-bin Zhan; zlbnj@njucm.edu.cn

Received 22 August 2020; Revised 26 December 2020; Accepted 8 January 2021; Published 31 January 2021

Academic Editor: Jason H. Huang

Background. Diabetes-associated cognitive decline (DACD) is one of the nervous system dysfunctions induced by diabetes mellitus with cognitive impairment as the major symptom. In a previous preliminary proteomic study, we found that endoplasmic reticulum processing and PI3K-Akt signaling pathway might be impaired in DACD pathogenesis. In addition, growth factor receptor-bound protein 2 might be a crucial protein as a molecular target of the neuroprotective effects of ZiBuPiYin recipe (ZBPYR). *Methods*. In this study, 6-8 weeks aged db/db mice were treated with excipients or ZBPYR for 6 weeks. Body weight and RBG were recorded weekly. Oral glucose tolerance and insulin tolerance tests were used to assess insulin sensitivity. Morris water maze (MWM) tests were used to assess memory function. The expression of Grb2, Gab2, Akt, and GSK3β in mouse hippocampus and cerebral cortex were analyzed by Western blotting. *Results*. ZBPYR not only significantly reduced RGB and improved glucose tolerance and insulin resistance, but also improved spatial cognition in DACD mice. The expression of Grb2 and Gab2 in hippocampus and cerebral cortex of db/db mice was upregulated after treated with ZBPYR, and then affected the PI3K/Akt signaling pathway, and inhibited GSK3β overactivity. *Conclusions*. This study showed that ZBPYR could enhance the memory and learning ability of db/db mice. Such neuroprotective effect might be related to the activation of Grb2-PI3K/Akt signaling which might provide a novel therapeutic target for the clinical treatment of DACD.

1. Introduction

Diabetes mellitus (DM) is the most common chronic metabolic disease with a high global prevalence. The global prevalence of diabetes has been increasing over recent decades. It was estimated that there were approximately 451 million people with DM worldwide in 2017 and was predicted to rise to 700 million in 2045 [1]. Diabetes-associated cognitive decline (DACD), also known as diabetes encephalopathy, is one of the most common neurological complications in DM patients [2]. The brain aging and neurodegenerative processes of DACD are similar to those of Alzheimer's disease (AD) [3]. Recent epidemiological studies suggested that people with DM have been associated with an increased risk of cognitive decline and dementia, including AD [4]. However, at present, the underlying pathophysiological mechanisms of DACD are not fully understood, and there is still no efficient cure or prevention [5]. Therefore, it is of great significance to study the pathogenesis of DACD and explore effective treatment options [6]. Animal studies may help to identify the mechanisms that underlie the adverse impact of diabetes on cognition and advance our understanding of its pathophysiology and may provide potential treatment on DACD. The leptin receptor-deficient db/db mice, one of the most widely used type 2 diabetes mellitus (T2DM) animal models, showed a series of diabetic symptoms such as obesity, hyperglycemia, hyperinsulinemia, insulin resistance, and diabetic complications like DACD as leptin plays a critical role in memory and learning [7, 8]. Therefore, db/db mice were used as DACD animal model in this study.

Traditional Chinese medicine (TCM) provides unique advantages in the treatment of complex metabolic diseases such as diabetes and its complications due to its multicomponent and multitarget characteristics [9]. ZiBuPiYin recipe (ZBPYR) is derived from a modification of ZiCheng decoction, a TCM recipe recorded in a TCM monograph named Bujuji written by Wu Cheng during Qing dynasty. Our preliminary study suggested that ZBPYR improved learning and memory ability in multiple animal models of diabetes [10–12]. We also found that ZBPYR protected hippocampal neurons against glutamate and amyloid beta-peptide- (Aβ-) induced neurotoxicity through blocking the serum-inducible kinase and spine-associated Rap GTPase-activating protein (SNK-SPAR) pathway [13, 14]. Moreover, in a previous preliminary proteomic study, we found that endoplasmic reticulum processing and PI3K-Akt signaling pathway might be impaired in DACD pathogenesis. In addition, growth factor receptor-bound protein 2 (Grb2) might be a crucial protein as a molecular target of the neuroprotective effects of ZBPYR [15].

Grb2 is an adaptor protein that transmits downward growth factor signals, consisting of an SH2 domain flanked by *N*- and *C*-terminal SH3 domain [16]. Grb2 recruits and mediates the interaction with the adaptor protein Grb2-associated binder Gab2, and the SH2 domain could bind tyrosine-phosphorylated proteins, such as tyrosine-phosphorylated Gab2 [17, 18]. Gab2 has been reported as an activator of phosphatidylinositol 3-kinase (PI3K) signaling pathway, since the interaction of SH2 domain of Grb2 with Gab2 recruited p85, which is the regulatory subunit of PI3K [19–21]. It has been demonstrated that PI3K activates its downstream effector Akt, which then promotes glycogen synthasekinase-3 (GSK3) phosphorylation [22]. Impaired PI3K/Akt/GSK3β signaling pathway modulates abnormal hyperphosphorylation of Tau protein which is one of the most important pathological lesions in AD [23–25]. The pathology of DACD is particularly similar to that of AD. Therefore, based on our previous study, we hypothesized that the cognitive dysfunction in diabetic mice might be related to the inhibition of the PI3K/Akt signaling pathway and neuroprotective effects of ZBPYR may be related to its upregulation of Grb2 in the brain and then activation of PI3K/Akt signaling pathway.

In this study, db/db mice (6 weeks old of age) were utilized to explore the improvement in memory and learning ability of ZBPYR and investigate its impact on Grb2 and PI3K/Akt signaling in the brain of db/db mice in order to interpret the neuroprotective effects and related mechanisms of ZBPYR.

2. Materials and Methods

2.1. Reagents. Primary antibodies p-Tyr452 Gab2 (#3882, 1 : 1000), PI3 kinase p85 (#4257, 1 : 1000), Akt (#9272, 1 : 1000), p-Ser473Akt (#4058, 1 : 1000), p-Ser9GSK3β (#9323, 1 : 1000), and beta-actin (#3700T, 1 : 2000) were purchased from Cell Signaling Technologies (Danvers, MA, USA). Primary antibody directed against Grb2 (#ab32111, 1 : 1000) and GSK3β (#ab131356, 1 : 1000) were from Abcam PLC (Cambridge, UK). Primary antibody Gab2 (sc-365590, 1 : 500) was from Santa Cruz (Santa Cruz, USA). Secondary antibodies were goat anti-rabbit (BA1054, 1 : 2000) (Boster Biological Technology Co. Itd, Wuhan, China) or anti-mouse (BA1050, 1 : 2000).

2.2. Animals. Male C57BLKS/J-db/db mice (6 weeks old of age) and age-matched nondiabetic littermates' db/m mice were obtained from Nanjing Qingzilan Technology Co., Ltd. (Nanjing, Jiangsu Province, China). Mice were housed in the Specific Pathogen Free (SPF) Animal Laboratory of Dalian Medical University. Specifically, mice were housed in a 12 h light/dark cycle (24°C ± 2°C and 65% ± 5% humidity) and received food and water ad libitum. All animal experiments were conducted in accordance with the NIH Principles of Laboratory Animal Care and the institutional guidelines for the care and use of laboratory animals at Dalian Medical University. All experiments were approved by the Committee on the Ethics of Animal Experiments of Dalian Medical University. All surgery was performed under anesthesia with ether (the usage of ether was approved by the Committee on the Ethics of Animal Experiments of Dalian Medical University), and all efforts were made to minimize suffering.

2.3. Preparation and Administration of ZBPYR. ZBPYR is consists of 12 Chinese Herbal Medicines: red ginseng (Radix Ginseng Rubra), common yam rhizome (Rhizoma Dioscoreae Oppositae), Indian Buead (PORIA), white peony root (Radix Paeoniae Alba), Dan shen root (Radix Salviae Miltiorrhizae), white hyacinth bean (Semen Lablab Album), lotus seed (Semen Nelumbinis), grassleaf sweetflag rhizome (Rhizoma Acori Tatarinowii), thinleaf milkwort root (Radix Palygalae), sandalwood (Lignum Santali Albi), tangerine red epicarp (Exocarpium Citri Rubrum), and liquorice root (Radix Glycyrrhizae). All herbs were purchased from Dalian Metro Pharmaceutical Co., Ltd., Dalian, Liaoning, China (the drug meets the 2015 National Pharmacopoeia Standard). The mixtures were soaked in distilled water (Milli-Q Integral Water Purification System, Millipore Corporation, Billerica, MA, USA) for 30 min and boiled in 8 volumes of water (v/w) for 90 min. The decoction was then concentrated to 3.29 g/ml and finally stored at 4°C.

We had done some works about the chemical components and quality control of the ZBPYR in the previous studies. For the quality control of ZBPYR, we combined high-performance liquid chromatography (HPLC) and electrospray ionisation quadrupole time-of-flight tandem mass spectrometry (HPLC-Q-TOF-MS) for fingerprint analysis and qualitative analysis. Seven common peaks (liquiritin, naringin, 3,6-disinapoylsucrose, 3,4,5-trimethoxycinnamic acid, rosmarinic acid, isoliquiritin apioside, and salvianolic acid B) were identified and detected [26]. In this experiment, ZBPYR was prepared according to the process described in the previous paper.

After one week of adaptive feeding, the db/db and db/m mice were randomly assigned to three groups: control group, DM group, and DM/ZBPYR group with 4 mice in each group. At 6th week, oral administration of ZBPYR treated

with DM/ZBPYR group at a dose of 10 ml/kg body weight per day, while an identical dose of ultrapure water (Milli-Q Integral Water Purification System, Millipore Corporation, Billerica, MA, USA) was administered to DM and control groups.

2.4. Random Blood Glucose and Fasting Serum Insulin. Body weight and random blood glucose (RBG) were measured weekly during the whole treatment to verify the development of diabetes in the db/db mice. At the end of the administration, mice were starved for 12 h and blood samples were obtained from the inner canthus vein of the eye after being anesthetized with ether. Blood samples were then centrifuged (4°C, 3000 rpm) for 15 min, and serum samples were obtained and stored at -80°C until measuring fasting serum insulin (FSI). FSI levels were assayed using an insulin radioimmunoassay kit (Atom High-tech, Beijing, China).

2.5. Oral Glucose Tolerance Test and Insulin Tolerance Test. Oral glucose tolerance test (OGTT) and insulin tolerance test (ITT) were performed at the end of the administration period. Mice received oral administration of 2 g/kg body weight of 50% (wt/wt) glucose solution after fasted for 14 h. Blood samples were collected at 0, 30, 60, and 120 min from tail vein after glucose administration. In insulin tolerance test, mice were injected intraperitoneally with regular human insulin (Novolin, Novo Nordisk Pharmaceutical Co., Ltd., Tianjin, China) at a dose of 0.75 U/kg body weight after fasted for 6 h. Glucose levels were monitored at 0, 15, 30, 60, 90, and 120 min after insulin injection. OGTT and ITT were determined using a strip-operated blood glucose sensor (Roche, Mannheim, Germany).

2.6. Morris Water Maze Test. Morris water maze test was performed for 6 days to assess spatial learning and memory performance of the mice. The water maze is consisted of a round tank (Institute of Materia Medica, Chinese Academy of Medical Sciences, Beijing, China), which was 100 cm in diameter, 50 cm in height, and filled with water and milk powder maintained at 26°C ± 1°C, a transparent platform, which was 9 cm in diameter, 29 cm in height, and located at 30 cm from the edge of the tank and hidden under water, and an automatic photographic recording and analysis system (EthoVision, Noldus Information Technology b.v., Wageningen, Netherlands). On the 1st day, mice were permitted to swim freely in the pool for 120 s without the platform. During the following 4 days, mice were trained on 4 trials per day at intervals of 60 s. The platform location was submerged 1 cm below the water surface, and the starting points were changed every trial. Each trial lasted until the mice swam to the platform or for a maximum observation time of 120 s. If the mice failed to swim to the platform within 120 s, they were guided to the platform. On the day after the last acquisition training session, mice were tested in a single 120 s probe test without the platform. Over this period, time in seeking the platform location (escape latency), time in the target quadrant where the platform had been located, and the number of platform location crossings were all measured automatically. On the 6th day, mice were trained on a visible-platform test. The platform was located 1 cm over the water surface and fixed at a position different from the previous ones. During this test, the experimental procedures were performed as same as previous tests, and escape latency and swimming distance were recorded.

2.7. Sample Preparation. The mice were anesthetized with ether and decapitated for Western blotting analysis. Hippocampus and cerebral cortex were rapidly dissected via surgery on ice. All samples were immediately frozen in liquid nitrogen and stored at -80°C until required. Hippocampus and cerebral cortex samples were homogenized in ice-cold lysis buffer (0.125 M Tris HCl (pH 6.8), 0.2 M DTT, 4% SDS, and 20% glycerol). The lysates were sonicated for 10 min and centrifuged (4°C and 15,000 rpm) for 5 min to remove insoluble debris. Protein concentrations in the supernatants were measured by a Minim Spectrophotometer (NanoVueTM Plus, GE Healthcare, Amersham Place, Little Chalfont, Buckinghamshire, HP79NA, UK).

2.8. Western Blotting. Protein (50 mg per sample) was loaded per line and separated on 8%–15% tris-glycine polyacrylamide gels and transferred to nitrocellulose membranes. Immunoblots were blocked for 2 h in Tris-buffered saline Tween-20 (TBST, 20 mM Tris-HCl, 150 mM NaCl, pH 7.5, and 0.05% Tween 20) containing 5% skim milk. The blots were then incubated with primary antibodies in TBST at 4°C overnight. Membranes were washed three times with TBST and then incubated with secondary antibody for 2 h at room temperature. Membranes were washed again and developed with enhanced chemiluminescence (ECL) and detected with X-ray films. The blots were visualized with ImageQuant TL 1D (GE Healthcare, USA). Primary antibodies used from Cell Signaling Technologies (Danvers, MA, USA) were as follows: p-Tyr452 Gab2 (#3882, 1 : 1000), PI3 kinase p85 (#4257, 1 : 1000), Akt (#9272, 1 : 1000), p-Ser473Akt (#4058, 1 : 1000), p-Ser9GSK3β (#9323, 1 : 1000), and beta-actin (#3700T, 1 : 2000). Primary antibody directed against Grb2 (Abcam PLC, Cambridge, UK, #ab32111, 1 : 1000), GSK3β (Abcam PLC, Cambridge, UK, #ab131356, 1 : 1000), and Gab2 (Santa Cruz, USA, sc-365590, 1 : 500) were also used in the experiments. Secondary antibodies were goat anti-rabbit (BA1054, 1 : 2000) (Boster Biological Technology Co. Itd, Wuhan, China) or anti-mouse (BA1050, 1 : 2000).

2.9. Statistical Analysis. Statistical analysis was performed using SPSS 17.0. All experimental data were statistically analyzed by one-way ANOVA and Student's t-test to compare all groups. The difference was considered to be statistically significant when $p < 0.05$.

3. Results

3.1. Effects of ZBPYR on Peripheral Glucose Homeostasis and Insulin Sensitivity. As shown in Figure 1(a), body weight of DM mice was significantly heavier compared to control mice while ZBPYR administration had no significant effects on body weight. RBG levels of DM/ZBPYR mice were significantly lower than DM mice from the 3rd week to the 6th

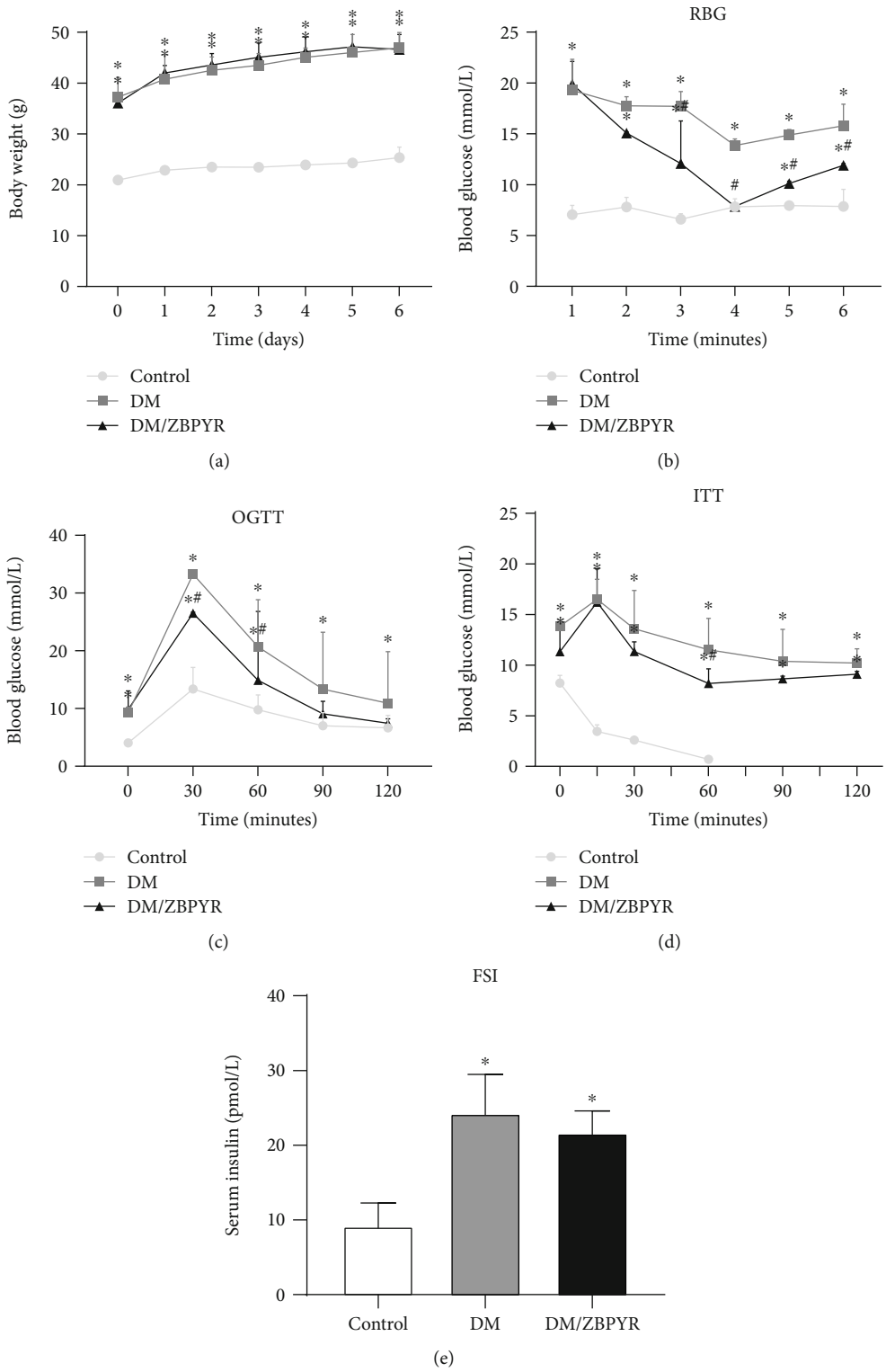

Figure 1: The antidiabetic effects of ZBPYR on db/db mice. (a) Body weight was recorded weekly. (b) RBG level was measured every week in the three groups during ZBPYR administration. (c–e) OGTT, ITT and FSI level were measured at the end of treating period. Values are means ± S.D. from 4 mice in each group. $^{*}p < 0.05$ compared to control; $^{\#}p < 0.05$ compared to DM.

week of treatment (Figure 1(b)). The OGTT results revealed that ZBPYR significantly reduced the blood glucose levels at 30 min (0.80 times) and 60 min (0.72 times) after glucose load (Figure 1(c)). Additionally, the administration of ZBPYR also significantly decreased the blood glucose levels at 60 min (0.64 times) after insulin injection (Figure 1(d)). DM mice exhibited impaired glucose tolerance and insulin sensitivity which are associated with the development of

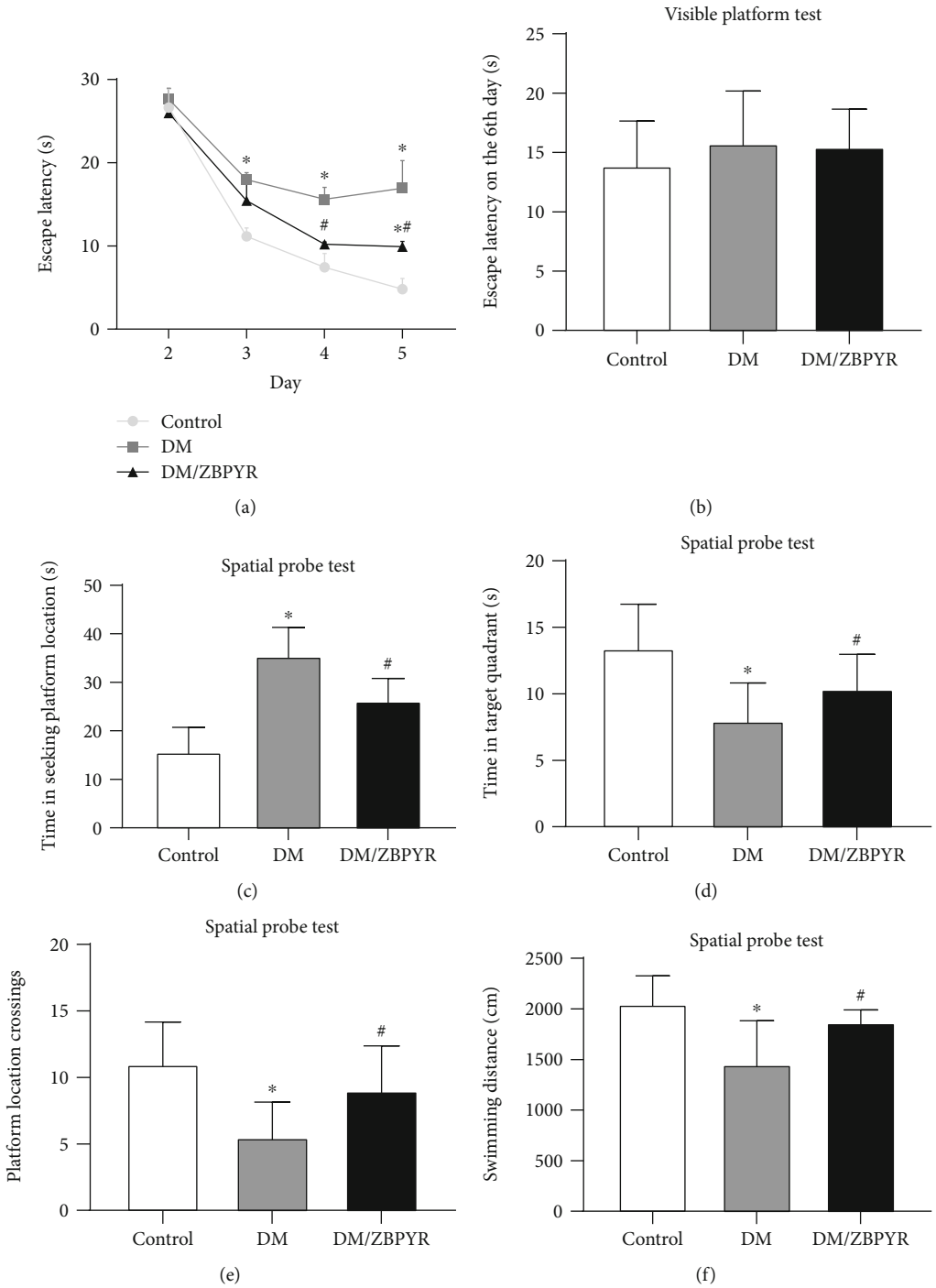

Figure 2: Effects of ZBPYR on DACD mice in Morris water maze test. (a) escape latency, (b) escape latency in the visible platform test, (c) time in searching original platforms, (d) time in target quadrant, (e and f) platform location crossings and swimming distance in spatial probe test. Values are means ± S.D. from 4 mice in each group. $^{*}p < 0.05$ compared to control; $^{\#}p < 0.05$ compared to DM.

cognitive decline and poor cognitive performance [27]. Treatment with ZBPYR could improve the impaired glucose tolerance and insulin sensitivity of DM mice. However, there was no significant difference in FSI levels between DM/ZBPYR and DM mice (Figure 1(e)).

3.2. ZBPYR Improves Spatial Learning and Memory Performance. Lesions in animals' brain regions, such as hippocampus and cerebral cortex, have an impairment on Morris water maze performance [22]. The results of Morris water maze test revealed that DM mice required significantly longer escape latency than the control ones between day 3 and day 5 (day 3 1.92 times, day 4 2.31 times, and day 5 5.41 times, respectively). The latency of DM/ZBPRY mice was shorter than that of DM mice on day 4 (0.70 times) and day 5 (0.59 times) (Figure 2(a)). In the visible platform

test on the 6th day, there was no significant difference among the three groups in escape latency (Figure 2(b)).

In the spatial probe test, the swimming time of DM/ZBPYR mice in seeking platform location was shorter (0.75 times) than that of DM mice (Figure 2(c)). And the moving time of DM/ZBPYR mice in the target quadrant was longer (1.25 times) than that of DM mice (Figure 2(d)). DM/ZBPYR mice exhibited more times (1.72 times) of crossing the platform location than DM mice (Figure 2(e)). Also, the swimming distance of DM/ZBPYR mice was enhanced 1.29 times compared to DM mice (Figure 2(f)).

3.3. ZBPYR Administration Increases the Expressions of Grb2 and Gab2 and Affects PI3K/Akt Signaling Pathway in the Hippocampus of db/db Mice. The hippocampus plays an especially important role on cognition and memory in mammals [28]. The result showed that expressions of Grb2, Gab2, p85, and Akt were different in hippocampus among the three groups. An obvious reduction in Grb2 expression was observed in the hippocampus of DM group compared with control group. Treatment with ZBPYR could significantly increase Grb2 expression. In addition, the expression of Gab2 showed no significant changes among the three groups (Figure 3(a)). As Tyr452 of Gab2 is a potential binding site of p85, the regulatory subunit of PI3 kinase [29], we detected the expression of p-Gab2 (Tyr452). Results revealed that the expression of p-Gab2 (Tyr452) modestly increased in the hippocampus of DM/ZBPYR mice compared to DM mice (Figure 3(a)). Moreover, ZBPYR affected PI3K/Akt signaling pathway in the hippocampus of db/db mice. Specifically, the levels of p85 and p-Akt (Ser473) were both decreased in the hippocampus of DM (Figure 3(b)) when compared to the control group, while ZBPYR treatment could enhance p85 (Figure 3(b)) and Akt hyperphosphorylation (Figure 3(b)).

3.4. ZBPYR Increases the Expressions of Grb2 and Gab2 and Affects PI3K/Akt Signaling Pathway in the Cerebral Cortex of db/db Mice. The cerebral cortex is also closely related to cognitive function [30, 31]. In this study, we did observe an obvious reduction in Grb2 and p-Gab2 (Tyr452) expressions in the cerebral cortex of DM mice compared to control (Figure 4(a)), and ZBPYR showed an ability to provide Grb2 and p-Gab2 (Tyr452) with varying degrees of increase (Figure 4(a)). Similarly, results revealed no statistically significant changes in the total levels of Gab2 (Figure 4(a)) and Akt (Figure 4(b)) in the cerebral cortex among the three groups. However, an apparent reduction in expression of p-Akt (Ser473) was detected in the cerebral cortex of DM mice when compared with control mice (Figure 4(b)), with an evident increase in DM/ZBPYR mice (Figure 4(b)). We also observed a significantly increased p85 in the cerebral cortex of DM/ZBPYR group compared to DM group (Figure 4(b)).

3.5. ZBPYR Inhibits GSK3β Overactivity. It has been clear that PI3K/Akt signaling pathway affects GSK3β activity in the brain [32]. In our study, we observed the alteration of GSK3β activity. However, we did not detect the statistically significant alterations in total GSK3β expressions among the three groups. Additionally, Western blotting results showed different extent of reduction in phosphorylated GSK3β at Ser9 in the hippocampus (Figure 3(c)) and cerebral cortex (Figure 4(c)) of DM group, while the levels of p-GSK3β (Ser9) increased in the hippocampus (Figure 3(c)) and cerebral cortex (Figure 4(c)) of DM/ZBPYR group.

4. Discussion

As DACD is a common complication of diabetes, the pathogenesis and effective treatment strategies of DACD have attracted increasing attention from researchers. DACD is associated with blood glucose and serum insulin level. Pharmaceutical therapy targeted on diabetic symptoms such as hyperglycemia, hyperinsulinemia, and insulin resistance and also treats some diabetic complications [33, 34]. Many studies have revealed that TCM has antidiabetic effects, providing multiple therapeutic effects on blood glucose and serum insulin level [35]. Here, we explored the effects of ZBPYR on blood glucose and serum insulin level. The results revealed that ZBPYR exhibited promising antidiabetic effects by moderating the increased RBG levels during the 3rd to 6th weeks of treatment and significantly improving the impaired glucose tolerance and insulin sensitivity.

Morris water maze test is widely used for testing spatial learning and memory [36]. T2DM mice exhibited severe cognitive deficits, seriously impair their Morris water maze performance [37]. Our results demonstrated that DM mice had severe cognitive impairment, and ZBPYR was able to improve these cognitive impairment and inferior learning and memory performance of DM mice, which could be seen in the training test (4th and 5th days) and spatial probe test.

Our previous studies have found that endoplasmic reticulum processing and PI3K-Akt signaling pathway might be impaired in DACD pathogenesis [15]. In addition, Grb2 might be a crucial protein as a molecular target of the neuroprotective effects of ZBPYR. The PI3K/Akt signaling pathway regulates cell proliferation, differentiation, metabolism, and cytoskeletal reorganization, leading to apoptosis and cancer cell survival. The PI3K/Akt pathway is the main pathway for insulin signal transduction and involved in the regulation of blood glucose [38]. Grb2 is a cytoplasmic connexin, and studies have shown that Grb2 can prevent AD by binding to insulin receptors to improve the expression of downstream molecules of insulin signaling to prevent diabetic peripheral neuropathy and interacting with NOX4 to protect the cytoskeletal disassembly [39, 40].

These studies indicated that Grb2 might play a key role in degenerative neuropathy. In the present study, we investigated the expression of Grb2, Gab2, p85, Akt, and GSK3β in the hippocampus and cerebral cortex, which are associated with cognitive function in humans and animals. Western blotting analysis results showed that ZBPYR affects the PI3K/Akt signaling pathway and increases the expression of p85 and p-Akt (Ser473) by enhancing the expression of Grb2 and Gab2 hyperphosphorylation in the hippocampus and cerebral cortex of db/db mice. Our study also found that ZBPYR could inhibit the downstream GSK3β over activity. All these results indicated that ZBPYR exerts a neuroprotective

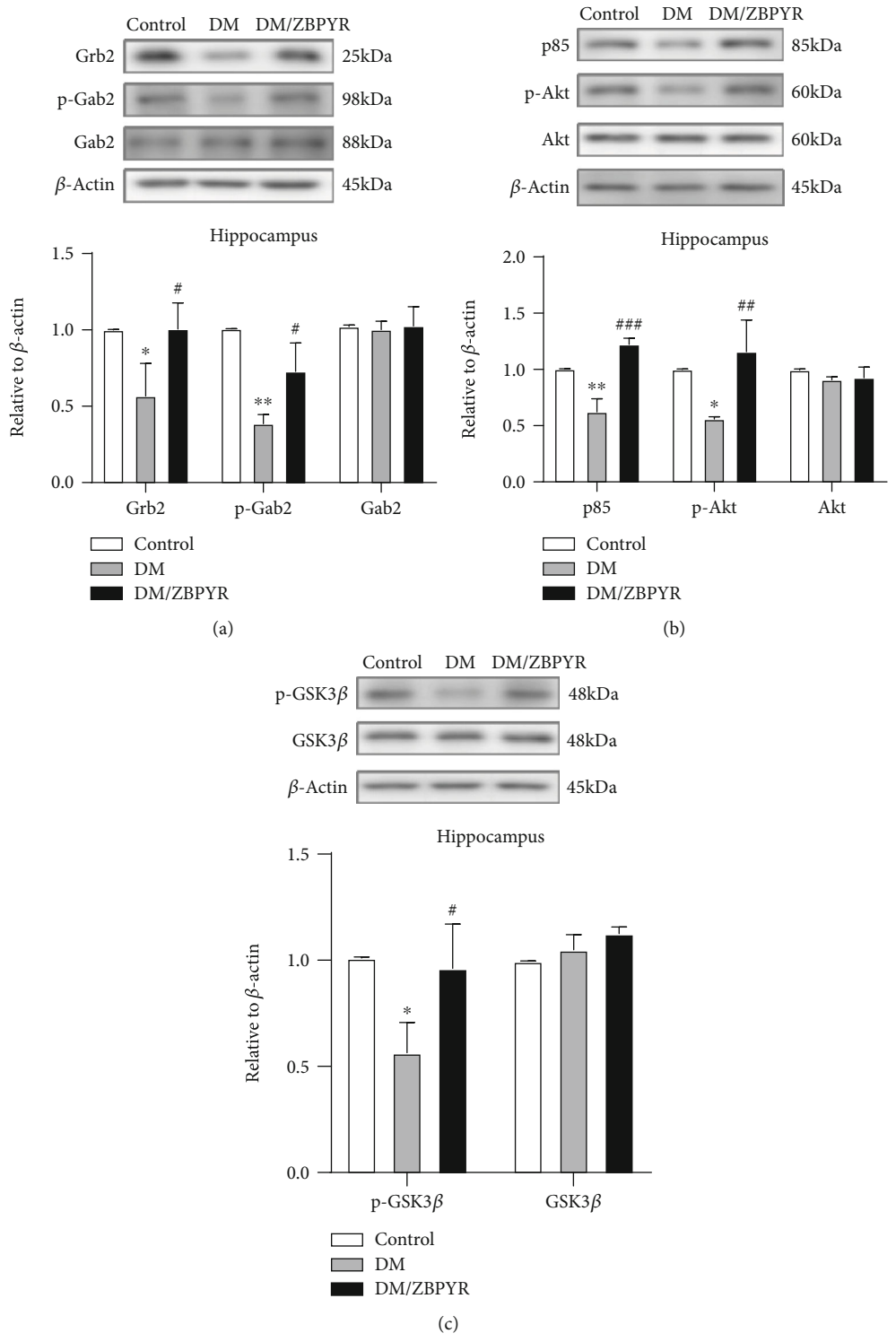

Figure 3: The effect of ZBPYR on the expression of Grb2, Gab2, Akt, p-Akt, and GSK3β in mouse hippocampus. (a) Compared with the control group, the expression of Grb2 in the hippocampus of the DM group was reduced. However, Grb2 levels increased after ZBPYR administration. The total level of Gab2 in the hippocampus did not change significantly between the three groups. The expression of p-Gab2 (Tyr452) in the hippocampus of DM/ZBPYR mice was moderately increased. (b) The levels of p85 and p-Akt (Ser473) were reduced in DM, while ZBPYR enhanced p85 and Akt hyperphosphorylation. The total Akt level was not different in the hippocampus between the three groups. (c) DM group hippocampus Ser9-phosphorylated GSK3β decreased, while p-GSK3β (Ser9) levels in the DM/ZBPYR group hippocampus increased. Values are means ± S.D. from 3 mice in each group. $^{*}p < 0.05$ and $^{**}p < 0.01$ compared to control; $^{\#}p < 0.05$, $^{\#\#}p < 0.01$, and $^{\#\#\#}p < 0.01$ compared to DM.

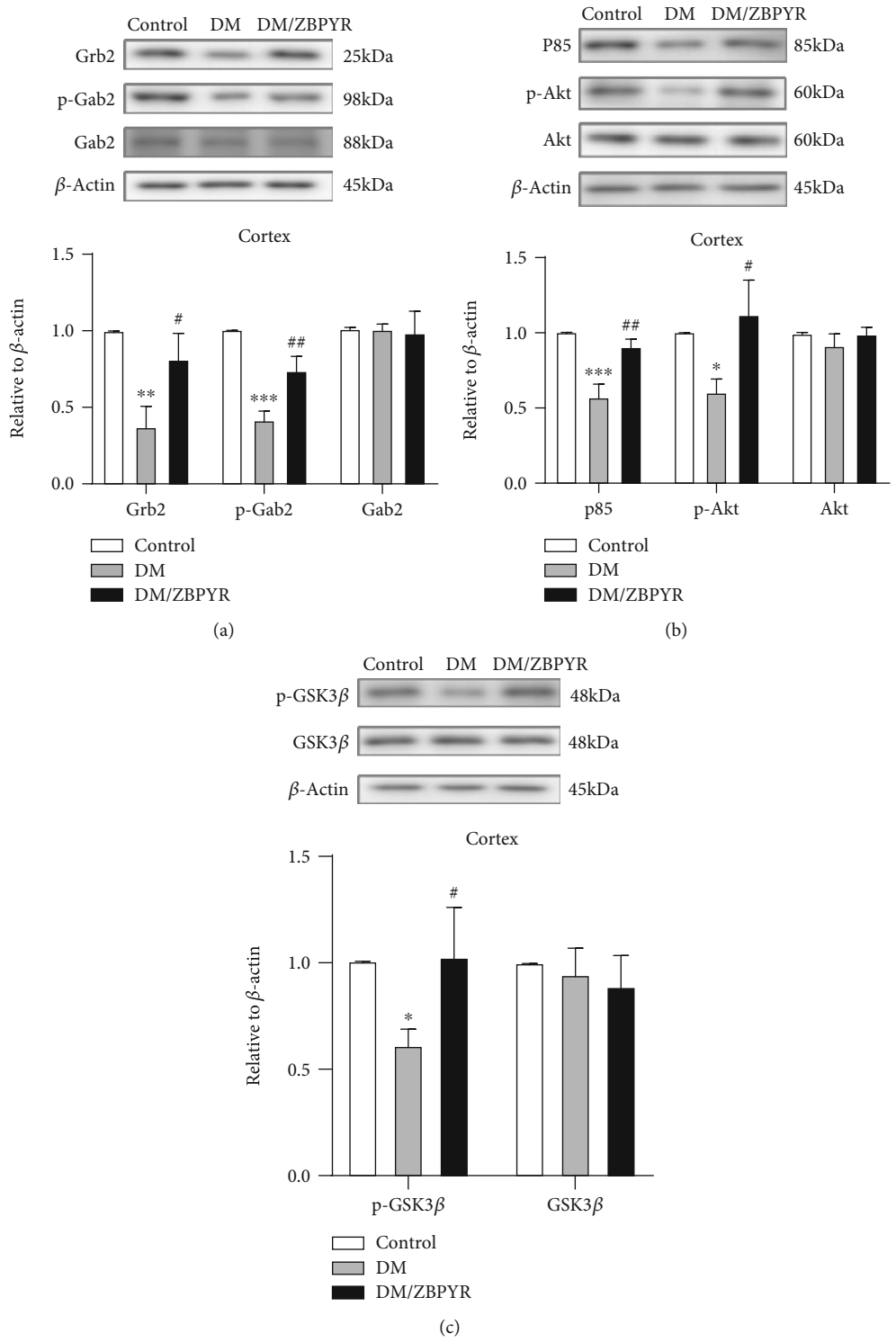

Figure 4: The effect of ZBPYR on the expression of Grb2, Gab2, Akt, p-Akt, and Gsk3β in mouse cerebral cortex. (a) The expression of Grb2 and p-Gab2 (Tyr452) in the cerebral cortex of DM mice was significantly reduced, and Grb2 and p-Gab2 (Tyr452) were increased to varying degrees after ZBPYR treatment. There were no statistically significant changes in the total levels of Gab2 and Akt in the three groups. (b) Compared with control mice, p-Akt (Ser473) expression in the cerebral cortex of DM mice was significantly reduced, while that of DM/ZBPYR mice was significantly increased. Compared with the DM group, p85 was significantly increased in the cerebral cortex of the DM/ZBPYR group. (c) The degree of Ser9 phosphorylation of GSK3β in the cerebral cortex of the DM group was reduced to varying degrees, and the level of p-GSK3β (Ser9) was increased in the cerebral cortex of the DM/ZBPYR group. Values are means ± S.D. from 3 mice in each group. $^{*}p < 0.05$, $^{**}p < 0.01$, and $^{***}p < 0.01$ compared to control; $^{\#}p < 0.05$ and $^{\#\#}p < 0.01$ compared to DM.

effect via PI3K-Akt signaling pathway by activating Grb2 on the brain of db/db mice.

5. Conclusions

In the present study, we investigated the neuroprotective effects of ZBPYR on db/db mice. The results demonstrated that ZBPYR could improve the learning and cognitive functions in DACD mice. The underlying mechanism may be related to the regulation of PI3K-Akt signaling pathway by activating Grb2.

Data Availability

The data used to support the findings of this study were supplied by Prof. Libin Zhan under license and so cannot be made freely available. Requests for access to these data should be made to Libin Zhan, zlbnj@njucm.edu.cn, School of Traditional Chinese Medicine & School of Integrated Chinese and Western Medicine, Nanjing University of Chinese Medicine, Nanjing 210023, China.

Conflicts of Interest

The authors declare that there is no conflict of interest regarding the publication of this paper.

Authors' Contributions

Li-bin Zhan contributed to the conceptualization, design, and project administration. Wei-ming Ren and Xin Li performed the experiments. Ze-bin Weng contributed to the statistical analysis and drafting of the manuscript. Wei-ming Ren and Ze-bin Weng contributed equally to this work.

Acknowledgments

This work was supported by the key project of the National Natural Science Foundation of China (No. 81730001, 81230084, and 81903940) and a project funded by the Priority Academic Program Development of Jiangsu Higher Education Institutions (Integration of Chinese and Western Medicine).

Supplementary Materials

Figure S1. Uncropped image of the original western blotting for p-Gab2/Gab2/Grb2/P85/p-Akt/Akt/p-GSK3β/GSK3β of hippocampus. Figure S2. Uncropped image of the original western blotting for p-Gab2/Gab2/Grb2/P85/p-Akt/Akt/p-GSK3β/ GSK3β of cortex. *(Supplementary Materials)*

References

[1] N. H. Cho, J. E. Shaw, S. Karuranga et al., "IDF Diabetes Atlas: global estimates of diabetes prevalence for 2017 and projections for 2045," *Diabetes Research and Clinical Practice*, vol. 138, pp. 271–281, 2018.

[2] Y. Wu, L. Ye, Y. Yuan et al., "Autophagy activation is associated with neuroprotection in diabetes-associated cognitive decline," *Aging and Disease*, vol. 10, no. 6, pp. 1233–1245, 2019.

[3] J. Weuve, L. L. Barnes, C. F. Mendes de Leon et al., "Cognitive aging in black and white Americans: cognition, cognitive decline, and incidence of Alzheimer disease dementia," *Epidemiology*, vol. 29, no. 1, pp. 151–159, 2018.

[4] C. C. Huang, C. M. Chung, H. B. Leu et al., "Diabetes mellitus and the risk of Alzheimer's disease: a nationwide population-based study," *PLoS One*, vol. 9, no. 1, article e87095, 2014.

[5] G. J. Biessels and F. Despa, "Cognitive decline and dementia in diabetes mellitus: mechanisms and clinical implications," *Nature Reviews. Endocrinology*, vol. 14, no. 10, pp. 591–604, 2018.

[6] A. Tumminia, F. Vinciguerra, M. Parisi, and L. Frittitta, "Type 2 diabetes mellitus and Alzheimer's disease: role of insulin signalling and therapeutic implications," *International Journal of Molecular Sciences*, vol. 19, no. 11, p. 3306, 2018.

[7] L. M. Yermakov, R. B. Griggs, D. E. Drouet et al., "Impairment of cognitive flexibility in type 2 diabetic db/db mice," *Behavioural Brain Research*, vol. 371, p. 111978, 2019.

[8] Y. Zheng, Y. Yang, B. Dong et al., "Metabonomic profiles delineate potential role of glutamate-glutamine cycle in db/db mice with diabetes-associated cognitive decline," *Molecular Brain*, vol. 9, no. 1, 2016.

[9] W. Zheng, G. Wang, Z. Zhang, Z. Wang, and K. Ma, "Research progress on classical traditional Chinese medicine formula Liuwei Dihuang pills in the treatment of type 2 diabetes," *Biomedicine & Pharmacotherapy*, vol. 121, p. 109564, 2020.

[10] T. Bi, L. Zhan, W. Zhou, and H. Sui, "Effect of the ZiBuPiYin recipe on diabetes-associated cognitive decline in Zucker diabetic fatty rats after chronic psychological stress," *Frontiers in Psychiatry*, vol. 11, p. 272, 2020.

[11] J. Chen, L. Liang, L. Zhan et al., "ZiBuPiYin recipe protects db/db mice from diabetes-associated cognitive decline through improving multiple pathological changes," *PLoS One*, vol. 9, no. 3, article e91680, 2014.

[12] J. Chen, L. Zhan, X. Lu, C. Xiao, and N. Sun, "The alteration of ZiBuPiYin recipe on proteomic profiling of forebrain postsynaptic density of db/db mice with diabetes-associated cognitive decline," *Journal of Alzheimer's Disease*, vol. 56, no. 2, pp. 471–489, 2017.

[13] L. B. Zhan, X. P. Niu, H. Sui, and X. Y. Gong, "Protective effect of spleen-yin-nourishing recipe on amyloid beta-peptide-induced damage of primarily cultured rat hippocampal neurons and its mechanism," *Zhong Xi Yi Jie He Xue Bao*, vol. 7, no. 3, pp. 242–248, 2009.

[14] L. B. Zhan, H. Sui, X. G. Lu, C. K. Sun, J. Zhang, and H. Ma, "Effects of Zibu Piyin recipe (滋补脾阴方药) on SNK-SPAR pathway in neuron injury induced by glutamate," *Chinese Journal of Integrative Medicine*, vol. 14, no. 2, pp. 117–122, 2008.

[15] X. Shi, X. G. Lu, L. B. Zhan et al., "The effects of the Chinese medicine ZiBu PiYin recipe on the hippocampus in a rat model of diabetes-associated cognitive decline: a proteomic analysis," *Diabetologia*, vol. 54, no. 7, pp. 1888–1899, 2011.

[16] T. J. Liao, H. Jang, R. Nussinov, and D. Fushman, "High-affinity interactions of the nSH3/cSH3 domains of Grb 2 with the C-terminal proline-rich domain of SOS1," *Journal of the American Chemical Society*, vol. 142, no. 7, pp. 3401–3411, 2020.

[17] D. H. Gu, J. H. Mao, X. D. Pan et al., "MicroRNA-302c-3p inhibits renal cell carcinoma cell proliferation by targeting

Grb2-associated binding 2 (Gab2)," *Oncotarget*, vol. 8, no. 16, pp. 26334–26343, 2017.

[18] H. E. Teal, S. Ni, J. Xu et al., "GRB2-mediated recruitment of GAB2, but not GAB1, to SF-STK supports the expansion of Friend virus-infected erythroid progenitor cells," *Oncogene*, vol. 25, no. 17, pp. 2433–2443, 2006.

[19] J. Tian, H. Zhang, L. Mu et al., "The miR-218/GAB2 axis regulates proliferation, invasion and EMT via the PI3K/AKT/GSK-3β pathway in prostate cancer," *Experimental Cell Research*, vol. 394, no. 1, p. 112128, 2020.

[20] C. Wang, C. Gu, K. J. Jeong et al., "YAP/TAZ-mediated upregulation of GAB2 leads to increased sensitivity to growth factor-induced activation of the PI3K pathway," *Cancer Research*, vol. 77, no. 7, pp. 1637–1648, 2017.

[21] Y. Wang, Q. Sheng, M. A. Spillman, K. Behbakht, and H. Gu, "Gab2 regulates the migratory behaviors and E-cadherin expression via activation of the PI3K pathway in ovarian cancer cells," *Oncogene*, vol. 31, no. 20, pp. 2512–2520, 2012.

[22] M. A. Hermida, J. Dinesh Kumar, and N. R. Leslie, "GSK3 and its interactions with the PI3K/AKT/mTOR signalling network," *Adv Biol Regul*, vol. 65, pp. 5–15, 2017.

[23] Y. Wang and Q. Chang, "MicroRNA miR-212 regulates PDCD4 to attenuate Aβ25–35-induced neurotoxicity via PI3K/AKT signaling pathway in Alzheimer's disease," *Biotechnology Letters*, vol. 42, no. 9, pp. 1789–1797, 2020.

[24] R. Xiong, X. L. Wang, J. M. Wu et al., "Polyphenols isolated from lychee seed inhibit Alzheimer's disease-associated Tau through improving insulin resistance via the IRS-1/PI3K/Akt/GSK-3β pathway," *Journal of Ethnopharmacology*, vol. 251, p. 112548, 2020.

[25] Y. Yao, Y. Wang, L. Kong, Y. Chen, and J. Yang, "Osthole decreases tau protein phosphorylation via PI3K/AKT/GSK-3β signaling pathway in Alzheimer's disease," *Life Sciences*, vol. 217, pp. 16–24, 2019.

[26] P. Dong, L. Zhang, L. Zhan, and Y. Liu, "Ultra high performance liquid chromatography with mass spectrometry for the rapid analysis and global characterization of multiple constituents from Zibu Piyin recipe," *Journal of Separation Science*, vol. 39, no. 3, pp. 595–602, 2016.

[27] L. Sun, X. Diao, X. Gang et al., "Risk factors for cognitive impairment in patients with type 2 diabetes," *Journal Diabetes Research*, vol. 2020, article 4591938, pp. 1–10, 2020.

[28] F. Novellino, M. E. Lopez, M. G. Vaccaro, Y. Miguel, M. L. Delgado, and F. Maestu, "Association between Hippocampus, thalamus, and caudate in mild cognitive impairment APOEε4 carriers: a structural covariance MRI study," *Frontiers in Neurology*, vol. 10, p. 1303, 2019.

[29] U. Strunk, D. G. Ramos, H. A. Saffran, and J. R. Smiley, "Role of Herpes simplex virus 1 VP11/12 tyrosine-based binding motifs for Src family kinases, p 85, Grb2 and Shc in activation of the phosphoinositide 3-kinase-Akt pathway," *Virology*, vol. 498, pp. 31–35, 2016.

[30] A. S. Mitchell, R. Czajkowski, N. Zhang, K. Jeffery, and A. J. D. Nelson, "Retrosplenial cortex and its role in spatial cognition," *Brain and Neuroscience Advances*, vol. 2, article 239821281875709, 2018.

[31] N. Sambuchi, Y. E. Geda, and B. F. Michel, "Cingulate cortex in pre-MCI cognition," *Handbook of Clinical Neurology*, vol. 166, pp. 281–295, 2019.

[32] A. Ozaita, E. Puighermanal, and R. Maldonado, "Regulation of PI3K/Akt/GSK-3 pathway by cannabinoids in the brain," *Journal of Neurochemistry*, vol. 102, no. 4, pp. 1105–1114, 2007.

[33] M. Bilal, M. S. Iqbal, S. B. Shah, T. Rasheed, and H. M. N. Iqbal, "Diabetic complications and insight into antidiabetic potentialities of ethno-medicinal plants: a review," *Recent Patents on Inflammation & Allergy Drug Discovery*, vol. 12, no. 1, pp. 7–23, 2018.

[34] H. Yaribeygi, A. E. Butler, G. E. Barreto, and A. Sahebkar, "Antioxidative potential of antidiabetic agents: a possible protective mechanism against vascular complications in diabetic patients," *Journal of Cellular Physiology*, vol. 234, no. 3, pp. 2436–2446, 2018.

[35] T. T. Zhang and J. G. Jiang, "Active ingredients of traditional Chinese medicine in the treatment of diabetes and diabetic complications," *Expert Opinion on Investigational Drugs*, vol. 21, no. 11, pp. 1625–1642, 2012.

[36] K. Bromley-Brits, Y. Deng, and W. Song, "Morris water maze test for learning and memory deficits in Alzheimer's disease model mice," *Journal of visualized experiments: JoVE*, vol. 53, no. 53, 2011.

[37] S. S. Tang, Y. Ren, X. Q. Ren et al., "ERα and/or ERβ activation ameliorates cognitive impairment, neurogenesis and apoptosis in type 2 diabetes mellitus mice," *Experimental Neurology*, vol. 311, pp. 33–43, 2019.

[38] Y. F. Gao, M. N. Zhang, T. X. Wang, T. C. Wu, R. D. Ai, and Z. S. Zhang, "Hypoglycemic effect of D-chiro-inositol in type 2 diabetes mellitus rats through the PI3K/Akt signaling pathway," *Molecular and Cellular Endocrinology*, vol. 433, pp. 26–34, 2016.

[39] P. Majumder, K. Roy, B. K. Singh, N. R. Jana, and D. Mukhopadhyay, "Cellular levels of Grb2 and cytoskeleton stability are correlated in a neurodegenerative scenario," *Disease Models & Mechanisms*, vol. 10, no. 5, pp. 655–669, 2017.

[40] M. S. Manu, K. S. Rachana, and G. M. Advirao, "Altered expression of IRS2 and GRB2 in demyelination of peripheral neurons: implications in diabetic neuropathy," *Neuropeptides*, vol. 62, pp. 71–79, 2017.

Hindawi
Neural Plasticity
Volume 2020, Article ID 8861903, 16 pages
https://doi.org/10.1155/2020/8861903

Review Article

Changes in Hippocampal Plasticity in Depression and Therapeutic Approaches Influencing These Changes

Wenbo Xu,[1] **Xiaoxiao Yao**,[1] **Fangyi Zhao**,[1] **Haisheng Zhao**,[1] **Ziqian Cheng**,[1] **Wei Yang**,[1] **Ranji Cui**,[1] **Songbai Xu**,[2] **and Bingjin Li**[1]

[1]*Jilin Provincial Key Laboratory on Molecular and Chemical Genetic, The Second Hospital of Jilin University, Changchun, China*
[2]*Department of Neurosurgery, First Hospital of Jilin University, Changchun, China*

Correspondence should be addressed to Songbai Xu; xusongbai@jlu.edu.cn and Bingjin Li; libingjin@jlu.edu.cn

Received 27 July 2020; Revised 30 September 2020; Accepted 11 November 2020; Published 27 November 2020

Academic Editor: Fushun Wang

Depression is a common neurological disease that seriously affects human health. There are many hypotheses about the pathogenesis of depression, and the most widely recognized and applied is the monoamine hypothesis. However, no hypothesis can fully explain the pathogenesis of depression. At present, the brain-derived neurotrophic factor (BDNF) and neurogenesis hypotheses have highlighted the important role of plasticity in depression. The plasticity of neurons and glial cells plays a vital role in the transmission and integration of signals in the central nervous system. Plasticity is the adaptive change in the nervous system in response to changes in external signals. The hippocampus is an important anatomical area associated with depression. Studies have shown that some antidepressants can treat depression by changing the plasticity of the hippocampus. Furthermore, caloric restriction has also been shown to affect antidepressant and hippocampal plasticity changes. In this review, we summarize the latest research, focusing on changes in the plasticity of hippocampal neurons and glial cells in depression and the role of BDNF in the changes in hippocampal plasticity in depression, as well as caloric restriction and mitochondrial plasticity. This review may contribute to the development of antidepressant drugs and elucidating the mechanism of depression.

1. Introduction

According to the latest epidemiological survey, the incidence of depression worldwide is 4.7%, and the incidence in China is 4%; depression is a serious disease, and only 10% of patients respond effectively to treatment [1]. Depression severely affects human health and quality of life, including but not limited to excessive negative emotions, anhedonia, and cognitive impairment. The hippocampus is a key anatomical brain region associated with depression. Numerous studies have confirmed that changes in hippocampal plasticity (hippocampal volume, number of synapses, synaptic plasticity, changes in glutamate receptors, neurogenesis, and glial cell plasticity) occur in patients with depression [2]. It has been reported that the volume of the hippocampus in patients with major depression disorder (MDD) is significantly reduced [3]. After using antidepressant drugs, patient hippocampal tail volume increases in proportion to symptom relief [4]. The change in volume could be due to changes in neurons and glial cells.

Studies have shown that stress (especially chronic stress and early life stress) is closely related to the development of depression [5]. Chronic stress can cause apoptosis in hippocampal subregions and affect the integrity of hippocampal cells [6]. Long-term potentiation (LTP) and long-term depression (LTD) are the two main forms of synaptic plasticity changes. Stress causes changes in synaptic efficacy and stimulates the hypothalamic-pituitary-adrenal (HPA) axis to increase the levels of glucocorticoid (cortisol in human, corticosterone in rodents), resulting in a decrease in hippocampal LTP [7] that contributes to LTD [8]. Cell-level studies have found that stress leads to decreases in dendritic complexity and dendritic spine density [9]. On the other hand, excitatory synaptic neurotransmission is also affected in

chronically stressed animals [10]. Central nervous system neurotransmitter dysfunction is one of the aspects of the pathogenesis of depression. Glutamate is widely distributed in the central nervous system and is an important excitatory neurotransmitter. Glutamate works by binding to the corresponding glutamate receptors, and pharmacological studies have shown that glutamate receptor modulators have antidepressant effects.

There are many hypotheses about the pathogenesis of depression, but the biological mechanisms remain unclear. The monoamine hypothesis is the most widely accepted hypothesis, and most current treatments for depression are based on the monoamine hypothesis. However, there are many limitations to the monoamine hypothesis. For example, the latency of antidepressant drugs cannot be explained, not all drugs that enhance monoamine functions have antidepressant activity, and a reduction in monoamines does not induce depression in healthy humans [11]. The neuroendocrine hypothesis proposes that abnormal function of the HPA axis leads to depression. Patients with depression often exhibit excessive secretion of glucocorticoids [12]. In a rodent model of chronic stress (classic depression model), plasma corticosterone levels are significantly increased [13]. Long-term administration of exogenous corticosterone can cause depression-like behavior in rodents [14]. With the development of immunological research, clinical studies have shown that chronic inflammation and some viral infectious diseases can significantly increase the incidence of depression, and the neuroinflammatory response hypothesis has thus been proposed. Studies have shown that the levels of proinflammatory cytokines in patients with depression are significantly increased [15]. Proinflammatory cytokines can affect the metabolism of monoamine transmitters and can also act on the HPA axis, impairing the negative feedback regulation of the HPA axis [16].

In recent years, people have gradually realized that information processing in the brain is not just the transfer of chemicals between neurons, but the result of the complex effects of neural networks. This finding puts forward the concept of neuroplasticity, that is, the ability of the nervous system to adapt and respond to the environment, including neurogenesis, neuronal remodeling, and synapse formation. The theory proposes that neuroplasticity disorders are involved in the pathological process of depression and that neurotrophic factors are important indicators for evaluating neuroplasticity. Brain-derived neurotrophic factor (BDNF) is a kind of neurotrophic factor. BDNF plays a key role in regulating synapse, hippocampal LTP, and neurogenesis [17].

Unfortunately, there is no single hypothesis that can explain the pathogenesis of depression. Moreover, the current clinical antidepressant treatment method is simplistic, the cure rate of antidepressant drugs is low, their side effects are high, and they are costly. The role of calorie restriction (CR) in depression has recently been revealed [18]. Previous research confirmed that CR is positively correlated with lifespan and negatively correlated with neurological diseases [19]. Studies have shown that CR can increase hippocampal neurogenesis and BDNF expression [20]. Neurogenesis is closely related to depression. Mitochondria are the sites at which cells metabolize energy and control programmed cell death [21]. The mitochondrial network plays a key role in CR [22]. Therefore, in addition to exploring the effect of CR on hippocampal plasticity, we also discuss the role of mitochondrial plasticity of the hippocampus.

At present, there have been many studies on antidepressants, and there are also different views on the pathogenesis of depression. However, the shortcomings of antidepressants are obvious to everyone. Because CR is simple to implement and has almost no side effects, it may be used to treat depression or to assist with existing antidepressant treatments to improve their efficacy. In this review, we introduce the various changes in hippocampal plasticity in depression and discuss the role of BDNF and CR in the treatment of depression. This review of hippocampal neuroplasticity may contribute to the development of new drugs and treatments.

2. Changes in Hippocampal Plasticity in Depression

The hippocampus is part of the limbic system and plays a vital role in depression. Numerous changes in hippocampal plasticity can be seen in both human depression patients and rodent depression models. There is a significant reduction in hippocampal volume. Depression can cause changes in various subregions, glutamate receptors, and glial cells in the hippocampus. Stress exists at the core of the many influencing factors. Some antidepressants also act through plasticity regulation. The different structures and functions of different hippocampal subregions may help to better understand hippocampal plasticity.

2.1. Hippocampal Volume. Clinical studies and neuroimaging results have shown that the hippocampal volume of patients with depression is reduced [23]. Similar results were observed in rodent models [24]. Both unipolar and bipolar depression (BD) patients have decreased hippocampal volume [25]. Telomere length is positively correlated with hippocampal volume, and reduced telomere length increases the risk of BD [26]. Chronic stress reduces hippocampal volume and inhibits neurogenesis in rats [27]. Early life stress increases the risk of MDD, which is associated with reduced left hippocampal volume [28]. The relationship between hippocampal volume and depression seems very complicated. Electroconvulsive therapy (ECT) increases the volume of the left hippocampus in patients, but there is no positive correlation with the treatment effect on depression [29]. The reduction in the hippocampus is not only caused by depression but is also a cause of depression [30]. Moreover, changes in hippocampal volume in depression are regulated by gene polymorphisms and gene expressions such as oxytocin receptor genes [31], monoamine-related genes [32], and neuroinflammatory genes [33].

2.2. Hippocampal Synaptic Neuroplasticity in the Different Subregions. In depression, the changes in hippocampal synaptic plasticity are also reflected in the hippocampal subregions, especially the cornu ammonis 3 (CA3) and the

dentate gyrus (DG). In this section, we summarize the relationship between different hippocampal subregions and LTP and LTD and introduce some antidepressant drugs or methods to improve depression (based on the plasticity of the different subregions).

2.2.1. Cornu Ammonis (CA1-CA3). CA1 neurons accept 2 different glutamatergic inputs: temporoammonic- (TA-) CA1 and the CA3 region and the Schaffer collateral- (SC-) CA1. The JAK-STAT signaling pathway plays a role in the LTD induced by both pathways [34]. Chronic unpredictable stress (CUS) and corticosterone administration can reduce the excitatory signaling of TA-CA1 in rats [35]. Long-term plasticity in CA1 is induced by GABAergic interneurons (parvalbumin-expressing (PV+), nitric oxide synthase-expressing (NOS+)) [36]. Acute stress activates μ-opioid receptors on GABAergic neurons to facilitate low-frequency stimulation-induced LTD at SC-CA1 glutamatergic synapses in mice [37]. Electroacupuncture (EA) can improve depression by restoring CA1 synaptic plasticity, which may be mediated by regulating 5-HT receptor levels [38]. The perineuronal net (PNN) restricts LTD in the CA1 area in mice [39]. Interlaminar CA1-CA1 networks exhibit NMDA receptor-dependent LTP rather than LTD [40].

CA2 is a region that tends to be overlooked. The volume of CA2 is negatively correlated with depressive symptoms [41]. It is difficult to induce LTP and LTD in the CA2 region, which showed unique synaptic stability compared with that of other regions. A study showed that neurons in CA2 require more current to generate action potentials [42]. The function of CA2 in regulating synaptic plasticity may be different from other CA regions. The inhibitory LTD of PV + interneurons in the CA2 region does not exist in young mice and may require the maturation of PNN and ErbB4 [43]. The plasticity of PV+ neurons is mediated by δ-opioid receptors [44].

CA3 pyramidal cells receive three types of excitatory synaptic afferent neurons: mossy fibers (MFs), perforant paths (PPs), and associational/commissural (AC) fibers. The MF-CA3 synapse has been reported to play a role in antidepressant drugs [45]. Novel spatial learning contributes to hippocampal plasticity and is termed learning-facilitated plasticity (LFP). When rats explore different environments, the MF-CA3 and AC-CA3 synapses show different responses to LTD. However, when exploring a new empty environment, both synapses promote LTP [46]. LFP-induced LTD and LTP in the MF-CA3 synapse require the activation of β-adrenergic receptors [47]. In addition, ECT treatment can increase dopamine regulation in MF [48]. The antidepressant drugs can enhance D1 receptor-dependent synaptic potentiation in the MF-CA3 [49]. Vagus nerve stimulation (a treatment for depression) can cause an increase in PP-CA3 synaptic transmission [50]. In an animal model of depression induced by chronic unpredictable mild stress (CUMS), LTP, basal synaptic transmission, and dendrite spine density were decreased in the CA3-CA1 synapse [51]. The CA3-CA1 synapse is also thought to be involved in the acquisition of associative learning [52]. CA3-CA3 synapses are widely distributed [53] and have strong plasticity [54]. Studies have shown that the spike timing-dependent plasticity of the CA3-CA3 synapses contributes to information storage and retrieval [55].

2.2.2. Dentate Gyrus. Apoptosis in the CA1 and CA4 regions and the DG can be observed in patients with MDD [56]. Patients with ECT treatment that had larger right CA4/DG volumes were associated with symptom remission [57]. DG plasticity changes are also involved in the mechanism of some antidepressant drugs. Tianeptine is a special tricyclic antidepressant. It mainly acts on the 5-HT system, which can increase the activity of hippocampal pyramidal cells and the reuptake of 5-HT by hippocampal neurons (as opposed to traditional antidepressants) [58]. Tianeptine was reported to reduce DG apoptosis in a tree shrew model of depression [59]. Maternal separation (MS) can impair learning and memory and cause depression-like behavior. Studies have shown that MS can induce the apoptosis in the DG and reduce cell proliferation in rats [60]. The expression of glutamate receptor 1 and protein kinase B phosphorylation in the DG were also decreased [60]. These factors may be involved in depression caused by MS. Fluoxetine, a selective 5-HT reuptake inhibitor widely used in clinical practice, can selectively inhibit 5-HT transporter and block the reuptake of 5-HT by the presynaptic membrane, thereby producing antidepressant effects. A study has shown that after 2 weeks of MS in rats, 7 days of fluoxetine treatment can reverse cell apoptosis, increase cell proliferation (reduce the number of terminal deoxynucleotidyl transferase-mediated dUTP gap terminal marker-positive cells), and has an antidepressant effect [61]. Chronic stress can damage LTP in the DG of rats, but this effect is reversible [62].

The effect of sirtuin (SIRT) 2 knockdown in the DG is similar to that of chronic stress, and both downregulate plasticity-related genes [63]. In addition, chronic stress reduces SIRT1 activity in mice, leading to depression-like behavior [64]. Physical activity can modulate LTP and LTD in DG of rodents, but the effects are complex and depend on the studies and the conditions (exercise regime, duration, and intensity) [65]. Both acute stress and dexamethasone injection increased the release of somatostatin (SST) in DG hilar cells [66]. Several studies have shown that SST promotes LTP in the DG [67]. However, the opposite effect has also been reported [68]. The reason for this phenomenon may be that SST has different effects on different hippocampal synapses.

There are other factors, such as dopamine [69], 5-HT [70], sex hormones (estradiol, testosterone) [71], paracrine signaling factor (Wnt [72], Notch1 [73]), proinflammatory cytokines [74], and epigenetic changes [75], that are also involved in regulating DG plasticity, which we will not elaborate here.

2.3. Glutamate Receptor Involvement in Synaptic Plasticity. Glutamate receptors are mainly divided into two categories: one is ionic receptors including the N-methyl-d-aspartate receptor (NMDAR), the α-amino-3-hydroxy-5-methyl-4-isoxazole propionic acid receptor (AMPAR), and the kainite receptor (KAR), and the metabolic receptor, mGluR. These

receptors are closely related to hippocampal plasticity to varying degrees.

2.3.1. N-Methyl-d-aspartate Receptor (NMDAR). NMDAR has multiple subtypes, including NR1 and NR2A-D. The function of NMDAR is determined by the different functions, structure and distribution of various subunits, and different combinations of subunits [76]. Generally, NR1 is considered to be an important component of NMDAR functionality [77]. NMDAR ligand-gated ion channels are regulated by glycine [78], and glycine has a binding site on NR1 [79]. Previous studies have shown that NMDAR is mainly distributed in the postsynaptic density (PSD) of the postsynaptic membrane. Studies in recent years have confirmed that NMDAR is also distributed in the presynaptic membrane and non-PSD areas [80]. PSD95 participates in NMDA receptor regulation [81]. PSD95 expression promotes the maturation of excitatory (glutamatergic) synapses, increasing the number and size of dendritic spines [82]. PSD95 stabilizes NMDAR by binding to GluN2B or degrading STEP61 [83]. The activity-dependent regulation of STEP61 and its substrates GluN2B and GluA2 (a subunit of AMPAR) may contribute to the homeostasis of excitatory synapses [84]. In the absence of stimulation, the NMDA ion channel is not opened due to the blocking of Mg2+. Under various stimuli, the postsynaptic membrane depolarizes. The blocking effect of Mg2+ disappears, and Ca2+ and Na+ enter the cell, increasing free Ca2+ in the cell and producing various biochemical reactions. NMDAR-dependent LTP is widely reported in the hippocampus [85]. Ketamine is an NMDAR antagonist, and its rapid antidepressant mechanism has been confirmed in human and animal models. Ketamine can reverse the decrease of hippocampal CA3 and DG dendritic spine density in depressed mice, activate AMPAR, and increase BDNF expression and release and activation of the mammalian target of rapamycin (mTOR) [86]. Depressed rats treated with ketamine exhibit increased LTP and levels of EPSCs mediated by NMDA receptors in the hippocampus [87]. In addition to PSD95, NMDAR also binds with multiple molecules including CaMKII [88] and microtubule-associated protein 2 [89], to form a multiprotein complex, which plays a role in plasticity, learning, and memory.

2.3.2. α-Amino-3-hydroxy-5-methyl-4-isoxazole Propionic Acid Receptor (AMPAR). AMPAR regulates synaptic plasticity through changes in the number of postsynaptic membranes (insertion or removal of AMPAR). AMPAR regulates synaptic transport during LTP through two ways: lateral movement and exocytosis [90]. Lateral diffusion exchanges AMPAR at the dendritic spines, depending on the spinal morphology [91]. AMPAR surface diffusion is the key to hippocampal LTP and learning [92]. Acute stress can increase the AMPAR phosphorylation and surface expression in the hippocampal CA1 region of mice and alleviate LTP impairment [93]. Another way to recruit AMPAR to the synapse is through exocytosis [94]. Cyclin Y inhibits AMPAR exocytosis of dendritic spines, thereby inhibiting LTP [95]. This exocytosis in LTP passes through the RAS/ERK signaling pathway [96]. In addition, the silent synapses (the synapse only expresses NMDAR before inducing LTP) express AMPAR after inducing LTP and then, they become a functional synapse [97]. Several studies have suggested that hippocampal LTD is associated with AMPAR endocytosis. Calcyon can regulate endocytosis, and knocking out the gene that encodes calcyon leads to the LTD disappearance in the hippocampal CA1 region [98]. Inhibition of AMPAR endocytosis can increase the AMPAR level and decrease LTD [99]. However, one study suggested that AMPAR-induced LTD was the result of inhibiting exocytosis rather than enhancing endocytosis [100].

2.3.3. Kainate Receptor (KAR). There has been less focus on KAR than on the other two ionic glutamate receptors. However, the function of KAR associated with plasticities such as the modulation of excitability [101], transmitter release [102], neuronal development [103], and neurogenesis [104]. The neto protein is an important auxiliary protein that regulates the KAR in many interneurons [105]. The distribution of KAR also shows some differences, and it is expressed in the presynaptic regions, in addition to the postsynaptic regions [106]. Furthermore, the bidirectional regulation of KAR is also considered to play an important role in plasticity [107]. Several studies have found a link between KAR subtypes and depression. GluR7 is a susceptibility gene associated with recurrent MDD [108]. GluK4 (a KAR subunit) deficiency is associated with increased cognitive ability [109]. Rodent models have also confirmed that GRIK4 (GluK4 gene) knockout causes an antidepressant phenotype [110].

Chronic stress and corticosteroids increase KAR subunit mRNA expression in rats [111]. KAR is reported to be involved in glutamate release in the CA1 and CA3 regions [112]. The short-term and long-term potentiation of KAR participation in the hippocampal MF synapse has been generally confirmed, in which presynaptic KAR plays a central role [113]. Similarly, KAR is also involved in the induction and expression of hippocampal LTD [114]. KAR regulates not only the glutamatergic system but also the GABAergic system. KAR inhibits GABA release and the synaptic transmission to CA1 [115]. However, another study came to the opposite conclusion. KAR increased the efficacy of GABAergic synapses [116]. This effect could be related to the agonist concentration, but the specific mechanism is still unclear.

2.3.4. Metabolic Receptor (mGluR). mGluR is a type of G-protein-coupled receptor and is divided into three categories (I, II, and III) with 8 subtypes (mGluR1-8). Type I mGluRs include two subtypes: mGluR1 and mGluR5. Chronic stress can increase type I mGluR-mediated LTD in the hippocampal CA1 region [117], while acute stress has only a promoting effect [118]. This phenomenon indicates that type I mGluR-mediated plasticity changes require repeated stress stimulation. Besides, DHPG (a type I glutamate receptor agonist) induced synaptic plasticity of the Schaffer collateral NMDAR (induced LTD) [119]. Studies on type I mGluRs mainly focus on the feedback circuit of the hippocampal stratum oriens, in which type I mGluRs induce LTP [120]. The type I mGluRs induced anti-Hebbian LTP in interneurons of rat

hippocampal stratum oriens [121]. Type I mGluRs are also involved in TEA-induced LTP in rat MF-CA3 synapses [122]. Studies have shown that type I mGluR-mediated synaptic plasticity occurs via the β-arrestin signaling pathway [123]. The TRPC1 channel plays a critical role in the process of mGluR5-regulated plasticity [124].

Although type II and III mGluRs are rarely reported in terms of hippocampal plasticity, their important role cannot be ignored. Fluoxetine combined with a low-dose ly379268 (a mGluR2/3 agonist) can increase cell proliferation and neurogenesis of cultured cerebellar granule neurotransmitters and shorten the incubation period required for the downregulation of hippocampal β-adrenergic receptors [125]. The study of type III mGluRs showed that MS significantly reduced the expression of mGluR4 in the hippocampus of rats, while fluoxetine reversed the changes induced by MS [126]. Behavioral pharmacology studies have shown that LSP4-2022 (a selective agonist of mGluR4) has a strong effect in promoting depression in mice. This effect does not exist in mGluR4-knockout mice, but whether an mGluR4 antagonist can induce an antidepressant effect needs further verification [127]. In mGluR4-knockout mice, improved spatial learning is associated with hippocampal LTP [128]. AMN082 (an mGluR7 allosteric agonist) produces antidepressant-like effects by regulating glutamatergic signaling [129]. mGluR7-knockout mice show antidepressant phenotype, causing HPA axis dysregulation and increasing hippocampal BDNF protein levels [130].

2.4. Hippocampal Apoptosis and Neurogenesis. The neurogenesis hypothesis is to some extent an extension of the BDNF hypothesis. Apoptosis of hippocampal neurons has been observed in MDD patients and rodent depression models [131, 132]. Apoptosis of hippocampal neurons may be one of the causes of depression. Venlafaxine is a dual inhibitor of 5-HT and norepinephrine reuptake, which can inhibit the reuptake of NA and 5-HT and slightly inhibit the reuptake of dopamine. Venlafaxine also inhibits hippocampal neuron apoptosis in depression by upregulating the expression of BDNF in the hippocampus of rats [133].

Hippocampal neurogenesis is the process by which adult neural stem cells become progenitor cells and then functional DG cells, providing functional and structural plasticity [134]. Although the number of newborn neurons is much smaller than that in the hippocampal granular cell layer, these cells have important implications in hippocampal function. Increased adult hippocampal neurogenesis can reduce depression-like behavior in mice [135]. Chronic corticosterone injection reduced the neurogenesis of DG in rats [136] and the dendritic complexity of mature granule cells [137]. Adult neurogenesis altered the excitability of the DG [138] and enforced chronic stress adaptability by inhibiting mature granulosa cells in the ventral DG [139]. Ketamine increased DG cell proliferation in depressed rats [140]. Stress and corticosterone also inhibit progenitor cell proliferation, possibly by increasing nitric oxide levels [141].

2.5. Glial Cell Plasticity. Glial cells are another prominent cell type in nerve tissue and are widely distributed in the central and peripheral nervous systems. The glial cells in the central nervous system mainly include astrocyte, oligodendrocyte, and microglia. There is evidence that astrocytes affect adult neurogenesis in hippocampal DG [142]. The activity of p38α mitogen-activated protein kinase (MAPK) in astrocytes is required for hippocampal LTD [143]. Chronic mild stress-induced depression may be related to a decrease in the number of astrocytes and the activation of microglia [144]. The pruning of synapses by microglia is necessary for brain development [145]. Microglia reshape synapses through presynaptic phagocytosis and spine head filopodia induction. Microglial inhibitors can eliminate the decrease in hippocampal LTP and LTD caused by peripheral inflammation [146]. In CUS-induced depression model rats, the number of oligodendrocytes in the hippocampal CA3 and DG regions is decreased [147]. Oligodendrocyte depolarization can induce short-term and long-term plasticity in hippocampal white matter [148]. Oligodendrocytes can regulate axonal excitability and nerve conduction [149]. The inhibition of oligodendrocyte formation impairs memory consolidation in mice [150]. Myelin basic protein is a marker of mature oligodendrocytes. Chronic social frustration stress can cause changes in the plasticity of ventral hippocampal myelin, but this effect depends on genetic background [151].

3. Role of Brain-Derived Neurotrophic Factor in Depression

The neurotrophic factor and neurogenesis hypotheses connect BDNF with plasticity and depression. Clinical studies have shown that plasma BDNF levels are reduced in patients with depression [152], and antidepressant treatment can increase BDNF levels [153]. BDNF is an indispensable factor in the antidepressant effects of ketamine [154]. BDNF plays an important role in regulating hippocampal plasticity. BDNF regulates LTP in the hippocampus by enhancing synaptic responses [155]. In addition, BDNF also affects the expression of monoamine genes in the hippocampus [156]. Current studies have mainly focused on BDNF and its precursor (proBDNF) and mature forms (mBDNF) [157]. CUMS caused a decrease in the BDNF/proBDNF ratio in the rodent's hippocampus: BDNF rescued CUMS-induced behaviors and spine loss, while proBDNF resulted in a decrease in spine density [158]. The high-affinity receptor of BDNF is tropomyosin receptor kinase B (TrkB), which has low affinity for p75 [159]. Furthermore, BDNF activates multiple signaling pathways (Figure 1). Therefore, in this section, we focus on these signaling pathways and discuss the role of the BDNF signaling pathway in hippocampal plasticity in depression and antidepressant drugs.

3.1. Mitogen-Activated Protein Kinase (MAPK) Pathway. After binding to TrkB, BDNF phosphorylates Shc and alters the conformation of the TrkB-Shc complex [160]. Phosphorylated Shc then acts on the downstream growth factor receptor-bound protein 2 (GRB2) and the son of sevenless (SOS), which in turn activate the MAPK signaling pathway, leading to ERK1/2 phosphorylation [161]. BDNF may increase nuclear CREB activity through 2 main pathways:

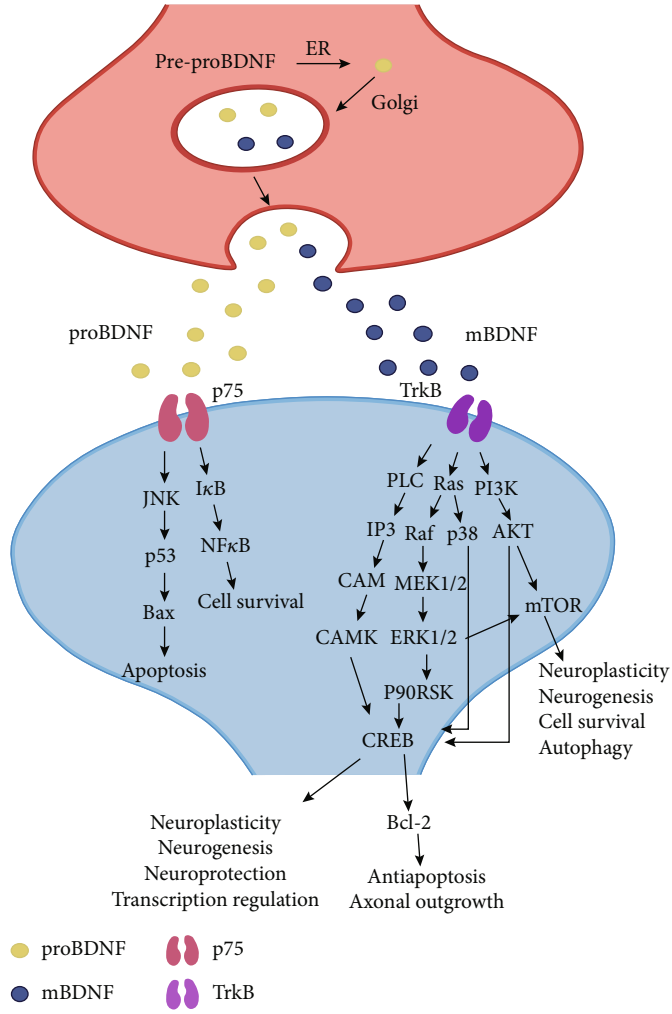

Figure 1: Diagrams of the BDNF-relevant signaling pathways. BDNF: brain-derived neurotrophic factor; ER: endoplasmic reticulum; TrkB: tropomyosin receptor kinase B; PLC: phospholipase C; IP3: inositol triphosphate; CAM: calmodulin; CAMK: CAM-dependent protein kinase; p90RSK: 90 kDa ribosomal S6 kinase; ERK1/2: extracellular-regulated kinase 1/2; PI3K: phosphoinositide 3-kinase; AKT: protein kinase B; mTOR: mammalian target of rapamycin; CREB: cAMP-response element binding protein; JNK: c-Jun N-terminal kinase; Bax: Bcl-2-associated X protein ; NF-κB: nuclear factor-κB; IκB: an inhibitor of NF-κB.

p38 phosphorylation and 90 kDa ribosomal S6 kinase (p90RSK) phosphorylation [162, 163]. CREB is an important hub in neuroplasticity and neuroprotection [164]. Many examples of antidepressants work through the BDNF/MAPK pathway. For example, the plant *Centella asiatica* supposed to have antidepressant properties improves the memory of chronic electrical stress rats (increased hippocampal BDNF levels) via the BDNF/TrkB/ERK pathway [165]. The plant *Angelica sinensis* plays a neuroprotective effect through the BDNF/CREB/p90RSK signaling pathway [162]. Imipramine, a selective inhibitor of monoamine reuptake, can exert neuroprotective effects via the BDNF/MAPK/Bcl-2 pathway [166].

3.2. Phospholipase Cγ (PLCγ). Activated PLC hydrolyzes the membrane component phosphatidylinositol 4,5-bisphosphate (PIP2) to produce a second messenger inositol triphosphate (IP3). IP3 promotes the release of Ca2+ from the cellular calcium reservoir and increases the concentration of Ca2+ in the cytoplasm. Ca2+ then binds to calmodulin (CAM) to transmit the signal. The signal transduction molecule downstream of the Ca2+/M complex is a protein kinase that can be activated by the Ca2+/CAM complex called CAM-dependent protein kinase [167]. One study showed that the TrkB/PLC pathway mediated mouse hippocampal LTP and regulated CREB activity [168].

3.3. Phosphoinositide 3-Kinase (PI3K) Pathway. Activated PI3K can catalyze the production of phosphatidylinositol 3,4,5-triphosphate (PIP3). PIP3 activates AKT by binding to its pleckstrin homology (PH) domain and can also activate AKT by activating 3-phosphoinositide-dependent protein kinase 1 (PDK1) [169]. BDNF has been reported to inhibit autophagy through the PI3K-Akt signaling pathway [170].

Most studies on downstream molecules of the BDNF-mediated PI3K-Akt signaling pathway have focused on mammalian target of rapamycin (mTOR). The BDNF/mTOR signaling pathway is involved in the rapid antidepressant

mechanism of the antidepressant drug ketamine [154], and ketamine enhances the structural plasticity of dopaminergic neurons through the AMPA receptor-driven BDNF/mTOR signaling pathway [171]. S 47445 (positive allosteric modulator of AMPAR) reduced the motor activity of olfactory bulb-excised mice, showing an antidepressant effect, and reversed the changes in the expression of BDNF/mTOR [172]. Hypidone hydrochloride (YL-0919) showed a faster antidepressant effect than fluoxetine and also reversed the activity of BDNF/mTOR signaling and some key synaptic proteins [173]. Sulforaphane can play an antidepressant effect in chronic mild stress mice and can block the elevation of corticosterone, corticotropin, IL-6, and TNF-α in serum of mice [174]. The antidepressant effect of sulforaphane may be through inhibition of the HPA axis and inflammatory response. Furthermore, sulforaphane can reverse the decrease of BDNF and dendritic spine density in depressed mice [175]. Knockdown of hyperpolarization-activated cyclic nucleotide-gated channel 1 (HCN1) increased the excitability of cells in the mouse CA1 region, resulting in showing an antidepressant phenotype [176]. Inhibition of HCN1 can reduce depression and improve learning ability in rats [177]. These effects are all related to the upregulation of the BDNF/mTOR signaling pathway and synaptic transmission. Studies on the binding of mTOR with different proteins to form functional polymer complexes suggested that BDNF/mTOR1 can be used as a research focus for a new generation of antidepressant drugs [178]. The BDNF/mTOR1 signaling pathway may be the target of the antidepressant effect of traditional prescriptions (lily bulb and Rehmannia decoction) [179].

4. Caloric Restriction as a Putative Treatment in Depression

The antidepressant effect of CR has been confirmed in rodent depression models (Figure 2). During aging, neuroinflammation and oxidative stress increase in the hippocampus, and synaptic plasticity and neurogenesis decrease, but these adverse reactions can be alleviated by CR [180]. CR reduces cell death in the hippocampal CA3 area after kainate administration [181]. At the genetic level, CR reduces basic DNA loss [182] and affects the expression of genes associated with synaptic plasticity in the hippocampal CA1 and CA3 region [183]. CR can stabilize the gene expression of presynaptic proteins [184] and prevent the reduction in key synaptic proteins in the CA3 [185]. In terms of neuroendocrine, CR increased the expression of adiponectin in rodent adipose tissue and blood adiponectin levels [186]. Patients with BD often have decreased plasma adiponectin levels [187]. Adiponectin and antidepressant drugs can improve the symptoms of depression [188]. Adiponectin has a beneficial effect in fighting neuroinflammation [189] and also plays an important role in the remodeling and neurogenesis of dendrites and dendritic spines of mouse hippocampal neurons [190]. All of these factors have beneficial effects on depression. Furthermore, CR can also lead to reduced leptin levels [191]. There have been different research results on the relationship between leptin and depression. Studies have shown that patients with depression have reduced leptin levels [192], and the same conclusions have been reached in animal models of depression [193]. However, in another study, it was found that patients with MDD had increased leptin levels [194]. Leptin is considered to be a proinflammatory factor, and the reduced level caused by CR may have a positive effect on depression [195]. CR also increases hippocampal synaptic plasticity by changing the morphology and function of astrocytes [196]. A study has confirmed that CR can preserve LTP that is lost in the hippocampus of aging rats [197]. cAMP and its response element-binding protein CREB are involved in the CR-mediated regulation of plasticity [198]. However, the regulation of plasticity by CR is bidirectional, as long-term CR decreased hippocampal neurogenesis and granulosa cell density [199] and leads to reduced levels of some lipids in the DG, impairing spatial memory [200], whereas short-term CR has beneficial effects on hippocampal plasticity. Proteomics analysis showed that CR could improve glutamate disorders, impaired protein synthesis, and mitochondrial dysfunction [201].

Depression may be related to impaired hippocampal mitochondrial plasticity, which is restored by antidepressant treatment [202]. Mitochondria contribute to increasing dendritic spines, synapse regeneration, and synaptic plasticity [203]. When mitochondria increase synaptic plasticity, BDNF levels increase [204]. Chronic stress leads to mitochondrial dysfunction and mitochondrial protein imbalance [205]. Importantly, LTP requires a rapid burst and fission of dendritic mitochondria [206]. In terms of treatment, physical exercise can improve posttraumatic stress disorder through an increase in hippocampal mitochondrial function [207]. Mitochondria are associated with BDNF-mediated synapses and vascular plasticity in ECT [208].

5. Conclusion

Different degrees of hippocampal plasticity changes have been observed in clinical depression patients and rodent depression models (Figure 3). BDNF plays a central role in hippocampal neuroplasticity, and a variety of changes involve the activation or inhibition of the BDNF signaling pathways. The downstream mTOR signaling pathway has received widespread attention since it was discovered to have a role in the antidepressant mechanism of ketamine. BDNF also promotes neurogenesis and remodeling of synaptic morphology and structure through the activation of the mTOR signaling pathway. However, due to the many side effects of ketamine and the fact that the direct activation or inhibition of the mTOR signaling pathway may have adverse effects on humans, the research on mTOR has been restrained to a certain extent. However, this does not affect its potential as a new generation, fast-acting antidepressant treatment target. The positive effects of CR on a variety of neurological diseases (including depression) have been confirmed. Because CR has almost no side effects and is simple to perform, it does not burden patients further with discomfort or treatment costs. CR may be used as a physical form of clinical antidepressant treatment in the future and support other antidepressant treatments to further reduce the suffering of

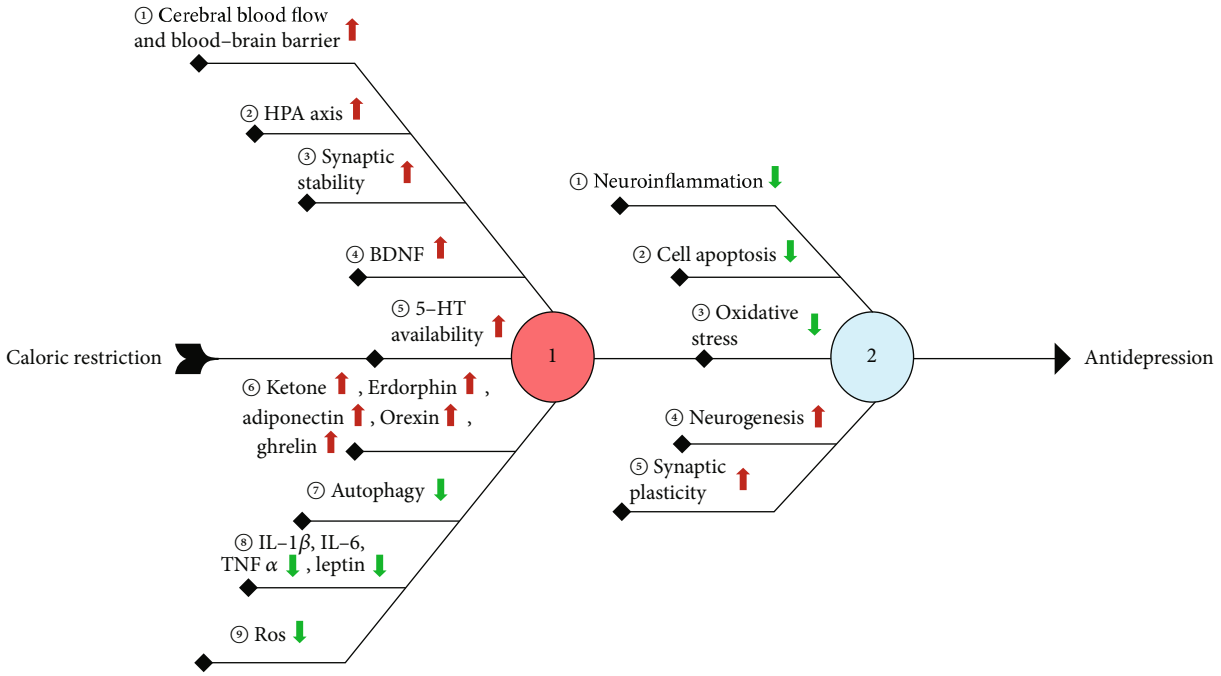

Figure 2: The molecular mechanism involved in the antidepressant effect of caloric restriction.

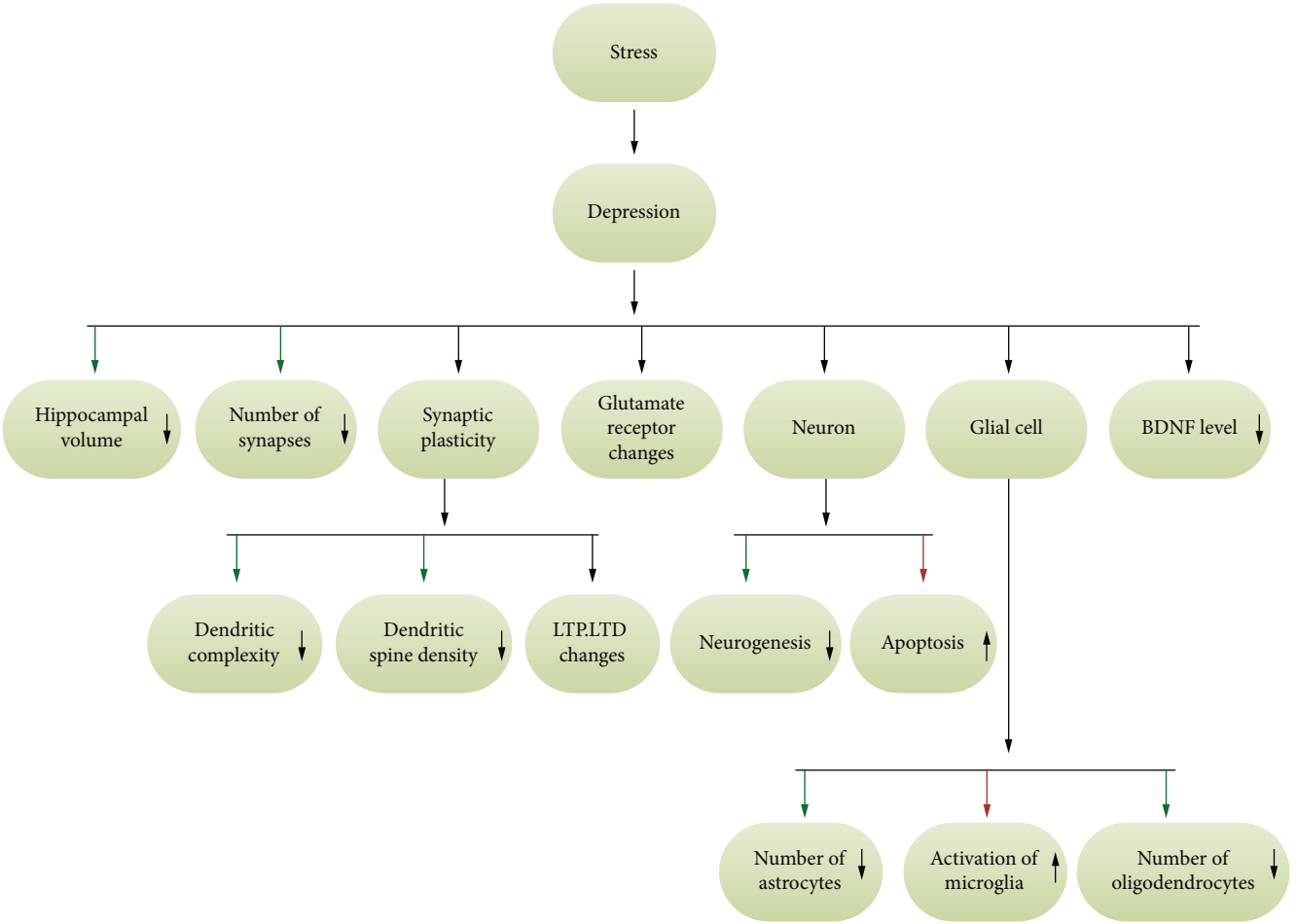

Figure 3: Changes in hippocampal plasticity in depression.

patients with depression. However, the deeper molecular and cellular mechanisms of CR need to be further explored, and its possible defects should be clarified.

Conflicts of Interest

The authors declare no conflict of interest.

Authors' Contributions

WX and RC contributed to the drafting of the article. WX, XY, FZ, HZ, ZC, WY, RC, SX, and BL provided comments. All authors have revised the manuscript critically for important intellectual content and approved the final version to be published.

Acknowledgments

This work was supported by the National Key R&D Program of China (Grant No. 2018YFC1311600), the Jilin Province Medical and Health Talents (2017F012, 2019SCZT007, and 2019SCZT013), the Jilin Science and Technology Agency (20180414050GH, 20190701078GH, 20200201465JC, and 20200301005RQ), and Scientific Research Foundation of the Education Department of Jilin Province (Grant Nos. JJKH20201038KJ and JJKH20201032KJ).

References

[1] Y. Huang, Y. Wang, H. Wang et al., "Prevalence of mental disorders in China: a cross-sectional epidemiological study," *Lancet Psychiatry*, vol. 6, no. 3, pp. 211–224, 2019.

[2] Y. I. Sheline, C. Liston, and B. S. McEwen, "Parsing the hippocampus in depression: chronic stress, hippocampal volume, and major depressive disorder," *Biological Psychiatry*, vol. 85, no. 6, pp. 436–438, 2019.

[3] B. Cao, I. C. Passos, B. Mwangi et al., "Hippocampal subfield volumes in mood disorders," *Molecular Psychiatry*, vol. 22, no. 9, pp. 1352–1358, 2017.

[4] J. J. Maller, K. Broadhouse, A. J. Rush, E. Gordon, S. Koslow, and S. M. Grieve, "Increased hippocampal tail volume predicts depression status and remission to anti-depressant medications in major depression," *Molecular Psychiatry*, vol. 23, no. 8, pp. 1737–1744, 2018.

[5] Y. Ding and J. Dai, "Advance in stress for depressive disorder," *Advances in Experimental Medicine and Biology*, vol. 1180, pp. 147–178, 2019.

[6] P. J. Lucassen, V. M. Heine, M. B. Muller et al., "Stress, depression and hippocampal apoptosis," *CNS & Neurological Disorders Drug Targets*, vol. 5, no. 5, pp. 531–546, 2006.

[7] H. Tamano, Y. Sato, M. Takiguchi et al., "CA1 LTP attenuated by corticosterone is canceled by effusol via rescuing intracellular Zn2+ dysregulation," *Cellular and Molecular Neurobiology*, vol. 39, no. 7, pp. 975–983, 2019.

[8] L. Xu, R. Anwyl, and M. J. Rowan, "Behavioural stress facilitates the induction of long-term depression in the hippocampus," *Nature*, vol. 387, no. 6632, pp. 497–500, 1997.

[9] B. Leuner and T. J. Shors, "Stress, anxiety, and dendritic spines: what are the connections," *Neuroscience*, vol. 251, pp. 108–119, 2013.

[10] A. J. Kallarackal, M. D. Kvarta, E. Cammarata et al., "Chronic stress induces a selective decrease in AMPA receptor-mediated synaptic excitation at hippocampal temporoammonic-CA1 synapses," *The Journal of Neuroscience*, vol. 33, no. 40, pp. 15669–15674, 2013.

[11] S. Boku, S. Nakagawa, H. Toda, and A. Hishimoto, "Neural basis of major depressive disorder: Beyond monoamine hypothesis," *Psychiatry and Clinical Neurosciences*, vol. 72, no. 1, pp. 3–12, 2018.

[12] C. M. Pariante, "Why are depressed patients inflamed? A reflection on 20 years of research on depression, glucocorticoid resistance and inflammation," *European Neuropsychopharmacology*, vol. 27, no. 6, pp. 554–559, 2017.

[13] S. Gong, Y. L. Miao, G. Z. Jiao et al., "Dynamics and correlation of serum cortisol and corticosterone under different physiological or stressful conditions in mice," *PLoS One*, vol. 10, no. 2, article e0117503, 2015.

[14] Y. Zhao, R. Ma, J. Shen, H. Su, D. Xing, and L. Du, "A mouse model of depression induced by repeated corticosterone injections," *European Journal of Pharmacology*, vol. 581, no. 1-2, pp. 113–120, 2008.

[15] R. Mao, C. Zhang, J. Chen et al., "Different levels of pro- and anti-inflammatory cytokines in patients with unipolar and bipolar depression," *Journal of Affective Disorders*, vol. 237, pp. 65–72, 2018.

[16] H. M. Abelaira, G. Z. Réus, F. Petronilho, T. Barichello, and J. Quevedo, "Neuroimmunomodulation in depression: a review of inflammatory cytokines involved in this process," *Neurochemical Research*, vol. 39, no. 9, pp. 1634–1639, 2014.

[17] T. Numakawa, H. Odaka, and N. Adachi, "Actions of brain-derived neurotrophin factor in the neurogenesis and neuronal function, and its involvement in the pathophysiology of brain diseases," *International Journal of Molecular Sciences*, vol. 19, no. 11, p. 3650, 2018.

[18] S. M. Manchishi, R. J. Cui, X. H. Zou, Z. Q. Cheng, and B. J. Li, "Effect of caloric restriction on depression," *Journal of Cellular and Molecular Medicine*, vol. 22, no. 5, pp. 2528–2535, 2018.

[19] C. Van Cauwenberghe, C. Vandendriessche, C. Libert, and R. E. Vandenbroucke, "Caloric restriction: beneficial effects on brain aging and Alzheimer's disease," *Mammalian Genome*, vol. 27, no. 7-8, pp. 300–319, 2016.

[20] J. Lee, W. Duan, J. M. Long, D. K. Ingram, and M. P. Mattson, "Dietary restriction increases the number of newly generated neural cells, and induces BDNF expression, in the dentate gyrus of rats," *Journal of Molecular Neuroscience*, vol. 15, no. 2, pp. 99–108, 2000.

[21] K. Yamada and K. Yoshida, "Mechanical insights into the regulation of programmed cell death by p53 via mitochondria," *Biochimica et Biophysica Acta (BBA) - Molecular Cell Research*, vol. 1866, no. 5, pp. 839–848, 2019.

[22] H. J. Weir, P. Yao, F. K. Huynh et al., "Dietary restriction and AMPK increase lifespan via mitochondrial network and peroxisome remodeling," *Cell Metabolism*, vol. 26, no. 6, pp. 884–896.e5, 2017.

[23] D. W. Roddy, C. Farrell, K. Doolin et al., "The hippocampus in depression: more than the sum of its parts? Advanced hippocampal substructure segmentation in depression," *Biological Psychiatry*, vol. 85, no. 6, pp. 487–497, 2019.

[24] R. Kalisch, M. Schubert, W. Jacob et al., "Anxiety and hippocampus volume in the rat," *Neuropsychopharmacology*, vol. 31, no. 5, pp. 925–932, 2006.

[25] P. Videbech and B. Ravnkilde, "Hippocampal volume and depression: a meta-analysis of MRI studies," *American Journal of Psychiatry*, vol. 161, no. 11, pp. 1957–1966, 2004.

[26] T. R. Powell, D. Dima, S. Frangou, and G. Breen, "Telomere length and bipolar disorder," *Neuropsychopharmacology*, vol. 43, no. 2, pp. 445–453, 2018.

[27] T. J. Schoenfeld, H. C. McCausland, H. D. Morris, V. Padmanaban, and H. A. Cameron, "Stress and loss of adult neurogenesis differentially reduce hippocampal volume," *Biological Psychiatry*, vol. 82, no. 12, pp. 914–923, 2017.

[28] A. Saleh, G. G. Potter, D. R. McQuoid et al., "Effects of early life stress on depression, cognitive performance and brain morphology," *Psychological Medicine*, vol. 47, no. 1, pp. 171–181, 2017.

[29] K. Gbyl and P. Videbech, "Electroconvulsive therapy increases brain volume in major depression: a systematic review and meta-analysis," *Acta Psychiatrica Scandinavica*, vol. 138, no. 3, pp. 180–195, 2018.

[30] S. W. Chan, C. J. Harmer, R. Norbury, U. O'Sullivan, G. M. Goodwin, and M. J. Portella, "Hippocampal volume in vulnerability and resilience to depression," *Journal of Affective Disorders*, vol. 189, pp. 199–202, 2016.

[31] K. S. Na, E. Won, J. Kang et al., "Interaction effects of oxytocin receptor gene polymorphism and depression on hippocampal volume," *Psychiatry Research: Neuroimaging*, vol. 282, pp. 18–23, 2018.

[32] J. L. Phillips, L. A. Batten, P. Tremblay, F. Aldosary, L. Du, and P. Blier, "Impact of monoamine-related gene polymorphisms on hippocampal volume in treatment-resistant depression," *Acta Neuropsychiatrica*, vol. 27, no. 6, pp. 353–361, 2015.

[33] G. J. Mahajan, E. J. Vallender, M. R. Garrett et al., "Altered neuro-inflammatory gene expression in hippocampus in major depressive disorder," *Progress in Neuro-Psychopharmacology and Biological Psychiatry*, vol. 82, pp. 177–186, 2018.

[34] G. McGregor, A. J. Irving, and J. Harvey, "Canonical JAK-STAT signaling is pivotal for long-term depression at adult hippocampal temporoammonic-CA1 synapses," *The FASEB Journal*, vol. 31, no. 8, pp. 3449–3466, 2017.

[35] M. D. Kvarta, K. E. Bradbrook, H. M. Dantrassy, A. M. Bailey, and S. M. Thompson, "Corticosterone mediates the synaptic and behavioral effects of chronic stress at rat hippocampal temporoammonic synapses," *Journal of Neurophysiology*, vol. 114, no. 3, pp. 1713–1724, 2015.

[36] P. Y. Lau, L. Katona, P. Saghy, K. Newton, P. Somogyi, and K. P. Lamsa, "Long-term plasticity in identified hippocampal GABAergic interneurons in the CA1 area in vivo," *Brain Structure and Function*, vol. 222, no. 4, pp. 1809–1827, 2017.

[37] K. M. Fan, L. J. Qiu, N. Ma et al., "Acute stress facilitates LTD induction at glutamatergic synapses in the hippocampal CA1 region by activating μ-opioid receptors on GABAergic neurons," *Frontiers in Neuroscience*, vol. 13, p. 71, 2019.

[38] X. Han, H. Wu, P. Yin et al., "Electroacupuncture restores hippocampal synaptic plasticity via modulation of 5-HT receptors in a rat model of depression," *Brain Research Bulletin*, vol. 139, pp. 256–262, 2018.

[39] G. H. Khoo, Y. T. Lin, T. C. Tsai, and K. S. Hsu, "Perineuronal nets restrict the induction of long-term depression in the mouse hippocampal CA1 region," *Molecular Neurobiology*, vol. 56, no. 9, pp. 6436–6450, 2019.

[40] D. G. Sun, H. Kang, H. Tetteh et al., "Long term potentiation, but not depression, in interlamellar hippocampus CA1," *Scientific Reports*, vol. 8, no. 1, p. 5187, 2018.

[41] O. Györfi, H. Nagy, M. Bokor et al., "Reduced CA2-CA3 hippocampal subfield volume is related to depression and normalized by l-DOPA in newly diagnosed Parkinson's disease," *Frontiers in Neurology*, vol. 8, p. 84, 2017.

[42] M. Zhao, Y. S. Choi, K. Obrietan, and S. M. Dudek, "Synaptic plasticity (and the lack thereof) in hippocampal CA2 neurons," *The Journal of Neuroscience*, vol. 27, no. 44, pp. 12025–12032, 2007.

[43] S. Domínguez, C. C. Rey, L. Therreau et al., "Maturation of PNN and ErbB4 signaling in area CA2 during adolescence underlies the emergence of PV interneuron plasticity and social memory," *Cell Reports*, vol. 29, no. 5, pp. 1099–1112.e4, 2019.

[44] F. Leroy, D. H. Brann, T. Meira, and S. A. Siegelbaum, "Input-timing-dependent plasticity in the hippocampal CA2 region and its potential role in social memory," *Neuron*, vol. 102, no. 1, pp. 260–262, 2019.

[45] K. Kobayashi, Y. Ikeda, E. Haneda, and H. Suzuki, "Chronic fluoxetine bidirectionally modulates potentiating effects of serotonin on the hippocampal mossy fiber synaptic transmission," *The Journal of Neuroscience*, vol. 28, no. 24, pp. 6272–6280, 2008.

[46] H. Hagena and D. Manahan-Vaughan, "Learning-facilitated synaptic plasticity at CA3 mossy fiber and commissural-associational synapses reveals different roles in information processing," *Cerebral Cortex*, vol. 21, no. 11, pp. 2442–2449, 2011.

[47] H. Hagena and D. Manahan-Vaughan, "Learning-facilitated long-term depression and long-term potentiation at mossy fiber-CA3 synapses requires activation of β-adrenergic receptors," *Frontiers in Integrative Neuroscience*, vol. 6, p. 23, 2012.

[48] K. Kobayashi, Y. Imoto, F. Yamamoto et al., "Rapid and lasting enhancement of dopaminergic modulation at the hippocampal mossy fiber synapse by electroconvulsive treatment," *Journal of Neurophysiology*, vol. 117, no. 1, pp. 284–289, 2017.

[49] K. Kobayashi, E. Haneda, M. Higuchi, T. Suhara, and H. Suzuki, "Chronic fluoxetine selectively upregulates dopamine D_1-like receptors in the hippocampus," *Neuropsychopharmacology*, vol. 37, no. 6, pp. 1500–1508, 2012.

[50] H. Shen, Y. Fuchino, D. Miyamoto, H. Nomura, and N. Matsuki, "Vagus nerve stimulation enhances perforant path-CA3 synaptic transmission via the activation of β-adrenergic receptors and the locus coeruleus," *International Journal of Neuropsychopharmacology*, vol. 15, no. 4, pp. 523–530, 2012.

[51] H. Qiao, S. C. An, W. Ren, and X. M. Ma, "Progressive alterations of hippocampal CA3-CA1 synapses in an animal model of depression," *Behavioural Brain Research*, vol. 275, pp. 191–200, 2014.

[52] A. Gruart, M. D. Muñoz, and J. M. Delgado-García, "Involvement of the CA3-CA1 synapse in the acquisition of associative learning in behaving mice," *The Journal of Neuroscience*, vol. 26, no. 4, pp. 1077–1087, 2006.

[53] X. G. Li, P. Somogyi, A. Ylinen, and G. Buzsáki, "The hippocampal CA3 network: an in vivo intracellular labeling study," *The Journal of Comparative Neurology*, vol. 339, no. 2, pp. 181–208, 1994.

[54] D. Debanne, B. H. Gähwiler, and S. M. Thompson, "Long-term synaptic plasticity between pairs of individual CA3 pyramidal cells in rat hippocampal slice cultures," *The Journal of Physiology*, vol. 507, no. 1, pp. 237–247, 1998.

[55] R. K. Mishra, S. Kim, S. J. Guzman, and P. Jonas, "Symmetric spike timing-dependent plasticity at CA3-CA3 synapses optimizes storage and recall in autoassociative networks," *Nature Communications*, vol. 7, no. 1, article 11552, 2016.

[56] P. J. Lucassen, M. B. Müller, F. Holsboer et al., "Hippocampal apoptosis in major depression is a minor event and absent from subareas at risk for glucocorticoid overexposure," *The American Journal of Pathology*, vol. 158, no. 2, pp. 453–468, 2001.

[57] A. Takamiya, E. Plitman, J. K. Chung et al., "Acute and long-term effects of electroconvulsive therapy on human dentate gyrus," *Neuropsychopharmacology*, vol. 44, no. 10, pp. 1805–1811, 2019.

[58] C. Alamo, P. García-Garcia, F. Lopez-Muñoz, and C. Zaragozá, "Tianeptine, an atypical pharmacological approach to depression," *Revista de Psiquiatría y Salud Mental*, vol. 12, no. 3, pp. 170–186, 2019.

[59] P. J. Lucassen, E. Fuchs, and B. Czéh, "Antidepressant treatment with tianeptine reduces apoptosis in the hippocampal dentate gyrus and temporal cortex," *Biological Psychiatry*, vol. 55, no. 8, pp. 789–796, 2004.

[60] S. S. Baek, T. W. Jun, K. J. Kim, M. S. Shin, S. Y. Kang, and C. J. Kim, "Effects of postnatal treadmill exercise on apoptotic neuronal cell death and cell proliferation of maternal-separated rat pups," *Brain and Development*, vol. 34, no. 1, pp. 45–56, 2012.

[61] H. J. Lee, J. W. Kim, S. V. Yim et al., "Fluoxetine enhances cell proliferation and prevents apoptosis in dentate gyrus of maternally separated rats," *Molecular Psychiatry*, vol. 6, no. 6, pp. 725–728, 2001.

[62] M. Radahmadi, N. Hosseini, and A. Nasimi, "Effect of chronic stress on short and long-term plasticity in dentate gyrus; study of recovery and adaptation," *Neuroscience*, vol. 280, pp. 121–129, 2014.

[63] S. E. Wang, S. Y. Ko, S. Jo et al., "Downregulation of SIRT2 by chronic stress reduces expression of synaptic plasticity-related genes through the upregulation of Ehmt2," *Experimental Neurobiology*, vol. 28, no. 4, pp. 537–546, 2019.

[64] N. Abe-Higuchi, S. Uchida, H. Yamagata et al., "Hippocampal sirtuin 1 signaling mediates depression-like behavior," *Biological Psychiatry*, vol. 80, no. 11, pp. 815–826, 2016.

[65] J. Triviño-Paredes, A. R. Patten, J. Gil-Mohapel, and B. R. Christie, "The effects of hormones and physical exercise on hippocampal structural plasticity," *Frontiers in Neuroendocrinology*, vol. 41, pp. 23–43, 2016.

[66] S. Arancibia, O. Payet, L. Givalois, and L. Tapia-Arancibia, "Acute stress and dexamethasone rapidly increase hippocampal somatostatin synthesis and release from the dentate gyrus hilus," *Hippocampus*, vol. 11, no. 4, pp. 469–477, 2001.

[67] A. Nakata, H. Saito, and N. Nishiyama, "Facilitatory role of somatostatin via muscarinic cholinergic system in the generation of long-term potentiation in the rat dentate gyrus in vivo," *Brain Research*, vol. 723, no. 1-2, pp. 135–140, 1996.

[68] M. V. Baratta, T. Lamp, and M. K. Tallent, "Somatostatin depresses long-term potentiation and Ca2+ signaling in mouse dentate gyrus," *Journal of Neurophysiology*, vol. 88, no. 6, pp. 3078–3086, 2002.

[69] T. J. Hamilton, B. M. Wheatley, D. B. Sinclair, M. Bachmann, M. E. Larkum, and W. F. Colmers, "Dopamine modulates synaptic plasticity in dendrites of rat and human dentate granule cells," *Proceedings of the National Academy of Sciences*, vol. 107, no. 42, pp. 18185–18190, 2010.

[70] D. Gruber, K. E. Gilling, A. Albrecht et al., "5-HT receptor-mediated modulation of granule cell inhibition after juvenile stress recovers after a second exposure to adult stress," *Neuroscience*, vol. 293, pp. 67–79, 2015.

[71] L. A. Galea, M. D. Spritzer, J. M. Barker, and J. L. Pawluski, "Gonadal hormone modulation of hippocampal neurogenesis in the adult," *Hippocampus*, vol. 16, no. 3, pp. 225–232, 2006.

[72] L. Muzio, V. Brambilla, L. Calcaterra, P. D'Adamo, G. Martino, and F. Benedetti, "Increased neuroplasticity and hippocampal microglia activation in a mice model of rapid antidepressant treatment," *Behavioural Brain Research*, vol. 311, pp. 392–402, 2016.

[73] X. Shang, Y. Shang, J. Fu, and T. Zhang, "Nicotine significantly improves chronic stress-induced impairments of cognition and synaptic plasticity in mice," *Molecular Neurobiology*, vol. 54, no. 6, pp. 4644–4658, 2017.

[74] M. Pickering and J. J. O'Connor, "Pro-inflammatory cytokines and their effects in the dentate gyrus," *Progress in Brain Research*, vol. 163, pp. 339–354, 2007.

[75] T. Y. Zhang, C. L. Keown, X. Wen et al., "Environmental enrichment increases transcriptional and epigenetic differentiation between mouse dorsal and ventral dentate gyrus," *Nature Communications*, vol. 9, no. 1, p. 298, 2018.

[76] G. Köhr, "NMDA receptor function: subunit composition versus spatial distribution," *Cell and Tissue Research*, vol. 326, no. 2, pp. 439–446, 2006.

[77] M. García-Gallo, J. Renart, and M. Díaz-Guerra, "The NR1 subunit of the N-methyl-D-aspartate receptor can be efficiently expressed alone in the cell surface of mammalian cells and is required for the transport of the NR2A subunit," *Biochemical Journal*, vol. 356, no. 2, pp. 539–547, 2001.

[78] D. W. Bonhaus, G. C. Yeh, L. Skaryak, and J. O. McNamara, "Glycine regulation of the N-methyl-D-aspartate receptor-gated ion channel in hippocampal membranes," *Molecular Pharmacology*, vol. 36, no. 2, pp. 273–279, 1989.

[79] C. Madry, I. Mesic, I. Bartholomäus, A. Nicke, H. Betz, and B. Laube, "Principal role of NR3 subunits in NR1/NR3 excitatory glycine receptor function," *Biochemical and Biophysical Research Communications*, vol. 354, no. 1, pp. 102–108, 2007.

[80] R. S. Petralia, Y. X. Wang, F. Hua et al., "Organization of NMDA receptors at extrasynaptic locations," *Neuroscience*, vol. 167, no. 1, pp. 68–87, 2010.

[81] K. W. Roche, S. Standley, J. McCallum, C. Dune Ly, M. D. Ehlers, and R. J. Wenthold, "Molecular determinants of NMDA receptor internalization," *Nature Neuroscience*, vol. 4, no. 8, pp. 794–802, 2001.

[82] A. E. El-Husseini, E. Schnell, D. M. Chetkovich, R. A. Nicoll, and D. S. Bredt, "PSD-95 involvement in maturation of excitatory synapses," *Science*, vol. 290, no. 5495, pp. 1364–1368, 2000.

[83] S. Won, S. Incontro, R. A. Nicoll, and K. W. Roche, "PSD-95 stabilizes NMDA receptors by inducing the degradation of STEP61," *Proceedings of the National Academy of Sciences of the United States of America*, vol. 113, no. 32, pp. E4736–E4744, 2016.

[84] S. S. Jang, S. E. Royston, J. Xu et al., "Regulation of STEP61 and tyrosine-phosphorylation of NMDA and AMPA receptors during homeostatic synaptic plasticity," *Molecular Brain*, vol. 8, no. 1, p. 55, 2015.

[85] A. Volianskis, G. France, M. S. Jensen, Z. A. Bortolotto, D. E. Jane, and G. L. Collingridge, "Long-term potentiation and the role of N-methyl-D-aspartate receptors," *Brain Research*, vol. 1621, pp. 5–16, 2015.

[86] G. Treccani, M. Ardalan, F. Chen et al., "S-Ketamine reverses hippocampal dendritic spine deficits in Flinders Sensitive Line rats within 1 h of administration," *Molecular Neurobiology*, vol. 56, no. 11, pp. 7368–7379, 2019.

[87] Y. Yang, W. Ju, H. Zhang, and L. Sun, "Effect of ketamine on LTP and NMDAR EPSC in hippocampus of the chronic social defeat stress mice model of depression," *Frontiers in Behavioral Neuroscience*, vol. 12, p. 229, 2018.

[88] Q. Nai, S. Li, S. H. Wang et al., "Uncoupling the D1-N-methyl-D-aspartate (NMDA) receptor complex promotes NMDA-dependent long-term potentiation and working memory," *Biological Psychiatry*, vol. 67, no. 3, pp. 246–254, 2010.

[89] Y. Kim, Y. N. Jang, J. Y. Kim et al., "Microtubule-associated protein 2 mediates induction of long-term potentiation in hippocampal neurons," *The FASEB Journal*, vol. 34, no. 5, pp. 6965–6983, 2020.

[90] H. Makino and R. Malinow, "AMPA receptor incorporation into synapses during LTP: the role of lateral movement and exocytosis," *Neuron*, vol. 64, no. 3, pp. 381–390, 2009.

[91] M. C. Ashby, S. R. Maier, A. Nishimune, and J. M. Henley, "Lateral diffusion drives constitutive exchange of AMPA receptors at dendritic spines and is regulated by spine morphology," *The Journal of Neuroscience*, vol. 26, no. 26, pp. 7046–7055, 2006.

[92] A. C. Penn, C. L. Zhang, F. Georges et al., "Hippocampal LTP and contextual learning require surface diffusion of AMPA receptors," *Nature*, vol. 549, no. 7672, pp. 384–388, 2017.

[93] M. Wang, V. S. Ramasamy, M. Samidurai, and J. Jo, "Acute restraint stress reverses impaired LTP in the hippocampal CA1 region in mouse models of Alzheimer's disease," *Scientific Reports*, vol. 9, no. 1, p. 10955, 2019.

[94] O. R. Buonarati, E. A. Hammes, J. F. Watson, I. H. Greger, and J. W. Hell, "Mechanisms of postsynaptic localization of AMPA-type glutamate receptors and their regulation during long-term potentiation," *Science Signaling*, vol. 12, no. 562, article eaar6889, 2019.

[95] E. Cho, D. H. Kim, Y. N. Hur et al., "Cyclin Y inhibits plasticity-induced AMPA receptor exocytosis and LTP," *Scientific Reports*, vol. 5, no. 1, article 12624, 2015.

[96] M. A. Patterson, E. M. Szatmari, and R. Yasuda, "AMPA receptors are exocytosed in stimulated spines and adjacent dendrites in a Ras-ERK-dependent manner during long-term potentiation," *Proceedings of the National Academy of Sciences of the United States of America*, vol. 107, no. 36, pp. 15951–15956, 2010.

[97] D. Liao, N. A. Hessler, and R. Malinow, "Activation of postsynaptically silent synapses during pairing-induced LTP in CA1 region of hippocampal slice," *Nature*, vol. 375, no. 6530, pp. 400–404, 1995.

[98] H. T. Davidson, J. Xiao, R. Dai, and C. Bergson, "Calcyon is necessary for activity-dependent AMPA receptor internalization and LTD in CA1 neurons of hippocampus," *The European Journal of Neuroscience*, vol. 29, no. 1, pp. 42–54, 2009.

[99] Y. Yu, Z. Huang, C. Dai et al., "Facilitated AMPAR endocytosis causally contributes to the maternal sleep deprivation-induced impairments of synaptic plasticity and cognition in the offspring rats," *Neuropharmacology*, vol. 133, pp. 155–162, 2018.

[100] S. Fujii, H. Tanaka, and T. Hirano, "Suppression of AMPA receptor exocytosis contributes to hippocampal LTD," *The Journal of Neuroscience*, vol. 38, no. 24, pp. 5523–5537, 2018.

[101] A. Ruiz, "Kainate receptors with a metabotropic signature enhance hippocampal excitability by regulating the slow after-hyperpolarization in CA3 pyramidal neurons," *Advances in Experimental Medicine and Biology*, vol. 717, pp. 59–68, 2011.

[102] E. Cherubini, M. D. Caiati, and S. Sivakumaran, "In the developing hippocampus kainate receptors control the release of GABA from mossy fiber terminals via a metabotropic type of action," *Advances in Experimental Medicine and Biology*, vol. 717, pp. 11–26, 2011.

[103] J. M. Marques, R. J. Rodrigues, S. Valbuena et al., "CRMP2 tethers kainate receptor activity to cytoskeleton dynamics during neuronal maturation," *The Journal of Neuroscience*, vol. 33, no. 46, pp. 18298–18310, 2013.

[104] S. Sharma, D. Darland, S. Lei, S. Rakoczy, and H. M. Brown-Borg, "NMDA and kainate receptor expression, long-term potentiation, and neurogenesis in the hippocampus of long-lived Ames dwarf mice," *Age (Dordrecht, Netherlands)*, vol. 34, no. 3, pp. 609–620, 2012.

[105] M. S. Wyeth, K. A. Pelkey, X. Yuan et al., "Neto auxiliary subunits regulate interneuron somatodendritic and presynaptic kainate receptors to control network inhibition," *Cell Reports*, vol. 20, no. 9, pp. 2156–2168, 2017.

[106] H. Kamiya, "Kainate receptor-dependent presynaptic modulation and plasticity," *Neuroscience Research*, vol. 42, no. 1, pp. 1–6, 2002.

[107] T. S. Sihra and A. Rodríguez-Moreno, "Presynaptic kainate receptor-mediated bidirectional modulatory actions: mechanisms," *Neurochemistry International*, vol. 62, no. 7, pp. 982–987, 2013.

[108] H. H. Schiffer and S. F. Heinemann, "Association of the human kainate receptorGluR7 gene (GRIK3) with recurrent major depressive disorder," *American Journal of Medical Genetics. Part B, Neuropsychiatric Genetics*, vol. 144B, no. 1, pp. 20–26, 2007.

[109] M. Koromina, M. Flitton, I. R. Mellor, and H. M. Knight, "A kainate receptor GluK4 deletion, protective against bipolar disorder, is associated with enhanced cognitive performance across diagnoses in the TwinsUK cohort," *The World Journal of Biological Psychiatry*, vol. 20, no. 5, pp. 393–401, 2019.

[110] J. S. Catches, J. Xu, and A. Contractor, "Genetic ablation of the GluK4 kainate receptor subunit causes anxiolytic and antidepressant-like behavior in mice," *Behavioural Brain Research*, vol. 228, no. 2, pp. 406–414, 2012.

[111] R. G. Hunter, R. Bellani, E. Bloss, A. Costa, K. McCarthy, and B. S. McEwen, "Regulation of kainate receptor subunit mRNA by stress and corticosteroids in the rat hippocampus," *PLoS One*, vol. 4, no. 1, p. e4328, 2009.

[112] A. Rodríguez-Moreno and T. S. Sihra, "Metabotropic actions of kainate receptors in the control of glutamate release in the hippocampus," *Advances in Experimental Medicine and Biology*, vol. 717, pp. 39–48, 2011.

[113] A. Contractor, G. Swanson, and S. F. Heinemann, "Kainate receptors are involved in short- and long-term plasticity at mossy fiber synapses in the hippocampus," *Neuron*, vol. 29, no. 1, pp. 209–216, 2001.

[114] Y. Park, J. Jo, J. T. Isaac, and K. Cho, "Long-term depression of kainate receptor-mediated synaptic transmission," *Neuron*, vol. 49, no. 1, pp. 95–106, 2006.

[115] I. Bureau, S. Bischoff, S. F. Heinemann, and C. Mulle, "Kainate receptor-mediated responses in the CA1 field of wild-type and GluR6-deficient mice," *The Journal of Neuroscience*, vol. 19, no. 2, pp. 653–663, 1999.

[116] L. Jiang, J. Xu, M. Nedergaard, and J. Kang, "A kainate receptor increases the efficacy of GABAergic synapses," *Neuron*, vol. 30, no. 2, pp. 503–513, 2001.

[117] T. Sengupta, R. Das, and S. Chattarji, "Chronic but not acute immobilization stress stably enhances hippocampal CA1 metabotropic glutamate receptor dependent long-term depression," *Neuroscience Letters*, vol. 633, pp. 101–105, 2016.

[118] F. Chaouloff, A. Hémar, and O. Manzoni, "Acute stress facilitates hippocampal CA1 metabotropic glutamate receptor-dependent long-term depression," *The Journal of Neuroscience*, vol. 27, no. 27, pp. 7130–7135, 2007.

[119] S. Fitzjohn, Z. Bashir, and P. Farrow, "Group I mGluR induced LTD of NMDAR-synaptic transmission at the Schaffer collateral but not temperoammonic input to CA1," *Current Neuropharmacology*, vol. 14, no. 5, pp. 435–440, 2016.

[120] M. Le Vasseur, I. Ran, and J. C. Lacaille, "Selective induction of metabotropic glutamate receptor 1- and metabotropic glutamate receptor 5-dependent chemical long-term potentiation at oriens/alveus interneuron synapses of mouse hippocampus," *Neuroscience*, vol. 151, no. 1, pp. 28–42, 2008.

[121] C. Le Duigou and D. M. Kullmann, "Group I mGluR agonist-evoked long-term potentiation in hippocampal oriens interneurons," *The Journal of Neuroscience*, vol. 31, no. 15, pp. 5777–5781, 2011.

[122] E. Suzuki and T. Okada, "Group I metabotropic glutamate receptors are involved in TEA-induced long-term potentiation at mossy fiber-CA3 synapses in the rat hippocampus," *Brain Research*, vol. 1313, pp. 45–52, 2010.

[123] A. G. Eng, D. A. Kelver, T. P. Hedrick, and G. T. Swanson, "Transduction of group I mGluR-mediated synaptic plasticity by β-arrestin2 signalling," *Nature Communications*, vol. 7, no. 1, p. 13571, 2016.

[124] X. Yerna, O. Schakman, I. Ratbi et al., "Role of the TRPC1 channel in hippocampal long-term depression and in spatial memory extinction," *International Journal of Molecular Sciences*, vol. 21, no. 5, p. 1712, 2020.

[125] F. Matrisciano, I. Panaccione, M. Zusso et al., "Group-II metabotropic glutamate receptor ligands as adjunctive drugs in the treatment of depression: a new strategy to shorten the latency of antidepressant medication," *Molecular Psychiatry*, vol. 12, no. 8, pp. 704–706, 2007.

[126] R. M. O'Connor, M. M. Pusceddu, T. G. Dinan, and J. F. Cryan, "Impact of early-life stress, on group III mGlu receptor levels in the rat hippocampus: effects of ketamine, electroconvulsive shock therapy and fluoxetine treatment," *Neuropharmacology*, vol. 66, pp. 236–241, 2013.

[127] K. Podkowa, S. Rzeźniczek, M. Marciniak, F. Acher, A. Pilc, and A. Pałucha-Poniewiera, "A novel mGlu4 selective agonist LSP4-2022 increases behavioral despair in mouse models of antidepressant action," *Neuropharmacology*, vol. 97, pp. 338–345, 2015.

[128] E. Iscru, H. Goddyn, T. Ahmed, Z. Callaerts-Vegh, R. D'Hooge, and D. Balschun, "Improved spatial learning is associated with increased hippocampal but not prefrontal long-term potentiation in mGluR4 knockout mice," *Genes, Brain, and Behavior*, vol. 12, no. 6, pp. 615–625, 2013.

[129] S. R. Bradley, J. M. Uslaner, R. B. Flick, A. Lee, K. M. Groover, and P. H. Hutson, "The mGluR7 allosteric agonist AMN082 produces antidepressant-like effects by modulating glutamatergic signaling," *Pharmacology, Biochemistry, and Behavior*, vol. 101, no. 1, pp. 35–40, 2012.

[130] K. Mitsukawa, C. Mombereau, E. Lötscher et al., "Metabotropic glutamate receptor subtype 7 ablation causes dysregulation of the HPA axis and increases hippocampal BDNF protein levels: implications for stress-related psychiatric disorders," *Neuropsychopharmacology*, vol. 31, no. 6, pp. 1112–1122, 2006.

[131] C. A. Stockmeier, G. J. Mahajan, L. C. Konick et al., "Cellular changes in the postmortem hippocampus in major depression," *Biological Psychiatry*, vol. 56, no. 9, pp. 640–650, 2004.

[132] G. Pei, L. Xu, W. Huang, and J. Yin, "The protective role of microRNA-133b in restricting hippocampal neurons apoptosis and inflammatory injury in rats with depression by suppressing CTGF," *International Immunopharmacology*, vol. 78, p. 106076, 2020.

[133] X. Huang, Y. S. Mao, C. Li, H. Wang, and J. L. Ji, "Venlafaxine inhibits apoptosis of hippocampal neurons by up-regulating brain-derived neurotrophic factor in a rat depression model," *Die Pharmazie*, vol. 69, no. 12, pp. 909–916, 2014.

[134] T. Toda, S. L. Parylak, S. B. Linker, and F. H. Gage, "The role of adult hippocampal neurogenesis in brain health and disease," *Molecular Psychiatry*, vol. 24, no. 1, pp. 67–87, 2019.

[135] A. S. Hill, A. Sahay, and R. Hen, "Increasing adult hippocampal neurogenesis is sufficient to reduce anxiety and depression-like behaviors," *Neuropsychopharmacology*, vol. 40, no. 10, pp. 2368–2378, 2015.

[136] S. Y. Yau, A. Li, J. B. Tong et al., "Chronic corticosterone administration reduces dendritic complexity in mature, but not young granule cells in the rat dentate gyrus," *Restorative Neurology and Neuroscience*, vol. 34, no. 5, pp. 849–857, 2016.

[137] S. Brummelte and L. A. Galea, "Chronic high corticosterone reduces neurogenesis in the dentate gyrus of adult male and female rats," *Neuroscience*, vol. 168, no. 3, pp. 680–690, 2010.

[138] T. Ikrar, N. Guo, K. He et al., "Adult neurogenesis modifies excitability of the dentate gyrus," *Frontiers in Neural Circuits*, vol. 7, p. 204, 2013.

[139] C. Anacker, V. M. Luna, G. S. Stevens et al., "Hippocampal neurogenesis confers stress resilience by inhibiting the ventral dentate gyrus," *Nature*, vol. 559, no. 7712, pp. 98–102, 2018.

[140] H. Michaëlsson, M. Andersson, J. Svensson et al., "The novel antidepressant ketamine enhances dentate gyrus proliferation with no effects on synaptic plasticity or hippocampal function in depressive-like rats," *Acta Physiologica (Oxford, England)*, vol. 225, no. 4, article e13211, 2018.

[141] S. B. Pinnock, R. Balendra, M. Chan, L. T. Hunt, T. Turner-Stokes, and J. Herbert, "Interactions between nitric oxide and corticosterone in the regulation of progenitor cell proliferation in the dentate gyrus of the adult rat," *Neuropsychopharmacology*, vol. 32, no. 2, pp. 493–504, 2007.

[142] C. E. Terrillion, B. Abazyan, Z. Yang et al., "DISC1 in astrocytes influences adult neurogenesis and hippocampus-dependent behaviors in mice," *Neuropsychopharmacology*, vol. 42, no. 11, pp. 2242–2251, 2017.

[143] M. Navarrete, M. I. Cuartero, R. Palenzuela et al., "Astrocytic p38α MAPK drives NMDA receptor-dependent long-term depression and modulates long-term memory," *Nature Communications*, vol. 10, no. 1, p. 2968, 2019.

[144] M. Hei, P. Chen, S. Wang et al., "Effects of chronic mild stress induced depression on synaptic plasticity in mouse hippocampus," *Behavioural Brain Research*, vol. 365, pp. 26–35, 2019.

[145] R. C. Paolicelli, G. Bolasco, F. Pagani et al., "Synaptic pruning by microglia is necessary for normal brain development," *Science*, vol. 333, no. 6048, pp. 1456–1458, 2011.

[146] K. Riazi, M. A. Galic, A. C. Kentner, A. Y. Reid, K. A. Sharkey, and Q. J. Pittman, "Microglia-dependent alteration of glutamatergic synaptic transmission and plasticity in the hippocampus during peripheral inflammation," *The Journal of Neuroscience*, vol. 35, no. 12, pp. 4942–4952, 2015.

[147] J. Tang, X. Liang, Y. Zhang et al., "The effects of running exercise on oligodendrocytes in the hippocampus of rats with depression induced by chronic unpredictable stress," *Brain Research Bulletin*, vol. 149, pp. 1–10, 2019.

[148] Y. Yamazaki, H. Fujiwara, K. Kaneko et al., "Short- and long-term functional plasticity of white matter induced by oligodendrocyte depolarization in the hippocampus," *GLIA*, vol. 62, no. 8, pp. 1299–1312, 2014.

[149] Y. Yamazaki, "Oligodendrocyte physiology modulating axonal excitability and nerve conduction," *Advances in Experimental Medicine and Biology*, vol. 1190, pp. 123–144, 2019.

[150] P. E. Steadman, F. Xia, M. Ahmed et al., "Disruption of oligodendrogenesis impairs memory consolidation in adult mice," *Neuron*, vol. 105, no. 1, pp. 150–164.e6, 2020.

[151] M. A. Laine, K. Trontti, Z. Misiewicz et al., "Genetic control of myelin plasticity after chronic psychosocial stress," *eNeuro*, vol. 5, no. 4, pp. ENEURO.0166–ENEU18.2018, 2018.

[152] P. Monteleone, C. Serritella, V. Martiadis, and M. Maj, "Decreased levels of serum brain-derived neurotrophic factor in both depressed and euthymic patients with unipolar depression and in euthymic patients with bipolar I and II disorders," *Bipolar Disorders*, vol. 10, no. 1, pp. 95–100, 2008.

[153] M. Polyakova, K. Stuke, K. Schuemberg, K. Mueller, P. Schoenknecht, and M. L. Schroeter, "BDNF as a biomarker for successful treatment of mood disorders: a systematic & quantitative meta-analysis," *Journal of Affective Disorders*, vol. 174, pp. 432–440, 2015.

[154] P. Zanos and T. D. Gould, "Mechanisms of ketamine action as an antidepressant," *Molecular Psychiatry*, vol. 23, no. 4, pp. 801–811, 2018.

[155] A. Figurov, L. D. Pozzo-Miller, P. Olafsson, T. Wang, and B. Lu, "Regulation of synaptic responses to high-frequency stimulation and LTP by neurotrophins in the hippocampus," *Nature*, vol. 381, no. 6584, pp. 706–709, 1996.

[156] K. Sakata and S. M. Duke, "Lack of BDNF expression through promoter IV disturbs expression of monoamine genes in the frontal cortex and hippocampus," *Neuroscience*, vol. 260, pp. 265–275, 2014.

[157] C. Diniz, P. C. Casarotto, L. Resstel, and S. Joca, "Beyond good and evil: a putative continuum-sorting hypothesis for the functional role of proBDNF/BDNF-propeptide/mBDNF in antidepressant treatment," *Neuroscience and Biobehavioral Reviews*, vol. 90, pp. 70–83, 2018.

[158] H. Qiao, S. C. An, C. Xu, and X. M. Ma, "Role of proBDNF and BDNF in dendritic spine plasticity and depressive-like behaviors induced by an animal model of depression," *Brain Research*, vol. 1663, pp. 29–37, 2017.

[159] T. Numakawa, S. Suzuki, E. Kumamaru, N. Adachi, M. Richards, and H. Kunugi, "BDNF function and intracellular signaling in neurons," *Histology and Histopathology*, vol. 25, no. 2, pp. 237–258, 2010.

[160] L. De Vries, F. Finana, F. Cachoux, B. Vacher, P. Sokoloff, and D. Cussac, "Cellular BRET assay suggests a conformational rearrangement of preformed TrkB/Shc complexes following BDNF-dependent activation," *Cellular Signalling*, vol. 22, no. 1, pp. 158–165, 2010.

[161] J. Q. Wang and L. Mao, "The ERK pathway: molecular mechanisms and treatment of depression," *Molecular Neurobiology*, vol. 56, no. 9, pp. 6197–6205, 2019.

[162] C. Y. Cheng, S. T. Kao, and Y. C. Lee, "Angelica sinensis extract protects against ischemia-reperfusion injury in the hippocampus by activating p38 MAPK-mediated p90RSK/p-Bad and p90RSK/CREB/BDNF signaling after transient global cerebral ischemia in rats," *Journal of Ethnopharmacology*, vol. 252, p. 112612, 2020.

[163] R. Katoh-Semba, R. Kaneko, S. Kitajima et al., "Activation of p38 mitogen-activated protein kinase is required for in vivo brain-derived neurotrophic factor production in the rat hippocampus," *Neuroscience*, vol. 163, no. 1, pp. 352–361, 2009.

[164] K. Sakamoto, K. Karelina, and K. Obrietan, "CREB: a multifaceted regulator of neuronal plasticity and protection," *Journal of Neurochemistry*, vol. 116, no. 1, pp. 1–9, 2011.

[165] D. Sari, N. Arfian, U. Tranggono, W. Setyaningsih, M. M. Romi, and N. Emoto, "Centella asiatica (Gotu kola) ethanol extract up-regulates hippocampal brain-derived neurotrophic factor (BDNF), tyrosine kinase B (TrkB) and extracellular signal-regulated protein kinase 1/2 (ERK1/2) signaling in chronic electrical stress model in rats," *Iranian Journal of Basic Medical Sciences*, vol. 22, no. 10, pp. 1218–1224, 2019.

[166] C. H. Peng, S. H. Chiou, S. J. Chen et al., "Neuroprotection by imipramine against lipopolysaccharide-induced apoptosis in hippocampus-derived neural stem cells mediated by activation of BDNF and the MAPK pathway," *European Neuropsychopharmacology*, vol. 18, no. 2, pp. 128–140, 2008.

[167] D. R. Kaplan and F. D. Miller, "Neurotrophin signal transduction in the nervous system," *Current Opinion in Neurobiology*, vol. 10, no. 3, pp. 381–391, 2000.

[168] L. Minichiello, A. M. Calella, D. L. Medina, T. Bonhoeffer, R. Klein, and M. Korte, "Mechanism of TrkB-mediated hippocampal long-term potentiation," *Neuron*, vol. 36, no. 1, pp. 121–137, 2002.

[169] G. Kharebava, D. Makonchuk, K. B. Kalita, J. J. Zheng, and M. Hetman, "Requirement of 3-phosphoinositide-dependent protein kinase-1 for BDNF-mediated neuronal survival," *The Journal of Neuroscience*, vol. 28, no. 44, pp. 11409–11420, 2008.

[170] V. Nikoletopoulou, K. Sidiropoulou, E. Kallergi, Y. Dalezios, and N. Tavernarakis, "Modulation of autophagy by BDNF underlies synaptic plasticity," *Cell Metabolism*, vol. 26, no. 1, pp. 230–242.e5, 2017.

[171] L. Cavalleri, E. Merlo Pich, M. J. Millan et al., "Ketamine enhances structural plasticity in mouse mesencephalic and human iPSC-derived dopaminergic neurons via AMPAR-driven BDNF and mTOR signaling," *Molecular Psychiatry*, vol. 23, no. 4, pp. 812–823, 2018.

[172] F. Pilar-Cuellar, E. Castro, S. Bretin, E. Mocaer, Á. Pazos, and Á. Díaz, "S 47445 counteracts the behavioral manifestations and hippocampal neuroplasticity changes in bulbectomized mice," *Progress in Neuro-Psychopharmacology & Biological Psychiatry*, vol. 93, pp. 205–213, 2019.

[173] L. J. Sun, L. M. Zhang, D. Liu et al., "The faster-onset antidepressant effects of hypidone hydrochloride (YL-0919)," *Metabolic Brain Disease*, vol. 34, no. 5, pp. 1375–1384, 2019.

[174] S. Wu, Q. Gao, P. Zhao et al., "Sulforaphane produces antidepressant- and anxiolytic-like effects in adult mice," *Behavioural Brain Research*, vol. 301, pp. 55–62, 2016.

[175] J. C. Zhang, W. Yao, C. Dong et al., "Prophylactic effects of sulforaphane on depression-like behavior and dendritic changes in mice after inflammation," *The Journal of Nutritional Biochemistry*, vol. 39, pp. 134–144, 2017.

[176] C. S. Kim, P. Y. Chang, and D. Johnston, "Enhancement of dorsal hippocampal activity by knockdown of HCN1 channels leads to anxiolytic- and antidepressant-like behaviors," *Neuron*, vol. 75, no. 3, pp. 503–516, 2012.

[177] L. Ni, Y. Xu, S. Dong et al., "The potential role of the HCN1 ion channel and BDNF-mTOR signaling pathways and synaptic transmission in the alleviation of PTSD," *Translational Psychiatry*, vol. 10, no. 1, p. 101, 2020.

[178] Y. F. Li, "A hypothesis of monoamine (5-HT) - Glutamate/-GABA long neural circuit: aiming for fast-onset antidepressant discovery," *Pharmacology & Therapeutics*, vol. 208, article 107494, 2020.

[179] H. Zhang, X. Chi, W. Pan et al., "Antidepressant mechanism of classical herbal formula lily bulb and Rehmannia decoction: insights from gene expression profile of medial prefrontal cortex of mice with stress-induced depression-like behaviore12649," *Genes, Brain, and Behavior*, vol. 19, no. 5, 2020.

[180] L. Bettio, L. Rajendran, and J. Gil-Mohapel, "The effects of aging in the hippocampus and cognitive decline," *Neuroscience and Biobehavioral Reviews*, vol. 79, pp. 66–86, 2017.

[181] S. Sharma and G. Kaur, "Neuroprotective potential of dietary restriction against kainate-induced excitotoxicity in adult male Wistar rats," *Brain Research Bulletin*, vol. 67, no. 6, pp. 482–491, 2005.

[182] L. C. Ribeiro, L. Rodrigues, A. Quincozes-Santos et al., "Caloric restriction improves basal redox parameters in hippocampus and cerebral cortex of Wistar rats," *Brain Research*, vol. 1472, pp. 11–19, 2012.

[183] Z. Zeier, I. Madorsky, Y. Xu, W. O. Ogle, L. Notterpek, and T. C. Foster, "Gene expression in the hippocampus: regionally specific effects of aging and caloric restriction," *Mechanisms of Ageing and Development*, vol. 132, no. 1-2, pp. 8–19, 2011.

[184] A. Mladenovic Djordjevic, M. Perovic, V. Tesic et al., "Long-term dietary restriction modulates the level of presynaptic proteins in the cortex and hippocampus of the aging rat," *Neurochemistry International*, vol. 56, no. 2, pp. 250–255, 2010.

[185] M. M. Adams, L. Shi, M. C. Linville et al., "Caloric restriction and age affect synaptic proteins in hippocampal CA3 and spatial learning ability," *Experimental Neurology*, vol. 211, no. 1, pp. 141–149, 2008.

[186] Q. Ding, C. Ash, T. Mracek, B. Merry, and C. Bing, "Caloric restriction increases adiponectin expression by adipose tissue and prevents the inhibitory effect of insulin on circulating adiponectin in rats," *The Journal of Nutritional Biochemistry*, vol. 23, no. 8, pp. 867–874, 2012.

[187] M. Platzer, F. T. Fellendorf, S. A. Bengesser et al., "Adiponectin is decreased in bipolar depression," *The World Journal of Biological Psychiatry*, vol. 20, no. 10, pp. 813–820, 2019.

[188] J. L. Furman, A. Soyombo, A. H. Czysz et al., "Adiponectin moderates antidepressant treatment outcome in the combining medications to enhance depression outcomes randomized clinical trial," *Personalized Medicine in Psychiatry*, vol. 9-10, pp. 1–7, 2018.

[189] S. Nicolas, J. Chabry, A. Guyon, H. Zarif, C. Heurteaux, and A. Petit-Paitel, "Adiponectin: an endogenous molecule with anti-inflammatory and antidepressant properties?," *Medical Science (Paris)*, vol. 34, no. 5, pp. 417–423, 2018.

[190] D. Zhang, X. Wang, and X. Y. Lu, "Adiponectin exerts neurotrophic effects on dendritic arborization, spinogenesis, and neurogenesis of the dentate gyrus of male mice," *Endocrinology*, vol. 157, no. 7, pp. 2853–2869, 2016.

[191] V. Lecoultre, E. Ravussin, and L. M. Redman, "The fall in leptin concentration is a major determinant of the metabolic adaptation induced by caloric restriction independently of the changes in leptin circadian rhythms," *The Journal of Clinical Endocrinology and Metabolism*, vol. 96, no. 9, pp. E1512–E1516, 2011.

[192] T. Kraus, M. Haack, A. Schuld, D. Hinze-Selch, and T. Pollmächer, "Low leptin levels but normal body mass indices in patients with depression or schizophrenia," *Neuroendocrinology*, vol. 73, no. 4, pp. 243–247, 2001.

[193] X. Y. Lu, C. S. Kim, A. Frazer, and W. Zhang, "Leptin: a potential novel antidepressant," *Proceedings of the National Academy of Sciences of the United States of America*, vol. 103, no. 5, pp. 1593–1598, 2006.

[194] Y. Milaneschi, F. Lamers, M. Bot, M. L. Drent, and B. W. Penninx, "Leptin dysregulation is specifically associated with major depression with atypical features: evidence for a mechanism connecting obesity and depression," *Biological Psychiatry*, vol. 81, no. 9, pp. 807–814, 2017.

[195] G. M. Lord, "Leptin as a proinflammatory cytokine," *Contributions to Nephrology*, vol. 151, pp. 151–164, 2006.

[196] A. Popov, P. Denisov, M. Bychkov et al., "Caloric restriction triggers morphofunctional remodeling of astrocytes and enhances synaptic plasticity in the mouse hippocampus," *Cell Death & Disease*, vol. 11, no. 3, p. 208, 2020.

[197] N. Hori, I. Hirotsu, P. J. Davis, and D. O. Carpenter, "Long-term potentiation is lost in aged rats but preserved by calorie restriction," *NeuroReport*, vol. 3, no. 12, pp. 1085–1088, 1992.

[198] S. Fusco, C. Ripoli, M. V. Podda et al., "A role for neuronal cAMP responsive-element binding (CREB)-1 in brain responses to calorie restriction," *Proceedings of the National Academy of Sciences of the United States of America*, vol. 109, no. 2, pp. 621–626, 2012.

[199] M. C. Staples, M. J. Fannon, K. K. Mysore et al., "Dietary restriction reduces hippocampal neurogenesis and granule cell neuron density without affecting the density of mossy fibers," *Brain Research*, vol. 1663, pp. 59–65, 2017.

[200] J. Maliković, H. Vuyyuru, H. Koefeler et al., "Moderate differences in common feeding diets change lipid composition in the hippocampal dentate gyrus and affect spatial cognitive flexibility in male rats," *Neurochemistry International*, vol. 128, pp. 215–221, 2019.

[201] H. F. Poon, H. M. Shepherd, T. T. Reed et al., "Proteomics analysis provides insight into caloric restriction mediated oxidation and expression of brain proteins associated with age-related impaired cellular processes: mitochondrial dysfunction, glutamate dysregulation and impaired protein synthesis," *Neurobiology of Aging*, vol. 27, no. 7, pp. 1020–1034, 2006.

[202] F. Chen, G. Wegener, T. M. Madsen, and J. R. Nyengaard, "Mitochondrial plasticity of the hippocampus in a genetic rat model of depression after antidepressant treatment," *Synapse*, vol. 67, no. 3, pp. 127–134, 2013.

[203] Z. Li, K. Okamoto, Y. Hayashi, and M. Sheng, "The importance of dendritic mitochondria in the morphogenesis and plasticity of spines and synapses," *Cell*, vol. 119, no. 6, pp. 873–887, 2004.

[204] F. Chen, J. Danladi, M. Ardalan et al., "A critical role of mitochondria in BDNF-associated synaptic plasticity after one-week vortioxetine treatment," *The International Journal of Neuropsychopharmacology*, vol. 21, no. 6, pp. 603–615, 2018.

[205] H. Xie, H. Huang, M. Tang et al., "iTRAQ-based quantitative proteomics suggests synaptic mitochondrial dysfunction in the hippocampus of rats susceptible to chronic mild stress," *Neurochemical Research*, vol. 43, no. 12, pp. 2372–2383, 2018.

[206] S. S. Divakaruni, A. M. van Dyke, R. Chandra et al., "Long-term potentiation requires a rapid burst of dendritic mitochondrial fission during induction," *Neuron*, vol. 100, no. 4, pp. 860–875.e7, 2018.

[207] J. H. Seo, H. S. Park, S. S. Park, C. J. Kim, D. H. Kim, and T. W. Kim, "Physical exercise ameliorates psychiatric disorders and cognitive dysfunctions by hippocampal mitochondrial function and neuroplasticity in post-traumatic stress disorder," *Experimental Neurology*, vol. 322, article 113043, 2019.

[208] F. Chen, M. Ardalan, B. Elfving, G. Wegener, T. M. Madsen, and J. R. Nyengaard, "Mitochondria are critical for BDNF-mediated synaptic and vascular plasticity of hippocampus following repeated electroconvulsive seizures," *The International Journal of Neuropsychopharmacology*, vol. 21, no. 3, pp. 291–304, 2018.

Hindawi
Neural Plasticity
Volume 2020, Article ID 8855822, 9 pages
https://doi.org/10.1155/2020/8855822

Research Article

Repressor Element 1 Silencing Transcription Factor (REST) Governs Microglia-Like BV2 Cell Migration via Progranulin (PGRN)

Tongya Yu, Yingying Lin, Yuzhen Xu, Yunxiao Dou, Feihong Wang, Hui Quan, Yanxin Zhao, and Xueyuan Liu

Shanghai Tenth People's Hospital of Tongji University, Tongji University, Middle Yanchang Rd. 301#, Jingan District, Shanghai, China 200072

Correspondence should be addressed to Yanxin Zhao; zhao_yanxin@tongji.edu.cn and Xueyuan Liu; liuxy@tongji.edu.cn

Received 18 August 2020; Revised 26 October 2020; Accepted 13 November 2020; Published 25 November 2020

Academic Editor: Fushun Wang

Microglia activation contributes to Alzheimer's disease (AD) etiology, and microglia migration is a fundamental function during microglia activation. The repressor element-1 silencing transcription factor (REST), a powerful transcriptional factor, was found to play a neuroprotective role in AD. Despite its possible role in disease progression, little is known about whether REST participates in microglia migration. In this study, we aimed to explore the function of REST and its molecular basis during microglia migration under $A\beta_{1\text{-}42}$-treated pathological conditions. When treated by $A\beta_{1\text{-}42}$ REST was upregulated through JAK2/STAT3 signal pathway in BV2 cells. And transwell coculture system was used to evaluate cell migration function of microglia-like BV2. Small interfering RNA (siRNA) targeting progranulin (PGRN) were delivered into BV2 cells, and results showed that PGRN functions to promote BV2 migration. REST expression was inhibited by sh-RNA, which induced BV2 cell migration obviously. On the contrary, REST was overexpressed by REST recombinant plasmid transfection, which repressed BV2 cell migration, indicating that REST may act as a repressor of cell migration. To more comprehensively examine the molecular basis, we analyzed the promoter sequence of PGRN and found that it has the potential binding site of REST. Moreover, knocking-down of REST can increase the expression of PGRN, which confirms the inhibiting effect of REST on PGRN expression. Further detection of double luciferase reporter gene also confirmed the inhibition of REST on the activity of PGRN promoter, indicating that REST may be an inhibitory transcription factor of PGRN which governs microglia-like BV2 cell migration. In conclusion, the present study demonstrates that transcription factor REST may act as a repressor of microglia migration through PGRN.

1. Introduction

Alzheimer's disease, the first leading cause of senile dementia, is characterized by amyloid-β deposition and tau hyperphosphorylation. Increasing evidence indicates that over activation of microglia plays an important role in the development of Alzheimer's disease [1]. Microglia, the resident immune cell of the brain, are considered to be the first line defense and respond quickly to infectious, inflammatory, and pathophysiological stimuli [2, 3]. As the guardian of the central nervous system, microglia are constantly sampling their environment to maintain homeostasis and respond to immune challenges [4].

The migration of microglia is mediated by the interaction of chemokine and its receptor. Previously published data showed that progranulin (PGRN), a multifunctional growth factor expressed in various tissues, may act as a chemoattractant for microglia that over expression of progranulin in

C57BL/6 mice lead to an increase of microglia around the injection site, and progranulin alone was sufficient to promote migration of primary mouse microglia in vitro [5].

The repressor element-1 silencing transcription factor (REST/NRSF) is a master transcriptional factor which played an important role in neurogenesis and neurodegenerative diseases. In the aging human brain, REST potently protects neurons from oxidative stress and amyloid β (Aβ) toxicity, while in AD brain, neuronal REST is lost from the nucleus resulting in the decline of cognitive function [6]. Abundance of study was focused on neuronal REST while function of REST in microglia remains unknown.

In this study, we reported that Aβ-induced REST upregulation in microglia-like BV2 cells and microglial REST represses migration. And we further show that REST regulated microglia migration through PGRN.

2. Methods

2.1. Preparation of Aggregated $A\beta_{1\text{-}42}$. It is generally believed that oligomer Aβ is more toxic than fibrillary Aβ. Therefore, in recent years, the research on the pathogenesis of AD is mainly based on oligomer Aβ stimulation. However, due to the poor stability of the oligomer Aβ which is easy to transform into fibrillary Aβ [1], the operation time window in vitro is relatively short of oligomer Aβ. So, in this study, fibrillary $A\beta_{1\text{-}42}$ was choosing to stimulate BV2 cells. And aggregated $A\beta_{1\text{-}42}$ was formed as previously described [7]. Synthetic human $A\beta_{1\text{-}42}$ peptides (ChinaPeptides, Shanghai, China) were dissolved in 0.4% DMSO-water to a concentration of 100 μM, then incubated at 37°C for 72 h to form fibrillary $A\beta_{1\text{-}42}$. Fibrillary $A\beta_{1\text{-}42}$ was frozen at -80°C for storage.

2.2. Cell Culture. BV-2 cells (Saiqi, Shanghai, China), PC12 cells (Chinese Academy of Sciences, Shanghai, China), and 293T cells (Chinese Academy of Sciences, Shanghai, China) were cultured in a humidified incubator with 5% CO_2 at 37°C. The culture medium was Dulbecco's modified Eagle medium (Gibco, New York, America) supplemented with 5% low-endotoxin fetal bovine serum (Gibco, New York, America), 100 units/ml penicillin (Gibco, New York, America), and 100 μg/ml streptomycin (Gibco, New York, America).

2.3. Transwell Migration Assay. BV-2 cells (3.5×10 [4]) were seeded in the inserts of transwells (Corning Costar Corp., Cambridge, MA, USA, 8.0 μm pore size). The transwell assay was performed as described. The insert was transferred into a well containing serum-free DMEM with or without $A\beta_{1\text{-}42}$ in the lower compartment and incubated for 24 h in 5% CO_2 at 37°C. Microglia that migrated to the lower surface were stained with Gentian Violet. Images were taken from four random fields with a florescent microscope at 4x magnification. The number of microglia on the lower surface of the insert was quantified. The experiments were repeated at least three times.

2.4. Plasmid Transfection. BV-2 cells were replanted 24 hours before transfection in 2 ml of fresh culture medium in a 6-well plastic plate. Plasmid were transfected when the cell density reached 70-80% by Lipofectamine 3000 (Thermo Fisher Scientific) according to the manufacturer's instructions. Before transfection, DMEM was removed and instead by Opti-MEM media. BV-2 cells were transfected with 2500 ng/well of the plasmid pCMV6XL4+sh-REST (Bio-link, Shanghai, China). Alternatively, the mock plasmid pcDNA 3.1 (Bio-link, Shanghai, China) was used as a control instead of the sh-REST plasmid. Six hours after transfection Opti-MEM media was removed, and BV-2 cells were culture for 48 h in DMEM before collecting for further Western blotting or qPCR.

2.5. Western Blotting. Before harvest, BV-2 cells were washed with cold PBS and then lysed with lysis buffer containing protease inhibitors for 30 min on ice. The samples were centrifuged at 12000 rpm, 4°C for 15 min. Then, the protein concentrations were determined by using a BCA protein assay kit (Beyotime Insititute of Biotechnology, Haimen, China). Proteins were electrophoresed using sodium dodecyl sulfate/polyacrylamide gel electrophoresis (SDS-PAGE Bio-Rad, CA, USA) and transferred electrophoretically to PVDF membranes. Then, the membranes were blocked with 5% skim milk at room temperature (RT) for 1 h and were incubated with primary antibodies overnight at 4°C. Subsequently, membranes were washed and incubated with the appropriate HRP-conjugated secondary antibodies at room temperature for 1 h. Finally, membranes were washed and detected with enhanced chemiluminescence. Primary antibodies were as follows: anti-β-tubulin (1 : 2000; Sangon Biotech, China), anti-REST (1 : 1000; Abcam, USA) [8], anti-lambin 1 (1 : 2000, Proteintech, China), Jak2 (1 : 5000, Abcam, USA), p-JAK2 (1 : 1000, abcam, USA), STAT3 (1 : 1000, Abcam, USA), p-STAT3 (1 : 1000, Abcam, USA), PGRN (1 : 1000; R&D systems, USA), and lamin B1 (1 : 1000, Abcam, USA).

2.6. qPCR. Total RNA was isolated from the BV2 cells using Trizol Reagent (Invitrogen Life Technologies, Carlsbad, CA, USA) according to the manufacturer's protocol. 1 mg of RNA was reverse-transcribed to cDNA using PrimeScript™ RT reagent Kit (TaKaRa Bio Inc., Beijing, China). Quantitative RT-PCR analysis was performed using a SYBR Green PCR Kit (KAPA Biosystems, South Africa) with 1 μl of cDNA template in 20 μl reaction mixture. Results were analyzed using the comparative CT method. Data are expressed throughout the study as $2^{-\Delta\Delta CT}$ for the experimental gene of interest normalized to β-actin [9]. The gene specific primer pairs were as follows: mouse REST gene forward 5′-GGCAGATGGCCGAATTGATG-3′ and reverse 5′-CTTTGAGGTCAGCCGACTCT-3′; β-actin gene forward 5′-ATCATGTTTGAGACCTTAAA-3′ and reverse 5′-CATCTCTTGCTCGAAGTCCA-3′.

2.7. Dual Luciferase Assay Experiments. PGRN 3′ UTR (2000 bp) containing REST target sequences was amplified from the BV-2 DNA with primers (forward: 5′-CGGGGTACCCAGCCTGGTCTACAAAGTGAG-3′; reverse: 5′-GAAGATCTCTGGCGGTCAGCTCCAGG-3′) and cloned into pGL3 Luciferase Reporter Vectors (Promega, Madison,

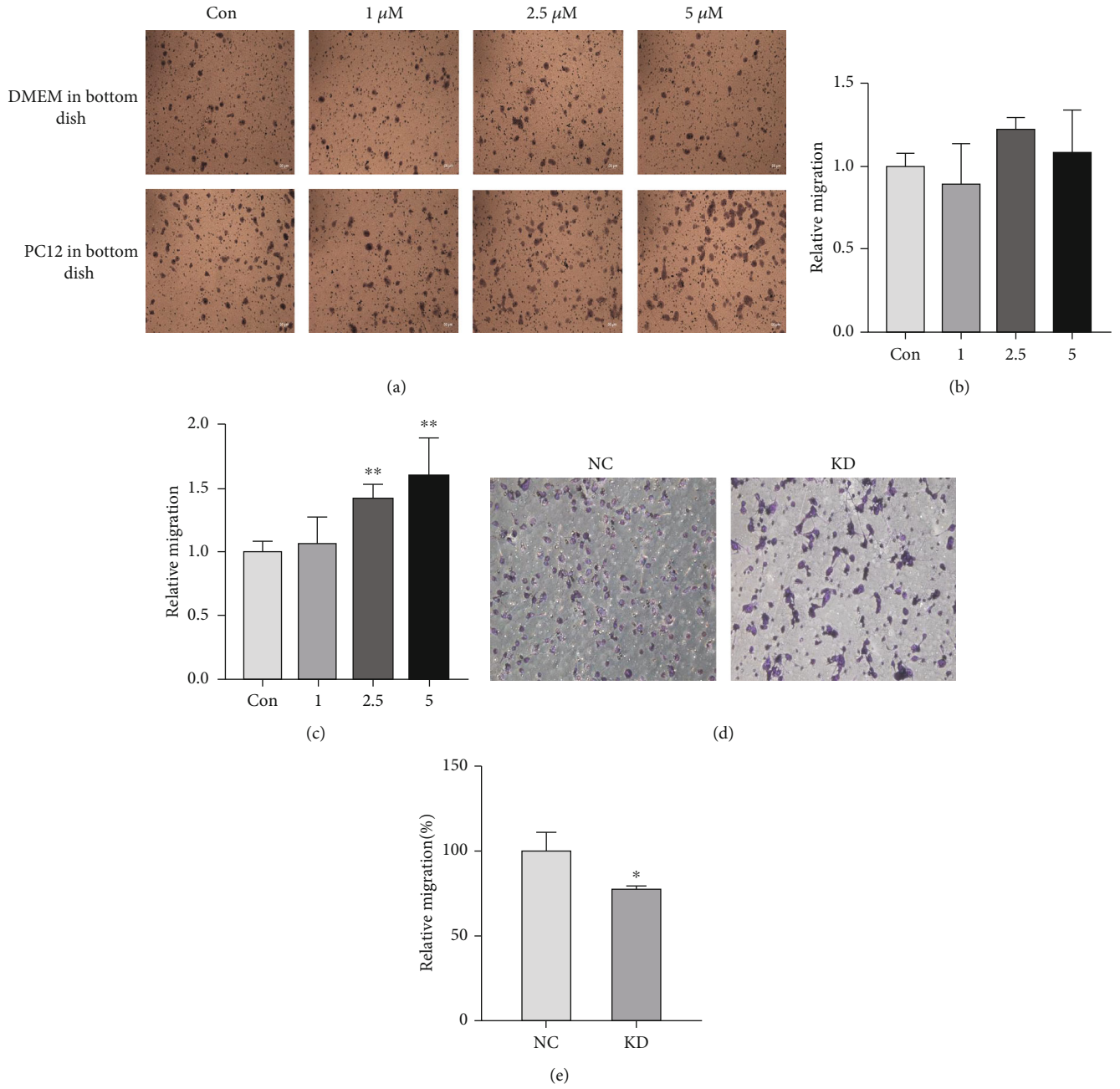

Figure 1: PGRN promotes BV-2 cell migration. (a–c) Different concentration of $A\beta_{1\text{-}42}$ (0-5 μM) contained in DMEM did not induced significant BV-2 cell migration. (d, e) Knocking down PGRN by siRNA repressed BV-2 cell migration. KD: knock down. $^{*}p < 0.05$, $^{**}p < 0.01$.

USA). pRL-TK-SV40 control plasmid was used as internal control. 293T cells were replanted in a 24-well plate. When the cell fusion degree reached 70%, REST constructed plasmids; the GRN gene promoter plasmids and the control plasmid PRL TK were cotransfected (pGL3 basic recombinant plasmid : PRL TK control plasmid transfection amount = 10 : 1). Luciferase activity was detected with a Dual-Luciferase Reporter Assay System (Promega, Madison, USA) 48 h after transfection. Luciferase reporter activity in relative light units (RLU) was expressed as firefly-to-renilla ratio.

2.8. Statistical Analysis. For the analysis among more than two experimental conditions, one-way ANOVA with Tukey's post hoc test was used, whereas for the analysis between two experimental groups, unpaired Student's t test was used. $p < 0.05$ was considered statistically significant.

3. Results

3.1. The Promoting Effect of PGRN on Migration of BV-2 Cells. To explore the mechanism of microglia migration,

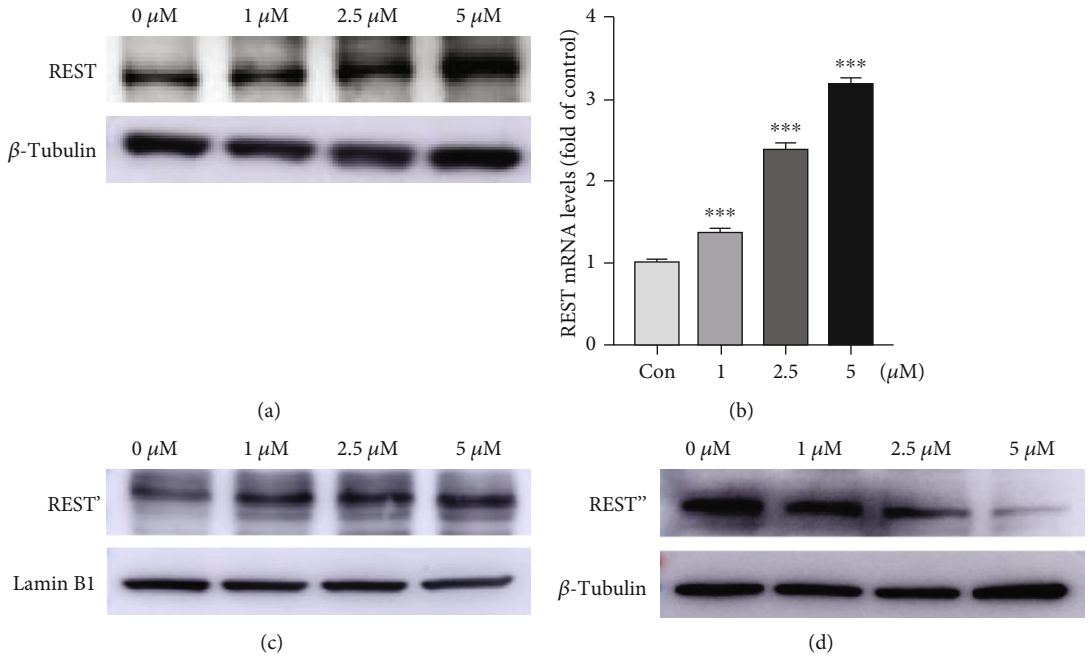

FIGURE 2: $A\beta_{1\text{-}42}$ induced REST expression. (a, b) REST mRNA and protein expression was upregulated with the increase of concentration of $A\beta_{1\text{-}42}$. (c) intranuclear REST was upregulated by treatment with $A\beta_{1\text{-}42}$. (d), Intracytoplasmic REST was downregulated by treatment with $A\beta_{1\text{-}42}$. $^{***}p < 0.001$.

in vitro transwell coculture system of BV-2 cells and PC12 was performed. In the transwell system, BV-2 cells were seeded in on the upper insert, and cell migration was analyzed by crystal violet staining. Results showed that DMEM cell culture medium in the bottom dish with different concentration of $A\beta_{1\text{-}42}$ did not cause a significant increase in the transmigration (Figures 1(a) and 1(b)). And PC12 cells cultivated in bottom dish treated with different concentration of $A\beta_{1\text{-}42}$ induced transmigration of BV2 cells significantly (Figures 1(a) and 1(c)). These results indicated that compared with $A\beta_{1\text{-}42}$ itself, impaired neurons are more likely to promote microglia migration.

Existing studies confirmed that PGRN may act as a chemoattractant to promote microglia migration [2]. In order to verify the effect of PGRN on the migration of microglia, small interfering RNA (siRNA) targeting PGRN were delivered into BV2 cells in the upper transwell dishes. Results were shown in Figures 1(d) and 1(e) that compared with the control group, silencing PGRN has repressed BV2 cell migration significantly, indicating the effect of PGRN on promoting BV-2 cell migration.

3.2. $A\beta_{1\text{-}42}$ Induced REST Expression through JAK2/STAT3 Pathway. Previous work established that REST is a master transcription factor of neurogenesis, which plays an important role in neuron. And Ilaria Prada's work found that, in microglia, REST is highly expressed in the nucleus [10]. In this study, when BV-2 cells were treated with $A\beta_{1\text{-}42}$, REST mRNA and protein expression was upregulated with the increase of concentration of $A\beta_{1\text{-}42}$ (Figures 2(a) and 2(b)), which indicated that REST may involve in Aβ-induced activation of microglia.

Meanwhile, a significant induction of JAK2 and STAT3 phosphorylation were observed when BV-2 cells were treated with $A\beta_{1\text{-}42}$ although JAK2 and STAT3 total protein level did not change significantly (Figures 3(a)–3(d)), which was consistent with previous researches [11, 12]. In order to verify whether the increase of REST expression is induced by JAK2/STAT3 pathway, we treated BV-2 cells with $A\beta_{1\text{-}42}$, and meanwhile, different concentrations of JAK2/STAT3 pathway-specific inhibitor WP1066 was added, and then, REST protein level was analyzed by Western blotting. The results showed that compared with the control group, REST in BV-2 cells treated with $A\beta_{1\text{-}42}$ was upregulated which was consisting with previous data. And with the existing of WP1066 at 4 μM or 6 μM, $A\beta_{1\text{-}42}$-induced REST upregulation was inhibited (Figures 3(e) and 3(f)), which suggested that $A\beta_{1\text{-}42}$ might induce REST upregulation through JAK2/-STAT3 pathway.

3.3. REST Repressed BV2 Cell Migration. In order to study the effect of REST on the migration function of BV-2 cells, sh-RNA was used to knock down REST in BV-2 cells in a transwell migration assay. As shown in Figures 4(a) and 4(b) that REST was downregulated about 75% compared with the control group by treatment with sh-RNA. And knocking down of REST induced BV2 cell migration (Figure 4(d)). This result indicated that REST may act as a repressor of BV-2 cell migration. On the contrary, when REST was overexpressed by recombinant plasmid, BV-2 cell migration was repressed significantly (Figures 4(c) and 4(e)).

3.4. REST Repressed PGRN Expression. The previous experimental results confirmed the inhibition of REST on cell

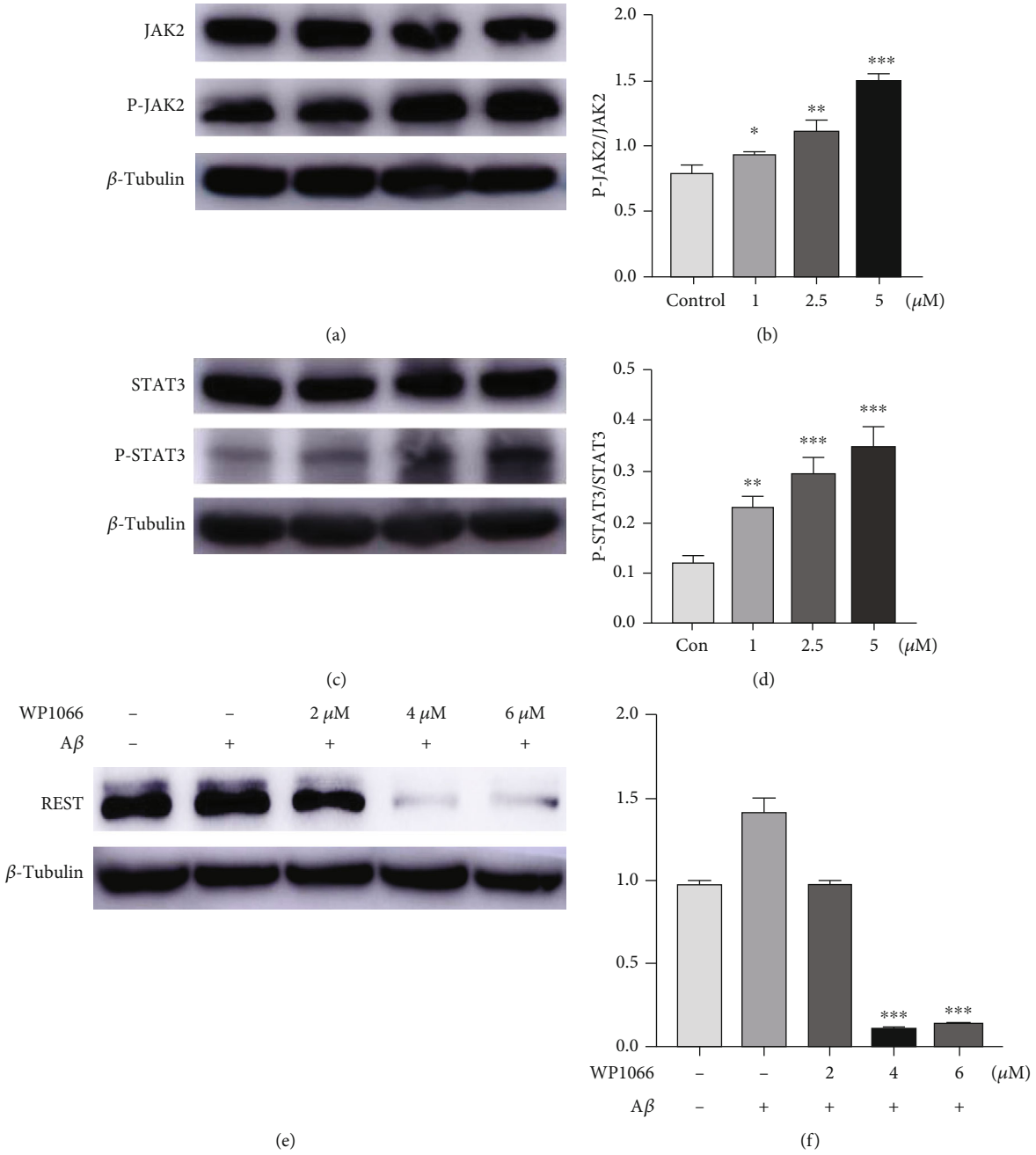

FIGURE 3: $A\beta_{1\text{-}42}$ induced REST expression through JAK2/STAT3 pathway. (a, b) $A\beta_{1\text{-}42}$ promotes JAK2 phosphorylation. (c, d) $A\beta_{1\text{-}42}$ promotes STAT3 phosphorylation. (e, f) Blocking JAK2/STAT3 signaling with WP1066 repressed $A\beta_{1\text{-}42}$-induced REST expression. $^{*}p < 0.05$, $^{**}p < 0.01$, $^{***}p < 0.001$.

migration [13]. Since REST is a powerful transcription factor regulating various neural functions, we speculated REST might inhibit the migration of BV-2 cells by silencing the expression of PGRN. Searching from JASPAR database (http://jaspar.genereg.net/), putative REST binding sequences in genomic regions upstream of the PGRN gene coding sequences was identified (Figure 5(a)).

In order to verify the regulatory effect of REST on PGRN, Western blotting was performed to analyze PGRN expression when REST was knocked down by sh-RNA transfection and overexpressed by REST recombinant plasmid transfection. Results were shown in Figures 5(b) and 5(c) that knocking down of REST induced PGRN protein while overexpression of REST leads to downregulation of PGRN. And, meanwhile, PGRN in culture supernatant PGRN protein level was upregulated when REST was knocked down (Figure 5(b)). Ultimately, these observations suggest that REST may repress PGRN expression and secretion.

3.5. REST Repress PGRN Promoter Activity. To more comprehensively examine the molecular mechanism of PGRN transcription regulation by REST, dual-luciferase reporter

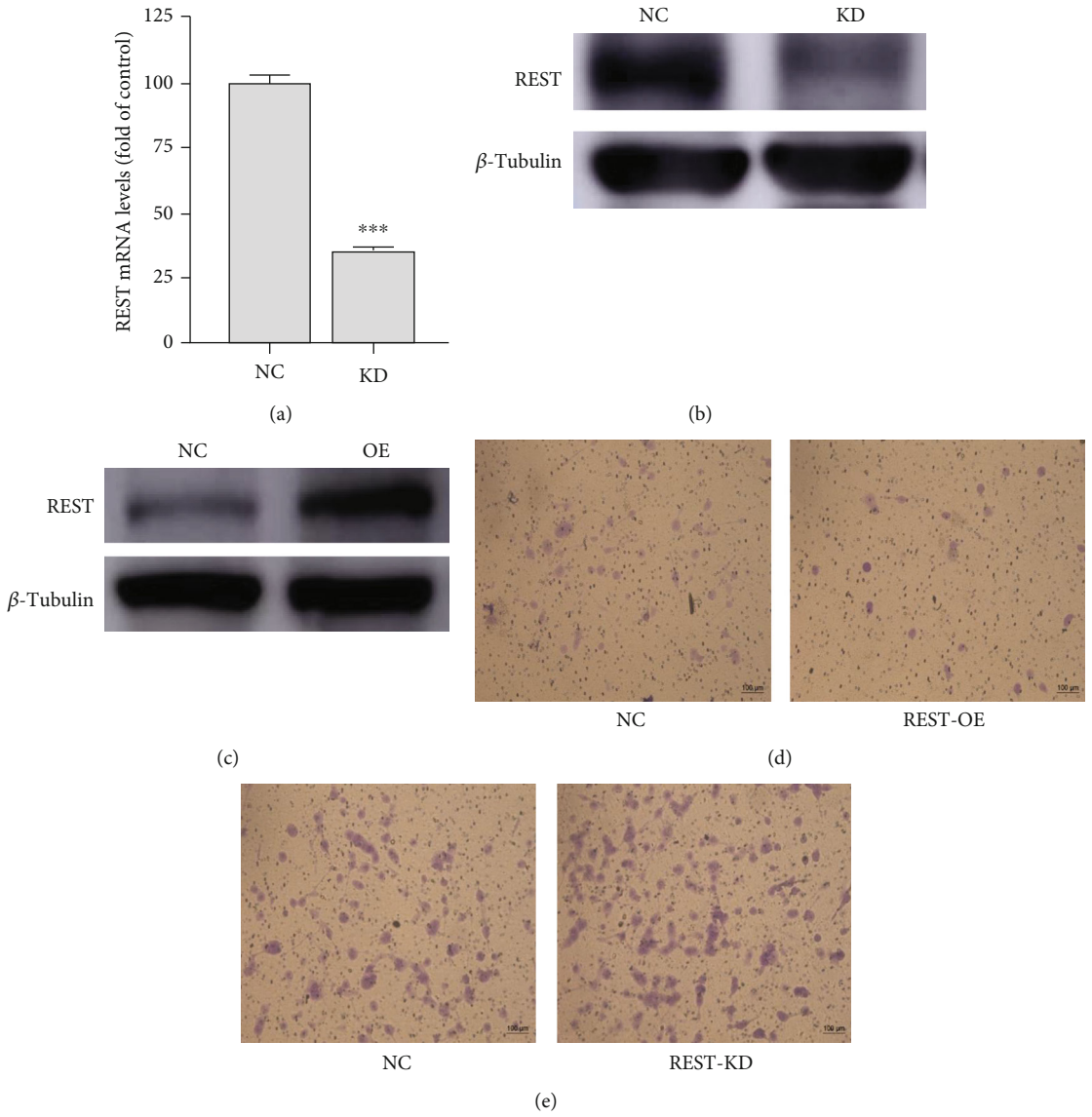

Figure 4: REST repressed BV2 cell migration. (a, b) REST was knock down by sh-RNA. (c) REST was overexpressed by recombinant plasmid transfection. (d), Overexpression of REST repressed BV-2 cell migration. (e), Knocking down of REST induced BV-2 cell migration. KD: knock down; OE: overexpression. $^{***}p < 0.001$.

gene assay was performed. The first base of the transcription start site (TSS) of PGRN was numbered +1, and 2000 BP (-1959~+41) upstream of TSS was selected as the promoter. Then, using BV-2 cell genomic DNA as template, we cloned the 5′ noncoding region (-1959~+41, PGRN promoter) of PGRN gene, and then, we insert the PGRN promoter into pGL3. Basic plasmid. Results were shown in Figure 5(d) that the luciferase activity of PGRN promoter transfected cells was significantly higher than that of the control group, which means gene segment we had cloned from BV-2 cells contains the functional region of PGRN promoter.

To investigate whether PGRN transcriptional activity could be regulated by REST, REST recombinant plasmid and PGRN promoter plasmid were cotransfected into 293T cells, and then, changes of luciferase activity were examined. Results were shown in Figure 5(e) that compared with the control group, overexpression of REST reduced luciferase activity significantly, which means that REST may repress PGRN promoter transcriptional activity.

4. Discussion

Overactivation of microglia is closely related to the progression of Alzheimer's disease, and microglial migration plays an important role in the activation of microglia. In Alzheimer's disease, microglial migration towards soluble Aβ is an important process of phagocytosis [14]. Furthermore, microglia migrate to senile plaques constituting a barrier which prevents outward plaque expansion and limits inward accumulation of protofibrillar Aβ aggregates [15]. Besides,

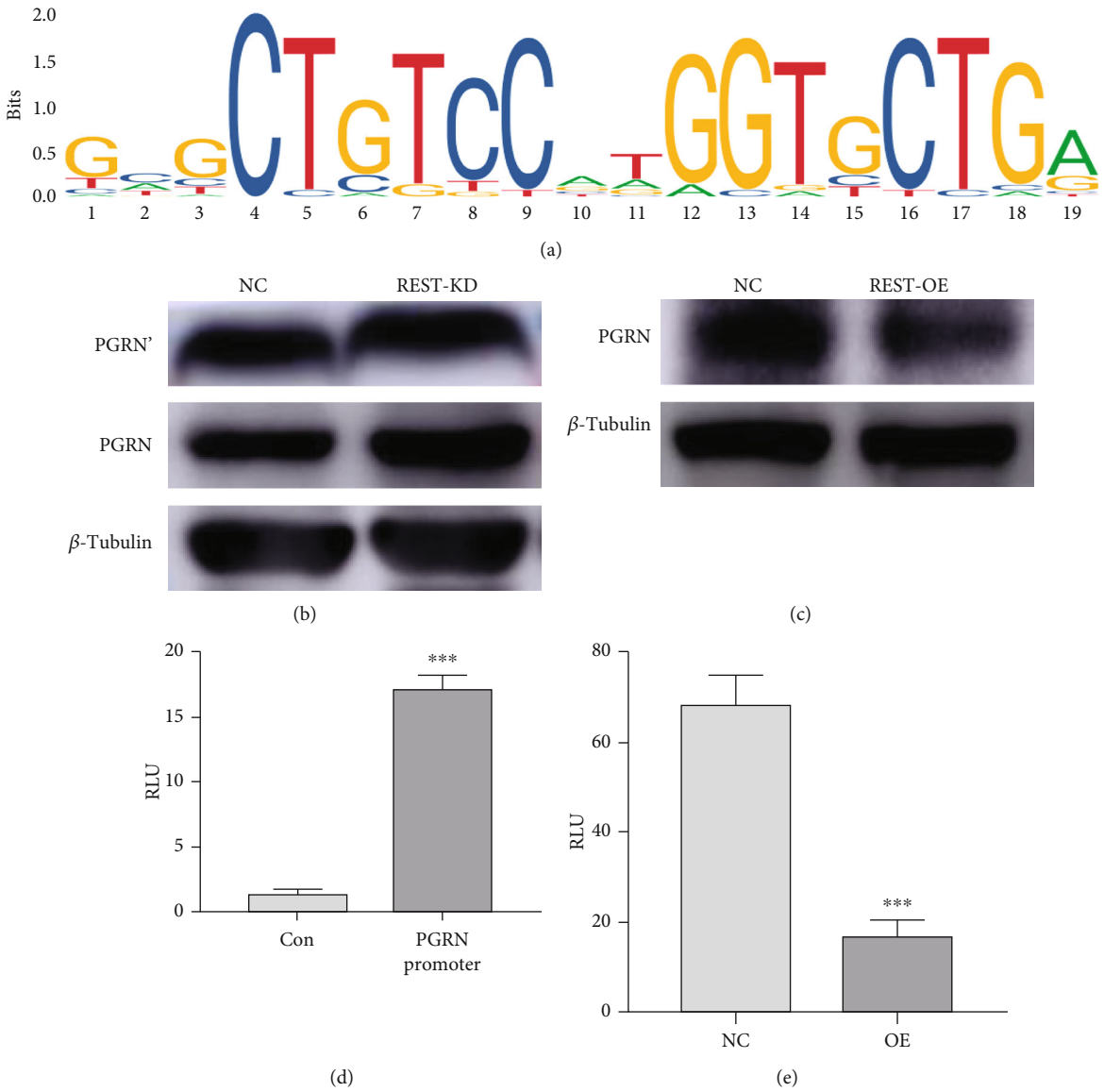

Figure 5: REST repress PGRN promoter activity. (a) Putative REST binding sequences in upstream of the PGRN gene coding sequences were predicted from JASPAR database. (b) Knocking down of REST induced PGRN expression and secretion. (c) Overexpression of REST repressed PGRN expression. (d, e) overexpression of REST repressed PGRN promoter transcriptional activity. KD: knock down; OE: overexpression.

synaptic pruning function of microglia is also carried out in a migration-dependent manner [16, 17]. And when neuronal damage occurs, the migration function facilitates microglial phagocytosis of unwanted self-debris, which is critical to maintain homeostasis in the brain [18, 19]. In this study, transwell system was used to explore the role of REST on Aβ-induced microglial migration, and our data suggested that REST repressed microglial migration through PGRN.

Microglial migration is regulated by many mechanisms; some of which promote migration while others inhibit migration. Microglial migration is dependent on interaction between cell surface receptors and diverse external stimuli. The mechanisms related to the microglial migration have been studied, including P2Y receptor-mediated Ca(2+) signalling [20], calcium-dependent purinergic signalling [21], TRPM7 and KCa2.3/SK3 channels [22], and TREM2/β-catenin signaling pathway [23]. It has been reported that ATP released from injured neurons and nerve terminals can affect the motor ability of microglia. ATP/ADP can induce the chemotaxis of microglia through P2Y12 or P2Y13 receptors [24]. In this study, REST was observed as a suppressor of migration.

REST is a powerful transcription factor which binds to a conserved 23 bp DNA motif known as repressor element 1 (RE1) blocking transcription of downstream genes [25]. Previous work established that REST also participates in cell migration and plays diverse roles both in the physiological and pathological condition. Mandel et al. have reported that

REST blocks radial migration during neurogenesis [13]. And in medulloblastoma (MB), REST is elevated promoting MB cell migration [26]. Beyond that, in glioblastoma (GBM) downregulation of REST by siRNA silencing could inhibit the migration of GBM cells [27]. Up to now, the role of REST in microglial migration in Alzheimer's disease is unclear. In this study, a significant induction of JAK2 and STAT3 phosphorylation were observed when BV-2 cells were treated with $A\beta_{1\text{-}42}$, and with the existing of WP1066, $A\beta_{1\text{-}42}$-induced REST upregulation was inhibited, which suggested that $A\beta_{1\text{-}42}$ might induce the increase of REST expression through JAK2/STAT3 pathway. And knocking-down of REST weakened the migration of BV2 cells, which indicated that REST may have played a role of repressor during $A\beta_{1\text{-}42}$-induced BV-2 cell migration.

In addition to REST, progranulin (PGRN) also regulates microglial migration. PGRN is a secreted glycoprotein expressed in peripheral organs and the central nervous system, which was reported to implicate in embryonic development, tumorigenesis, wound defense, and inflammation, and PGRN was proved to promote cell migration as well. Previous work established that PGRN promotes migration of epithelial ovarian cancer cells [28], breast cancer cells [29], and *H. pylori* infected gastric cell migration [30]. In this study, PC12 cells stimulated by $A\beta_{1\text{-}42}$ were observed to promote microglial migration, which was consisting with previous study. And PGRN-specific siRNA was used to knockdown PGRN, which results in decreased BV2 cell migration. These data showed that PGRN can promote BV2 cell migration under the condition of treatment with $A\beta_{1\text{-}42}$. This observation was not surprising as previously published data showed that PGRN acts as a chemoattractant in the brain to recruit or activate microglia [2].

By analyzing the promoter sequence of PGRN, we found that it has the potential binding site of REST. Moreover, the knockdown of REST can increase the expression of PGRN, which confirms the inhibiting effect of REST on PGRN. Further detection of double luciferase reporter gene also confirmed the inhibition of REST on the activity of PGRN promoter, indicating that REST may be an inhibitory transcription factor of PGRN which governs microglia-like BV2 cell migration. In conclusion, the present study demonstrates that PGRN can promote microglia migration and transcription factor REST may act as a repressor of microglia migration through PGRN.

5. Conclusions

Our findings raise the possibility that $A\beta_{1\text{-}42}$-induced REST expression has a repressing effect on BV-2 cell migration through PGRN.

Data Availability

The data used to support the findings of this study are available from the corresponding author upon reasonable request.

Disclosure

Tongya Yu, Yingying Lin, and Yuzhen Xu are co-first authors.

Conflicts of Interest

The authors declare that they have no competing interests.

Authors' Contributions

Tongya Yu, Yingying Lin, and Yuzhen Xu contributed equally to this work.

Acknowledgments

This work was supported by grants from the National Natural Science Foundation of China (81771131), the Major Projects of Science and Technology Commission of Shanghai Municipality (17411950100), and Shanghai Municipal Key Clinical (shslczdzk06102).

References

[1] T. Yu, H. Quan, Y. Xu et al., "Aβ-induced repressor element 1-silencing transcription factor (REST) gene delivery suppresses activation of microglia-like BV-2 cells," *Neural Plasticity*, vol. 2020, Article ID 8888871, 8 pages, 2020.

[2] Q. Wang, W. Yang, J. Zhang, Y. Zhao, and Y. Xu, "TREM2 overexpression attenuates cognitive deficits in experimental models of vascular dementia," *Neural Plasticity*, vol. 2020, Article ID 8834275, 10 pages, 2020.

[3] X. Du, Y. Xu, S. Chen, and M. Fang, "Inhibited CSF1R alleviates ischemia injury via inhibition of microglia M1 polarization and NLRP3 pathway," *Neural Plasticity*, vol. 2020, Article ID 8825954, 11 pages, 2020.

[4] Q. Wang, Y. Xu, C. Qi, A. Liu, and Y. Zhao, "Association study of serum soluble TREM2 with vascular dementia in Chinese Han population," *The International Journal of Neuroscience*, vol. 130, no. 7, pp. 708–712, 2020.

[5] F. Pickford, J. Marcus, L. M. Camargo et al., "Progranulin is a chemoattractant for microglia and stimulates their endocytic activity," *The American Journal of Pathology*, vol. 178, no. 1, pp. 284–295, 2011.

[6] T. Lu, L. Aron, J. Zullo et al., "REST and stress resistance in ageing and Alzheimer's disease," *Nature*, vol. 507, no. 7493, pp. 448–454, 2014.

[7] D. Roy, G. J. Steyer, M. Gargesha, M. E. Stone, and D. L. Wilson, "3D cryo-imaging: a very high-resolution view of the whole mouse," *Anatomical Record*, vol. 292, no. 3, pp. 342–351, 2009.

[8] Y. Xu, Q. Wang, Z. Wu et al., "The effect of lithium chloride on the attenuation of cognitive impairment in experimental hypoglycemic rats," *Brain Research Bulletin*, vol. 149, pp. 168–174, 2019.

[9] Y. Xu, Q. Wang, D. Li et al., "Protective effect of lithium chloride against hypoglycemia-induced apoptosis in neuronal PC12 cell," *Neuroscience*, vol. 330, pp. 100–108, 2016.

[10] I. Prada, J. Marchaland, P. Podini et al., "REST/NRSF governs the expression of dense-core vesicle gliosecretion in

astrocytes," *The Journal of Cell Biology*, vol. 193, no. 3, pp. 537–549, 2011.

[11] M. Eufemi, R. Cocchiola, D. Romaniello et al., "Acetylation and phosphorylation of STAT3 are involved in the responsiveness of microglia to beta amyloid," *Neurochemistry International*, vol. 81, pp. 48–56, 2015.

[12] J. Xiong, C. Wang, H. Chen et al., "Aβ-induced microglial cell activation is inhibited by baicalin through the JAK2/STAT3 signaling pathway," *The International Journal of Neuroscience*, vol. 124, no. 8, pp. 609–620, 2014.

[13] G. Mandel, C. G. Fiondella, M. V. Covey, D. D. Lu, J. J. Loturco, and N. Ballas, "Repressor element 1 silencing transcription factor (REST) controls radial migration and temporal neuronal specification during neocortical development," *Proceedings of the National Academy of Sciences of the United States of America*, vol. 108, no. 40, pp. 16789–16794, 2011.

[14] Y. Fang, J. Wang, L. Yao et al., "The adhesion and migration of microglia to β-amyloid (Aβ) is decreased with aging and inhibited by Nogo/NgR pathway," *Journal of Neuroinflammation*, vol. 15, no. 1, p. 210, 2018.

[15] C. Condello, P. Yuan, A. Schain, and J. Grutzendler, "Microglia constitute a barrier that prevents neurotoxic protofibrillar Aβ42 hotspots around plaques," *Nature Communications*, vol. 6, no. 1, article 6176, 2015.

[16] H. Kettenmann, F. Kirchhoff, and A. Verkhratsky, "Microglia: new roles for the synaptic stripper," *Neuron*, vol. 77, no. 1, pp. 10–18, 2013.

[17] C. N. Parkhurst, G. Yang, I. Ninan et al., "Microglia promote learning-dependent synapse formation through brain-derived neurotrophic factor," *Cell*, vol. 155, no. 7, pp. 1596–1609, 2013.

[18] A. F. Lloyd, C. L. Davies, and V. E. Miron, "Microglia: origins, homeostasis, and roles in myelin repair," *Current Opinion in Neurobiology*, vol. 47, pp. 113–120, 2017.

[19] M. Fricker, A. Vilalta, A. M. Tolkovsky, and G. C. Brown, "Caspase inhibitors protect neurons by enabling selective necroptosis of inflamed microglia," *The Journal of Biological Chemistry*, vol. 288, no. 13, pp. 9145–9152, 2013.

[20] A. Langfelder, E. Okonji, D. Deca, W. C. Wei, and M. D. Glitsch, "Extracellular acidosis impairs P2Y receptor-mediated Ca(2+) signalling and migration of microglia," *Cell Calcium*, vol. 57, no. 4, pp. 247–256, 2015.

[21] A. Sunkaria, S. Bhardwaj, A. Halder, A. Yadav, and R. Sandhir, "Migration and phagocytic ability of activated microglia during post-natal development is mediated by calcium-dependent purinergic signalling," *Molecular Neurobiology*, vol. 53, no. 2, pp. 944–954, 2016.

[22] T. Siddiqui, S. Lively, R. Ferreira, R. Wong, and L. C. Schlichter, "Expression and contributions of TRPM7 and KCa2.3/SK3 channels to the increased migration and invasion of microglia in anti-inflammatory activation states," *PLoS One*, vol. 9, no. 8, article e106087, 2014.

[23] H. Zheng, L. Jia, C. C. Liu et al., "TREM2 promotes microglial survival by activating Wnt/β-catenin pathway," *The Journal of neuroscience : the official journal of the Society for Neuroscience*, vol. 37, no. 7, pp. 1772–1784, 2017.

[24] P. Jiang, F. Xing, B. Guo et al., "Nucleotide transmitters ATP and ADP mediate intercellular calcium wave communication via P2Y12/13 receptors among BV-2 microglia," *PLoS One*, vol. 12, no. 8, article e0183114, 2017.

[25] J. A. Chong, J. Tapia-Ramírez, S. Kim et al., "REST: a mammalian silencer protein that restricts sodium channel gene expression to neurons," *Cell*, vol. 80, no. 6, pp. 949–957, 1995.

[26] K. Callegari, S. Maegawa, J. Bravo-Alegria, and V. Gopalakrishnan, "Pharmacological inhibition of LSD1 activity blocks REST-dependent medulloblastoma cell migration," *Cell Communication and Signaling*, vol. 16, no. 1, p. 60, 2018.

[27] D. Zhang, Y. Li, R. Wang et al., "Inhibition of REST suppresses proliferation and migration in glioblastoma cells," *International Journal of Molecular Sciences*, vol. 17, no. 5, p. 664, 2016.

[28] T. Dong, D. Yang, R. Li et al., "PGRN promotes migration and invasion of epithelial ovarian cancer cells through an epithelial mesenchymal transition program and the activation of cancer associated fibroblasts," *Experimental and Molecular Pathology*, vol. 100, no. 1, pp. 17–25, 2016.

[29] M. Swamydas, D. Nguyen, L. D. Allen, J. Eddy, and D. Dréau, "Progranulin stimulated by LPA promotes the migration of aggressive breast cancer cells," *Cell Communication & Adhesion*, vol. 18, no. 6, pp. 119–130, 2011.

[30] H. Wang, Y. Sun, S. Liu et al., "Upregulation of progranulin by Helicobacter pylori in human gastric epithelial cells via p38MAPK and MEK1/2 signaling pathway: role in epithelial cell proliferation and migration," *FEMS Immunology and Medical Microbiology*, vol. 63, no. 1, pp. 82–92, 2011.

Hindawi
Neural Plasticity
Volume 2020, Article ID 8894372, 11 pages
https://doi.org/10.1155/2020/8894372

Review Article

Stress-Sensitive Protein Rac1 and Its Involvement in Neurodevelopmental Disorders

Xiaohui Wang[1], **Dongbin Liu**[1], **Fangzhen Wei**[2], **Yue Li**[3], **Xuefeng Wang**[3], **Linjie Li**[4], **Guan Wang**[5], **Shuli Zhang**[6] and **Lei Zhang**[7]

[1]*Department of General Surgery, Xuanwu Hospital, Capital Medical University, Beijing 100053, China*
[2]*Peking University Hospital, Beijing 100870, China*
[3]*Guangwai Community Health Service Center of Xicheng District, Beijing 100055, China*
[4]*Department of Epidemiology, Emory University, Atlanta, GA, USA*
[5]*School of Pharmaceutical Sciences, Tsinghua University, Beijing, China*
[6]*State Key Laboratory of Brain and Cognitive Sciences, Institute of Biophysics, Chinese Academy of Sciences, Beijing 100101, China*
[7]*Neurological Research Unit, Staidson (Beijing) Biopharmaceuticals Co., Ltd., Beijing 100176, China*

Correspondence should be addressed to Guan Wang; wangguan@bu.edu, Shuli Zhang; shulizhang@ibp.ac.cn, and Lei Zhang; leizhang3030@hotmail.com

Received 4 July 2020; Revised 1 November 2020; Accepted 12 November 2020; Published 24 November 2020

Academic Editor: Fushun Wang

Ras-related C3 botulinum toxin substrate 1 (Rac1) is a small GTPase that is well known for its sensitivity to the environmental stress of a cell or an organism. It senses the external signals which are transmitted from membrane-bound receptors and induces downstream signaling cascades to exert its physiological functions. Rac1 is an important regulator of a variety of cellular processes, such as cytoskeletal organization, generation of oxidative products, and gene expression. In particular, Rac1 has a significant influence on certain brain functions like neuronal migration, synaptic plasticity, and memory formation *via* regulation of actin dynamics in neurons. Abnormal Rac1 expression and activity have been observed in multiple neurological diseases. Here, we review recent findings to delineate the role of Rac1 signaling in neurodevelopmental disorders associated with abnormal spine morphology, synaptogenesis, and synaptic plasticity. Moreover, certain novel inhibitors of Rac1 and related pathways are discussed as potential avenues toward future treatment for these diseases.

1. Introduction

As a member of the Ras-homologous (Rho) small GTPase family, Rac1 is well known for its versatility in mediating the response of cells or organisms when facing external disturbances or environmental challenges, such as heat shock [1], oxidative stress [2], mechanical stress [3], genotoxic stress [4], hypoxic stress [5], or even higher-level mental stress from social confrontation and fear [6–9]. In the last decade, Rac1 has gained increased attention in the field of neuroscience with its roles in brain structure and function becoming more widely appreciated. It is commonly accepted that Rac1 and related signaling pathways are prominently involved in the maintenance and regulation of basic nervous system functions including neurite outgrowth, neuronal migration, synaptogenesis, synaptic plasticity, and learning memory [10–13]. Moreover, Rac1 is believed to contribute to the formation of addictive behavior [14]. However, not until recently have studies revealed that Rac1 may be relevant for certain inherited neurodevelopmental disorders, likely due to its essential role in the regulation of neuronal cell structure and development [15–19]. In this review, we aim

to sketch a picture of the newly identified roles of Rac1 in these diseases and to shed light on the potential of specific inhibitors for Rac1 as novel therapeutics.

2. Basic Molecular Mechanism of Rac1 Signaling

Rac1 belongs to the Rac subfamily of Rho small GTPases (~21 kDa), whose primary function is to transduce external signals to the inside of a cell. Rac proteins are among the frontline responders to external stress signals [20]. To date, three Rac proteins (Rac1–3) have been identified in vertebrates, which share a high degree of homology in amino acid sequences (88–92%) [21]. Rac1 participates in a wide spectrum of physiological processes, including actin cytoskeleton organization, cell adhesion and migration, gene expression, neurodevelopment, and synaptic plasticity [12, 22–24]. Rac1 was first identified in the human leukemia cell line HL-60 as a substrate of botulinum C3 ADP-ribosyltransferase [25, 26]. Similar to other small GTPases, Rac1 possesses a G core domain and an effector binding domain [27]. It is expressed in both the eukaryotic cytoplasm and the nucleus and cycles between the GTP-bound and GDP-bound states, marking the active and inactive forms of Rac1, respectively. To enter the active form, the bound GDP on Rac1 is replaced by GTP which is catalyzed by specific guanine nucleotide exchange factors (GEFs). Conversely, bound GTP is hydrolyzed to GDP by GTPase-activating proteins (GAPs) to produce the inactive form of Rac1 [28, 29]. Rac1 shares an identical amino acid sequence between murine, bovine, and human [30, 31]. The high degree of conservation with Rac1 protein structure and its downstream signaling cascades highlights its physiological relevance across different species. Rac1 exerts its functional impacts mainly *via* a downstream effector named p21-activated kinase (PAK). PAK directly phosphorylates and activates the LIM kinase (LIMK), which in turn phosphorylates and inactivates the actin-depolymerizing factor, cofilin, leading to actin depolymerization and cytoskeleton reorganization (Figure 1). In addition to the PAK-LIMK-cofilin pathway, Rac1 can also act directly through the WAVE1 and actin-related protein 2/3 (Arp2/3) complex to regulate actin nucleation and thus cellular structure, movement, and functions [32–36].

3. Rac1 and Neurodevelopmental Disorders

Given the vital role that actin dynamics plays in multiple key physiological processes in the brain, it is no surprise that Rac1 influences a wide variety of nervous system functions, including synaptogenesis, neuronal migration, neurite outgrowth, synaptic transmission and plasticity, memory, and addictive behavior formation [14, 37–41]. Aberrant Rac1 expression or activity regulation or even small alterations to its downstream signaling may lead to severe neurodevelopmental disorders (Figure 2). Here, we briefly summarize recent findings on a few hereditary neurodevelopmental disorders that involve dysregulated Rac1 expression/activity, which have not been systemically covered previously in other reviews.

3.1. Autism Spectrum Disorders. Autism spectrum disorders (ASD) refer to a group of neurodevelopmental disorders characterized by impaired social interaction and communication along with restricted or repetitive behaviors [16, 42]. ASD can be diagnosed at any age; however, they are described as developmental disorders because they become apparent mostly in the first two years of life. A number of high-risk genes linked to the etiology of ASD have been identified and characterized, including the Autism susceptibility candidate 2 (AUTS2), SH3 and multiple ankyrin repeat domains 3 (SHANK3), Ubiquitin-protein ligase E3A (UBE3A), and Methyl-CpG-binding protein 2 (MECP2) [19, 43–49]. Some of these autism-risk genes were recently found to be linked to ASD *via* the Rac1-associated signaling network in the brain.

The *AUTS2* gene was first found to be disrupted by a *de novo* balanced translocation in two monozygotic twins with ASD [50]. It was later found to contribute to ASD by influencing synaptogenesis and neuron migration *via* Rac1. The AUTS2 protein activates Rac1 by interacting with different GEFs, such as P-Rex-1 and Elmo2/Dock180 complex, to promote the formation of lamellipodia in neurons [18, 43, 44]. Rac1 is also essential for AUTS2-mediated neuronal migration and neuritogenesis in the process of corticogenesis. At the early stages of cerebral cortex development, AUTS2 deficiency in mice results in retarded cortical neuronal migration that can be rescued by the overexpression of wild-type Rac1 [18, 44].

SHANK3 is another highly studied risk gene for ASD. The link between *SHANK3* haploinsufficiency and ASD has been extensively studied in human and animal models [42, 51, 52]. *SHANK3*-deficient mice exhibit typical autistic cellular and behavioral phenotypes [52]. It was recently shown that the social deficits and diminished synaptic *N*-methyl-D-aspartate (NMDA) receptor function in *SHANK3*-deficient mice resulted from actin filament disorganization, caused by reduced Rac1/PAK activity and increased cofilin activity in the prefrontal cortex. To support this conclusion, it was found that both behavioral deficits and NMDA receptor malfunction were rescued by restoring Rac1/PAK activity in these mice [16, 45].

Impaired reversal learning caused by behavioral inflexibility is another hallmark symptom of ASD [53]. In a recent study with fruit flies (*Drosophila melanogaster*), Rac1 was a functional converging point for multiple autism risk genes, including Fragile X mental retardation 1 (*FMR1*), *UBE3A*, Neurexin-1 (*Nrx-1*), Neuroligin-4 (*Nlg4*), and Tuberous sclerosis complex 1 (*TSC1*). Mutations on these genes all caused similar autistic behavioral inflexibility related to Rac1-dependent memory impairment, which led to impaired reversal learning [47].

3.2. Schizophrenia. Schizophrenia is an inherited, severe psychiatric disorder that is thought to be associated with disturbances in neural network connectivity [54, 55]. An examination of postmortem brains from schizophrenia patients revealed the reduced density of dendritic spines and fewer glutamatergic synapses [56]. In the past decade, several schizophrenia risk genes have been reported, such

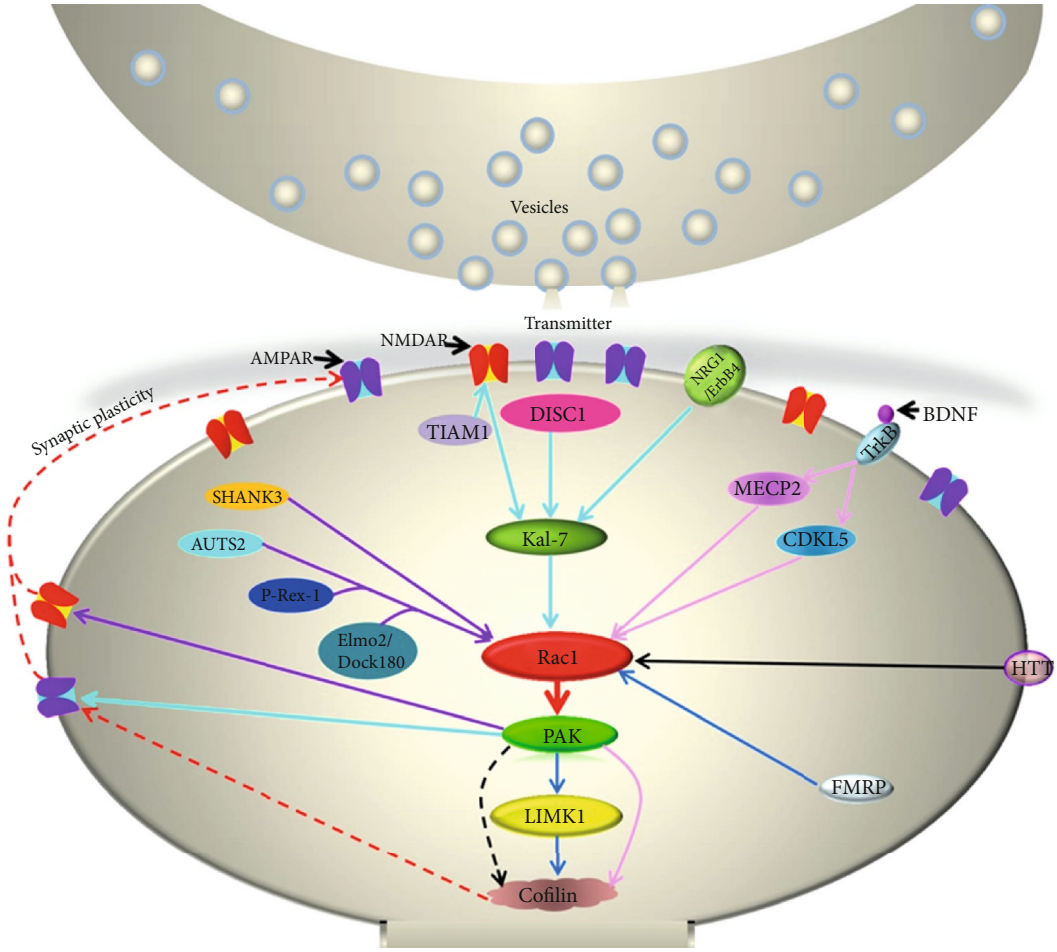

Figure 1: Regulation and interaction of Rac1-related signaling pathways at the postsynaptic terminal. Effectors of FXS and Huntington's disease, such as FMRP and HTT, can directly activate or inhibit Rac1 activity to modulate its downstream signaling cascades, mainly *via* the Rac1-PAK-cofilin pathway, which subsequently influences synaptic plasticity. In schizophrenia, NMDA receptors activate Kal-7 *via* TIAM1, while DISC1 and NRG1/ErbB4 interact with Kal-7 to activate or inhibit Rac1. In ASD, SHANK3 directly modulates Rac1 activity, while other effectors like AUTS2, P-Rex-1, and Elmo2/Dock180 form a complex to modulate Rac1 activity and then affect NMDA receptor activity through the PAK pathway. In Rett syndrome, BDNF activates TrkB receptors to modulate the activity of CDKL5 and MECP2 that further regulate the function of the Rac1-cofilin pathway. Abnormalities of these proteins in any pathways may affect neuroplasticity and cause neurodevelopmental disorders.

as Disrupted-in-Schizophrenia 1 (*DISC1*), NMDA receptor subunit genes, Neuregulin 1/ErbB4 (*NRG1/ErbB4*), and Brain-derived neurotrophic factor (*BDNF*), which participate in the regulation of neuroplasticity and neural connectivity [15, 57–60]. Rac1 functions mostly as a downstream signaling hub molecule of these genes [11, 15, 57, 61].

Kalirin 7 (Kal-7) is a Rac1 GEF that was found to be transcriptionally downregulated in the prefrontal cortices of patients with schizophrenia [56]. Multiple lines of evidence support a critical role for Kal-7 in the modulation of spine morphology, driven mainly by the Rac1-dependent regulation of actin cytoskeleton [61–63]. Kal-7 interacts with DISC1 as a signalosome to control the duration and intensity of Rac1 activation in response to NMDA receptor activation. In rodent primary cortical neurons, DISC1 deficiency activates Rac1 and leads to rapid spine growth, while the overexpression of DISC1 suppresses Rac1 activity to reduce spine size [15]. Kal-7 also interacts with NR2B, an NMDA receptor subunit extensively involved in nervous system function and neurological diseases [10, 64–66]. It was noted that the NR2B-dependent NMDA receptor currents are diminished in neurons lacking Kal-7 [10, 61]. Additionally, Kal-7 is also involved in signaling cascades mediated by synaptic receptors like Ephrin B (EphB), Erb-B2 receptor tyrosine kinase 4 (ErbB4), and 5-Hydroxytryptamine (serotonin) receptor 2A (5HT2A), which regulate structural and functional plasticity of synapses [60, 62, 67, 68].

Like Kal-7, TIAM1 (TIAM Rac1-associated GEF 1) is a Rac1 GEF that colocalizes with the NR1 subunit of NMDA receptors. TIAM1 deficiency leads to reduced spine size, a result of TIAM1 binding to NMDA receptors and induction of local Rac1-dependent spine morphogenesis [69]. Moreover, other studies suggest that the inhibition of PAK prevents the progressive synaptic deterioration in rodent

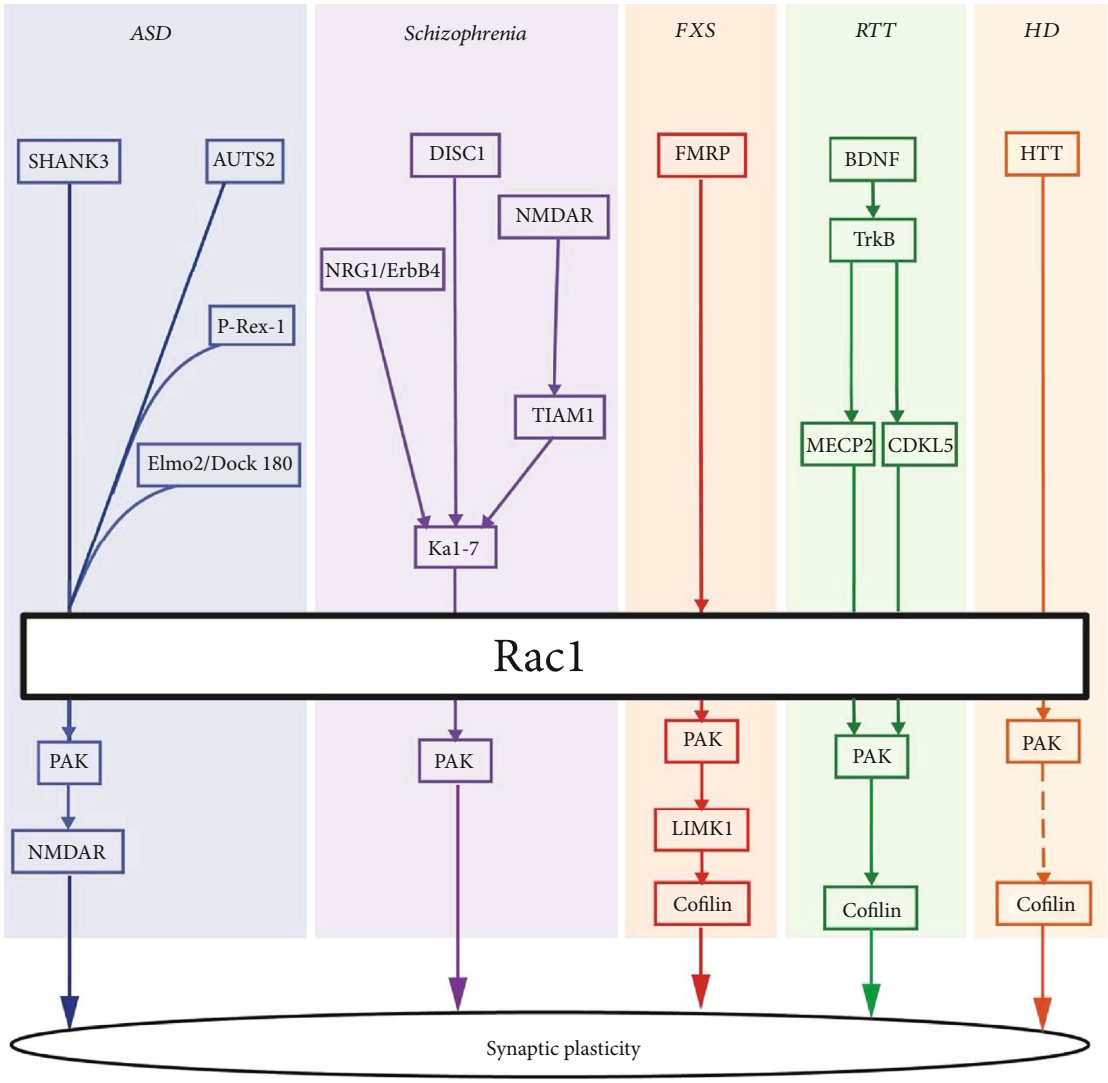

Figure 2: Putative schematic of the Rac1 signaling pathways involved in different neurodevelopmental disorders. The upstream effector, such as Kal-7, AUTS2, NMDAR, or FMRP, activates or inhibits Rac1 activity to modulate its downstream signaling cascades, primarily *via* the PAK-cofilin pathway, which orchestrates neuronal cell migration, spinogenesis, and synaptic plasticity. Abnormalities in this Rac1-related signaling complex are common features of neurodevelopmental disorders. The dashed lines indicate certain mechanisms that remain unclear and require further investigation.

models of schizophrenia [57, 70, 71]. These studies collectively demonstrate a role for Rac1 and its regulators/effectors in the pathogenesis of schizophrenia, suggesting that Rac1 and related signaling pathways can be novel therapeutic targets.

3.3. Fragile X Syndrome. Fragile X syndrome (FXS) is a hereditary neurodevelopmental disability that results from an abnormal expansion of the CGG trinucleotide repeat in the *FMR1* gene on the X chromosome. The expansion leads to promoter hypermethylation and transcriptional silencing that prevents the expression of FMR1 protein (FMRP). FXS is characterized by abnormalities in dendritic spine structure, learning disabilities, and cognitive impairment. As an X-linked disorder, FXS occurs in males about two times more frequently compared to females [72–77].

Rac1 is found physically and functionally associated with FMRP. FMRP acts as a negative regulator of Rac1 synthesis [78]. Abnormally high Rac1 activity has been observed in the neocortices of FXS patients and animal models [79]. In the actin ring of murine fibroblasts, Rac1 colocalizes and interacts with FMRP and its partners, which serve as regulators of Rac1-dependent actin remodeling [80]. In developing *Drosophila* brains, Rac1 interacts with the homolog of FMRP to influence the cytoskeletal dynamics and neuronal outgrowth as well as synaptic morphology at neuromuscular junctions (NMJ). Loss-of-function mutations in FMRP increase the number of higher-order dendritic branches. Conversely, expression of normal FMRP dramatically decreases dendritic branching in *Drosophila* dendritic arborization (DA) neurons [81]. Comery et al. generated *FMR1* knockout (KO) mice and observed a larger proportion of

long but thin dendritic spines in the occipital cortex with elevated Rac1, similar to what was observed in humans [79]. Another study demonstrated that Rac1 expression levels are unusually high in brain stems, hippocampi, and cortices of 3-month-old mice lacking *FMR1* [78].

Rac1-related signaling pathways have also been extensively investigated in FXS animal models. When Rac1 is absent in the synapses of certain brain regions, PAK activity is also downregulated. Partial inhibition of PAK by introducing dominant-negative PAK in mice results in a shift in the overall spine distribution toward shorter spines with a lower proportion of longer spines relative to wild-type neurons [82]. Opposite phenotypes have been observed in *FMR1* KO mice [78]. In a separate study, the application of a small-molecule PAK inhibitor FRAX486 rescued most of the FXS phenotypes in *FMR1* KO mice [83]. The activity of cofilin was also found to be suppressed in the somatosensory cortex of *FMR1* KO mice, due to the hyperactivity of Rac1 [84]. These studies revealed a previously unappreciated role for impaired Rac1-PAK1-cofilin-LIMK1 signaling in abnormal spine morphology and density associated with FXS and pointed to Rac1 as a promising target for these specific abnormalities.

3.4. Rett Syndrome. Rett syndrome (RTT) is a severe progressive developmental intellectual disability that affects almost exclusively girls [85, 86]. Autopsy studies of six girls that died between the ages of 2.9 and 35 revealed excessive amounts of immature dendrites in the motor and frontal cortices [87]. Two high-risk genes linked to RTT have been identified: *MECP2* and the X-linked cyclin-dependent kinase-like 5 (*CDKL5*). It was reported that mutations on *MECP2* account for ~20% of classical RTT along with 60~80% of RTT variants [88, 89], while mutations on *CDKL5* were identified in patients with the Hanefeld variant of RTT [90, 91].

In patients with *MECP2* mutations, significant decreases in spine density were observed in hippocampal CA1 pyramidal neurons. Similarly, reductions of spine density were observed in the motor cortices and hippocampi of mice lacking *MECP2* [92–94], which was found to be at least partially attributed to the deregulation of BDNF, a protein well known for its vital role in spine growth and synaptogenesis by binding and activating the tropomyosin-receptor kinase B (TrkB) receptor and its downstream signaling pathways [95–99]. Although more evidence is needed, Rac1 has been proposed to act as a downstream signaling effector of BDNF [100, 101]. Moreover, in the brains of RTT model mice, activation of certain Rac1 downstream proteins such as PAK and cofilin directly activates mTOR in *MECP2* mutant neurons, which is responsible for the translational control of altered proteins in RTT [102].

Patients with *CDKL5* mutations exhibit prominent intellectual disabilities. Knocking down *CDKL5* in the rat brain results in delayed neuronal migration and severely impairs dendritic arborization. Overexpression of Rac1 rescues the dendritic growth inhibited by CDKL5 knockdown. Moreover, CDKL5 is required for the BDNF-induced activation of Rac1 [103, 104].

Taken together, Rac1 mediates the dendritic development through BDNF regulation, which may be a common mechanism in cases of RTT involving *MECP2* or *CDKL5* mutations. Rac1 is also responsible for the posttranslational control of altered proteins in cases of RTT involving *MECP2* mutations. The modulation of Rac1-dependent spine development is potentially beneficial as a treatment for RTT.

3.5. Huntington's Disease. Huntington's disease (HD) is a hereditary and progressive nervous system disorder that is caused by a CAG trinucleotide repeat expansion in the first exon of the *HTT* gene, which encodes for the huntingtin protein (HTT) [105]. HD patients manifest with progressive motor, cognitive, and emotional impairments, coupled with abnormal spine morphogenesis in the cortex and striatum [106–108].

Recent studies suggest that Rac1 may contribute to the pathogenesis and symptoms of HD. In a large-scale screening study with the yeast two-hybrid system, over 2000 HTT-interacting proteins were analyzed. A few Rho GTPase signaling components, including Rac1 and PAK2, were identified as modifiers of mutant HTT toxicity, which implicates Rac1 and related signaling cascades in the onset of HD [109]. Consistent with this screen, Rac1 activity was found to be drastically enhanced in both primary human fibroblasts lacking HTT and the striatum of 1.5-month-old HD Q140/Q140 knock-in mice [110, 111]. Moreover, consistent with the conventional role of Rac1 in oxidative stress, multiple recent studies suggest that Rac1 modulates the generation of reactive oxygen species (ROS) in HD models [112, 113]. Nevertheless, even though studies suggest that Rac1 is involved in actin-dependent morphological changes of neurons during the pathogenesis of HD [110], whether Rac1 contributes to the crucial early development of HD remains unclear and requires further investigation.

4. Screening Novel Rac1 Inhibitors for the Treatment of Neurodevelopmental Disorders

Due to the multifaceted roles that Rac1 plays in brain function and neurodevelopmental disease etiology, enormous efforts have been made to screen for effective Rac1 inhibitors with the hope to develop novel medications for relevant neurodevelopmental diseases (Table 1). A good number of small-molecule compounds targeting Rac1 and related signaling pathways have been developed. NSC23766 and its derivatives have been extensively investigated in multiple disease models, both *in vitro* and *in vivo*. NSC23766 inhibits Rac1 activity by disrupting its physical binding with its interacting proteins, such as GEFs, TIAM1, and triple functional domain protein (TRIO), without affecting RhoA or Cdc42 activity. Preclinically, NSC23766 has demonstrated positive effects in several disease models, including in models of cancers, cognitive disorders, brain injuries, and neurodegenerative and kidney diseases [112–118]. Based on its structure and characteristics, further optimization of NSC23766 has been performed. AZA1 is a compound structurally based on NSC23766 that has greater inhibitory potency on Rho GTPase activity, which was shown to inhibit both Rac1 and

Table 1: List of small-molecule compounds that inhibit Rac1 activity.

Compound name	Formula	Molecular weight	Target Rac1 signaling	Target other Rho GTPases	Reference
NSC23766	$C_{24}H_{35}N_{73}HCl$	530.96	Inhibit TIAM1 and TRIO	None	[114]
ITX3	$C_{22}H_{17}N_3OS$	371.45	TRIO	RhoG and Rac1	[122]
EHop-016	$C_{25}H_{30}N_{60}$	430.55	Inhibit Vav2	Rac3, Cdc42	[120]
AZA1	$C_{22}H_{20}N_6$	368.43	Rac1/PAK1	Cdc42	[119]
1A-116	$C_{16}H_{16}F_3N_3$	307.31	Rac1/P-Rex-1	None	[123, 127]
ETH 1864	$C_{25}H_{27}F_3N_{204}S_2HCI$	581.47	Rac1/TIAM1	Rac1b, Rac2, Rac3	[128]
FRAX486	$C_{25}H_{23}C_{l2}FN_6O$	513.39	PAK1-3	None	[71, 83]

Cdc42 activity in prostate cancer cells and improve the survival rate of mice bearing human prostate cancer xenografts [119]. EHop-016 is another potent Rac inhibitor derived from NSC23766 that targets the association between Rac1 and the Rac GEF Vav2. EHop-016 is highly effective at inhibiting Rac1 activity and suppressing Rac-directed lamellipodia formation in MDA-MB-435 metastatic cancer cells and MDA-MB-231 metastatic breast cancer cells [120].

Even though much work has been done to optimize NSC23766-based molecules, a big gap still remains with further development into clinical testing, possibly due to their low binding capacity to the target proteins.

Unraveling the crystal structures of Rac1 and its interacting proteins opened another door to identify inhibitory compounds [121]. ITX3 was identified as a selective inhibitor of TRIO and N-terminal TRIO-dependent cell structures *in vitro* based on the crystal structures and characteristics of the target proteins. However, the efficacy of ITX3 in animal models appears to be not ideal [122]. A thorough screening of the ZINC database containing more than 200,000 compounds led to the discovery of a number of novel Rac1 inhibitors. 1A-116 shows a robust antimetastatic effect by blocking Rac GEF P-Rex-1 (PIP3-dependent Rac exchanger 1) binding to suppress Rac1 activation [123]. In addition, ETH 1864 was identified to be a potent suppressor of Rac1a and its GEF, TIAM1, as well as the other Rac1 isoforms, Rac1b, Rac2, and Rac3. ETH 1864 has been demonstrated to decrease the NMDAR current density in rat cortical neurons and reduce spine density in the early stages of hippocampal neuronal development [124]. Consistent with this, LTP and LTD were both abolished by the treatment of ETH 1864 and NSC23766, respectively, on mouse hippocampus slices [11]. The downstream effectors of Rac1, such as PAK, have also been targets for novel inhibitor screening. Through a traditional, two-part structure-activity relationship approach, a series of PAK inhibitors were found in a library of 12,000 compounds using a FRET-based assay. Among them, FRAX486 was identified to show a potent inhibitory effect to PAK with good PK properties and brain penetration. The small molecule was demonstrated to reverse the spine abnormalities seen in animal models of FXS and schizophrenia. Behavioral phenotypes, such as hyperactivity and repetitive movements, were also rescued after treatment with FRAX486 [71, 83].

So far, although no small-molecule inhibitors have moved into clinical trials, recent alternative approaches to targeting Rac1 offer more optimism for this approach. A polypeptide that inhibits Rac1 and a few other RhoA GTPases is in preclinical testing with positive effects shown on treating neurodegenerative diseases and cancer [125]. An antisense RNAi oligonucleotide drug for Kaposi's sarcoma developed by researchers from the University of Miami has also been reported [126]. Although no drugs have been tested in humans at this moment, the application of these Rac1 inhibitors in neurodevelopmental disease models may provide new leads for diseases featuring synaptic abnormalities.

5. Conclusions

The dysregulation of Rac1 has been indicated in the processes of neuronal morphogenesis, migration, and synaptic plasticity in neurodevelopmental disorders such as schizophrenia, ASD, and FXS, as highlighted in the review. Given the lack of effective medications for these diseases, Rac1 presents an opportunity for therapeutic intervention by targeting the abnormalities in synaptic morphology and plasticity. Further exploration of the expression and modulation of specific Rac1 regulators as well as Rac1 itself under physiological and pathological conditions will be beneficial to our understanding of the underlying mechanisms of these diseases as well as the development of novel therapeutic approaches.

Data Availability

No data were used to support this study.

Conflicts of Interest

The authors declare no conflict of interest.

Authors' Contributions

The contributions of the authors involved in this study are as follows: conceptualization: Lei Zhang, Shuli Zhang, and Guan Wang; writing-original draft for the basic molecular mechanism of Rac1 and autism spectrum disorders: Xiaohui Wang; writing-original draft about Huntington's disease: Dongbin Liu; writing-original draft about Rac1 inhibitors for neurodevelopmental disease treatment: Fangzhen Wei; writing-original draft about fragile X syndrome: Linjie Li; writing-original draft for Rett syndrome: Xuefeng Wang;

writing-original draft for schizophrenia: Yue Li; and supervision, figures, and editing: Lei Zhang, Shuli Zhang, and Guan Wang. Xiaohui Wang, Dongbin Liu, and Fangzhen Wei contributed equally to this work.

Acknowledgments

The work was supported by the grants of the National Science Foundation of China (Nos. 31527802 and 31871033) (S. Z.), the Beijing Natural Science Foundation (7182063), the Beijing Health System High-Level Health Technical Personnel (2014-3-058), and the Fund for Incubating Program of Capital Medical University (No. PYZ2018058) (X. H. W.).

References

[1] S. I. Han, S. Y. Oh, S. H. Woo et al., "Implication of a small GTPase Rac1 in the activation of c-Jun N-terminal kinase and heat shock factor in response to heat shock," *The Journal of Biological Chemistry*, vol. 276, no. 3, pp. 1889–1895, 2001.

[2] G. Mohammad, A. J. Duraisamy, A. Kowluru, and R. A. Kowluru, "Functional regulation of an oxidative stress mediator, Rac1, in diabetic retinopathy," *Molecular Neurobiology*, vol. 56, no. 12, pp. 8643–8655, 2019.

[3] X. Huang, Y. Shen, Y. Zhang et al., "Rac1 mediates laminar shear stress-induced vascular endothelial cell migration," *Cell Adhesion & Migration*, vol. 7, no. 6, pp. 462–468, 2013.

[4] S. C. Huelsenbeck, A. Schorr, W. P. Roos et al., "Rac1 protein signaling is required for DNA damage response stimulated by topoisomerase II poisons," *The Journal of Biological Chemistry*, vol. 287, no. 46, pp. 38590–38599, 2012.

[5] J. Du, R. Xu, Z. Hu et al., "PI3K and ERK-induced Rac1 activation mediates hypoxia-induced HIF-1α expression in MCF-7 breast cancer cells," *PLoS One*, vol. 6, no. 9, article e25213, 2011.

[6] J. Wang, G. E. Hodes, H. Zhang et al., "Epigenetic modulation of inflammation and synaptic plasticity promotes resilience against stress in mice," *Nature Communications*, vol. 9, no. 1, p. 477, 2018.

[7] S. A. Golden, D. J. Christoffel, M. Heshmati et al., "Epigenetic regulation of RAC1 induces synaptic remodeling in stress disorders and depression," *Nature Medicine*, vol. 19, no. 3, pp. 337–344, 2013.

[8] Z. Liao, Y. Tao, X. Guo et al., "Fear conditioning downregulates Rac1 activity in the basolateral amygdala astrocytes to facilitate the formation of fear memory," *Frontiers in Molecular Neuroscience*, vol. 10, p. 396, 2017.

[9] Q. Gao, W. Yao, J. Wang et al., "Post-training activation of Rac1 in the basolateral amygdala is required for the formation of both short-term and long-term auditory fear memory," *Frontiers in Molecular Neuroscience*, vol. 8, 2015.

[10] F. Lemtiri-Chlieh, L. Zhao, D. D. Kiraly, B. A. Eipper, R. E. Mains, and E. S. Levine, "Kalirin-7 is necessary for normal NMDA receptor-dependent synaptic plasticity," *BMC Neuroscience*, vol. 12, no. 1, p. 126, 2011.

[11] L. A. Martinez and M. V. Tejada-Simon, "Pharmacological inactivation of the small GTPase Rac1 impairs long-term plasticity in the mouse hippocampus," *Neuropharmacology*, vol. 61, no. 1-2, pp. 305–312, 2011.

[12] K. F. Tolias, J. G. Duman, and K. Um, "Control of synapse development and plasticity by Rho GTPase regulatory proteins," *Progress in Neurobiology*, vol. 94, no. 2, pp. 133–148, 2011.

[13] M. V. Tejada-Simon, L. E. Villasana, F. Serrano, and E. Klann, "NMDA receptor activation induces translocation and activation of Rac in mouse hippocampal area CA1," *Biochemical and Biophysical Research Communications*, vol. 343, no. 2, pp. 504–512, 2006.

[14] D. M. Dietz, H. Sun, M. K. Lobo et al., "Rac1 is essential in cocaine-induced structural plasticity of nucleus accumbens neurons," *Nature Neuroscience*, vol. 15, no. 6, pp. 891–896, 2012.

[15] A. Hayashi-Takagi, M. Takaki, N. Graziane et al., "Disrupted-in-Schizophrenia 1 (DISC1) regulates spines of the glutamate synapse via Rac1," *Nature Neuroscience*, vol. 13, no. 3, pp. 327–332, 2010.

[16] L. J. Duffney, P. Zhong, J. Wei et al., "Autism-like deficits in Shank3-deficient mice are rescued by targeting actin regulators," *Cell Reports*, vol. 11, no. 9, pp. 1400–1413, 2015.

[17] D. Tropea, N. Hardingham, K. Millar, and K. Fox, "Mechanisms underlying the role of DISC1 in synaptic plasticity," *The Journal of Physiology*, vol. 596, no. 14, pp. 2747–2771, 2018.

[18] K. Hori and M. Hoshino, "Neuronal migration and AUTS2 syndrome," *Brain Sciences*, vol. 7, no. 12, p. 54, 2017.

[19] C. Tian, Y. Kay, A. Sadybekov, S. Rao, V. Katritch, and B. E. Herring, "An intellectual disability-related missense mutation in Rac1 prevents LTP induction," *Frontiers in Molecular Neuroscience*, vol. 11, p. 223, 2018.

[20] G. Fritz and B. Kaina, "Rac1 GTPase, a multifunctional player in the regulation of genotoxic stress response," *Cell Cycle*, vol. 12, no. 16, pp. 2521-2522, 2014.

[21] S. Corbetta, S. Gualdoni, C. Albertinazzi et al., "Generation and characterization of Rac3 knockout mice," *Molecular and Cellular Biology*, vol. 25, no. 13, pp. 5763–5776, 2005.

[22] A. Abdrabou and Z. Wang, "Post-Translational Modification and Subcellular Distribution of Rac1: An Update," *Cells*, vol. 7, no. 12, p. 263, 2018.

[23] A. Payapilly and A. Malliri, "Compartmentalisation of RAC1 signalling," *Current Opinion in Cell Biology*, vol. 54, pp. 50–56, 2018.

[24] L. Liu, J. Li, L. Zhang et al., "Cofilin phosphorylation is elevated after F-actin disassembly induced by Rac1 depletion," *BioFactors*, vol. 41, no. 5, pp. 352–359, 2015.

[25] J. Didsbury, R. F. Weber, G. M. Bokoch, T. Evans, and R. Snyderman, "rac, a novel ras-related family of proteins that are botulinum toxin substrates," *The Journal of Biological Chemistry*, vol. 264, no. 28, pp. 16378–16382, 1989.

[26] P. G. Polakis, R. F. Weber, B. Nevins, J. R. Didsbury, T. Evans, and R. Snyderman, "Identification of the ral and rac1 gene products, low molecular mass GTP-binding proteins from human platelets," *The Journal of Biological Chemistry*, vol. 264, no. 28, pp. 16383–16389, 1989.

[27] Z. Yang, "Small GTPases: versatile signaling switches in plants," *Plant Cell*, vol. 14, suppl 1, pp. S375–S388, 2002.

[28] H. Marei, A. Carpy, B. Macek, and A. Malliri, "Proteomic analysis of Rac1 signaling regulation by guanine nucleotide exchange factors," *Cell Cycle*, vol. 15, no. 15, pp. 1961–1974, 2016.

[29] H. Marei, A. Carpy, A. Woroniuk et al., "Differential Rac1 signalling by guanine nucleotide exchange factors implicates

FLII in regulating Rac1-driven cell migration," *Nature Communications*, vol. 7, no. 1, 2016.

[30] A. Jia and X. H. Zhang, "cDNA cloning, characterization, and expression analysis of the Rac1 gene from Scophthalmus maximus," *Comparative Biochemistry and Physiology. Part B, Biochemistry & Molecular Biology*, vol. 154, no. 1, pp. 80–84, 2009.

[31] D. García-Weber and J. Millán, "Parallels between single cell migration and barrier formation: the case of RhoB and Rac1 trafficking," *Small GTPases*, vol. 9, no. 4, pp. 332–338, 2016.

[32] A. J. Ridley, "Rho GTPases and actin dynamics in membrane protrusions and vesicle trafficking," *Trends in Cell Biology*, vol. 16, no. 10, pp. 522–529, 2006.

[33] N. Yang, O. Higuchi, K. Ohashi et al., "Cofilin phosphorylation by LIM-kinase 1 and its role in Rac-mediated actin reorganization," *Nature*, vol. 393, no. 6687, pp. 809–812, 1998.

[34] D. C. Edwards, L. C. Sanders, G. M. Bokoch, and G. N. Gill, "Activation of LIM-kinase by Pak1 couples Rac/Cdc42 GTPase signalling to actin cytoskeletal dynamics," *Nature Cell Biology*, vol. 1, no. 5, pp. 253–259, 1999.

[35] T. D. Pollard, "Regulation of actin filament assembly by Arp2/3 complex and formins," *Annual Review of Biophysics and Biomolecular Structure*, vol. 36, no. 1, pp. 451–477, 2007.

[36] A. M. Sanchez, M. I. Flamini, X. D. Fu et al., "Rapid signaling of estrogen to WAVE1 and moesin controls neuronal spine formation via the actin cytoskeleton," *Molecular Endocrinology*, vol. 23, no. 8, pp. 1193–1202, 2009.

[37] L. Zhang, F. Zhang, T. Yang et al., "The B-cell receptor BR3 modulates cellular branching via Rac1 during neuronal migration," *Journal of Molecular Cell Biology*, vol. 8, no. 4, pp. 363–365, 2016.

[38] L. Z. Li, N. Yin, X. Y. Li et al., "Rac1 modulates excitatory synaptic transmission in mouse retinal ganglion cells," *Neuroscience Bulletin*, vol. 35, no. 4, pp. 673–687, 2019.

[39] J. F. Costa, M. Dines, and R. Lamprecht, "The role of Rac GTPase in dendritic spine morphogenesis and memory," *Front Synaptic Neurosci*, vol. 12, 2020.

[40] R. Pennucci, I. Gucciardi, and I. de Curtis, "Rac1 and Rac3 GTPases differently influence the morphological maturation of dendritic spines in hippocampal neurons," *PLoS One*, vol. 14, no. 8, article e0220496, 2019.

[41] L. Lv, Y. Liu, J. Xie et al., "Interplay between α2-chimaerin and Rac1 activity determines dynamic maintenance of long-term memory," *Nature Communications*, vol. 10, no. 1, p. 5313, 2019.

[42] S. De Rubeis, T. D. D. D. Study, X. He et al., "Synaptic, transcriptional and chromatin genes disrupted in autism," *Nature*, vol. 515, no. 7526, pp. 209–215, 2014.

[43] K. Hori, T. Nagai, W. Shan et al., "Heterozygous disruption of autism susceptibility candidate 2 causes impaired emotional control and cognitive memory," *PLoS One*, vol. 10, no. 12, p. e0145979, 2015.

[44] K. Hori, T. Nagai, W. Shan et al., "Cytoskeletal regulation by AUTS2 in neuronal migration and neuritogenesis," *Cell Reports*, vol. 9, no. 6, pp. 2166–2179, 2014.

[45] L. J. Duffney, J. Wei, J. Cheng et al., "Shank3 deficiency induces NMDA receptor hypofunction via an actin-dependent mechanism," *The Journal of Neuroscience*, vol. 33, no. 40, pp. 15767–15778, 2013.

[46] J. H. Lee, A. R. Espinera, D. Chen et al., "Neonatal inflammatory pain and systemic inflammatory responses as possible environmental factors in the development of autism spectrum disorder of juvenile rats," *Journal of Neuroinflammation*, vol. 13, no. 1, p. 109, 2016.

[47] T. Dong, J. He, S. Wang, L. Wang, Y. Cheng, and Y. Zhong, "Inability to activate Rac1-dependent forgetting contributes to behavioral inflexibility in mutants of multiple autism-risk genes," *Proceedings of the National Academy of Sciences of the United States of America*, vol. 113, no. 27, pp. 7644–7649, 2016.

[48] A. Astrinidis, T. P. Cash, D. S. Hunter, C. L. Walker, J. Chernoff, and E. P. Henske, "Tuberin, the tuberous sclerosis complex 2 tumor suppressor gene product, regulates Rho activation, cell adhesion and migration," *Oncogene*, vol. 21, no. 55, pp. 8470–8476, 2002.

[49] A. Sadybekov, C. Tian, C. Arnesano, V. Katritch, and B. E. Herring, "An autism spectrum disorder-related de novo mutation hotspot discovered in the GEF1 domain of Trio," *Nature Communications*, vol. 8, no. 1, p. 601, 2017.

[50] R. Sultana, C. E. Yu, J. Yu et al., "Identification of a novel gene on chromosome 7q11.2 interrupted by a translocation breakpoint in a pair of autistic twins," *Genomics*, vol. 80, no. 2, pp. 129–134, 2002.

[51] C. Betancur and J. D. Buxbaum, "SHANK3 haploinsufficiency: a "common" but underdiagnosed highly penetrant monogenic cause of autism spectrum disorders," *Molecular Autism*, vol. 4, no. 1, p. 17, 2013.

[52] M. Kouser, H. E. Speed, C. M. Dewey et al., "Loss of predominant Shank3 isoforms results in hippocampus-dependent impairments in behavior and synaptic transmission," *The Journal of Neuroscience*, vol. 33, no. 47, pp. 18448–18468, 2013.

[53] D. R. Dajani and L. Q. Uddin, "Demystifying cognitive flexibility: implications for clinical and developmental neuroscience," *Trends in Neurosciences*, vol. 38, no. 9, pp. 571–578, 2015.

[54] A. Ramos-Miguel, A. M. Barr, and W. G. Honer, "Spines, synapses, and schizophrenia," *Biological Psychiatry*, vol. 78, no. 11, pp. 741–743, 2015.

[55] D. Datta, D. Arion, J. P. Corradi, and D. A. Lewis, "Altered expression of CDC42 signaling pathway components in cortical layer 3 pyramidal cells in schizophrenia," *Biological Psychiatry*, vol. 78, no. 11, pp. 775–785, 2015.

[56] L. A. Glantz and D. A. Lewis, "Decreased dendritic spine density on prefrontal cortical pyramidal neurons in schizophrenia," *Archives of General Psychiatry*, vol. 57, no. 1, pp. 65–73, 2000.

[57] S. Y. Chen, P. H. Huang, and H. J. Cheng, "Disrupted-in-Schizophrenia 1-mediated axon guidance involves TRIO-RAC-PAK small GTPase pathway signaling," *Proceedings of the National Academy of Sciences of the United States of America*, vol. 108, no. 14, pp. 5861–5866, 2011.

[58] E. Moutin, I. Nikonenko, T. Stefanelli et al., "Palmitoylation of cdc42 promotes spine stabilization and rescues spine density deficit in a mouse model of 22q11.2 deletion syndrome," *Cerebral Cortex*, vol. 27, no. 7, pp. 3618–3629, 2017.

[59] D. Han, L. Xu, H. Xiao, G. C. Prado Schmidt, and S. Shi, "Dizocilpine reduces head diameter of dendritic spines in the hippocampus of adolescent rats," *Psychiatry Research*, vol. 210, no. 1, pp. 351–356, 2013.

[60] M. Cahill and P. Penzes, "Colocalization between endogenous erbB4 and endogenous kalirin-7 in interneuronal dendrites," *Molecular Psychiatry*, vol. 17, no. 1, p. 1, 2012.

[61] D. D. Kiraly, F. Lemtiri-Chlieh, E. S. Levine, R. E. Mains, and B. A. Eipper, "Kalirin binds the NR2B subunit of the NMDA receptor, altering its synaptic localization and function," *The Journal of Neuroscience*, vol. 31, no. 35, pp. 12554–12565, 2011.

[62] Z. Xie, D. P. Srivastava, H. Photowala et al., "Kalirin-7 controls activity-dependent structural and functional plasticity of dendritic spines," *Neuron*, vol. 56, no. 4, pp. 640–656, 2007.

[63] P. Penzes, R. C. Johnson, V. Kambampati, R. E. Mains, and B. A. Eipper, "Distinct roles for the two Rho GDP/GTP exchange factor domains of kalirin in regulation of neurite growth and neuronal morphology," *The Journal of Neuroscience*, vol. 21, no. 21, pp. 8426–8434, 2001.

[64] S. Berberich, P. Punnakkal, V. Jensen et al., "Lack of NMDA receptor subtype selectivity for hippocampal long-term potentiation," *The Journal of Neuroscience*, vol. 25, no. 29, pp. 6907–6910, 2005.

[65] C.-I. Sze, H. Bi, B. K. Kleinschmidt-DeMasters, C. M. Filley, and L. J. Martin, "N-Methyl-D-aspartate receptor subunit proteins and their phosphorylation status are altered selectively in Alzheimer's disease," *Journal of the Neurological Sciences*, vol. 182, no. 2, pp. 151–159, 2001.

[66] J. Ma, B. R. Choi, C. H. Chung, S. Min, W. Jeon, and J. S. Han, "Chronic brain inflammation causes a reduction in GluN2A and GluN2B subunits of NMDA receptors and an increase in the phosphorylation of mitogen-activated protein kinases in the hippocampus," *Molecular Brain*, vol. 7, no. 1, p. 33, 2014.

[67] K. A. Jones, D. P. Srivastava, J. A. Allen, R. T. Strachan, B. L. Roth, and P. Penzes, "Rapid modulation of spine morphology by the 5-HT2A serotonin receptor through kalirin-7 signaling," *Proceedings of the National Academy of Sciences of the United States of America*, vol. 106, no. 46, pp. 19575–19580, 2009.

[68] P. Penzes and K. A. Jones, "Dendritic spine dynamics–a key role for kalirin-7," *Trends in Neurosciences*, vol. 31, no. 8, pp. 419–427, 2008.

[69] K. F. Tolias, J. B. Bikoff, A. Burette et al., "The Rac1-GEF Tiam1 couples the NMDA receptor to the activity-dependent development of dendritic arbors and spines," *Neuron*, vol. 45, no. 4, pp. 525–538, 2005.

[70] Z. Xie, H. Photowala, M. E. Cahill et al., "Coordination of synaptic adhesion with dendritic spine remodeling by AF-6 and kalirin-7," *The Journal of Neuroscience*, vol. 28, no. 24, pp. 6079–6091, 2008.

[71] A. Hayashi-Takagi, Y. Araki, M. Nakamura et al., "PAKs inhibitors ameliorate schizophrenia-associated dendritic spine deterioration in vitro and in vivo during late adolescence," *Proceedings of the National Academy of Sciences of the United States of America*, vol. 111, no. 17, pp. 6461–6466, 2014.

[72] S. Stefanovic, B. A. DeMarco, A. Underwood, K. R. Williams, G. J. Bassell, and M. R. Mihailescu, "Fragile X mental retardation protein interactions with a G quadruplex structure in the 3'-untranslated region of NR2B mRNA," *Molecular BioSystems*, vol. 11, no. 12, pp. 3222–3230, 2015.

[73] C. M. Bonaccorso, M. Spatuzza, B. di Marco et al., "Fragile X mental retardation protein (FMRP) interacting proteins exhibit different expression patterns during development," *International Journal of Developmental Neuroscience*, vol. 42, no. 1, pp. 15–23, 2015.

[74] I. Heulens, "Fragile X syndrome: from gene discovery to therapy," *Frontiers in Bioscience*, vol. 16, no. 1, p. 1211, 2011.

[75] F. Bolduc, "Fragile X mental retardation 1 and filamin A interact genetically in Drosophila long-term memory," *Front Neural Circuits*, vol. 3, 2010.

[76] R. J. Hagerman, E. Berry-Kravis, H. C. Hazlett et al., "Fragile X syndrome," *Nature Reviews. Disease Primers*, vol. 3, no. 1, 2017.

[77] A. Rajaratnam, J. Shergill, M. Salcedo-Arellano, W. Saldarriaga, X. Duan, and R. Hagerman, "Fragile X syndrome and fragile X-associated disorders," *F1000Res*, vol. 6, p. 2112, 2017.

[78] O. Y. N. Bongmba, L. A. Martinez, M. E. Elhardt, K. Butler, and M. V. Tejada-Simon, "Modulation of dendritic spines and synaptic function by Rac1: a possible link to fragile X syndrome pathology," *Brain Research*, vol. 1399, pp. 79–95, 2011.

[79] T. A. Comery, J. B. Harris, P. J. Willems et al., "Abnormal dendritic spines in fragile X knockout mice: maturation and pruning deficits," *Proceedings of the National Academy of Sciences of the United States of America*, vol. 94, no. 10, pp. 5401–5404, 1997.

[80] M. Castets, C:. Schaeffer, E. Bechara et al., "FMRP interferes with the Rac1 pathway and controls actin cytoskeleton dynamics in murine fibroblasts," *Human Molecular Genetics*, vol. 14, no. 6, pp. 835–844, 2005.

[81] A. Lee, W. Li, K. Xu, B. A. Bogert, K. Su, and F. B. Gao, "Control of dendritic development by the Drosophila fragile X-related gene involves the small GTPase Rac1," *Development*, vol. 130, no. 22, pp. 5543–5552, 2003.

[82] M. L. Hayashi, S. Y. Choi, B. S. S. Rao et al., "Altered cortical synaptic morphology and impaired memory consolidation in forebrain- specific dominant-negative PAK transgenic mice," *Neuron*, vol. 42, no. 5, pp. 773–787, 2004.

[83] B. M. Dolan, S. G. Duron, D. A. Campbell et al., "Rescue of fragile X syndrome phenotypes in Fmr1 KO mice by the small-molecule PAK inhibitor FRAX486," *Proceedings of the National Academy of Sciences of the United States of America*, vol. 110, no. 14, pp. 5671–5676, 2013.

[84] A. Pyronneau, Q. He, J. Y. Hwang, M. Porch, A. Contractor, and R. S. Zukin, "Aberrant Rac1-cofilin signaling mediates defects in dendritic spines, synaptic function, and sensory perception in fragile X syndrome," *Science Signaling*, vol. 10, no. 504, article eaan0852, 2017.

[85] B. De Filippis, L. Ricceri, A. Fuso, and G. Laviola, "Neonatal exposure to low dose corticosterone persistently modulates hippocampal mineralocorticoid receptor expression and improves locomotor/exploratory behaviour in a mouse model of Rett syndrome," *Neuropharmacology*, vol. 68, pp. 174–183, 2013.

[86] B. Hagberg, "Rett's syndrome: prevalence and impact on progressive severe mental retardation in girls," *Acta Paediatrica Scandinavica*, vol. 74, no. 3, pp. 405–408, 1985.

[87] R. Cianfaglione, A. Clarke, M. Kerr et al., "A national survey of Rett syndrome: behavioural characteristics," *Journal of Neurodevelopmental Disorders*, vol. 7, no. 1, p. 11, 2015.

[88] J. P. Cheadle, H. Gill, N. Fleming et al., "Long-read sequence analysis of the MECP2 gene in Rett syndrome patients: correlation of disease severity with mutation type and location,"

Human Molecular Genetics, vol. 9, no. 7, pp. 1119–1129, 2000.

[89] H. Gill, J. P. Cheadle, J. Maynard et al., "Mutation analysis in the MECP2 gene and genetic counselling for Rett syndrome," *Journal of Medical Genetics*, vol. 40, no. 5, pp. 380–384, 2003.

[90] C. Keogh, G. Pini, A. H. Dyer et al., "Clinical and genetic Rett syndrome variants are defined by stable electrophysiological profiles," *BMC Pediatrics*, vol. 18, no. 1, p. 333, 2018.

[91] G. Pini, S. Bigoni, I. W. Engerström et al., "Variant of Rett syndrome and CDKL5 gene: clinical and autonomic description of 10 cases," *Neuropediatrics*, vol. 43, no. 1, pp. 37–43, 2012.

[92] Y. Sun, Y. Gao, J. J. Tidei et al., "Loss of MeCP2 in immature neurons leads to impaired network integration," *Human Molecular Genetics*, vol. 28, no. 2, pp. 245–257, 2019.

[93] S. Balakrishnan and S. L. Mironov, "CA1 neurons acquire Rett syndrome phenotype after brief activation of glutamatergic receptors: specific role of mGluR1/5," *Frontiers in Cellular Neuroscience*, vol. 12, p. 363, 2018.

[94] K. Gulmez Karaca, D. V. C. Brito, B. Zeuch, and A. M. M. Oliveira, "Adult hippocampal MeCP2 preserves the genomic responsiveness to learning required for long-term memory formation," *Neurobiology of Learning and Memory*, vol. 149, pp. 84–97, 2018.

[95] K. N. McFarland, M. N. Huizenga, S. B. Darnell et al., "MeCP2: a novel huntingtin interactor," *Human Molecular Genetics*, vol. 23, no. 4, pp. 1036–1044, 2014.

[96] W. Li and L. Pozzo-Miller, "BDNF deregulation in Rett syndrome," *Neuropharmacology*, vol. 76, pp. 737–746, 2014.

[97] R. Klein, V. Nanduri, S. Jing et al., "The Trkb tyrosine protein-kinase is a receptor for brain-derived neurotrophic factor and neurotrophin-3," *Cell*, vol. 66, no. 2, pp. 395–403, 1991.

[98] B. Lu, P. T. Pang, and N. H. Woo, "The yin and yang of neurotrophin action," *Nature Reviews. Neuroscience*, vol. 6, no. 8, pp. 603–614, 2005.

[99] C. Zuccato and E. Cattaneo, "Brain-derived neurotrophic factor in neurodegenerative diseases," *Nature Reviews. Neurology*, vol. 5, no. 6, pp. 311–322, 2009.

[100] A. Bellot, B. Guivernau, M. Tajes, M. Bosch-Morató, V. Valls-Comamala, and F. J. Muñoz, "The structure and function of actin cytoskeleton in mature glutamatergic dendritic spines," *Brain Research*, vol. 1573, pp. 1–16, 2014.

[101] Q. Chen, Y. C. Zhu, J. Yu et al., "CDKL5, a protein associated with rett syndrome, regulates neuronal morphogenesis via Rac1 signaling," *The Journal of Neuroscience*, vol. 30, no. 38, pp. 12777–12786, 2010.

[102] B. De Filippis, P. Nativio, A. Fabbri et al., "Pharmacological stimulation of the brain serotonin receptor 7 as a novel therapeutic approach for Rett syndrome," *Neuropsychopharmacology*, vol. 39, no. 11, pp. 2506–2518, 2014.

[103] C. Fuchs, G. Medici, S. Trazzi et al., "CDKL5 deficiency predisposes neurons to cell death through the deregulation of SMAD3 signaling," *Brain Pathology*, vol. 29, no. 5, pp. 658–674, 2019.

[104] C. Fuchs, L. Gennaccaro, S. Trazzi et al., "Heterozygous CDKL5 knockout female mice are a valuable animal model for CDKL5 disorder," *Neural Plasticity*, vol. 2018, Article ID 9726950, 18 pages, 2018.

[105] B. L. Tang, "Unconventional secretion and intercellular transfer of mutant huntingtin," *Cell*, vol. 7, no. 6, p. 59, 2018.

[106] R. K. Graham, M. A. Pouladi, P. Joshi et al., "Differential susceptibility to excitotoxic stress in YAC128 mouse models of Huntington disease between initiation and progression of disease," *The Journal of Neuroscience*, vol. 29, no. 7, pp. 2193–2204, 2009.

[107] M. E. Schmidt, C. Buren, J. P. Mackay et al., "Altering cortical input unmasks synaptic phenotypes in the YAC128 corticostriatal co-culture model of Huntington disease," *BMC Biology*, vol. 16, no. 1, p. 58, 2018.

[108] A. Reiner, R. L. Albin, K. D. Anderson, C. J. D'Amato, J. B. Penney, and A. B. Young, "Differential loss of striatal projection neurons in Huntington disease," *Proceedings of the National Academy of Sciences of the United States of America*, vol. 85, no. 15, pp. 5733–5737, 1988.

[109] C. Tourette, B. Li, R. Bell et al., "A large scale huntingtin protein interaction network implicates Rho GTPase signaling pathways in Huntington disease," *The Journal of Biological Chemistry*, vol. 289, no. 10, pp. 6709–6726, 2014.

[110] A. Tousley, M. Iuliano, E. Weisman et al., "Rac1 activity is modulated by huntingtin and dysregulated in models of Huntington's disease," *Journal of Huntington's Disease*, vol. 8, no. 1, pp. 53–69, 2019.

[111] A. Valencia, E. Sapp, J. S. Kimm et al., "Elevated NADPH oxidase activity contributes to oxidative stress and cell death in Huntington's disease," *Human Molecular Genetics*, vol. 22, no. 6, pp. 1112–1131, 2013.

[112] H. Marei and A. Malliri, "GEFs: dual regulation of Rac1 signaling," *Small GTPases*, vol. 8, no. 2, pp. 90–99, 2016.

[113] H. Marei and A. Malliri, "Rac1 in human diseases: the therapeutic potential of targeting Rac1 signaling regulatory mechanisms," *Small GTPases*, vol. 8, no. 3, pp. 139–163, 2016.

[114] Y. Gao, J. B. Dickerson, F. Guo, J. Zheng, and Y. Zheng, "Rational design and characterization of a Rac GTPase-specific small molecule inhibitor," *Proceedings of the National Academy of Sciences of the United States of America*, vol. 101, no. 20, pp. 7618–7623, 2004.

[115] Q. G. Zhang, R. Wang, D. Han, Y. Dong, and D. W. Brann, "Role of Rac1 GTPase in JNK signaling and delayed neuronal cell death following global cerebral ischemia," *Brain Research*, vol. 1265, pp. 138–147, 2009.

[116] Z. Zhou, J. Hu, M. Passafaro, W. Xie, and Z. Jia, "GluA2 (GluR2) regulates metabotropic glutamate receptor-dependent long-term depression through N-cadherin-dependent and cofilin-mediated actin reorganization," *The Journal of Neuroscience*, vol. 31, no. 3, pp. 819–833, 2011.

[117] I. H. Kim, S. K. Park, S. T. Hong et al., "Inositol 1,4,5-trisphosphate 3-kinase A functions as a scaffold for synaptic Rac signaling," *The Journal of Neuroscience*, vol. 29, no. 44, pp. 14039–14049, 2009.

[118] P. Wu, Z. B. Ding, S. Q. Meng et al., "Differential role of Rac in the basolateral amygdala and cornu ammonis 1 in the reconsolidation of auditory and contextual Pavlovian fear memory in rats," *Psychopharmacology*, vol. 231, no. 15, pp. 2909–2919, 2014.

[119] K. Zins, T. Lucas, P. Reichl, D. Abraham, and S. Aharinejad, "A Rac1/Cdc42 GTPase-specific small molecule inhibitor suppresses growth of primary human prostate cancer xenografts and prolongs survival in mice," *PLoS One*, vol. 8, no. 9, article e74924, 2013.

[120] B. L. Montalvo-Ortiz, L. Castillo-Pichardo, E. Hernández et al., "Characterization of EHop-016, novel small molecule

inhibitor of Rac GTPase," *The Journal of Biological Chemistry*, vol. 287, no. 16, pp. 13228–13238, 2012.

[121] D. K. Worthylake, K. L. Rossman, and J. Sondek, "Crystal structure of Rac1 in complex with the guanine nucleotide exchange region of Tiam1," *Nature*, vol. 408, no. 6813, pp. 682–688, 2000.

[122] N. Bouquier, E. Vignal, S. Charrasse et al., "A cell active chemical GEF inhibitor selectively targets the Trio/Rho-G/Rac1 signaling pathway," *Chemistry & Biology*, vol. 16, no. 6, pp. 657–666, 2009.

[123] G. Cardama, M. Comin, L. Hornos et al., "Preclinical development of novel Rac1-GEF signaling inhibitors using a rational design approach in highly aggressive breast cancer cell lines," *Anti-Cancer Agents in Medicinal Chemistry*, vol. 14, no. 6, pp. 840–851, 2014.

[124] C. Onesto, A. Shutes, V. Picard, F. Schweighoffer, and C. J. der, "Characterization of EHT 1864, a novel small molecule inhibitor of Rac family small GTPases," *Methods in Enzymology*, vol. 439, pp. 111–129, 2008.

[125] A. Klaus et al., *A polypeptide capable of glycosylating tyrosine residues of target proteins*, WO, 2014.

[126] C. Dong et al., *Use of Rac1 inhibitors to treat Kaposi's sarcoma*, 2009, US2008/011916.

[127] N. Gonzalez, G. A. Cardama, M. J. Comin et al., "Pharmacological inhibition of Rac1-PAK1 axis restores tamoxifen sensitivity in human resistant breast cancer cells," *Cellular Signalling*, vol. 30, pp. 154–161, 2017.

[128] F. Raynaud, E. Moutin, S. Schmidt et al., "Rho-GTPase-activating protein interacting with Cdc-42-interacting protein 4 homolog 2 (Rich2): a new Ras-related C3 botulinum toxin substrate 1 (Rac1) GTPase-activating protein that controls dendritic spine morphogenesis," *The Journal of Biological Chemistry*, vol. 289, no. 5, pp. 2600–2609, 2014.

Hindawi
Neural Plasticity
Volume 2020, Article ID 8872296, 14 pages
https://doi.org/10.1155/2020/8872296

Research Article

Pretreatment of Ascorbic Acid Inhibits MPTP-Induced Astrocytic Oxidative Stress through Suppressing NF-κB Signaling

Xiaokang Zeng,[1] **Kai Xu**,[2,3,4] **Ji Wang**,[2,3,4] **Yunqi Xu**,[2] **and Shaogang Qu**[2,3,4]

[1]*Central Laboratory, Shunde Hospital, Southern Medical University (The First People's Hospital of Shunde Foshan), Foshan, 528300 Guangdong, China*
[2]*Department of Neurology, Nanfang Hospital, Southern Medical University/The First School of Clinical Medicine, Southern Medical University, Guangzhou, Guangdong 510515, China*
[3]*Central Laboratory and Department of Neurology, Shunde Hospital, Southern Medical University (The First People's Hospital of Shunde Foshan), Foshan, Guangdong, China*
[4]*Key Laboratory of Mental Health of the Ministry of Education, Southern Medical University, Guangzhou, China*

Correspondence should be addressed to Yunqi Xu; 358353103@qq.com and Shaogang Qu; sgq9528@163.com

Received 24 July 2020; Revised 21 September 2020; Accepted 14 October 2020; Published 17 November 2020

Academic Editor: Fushun Wang

Astrocytes are a major constituent of the central nervous system (CNS). Astrocytic oxidative stress contributes to the development of Parkinson's disease (PD). Maintaining production of antioxidant and detoxification of reactive oxygen and nitrogen species (ROS/RNS) in astrocytes is critical to prevent PD. Study has illuminated that ascorbic acid (AA) stimulates dopamine synthesis and expression of tyrosine hydroxylase in human neuroblastoma cells. However, the role and regulatory mechanisms of AA on detoxification of astrocytes are still unclear. The purpose of our study is in-depth study of the regulatory mechanism of AA on detoxification of astrocytes. We found that AA pretreatment decreased the expression of ROS and inducible nitric oxide synthase (iNOS) in MPP^+-treated astrocytes. In contrast, the expression levels of antioxidative substances—including superoxide dismutase (SOD), glutathione (GSH), and glutamate-cysteine ligase modifier (GCLM) subunit—were upregulated after AA pretreatment in MPP^+-treated astrocytes. However, inhibition of NF-κB prevented such AA induced increases in antioxidative substances following MPP^+ treatment in astrocytes, suggesting that AA improved antioxidative function of astrocytes through inhibiting NF-κB-mediated oxidative stress. Furthermore, *in vivo* studies revealed that AA preadministration also suppressed NF-κB and upregulated the expression levels of antioxidative substances in the midbrain of MPTP-treated mice. Additionally, pretreatment of AA alleviated MPTP-induced PD-like pathology in mice. Taken together, our results demonstrate that preadministration of AA improves the antioxidative function of astrocytes through suppressing NF-κB signaling, following alleviated the pathogenesis of PD which induced by MPTP. Hence, our findings elucidate a novel protective mechanism of AA in astrocytes.

1. Introduction

Parkinson's disease (PD) is the second-most prevalent neurodegenerative disease following Alzheimer's disease and is the most common movement-disorder disease worldwide [1]. Approximately 2% of individuals over 65 years old are afflicted with PD. The prevention situation of PD is very grim. The motor symptoms of PD include bradykinesia, cogwheel rigidity, resting tremor, a slow shuffling gait, and difficulty maintaining balance. Nonmotor symptoms of PD include cognitive decline, depression, anxiety, and sleep disturbances [2]. The pathological hallmarks of PD include depigmentation of the substantia nigra, dopaminergic neuronal loss in the pars compacta of the substantia nigra, and formation of Lewy bodies/cytoplasmic inclusions containing fibrillar α-synuclein in the substantia nigra compacta (SNpc) [3]. Currently, levodopa coupled with a DOPA decarboxylase inhibitor is the most effective therapy for PD. However, there are some side effects during levodopa therapy, such as dizziness and gastrointestinal disturbances. Thus, there is a

continued need to further identify and develop novel therapeutic agents for PD [4].

Astrocyte is the major class of glial cells in the CNS, providing critical structural and metabolic support for neurons. However, growing evidence shows that oxidative stress of astrocytes contributes to PD pathogenesis. Astrocytes may play a key role in the pathogenesis of PD via oxidative and nitrosative stress [5]. Postmortem analysis of the brains of PD patients and experimental animal models indicate that astrocyte activation and elevated ROS/RNS levels are the pathogenic features of PD [6]. Toxins can trigger excessive formation of reactive oxygen species (ROS), the byproducts of oxygen metabolism including superoxides, hydroxyl radicals, and nitric monoxide, play essential roles in cell signaling, gene transcription, and microbial defense [7]. When the levels of ROS exceed the detoxification capacity of the astrocytic antioxidant system, it leads to pathological oxidative stress [8]. Exposure to environmental toxicants such as 1-methyl-4-phenyl-1,2,3,6-tetrahydropyridine (MPTP), rotenone, and manganese (Mn) may induce reactive astrogliosis and subsequent astrocytic oxidative/nitrosative stress [9–11]. Therefore, elucidating the role of astrocytic oxidative/nitrosative stress in the pathogenesis of PD may greatly expand our understanding of PD. Although the contribution of astrocytic oxidative stress to PD needs to elucidated, the presence of oxidative metabolites in PD patients is related to the in vitro aggregation of α-synuclein [12]. In the SNpc of PD patients, the level of the antioxidant molecule GSH secreted mainly by astrocytes is significantly decreased, and the activities of astrocyte-secreted antioxidant enzymes such as SOD, GSH peroxidase (GSH-Px), and catalase (CAT) are significantly decreased compared to healthy controls [13]. Taken together, these findings suggest that there is a need to continue to explore treatments for PD by targeting oxidative/nitrosative stress in astrocytes.

Ascorbic acid (AA) has many different functions in the CNS, including the following: (1) it crosses the blood-brain barrier and has been tested as a potential drug for treating degenerative diseases; (2) it promotes neuronal differentiation, maturation, and survival; and (3) it participates in catecholaminergic synthesis and modulates neurotransmission [14]. However, its role in the astrocytic oxidative stress is still clear. Lee et al. found that AA promoted differentiation of astrocytes by enhancing the expression of NeuroD, Notch, bone morphogenetic protein 2 (BMP2), and bone morphogenetic protein 7 (BMP7) [15]. Secretion of brain-derived neurotrophic factor (BDNF) by astrocytes is also increased after administration of AA *in vitro*, which contributes to cellular survival by enhancing the expression of SOD and GSH [16]. However, there are some different views, Kao et al. found that rat brain astrocytes (RBA-1 cells) incubated with AA for 2 days or 7 days, the SOD activity, SOD mRNA level, and SOD protein level were significantly decreased [17]. But Sanchez-Moreno et al. found that AA has a protective effect against the ethanol-mediated toxic effects on human brain glial cells by reducing the expression of cyclooxygenase-2 (COX-2) and synthesis of prostaglandin E2 (PGE2) [18]. Thus, we hypothesize that AA may have a protective effect on PD by inhibiting astrocytic oxidative stress.

In the present study, we revealed that AA decreased ROS production in astrocytes *in vitro* via inhibition of NF-κB-mediated oxidative stress. Pretreatment of AA improved behavioral performance and restored tyrosine dehydrogenase expression in MPTP-treated mice *in vivo*. Thus, our findings demonstrated that pretreatment of AA alleviated MPTP-induced PD symptoms through inhibiting astrocytic oxidative stress. Collectively, our findings unveil a protective role of AA in astrocytic oxidative stress and suggest that AA may represent a therapeutic drug for PD.

2. Materials and Methods

2.1. Animals and Treatments. The protocols used for animal experiments were approved by the Institutional Animal Care and Use Committee of Southern Medical University. All procedures involving animals were approved by the Animal Ethics Committee of Southern Medical University. Male C57BL/6 mice (8-week old) were used in our experiments. The mice were from Guangdong Medical Animal Laboratory (Foshan, China). All animals were provided food and water *ad libitum*, under a 12/12-hour light/dark cycle. Age- and weight-matched animals were randomly assigned to each group. Animal experiments were conducted in the following four groups ($n = 20$ for each group): a saline-treated control group, AA-treated group, MPTP-treated group, and AA+MPTP-treated group. AA (Sigma, A7506, MO, US) was dissolved in saline solution. Mice received intraperitoneal injections of AA at 100 mg/kg every three days for 60 days. After supplementation with AA for two months, mice simultaneously received AA and intraperitoneal injections of MPTP (Sigma, M0896, MO, US) every three days (25 mg/kg in saline) for 35 days, the animals received AA during MPTP injection. After MPTP lesion, behavioral experiments were conducted. Subsequently, mice were euthanized, and their midbrains were quickly dissected for analyses in various assays. The mortality rate in the MPTP-treated group was approximately 20%; however, no mice died in any of the other groups.

2.2. Cell Culture. Primary midbrain astrocytes were obtained from one-day-old C57BL/6 pups, as previously described by our group [19]. Mice pups were anesthetized with isoflurane and then the cerebral hemispheres were removed, after which midbrains were collected in ice-cold phosphate-buffered solution (PBS). Tissue was thoroughly chopped with scissors and was then incubated in 0.25% trypsin–EDTA for 10 min at 37°C. DMEM/F12 (Gibco, 11330057, MA, US) supplemented with 10% fetal bovine serum (FBS) (Gibco, 26010074, MA, US) was then added to stop digestion. After centrifugation (1,000 rpm) for 5 min, each pellet was resuspended and seeded into a T75 flask (Corning, 43072, NY, US). The culture medium was changed every three days. Cells were cultured for seven days, and the microglia and oligodendrocytes were then removed by thermostatic oscillation at 200 rpm for 18 h. Astrocytes were identified by immunofluorescence with an antibody against glial fibrillary acidic protein (GFAP) (CST, #3670, MA, US).

2.3. Detection of Intracellular Reactive Oxygen Species. Intracellular ROS were detected by a 2,7dichlorodi-hydrofluorescein diacetate (DCFH-DA) fluorescence assay (Beyotime, S003M, Shanghai, China). Briefly, astrocytes were seeded into confocal dish at a density of 2×10^5 cells/well and were cultured overnight. After treatment with AA and/or MPTP, cells were incubated in serum-free medium containing 10 mM of DCFH-DA at 37°C in an incubator for 6 h. Each dish was subsequently washed three times with cold PBS to remove unbound DCFH-DA. Images were acquired vial laser-scanning confocal microscopy (Leica, SP8, Wetzlar, Germany), and the same settings were used for all samples in each experiment. Fluorescent intensities were calculated using the Image-Pro Plus 6.0 software (Silver Spring, MD, US).

2.4. Immunohistochemistry. For immunohistochemistry, mice were anesthetized and transcardially perfused with both freshly prepared PBS and, subsequently, 4% paraformaldehyde (Sangon, E672002, Shanghai, China) in PBS. After mice were decapitated, their brains were dissected. Brain tissue samples were embedded in optimum-cutting temperature compound (Leica, DJ-LDB-004, Nussloch, Germany) and stored at -80°C. Serial 10 μm-thick coronal tissue sections were cut using a freezing microtome (Leica, CM1950, Nussloch, Germany). Citrate buffer (Sangon, E673002, Shanghai, China) was added to the sections to retrieve antigens. Sections were treated with 3% hydrogen peroxide (Sigma, 323381, MO, USA) for 10 min to enable penetration and were then blocked with 5% BSA (Sangon, E661003, Shanghai, China) for 30 min at room temperature. Sections were incubated overnight at 4°C with primary antibodies as follows: tyrosine hydroxylase (TH) antibody (Santa Cruz, sc-25269). After washing three times with PBS (5 min each wash). Sections were incubated sequentially in HRP-conjugated goat anti-mouse (Beyotime, A0208) and goat anti-rabbit secondary antibody (Beyotime, A0216) for 2 h at 37°C. Sections were visualized with a 3,3-diaminobenzidine (DAB) peroxidase substrate kit (Boster, AR1022). Integrated optical density (IOD) was determined using an Image-Pro Plus 6.0 photogram analysis system (IPP 6.0; Media Cybernetics, Bethesda, MD, US).

2.5. Western Blotting. Cells or midbrain tissues were added to 100 μl/10^6 cells or 500 μl/g tissue of RIPA buffer (Beyotime, P0013E) containing 1 mM of phenylmethanesulfonyl fluoride (PMSF) (Beyotime, ST506) and were then lysed for 1 h on ice. Extracts were centrifuged for 10 min at 14,000 rpm. Protein concentrations were measured by BCA assays (Beyotime, P0012S). Samples were diluted with protein loading buffer and heated to 95°C for 10 min and were stored at -80°C prior to Western blotting. Protein extracts were separated by SDS-PAGE on 12% polyacrylamide gels and were subsequently electrophoretically transferred to a PVDF membrane (Millipore, GVHP29325). After blocking with 5% (w/v) BSA in Tris-buffered saline with tween (TBST) at room temperature for 2 h, membranes were then incubated with an appropriate specific primary antibody from Santa Cruz (anti-TH, sc-25269; anti-SOD1, sc-101523; anti-gp91phox, sc-130543; anti-p47phox, sc-17844; anti-GCLM, sc-55586; anti-HO-1, sc-390991; anti-PGC-1α, sc-518025; anti-pp65, sc-166748; anti-p65, sc-8008; anti-piκBα, sc-52943; anti-iκBα, sc-1643; anti-pp38, sc-166182; anti-p38, sc-81621; anti-p-ERK1/2, sc-81492; anti-ERK1/2, sc-135900; anti-pJNK1/2, sc-293136; anti-JNK1/2, sc-137019; and anti-β-actin, sc-8432) at 4°C overnight, followed by incubation with an HRP-conjugated secondary antibody [anti-mouse, -rabbit, or -goat (Beyotime, A0208; A0216); or anti-sheep, (Abcam, ab6764)]. Detection was performed using an enhanced chemiluminescence kit (Thermo Scientific, 32106) according to the manufacturer's instructions. For analysis of phosphorylated protein, total protein was set as a loading control, and for other protein, β-actin was set as a loading control. Protein-band density values of total proteins were normalized to β-actin, and protein-band density values of phosphorylated proteins were normalized to their total proteins. Protein-band densities were measured using the ImageJ software. Data were collected from at least three independent experiments.

2.6. Determination of Intracellular Superoxide Dismutase and Glutathioneactivity. Total SOD and GSH activities in cell culture supernatants were determined using total SOD and GSH assay kits with WST-8 (Beyotime, S0101M; S0053), based on the protocols provided by the manufacturer [20].

2.7. Open-Field Test. Locomotion behavior was evaluated in a square open field [21]. The open-field apparatus consisted of a black PVC box (Ugo Basile, Italy) with the following dimensions: 44 cm (l) × 44 cm (w) × 30 cm (h). The floor was divided into nine equal squares using brightly colored tape to facilitate quantification of locomotion. Mice were transported to the testing room before testing. For each test, pups were placed in the center of the box and allowed to explore the arena for 1 min.

2.8. Rotarod Test. Motor coordination and balance were assessed by an automated four-lane rotarod unit (Ugo Basile, Italy) every three days after MPTP lesion. The mice were pretrained for three days (at 8 rpm on day 1, at 10 rpm on day 2, and 12 rpm on day 3) to reach a stable performance. The mice were placed on the rod, and the rotation speed was started at 4 rpm and was then accelerated to 40 rpm within 2 min. The latency to fall from the rod was automatically recorded.

2.9. Grip Strength Test. Muscle strength in all four limbs was determined using a grip strength meter (Ugo Basile, 47200, Italy) after MPTP-induced lesions.

2.10. Pole Test. Mice were placed on the peak of a foam ball (diameter: 2.0 cm) fixed on a stick (diameter: 1.0 cm; length: 50 cm). The climbing time from the peak to the bottom of the stick was then recorded for each mouse, and each mouse had to have at least three successful trials.

2.11. Statistical Analysis. All experimental results are expressed as the mean ± standard deviation (SD) and were plotted using the GraphPad Prism 7 software (IBM Corp., Armonk, NY, US). Statistical analysis of data was performed by LSD or Dunnett's posttests based on the ANOVA for multivariate data analysis using SPSS 22.0 (SPSS Inc., Chicago, IL, US). A P

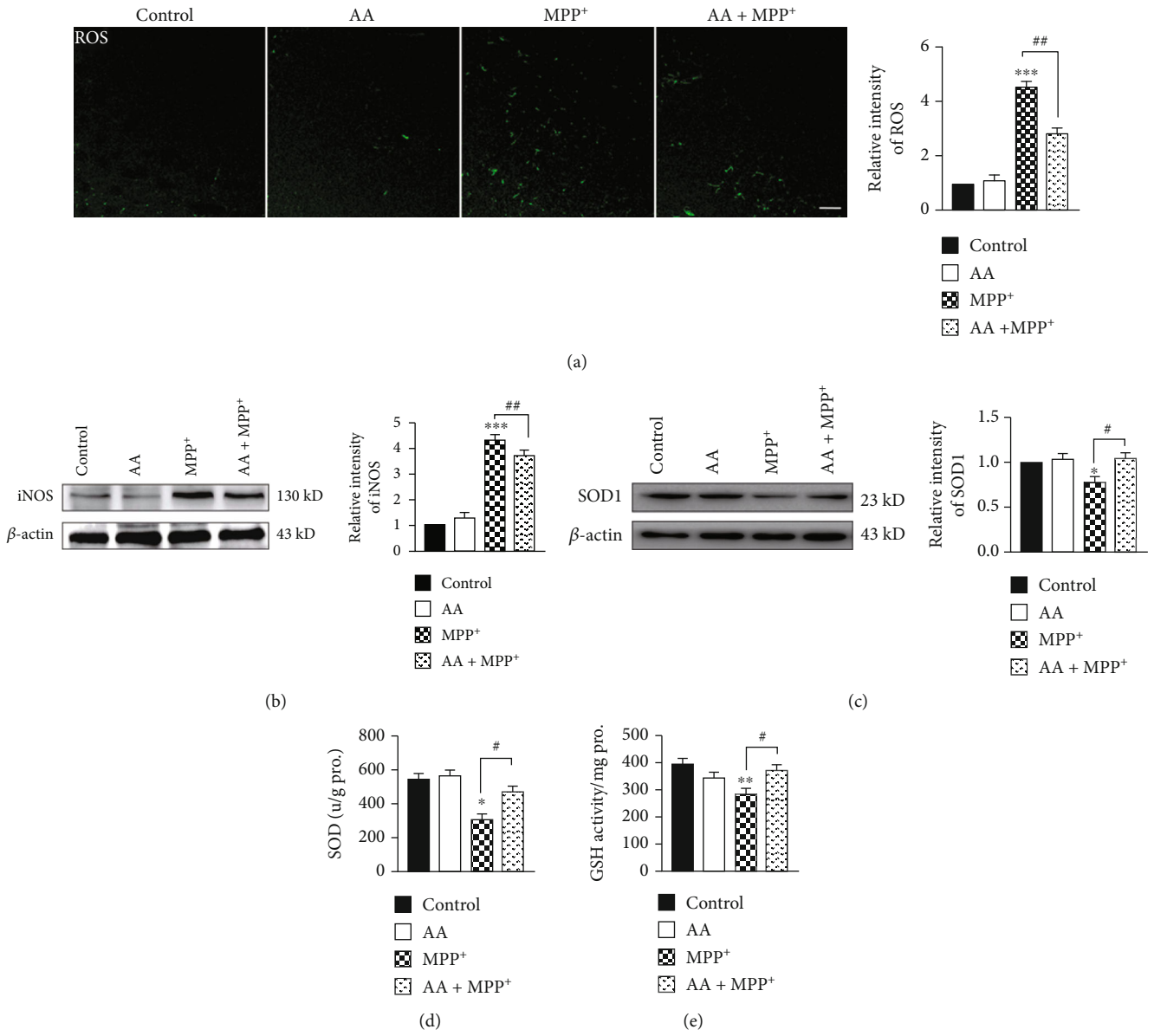

Figure 1: Ascorbic acid reduces MPP^+-induced reactive oxygen species (ROS) and inducible nitric oxide synthase (iNOS) production and increases antioxidant expression in astrocytes *in vitro*. Primary astrocytes were treated with 1 mM of AA for 24 h and/or 1 mM of MPP^+ for another 24 h. (a) Intracellular ROS was measured using the carboxy-H2DCFDA method (scale bar, 20 μm) ($n = 3$). (b) The expression of iNOS was detected by Western blotting ($n = 3$). (c) The expression of SOD1 was detected by Western blotting ($n = 3$). (d) The concentration of SOD in the supernatant from primary astrocytes was detected by ELISAs ($n = 3$). (e) The concentration of GSH in the supernatant from primary astrocytes was detected by ELISAs ($n = 3$). Data were obtained from three independent experiments. One-way ANOVAs followed by LSD pairwise comparisons were performed. * was considered significant compared to control ($^*P < 0.05$, $^{**}P < 0.01$, and $^{***}P < 0.001$). # was considered significant compared to MPTP or MPP^+ ($^{\#}P < 0.05$, $^{\#\#}P < 0.01$, and $^{\#\#\#}P < 0.001$).

value of less than 0.05 was considered statistically significant (* denotes significance compared to control: $^*P < 0.05$, $^{**}P < 0.01$, and $^{***}P < 0.001$; # denotes significance compared to MPTP or MPP^+: $^{\#}P < 0.05$, $^{\#\#}P < 0.01$, and $^{\#\#\#}P < 0.001$).

3. Results

3.1. Ascorbic Acid Reduces MPP^+-Induced Reactive Oxygen Species and Inducible Nitric Oxide Synthase Production and Enhances Antioxidant Expression in Astrocytes In Vitro. MPP^+ is known to induce oxidative stress *in vitro*. After MPP^+ treatment, a large quantity of ROS accumulated in primary astrocytes *in vitro*. To examine whether AA prevents the production of ROS after MPP^+ treatment, the accumulation of ROS in astrocytes was measured using the fluorescent probe, DCFH-DA. We found that 1 mM of MPP^+ induced increased intracellular ROS production in astrocytes after 24 h of treatment. However, pretreatment with AA inhibited MPP^+-induced production of ROS (Figure 1(a)). Oxidative stress plays an important role in

the onset of PD, as it induces glial cells to overexpress inducible nitric oxide synthase (iNOS), which results in the production of toxic levels of NO in neurons. In our present study, we found that after MPP^+ treatment, the iNOS expression was significantly increased. However, AA pretreatment significantly decreased MPP^+-induced iNOS expression compared to that of the MPP^+ group not receiving AA (Figure 1(b)). The antioxidant system is responsible for removing oxidizing substances. The main antioxidant enzymes are SOD, POD, and glutathione reductase. We found that the expression of SOD1 was decreased in astrocytes after MPP^+ treatment. In contrast, AA pretreatment significantly increased SOD1 expression compared to that of the MPP^+ group not receiving AA (Figure 1(c)). We also detected antioxidants in the supernatant of astrocytes. We found that the released levels of SOD and GSH from astrocytes in the AA-pretreated MPP^+ group were higher than those in the MPP^+ group (Figures 1(d) and 1(e)). These results indicate that AA improved antioxidative function in MPP^+-treated astrocytes.

3.2. Ascorbic Acid Inhibits MPP^+-Induced Nicotinamide Adenine Dinucleotide Phosphate (NADPH) Activation and Enhances the Expression of Antioxidative Proteins in Astrocytes In Vitro. Many glial enzymes are involved in the formation of ROS. NADPH oxidase plays an important role in producing ROS in the brain. In our present study, we found that the NADPH oxidase subunit, gp91phox, was activated after MPP^+ treatment. In contrast, AA pretreatment reduced the MPP^+-induced expression of gp91phox. However, the expression of another NADPH oxidase subunit, p47phox, was not changed from any treatment (Figures 2(a) and 2(b)). These results suggest that AA decreased MPP^+-induced NADPH oxidase activity through inhibiting gp91phox expression. Glutamate-cysteine ligase modifier (GCLM) subunit belongs to the aldo/keto reductase family. GCLM catalyzes the first step of GSH synthesis. In our present study, we found that MPP^+ treatment decreased the expression of GCLM in astrocytes after 24 h of stimulation, which was reversed by AA pretreatment (Figure 2(c)). Heme oxygenase-1 (HO-1) is expressed in many cell types, including astrocytes, and has been identified as an important endogenous protective factor induced by various stimulants, such as oxidative stress, heat shock, and endotoxins. Herein, we found that the expression of HO-1 in astrocytes exposed to MPP^+ was significantly increased. Compared to that in the MPP^+ group, the expression of HO-1 was significantly increased in the AA-pretreated MPP^+ group (Figure 2(d)). Peroxisome proliferator-activated receptor gamma coactivator-1 alpha (PGC-1α) is a newly characterized transcriptional regulator that plays a key role in antioxidant stress systems. To investigate the effect of AA on PGC-1α, we examined the protein level of PGC-1α in astrocytes. Treatment with 0.5 mM of MPP^+ increased the expression of PGC-1α. Preadministration of AA could further enhanced MPP^+-induced expression of PGC-1α (Figure 2(e)). These results indicate that AA inhibited NADPH oxidase and upregulated the expression of antioxidative proteins in MPP^+-treated astrocytes *in vitro*.

3.3. Ascorbic Acid Inhibits MPP^+-Induced Nuclear Factor-κB (NF-κB) Activation but Does Not Affect Mitogen-Activated Protein Kinasep38/Extracellular-Regulated Protein Kinases (ERK) or c-Jun N-Terminal Kinase (JNK) Signaling in Astrocytes In Vitro. In our present study, we found that AA decreased the MPP^+-induced activation of NADPH oxidase, which inhibited the production of ROS and eventually led to increased expression of antioxidant proteins. However, which signal pathways are involved in this process remain unclear. Therefore, we next assayed the classical MAPK signaling pathway and its downstream NK-κB signaling pathway. We found that MPP^+ stimulation elevated the expression levels of phosphorylated p65 and iκBα. However, preadministration with AA reversed the MPP^+-induced expression of phosphorylated p65 and iκBα (Figures 3(a) and 3(b)). MPP^+ treatment elevated the expression levels of phosphorylated JNK, ERK, and p38, but pretreated with AA did not change any of these MPP^+-induced changes in expression levels (Figures 3(c)–3(e)). These results indicate that AA administration decreased the MPP^+-induced activation of p65, decreasing the level of astrocytic oxidative stress.

3.4. Inhibition of NF-κB Signaling Blocks the Antioxidative Effects of Ascorbic Acid and Perpetuates Cytotoxicity in MPP^+-Treated Astrocytes In Vitro. To determine the role of NF-κB in the antioxidation of AA in MPP^+-treated astrocytes, we administrated QNZ (Selleck, EVP4593) to inhibit NK-κB activation. We found that after QNZ administration, MPP^+-induced expression of phosphorylated p65 was decreased significantly (Figure 4(a)). Next, we tested whether inhibition of NF-κB affected the production of ROS in astrocytes. We found that after QNZ administration, the production of ROS in astrocytes was significantly reduced in the MPP^+ group but AA-pretreatment MPP^+ group was unaffected in the control group and AA group (Figure 4(b)). We also detected the expression of iNOS in astrocytes with or without NF-κB inhibition. The results showed that the expression of iNOS was decreased in the AA-pretreatment MPP^+ group compared to that in the MPP^+ group. However, the expression of iNOS was comparable between the AA-pretreatment MPP^+ group and MPP^+ group after NF-κB inhibition (Figure 4(c)). Since the MPP^+-induced productions of ROS and iNOS were reduced after NF-κB inhibition, we next investigated whether inhibition NF-κB disturbs the expression of antioxidative enzymes in MPP^+-treated astrocytes. We found that the MPP^+-induced expression of SOD1 was reduced after NF-κB inhibition. Additionally, there was no significant difference in SOD1 expression between the AA-pretreatment MPP^+ group and MPP^+ group following NF-κB inhibition (Figure 4(d)). Furthermore, we determined whether NF-κB inhibition changed the release of SOD and GSH from astrocytes. We found that the MPP^+-induced levels of released SOD1 and GSH were decreased after NF-κB inhibition. Furthermore, there was no difference in SOD and GSH levels between the AA-pretreatment MPP^+ group and MPP^+ group following NF-κB inhibition (Figures 4(e) and 4(f)). These results indicate that AA exerted antioxidative

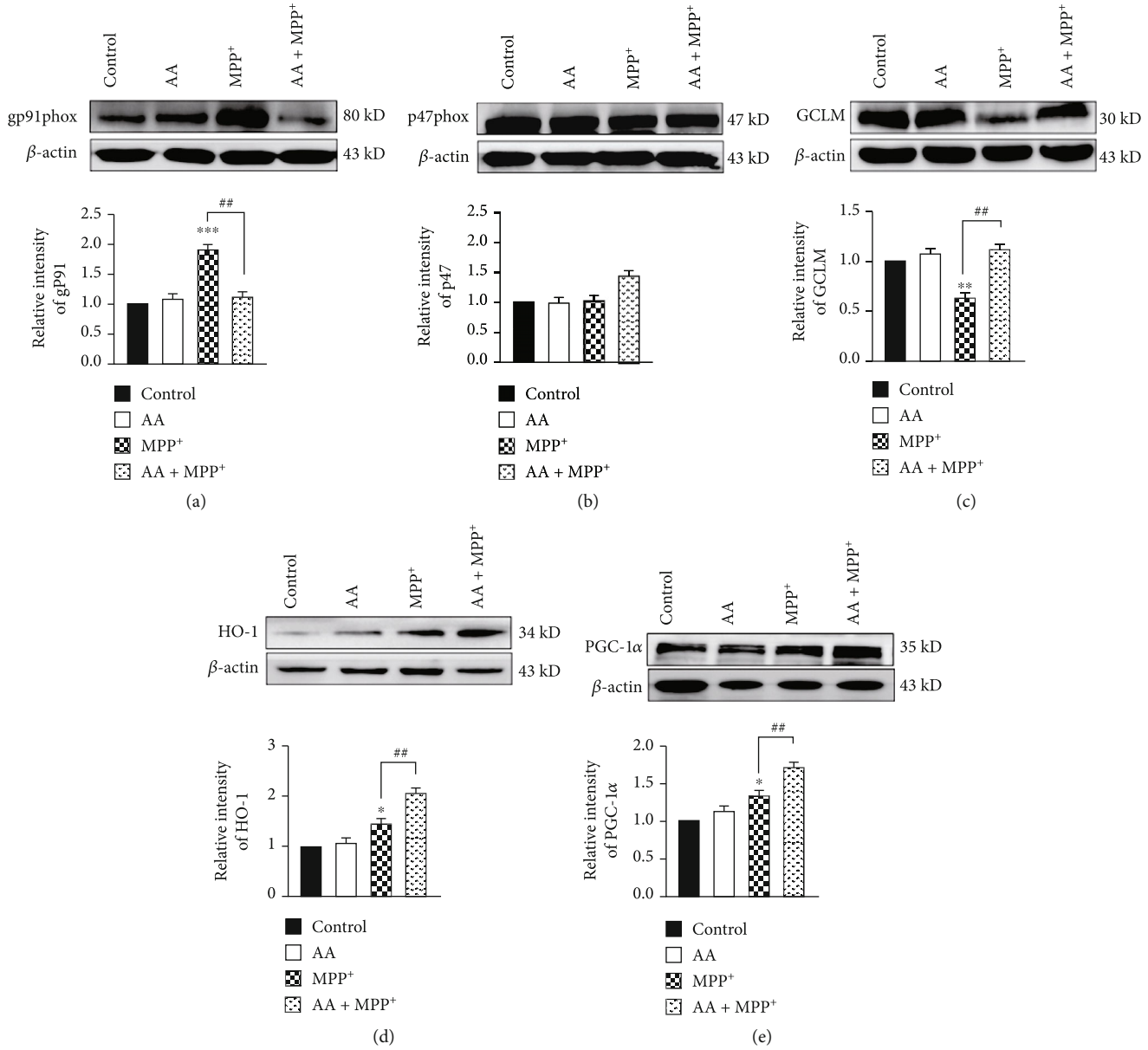

Figure 2: Ascorbic acid inhibits MPP^+-induced nicotinamide adenine dinucleotide phosphate (NADPH) oxidase activation and enhances the expression of antioxidative proteins in astrocytes *in vitro*. Primary astrocytes were treated with 1 mM of AA for 24 h and/or 1 mM of MPP^+ for another 24 h. (a) The expression of total gp91phox was detected by Western blotting ($n = 3$). (b) The expression of total p47phox was detected by Western blotting ($n = 3$). (c) The expression of GCLM was detected by Western blotting ($n = 3$). (d) The expression of HO-1 was detected by Western blotting ($n = 3$). (e) The expression of PGC-1α was detected by Western blotting ($n = 3$). Data were obtained from three independent experiments. One-way ANOVAs followed by LSD pairwise comparisons were performed. * was considered significant compared to control ($^*P < 0.05$, $^{**}P < 0.01$, and $^{***}P < 0.001$). # was considered significant compared to MPTP or MPP^+ ($^{\#}P < 0.05$, $^{\#\#}P < 0.01$, and $^{\#\#\#}P < 0.001$).

effects in MPP^+-treated astrocytes *in vitro* through NF-κB signaling.

3.5. Inhibition of NF-κB Signaling Blocks the Protective Effects of Ascorbic Acid in MPP^+-Induced Astrocytes In Vitro through Suppressing the Expression of Antioxidative Proteins. We demonstrated that AA exerted its role in inhibiting MPP^+-induced oxidative stress via the NF-κB pathway. Next, we assessed whether blocking NF-κB disrupted the expression of antioxidative proteins. We first inhibited p65 phosphorylation by QNZ, and then administered AA and/or MPP^+ to primary astrocytes *in vitro*. Finally, we collected the total protein from each group and detected the expression of GCLM, HO-1, and PGC-1α via Western blotting. We found that inhibition of NF-κB did not affect the expression of these proteins under control conditions. However, inhibition of NF-κB eliminated the differences in expression levels of GCLM, HO-1, and PGC-1α between the AA-pretreatment MPP^+ group and MPP^+ group (Figures 5(a)–5(c)). These results suggest that blocking NF-

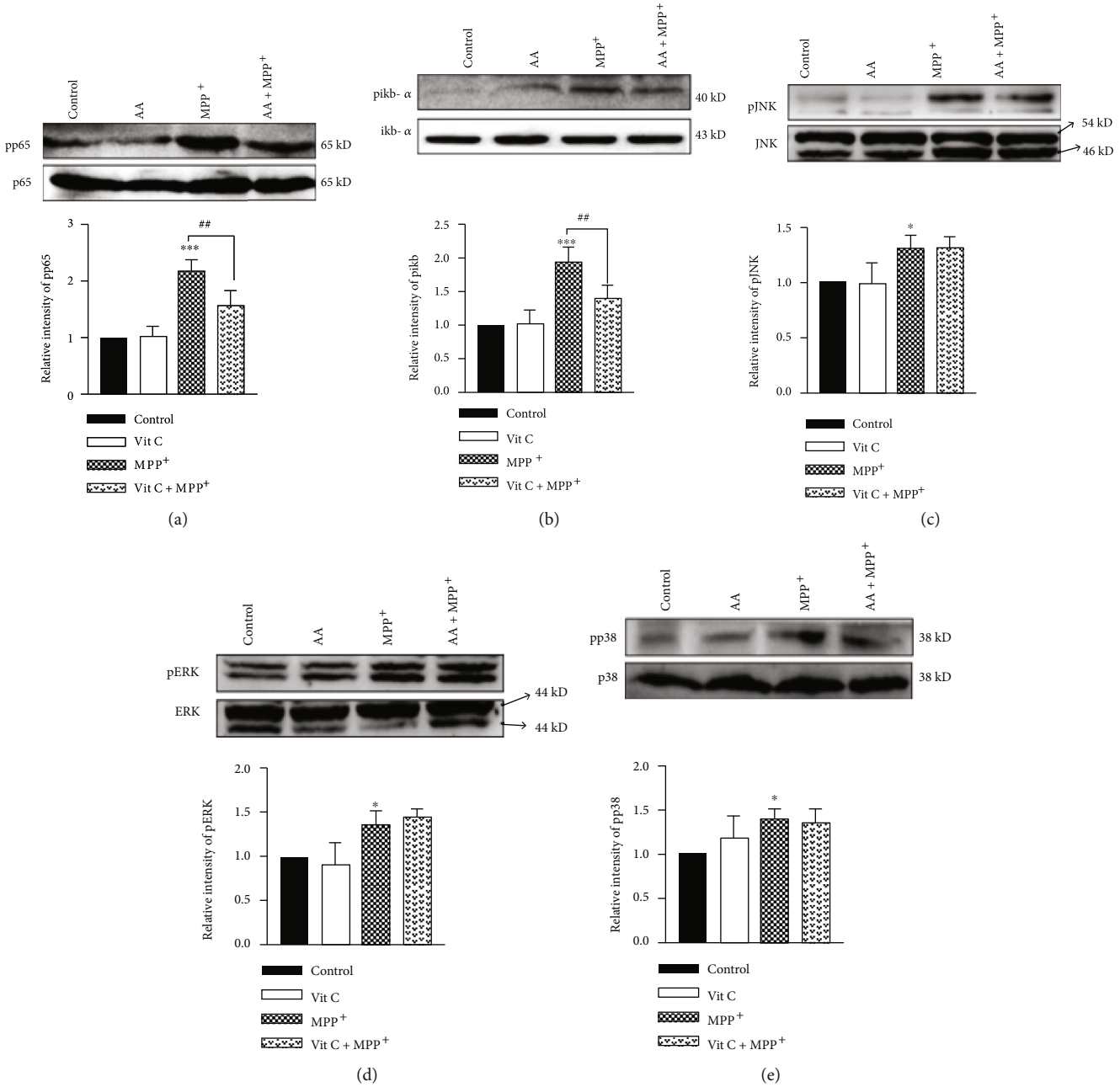

Figure 3: Ascorbic acid inhibits MPP^+-induced nuclear factor-kappaB (NF-κB) activation but does not affect p38/ERK or JNK signaling in astrocytes *in vitro*. Primary cells were treated with 1 mM of AA for 24 h and/or 1 mM of MPP^+ for another 24 h. (a) The expression of phosphorylated p65 (pp65) was detected by Western blotting ($n = 3$). (b) The expression of phosphorylated iκBα (piκBα) was detected by Western blotting ($n = 3$). (c) The expression of phosphorylated JNK (pJNK) was detected by Western blotting ($n = 3$). (d) The expression of phosphorylated ERK (pERK) was detected by Western blotting ($n = 3$). (e) The expression of phosphorylated p38 (pp38) was detected by Western blotting ($n = 3$). Data were obtained from three independent experiments. One-way ANOVAs followed by LSD pairwise comparisons were performed. * was considered significant compared to control ($^*P < 0.05$, $^{**}P < 0.01$, and $^{***}P < 0.001$). $^\#$ was considered significant compared to MPTP or MPP^+ ($^\#P < 0.05$, $^{\#\#}P < 0.01$, and $^{\#\#\#}P < 0.001$).

κB signaling occluded the protective effects of AA in MPP^+-treated astrocytes through suppressing the expression of antioxidative proteins.

3.6. Ascorbic Acid Enhances Antioxidant Function through Decreasing NK-κB Activation in the Midbrain of MPTP-Treated Mice. Our *in vitro* experiments demonstrated that AA pretreatment improved antioxidant function and reduced oxidative stress in MPP^+-treated astrocytes via increasing expression levels of GCLM, HO-1, and PGC-1α via inhibition of the NK-κB signal pathway. However, the molecular mechanisms for such AA-induced neuroprotection *in vivo* remained unclear. Hence, we next assayed relevant signaling molecules in the midbrains of

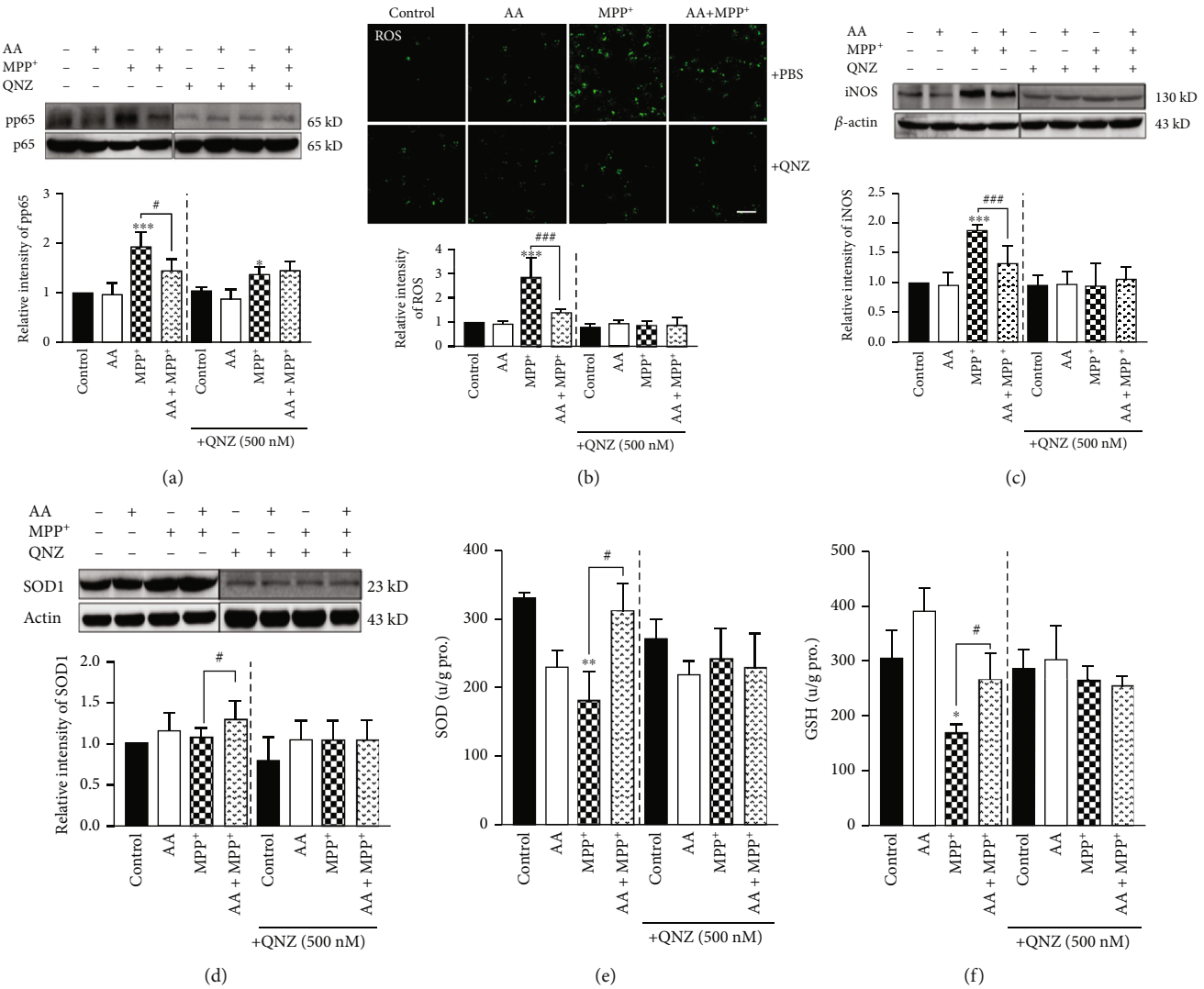

FIGURE 4: Inhibition of NF-κB signaling blocks the antioxidative effects of ascorbic acid and perpetuates cytotoxicity in MPP^+-treated astrocytes *in vitro*. Primary astrocytes were copretreated with 1 mM of AA and 0.5 mM of QNZ (EVP4593) for 24 h and/or 1 mM of MPP^+ for another 24 h. (a) The NF-κB-inhibition efficiency was detected by measuring the phosphorylation of p65 by Western blotting ($n = 3$). (b) Intracellular ROS was measured using the carboxy-H2DCFDA method (scale bar, 100 μm) ($n = 3$). (c) The expression of iNOS was detected by Western blotting ($n = 3$). (d) The expression of SOD1 was detected by Western blotting ($n = 3$). (e) The concentration of SOD in the supernatant from primary astrocytes was detected by ELISAs ($n = 3$). (f) The concentration of GSH in the supernatant from primary astrocytes was detected by ELISAs ($n = 3$). Data were obtained from three independent experiments. One-way ANOVAs followed by LSD pairwise comparisons were performed. * was considered significant compared to control ($^*P < 0.05$, $^{**}P < 0.01$, and $^{***}P < 0.001$). # was considered significant compared to MPTP or MPP^+ ($^{\#}P < 0.05$, $^{\#\#}P < 0.01$, and $^{\#\#\#}P < 0.001$).

mice from each experimental group. We found that the expression of iNOS was significantly elevated in the MPTP group, whereas this MPTP-induced increase was significantly reduced in the AA-pretreatment MPTP group (Figure 6(a)). On the contrary, the expression the antioxidant protein, SOD1, in the AA-pretreatment MPTP group was significantly higher compared to that in the MPTP group (Figure 6(b)). We further detected the expression levels of several antioxidant proteins—namely, GCLM, HO-1, and PGC-1α—via Western blotting and found that MPTP treatment increased these expression levels, while AA pretreatment further increased the MPTP-induced expression levels of GCLM, HO-1, and PGC-1α (Figure 6(c)). These results indicated that AA pretreatment enhanced the expression levels of antioxidant proteins and reduced oxidative stress in MPTP-treated mice. We further explored the molecular mechanisms underlying this AA-induced phenotype in MPTP-treated mice. Interestingly, we found that AA pretreatment also inhibited MPTP-induced NF-κB activation in the midbrain (Figure 6(d)). However, AA did not alter MPTP-induced changes in the expression levels of components of the JNK, ERK, and p38 signaling pathways (Figure 6(e)). Collectively, these results indicate that AA inhibits MPTP-induced activation of NF-κB and enhances antioxidant function to protect MPTP-treated mice.

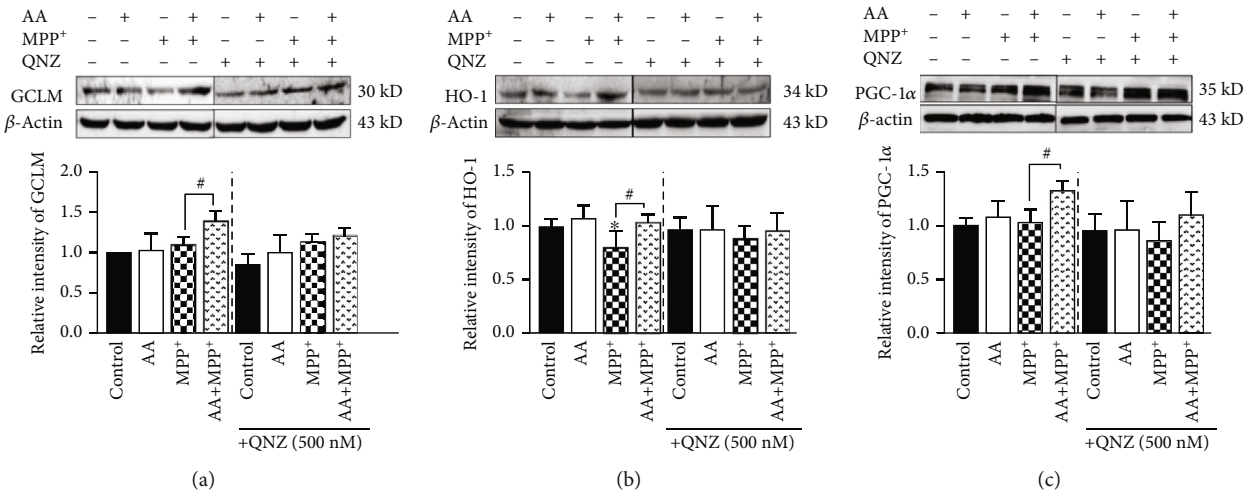

Figure 5: Inhibition of NF-κB signaling suppresses the expression of antioxidative proteins and blocks the protective effects of ascorbic acid to perpetuate cytotoxicity in MPP^+-treated in astrocytes *in vitro*. Primary astrocytes were copretreated with 1 mM of AA and 0.5 mM of QNZ (EVP4593) for 24 h and/or 1 mM of MPP^+ for another 24 h. (a) The expression of GCLM was detected by Western blotting ($n = 3$). (b) The expression of HO-1 was detected by Western blotting ($n = 3$). (c) The expression of PGC-1α was detected by Western blotting ($n = 3$). Data were obtained from three independent experiments. One-way ANOVAs followed by LSD pairwise comparisons were performed. * was considered significant compared to control ($^*P < 0.05$, $^{**}P < 0.01$, and $^{***}P < 0.001$). $^\#$ was considered significant compared to MPTP or MPP^+ ($^\#P < 0.05$, $^{\#\#}P < 0.01$, and $^{\#\#\#}P < 0.001$).

3.7. Ascorbic Acid Ameliorates MPTP-Induced Behavioral Deficits and Pathophysiology in Mice. To explore the effects of AA on behavioral performance in MPTP-treated mice, we tested mice in the rotarod test, grip power test, pole test, and open-field test. Mice were assigned to the following four treatment groups: saline+vehicle (control), AA+vehicle (AA), MPTP+vehicle (MPTP), and AA+MPTP (AA+MPTP). AA treatment alone had no effects compared to those of control treatment. In contrast, MPTP treatment induced poor behavioral performance, including a reduced holding time in the rotarod test, decreased grip strength in the grip strength test, prolonged pole-climbing time in the pole test, and shortened the movement distance in the open-field test. AA pretreatment in MPTP-treated mice ameliorated MPTP-induced behavioral deficits compared with performances in vehicle-treated MPTP mice (Figures 7(a)–7(d)). We also explored whether AA ameliorated MPTP-induced pathology. We detected tyrosine hydroxylase- (TH-) positive cells in the SNpc via immunohistochemistry. We found that AA pretreatment in MPTP-treated mice significantly reversed MPTP-induced loss of TH-positive cells in the SNpc compared to that of vehicle treatment in MPTP-treated mice (Figure 7(e)). We also confirmed this result by measured total TH expression in the midbrain. The expression of TH in the vehicle-treated MPTP group was significantly lower than that in the control group. In contrast, AA pretreatment restored expression of TH in MPTP-treated mice (Figure 7(f)). These results confirm the protective effects of AA in MPTP-treated mice.

4. Discussion

The current understanding of the pathogenesis of PD involves the formation of ROS and the onset of oxidative stress leading to oxidative damage in the SNpc [22]. Extensive postmortem studies have provided evidence to support the involvement of oxidative stress in the pathogenesis of PD; in particular, these forms of oxidative stress include alterations in brain iron content, impaired mitochondrial function, alterations in antioxidant protective systems, and oxidative damage to lipids, proteins, and DNA [23, 24]. Therefore, use of antioxidants is considered to represent a promising approach for inhibiting astrocytic oxidative stress and slowing the progression of PD.

AA is an important antioxidant in the human brain. A previous study reported that frequent AA supplementation can reduce 20% of oxidative damage in the body [14]. During central nervous system (CNS) injury or disease, the overproduction of ROS and/or insufficient detoxification can result in the activation of a coordinated astrocytic response, which involves a series of biochemical and morphological changes collectively referred to as reactive astrogliosis [25]. Reactive astrocytes respond to acute cellular stress and work to limit CNS damage, but chronic astrogliosis can result in the sustained production of ROS and the release of proinflammatory molecules, which promote neuronal injury and neurotoxicity. Our present study found that AA pretreatment reduced MPP^+-induced ROS production and iNOS expression in astrocytes *in vitro*. Further results indicated that AA pretreatment increased the expression of the antioxidant molecules, SOD and GSH, in MPP^+-treated astrocytes. These findings indicate that AA reduced MPP^+-induced excessive ROS levels by increasing antioxidant activities in astrocytes *in vitro*.

A significant source of ROS in PD-like pathology derives from NADPH oxidase, which is a multimeric enzyme composed of gp91phox, p47phox, p22phox, p67phox, and p40phox subunits. Upon cellular activation, p47phox assembles with gp91phox and p22phox, thus forming a NADPH-oxidase entity capable of reducing oxygen to superoxide radicals [26]. A previous study found that the expression of

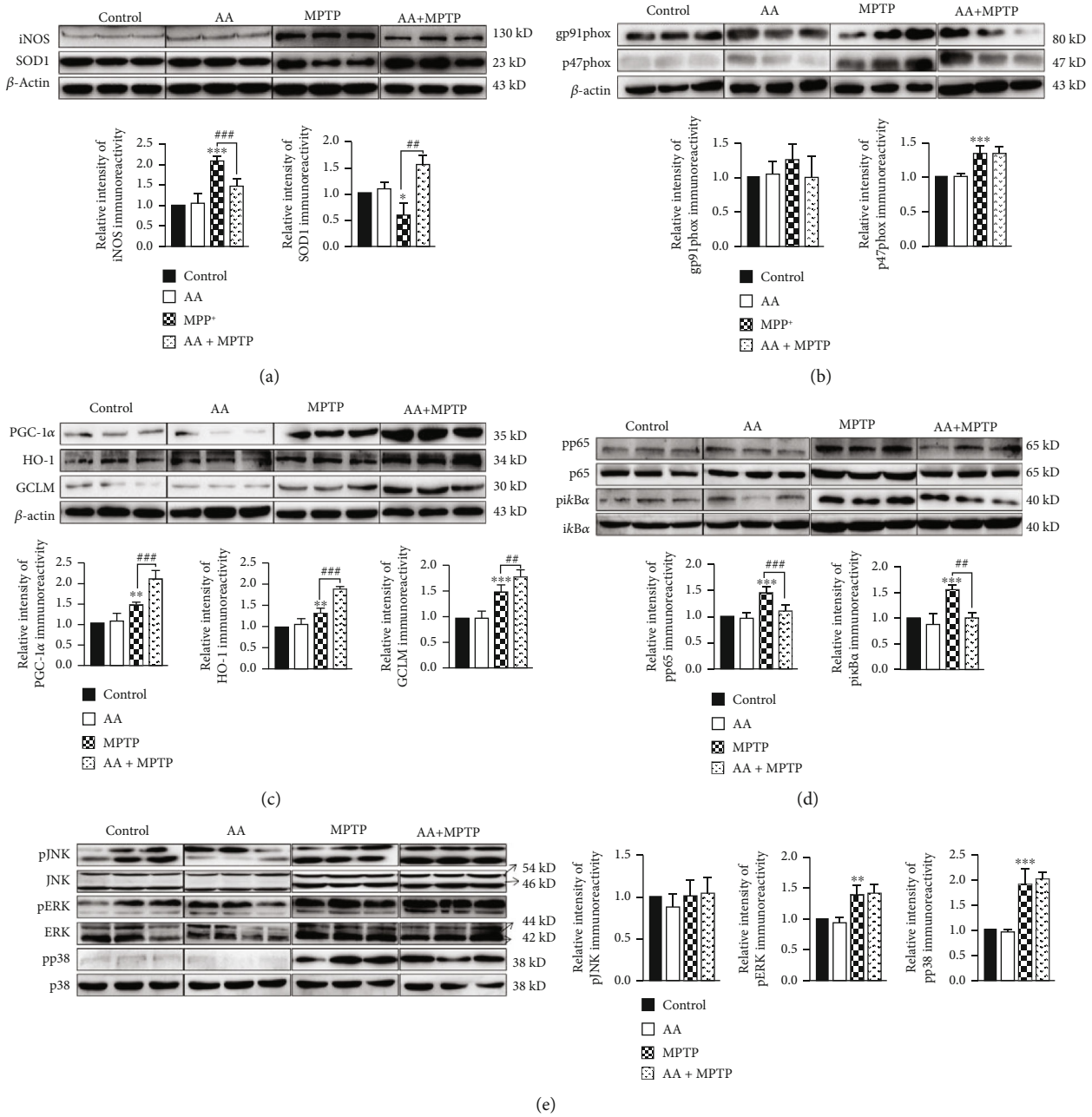

Figure 6: Ascorbic acid enhances antioxidant function and decreases NK-κB activation in the midbrains of MPTP-treated mice. Wild-type mice were intraperitoneally treated with 500 mg/kg of AA for 60 days, following by coinjected with 25 mg/kg of MPTP every 3.5 days for five weeks. After behavioral testing, midbrains were removed and total proteins were extracted. (a) The expression levels of iNOS and SOD1 were detected by Western blotting ($n = 3$). (b) The expression of gp9phox and p47phox was detected by Western blotting ($n = 3$). (c) The expression levels of PGC-1α, HO-1, and GCLM were detected by Western blotting ($n = 3$). (d) The expression levels of phosphorylated p65 and iκBα were detected by Western blotting ($n = 3$). (e) The expression levels of phosphorylated JNK, ERK, and p38 were detected by Western blotting ($n = 3$). Data were obtained from three independent experiments. One-way ANOVAs followed by LSD pairwise comparisons were performed. * was considered significant compared to control ($^{*}P < 0.05$, $^{**}P < 0.01$, and $^{***}P < 0.001$). $^{\#}$ was considered significant compared to MPTP or MPP^{+} ($^{\#}P < 0.05$, $^{\#\#}P < 0.01$, and $^{\#\#\#}P < 0.001$).

gp91phox was increased in the midbrain of MPTP-treated mice [27]. Additionally, inhibition of gp91phox may prevent MPTP-associated ROS production. A previous study found that NADPH oxidase plays an important role in ROS production [28]. Another study found that NADPH oxidase (NOX2) was upregulated in a rotenone-induced cellular model of PD. Furthermore, inhibition of NOX2-dependent oxidative stress attenuates aberrant autophagy and cellular death in a rotenone-induced cellular model of PD [29]. Lv et al. found that GCLM deletion led to a decrease in GSH in the striatum, indicating that GCLM is important for maintaining GSH expression in the midbrain. Growing evidence has indicated that induction of HO-1 expression via activation of Nrf2 signaling exerts neuroprotection against

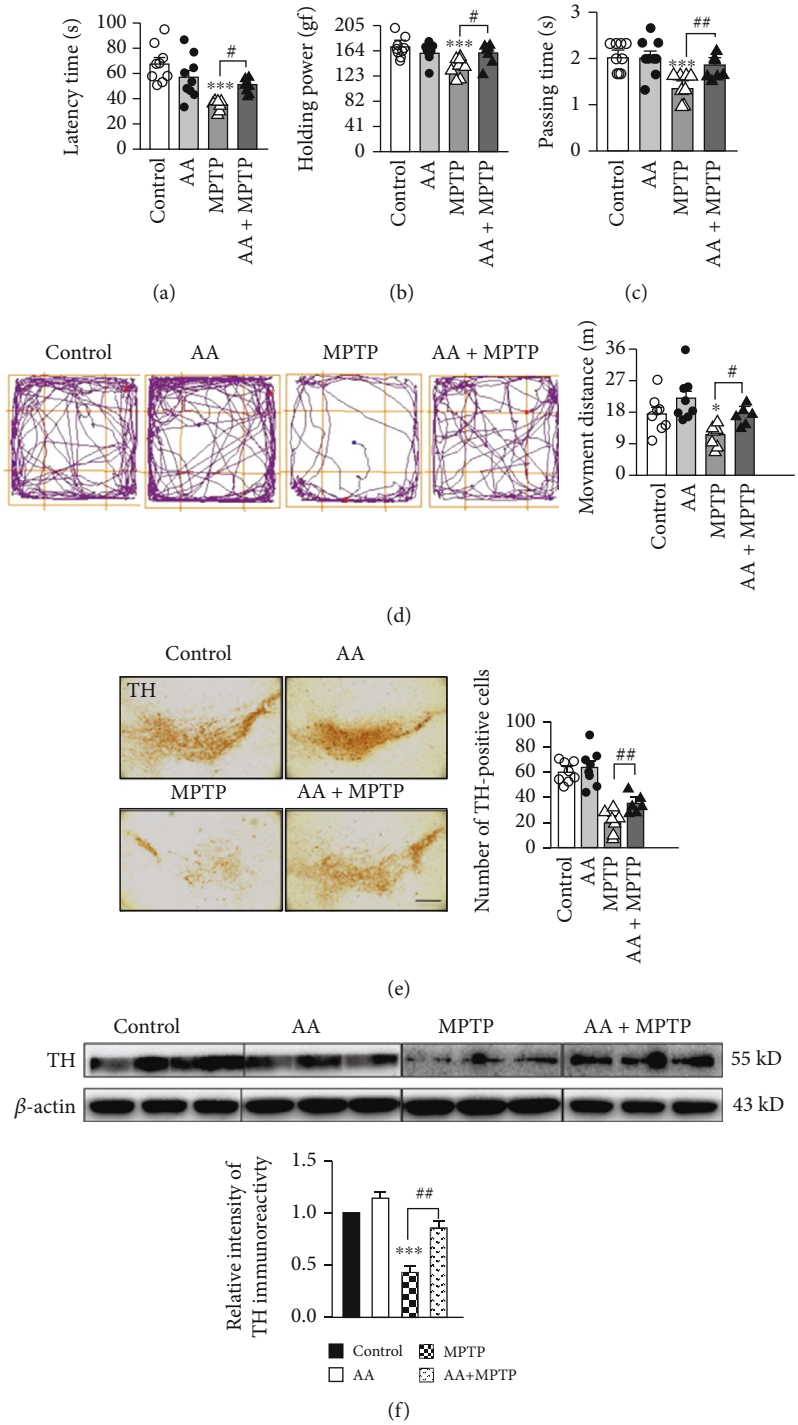

Figure 7: Ascorbic acid pretreatment ameliorates PD-like behavioral deficits and pathophysiology in an MPTP-induced mouse model of PD. (a) Holding times in the rotarod test were recorded after training mice for three days ($n = 6$). (b) Grasping strengths were measured using a grip meter after training mice for three days ($n = 6$). (c) Pole-climbing times were recorded after training mice for three days ($n = 6$). (d) Motion tracking was monitor in the open-field test ($n = 6$). (e) The expression of TH in the midbrain was detected by immunohistochemistry (scale bar, 50 μm) ($n = 3$). (f) The expression level of TH in the midbrain was detected by Western blotting ($n = 3$). Data were obtained from three independent experiments. One-way ANOVAs followed by LSD pairwise comparisons were performed. * was considered significant compared to control ($^{*}P < 0.05$, $^{**}P < 0.01$, and $^{***}P < 0.001$). $^{\#}$ was considered significant compared to MPTP or MPP^{+} ($^{\#}P < 0.05$, $^{\#\#}P < 0.01$, and $^{\#\#\#}P < 0.001$).

oxidative injury in neurons [30]. Recent studies have highlighted important roles of PGC-1α in neurodegenerative diseases. One such study found that overexpression of PGC-1α improved in motor behavior and increased in TH expression in the substantia nigra of MPTP-treated mice [31]. Our present results demonstrated that AA facilitated the

clearance of MPP^+-induced excessive ROS in astrocytes *in vitro* by reducing the expression of gp91phox and increasing the expression of the antioxidant molecules, GCLM, HO-1, and PGC-1α.

Which signaling pathways are involved in AA-induced enhancement of antioxidative function in MPP^+-treated astrocytes? A previous study found that rosmarinic acid attenuated inflammatory responses through suppressing the HMGB1/TLR4/NF-kappaB signaling pathway, which may have contributed to its anti-PD-like activity [32]. Glaucocalyxin B has been shown to suppress LPS-induced PD-like symptoms via modification of TLR/NF-kappaB and Nrf2/HO-1 pathways both *in vivo* and *in vitro* [33]. In the present study, we found that AA pretreatment significantly reduced MPP^+-induced expression of NF-κB in astrocytes *in vitro*, whereas there was no significant effect on the phosphorylation levels of JNK, ERK, or p38. From these findings, we hypothesized that AA enhanced antioxidant function in MPP^+-treated astrocytes via inhibition of NF-κB expression. Hence, we subsequently inhibited the NF-κB signaling pathway and explored whether the protective effects of AA remained. We found that the MPP^+-induced expression of ROS and iNOS decreased after inhibition of NF-κB, which also eliminated any such differences between the AA-pretreatment MPP^+ group and MPP^+ group. The antioxidant system also exhibited similar effects after NF-κB inhibition in MPP^+-treated astrocytes, in which AA pretreatment no longer restored the MPP^+-altered expression of SOD1 and GSH. Interestingly, inhibition of NF-κB did not significantly inhibit GCLM, HO-1, or PGC-1α. However, inhibition of NF-κB eliminated the differences in these levels between the AA-pretreatment MPP^+ group and MPP^+ group.

In vitro experiments have shown that AA increases the antioxidative activity of MPP^+-treated astrocytes. One study found that plasma rich in growth factors-Endoret (PRGF-Endoret) improved motor performance in MPTP-treated mice [34]; these effects were associated with a robust reduction in NF-κB activation and nitric oxide (NO) expression in the substantia nigra. Quercetin has been demonstrated to play an important role in altering the progression of neurodegenerative diseases by protecting against oxidative stress [35]. Furthermore, dietary vitamin C intake is significantly associated with reduced PD risk [36]. However, Martinovits et al. found that systemic administration of AA for a short time (two days) does not protect mice against the dopaminergic neurotoxicity of MPTP [37]. But many researchers reported that AA exerts neuroprotective effects against MPTP-induced neurotoxic [38, 39]. Our present study demonstrated that AA alleviated pathology and behavioral deficits in MPTP-treated mice. We found that AA pretreatment increased the expression of TH in the midbrain of MPTP-treated mice. Behavioral studies—including assessments in the rotarod test, grasping strength test, pole-climbing test, and open-field test—showed that AA pretreatment ameliorated behavioral deficits in MPTP-treated mice. We found that AA pretreatment reduced oxidative stress in MPP^+-treated primary astrocytes in vitro. Pretreatment with AA reduced MPP^+-induced ROS and iNOS production in astrocytes in vitro, which may have been due to decreasing MPP^+-induced expression of the NADPH oxidase subunit, gp91phox. Finally, we found that inhibition of MPP^+-induced NF-κB activation led to an increase in the expression levels of antioxidant molecules, such as SOD, GSH, GCLM, HO-1, and PGC-1α. Hence, our present study reveals a new role of AA in inhibiting astrocytic oxidative stress.

5. Conclusion

Taken together, our present study demonstrates that AA inhibits astrocytic oxidative stress in MPP^+-treated astrocytes through suppressing NF-κB, which ultimately leads to increased expression levels of antioxidant proteins to scavenge ROS to further decrease MPTP/MPP^+-induced apoptosis. Thus, AA may represent a potential therapeutic agent for ameliorating PD symptoms. However, further research is needed to elucidate the antioxidative capacity of AA in a primate model of PD and, if efficacious, in human PD patients. Collectively, our present findings provide insight into the role of AA in ameliorating MPTP-induced PD-like behavioral deficits and pathophysiology in mice. This data suggests that AA may be advantageous in exerting neuroprotection to slow the progression of PD in humans.

Data Availability

The data used to support the findings of this study are available from the corresponding author upon reasonable request.

Conflicts of Interest

The authors declare that they have no competing interests.

Authors' Contributions

Xiaokang Zeng, Yunqi Xu, Kai Xu, and Ji Wang performed and analyzed the experiments. Shaogang Qu conceived and designed the study. Xiaokang Zeng and Shaogang Qu wrote the paper. All authors read and approved the final manuscript. All authors have agreed to be accountable for all aspects of this work.

Acknowledgments

This work was funded by grants from the National Natural Science Foundation of China (81870991, U1603281, and 31570716), the Guangdong Basic and Applied Basic Research Foundation (2019A1515110956 to X. Zeng), the Fund of Guangdong Medical Science and Technology Research (A2020557 to X. Zeng), Scientific Research Start Plan of Shunde Hospital, Southern Medical University (SRSP2019002 to X. Zeng), and the key innovational technology project of Guangzhou (2018-1202-SF-0019).

References

[1] X. S. Zeng, W. S. Geng, J. J. Jia, L. Chen, and P. P. Zhang, "Cellular and molecular basis of neurodegeneration in Parkinson disease," *Frontiers in Aging Neuroscience*, vol. 10, p. 109, 2018.

[2] M. Vila and S. Przedborski, "Genetic clues to the pathogenesis of Parkinson's disease," *Nature Medicine*, vol. 10, no. S7, pp. S58–S62, 2004.

[3] M. T. Hayes, "Parkinson's disease and parkinsonism," *The American Journal of Medicine*, vol. 132, no. 7, pp. 802–807, 2019.

[4] I. Yazawa, Y. Terao, I. Sai, K. Hashimoto, and M. Sakuta, "Gastric acid secretion and absorption of levodopa in patients with Parkinson's disease–the effect of supplement therapy to gastric acid," *Rinshō Shinkeigaku*, vol. 34, no. 3, pp. 264–266, 1994.

[5] P. M. Rappold and K. Tieu, "Astrocytes and therapeutics for Parkinson's disease," *Neurotherapeutics*, vol. 7, no. 4, pp. 413–423, 2010.

[6] Z. I. Alam, A. Jenner, S. E. Daniel et al., "Oxidative DNA damage in the parkinsonian brain: an apparent selective increase in 8-hydroxyguanine levels in substantia nigra," *Journal of Neurochemistry*, vol. 69, no. 3, pp. 1196–1203, 1997.

[7] A. H. K. Tsang and K. K. K. Chung, "Oxidative and nitrosative stress in Parkinson's disease," *Biochimica et Biophysica Acta*, vol. 1792, no. 7, pp. 643–650, 2009.

[8] A. Umeno, V. Biju, and Y. Yoshida, "In vivo ROS production and use of oxidative stress-derived biomarkers to detect the onset of diseases such as Alzheimer's disease, Parkinson's disease, and diabetes," *Free Radical Research*, vol. 51, no. 4, pp. 413–427, 2017.

[9] S. S. Karuppagounder, Y. Xiong, Y. Lee et al., "LRRK2 G2019S transgenic mice display increased susceptibility to 1-methyl-4-phenyl-1,2,3,6-tetrahydropyridine (MPTP)-mediated neurotoxicity," *Journal of Chemical Neuroanatomy*, vol. 76, no. Part B, pp. 90–97, 2016.

[10] M. Inden, T. Taira, Y. Kitamura et al., "PARK7 DJ-1 protects against degeneration of nigral dopaminergic neurons in Parkinson's disease rat model," *Neurobiology of Disease*, vol. 24, no. 1, pp. 144–158, 2006.

[11] H. Mirzaei, J. L. Schieler, J. C. Rochet, and F. Regnier, "Identification of rotenone-induced modifications in alpha-synuclein using affinity pull-down and tandem mass spectrometry," *Analytical Chemistry*, vol. 78, no. 7, pp. 2422–2431, 2006.

[12] D. A. Bosco, D. M. Fowler, Q. Zhang et al., "Elevated levels of oxidized cholesterol metabolites in Lewy body disease brains accelerate alpha-synuclein fibrilization," *Nature Chemical Biology*, vol. 2, no. 5, pp. 249–253, 2006.

[13] A. Baillet, V. Chanteperdrix, C. Trocmé, P. Casez, C. Garrel, and G. Besson, "The role of oxidative stress in amyotrophic lateral sclerosis and Parkinson's disease," *Neurochemical Research*, vol. 35, no. 10, pp. 1530–1537, 2010.

[14] F. E. Harrison and J. M. May, "Vitamin C function in the brain: vital role of the ascorbate transporter SVCT2," *Free Radical Biology & Medicine*, vol. 46, no. 6, pp. 719–730, 2009.

[15] J. Y. Lee, M. Y. Chang, C. H. Park et al., "Ascorbate-induced differentiation of embryonic cortical precursors into neurons and astrocytes," *Journal of Neuroscience Research*, vol. 73, no. 2, pp. 156–165, 2003.

[16] M. M. Grant, V. S. Barber, and H. R. Griffiths, "The presence of ascorbate induces expression of brain derived neurotrophic factor in SH-SY5Y neuroblastoma cells after peroxide insult, which is associated with increased survival," *Proteomics*, vol. 5, no. 2, pp. 534–540, 2005.

[17] P. F. Kao, W. S. Lee, J. C. Liu et al., "Downregulation of superoxide dismutase activity and gene expression in cultured rat brain astrocytes after incubation with vitamin C," *Pharmacology*, vol. 69, no. 1, pp. 1–6, 2003.

[18] C. Sánchez-Moreno, M. Paniagua, A. Madrid, and A. Martín, "Protective effect of vitamin C against the ethanol mediated toxic effects on human brain glial cells," *The Journal of Nutritional Biochemistry*, vol. 14, no. 10, pp. 606–613, 2003.

[19] Y. Zhang, X. He, X. Meng et al., "Regulation of glutamate transporter trafficking by Nedd4-2 in a Parkinson's disease model," *Cell Death & Disease*, vol. 8, no. 2, article e2574, 2017.

[20] W. Chen, H. Su, Y. Xu, and C. Jin, "In vitro gastrointestinal digestion promotes the protective effect of blackberry extract against acrylamide-induced oxidative stress," *Scientific Reports*, vol. 7, no. 1, 2017.

[21] T. C. H. Leung, C. N. P. Lui, L. W. Chen, W. H. Yung, Y. S. Chan, and K. K. L. Yung, "Ceftriaxone ameliorates motor deficits and protects dopaminergic neurons in 6-hydroxydopamine-lesioned rats," *ACS Chemical Neuroscience*, vol. 3, no. 1, pp. 22–30, 2011.

[22] K. Sudha, A. V. Rao, S. Rao, and A. Rao, "Free radical toxicity and antioxidants in Parkinson's disease," *Neurology India*, vol. 51, no. 1, pp. 60–62, 2003.

[23] G. Cohen, "Oxidative stress, mitochondrial respiration, and Parkinson's disease," *Annals of the New York Academy of Sciences*, vol. 899, no. 1, pp. 112–120, 2000.

[24] K. C. Luk, "Oxidative stress and α-synuclein conspire in vulnerable neurons to promote Parkinson's disease progression," *The Journal of Clinical Investigation*, vol. 129, no. 9, pp. 3530-3531, 2019.

[25] E. H. Joe, D. J. Choi, J. An, J. H. Eun, I. Jou, and S. Park, "Astrocytes, microglia, and Parkinson's disease," *Exp Neurobiol*, vol. 27, no. 2, pp. 77–87, 2018.

[26] B. M. Babior, "NADPH oxidase: an update," *Blood*, vol. 93, no. 5, pp. 1464–1476, 1999.

[27] D. C. Wu, P. Teismann, K. Tieu et al., "NADPH oxidase mediates oxidative stress in the 1-methyl-4-phenyl-1,2,3,6-tetrahydropyridine model of Parkinson's disease," *Proceedings of the National Academy of Sciences of the United States of America*, vol. 100, no. 10, pp. 6145–6150, 2003.

[28] Q. Liu, J. H. Kang, and R. L. Zheng, "NADPH oxidase produces reactive oxygen species and maintains survival of rat astrocytes," *Cell Biochemistry and Function*, vol. 23, no. 2, pp. 93–100, 2005.

[29] R. Pal, L. Bajaj, J. Sharma et al., "NADPH oxidase promotes Parkinsonian phenotypes by impairing autophagic flux in an mTORC1-independent fashion in a cellular model of Parkinson's disease," *Scientific Reports*, vol. 6, no. 1, 2016.

[30] J. Lv, S. Jiang, Z. Yang et al., "PGC-1α sparks the fire of neuroprotection against neurodegenerative disorders," *Ageing Research Reviews*, vol. 44, pp. 8–21, 2018.

[31] Y. Wang, C. Chen, W. Huang et al., "Beneficial effects of PGC-1α in the substantia nigra of a mouse model of MPTP-induced dopaminergic neurotoxicity," *Aging*, vol. 11, no. 20, pp. 8937–8950, 2019.

[32] R. Lv, L. du, X. Liu, F. Zhou, Z. Zhang, and L. Zhang, "Rosmarinic acid attenuates inflammatory responses through inhibiting HMGB1/TLR4/NF-κB signaling pathway in a mouse model of Parkinson's disease," *Life Sciences*, vol. 223, pp. 158–165, 2019.

[33] W. Xu, D. Zheng, Y. Liu, J. Li, L. Yang, and X. Shang, "Glaucocalyxin B alleviates lipopolysaccharide-induced Parkinson's

disease by inhibiting TLR/NF-κB and activating Nrf2/HO-1 pathway," *Cellular Physiology and Biochemistry*, vol. 44, no. 6, pp. 2091–2104, 2018.

[34] E. Anitua, C. Pascual, R. Pérez-Gonzalez, G. Orive, and E. Carro, "Intranasal PRGF-Endoret enhances neuronal survival and attenuates NF-κB-dependent inflammation process in a mouse model of Parkinson's disease," *Journal of Controlled Release*, vol. 203, pp. 170–180, 2015.

[35] E. Bahar, J. Y. Kim, and H. Yoon, "Quercetin attenuates manganese-induced neuroinflammation by alleviating oxidative stress through regulation of apoptosis, iNOS/NF-κB and HO-1/Nrf2 pathways," *International Journal of Molecular Sciences*, vol. 18, no. 9, p. 1989, 2017.

[36] K. C. Hughes, X. Gao, I. Y. Kim et al., "Intake of antioxidant vitamins and risk of Parkinson's disease," *Movement Disorders*, vol. 31, no. 12, pp. 1909–1914, 2016.

[37] G. Martinovits, E. Melamed, O. Cohen, J. Rosenthal, and A. Uzzan, "Systemic administration of antioxidants does not protect mice against the dopaminergic neurotoxicity of 1-methyl-4-phenyl-1,2,5,6-tetrahydropyridine (MPTP)," *Neuroscience Letters*, vol. 69, no. 2, pp. 192–197, 1986.

[38] H. Sershen, M. E. A. Reith, A. Hashim, and A. Lajtha, "Protection against 1-methyl-4-phenyl-1,2,3,6-tetrahydropyridine neurotoxicity by the antioxidant ascorbic acid," *Neuropharmacology*, vol. 24, no. 12, pp. 1257–1259, 1985.

[39] G. C. Wagner, M. F. Jarvis, and R. M. Carelli, "Ascorbic acid reduces the dopamine depletion induced by MPTP," *Neuropharmacology*, vol. 24, no. 12, pp. 1261-1262, 1985.

Hindawi
Neural Plasticity
Volume 2020, Article ID 8880543, 13 pages
https://doi.org/10.1155/2020/8880543

Research Article

Based on Systematic Pharmacology: Molecular Mechanism of Siwei Jianbu Decoction in Preventing Oxaliplatin-Induced Peripheral Neuropathy

Peng Zhang,[1] Yuting Lu,[1] Chao Yang,[1] Qiuyan Zhang,[1] Yangyan Qian,[1] Jinshuai Suo,[1] Peng Cheng,[1] and Jing Zhu[1,2]

[1]*Jiangsu Key Laboratory for Pharmacology and Safety Evaluation of Chinese Materia Medica, Department of Pharmacy, Nanjing University of Chinese Medicine, Nanjing210023, China*
[2]*Departments of Neurology and Neuroscience, Johns Hopkins University School of Medicine, Baltimore, MD, USA*

Correspondence should be addressed to Jing Zhu; 830640@njucm.edu.cn

Received 22 June 2020; Revised 18 September 2020; Accepted 21 September 2020; Published 6 October 2020

Academic Editor: Fushun Wang

Chemotherapy-induced peripheral neuropathy (CIPN) is a dose-limiting side effect caused by chemotherapy drugs, and its existence seriously affects the quality of life of patients. We first established an oxaliplatin-induced peripheral neuropathy (OIPN) model and then measured and evaluated mechanical hyperalgesia, thermal nociception, cold allodynia, and intraepidermal nerve fiber (IENF) density to determine Siwei Jianbu Decoction's role in preventing OIPN. Then, we conducted a systematic pharmacological study that revealed important roles for the MAPK signaling pathway and proinflammatory immune pathway and confirmed these roles by western blot, immunofluorescence, and qPCR. The data show that Siwei Jianbu Decoction can effectively prevent oxaliplatin-induced neuroinflammation by inhibiting an increase in NF-κB expression via downregulation of p-ERK1/2 and p-p38. The present study showed that SWJB may be beneficial in preventing oxaliplatin-induced peripheral neuropathy.

1. Introduction

Currently, colorectal cancer has become a common type of cancer, and its present global incidence and mortality rate are among the highest. Oxaliplatin is an antitumor drug combined with 5-fluorouracil (5-FU) and leucovorin (LV), which is used as an adjuvant treatment for patients with colon cancer reoperation [1, 2]. However, severe peripheral neuropathy is induced in approximately 90% of patients during the course of treatment [3]. Common symptoms include allodynia, hyperalgesia, dysesthesia, and paranaesthesia [4]. These side effects limit the use of oxaliplatin. It has been shown that the activation of glial cells and the upregulation of proinflammatory cytokines play a crucial role in the occurrence and development of chemotherapy-induced neuropathic pain [5]. In particular, oxaliplatin induces neuropathic pain via astrocyte-activated cosignaling and the mitogen-activated protein kinase (MAPK) pathway [6, 7]. We know that the MAPK signaling system is activated by extracellular stimuli, leading to an intracellular response. These stimuli provide links between transmembrane signal transduction and transcriptional changes in different environmental signals, such as cytokines, growth factors, oxidative stress, and inflammation [8]. In our study, we found that inflammation may be related to nuclear factor kappa-B (NF-κB) and extracellular regulated protein kinases (ERK/p38) MAPK signaling pathways in mouse models of oxaliplatin-induced peripheral neuropathic pain (OIPN). Similarly, studies have found that celecoxib reduces oxaliplatin-induced hyperalgesia by inhibiting ERK1/2 signaling in the spinal cord [9], and the major drugs used clinically for the prevention and treatment of OIPN, such as glutathione, vitamin E, amifolin, amantadine, mannitrite, and norepinephrine reuptake inhibitors, are not effective against neuroinflammation in OIPN [10, 11].

As a result of the overall concept of traditional Chinese medicine theory and the historical clinical practice of treating

complex diseases, traditional Chinese medicine (TCM) is attracting attention worldwide. Siwei Jianbu Decoction is a well-known recipe created by Professor Huang Huang of Nanjing University of Chinese Medicine. In the following, J12 will be used as an abbreviation for Siwei Jianbu Decoction. This recipe is made up of four herbs: *Paeonia veitchii* Lynch, *Salvia miltiorrhiza* Bge, *Achyranthes bidentata* Blume, and *Dendrobium nobile* Lindl, and its main effect is to activate blood circulation, relieve stasis and pain, improve blood supply to the lower limbs, and restore lower limb function. J12 is commonly used in the treatment of diabetic peripheral neuritis, diabetic foot, lower extremity thrombosis, and other diseases [12]. However, the therapeutic mechanism of J12 is not clear, and there are few studies on the analgesic effect of J12 on OIPN.

Therefore, the purpose of our present study was to elucidate the roles of J12 in peripheral neuropathic pain caused by oxaliplatin and whether the MAPK and ERK/p38 signaling pathways of oxaliplatin are related to the preventive effect of J12 on OIPN. First, the oxaliplatin-induced neuropathy model was established. The OIPN prevention effect of J12 was then confirmed by measurement of mechanical hyperalgesia, measurement of thermal nociception, measurement of cold allodynia, and plantar nerve fiber (IENF) density determination. In addition, because of the complexity and diversity of traditional Chinese medicine formula ingredients, we adopted a systematic approach to study the possible mechanisms, and it was finally determined that the major pathways of MAPK and proinflammatory immunity play an important role. Based on the findings of systemic pharmacology, we also validated the prediction of systemic pharmacology on the mechanism of J12 prevention and treatment of OIPN by studying the expression of NF-κB and proinflammatory factors (TNF-α, IL-1β, IL-6).

2. Materials and Methods

2.1. Reagents. Oxaliplatin (Sigma, USA) was dissolved in 5% glucose and formulated to a final concentration of 0.4 mg/mL. J12, containing four Chinese herbs, was purchased from Jiangsu Provincial Hospital (Nanjing, Jiangsu, China) and deposited at Nanjing University of Chinese Medicine. The component herbs were decocted twice, each for 1 h. The decoction was filtered, and the filtrates were combined and concentrated by rotary evaporation under reduced pressure to 120 mL, which is equivalent to 1 g/mL of the original drug. To ensure its quality and stability, we purchased different batches of raw medicinal materials, divided them into ten parts of the same specification, made the original liquid according to the same decoction method, and tested its fingerprint. The results are shown in the supplementary material (Figure S1-S2).

2.2. Animals. Male adult C57BL/6 mice between 6 and 8 weeks of age were purchased from Qinglong Mountain Animal Breeding Farm (Nanjing, China) and were kept under specific pathogen-free conditions with air conditioning and a 12 h light/dark cycle. The mice were housed in cages with free access to food and water at a constant temperature (20°C ± 2). The experimental protocols were approved by the Animal Committee of Nanjing University of Chinese Medicine. All experiments were tested in a blinded manner.

After one week of adaptation to the environment, thirty-two C57 mice were randomly divided into 4 groups as follows: normal control group (normal saline), OXA group (4 mg/kg of body weight), and O+J12 (H) and O+J12 (L) groups (daily dose 10 g/kg and 5 g/kg of body weight, respectively). The O+J12 (L, H) group was given J12 by oral enema for 6 weeks. From the third week, the OXA group and O+J12 (L, H) group received i.p. injections of 100 μL/10 g oxaliplatin (Sigma, USA) solution (prepared with 5% glucose) on Mondays and Thursdays (1 hour after J12) for 4 weeks [13]. A total of 8 injections at a cumulative dose of 32 mg/kg of OHP were given. The dose of the J12 decoction was converted from Professor Huang Huang's outpatient medical records and combined with the equivalent dose conversion between humans and animals [12].

2.3. Animal Behavior Tests. Behavioral tests were performed on days 0, 7, 14, 21, 28, 35, and 42. Body weight was recorded before the beginning of each behavioral study. Measurements were repeated three times for each mouse, and the mean was the behavioral threshold for each mouse. The investigators were unaware of the treatment group.

2.3.1. Measurement of Mechanical Hyperalgesia. A dynamic plantar aesthesiometer (DPA, Ugo Basile, Italy) was used to measure the mechanical retraction threshold of the mice. The mice were placed in a plexiglass box on a metal sieve for 30 minutes, and the tactometer was calibrated with a 0.5 mm filament. The intensity of the stimulus to the middle of the plantar foot of the mouse was increased (the setting frequency was 1 g/s, the maximum force was 10 g) while slowly increasing the stimulus pressure. When a foot withdrawal reaction occurs, the system records the latency time and the animal's foot withdrawal reaction pressure. Each mouse was repeatedly measured 3 times, and the average value was the mechanical withdrawal threshold of each mouse.

2.3.2. Measurement of Thermal Nociception. A plantar stimulation pain meter (37370, Ugo Basile Plantar Test Apparatus, Italy) was used to measure the reflex threshold of heat pain and contraction. The mice were placed in a plexiglass box on a glass plate for 30 minutes. The response time to irradiation until the mice withdraw their feet was measured. To prevent the skin of the mice from being burned, the automatic cut-off time was set to 30 s. Each mouse was repeatedly measured 3 times, and the average value was the heat pain threshold of each mouse.

2.3.3. Measurement of Cold Allodynia. Determination of cold pain threshold: the upper body of the mouse was fixed, and 1/3 of the tail tip was placed in an ice water bath at 4°C. The time from the tail tip entering the water to tail swing was recorded. To prevent the tail from frostbite, the cut-off time was set to 30 s. Each mouse was repeatedly measured 3 times, and the average value was the cold pain tail flick threshold of each mouse.

2.4. Intraepidermal Nerve Fiber (IENF) Density Determination. According to reports, the lack of IENFs plays a key role in neuropathy caused by various chemotherapy drugs (such as oxaliplatin) [14]. On the last day of the sixth week, the plantar skin tissues of the mice were removed, fixed in a periodate-lysine-paraformaldehyde (PLP) solution for 18-22 hours, and then transferred to a 30% sucrose-containing PBS solution to dehydrate until the tissue subsided, and frozen sections were made within one week. The tissue was embedded with optimal cutting temperature compound (OCT) and sectioned frozen (continuously cut perpendicular to the epidermis) with a thickness of approximately 30 μm. The sections were subsequently stained, and the state of the epidermal nerve fibers was observed under an inverted microscope.

2.5. Acquisition of Compounds in J12. The compounds of four herbs in J12 were gathered from the Traditional Chinese Medicine Systems Pharmacology Database and Analysis Platform (TCMSP, https://tcmspw.com/tcmsp.php) and Shanghai Institute of Organic Chemistry of CAS, Chemistry Database [DB/OL] (http://www.organchem.csdb.cn) for further screening [15].

2.5.1. Screening of Parameters of Active Compounds. J12 is composed of four medicinal herbs, including Achyranthes bidentata, Akabane, Salvia miltiorrhiza, and Dendrobium. Therefore, we combined drug half-life (t1/2) (HL), drug-likeness (DL), oral bioavailability (OB), and blood–brain barrier (BBB) screening with Caco-2 permeability (Caco-2) evaluation to identify the active compounds in J12 [16].

Ultimately, we screened the active compounds by setting the following parameters: HL $\geq$ 4, DL $\geq$ 0.18, OB $\geq$ 30%, BBB ≥ -0.3, and Caco-2 ≥ -0.4 [17].

2.5.2. Drug Target Prognostication for J12 and Construction of Compound–Target. To predict the potential targets of the active compounds in J12 screened above, we employed a systematic drug targeting method developed by Yu and others [18]: that is, we combined computer prediction model (combining two effective methods: support vector machine and random forest), SEA search tool (http://sea.bkslab.org/), and TCMSP database (http://lsp.nwu.edu.cn/tcmsp.php) and finally obtained the potential of the J12 target.

To gain a deeper understanding of the relationship between compounds and targets, we used Cytoscape (https://cytoscape.org/) software to build a composite target network.

2.5.3. Recognition of OIPN Targets. To further analyze known targets associated with oxaliplatin-induced peripheral neuropathy, we searched five databases: DrugBank (http://www.drugbank.ca/), OMIM (http://www.omim.org/), GAD (http://geneticassociationdb.nih.gov/), PharmGKB (https://www.pharmgkb.org/index.jsp), and TTD (http://database.idrb.cqu.edu.cn/TTD/) [15]. We searched these databases using the keyword "oxaliplatin-induced peripheral neuropathy" and collected oxaliplatin-induced peripheral neuropathy-related targets.

2.5.4. Construction of the Protein–Protein Interaction (PPI) Network and Recognition of Topological Features. An interactive network for potential J12 targets was constructed using the Cytoscape built-in plugin, Bisogenet, and Cytoscape software was used for visualization (version 3.7.1) [19]. In the same way, we built an interactive network for OIPN-related targets. The two networks were then combined to form a core protein-protein interaction (CPPI) network. To identify the necessary proteins in this PPI network, subsequent concentration analysis was performed using the Cytoscape plugin CytoNCA [20]. We filtered the major hubs of the network by the following six topology characteristics: "degree center (DC)," "intermediate center (BC)," "compact center (CC)," "feature vector center (EC)," "network center (NC)," and "local average connection (LAC)." These parameters are defined and computed in predefined formulas that represent the topological significance of the nodes in the network.

2.5.5. Pathway Enrichment Analysis. We then applied the DAVID database (http://david.ncifcrf.gov) and the Metascape database (https://metascape.org/) for KEGG annotation of nodes in J12 and Omicshare Tools to construct visual enrichment results to analyze potential targets, signaling pathways, and related biological processes in the gene network that may be involved in the regulation of active components in J12.

2.6. Western Blotting. Extraction of total tissue protein: all operations were performed on ice. Mouse DRG tissue and sciatic nerve tissue were removed from the -80°C ultralow temperature refrigerator, and 500 μL RIPA strong lysate and 5 μL protease were added to the tissue of each mouse at a ratio of 100 : 1 inhibitor (PMSF) mixture. After grinding the homogenate, centrifugation was performed in a low temperature centrifuge at 12000 rpm and 4°C for 15 min, the supernatant was slowly removed, and the protein concentration was measured using a BCA kit (P0010; Beyotime, China) on a microplate reader (Infinite M200 Pro; Tecan, Switzerland). The proteins were analyzed by 8-12% SDS-PAGE gels and transferred to polyvinylidene fluoride membranes (Millipore, Billerica, MA). Nonspecific binding sites were blocked with 5% (w/v) BSA (4240GR100; BioFroxx), and the membranes were incubated with the primary antibodies NF-κB, ERK1/2 (Abcam), phospho-p38, phospho-SAPK/JNK, phospho-ERK1/2, p38, SAPK/JNK, and GAPDH (Cell Signaling Tech). The membranes were washed 4 times in TBST and then incubated with the secondary antibodies for 1 h at room temperature on a shaker. Protein expression was measured by using an ECL system (UV200R; Tanon).

2.7. Immunofluorescence. At the end of week 6, L4 and L5 DRGs were taken from mice for immunohistochemical analysis. The sample tissue was placed in a paraformaldehyde fixative solution and placed at a temperature of 4°C. The tissue was then transferred to 20% sucrose for dehydration for 24 h, and then, the DRG was cut to a thickness of 10 μm and mounted on a glass slide. Briefly, sections were blocked for 1 hour at room temperature in 5% normal goat serum and 0.5% Tween-20 in PBS and incubated overnight at 4°C with

a primary antibody containing NF-κB (1 : 1000; Abcam). The sections remained overnight at 4°C. After being washed three times with PBS, sections were incubated with FITC-conjugated secondary antibodies (1 : 100) in the dark at room temperature for 1 hour. After extensive washing, the sections were stained with DAPI. The immunostained DRGs were then observed under an inverted fluorescence microscope.

2.8. Real-Time Quantitative Polymerase Chain Reaction (PCR). Total RNA was extracted from DRG tissue using a TRIzol extraction kit (Invitrogen, Carlsbad, USA). CDNA was synthesized using the reverse transcription kit TransStart Top Green qPCR SuperMix (TransGen Biotech, China). Real-time PCR was performed using an Applied Biosystems 7500 RealTime PCR System (Life Technologies, USA). Due to different species, qPCR-related primers were provided by Shanghai Shenggong Co., Ltd. The sequences are as follows:

GAPDH (forward: 5′ TTCCTACCCCCAATTATCCG 3′; reverse: 5′ CATGAGGTCCACCACCCTGTT 3′).

TNF-α (forward: 5′ GCGACGTGGAACTGGCAGAAG 3′; reverse: 5′ GAATGAGAAGAGGCTGAGACATAGGC 3′).

IL-6 (forward: 5′-AGACTTCCATCCAGTTGCC TTCT TG-3′

reverse: 5′-CATGTGTAATTAAGCCTCCGACTTGTG-3′).

IL-1β (forward: 5′ TTCAGGCAGGCAGTATCACTC ATTG 3′;

reverse: 5′ ACACCAGCAGGTTATCATCATCATCC 3′).

NF-κB (forward: 5′ CTGGTGCATTCTGACCTTGC 3′; reverse: 5′ GGTCCATCTCCTTGGTCTGC 3′).

2.9. ELISA Measurements. Approximately 200 μL of blood sample was collected from the eye socket of the mouse, and the supernatant of the blood sample was gathered after centrifugation at 3,000 × g for 15 minutes. According to the manufacturer's instructions, ELISA analysis kits (NF-κB, MBE10044; TNF-α, MBE10037; IL-6, MBE10288; and IL-1β, MBE10289) were used to measure the concentration of IL-1β, NF-κB, TNF-α, and IL-6 in the supernatant of the blood.

3. Statistical Analysis

All the experimental data are presented as the mean ± standard deviation (SD) and were analyzed with GraphPad Prism 8. The p values were tested by one-way analysis of variance (ANOVA) with the Tukey post hoc test for multiple comparisons. Data comparisons were considered to be significant if $p < 0.05$.

4. Results

4.1. J12 Prevents Oxaliplatin-Induced Hypersensitivity to Pain in Mice. To verify whether J12 prevented oxaliplatin-induced peripheral neuropathy, we followed the behavioral experiment plan, as shown in Figure 1(a). There was a significant difference in the paw withdrawal threshold between the OXA group and the CONTROL group from the third week. In the line chart, J12 was effective from the third week by comparing the treatment groups and the OXA group. However, the preventive treatment groups and the OXA group showed significant differences in weeks 5 and 6 from the data analysis (Figure 1(a)).

The data on heat hyperalgesia of mice in each group showed significant differences in the sixth week. The OXA group mice were more sensitive than the control. Moreover, the difference between the OXA group and O+J12(L) group demonstrated that the prophylactic administration of J12 could attenuate oxaliplatin-induced heat hyperalgesia (Figure 1(b)).

The line chart shows subtle differences between the groups from the fourth week to the sixth week. The O +J12(L) group showed better preventive effects than the O +J12(H) group (Figure 1(c)). In summary, these results indicated that J12(L) successfully prevented OXA-induced neuropathic pain in mice.

4.2. J12 Prevented Oxaliplatin-Induced Loss of IENFs. The immunofluorescence detection of PGP9.5 (a marker of IENFs) showed that compared with the control group (Figure 2(a)), the IENF density of the OXA group obviously decreased (Figure 2(b)). However, the prophylaxis groups reflected significant preventive effects, preventing the loss of epidermal innervation (Figures 2(c) and 2(d)). The results of our study demonstrated that J12 could prevent the loss of epidermal nerve fibers induced by oxaliplatin.

4.3. Systems Pharmacology Revealed Potential Therapeutic Effects of the MAPK Signaling Pathway in OIPN. J12 contains four herbs, but the mechanism of J12 treatment of OIPN remains unclear because of the multicomponent, multitarget nature of the herbal component. Therefore, we conducted a systematic approach to investigate the possible pharmacological mechanisms of J12.

A total of 471 compounds were collected from J12 to screen for active compounds by indicator, including drug half-life (HL), drug similarity (DL), oral bioavailability (OB), blood-brain barrier (BBB), and Coco-2 permeability (Coco-2) with the following criteria: HL ≥ 4, DL ≥ 0.18, OB% ≥ 30%, BBB ≥ -0.3, and Caco-2 ≥ -0.4 [17]. Finally, 64 potential compounds were screened. TCM compounding can play a therapeutic role through multiple targets. Therefore, we adopt a systematic approach to predict the potential targets of J12, and 88 potential targets were predicted: 49 for Salvia miltiorrhiza Bge, 73 for Achyranthes bidentata Blume, 62 for Paeonia veitchii Lynch, and 39 for Dendrobium nobile Lindl. It is worth noting that some herbs have similar targets; for example, four herbs can affect mitogen-activated protein kinase 14 (a key enzyme in the p38-MAPK signaling pathway), which is a key regulator of proinflammatory cytokine biosynthesis, making different components of the pathway a therapeutic potential target for autoimmune and inflammatory diseases.

Then, we erected a compound-target network from the selected active compounds and their potential targets to identify the complex interactions between them (Figure 3). Throughout the network, we found that most compounds are involved in the regulation of multiple targets (for

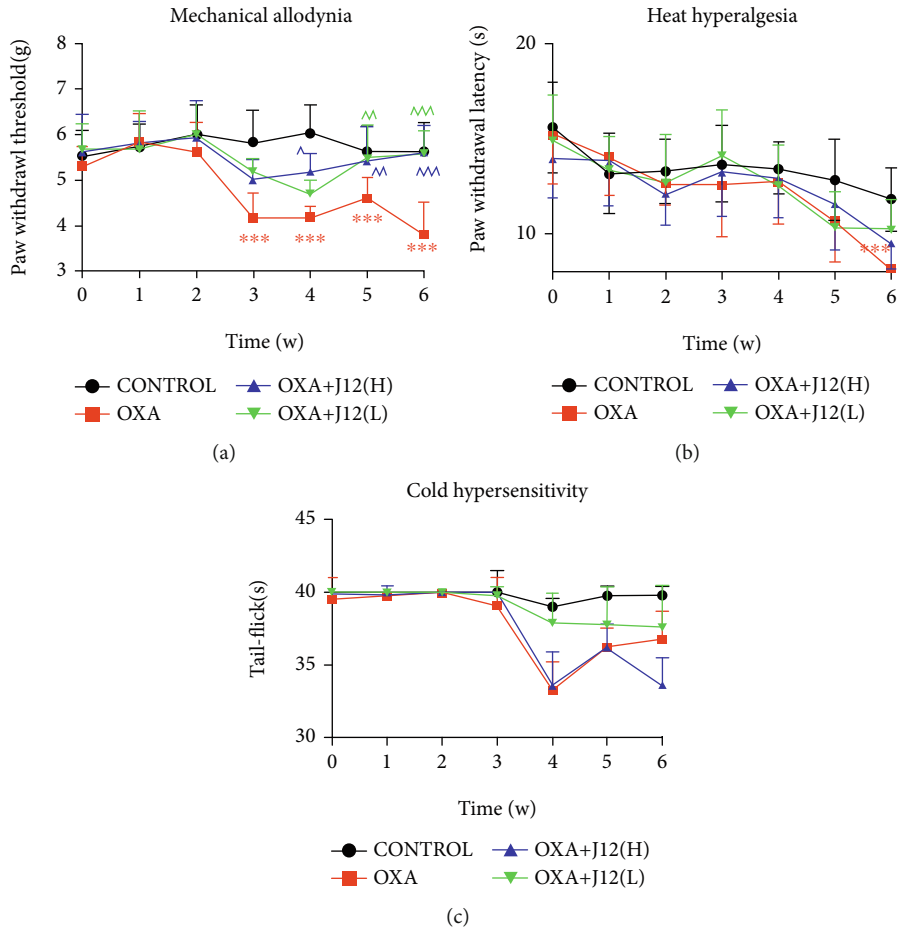

Figure 1: J12 treatment prevented OXA-induced inflammatory pain. J12 treatment prevented OXA-induced mechanical allodynia (a), heat hyperalgesia (b), and cold hypersensitivity (c). ** vs. Control, $p < 0.01$; *** vs. Control, $p < 0.001$; ^ vs. OXA, $p < 0.05$; ^^ vs. OXA, $p < 0.01$; ^^^ vs. OXA, $p < 0.001$, $\alpha = 0.05$; $n \geq 6$.

example, beta-sitosterol, stigmasterol, 1,2,5,6-tetrahydrotanshinone, sugiol, and wogonin). They may be the key multieffect compounds of J12 and play a pharmacological role in OIPN and other diseases.

We used the screened active compounds and potential targets to construct a compound-target network to elucidate the complex interactions between them. Eighty-seven genes were gathered from five databases (GAD, PharmGKB, DrugBank, TTD, and OMIM) and recognized as CIPN-related targets. Genes and proteins do not act by acting independently of each other but through interconnected molecular networks and pathways acting at multiple levels [21]. Therefore, we selected proteins as nodes to generate the network (Figure 4). First, through previous screening and prediction, we constructed a protein-protein interaction (PPI) network for J12-related targets (3955 nodes and 96391 edges) (Figure 4(a)). Next, we constructed a PPI network of OIPN-related targets (3877 nodes and 88138 edges) (Figure 4(b)). We then combined the two networks to form a core protein-protein interaction (CPPI) network. To determine the important proteins in the CPPI network, the Cytoscape plugin CytoNCA was then used for concentration analysis [22]. .DC," "BC," "CC," "EC," "NC," and "LAC" are set to medians of 80, 3398.987, 0.474, 0.0169, 20.668, and 14.984, respectively. Finally, we considered the 170 candidate targets as the main hubs (Figure 4(c)).

Through the DAVID and Metascape databases, further research on potential pathways involving candidate targets, the results were divided into two categories, namely, molecular functions/biological processes and signaling pathways. As shown in Figure 5, gene ontology (GO) analysis showed that J12 participation in the biological process ranked top: protein ubiquitination was involved, including in ubiquitin-dependent protein catabolic process, MAPK cascade, apoptotic process, positive regulation of ERK1 and ERK2 cascade, and negative regulation of neuron death. The analysis showed that the molecular functions involved were protein binding, protein kinase binding, and NF-kappaB binding.

The results of KEGG annotation analysis showed that J12 participates in signaling pathways, including the MAPK signaling pathway, ubiquitin-mediated proteolysis, and neurotrophin signaling pathway (Figure 6). Based on these data, we speculate that J12 may inhibit OIPN by participating in the regulation of the MAPK pathway. Therefore, to verify the influence of J12 in the MAPK pathway, we conducted relevant molecular biological assays.

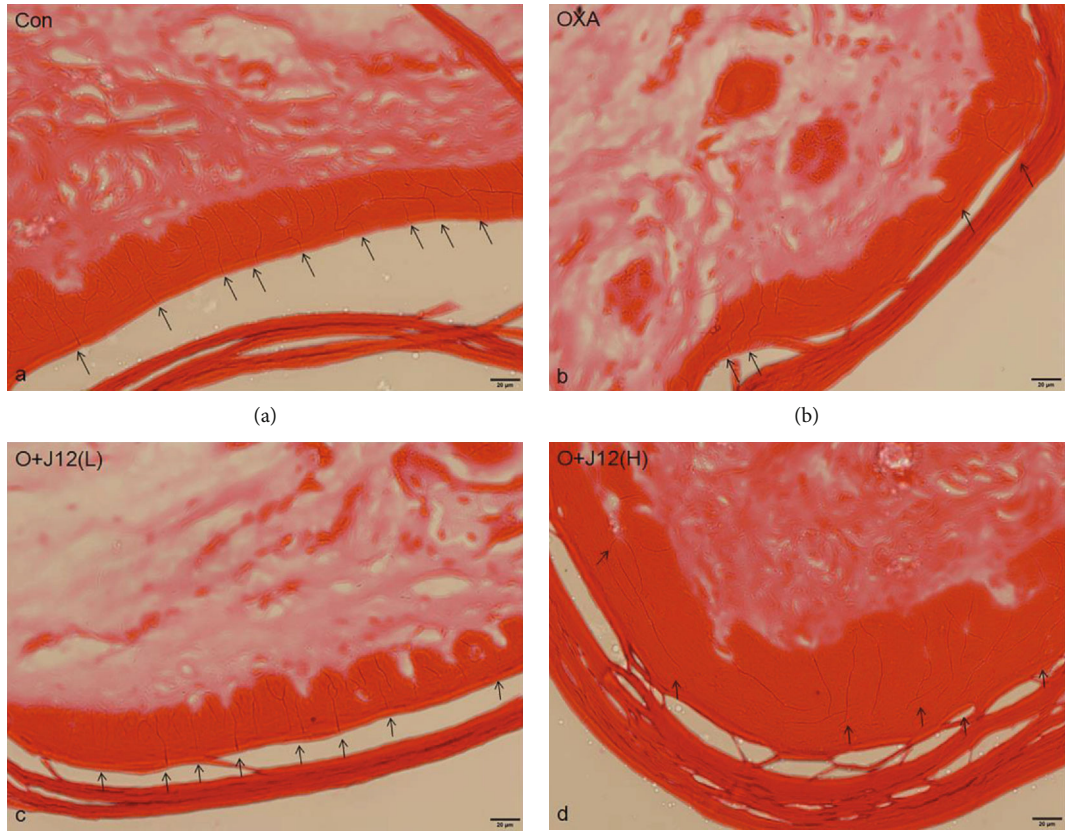

(a) (b) (c) (d)

Figure 2: Animals were sectioned and stained with PGP9.5. Hindpaw skin tissue from control (a), OXA (b), O+J12 (L) (c), and O+J12 (H) (d) demonstrated that J12 could prevent oxaliplatin-induced loss of intraepidermal nerve fiber (IENF) density (scale bar = 20 μm).

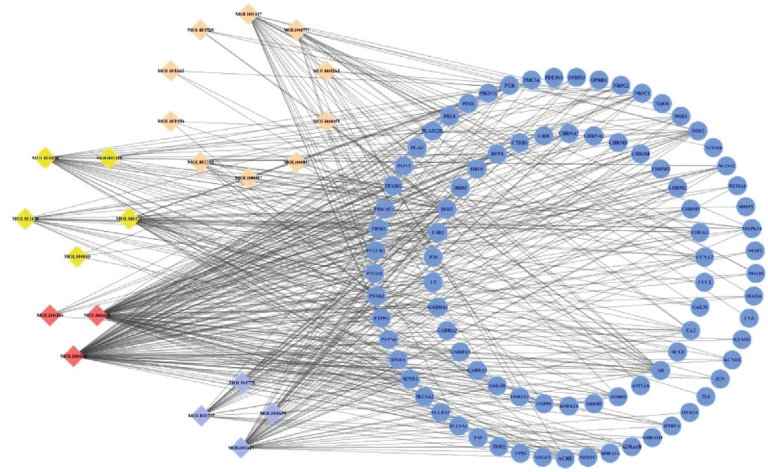

Figure 3: Construction of the J12 compound-putative target network. The candidate compounds of the four herbs and their putative targets were connected to construct a putative target network of compounds. The nodes representing the candidate compounds are shown as multicolored quadrilateral, and the targets are represented by blue circles.

4.4. J12 Prevents Oxaliplatin-Induced p-ERK1/2, p-p38 and NF-κB Activation in DRGs. Based on the above analysis, to verify whether the MAPK signaling pathway and NF-κB are involved in oxaliplatin-induced neuroinflammation, western blot analysis was performed to detect the protein expression levels of MAPK and NF-κB in the DRG. Compared to control mice, p-p38, p-ERK1/2, and NF-κB were activated in the OXA group. Compared to the OXA group, most of the same proteins were reduced in the treatment group (Figures 7(a), 7(b), and 7(d)).

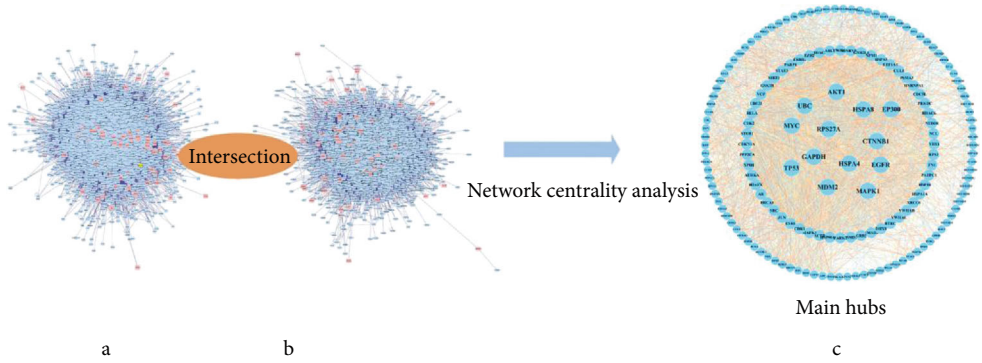

Figure 4: Network centrality analysis: prediction of compound targets and construction of known OIPN-related targets (a, b). Identification of advertising and screening therapeutic targets for J12 (c).

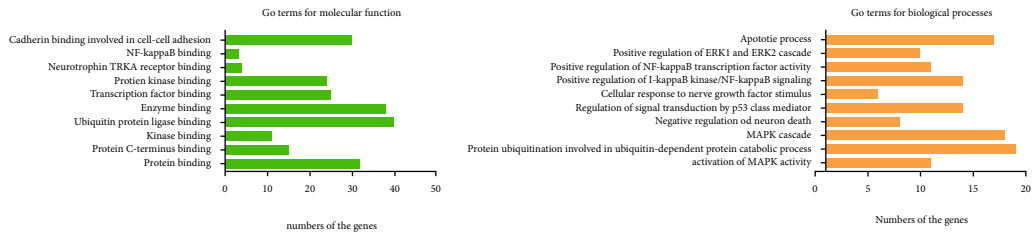

Figure 5: GO analysis shows representative molecular functions (a) and biological processes (b).

Immunofluorescence results also revealed the role of NF-κB in oxaliplatin-induced neuropathic pain (Figure 8). These results suggest that J12 prevents oxaliplatin-induced neuropathic pain by activating p38, ERK1/2, and NF-κB signaling pathways without activating p-JNK/JNK (Figure 7(c)).

4.5. J12 Attenuates Oxaliplatin-Induced TNF-α, IL-6, and IL-1β Activation in DRGs. By measuring quantitative RT-PCR, we found that the mRNA of TNF-α, IL-6, and IL-1β were activated in the OXA group comparing with control group. However, the prophylactic administration of J12 could effectively prevent these upregulations, and the preventive effect of the low-dose (5 g/kg) prophylaxis group was significantly better than that of the high-dose (10 g/kg) group (Figures 9(a), 9(b), and 9(c)).

4.6. J12 Prevents the Increase in Oxaliplatin-Induced Inflammatory-Related Factors in the Serum of Mice. ELISA results show that compared with the control group, inflammatory-related factors of the mouse serum were significantly elevated by injecting oxaliplatin. This phenomenon was significantly improved in the preventive treatment group (Figure 10). However, it is interesting to find that in the serum, the preventive effect of the high-dose (10 g/kg) prophylaxis group was significantly better than that of the low-dose (5 g/kg) group. This is different from the results of those factors in DRG.

5. Discussion

Oxaliplatin is still one of the main treatments for colorectal cancers [23]. However, its anticancer efficacy is related to adverse drug reactions, especially chemotherapy-induced peripheral neuropathy (CIPN), which is the main dose-limiting toxicity of this therapy [24]. OIPN presents specific sensory disturbances, pain induced by cold and warmth, and decreased vibration perception of the hands and feet [25]. Therefore, finding a way to protect against this neuropathic pain is critical. According to an analysis of the literature, despite many neuron disease therapeutic clinical trials, no standard evidence-based treatment exists. In 2012, ASCO reported that the antidepressant duloxetine can slow down the associated numbness and tingling symptoms caused by *Taxol* or platinum but lacks systematic research evidence. However, colorectal cancer survivors now account for the third largest group of cancer survivors [26], and efficient strategies are needed to improve the prevention and/or treatment of OIPN. Therefore, we started to explore Chinese herbal medicine, which is much less toxic.

J12 has been proven to strengthen bones and tendons, to promote blood circulation, and to remove blood stasis in the clinic. Moreover, J12 is often used to treat the symptoms of weakness, pain, and edema of the lower limbs, which result from blood stasis [12]. J12 could prevent oxaliplatin-induced peripheral neuralgia based on our behavioral tests. However, there are no articles on

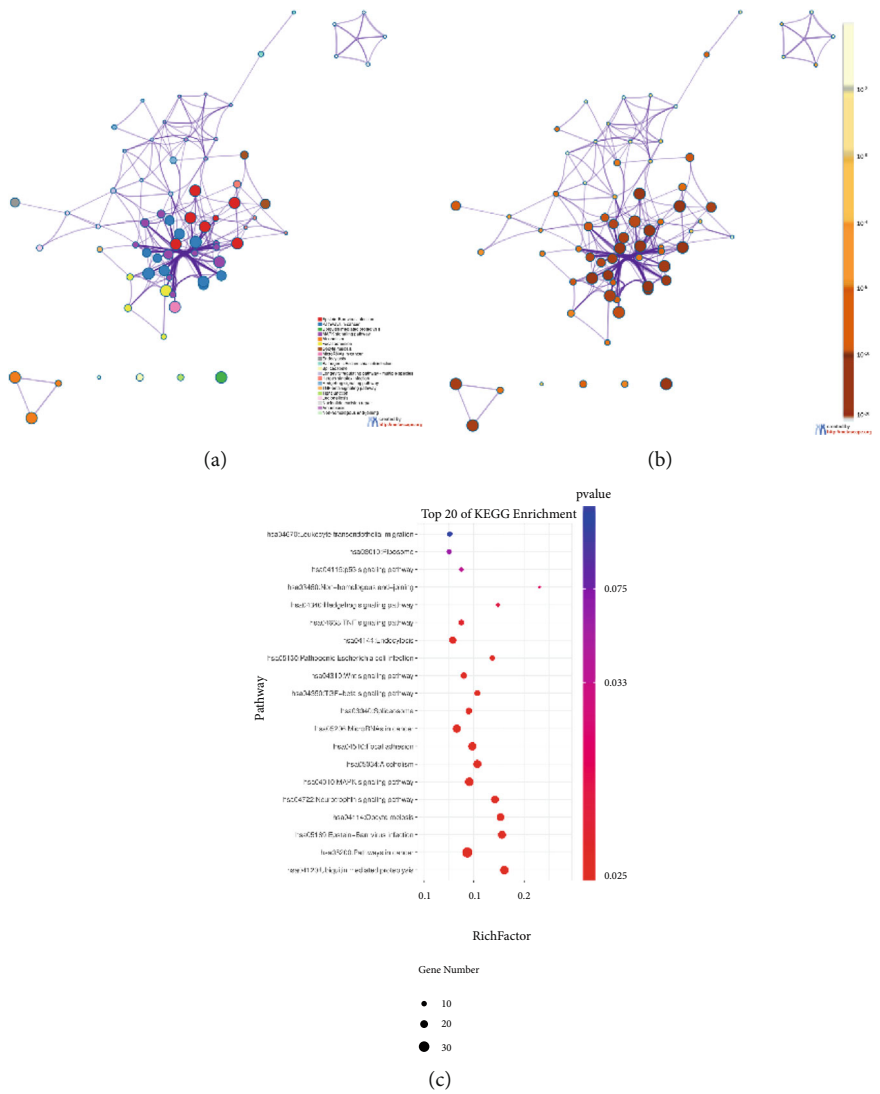

FIGURE 6: Pathway enrichment analysis: Enriched representative signal transduction pathways. Nodes in the same enriched network are colored with p values. The darker the color is, the more statistically important the node is. The larger the Rich factor is, the higher the enrichment degree is.

the roles of J12 in the prevention and treatment of oxaliplatin-induced neuroinflammation.

Considering the complexity and diversity of herbal formulation components, it may be difficult to elucidate the mechanism of J12 treatment for CIPN; hence, the systematic approach was carried out first. First, we gathered a batch of active compounds in J12 by screening absorption, distribution, metabolism, and excretion (ADME). After that, the target of J12 is predicted, and a composite target network is constructed to further understand the interaction of composite targets, to further identify the key regulatory factors that these targets play as an important role in CIPN therapy. We combined two PPI networks to generate a CPPI network, one for J12 targets and the other for CIPN-related targets. By screening the topological characteristics of the CPPI network, we obtained key proteins that may contribute to CIPN therapy. Using the DAVID database and Omicshare software, the MAPK signaling pathway was identified as the main pathway.

Nuclear factor kappa light chain enhancer of activated B cells (NF-κB) is a ubiquitous transcription factor well known for its role in the innate immune response. As such, NF-κB is a transcriptional activator of inflammatory mediators, such as cytokines. It has been reported that downregulating NF-κB can reduce inflammation [27]. Tumor necrosis factor α (TNF-α) is a master cytokine that mediates inflammatory responses and innate immunity. Guadalupe Sabio [28] has reviewed the mechanisms that mediate this dual role of MAP kinases in signal transduction mediated by TNF-α. It was stated that the activation of MAP kinases and TNF-α is synchronized. Interestingly, p38 MAP kinases can also inhibit NF-κB activity following exposure to TNF-α [29, 30]. It has long been proven that reducing IL-6 and IL-1β expression can reduce

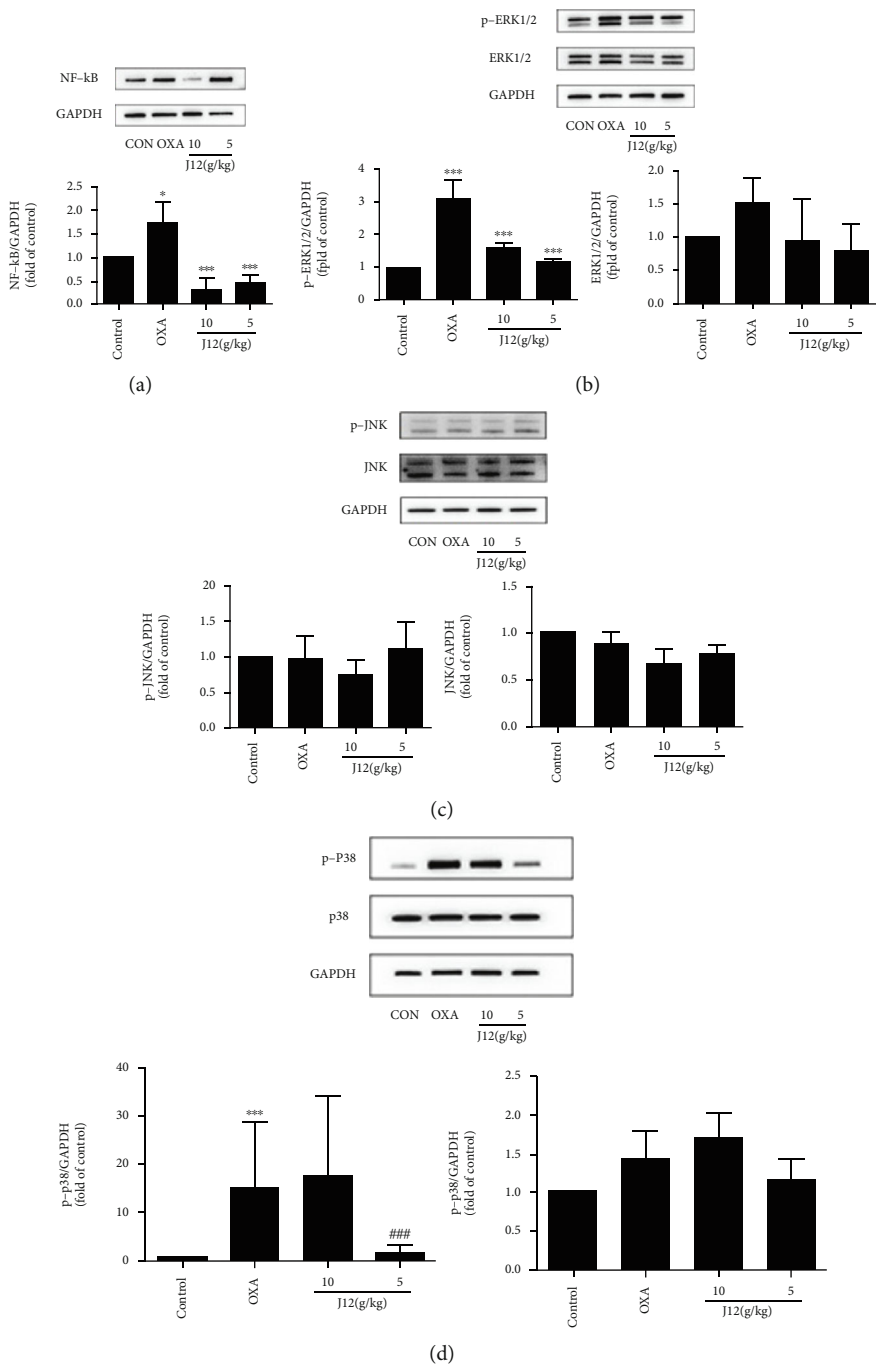

Figure 7: Compared with mice in the CONTROL group, p-p38, p-ERK1/2, and NF-κB in the OXA group were activated. Compared with the OXA group, the same proteins in the treatment groups were mostly decreased (a, c, and d). The O+J12(L) group showed better preventive effects than the O+J12(H) group in p-p38 (d). Otherwise, the high-dose group was better than the NF-κB (a) group. In conclusion, J12 prevents oxaliplatin-induced NF-κB (a), p-ERK1/2 (b), and p-p38 (d) activation in the DRG. * vs. Control, $p < 0.05$; ** vs. Control, $p < 0.01$; $^{\#}$ vs. OXA, $p < 0.05$; $^{\#\#}$ vs. OXA, $p < 0.01$, $^{\#\#\#}$ vs. OXA, $p < 0.001$, $\alpha = 0.05$.

inflammation [31, 32], similar to the data in this article. Another interesting finding is that in our results, it was shown that the prevention and treatment effects of J12 low-dose and high-dose groups are completely different in DRG and serum. Our hypothesis is that chemotherapy drugs affected this result in mice because chemotherapeutic drugs can accumulate in the dorsal root ganglia (DRG) [33, 34] and are considered to be used to deliver noxious stimuli [35, 36].

6. Conclusions

In our study, we investigated the effect of J12 on oxaliplatin-induced inflammatory pain and the potential

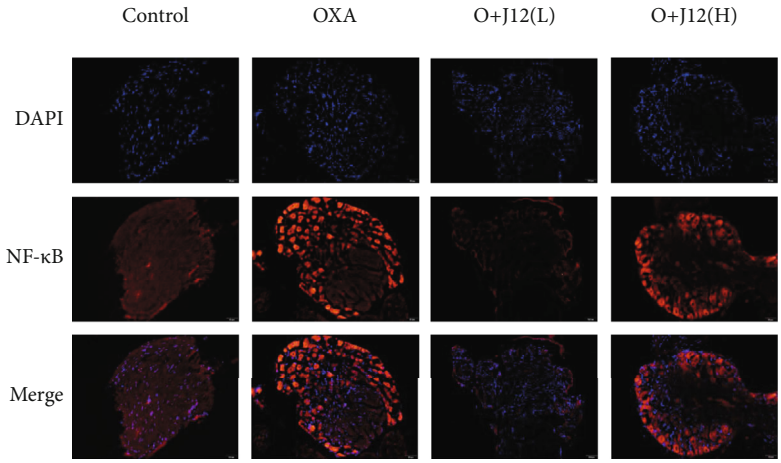

Figure 8: In general, the expression of NF-κB in normal nerve cells is rare. From the figure, we found that the activation of NF-κB was induced by OXA. The immunofluorescence results demonstrated that J12 could prevent oxaliplatin-induced NF-κB activation in the DRG (scale bar = 50 μm).

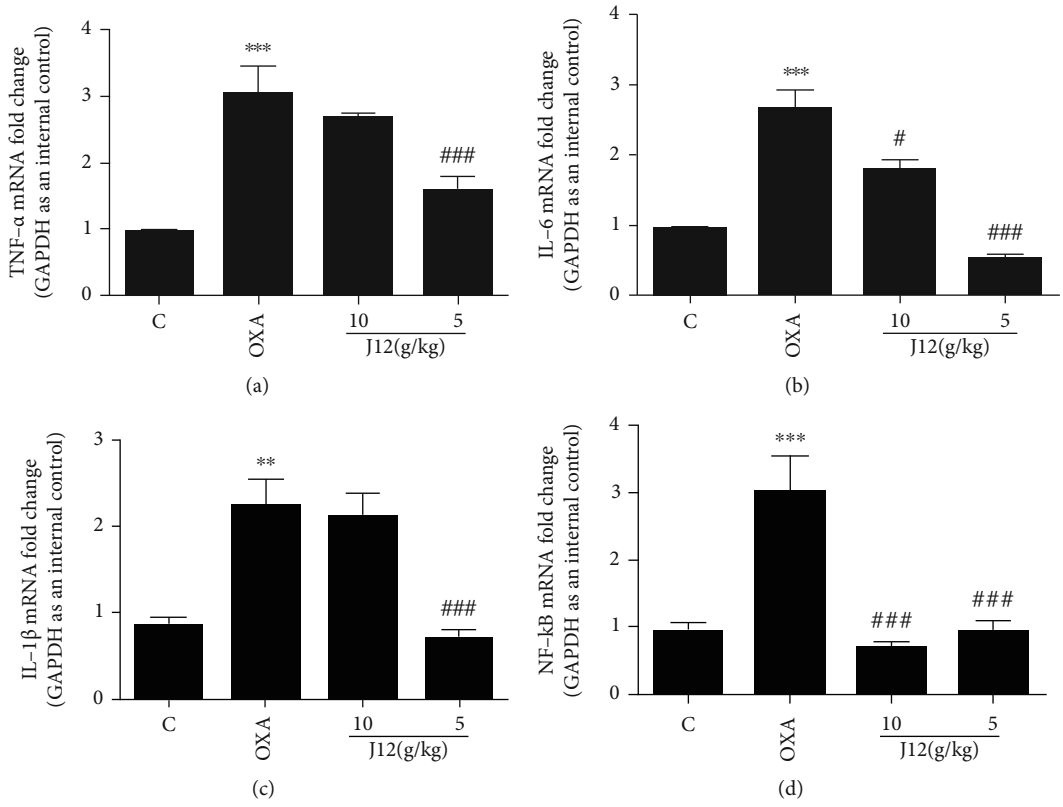

Figure 9: Quantitative RT-PCR showed that J12 could prevent oxaliplatin-induced TNF-α (a), IL-6 (b), IL-1β (c), and NF-κB (d) activation in the DRG. * vs. Control, $p < 0.05$; ** vs. Control, $p < 0.01$; *** vs. Control, $p < 0.001$; $^{\#}$ vs. OXA, $p < 0.05$; $^{\#\#}$ vs. OXA, $p < 0.01$; $^{\#\#\#}$ vs. OXA, $p < 0.001$, $\alpha = 0.05$.

underlying mechanisms. The results suggested that J12 had an anti-inflammatory effect in mice, inhibited by the activation of p38/NF-κB and/or ERK/NF-κB induced by oxaliplatin. J12 could reduce the oxaliplatin-induced production of TNF-α, IL-6, and IL-1β in the dorsal root ganglion. Overall, these data suggested that J12 may be effective in attenuating neuroinflammation in mice. These findings may aid in further exploration of the mechanism of J12 prevention of oxaliplatin-induced inflammation.

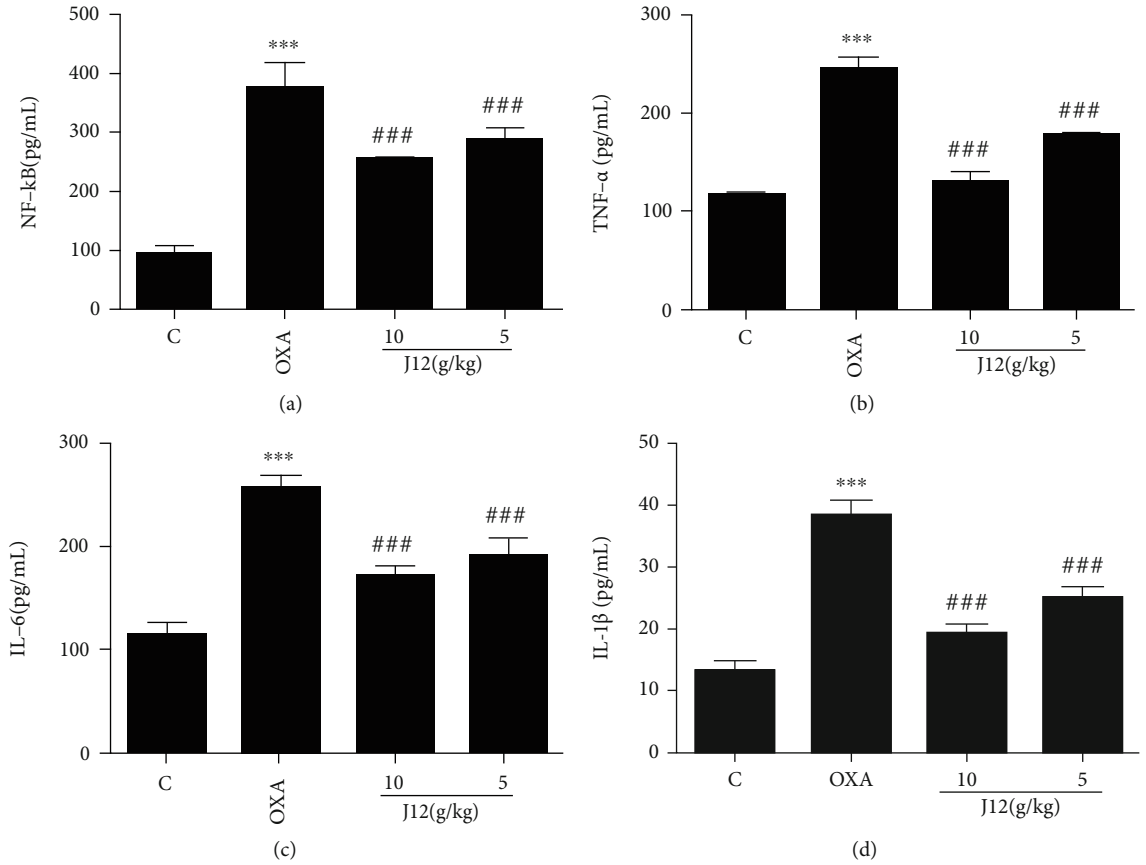

Figure 10: ELISA showed that J12 could prevent oxaliplatin-induced NF-κB (a), TNF-α (b), IL-6 (c), and IL-1β (d) activation in the serum of mice. *** vs. Control, $p < 0.001$; ### vs. OXA, $p < 0.001$, $n = 6$.

Data Availability

The data used to support the findings of this study are available from the corresponding author upon reasonable request.

Ethical Approval

All experiments were performed in accordance with protocols approved by the Animal Care and Use Committee at the Nanjing University of Chinese Medicine (Approval number AUC171001).

Conflicts of Interest

The authors declare that they have no conflicts of interest.

Authors' Contributions

Peng Zhang and Yuting Lu contributed equally to this work.

Acknowledgments

This study was supported by Key Project of Jiangsu Province for Fundamental Research and Development (BE2018717), The dual creative team of Jiangsu Province (2018-2020, 013033004008A), Specially-appointed Professor Grant by JiangSu province (2014, Prof. Jing Zhu), and Jiangsu Six Talent Peak Award (2015, Prof. Jing Zhu, 013034001002).

Supplementary Materials

Figure S1: fingerprint of Siwei Jianbu Decoction and its common pattern. Taking the shared model as a reference, taking the shared model as a reference, the similarities between S1 and S10 are 0.930, 0.951, 0.937, 0.943, 0.834, 0.931, 0.936, 0.958, 0.886, and 0.919, respectively. Figure S2: fingerprint common peak and reference spectrum: 14 main common peaks can be seen in the fingerprint spectrum, accounting for more than 90% of the total peak area. Comparing the retention time with the chromatogram of the reference substance, the common peaks 4, 5, and 10 are, respectively, identified as paeoniflorin, β-ecdysterone, and salvianolic acid B. *(Supplementary Materials)*

References

[1] T. André, C. Boni, L. Mounedji-Boudiaf et al., "Oxaliplatin, fluorouracil, and leucovorin as adjuvant treatment for colon cancer," *New England Journal of Medicine*, vol. 350, pp. 2343–2351, 2004.

[2] I. Chau and D. Cunningham, "Adjuvant therapy in colon cancer–what, when and how?," *Annals of Oncology*, vol. 17, no. 9, pp. 1347–1359, 2006.

[3] D. Balayssac, J. Ferrier, B. Pereira et al., "Prevention of oxaliplatin-induced peripheral neuropathy by a polyamine-reduced diet-NEUROXAPOL: protocol of a prospective, randomised, controlled, single-blind and monocentric trial," *BMJ Open*, vol. 5, no. 4, article e7479, p. e007479, 2015.

[4] S. Wolf, D. Barton, L. Kottschade, A. Grothey, and C. Loprinzi, "Chemotherapy-induced peripheral neuropathy: Prevention and treatment strategies," *European Journal of Cancer*, vol. 44, no. 11, pp. 1507–1515, 2008.

[5] X.-M. Wang, T. J. Lehky, J. M. Brell, and S. G. Dorsey, "Discovering cytokines as targets for chemotherapy-induced painful peripheral neuropathy," *Cytokine*, vol. 59, no. 1, pp. 3–9, 2012.

[6] A. Scuteri, A. Galimberti, D. Maggioni et al., "Role of MAPKs in platinum-induced neuronal apoptosis," *Neurotoxicology*, vol. 30, no. 2, pp. 312–319, 2009.

[7] L. D. C. Mannelli, A. Pacini, L. Micheli, A. Tani, M. Zanardelli, and C. Ghelardini, "Glial role in oxaliplatin-induced neuropathic pain," *Experimental Neurology*, vol. 261, pp. 22–33, 2014.

[8] M. L. Slattery, A. Lundgreen, and R. K. Wolff, "MAP kinase genes and colon and rectal cancer," *Carcinogenesis*, vol. 33, no. 12, pp. 2398–2408, 2012.

[9] H. Chen, Q. Wang, D. Shi et al., "Celecoxib alleviates oxaliplatin-induced hyperalgesia through inhibition of spinal ERK1/2 signaling," *Journal of Toxicologic Pathology*, vol. 29, no. 4, pp. 253–259, 2016.

[10] P. Milla, M. Airoldi, G. Weber, A. Drescher, U. Jaehde, and L. Cattel, "Administration of reduced glutathione in FOLFOX4 adjuvant treatment for colorectal cancer: effect on oxaliplatin pharmacokinetics, Pt-DNA adduct formation, and neurotoxicity," *Anticancer Drugs*, vol. 20, no. 5, pp. 396–402, 2009.

[11] R. Coriat, J. Alexandre, C. Nicco et al., "Treatment of oxaliplatin-induced peripheral neuropathy by intravenous mangafodipir," *Journal of Clinical Investigation*, vol. 124, no. 1, pp. 262–272, 2014.

[12] C. Wen-Ji, "Professor Huang Huang's Experience in Application of 'Siwei Jianbu Decoction," *Shanghai Journal of Traditional Chinese Medicine*, vol. 42, no. 4, pp. 10–12, 2008.

[13] Y. Yang, L. Luo, X. Cai et al., "Nrf2 inhibits oxaliplatin-induced peripheral neuropathy via protection of mitochondrial function," *Free Radical Biology and Medicine*, vol. 120, pp. 13–24, 2018.

[14] J. Boyette-Davis, W. Xin, H. Zhang, and P. M. Dougherty, "Intraepidermal nerve fiber loss corresponds to the development of Taxol-induced hyperalgesia and can be prevented by treatment with minocycline," *Pain*, vol. 152, no. 2, pp. 308–313, 2011.

[15] J. Wu, T. Zhang, L. Yu et al., "Zhile Capsule Exerts Antidepressant-Like Effects through Upregulation of the BDNF Signaling Pathway and Neuroprotection," *International Journal of Molecular Sciences*, vol. 20, no. 1, p. 195, 2019.

[16] C. Zheng, T. Pei, C. Huang et al., "A novel systems pharmacology platform to dissect action mechanisms of traditional Chinese medicines for bovine viral diarrhea disease," *European Journal of Pharmaceutical Sciences*, vol. 94, pp. 33–45, 2016.

[17] H. Liu, J. Wang, W. Zhou, Y. Wang, and L. Yang, "Systems approaches and polypharmacology for drug discovery from herbal medicines: an example using licorice," *Journal of Ethnopharmacology*, vol. 146, no. 3, pp. 773–793, 2013.

[18] H. Yu, J. Chen, X. Xu et al., "A systematic prediction of multiple drug-target interactions from chemical, genomic, and pharmacological data," *PLoS One*, vol. 7, no. 5, article e37608, 2012.

[19] A. Martin, M. E. Ochagavia, L. C. Rabasa, J. Miranda, J. Fernandez-de-Cossio, and R. Bringas, "BisoGenet: a new tool for gene network building, visualization and analysis," *BMC Bioinformatics*, vol. 11, no. 1, p. 91, 2010.

[20] Y. Tang, M. Li, J. Wang, Y. Pan, and F. X. Wu, "CytoNCA: a cytoscape plugin for centrality analysis and evaluation of protein interaction networks," *Bio Systems*, vol. 127, pp. 67–72, 2015.

[21] D. Greenbaum, C. Colangelo, K. Williams, and M. Gerstein, "Comparing protein abundance and mRNA expression levels on a genomic scale," *Genome Biology*, vol. 4, no. 9, p. 117, 2003.

[22] A. J. Beijers, F. Mols, and G. Vreugdenhil, "A systematic review on chronic oxaliplatin-induced peripheral neuropathy and the relation with oxaliplatin administration," *Supportive Care in Cancer*, vol. 22, no. 7, pp. 1999–2007, 2014.

[23] B. Nordlinger, H. Sorbye, B. Glimelius et al., "Perioperative FOLFOX4 chemotherapy and surgery versus surgery alone for resectable liver metastases from colorectal cancer (EORTC 40983): long-term results of a randomised, controlled, phase 3 trial," *Lancet Oncology*, vol. 14, no. 12, pp. 1208–1215, 2013.

[24] A. J. Beijers, J. L. Jongen, and G. Vreugdenhil, "Chemotherapy-induced neurotoxicity: the value of neuroprotective strategies," *Netherlands Journal of Medicine*, vol. 70, no. 1, pp. 18–25, 2012.

[25] N. Attal, D. Bouhassira, M. Gautron et al., "Thermal hyperalgesia as a marker of oxaliplatin neurotoxicity: a prospective quantified sensory assessment study," *Pain*, vol. 144, no. 3, pp. 245–252, 2009.

[26] P. A. Ganz, "Why and how to study the fate of cancer survivors: observations from the clinic and the research laboratory," *European Journal of Cancer*, vol. 39, no. 15, pp. 2136–2141, 2003.

[27] T. Watanabe, N. Asano, G. Meng et al., "NOD2 downregulates colonic inflammation by IRF4-mediated inhibition of K63-linked polyubiquitination of RICK and TRAF6," *Mucosal Immunology*, vol. 7, no. 6, pp. 1312–1325, 2014.

[28] G. Sabio and R. J. Davis, "TNF and MAP kinase signalling pathways," *Seminars in Immunology*, vol. 26, no. 3, pp. 237–245, 2014.

[29] A. G. Bowie and L. A. O'Neill, "Vitamin C inhibits NF-kappa B activation by TNF via the activation of p38 mitogen-activated protein kinase," *Journal of Immunology*, vol. 165, no. 12, pp. 7180–7188, 2000.

[30] D. Alpert, P. Schwenger, J. Han, and J. Vilcek, "Cell stress and MKK6b-mediated p38 MAP kinase activation inhibit tumor necrosis factor-induced IkappaB phosphorylation and NF-kappaB activation," *Journal of Biological Chemistry*, vol. 274, no. 32, pp. 22176–22183, 1999.

[31] V. Tiwari and K. Chopra, "Attenuation of oxidative stress, neuroinflammation, and apoptosis by curcumin prevents cognitive deficits in rats postnatally exposed to ethanol," *Psychopharmacology*, vol. 224, no. 4, pp. 519–535, 2012.

[32] J. Vink, J. Auth, D. T. Abebe, D. E. Brenneman, and C. Y. Spong, "Novel peptides prevent alcohol-induced spatial learning deficits and proinflammatory cytokine release in a mouse model of fetal alcohol syndrome," *American journal of Obstetrics and Gynecology*, vol. 193, no. 3, Part 1, pp. 825–829, 2005.

[33] S. R. Mcwhinney, R. M. Goldberg, and H. L. Mcleod, "Platinum neurotoxicity pharmacogenetics," *Molecular Cancer Therapeutics*, vol. 8, no. 1, pp. 10–16, 2009.

[34] S. B. Park, D. Goldstein, A. V. Krishnan et al., "Chemotherapy-induced peripheral neurotoxicity: a critical analysis," *Ca A Cancer Journal for Clinicians*, vol. 63, no. 6, pp. 419–437, 2013.

[35] M. P. Caulfield, "Muscarinic receptors–characterization, coupling and function," *Pharmacology & Therapeutics*, vol. 58, no. 3, pp. 319–379, 1993.

[36] W. Jürgen, A. Duttaroy, J. Gomeza et al., "Muscarinic receptor subtypes mediating central and peripheral antinociception studied with muscarinic receptor knockout mice," *Life Sciences*, vol. 72, no. 18-19, pp. 2047–2054, 2003.

Hindawi
Neural Plasticity
Volume 2020, Article ID 8888871, 8 pages
https://doi.org/10.1155/2020/8888871

Research Article

Aβ-Induced Repressor Element 1-Silencing Transcription Factor (REST) Gene Delivery Suppresses Activation of Microglia-Like BV-2 Cells

Tongya Yu,[1] Hui Quan,[1] Yuzhen Xu,[1] Yunxiao Dou,[1] Feihong Wang,[2] Yingying Lin,[1] Xue Qi,[1] Yanxin Zhao,[1] and Xueyuan Liu[1]

[1]*Shanghai Tenth People's Hospital of Tongji University, Tongji University, Middle Yanchang Rd. 301#, Jingan District, Shanghai, China 200072*
[2]*Shanghai Tenth People's Hospital of Tongji University, Nanjing Medical University, Middle Yanchang Rd. 301#, Jingan District, Shanghai, China 200072*

Correspondence should be addressed to Yanxin Zhao; zhao_yanxin@tongji.edu.cn and Xueyuan Liu; liuxy@tongji.edu.cn

Received 28 June 2020; Revised 18 August 2020; Accepted 24 August 2020; Published 22 September 2020

Academic Editor: Fushun Wang

Compelling evidence from basic molecular biology has demonstrated the crucial role of microglia in the pathogenesis of Alzheimer's disease (AD). Microglia were believed to play a dual role in both promoting and inhibiting Alzheimer's disease progression. It is of great significance to regulate the function of microglia and make them develop in a favorable way. In the present study, we investigated the function of repressor element 1-silencing transcription factor (REST) in $A\beta_{1\text{-}42}$-induced BV-2 cell dysfunction. We concluded that $A\beta_{1\text{-}42}$ could promote type I activation of BV-2 cells and induce cell proliferation, migration, and proinflammation cytokine TNF-α, IL-1β, and IL-6 expression. Meanwhile, REST was upregulated, and nuclear translocalization took place due to $A\beta_{1\text{-}42}$ stimulation. When REST was knocked down by a specific short hairpin RNA (sh-RNA), BV-2 cell proliferation, migration, and proinflammation cytokine expression and secretion induced by $A\beta_{1\text{-}42}$ were increased, demonstrating that REST may act as a repressor of microglia-like BV-2 cell activation.

1. Introduction

Alzheimer's disease (AD), a chronic and neurodegenerative disease, is currently the most prevalent cause of dementia of aging people. The neuropathological hallmarks of AD include extracellular Aβ deposits, intracellular neurofibrillary tangles, and marked inflammation [1, 2]. As a chronic and degenerative disease, Alzheimer's disease progress is coupled with continuous activation of microglia [3]. Microglia, the main innate immune cells in the central nervous system, play a pivotal role in the process of AD including secretion of proinflammation cytokines, clearance of amyloid plaques, and synaptic pruning [4–6]. In the pathogenesis of AD, microglia have both advantages and disadvantages. Selective modulation of microglia phenotype function could be a promising strategy in AD.

Repressor element 1-silencing transcription factor (REST), also named neuron-restricted silencing factor (NRSF), is a zinc finger protein which binds to a 21 bp repressor element-1 (RE-1) to keep silence of hundreds of genes, many of which are neurally expressed genes [7, 8]. REST is known to play a key role in neuronal differentiation, including neurogenesis, synaptogenesis, excitability, and synaptic transmission [9, 10]. Importantly, REST dysregulation has been associated with neurodegenerative diseases, such as Alzheimer's disease [11–13]. In an aging neuron, REST is induced strikingly in the nucleus of cortical and hippocampus neurons to repress genes associated with cell death and AD pathology and protects neurons from oxidative stress and amyloid β-protein (Aβ) toxicity, while REST is almost absent from the nucleus in AD leading to neuron damage thus cognitive impairment [12]. Up to now, existing studies

are mainly about functions of REST in neurons or astrocytes; nevertheless, the function of REST protein in microglia remains unknown even though REST also has high expression abundance in microglia [14]. In this study, we evaluated the levels of REST protein in A$\beta_{1\text{-}42}$-treated BV-2 cells and characterized the effect of REST on the function of microglia including proliferation, cell migration, and expression and secretion of proinflammation cytokines.

2. Materials and Methods

2.1. Cell Culture and Treatment. Mouse microglia-like BV-2 cells were cultured in Dulbecco's modified Eagle's medium (DMEM) containing 10% fetal bovine serum (FBS) at 37°C in an atmosphere containing 5% CO_2. BV-2 cells were cultured for 24 h or 48 h with different concentrations of A$\beta_{1\text{-}42}$ oligomers (ChinaPeptides, Shanghai, China). Synthetic A$\beta_{1\text{-}42}$ power was dissolved in 0.4% DMSO water to 100 μM, then incubated at 37°C for 72 h for oligomerization.

2.2. Cell Viability Assay. BV-2 cells were seeded into 96-well plates in 100 μL complete media at a density of 4×10^5 cells/mL and treated with A$\beta_{1\text{-}42}$ (0, 1, 2.5, or 5 μM) for 24 or 48 h. Cell viability was evaluated by Cell Counting Kit-8 (CCK8, Beyotime, Haimen, China) on the basis of our previous studies [15]. After incubation at 37°C in 5% CO_2 for 24 or 48 h, the 10 μL CCK8 reagent was added to each well under a lightproof condition, and incubation continued for a further 2 h. The cell viability was evaluated by measuring absorbance at 450 nm using a microplate reader. The experiments were carried out at least three times.

2.3. Western Blot. Before harvest, BV-2 cells were washed with cold PBS and then lysed with lysis buffer containing protease inhibitors for 30 min on ice. The samples were centrifuged at 12000 rpm, 4°C for 15 min. Then, the protein concentrations were determined by a BCA protein assay kit (Beyotime Institute of Biotechnology, Haimen, China) as previously described [16]. Proteins were electrophoresed using sodium dodecyl sulfate/polyacrylamide gel electrophoresis (SDS-PAGE, Bio-Rad, CA, USA) and transferred electrophoretically to PVDF membranes. Then, the membranes were blocked with 5% skim milk at room temperature (RT) for 1 h and then incubated with primary antibodies overnight at 4°C. Subsequently, membranes were washed and incubated with the appropriate HRP-conjugated secondary antibodies at room temperature for 1 h. Finally, membranes were washed and detected with enhanced chemiluminescence. Primary antibodies were as follows: anti-GAPDH (1 : 2000; Sangon Biotech), anti-β-actin (1 : 2000; Santa Cruz), anti-REST (1 : 1000; Abcam), anti-MHC II (1 : 1000, Abcam), and anti-Arg1 (1 : 1000; Sigma).

2.4. Real-Time RT-PCR. Total RNA was isolated from the BV-2 cells using the TRIzol reagent (Invitrogen Life Technologies, Carlsbad, CA, USA) according to the manufacturer's protocol. 1 mg of RNA was reverse-transcribed to cDNA using a PrimeScript™ RT reagent kit (TaKaRa Bio Inc., Beijing, China). Quantitative RT-PCR analysis was performed using a SYBR Green PCR Kit (KAPA Biosystems, South Africa) with 1 μL of cDNA template in 20 μL reaction mixture. Results were analyzed using the comparative CT method. Data are expressed throughout the study as $2^{-\Delta\Delta CT}$ for the experimental gene of interest normalized to β-actin. The gene-specific primer pairs were as follows: mouse REST gene forward 5′-GGCAGATGGCCGAATTGATG-3′ and reverse 5′-CTTTGAGGTCAGCCGACTCT-3′, actin gene forward 5′-ATCATGTTTGAGACCTTAAA-3′ and reverse 5′-CATCTCTTGCTCGAAGTCCA-3′, TNF-α gene forward 5′-CCTCTCTCTAATCAGCCCTCTG-3′ and reverse 5′-GAGGACCTGGGAGTAGATGAG-3′, IL-1β gene forward 5′-CCAGGGACAGGATATGGAGCA-3′ and reverse 5′-TTCAACACGCAGGACAGGTACG-3′, and IL-6 gene forward 5′-AAGCCAGA GCTGTGCAGATGAGTA-3′ and reverse 5′-TGTCCTGCAG CCACTGGTTC-3′.

2.5. Transwell Assay. BV-2 cells (2×10^4) were seeded in the inserts of transwells (Corning Costar Corp., Cambridge, MA, USA, 8.0 μm pore size), and the insert was transferred into a well with PC12 cells seeded in the lower chamber. PC12 cells were treated with or without Aβ, and the transwell system was incubated for 24 h in 5% CO_2 at 37°C. BV-2 cells that migrated to the lower surface were stained with gentian violet. Images were taken from four random fields at 40x magnification. The number of BV-2 cells on the lower surface of the insert was quantified. The experiments were repeated at least three times.

2.6. Plasmid Transfection. BV-2 cells were replanted 24 hours before transfection in 2 mL of fresh culture medium in a 6-well plastic plate. Plasmids were transfected when the cell density reached 70-80% by Lipofectamine 3000 (Thermo Fisher Scientific), according to the manufacturer's instructions. Before transfection, DMEM was removed, and Opti-MEM media were used instead. BV-2 cells were transfected with 2500 ng/well of the pLenR-GPH vector carrying shRNA against REST (bio-link, Shanghai, China). Alternatively, the mock plasmid pLenR-GPH (bio-link, Shanghai, China) was used as a control instead of the sh-REST plasmid. Six hours after transfection, Opti-MEM media were removed and BV-2 cells were cultured for 48 h in DMEM before collecting for further Western blotting or qPCR. The specific primer pairs were as follows: forward: 5′-GATCCGCAAGC TTCTGAAGGGAAACACTTCCTGTCAGATGTTTCCC TTCAGAAGCTTGCTTTTTG-3′ and reverse 5′-AATTCA AAAAGCAAGCTTCTGAAGGGAAACATCTGACAGGA AGTGTTTCCCTTCAGAAGCTTGCG-3′.

2.7. Enzyme-Linked Immunosorbent Assay (ELISA). Proinflammation cytokine TNF-α, IL-1β, and IL-6 levels of cellular supernatant were measured with commercial mouse ELISA kits according to the manufacturer's instructions (eBioscience Inc., CA, USA). The concentration of target proteins was indexed by absorbance measured at 450 nm.

2.8. Statistical Analyses. Results were expressed as the mean ± standard deviations (SD). Student's t-test was used for

the determination of statistical significance among groups. The level of statistical significance was $P < 0.05$.

3. Results

3.1. $A\beta_{1\text{-}42}$ Induced BV-2 Cell Activation. We investigated the effect of synthetic $A\beta_{1\text{-}42}$ on BV-2 cell proliferation using the CCK8 assay. BV-2 cells were treated with different concentrations of synthetic $A\beta_{1\text{-}42}$ (0-5 μM) for 24 and 48 hours. When BV-2 cells were treated for 24 h, 1 or 2.5 μM $A\beta_{1\text{-}42}$ did not induce cell proliferation while 5 μM $A\beta_{1\text{-}42}$ promotes cell proliferation significantly ($P < 0.05$). When BV-2 cells were treated with $A\beta_{1\text{-}42}$ for 48 h, 1 μM $A\beta_{1\text{-}42}$ did not induce cell proliferation while 2.5 and 5 μM $A\beta$ both promote cell proliferation significantly ($P < 0.05$ and $P < 0.05$) (Figure 1(a)).

In addition to cell proliferation, morphological changes were observed in BV-2 cells treated with $A\beta_{1\text{-}42}$. As shown in Figure 2(b), in the control group, BV-2 cells presented oval or round with short branches. When treated with 1 μM $A\beta_{1\text{-}42}$, short branches of BV-2 cells prolonged and the cell body enlarged. When treated with 2.5 μM $A\beta_{1\text{-}42}$, BV-2 cell branches further extended appearing amebic morphology with extended pseudopodia (Figure 1(b)). When treated with 5 μM $A\beta_{1\text{-}42}$, amebic cell proportions were increased (Figure 1(c)).

After BV-2 cells were treated with $A\beta_{1\text{-}42}$ for 24 h, Western blotting was used to analyze the changes of MHC II and Arg1 protein levels which represent different activation phenotypes of microglia. MHC II was upregulated in a concentration-dependent manner while Arg1 was downregulated (Figures 1(d) and 1(e)) indicating that BV-2 cells demonstrated an acute M1-like response to $A\beta_{1\text{-}42}$ after 24 hours' treatments.

3.2. Aβ Induced REST Expression and Nuclear Translocalization. REST expression was analyzed by Western blotting and qPCR after 24 hours of treatment with 0, 1, 2.5, and 5 μM $A\beta_{1\text{-}42}$. The results showed that compared with the control group, both the REST protein level and mRNA level of the $A\beta_{1\text{-}42}$ treatment group increased gradually with the increase of $A\beta_{1\text{-}42}$ concentration (Figures 2(a) and 2(b)). Consistent with the total REST protein level, intranuclear distribution of REST protein increased significantly with the increase of $A\beta_{1\text{-}42}$ concentration, indicating that $A\beta_{1\text{-}42}$ could promote REST nuclear translocalization (Figure 2(c)).

3.3. REST Repressed Aβ-Induced BV-2 Cell Proliferation. To study the effect of REST on cell proliferation, a specific short hairpin RNA (sh-RNA) was used to knock down the REST gene in BV-2 cells confirmed by Western blotting and qPCR. As shown in Figures 3(a) and 3(b), REST was downregulated for about 75% compared with the control group. Then, we treated BV-2 cells with $A\beta_{1\text{-}42}$ for 24 hours and detected the proliferation of BV-2 cells by a CCK8 kit. The results showed that cell proliferation in the control group was similar to that in Figure 1(a) that the cell proliferation increased in a concentration-dependent manner with statistical difference at 5 μM. And compared with the control group, $A\beta_{1\text{-}42}$ induced a marked increase in cell proliferation in the REST-knockdown group, indicating that REST may repress $A\beta$-induced BV-2 cell proliferation (Figure 3(c)).

3.4. REST Repressed BV-2 Cell Migration. As the main innate immune cells in the brain, microglia always detect the changes in the surrounding environment through continuous contraction and extension [17]. When there are adverse factors to activate microglia, chemokines in the microenvironment can promote the migration of microglia to lesions [18–20]. The migration ability of glial cells plays a major role in the function of microglia. In order to study the effect of REST on cell migration, BV-2 cell migration was tested by the transwell assay while REST was knocked down by sh-RNA in the experimental group. PC12 cells were inoculated in the lower chamber of the transwell system and treated with 5 μM $A\beta_{1\text{-}42}$ while BV-2 cells were inoculated in the upper chamber. Results are shown in Figure 3(d) that compared with the control group, migration of BV-2 cells with REST low expression was increased significantly ($P < 0.001$, $P < 0.001$) regardless of whether the PC12 cells in the lower chamber were treated with $A\beta_{1\text{-}42}$ or not, suggesting that REST may function as a repressor of BV-2 cell migration.

3.5. REST Repressed the Expression and Secretion of Proinflammatory Cytokines. As a chronic and progressive disease, AD is characterized by neuroinflammation throughout the disease. Expression of inflammatory cytokines is a major feature of AD [21]. To evaluate inflammation cytokine gene expression changes induced by $A\beta_{1\text{-}42}$, qPCR was used to analyze mRNA levels of proinflammatory cytokines in BV-2 cells. Results are shown in Figure 4(a) that $A\beta_{1\text{-}42}$ promoted proinflammatory cytokine TNF-α, IL-1β, and IL-6 expression. As shown in Figure 4(a) that with the increase of concentration of $A\beta_{1\text{-}42}$, the TNF-α mRNA level was induced; upregulation was statistically significant when concentration of $A\beta_{1\text{-}42}$ reached 5 μM ($P < 0.01$). The mRNA levels of IL-1β in the three $A\beta_{1\text{-}42}$ treatment groups were significantly higher than those in the control group ($P < 0.01$, $P < 0.001$, and $P < 0.01$). So was IL-6 that the mRNA levels of IL-6 in the three $A\beta_{1\text{-}42}$ treatment groups were significantly higher than those in the control group ($P < 0.05$, $P < 0.05$, and $P < 0.01$).

When REST gene was knocked down, proinflammatory cytokine TNF-α, IL-1β, and IL-6 mRNA levels were significantly upregulated compared with the control group (Figure 4(b)). And ELISA analysis showed that downexpression of REST gene leads to significant upregulation of proinflammation cytokines TNF-α, IL-1β, and IL-6 secreted to cell supernatant (Figure 4(c)). These observations suggest that REST may repress the expression and secretion of proinflammatory cytokines TNF-α, IL-1β, and IL-6.

4. Discussion

Alzheimer's disease is a common neurodegenerative disease and the most common type of senile dementia, whose main symptoms are progressive cognitive decline and memory loss. Extracellular beta-amyloid ($A\beta$) plaques and

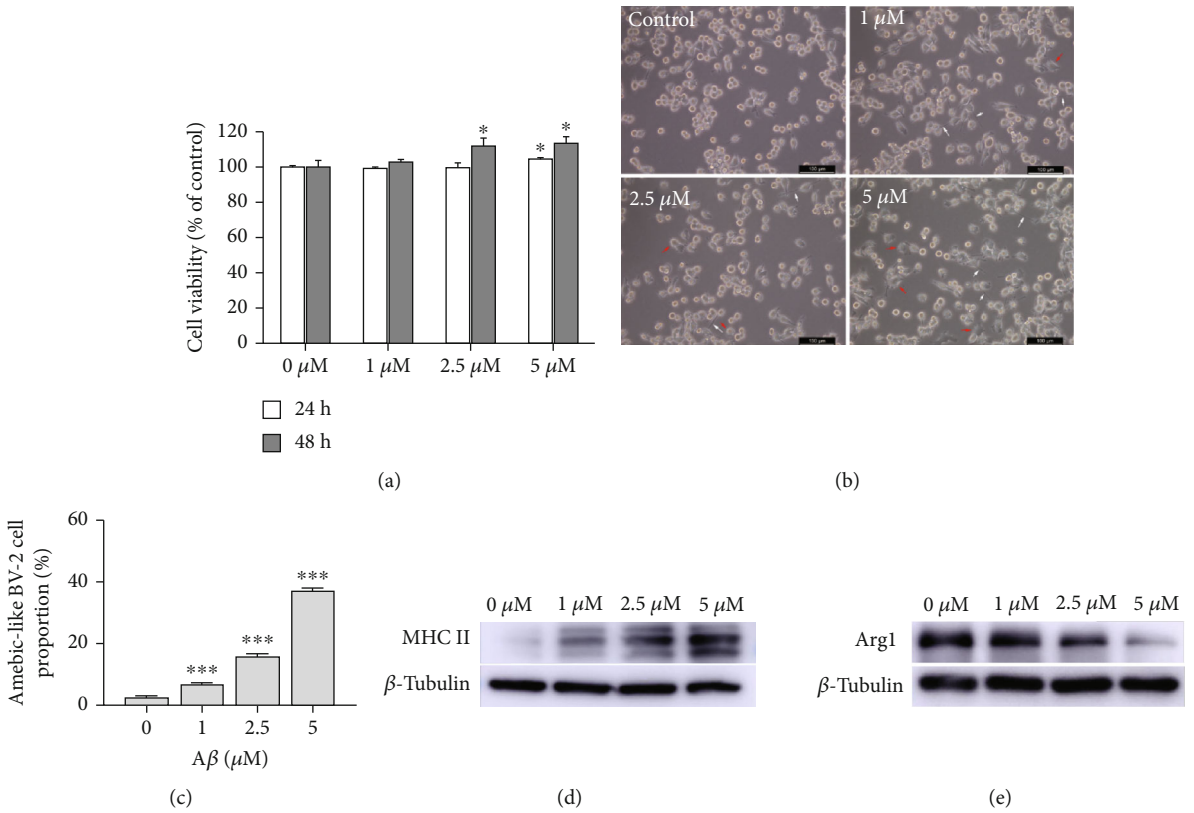

FIGURE 1: $A\beta_{1\text{-}42}$ induced BV-2 cell activation. (a) $A\beta_{1\text{-}42}$ promotes BV-2 cell proliferation. The proliferation of BV-2 cells increased with the increase of $A\beta_{1\text{-}42}$ treatment time and concentration. Both 24 h and 48 h treatment of $A\beta_{1\text{-}42}$ could induce the proliferation of BV-2 cells. Only 5 μM $A\beta_{1\text{-}42}$ induced BV-2 cell proliferation significantly at the treatment time of 24 h, while both 2.5 μM and 5 μM could promote BV-2 cell proliferation at the treatment time of 48 h. (b) $A\beta_{1\text{-}42}$ induced morphological changes in BV-2 cells. Under the action of $A\beta_{1\text{-}42}$, BV-2 cells presented shortening of the processes and swelling of the soma. (c) Quantitative statistics of the increase of ameba-like cell proportion under treatment of $A\beta_{1\text{-}42}$. (d, e) Under the treatment of $A\beta_{1\text{-}42}$, MHC II protein levels were upregulated while Arg1 was downregulated with the increase of concentration of $A\beta_{1\text{-}42}$. $^{*}P < 0.05$ vs. control; $^{***}P < 0.001$ vs. control.

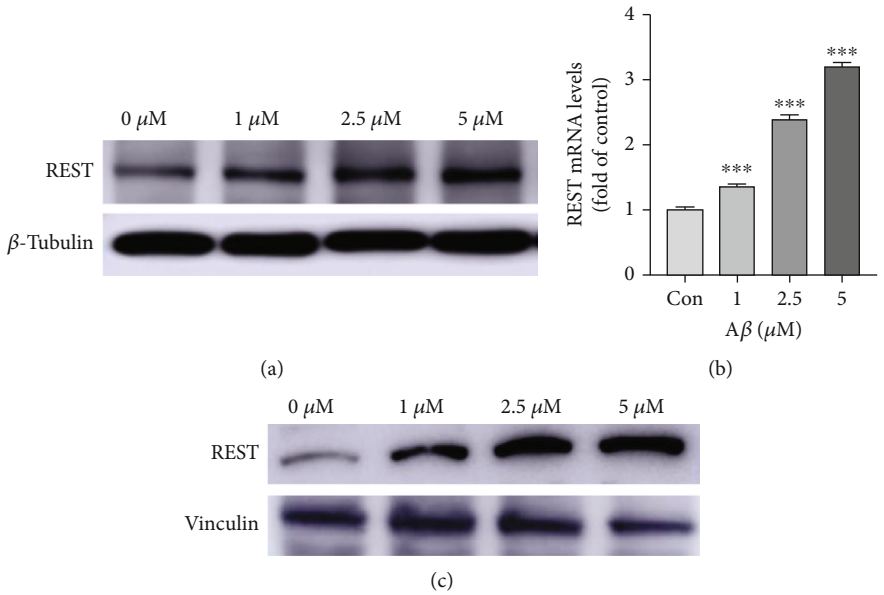

FIGURE 2: Aβ induced REST expression and nuclear translocalization. (a, b) Under the treatment of $A\beta_{1\text{-}42}$, both the REST protein level and the mRNA level were upregulated. (c) With the increase of concentration of $A\beta_{1\text{-}42}$, intranuclear distribution of REST protein increased. $^{***}P < 0.001$ vs. control.

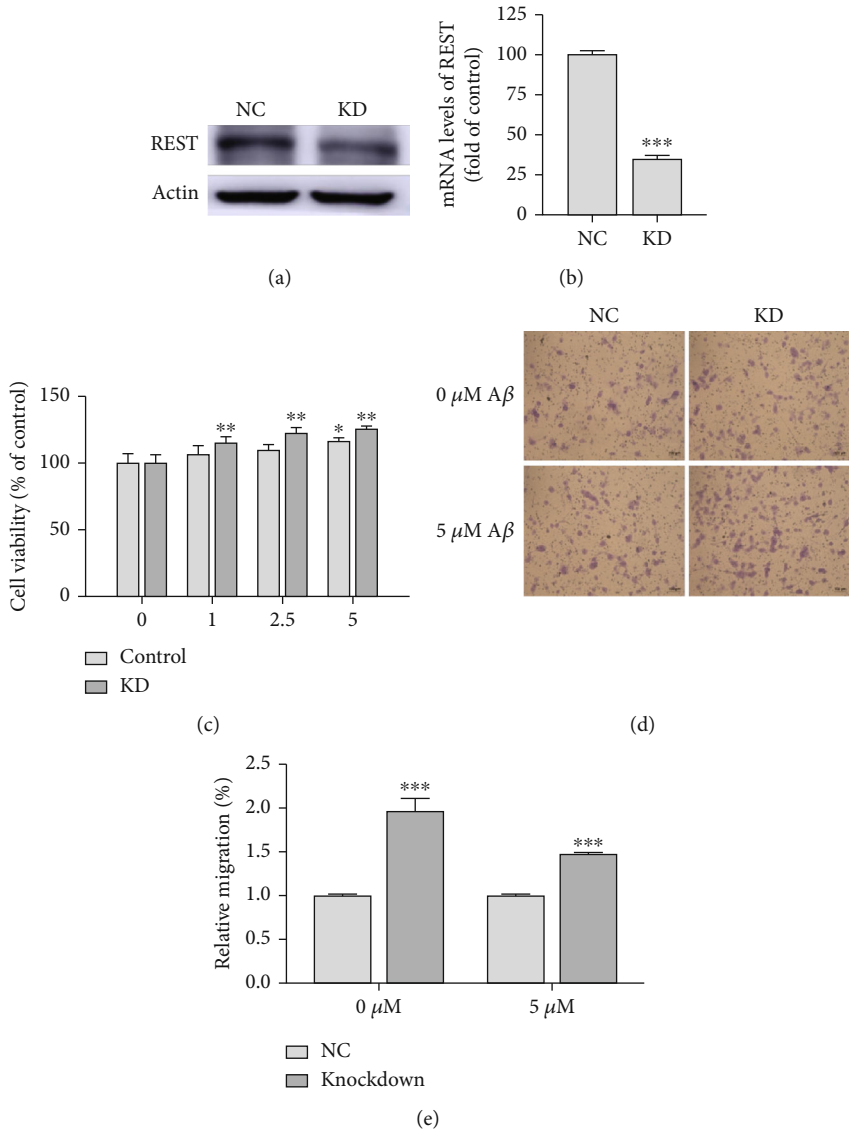

FIGURE 3: Knockdown of REST by short hairpin RNA increased A$\beta_{1\text{-}42}$-induced BV-2 cell proliferation and migration. (a, b) REST gene was knocked down by short hairpin RNA about 75% at the mRNA level and 50% at the protein level. (c) Knockdown REST gene by short hairpin RNA promoted A$\beta_{1\text{-}42}$-induced cell proliferation. (d, e) When PC12 cells were inoculated in the lower chamber of the transwell system, knockdown REST gene promotes BV-2 cell migration in the upper chamber no matter if PC12 cells were treated with A$\beta_{1\text{-}42}$ or not. $^{*}P < 0.05$ vs. control, $^{**}P < 0.01$ vs. control, and $^{***}P < 0.001$ vs. control.

intracellular neurofibrillary tangles in the brain are two classical pathological features of AD. With the gradual deepening of the understanding of the toxicity of Aβ, Hardy and Higgins put forward the "Aβ theory" of the etiology of AD in the 1990s, which suggests that the central mechanism of AD is the corresponding neurotoxicity caused by abnormal deposition of Aβ in the brain and has a profound impact on the later research [22]. Besides Aβ toxicity, scientists also noticed that there was obvious microglia proliferation in the brain of AD patients and extensive activation of microglia in AD [23, 24]. The proliferation and activation of microglia were proved to have important effects on the course of AD [5]. In this study, BV-2 cells treated with synthetic A$\beta_{1\text{-}42}$ presented obvious proliferation and activation. Active BV-2 cells presented shortening of the processes and swelling of the soma, as well as activation phenotype marker alteration that MHC II expression was significantly upregulated, suggesting that microglia were activated to become antigen-presenting cells. Arginase 1 (Arg1) which has inhibitory effect on microglia activation due to its ability to decompose arginine which was necessary for microglia activation was significantly downregulated by the stimulation of A$\beta_{1\text{-}42}$, suggesting that A$\beta_{1\text{-}42}$ can promote type I activation of microglia but inhibit type II activation.

RE-1 silencing transcription factor (REST) has been proved to play an important neuroprotective role in AD [11, 12]. Normal elderly neurons have a high level of REST in order to inhibit the expression of genes related to neuronal death and AD progression, while in AD patients and animal models, neuronal REST is significantly downregulated, or

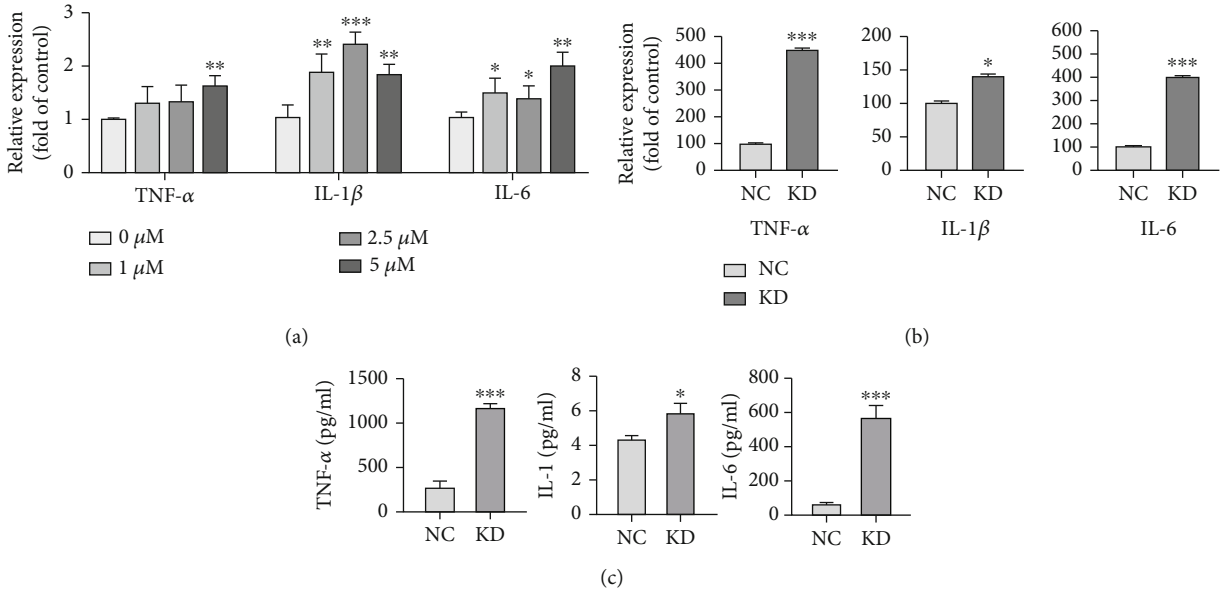

Figure 4: REST repressed proinflammation cytokine TNF-α, IL-1β, and IL-6 expression and secretion. (a) A$\beta_{1\text{-}42}$ induced proinflammation cytokine TNF-α, IL-1β, and IL-6 upregulation and anti-inflammation cytokine IL-12 downregulation. (b) Knockdown REST gene induced proinflammation cytokine TNF-α, IL-1β, and IL-6 mRNA upregulation with the treatment of A$\beta_{1\text{-}42}$. (c) Knockdown REST gene increased secretion of proinflammation cytokines TNF-α, IL-1β, and IL-6. $^{*}P < 0.05$ vs. control, $^{**}P < 0.01$ vs. control, and $^{***}P < 0.001$ vs. control.

even missing, leading to a large number of neuronal death and cognitive decline [12]. In this study, synthetic A$\beta_{1\text{-}42}$ induced microglial REST upregulation and nuclear translocalization in BV-2 cells, which was observed to play an important role in microglia.

Microglia, the innate immune cells in the brain, have been constantly moving to detect the changes of the microenvironment in the brain and play a role as a guardian of the central nervous system [25, 26]. The migration function is of great importance to microglia. In this study, PC12 cells were used as an alternate of neurons to coculture with BV-2 cells in the transwell system. PC12 cells are a cell line cloned from rat adrenal pheochromocytoma, which were widely used in the in vitro study of nervous system diseases due to their similar characteristics to neurons. Previous studies have revealed that Aβ can promote microglia migration. And in this study, when PC12 cells in the lower chamber were treated with A$\beta_{1\text{-}42}$, BV-2 cells migrate more than the control group, indicating that PC12 cells suffering from A$\beta_{1\text{-}42}$ can promote BV-2 cell migration. That is, both A$\beta_{1\text{-}42}$ and PC12 suffering from A$\beta_{1\text{-}42}$ can promote BV-2 cell migration. In this study, knocking down REST promoted the migration of BV-2 cells no matter if PC12 cells in the lower chamber were treated with A$\beta_{1\text{-}42}$, suggesting that REST has the function of inhibiting migration of BV-2 cells. In AD brains, microglia are often found near Aβ plaques [5, 27]. One explanation might be that microglia and neurons stimulated by Aβ release chemokines to recruit microglia or macrophages in the blood while the REST is upregulated as a result of Aβ neurotoxicity in the recruited microglia or macrophages, which limit the migration of microglia in turn. Thus, microglia stay around the Aβ plate limiting the spread of senile plaque. In addition, chronic monocyte transmigration could also result in subtle damage to the blood-brain barrier (BBB) [28]; the function of repressing migration of microglia has a protective effect on the blood-brain barrier (BBB) to some extent.

As a chronic and progressive disease, chronic neuroinflammatory response exists throughout the course of AD [29–31]. In this study, the expression of TNF-α, IL-1β, and IL-6 increased significantly in A$\beta_{1\text{-}42}$-treated BV-2 cells. Long-term sustained inflammatory factors can damage the brain and strengthen synaptic degeneration and neuronal apoptosis [32]. In this study, knocking down REST can promote the expression and secretion of proinflammatory cytokines TNF-α, IL-1β, and IL-6 suggesting that REST may play a protective role in the course of AD by inhibiting the expression and secretion of inflammatory factors.

5. Conclusions

Our findings raise the possibility that Aβ-induced REST expression in microglia has a protective effect of repressing microglia activation including cell proliferation, migration, and inflammation cytokine secretion.

Data Availability

The data used to support the findings of this study are available from the corresponding author upon reasonable request.

Conflicts of Interest

The authors declare that they have no competing interests.

Authors' Contributions

Tongya Yu, Hui Quan, and Yuzhen Xu are co-first authors of the article, and they contributed equally to this work.

Acknowledgments

This work was supported by grants from the National Natural Science Foundation of China (81771131) and the Major Projects of Science and Technology Commission of Shanghai Municipality (17411950100).

References

[1] D. T. Jones, J. Graff-Radford, V. J. Lowe et al., "Tau, amyloid, and cascading network failure across the Alzheimer's disease spectrum," *Cortex*, vol. 97, pp. 143–159, 2017.

[2] H. Sarlus and M. T. Heneka, "Microglia in Alzheimer's disease," *The Journal of Clinical Investigation*, vol. 127, no. 9, pp. 3240–3249, 2017.

[3] S. Prokop, K. R. Miller, and F. L. Heppner, "Microglia actions in Alzheimer's disease," *Acta Neuropathologica*, vol. 126, no. 4, pp. 461–477, 2013.

[4] M. Bolós, J. R. Perea, and J. Avila, "Alzheimer's disease as an inflammatory disease," *Biomolecular Concepts*, vol. 8, no. 1, pp. 37–43, 2017.

[5] S. H. Baik, S. Kang, S. M. Son, and I. Mook-Jung, "Microglia contributes to plaque growth by cell death due to uptake of amyloid β in the brain of Alzheimer's disease mouse model," *Glia*, vol. 64, no. 12, pp. 2274–2290, 2016.

[6] H. Lui, J. Zhang, S. R. Makinson et al., "Progranulin deficiency promotes circuit-specific synaptic pruning by microglia via complement activation," *Cell*, vol. 165, no. 4, pp. 921–935, 2016.

[7] S. Mukherjee, R. Brulet, L. Zhang, and J. Hsieh, "REST regulation of gene networks in adult neural stem cells," *Nature Communications*, vol. 7, no. 1, article 13360, 2016.

[8] J. Y. Hwang and R. S. Zukin, "REST, a master transcriptional regulator in neurodegenerative disease," *Current Opinion in Neurobiology*, vol. 48, pp. 193–200, 2018.

[9] K. Cortés-Sarabia, Y. Medina-Flores, L. D. C. Alarcón-Romero et al., "Production and characterization of monoclonal antibodies against the DNA binding domain of the RE1-silencing transcription factor," *Journal of Biochemistry*, vol. 166, no. 5, pp. 393–402, 2019.

[10] A. Mozzi, F. R. Guerini, D. Forni et al., "*REST*, a master regulator of neurogenesis, evolved under strong positive selection in humans and in non human primates," *Scientific Reports*, vol. 7, no. 1, article 9530, 2017.

[11] E. Orta-Salazar, A. Aguilar-Vázquez, H. Martínez-Coria et al., "REST/NRSF-induced changes of ChAT protein expression in the neocortex and hippocampus of the 3xTg-AD mouse model for Alzheimer's disease," *Life Sciences*, vol. 116, no. 2, pp. 83–89, 2014.

[12] T. Lu, L. Aron, J. Zullo et al., "REST and stress resistance in ageing and Alzheimer's disease," *Nature*, vol. 507, no. 7493, pp. 448–454, 2014.

[13] F. Paonessa, S. Criscuolo, S. Sacchetti et al., "Regulation of neural gene transcription by optogenetic inhibition of the RE1-silencing transcription factor," *Proceedings of the National Academy of Sciences*, vol. 113, no. 1, pp. E91–E100, 2016.

[14] I. Prada, J. Marchaland, P. Podini et al., "REST/NRSF governs the expression of dense-core vesicle gliosecretion in astrocytes," *The Journal of Cell Biology*, vol. 193, no. 3, pp. 537–549, 2011.

[15] Y. Xu, Q. Wang, D. Li et al., "Protective effect of lithium chloride against hypoglycemia-induced apoptosis in neuronal PC12 cell," *Neuroscience*, vol. 330, pp. 100–108, 2016.

[16] Y. Xu, Q. Wang, Z. Wu et al., "The effect of lithium chloride on the attenuation of cognitive impairment in experimental hypoglycemic rats," *Brain Research Bulletin*, vol. 149, pp. 168–174, 2019.

[17] C. A. Mosser, S. Baptista, I. Arnoux, and E. Audinat, "Microglia in CNS development: shaping the brain for the future," *Progress in Neurobiology*, vol. 149-150, pp. 1–20, 2017.

[18] S. Zhou, W. Zhu, Y. Zhang, S. Pan, and J. Bao, "S100B promotes microglia M1 polarization and migration to aggravate cerebral ischemia," *Inflammation Research*, vol. 67, no. 11-12, pp. 937–949, 2018.

[19] Y.-H. Kwon, J. Kim, C.-S. Kim et al., "Hypothalamic lipid-laden astrocytes induce microglia migration and activation," *FEBS Letters*, vol. 591, no. 12, pp. 1742–1751, 2017.

[20] M. Huang, Y. Wan, L. Mao et al., "Inhibiting the migration of M1 microglia at hyperacute period could improve outcome of tMCAO rats," *CNS Neuroscience & Therapeutics*, vol. 23, no. 3, pp. 222–232, 2017.

[21] C. Villegas-Llerena, A. Phillips, P. Garcia-Reitboeck, J. Hardy, and J. M. Pocock, "Microglial genes regulating neuroinflammation in the progression of Alzheimer's disease," *Current Opinion in Neurobiology*, vol. 36, pp. 74–81, 2016.

[22] T. Daly, M. Houot, A. Barberousse, Y. Agid, and S. Epelbaum, "Amyloid-β in Alzheimer's disease: a study of citation practices of the amyloid cascade hypothesis between 1992 and 2019," *Journal of Alzheimer's Disease*, vol. 74, no. 4, pp. 1309–1317, 2020.

[23] M. W. Marlatt, J. Bauer, E. Aronica et al., "Proliferation in the Alzheimer hippocampus is due to microglia, not astroglia, and occurs at sites of amyloid deposition," *Neural Plasticity*, vol. 2014, Article ID 693851, 12 pages, 2014.

[24] Y. Yoshiyama, M. Higuchi, B. Zhang et al., "Synapse loss and microglial activation precede tangles in a P301S tauopathy mouse model," *Neuron*, vol. 53, no. 3, pp. 337–351, 2007.

[25] Q. Wang, W. Yang, J. Zhang, Y. Zhao, and Y. Xu, "TREM2 overexpression attenuates cognitive deficits in experimental models of vascular Dementia," *Neural Plasticity*, vol. 2020, Article ID 8834275, 10 pages, 2020.

[26] C. Condello, P. Yuan, A. Schain, and J. Grutzendler, "Microglia constitute a barrier that prevents neurotoxic protofibrillar Aβ42 hotspots around plaques," *Nature Communications*, vol. 6, no. 1, article 6176, 2015.

[27] M. Noda and A. Suzumura, "Sweepers in the CNS: microglial migration and phagocytosis in the Alzheimer disease pathogenesis," *International Journal of Alzheimer's Disease*, vol. 2012, article 891087, 11 pages, 2012.

[28] H. A. Seifert, W. Zhu, A. A. Vandenbark, N. J. Alkayed, and H. Offner, "Sex differences in the therapeutic effects of anti-PDL2 neutralizing antibody on stroke," *Metabolic Brain Disease*, vol. 34, no. 6, pp. 1705–1712, 2019.

[29] E. E. Spangenberg and K. N. Green, "Inflammation in Alzheimer's disease: lessons learned from microglia-depletion models," *Brain, Behavior, and Immunity*, vol. 61, pp. 1–11, 2017.

[30] F. L. Heppner, R. M. Ransohoff, and B. Becher, "Immune attack: the role of inflammation in Alzheimer disease," *Nature Reviews Neuroscience*, vol. 16, no. 6, pp. 358–372, 2015.

[31] M. T. Heneka, D. T. Golenbock, and E. Latz, "Innate immunity in Alzheimer's disease," *Nature Immunology*, vol. 16, no. 3, pp. 229–236, 2015.

[32] Z. Cai, M. D. Hussain, and L. J. Yan, "Microglia, neuroinflammation, and beta-amyloid protein in Alzheimer's disease," *The International Journal of Neuroscience*, vol. 124, no. 5, pp. 307–321, 2013.

Hindawi
Neural Plasticity
Volume 2020, Article ID 8837024, 13 pages
https://doi.org/10.1155/2020/8837024

Research Article

Stress Reactivity Influences the Relationship between Emotional Labor Strategies and Job Burnouts among Chinese Hospital Nurses

Huihua Deng,[1,2] **Hanyao Wu**,[1,2,3] **Xingliang Qi**,[2,4] **Caixiang Jin**,[5] **and Jianmei Li**[2,6]

[1]*Key Laboratory of Child Development and Learning Science (Southeast University), Ministry of Education, Nanjing 210096, China*
[2]*Institute of Child Development and Education, Southeast University, Nanjing 210096, China*
[3]*Department of Medical Humanity, School of Humanities, Southeast University, Nanjing 211189, China*
[4]*College of Pro-School Education, Nanjing Xiaozhuang University, Nanjing 211171, China*
[5]*Department of Nursing, Nanjing Integrated Traditional Chinese and Western Medicine Hospital, Nanjing 210014, China*
[6]*Office of Social Science, Southeast University, Nanjing 210096, China*

Correspondence should be addressed to Huihua Deng; dengrcls@seu.edu.cn

Received 5 April 2020; Revised 10 August 2020; Accepted 18 August 2020; Published 22 September 2020

Academic Editor: Fushun Wang

Extant studies mostly focused on the buffering role of social and external organizational resources and personal mental resources. However, there is no research exploring the moderating role of personal physiological resources (e.g., stress reactivity). The present study is aimed at examining the interactive effect of emotional labor and stress reactivity on job burnout. The present study utilized cortisol content in a 1 cm hair segment as the biomarker of total stress reactivity in one month. The participants were 229 female hospital nurses randomly recruited from city hospitals, China. They self-reported their emotional labor strategies and job burnout syndromes and provided 1 cm hair segments closest to the scalp two weeks later after the survey. Hair cortisol content was determined with high-performance liquid chromatography-tandem mass spectrometry. The results revealed that hair cortisol can moderate the associations of surface acting with emotional exhaustion and personal burnout; of deep acting with emotional exhaustion, depersonalization, and personal burnout; and of expression of naturally felt emotions with professional inefficacy. In particular, nurses with high cortisol levels not only showed higher emotional exhaustion than those with low cortisol levels under high surface acting but also showed lower emotional exhaustion under low surface acting. A similar situation was true for nurses' emotional exhaustion and depersonalization in the context of deep acting. Nurses with low hair cortisol levels not only showed higher professional inefficacy than those with high hair cortisol levels under low expression of naturally felt emotions but also showed lower professional inefficacy under high expression of naturally felt emotions. Additionally, nurses with high hair cortisol levels showed lower personal burnout than those with low hair cortisol levels under low surface acting or high deep acting. In summary, the interaction pattern between stress reactivity and emotional labor was varied with the nature of emotional labor strategy and job burnout.

1. Introduction

Job burnout is a typical syndrome that results from chronic stress elicited by high job demands [1, 2]. Emotional labor is a particular aspect of job demands, requiring employees to modify their affective displays at work [3]. Intense emotional labor in a long time has been associated with higher job burnout [4] as work tasks with highly physical and other mental demands do [1]. *Nevertheless,* the relationship between emotional labor and job burnout may vary with the nature of emotional labor strategy that is required across numerous occupations and with employees' personal resources. Among various personal resources, stress reactivity conceptualized as a high biological sensitivity to context [5] may be one of the important personal physiological resources improving employees' sensitivity to organizational

requirements in emotional labor. However, it is unclear yet whether stress reactivity can buffer the deleterious effect of high emotional labor as personal mental resources buffer the deleterious effect of high job demands, such as self-esteem, self-efficacy, and optimism [6, 7]. Thus, determining the buffering role of stress reactivity will be helpful for understanding more fully the importance of the biological processes in employees dealing with job-related emotional labor. Therefore, the current study is aimed at examining how an emotional labor strategy interacts with employees' stress reactivity in predicting employees' job burnout.

Emotional labor has been conceptualized as a three-dimensional structure separating three strategies: surface acting, deep acting, and the expression of naturally felt emotions [8, 9]. Surface acting refers to employees hiding felt emotions or faking unfelt emotions without shaping inner feelings (acting in bad faith) to fit the desired emotion display at the workplace, and deep acting refers to employees modifying their actual inner emotion states (acting in good faith) while the expression of naturally felt emotions refers to employees spontaneously and genuinely experiencing and displaying the felt emotions [8]. Surface acting entails the consumption of a substantial amount of energy and resources in suppressing the true emotions at the behavioral level. Thus, surface acting perhaps leads to an imbalance between emotional demands and the resource expenditure because employees have strong motivations to conserve and establish their resources to minimize the extent to which they spend resources in their emotional labor at work as suggested by the conservation of resources model [10]. In contrast, deep acting spends very limited resources in the internalization of job demands on one's emotion, and natural feelings are often consistent with the expression normally demanded by the work. Therefore, surface acting is more likely positively associated with burnout symptoms and negative stressful reactions than deep acting and the expression of naturally felt emotion. Indeed, previous empirical studies mostly demonstrated positive associations of surface acting with burnout syndromes (e.g., emotional exhaustion and depersonalization) [11–17] and negative associations of the expression of naturally felt emotion with burnout syndromes [14, 16]. However, the association between deep acting and job burnout was less consistent in the previous, with studies demonstrating negative, positive, or no associations [11, 13, 14, 16–20]. One of the main reasons for the inconsistency might be that the amount and nature of emotional labor demand that employees face varied across numerous occupations requiring employees to perform the form of emotional labor differing in interpersonal interactions, such as mass service and high commitment service [21]. For example, nurses have little chance to establish stable relationships with their massive outpatients during short-term and one-off encounters, thereby having less autonomy to express naturally felt emotions than teachers who can establish relatively stable relationships with the students they well know. Another reason might be that the amount and form of emotional labor strategy employees perform varied with employees' stress reactivity or their sensitivity to organizational requirements in emotional labor. Therefore, it is necessary to separately validate the relationship between each emotional labor strategy and job burnout and examine whether the relationship shows the pattern differing in three emotional labor strategies and whether the relationship is moderated by stress reactivity.

As one of the stress-sensitive nervous systems, the hypothalamic-pituitary-adrenal (HPA) axis is responsible for the cortisol secretion to help organs adapt to stressful events [22]. Naturally, cortisol is considered as a biomarker of the HPA activity. It is also regarded as one of the reliable biomarkers for assessing an individual's stress reactivity [5, 23]. Salivary cortisol levels within one day were ever utilized as a biomarker of stress reactivity [23]. However, salivary or urinary cortisol levels reflect the acute or short-term activity of the HPA axis (or stress reactivity) over several hours or up to one day [24]. These traditional biomarkers do not reliably reflect long-term HPA activity (or stress reactivity) enough to match the time span (e.g., one-month period) that most psychological measurements cover in their questions. Alternatively, hair cortisol has been proven to be a novel biomarker reliably assessing basal cortisol levels and the long-term activity of the HPA axis [25]. That is, if the hair growth rate is 1 cm per month [26], the cortisol content in the 1 cm hair segment would reliably reflect the HPA activity over one month or the total reactivity to all daily stressful events over one month. Moreover, it shows high consistency with the average level of multiple-day salivary cortisols within one month [27, 28]. We therefore used the hair cortisol content as a biomarker of one-month stress reactivity to better match the time span that psychological measurements cover.

Previous empirical studies on this topic were done under the Job Demands-Resources (JDR) model [1] and mostly demonstrated that job resources can buffer the harmful effect of job demands [29, 30]. As health-protecting factors, job sources refer to those physical, psychological, social, or organizational aspects of the job that may be functional in achieving work goals, or reduce job demands at the associated physiological and psychological costs, or stimulate personal growth and development [1]. Moreover, it is emphasized that job resources can be catalogued into external resources (i.e., organizational and social resources) and internal personal resources, such as cognitive features and action patterns [31]. As aspects of the self at the cognitive level, emotional level, and biological level, personal resources that are generally linked to resiliency refer to individuals' sense of their ability to control and impact their environment successfully [32, 33]. Traditionally, regarding the job resources buffering the deleterious effect of job demands, extant studies mostly focused on the external organizational resources related to job characteristics, such as social support, job autonomy, quality of the relationship with the supervisor, and performance feedback [1, 29, 34]. Comparatively, limited studies have examined the buffering role of personal mental resources, such as organizational-based self-esteem, self-efficacy, optimism, compassion satisfaction, and recovery experience as resource replenishment [6, 7, 12, 15, 31, 35, 36]. However, to date, there is little research exploring the moderating role of stress reactivity in the association between job demands (e.g., emotional labor) and job burnout.

Stress reactivity as personal physiological resources might play a moderating role as personal mental resources do. This theoretical hypothesis on stress reactivity possibly obtains additional support from recent empirical studies finding that stress reactivity can moderate the relationship between environmental factors and psychological adaptations [23, 37–40]. It found that compared to those with lower cortisol levels (i.e., lower stress reactivity), adolescents with higher cortisol levels (i.e., higher stress reactivity) not only showed less prosocial behaviors and worse execute functions under more family adversities [23, 37] and more internalizing problems under more stressful events [38, 40] but also showed more prosocial behaviors and better execute functions under less family adversities and less internalizing problems under less stressful events, which was consistent with the differential susceptibility model recently developed by Belsky and collaborators [41, 42]. These results implied that high stress reactivity is a plasticity factor (i.e., it is not only a risk factor under adverse environments but also a promoting factor under supportive environments) or that low stress reactivity is a protective factor under adverse environments. Of course, whether the notions are true in the context of high emotional labor demands is needed to be validated.

Taken together, the present study is aimed at independently examining the interactive effects of three emotional labor strategies and stress reactivity on job burnout under the frame of the JDR model where emotional labor is a particular aspect of job demands and stress reactivity might be the most representative personal physiological resources. The cortisol content in the 1 cm hair segment was utilized as the biomarker of one-month stress reactivity, ensuring that the time span the hair cortisol content reflects matched that the measurements of psychological variables cover. We focused our study on Chinese hospital nurses. This is because the nursing profession is an emotionally demanding occupation. Hospital nurses currently in China utilize emotional labor and control their emotional expressions to meet patients' needs in the increasing demand for quality health care services [43]. In order to make the results more generalized, we examined job burnout syndromes that are measured with compulsory questionnaires, Maslach Burnout Inventory-General Survey (MBIGS) [44] and Copenhagen Burnout Inventory (CBI) [45] where MBI focuses on the long-term consequences under continuous job stress in emotions and interpersonal relationships, such as emotional exhaustion, depersonalization, and professional efficacy, and CBI on the different domains of burnout itself, such as personal burnout, work-related burnout, and client-related burnout. Based on the above background, we expected that each emotional labor strategy and hair cortisol would interact to predict nurses' job burnout syndromes and that high hair cortisol (i.e., high stress reactivity) would be the plasticity factor or that lower hair cortisol (i.e., lower stress reactivity) would be a protective factor in the context of high emotional labor demands.

2. Method

2.1. Participants. The initial sample consisted of 500 female nurses randomly recruited from nine hospitals in Nanjing City, China. All participants provided written informed consent before inclusion. This study followed the Declaration of Helsinki and was approved by the Health Science Research Ethics Board of Southeast University.

Among them, 456 nurses (91.20%) completed all the questionnaires including demographic information, emotional labor strategy, and job burnouts. 341 out of 456 nurses provided their hair strands and the hair-related information. 112 participants were excluded because they were smokers, alcoholics, or obese (body mass indexes ≥ 30), or with shorter hair (<1 cm) or treated hair (e.g., coloring, perm, or bleached), or had medicine intake (e.g., glucocorticoid and antibiotic drugs) or diseases (e.g., canker sores and inflammation), which might influence the contents of cortisol in hair [46]. Finally, 229 nurses participated in the present study. They worked in different types of working departments: intensive care unit (ICU, 20.96%), emergency intensive care unit (EICU, 8.30%), emergency department (33.62%), radiotherapy department (6.99%), rehabilitation department (16.59%), and others (13.54%) including paediatrics, internal medicine, department of medical psychology, Chinese medicine surgery, neurology, neurosurgery, struma, dental department, orthopaedics, endocrine department, and operating theatre over the past one year. They gave a range of years of working as a nurse, in which 50.22% served less than 5 years, 34.06% served 5-15 years, and 15.72% served over 15 years. Of those, 83.84% nurses were in the 8 h three-shift scheduling and 16.16% nurses in the 12 h two-shift scheduling.

2.2. Procedures. After signing the informed consent, participants self-reported with the questionnaires their demographic information including the working department, working duration and shift scheduling, emotional labor strategy, and the status of job burnout over the past one month. In order to match survey data in time span, hair samples (about 20 mg in weight) were collected by a well-trained research assist two weeks later after the questionnaires' collection. This is because 1-3 mm of the hair strands embeds in the skin and the 1-2 mm hair strands closest to the scalp cannot be completely cut with scissors [47] if the hair growth rate is 1 cm per month. As-collected hair samples were sealed with foil to avoid from direct irradiation of the sunlight and then were stored in a dry and dark environment at room temperature until the analysis.

2.3. Measures

2.3.1. Emotional Labor Strategy. The 14-item emotional labor strategy scale developed by Diefendorff and his colleagues [8] and translated into Chinese by Bai [48] and Cheung and Tang [49] was used to measure three types of emotional labor strategies: surface acting (7 items), deep acting (4 items), and expression of naturally felt emotions (3 items). These items were slightly modified to make the wording match the job characteristics and context of nurses, for example, "put on an act to deal with patients in an appropriate way" (surface acting), "try to actually experience the emotions that I must show to patients" (deep acting), and "the emotions I express

to patients are genuine" (expression of naturally felt emotions). Each item is rated on a 5-point Likert scale ranging from 1 (strongly disagree) to 5 (strongly agree). Higher scores indicate a higher emotional labor strategy. The scale was proven to have good reliability and validity in Chinese workers (e.g., Bai, 2006 for employees in supermarkets, hotels, and hospitals; Cheung and Tang, 2009 for human service professionals; and Yin et al., 2012 for teachers). In the present study, the average score for each subscale was utilized, and Cronbach's alpha coefficient was 0.86, 0.76, and 0.85 for the three subscales.

2.3.2. Job Burnout. Job burnout was measured with Maslach Burnout Inventory-General Survey (MBIGS) developed by Schaufeli et al. [44] and translated into Chinese by Li and Shi [50] and with Copenhagen Burnout Inventory (CBI) developed by Kristensen et al. [45] and translated into Chinese by Yeh et al. [51]. The Chinese version of MBIGS includes 16 items assessing the frequency of nurses experiencing burnout and consists of three subscales measuring emotional exhaustion (5 items), depersonalization (5 items), and professional efficacy (6 items) which we renamed and rated as professional inefficacy for the convenience and consistency with the other five burnout subscales in the results' description. Each item is rated on a 7-point Likert scale ranging from 1 (never) to 7 (always), higher scores indicating heavier burnout. The scale was proven to have good reliability and validity in Chinese workers [50]. In the present study, the average score for each subscale was utilized, and Cronbach's alpha coefficient was 0.94, 0.86, and 0.81 for the three subscales.

The Chinese version of CBI also contains 16 items assessing the degree of physical and psychological fatigue and exhaustion perceived by the nurses in three different aspects, personal burnout (5 items), work-related burnout (5 items), and client-related burnout (6 items). The items in the client-related burnout subscale were slightly modified to make the wording match the job context of nurses. Each item is rated on a 5-point Likert scale ranging from 0 (never) to 4 (always), higher scores indicating heavier burnout. The scale was proven to have good reliability and validity in Chinese workers [51]. In the present study, the average score enlarged 25 times for each CBI subscale was utilized to distinguish MBI and CBI, and Cronbach's alpha coefficient was 0.92, 0.90, and 0.90 for the three subscales.

2.3.3. The Analysis of Hair Cortisol Contents. The detailed procedures of analyzing hair cortisol contents (HCC) were described elsewhere [28]. Briefly, the 1 cm hair strands closest to the scalp were treated by a standard protocol: washing with methanol, cutting into pieces, incubation in methanol, centrifugation, solid-phase extraction, and drying at pure nitrogen gas. The dried residue was redissolved in 50-microliter methanol for cortisol analysis that was done on a Qtrap 3200 liquid chromatography-tandem mass spectrometer (ABI, USA). Cortisol was ionized with atmospheric pressure chemical ionization and identified in the positive ion mode using the multiple reaction monitoring mode. The assay method had good linearity in the range of 0.8-250.0 pg/mg, showing the square coefficient of correlation at 0.99. It also had good sensitivity, accuracy, and precision, showing limits of detection and quantitation at 0.3 and 0.8 pg/mg and intraday and interday coefficients of variation less than 15% and recovery ranging between 85 and 115% [28], which fit the requirements of hair cortisol measurement.

2.4. Data Preparation and Analysis Procedures. Prior to analyses, all variables were examined for accuracy of data entry, missing data, data normality, and common-method bias. Data were analyzed by the statistical package SPSS 22.0 for windows. Confirmatory factor analysis was performed by Lisrel 8.70. Percentages of missing data were less than 1.0% for all the predictive and outcome variables, and there was no missing data for the moderating variable. Missing data for all the predictive and outcome variables were handled using the expectation-maximization algorithm [52]. The data distribution normality was examined with a one-sample Shapiro-Wilk test. HCC showed nonnormally distributed ($p < 0.001$) and became normally distributed ($p = 0.200$) after a log transformation that could effectively reduce the skewness and kurtosis. The log-transformed HCC data were used for the next Pearson's correlation analysis and the hierarchical multiple regression analysis. All hierarchical multiple regression analyses were conducted controlling for the nurse's working department, shift pattern, and work duration for nursing.

3. Results

3.1. Descriptive Statistics. Harman's single-factor test was performed to assess the common method variance biases [53]. An exploratory factor analysis (EFA) (principal components extraction) showed that items on surface acting and each subscale of job burnouts did not generate the unique factor with the explained variance more than 40% for all six subscales of job burnouts. A confirmatory factor analysis (CFA) also demonstrated that the items did not converge on a single factor for all six subscales of job burnouts (RMSEAs > 0.150). Similarly, the other predictors and outcome variables did not generate a single factor. Thus, it was assumed that the common method variance bias was not serious in the present study. The details on EFA and CFA were seen in Tables S1 and S2 in the supplemental materials.

As listed in Table 1, surface acting showed significantly positive correlations with emotional exhaustion, depersonalization, personal burnout, work-related burnout, and client-related burnout (p's < 0.01) but did not correlate with professional inefficacy ($p > 0.05$). Deep acting showed significantly negative correlations with all six aspects of job burnouts (p's < 0.01). Expression of naturally felt emotion also showed significantly negative correlations with all six aspects of job burnouts (p's < 0.05). There were no correlations between emotional labor strategies and hair cortisol content and between hair cortisol content and six aspects of job burnouts (p's > 0.05). Additionally, these variables were not correlated with working duration as a nurse (p's > 0.128). Expression of naturally felt emotion, emotional exhaustion, depersonalization, personal burnout, work-related burnout, and client-

Table 1: Means, standard deviations, and coefficients of correlations for the study variables ($n = 229$).

		1	2	3	4	5	6	7	8	9	10
1 Surface acting	—	—	—	—	—	—	—	—	—	—	
2 Deep acting	-0.100	—	—	—	—	—	—	—	—	—	
3 Natural expression[a]	-0.425**	0.554**	—	—	—	—	—	—	—	—	
4 HCC[b]	0.067	-0.001	0.036	—	—	—	—	—	—	—	
5 Emotional exhaustion	0.383**	-0.201**	-0.194**	0.035	—	—	—	—	—	—	
6 Professional inefficacy	0.002	-0.363**	-0.246**	-0.006	0.108	—	—	—	—	—	
7 Depersonalization	0.306**	-0.265**	-0.311**	-0.046	0.654**	0.190**	—	—	—	—	
8 Personal burnout	0.234**	-0.253**	-0.168*	-0.072	0.658**	0.175**	0.472**	—	—	—	
9 Work-related burnout	0.285**	-0.265**	-0.259**	0.013	0.699**	0.282**	0.566**	0.858**	—	—	
10 Client-related burnout	0.329**	-0.330**	-0.333**	0.010	0.567**	0.284**	0.562**	0.621**	0.754**	—	
M[c]	2.59	3.13	3.44	3.2	3.59	3.00	2.63	52.45	46.63	41.45	
SD[c]	0.65	0.63	0.74	0.8-48.7	1.45	1.22	1.32	21.40	20.74	19.28	

Notes: $^{*}p < 0.05$, $^{**}p < 0.01$, and $^{***}p < 0.001$. [a]Natural expression referred to expression of naturally felt emotions. [b]HCC was log-transformed for Pearson correlation analysis. [c]HCC was presented as median and range (pg/mg) because HCC has nonnormal distribution, and the other variables were presented as M and SD where M was mean and SD was standard deviation. Subscales, surface acting, deep acting, and expression of naturally felt emotions in emotional labor, and three subscales, emotional exhaustion, depersonalization, and professional inefficacy, in Maslach Burnout Inventory (MBI) were presented with average scores, but three subscales, personal burnout, work-related burnout, and client-related burnout, in Copenhagen Burnout Inventory (CBI) were presented with 25 times average scores each subscale to distinguish MBI and CBI throughout the text.

related burnout were varied with the working department (p's < 0.05), but it was not true for surface acting, deep acting, HCC, and professional inefficiency (p's > 0.05). Emotional exhaustion, personal burnout, and work-related burnout were varied with shift scheduling patterns (p's < 0.05), but it was not true for emotional labor strategies, HCC, and the other burnouts (p's > 0.246). The details are seen in Table S3 in the supplemental materials.

3.2. Multiple Linear Regression Analyses. A total of eighteen 4-step moderated hierarchical regressions were conducted to examine the unique effects of emotional labor strategies and interactive effects between emotional labor strategies and hair cortisol content on six aspects of job burnouts. Prior to the regression analyses, all the predictors except for type variables and moderator were centralized to reduce multicollinearity [54]. Demographic variables (i.e., working department, shift pattern, and working duration as a nurse) were entered into the regression in Step 1 to control for their respective effects. The emotional labor strategy as the predictive variable was separately entered into the equation in Step 2. Hair cortisol content as the moderator variable was entered in Step 3. Lastly, the interaction term between each emotional labor strategy and hair cortisol content was separately entered in Step 4. The amount of an additional explained variance was estimated after each step. The collinearity diagnoses revealed that tolerance was more than 0.2 and the variance inflation factor was less than 5 for all the regression equations, indicating that collinearity was not serious in the present models [55]. Subsequently, the nature and directionality of the significant interactions were investigated using the simple slope analyses proposed by Aiken et al. [54] where the effect of high and low levels (i.e., 1 SD above the mean, $M + 1$ SD, and 1 SD below the mean, $M - 1$ SD) of emotional labor was done in female nurses with high and low levels (i.e., $M + 1$ SD and $M - 1$ SD) of hair cortisol content.

The regression results revealed that surface acting could positively predict emotional exhaustion, depersonalization, personal burnout, work-related burnout, and client-related burnout (p's < 0.01), but it was not true for professional inefficacy ($p > 0.05$) as listed in Tables 2 and 3. Deep acting could negatively predict all six aspects of job burnouts (p's < 0.01) as listed in Tables 4 and 5. Expression of naturally felt emotion could also negatively predict all six aspects of job burnouts (p's < 0.01) as listed in Tables 6 and 7. HCC could not predict any aspects of job burnouts (p's > 0.05). Moreover, the Fisher Z test on the regression coefficients revealed that the impact patterns of surface acting on emotional exhaustion, depersonalization, professional inefficacy, personal burnout, work-related burnout, and client-related burnout were distinctly different from those of deep acting and expression of naturally felt emotion ($Z = 5.611$, $Z = 4.083$, $Z = 5.842$, $Z = 4.202$, $Z = 5.148$, and $Z = 6.417$, p's < 0.05 and $Z = 5.666$, $Z = 2.649$, $Z = 6.465$, $Z = 3.367$, $Z = 5.215$, and $Z = 6.546$, p's < 0.05), but there were no differences between deep acting and expression of naturally felt emotion (Z's < 1.96, p's > 0.05). Additionally, surface acting showed the association pattern differing between professional inefficacy and the other two MBIGS dimensions, emotional exhaustion and depersonalization ($Z = 3.74$, $Z = 3.09$, p's < 0.05), and deep acting between professional inefficacy and emotional exhaustion ($Z = 2.26$, $p < 0.05$).

Notably, the interaction terms between surface acting and HCC could positively predict emotional exhaustion and personal burnout (p's < 0.05) as listed in Tables 2 and 3. The interaction terms between deep acting and HCC could negatively predict emotional exhaustion, depersonalization, and personal burnout (p's < 0.05) as listed in Tables 4 and

Table 2: Coefficients of multiple linear regression of surface acting, hair cortisol content, and their interaction against Maslach job burnout ($n = 229$).

	Independent variable	Emotional exhaustion				Professional inefficacy				Depersonalization			
	Predictive variable	ΔR^2	β	B	SE	ΔR^2	β	B	SE	ΔR^2	β	B	SE
Step 1	Demographic variables[a]		0.105**				0.015				0.068*		
	ICU		0.268**	0.955	0.339		0.073	0.217	0.299		0.232*	0.751	0.315
	EICU		0.228**	1.199	0.434		-0.008	-0.037	0.383		0.173*	0.828	0.403
	Emergency		0.364**	1.116	0.299		-0.004	-0.010	0.264		0.219*	0.610	0.278
	Radiotherapy		0.065	0.368	0.430		-0.011	-0.053	0.379		-0.076	-0.391	0.400
	Rehabilitation		0.071	0.276	0.339		-0.083	-0.273	0.299		0.047	0.167	0.315
	Shift pattern		0.068	0.269	0.278		0.005	0.016	0.245		-0.045	-0.160	0.258
	Working duration		0.011	0.003	0.015		0.006	0.001	0.013		0.065	0.014	0.014
Step 2	Surface acting	0.110**	0.340**	0.762	0.137	0.000	-0.002	-0.003	0.129	0.077**	0.285**	0.581	0.131
Step 3	HCC[b]	0.000	-0.011	-0.045	0.259	0.000	-0.000	-0.001	0.243	0.005	-0.070	-0.271	0.245
Step 4	SA×HCC[c]	0.014*	0.123*	0.801	0.396	0.004	0.063	0.344	0.376	0.000	0.014	0.081	0.379

Notes: $^*p < 0.05$, $^{**}p < 0.01$, and $^{***}p < 0.001$. ΔR^2 was the change of R square, β was standardized regression coefficients, B was unstandardized regression coefficients, and SE was standard error of mean (the same below). [a]Demographic variables include type variables, working department, and shift pattern (i.e., the 8 h three-shift or 12 h two-shift scheduling pattern) and continuous variable (i.e., working duration as a nurse). Because the working department containing six types of departments was a dummy variable, the intensive care unit (ICU), emergency intensive care unit (EICU), emergency department, radiotherapy department, and rehabilitation department were coded as 1 in turn while the other departments as a reference were coded as 0. The 8 h three-shift and 12 h two-shift scheduling patterns were coded as 0 and 1, respectively. [b]HCC referred to hair cortisol content. [c]SA×HCC referred to the interaction between surface acting and hair cortisol content.

Table 3: Coefficients of multiple linear regression of surface acting, hair cortisol content, and their interaction against Copenhagen job burnout ($n = 229$).

	Independent variable	Personal burnout				Work-related burnout				Client-related burnout			
	Predictive variable	ΔR^2	β	B	SE	ΔR^2	β	B	SE	ΔR^2	β	B	SE
Step 1	Demographic variables[a]		0.120**				0.095**				0.127**		
	ICU		0.227*	11.912	4.955		0.185*	9.391	4.871		0.262**	12.377	4.446
	EICU		0.167	12.926	6.350		0.105	7.890	6.241		0.059	4.121	5.697
	Emergency		0.408**	18.454	4.373		0.286**	12.515	4.298		0.361**	14.683	3.923
	Radiotherapy		0.062	5.153	6.295		-0.015	-1.227	6.188		-0.075	-5.647	5.648
	Rehabilitation		0.090	5.141	4.958		0.035	1.971	4.873		0.132	6.837	4.448
	Shift pattern		0.130	7.543	4.067		0.148	8.349	3.998		0.057	2.998	3.649
	Working duration		0.045	0.152	0.220		-0.005	-0.016	0.216		0.132*	0.400	0.198
Step 2	Surface acting	0.028**	0.173**	5.701	2.111	0.057*	0.245**	7.831	2.042	0.018**	0.291**	8.673	1.834
Step 3	HCC[b]	0.013	-0.118	-7.366	3.944	0.000	-0.018	-1.029	3.844	0.000	-0.011	-0.644	3.453
Step 4	SA×HCC[c]	0.016*	0.127*	12.251	6.040	0.004	0.062	5.821	5.930	0.001	0.035	3.028	5.335

Notes: $^*p < 0.05$, $^{**}p < 0.01$, and $^{***}p < 0.001$. [a]The same coding as Table 2. [b]HCC referred to hair cortisol content. [c]SA×HCC referred to the interaction between surface acting and hair cortisol content.

5. The interaction terms between expression of naturally felt emotion and HCC could negatively predict professional inefficacy ($p < 0.05$) as listed in Tables 6 and 7. Subsequently, examination of simple slopes revealed that association of emotional labor with job burnout varied across different levels of hair cortisol as shown in Figure 1. A stronger correlation between surface acting and emotional exhaustion was observed in nurses with high cortisol levels ($B = 1.030$, $p < 0.01$) than those with low cortisol levels ($B = 0.488$, $p < 0.05$) although the positive correlation was significant for both nurses with high and low cortisol levels (p's < 0.05). Nurses with high cortisol levels showed higher emotional exhaustion than those with low cortisol levels in the context of high surface acting under which nurses in both groups showed elevated emotional exhaustion but had lower emotional exhaustion in the context of low surface acting (Figure 1(a)). Surface acting was significantly related to higher personal burnout for nurses with high cortisol levels ($B = 9.984$, $p < 0.01$), but it was not true for nurses with low cortisol levels ($B = 1.784$, $p > 0.05$). In comparison to those with low cortisol levels, nurses with high cortisol levels showed lower personal burnout in the context

Table 4: Coefficients of multiple linear regression of deep acting, hair cortisol content, and their interaction against Maslach job burnout ($n = 229$).

	Independent variable	Emotional exhaustion				Professional inefficacy				Depersonalization			
	Predictive variable	ΔR^2	β	B	SE	ΔR^2	β	B	SE	ΔR^2	β	B	SE
Step 1		Demographic variables[a]											
Step 2	Deep acting	0.028**	-0.172**	-0.393	0.147	0.130**	-0.368**	-0.708	0.122	0.061**	-0.251**	-0.524	0.134
Step 3	HCC[b]	0.000	0.002	0.010	0.272	0.000	-0.002	-0.008	0.227	0.003	-0.060	-0.231	0.247
Step 4	DA×HCC[c]	0.017*	-0.133*	-0.845	0.400	0.001	0.026	0.137	0.337	0.030**	-0.174**	-1.010	0.362

Notes: $^{*}p < 0.05$, $^{**}p < 0.01$, and $^{***}p < 0.001$. [a]Demographic variables showed the same results as Table 2. [b]HCC referred to hair cortisol content. [c]DA×HCC referred to the interaction between deep acting and hair cortisol contents.

Table 5: Coefficients of multiple linear regression of deep acting, hair cortisol content, and their interaction against Copenhagen job burnout ($n = 229$).

	Independent variable	Personal burnout				Work-related burnout				Client-related burnout			
	Predictive variable	ΔR^2	β	B	SE	ΔR^2	β	B	SE	ΔR^2	β	B	SE
Step 1		Demographic variables[a]											
Step 2	Deep acting	0.045**	-0.217**	-7.313	2.123	0.051**	-0.230**	-7.530	2.082	0.083**	-0.295**	-8.959	1.860
Step 3	HCC[b]	0.012	-0.112	-6.988	3.904	0.000	-0.009	-0.562	3.855	0.000	0.001	-0.060	3.445
Step 4	DA×HCC[c]	0.024*	-0.155*	-14.564	5.727	0.011	-0.107	-9.733	5.700	0.001	-0.030	-2.537	5.125

Notes: $^{*}p < 0.05$, $^{**}p < 0.01$, and $^{***}p < 0.001$. [a]Demographic variables showed the same results as Table 3. [b]HCC referred to hair cortisol content. [c]DA×HCC referred to the interaction between deep acting and hair cortisol content.

Table 6: Coefficients of multiple linear regression of expression of naturally felt emotions, hair cortisol content, and their interaction against Maslach job burnout ($n = 229$).

	Independent variable	Emotional exhaustion				Professional inefficacy				Depersonalization			
	Predictive variable	ΔR^2	β	B	SE	ΔR^2	β	B	SE	ΔR^2	β	B	SE
Step 1		Demographic variables[a]											
Step 2	Natural expression[b]	0.030**	-0.177**	-0.347	0.126	0.058**	-0.246**	-0.406	0.110	0.088**	-0.305**	-0.544	0.113
Step 3	HCC[c]	0.000	0.007	0.031	0.271	0.000	0.006	0.020	0.236	0.003	-0.051	-0.198	0.244
Step 4	NE×HCC[d]	0.014	-0.122	-0.725	0.377	0.024*	0.159*	0.793	0.326	0.002	-0.042	-0.229	0.341

Notes: $^{*}p < 0.05$, $^{**}p < 0.01$, and $^{***}p < 0.001$. [a]Demographic variables showed the same results as seen in Table 2. [b]Natural expression referred to expression of naturally felt emotions. [c]HCC referred to hair cortisol content. [d]NE×HCC referred to the interaction between expression of naturally felt emotions and hair cortisol content.

Table 7: Coefficients of multiple linear regression of expression of naturally felt emotions, hair cortisol content, and their interaction against Copenhagen job burnout ($n = 229$).

	Independent variable	Personal burnout				Work-related burnout				Client-related burnout			
	Predictive variable	ΔR^2	β	B	SE	ΔR^2	β	B	SE	ΔR^2	β	B	SE
Step 1		Demographic variables[a]											
Step 2	Natural expression[b]	0.019**	-0.141**	-4.095	1.857	0.053**	-0.236**	-6.611	1.791	0.089**	-0.306**	-7.968	1.596
Step 3	HCC[c]	0.011	-0.107	-6.711	3.969	0.000	-0.002	-0.150	0.852	0.000	0.008	0.431	3.433
Step 4	NE×HCC[d]	0.013	-0.115	-10.038	5.513	0.000	-0.019	-1.640	5.389	0.000	0.017	1.310	4.804

Notes: $^{*}p < 0.05$, $^{**}p < 0.01$, and $^{***}p < 0.001$. [a]Demographic variables showed the same results as seen in Table 3. [b]Natural expression referred to expression of naturally felt emotions. [c]HCC referred to hair cortisol content. [d]NE×HCC referred to the interaction between expression of naturally felt emotions and hair cortisol content.

of low surface acting but showed slightly higher personal burnout in the context of high surface acting under which nurses in both groups showed elevated personal burnout (Figure 1(b)).

Deep acting was significantly related to lower emotional exhaustion, depersonalization, and personal burnout for nurses with high cortisol levels ($B = -0.683$, $B = -0.869$, and $B = -12.183$, p's < 0.01), but it was not true for nurses with

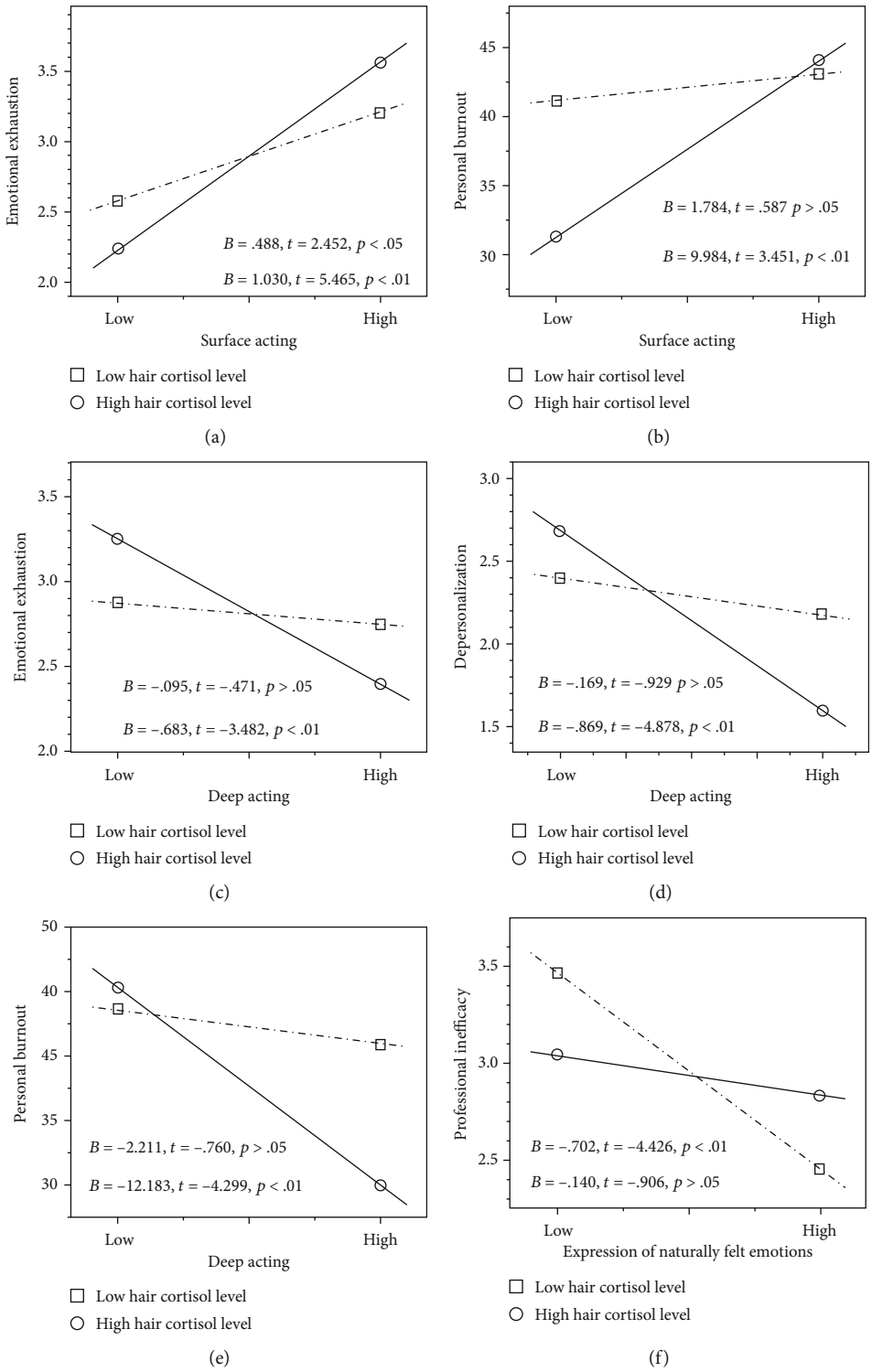

Figure 1: The moderating role of hair cortisol in the relationship between emotional labor strategies and job burnout: (a) surface acting and emotional exhaustion, (b) surface acting and personal burnout, (c) deep acting and emotional exhaustion, (d) deep acting and depersonalization, (e) deep acting and personal burnout, and (f) expression of naturally felt emotions and professional inefficacy.

low cortisol levels ($B = -0.095$, $B = -0.169$, and $B = -2.211$, p's > 0.05). Nurses with high cortisol levels showed higher emotional exhaustion and depersonalization than those with low cortisol levels in the context of low deep acting under which nurses in both groups showed elevated emotional exhaustion and depersonalization but had lower emotional exhaustion and depersonalization in the context of high deep acting (Figures 1(c) and 1(d)). In comparison to those with

low cortisol levels, nurses with high cortisol levels had lower personal burnout in the context of high deep acting but showed slightly higher personal burnout in the context of low deep acting under which nurses in both groups showed elevated personal burnout (Figure 1(e)). Expression of naturally felt emotions was significantly related to lower professional inefficacy for nurses with low cortisol levels ($B = -0.702$, $p < 0.01$), but it was not true for nurses with high cortisol levels ($B = -0.140$, $p > 0.05$). Nurses with low cortisol levels showed higher professional inefficacy than those with high cortisol levels in the context of low expression of naturally felt emotions under which nurses in both groups showed elevated professional inefficacy but had lower professional inefficacy in the context of high expression of naturally felt emotions (Figure 1(f)).

4. Discussions

The present study found that stress reactivity interacted with emotional labor in predicting emotional exhaustion, depersonalization, professional inefficacy, and personal burnout among Chinese female hospital nurses. Their interaction patterns were varied with the nature of emotional labor strategy and job burnout. Specifically, stress reactivity interacted with surface acting in predicting emotional exhaustion and personal burnout, and with deep acting in predicting emotional exhaustion, depersonalization, and personal burnout, and with the expression of naturally felt emotion in predicting professional inefficacy. The present study further found that low stress reactivity might be a protective factor for Chinese nurses' emotional exhaustion and depersonalization in the context of high job stress due to high surface acting or low deep acting, and high stress reactivity might be a protective factor for Chinese nurses' professional inefficacy in the context of high job stress due to low expression of naturally felt emotions. These findings provided new evidence for the extension of the JDR model to personal physiological resources from social and organizational resources and personal mental resources previous studies had already verified [1, 6, 7, 12, 15, 29, 30, 34–36].

Nurses with high cortisol levels (i.e., high stress reactivity) not only showed higher emotional exhaustion than those with low cortisol levels (i.e., low stress reactivity) when they underwent more stress experience resulting from high surface acting but also showed lower emotional exhaustion when undergoing less stress experience from low surface acting. Similarly, nurses with high stress reactivity not only showed higher emotional exhaustion and depersonalization than those with low cortisol levels under high job stress due to low deep acting but also showed lower emotional exhaustion and depersonalization under low job stress due to high deep acting. Nurses with low stress reactivity not only showed higher professional inefficacy than those with high stress reactivity under high job stress due to low expression of naturally felt emotions but also showed lower professional inefficacy under low job stress due to high expression of naturally felt emotions. These results together with the abovementioned previous findings on the interaction between stress reactivity and stressful environmental factors in predicting adolescents' psychological adaptations [23, 37, 38, 40] supported the differential susceptibility model. It implied that stress reactivity might be the plasticity factor for Chinese nurses' emotional exhaustion, depersonalization, and professional inefficacy in MBI burnouts. *Nevertheless*, stress reactivity showed the moderating patterns differing between the expression of naturally felt emotions and the other two emotional labor strategies in association with MBI burnout syndromes. For Chinese nurses' emotional exhaustion and depersonalization, high stress reactivity might be the plasticity factor in the context of surface acting and deep acting; that is, high stress reactivity might be a risk factor in the context of high job stress from high surface acting or low deep acting but be a promotive factor in the context of low job stress from low surface acting or high deep acting. In contrast, for Chinese nurses' professional inefficacy, low stress reactivity might be the plasticity factor in the context of the expression of naturally felt emotions. We discuss each of these findings in turn below.

The strengthening effect of high stress reactivity on the association of emotional labor and burnout is possibly attributed to the fact that individuals with higher stress reactivity are more sensitive to the context [5] and are more frequently in the allostasis upon the occurrence of stress [56], thereby being in a relatively higher stress-related arousal state. This might make them more easily influenced by external factors, for example, more easily suffer from adverse environments, thereby undergoing more stress experiences [40, 57]. In the present study, nurses with higher stress reactivity are also more susceptible to the context related to job demands and are more easily affected by job stress, such as stressful emotional labor demands in work environments. This explanation obtains the support from previous findings demonstrating that individuals with high stress reactivity are more likely to show more maladaptive outcomes (e.g., lower prosocial behaviors and more anxiety symptoms) under adverse environments but more adaptive outcomes under supportive environments [23, 37, 38, 40]. However, the explanation is held for associations of surface acting and deep acting with emotional exhaustion and depersonalization, but not for the association between the expression of naturally felt emotions and professional inefficacy. This is perhaps because both surface acting and deep acting need to consume resources to some extent [8]. Surface acting consumes a substantial amount of resources in order to suppress the true emotions at the behavioral level. Deep acting also spends considerable resources in the internalization of job demands on one's emotion through a cognitive regulation and reappraisal although its consumption in resources is relatively limited. In contrast, the expression of naturally felt emotions spends few resources because natural feelings are often consistent with the expression normally demanded by the work. When higher surface acting is exerted, the heavier imbalance between emotional demands and the resource expenditure happens, thereby giving rise to higher stress experience [14] and higher cortisol secretion [58] and more negative outcomes, such as more burnout syndromes as demonstrated in the current study. The resulting major resource's consumption and relatively more burnout

syndromes make employees greatly reduce resources to put into improving professional efficacy as suggested by the conservation of resources model [10], thereby weakening the association of surface acting with professional inefficacy as observed in the current study. A similar situation occurs in the context of deep acting that consumes relatively fewer resources than surface acting, but not for the expression of naturally felt emotions. Moreover, because their sensitivity and attention bias to the stressful context, nurses with high stress reactivity would put more physical and cognitive resources to cope with higher stressful emotional labor demands, thereby providing relatively fewer resources to improve their professional efficacy, especially in the context of surface acting and deep acting. On the contrary, because of their insensitivity to job stress, nurses with low stress reactivity would maintain more physical and cognitive resources, thereby having excess resources for improving their professional efficacy, especially in the context of the expression of naturally felt emotions. Additionally, according to the MBI definition of burnout [44], emotional exhaustion, depersonalization, and professional inefficacy are conceptualized as three dimensions that simultaneously occur. Actually, they are independently measured as three distinct and different dimensions as confirmed by many empirical studies [59]. In particular, professional inefficacy is largely independent of the other two dimensions [59]. Emotional exhaustion is seen as an individual state, depersonalization as a coping strategy, and professional inefficacy as one of many consequences of long-term stress as argued in previous studies [45]. Thus, they might have their own characteristic precursors, thereby showing the pattern of associations with emotional labor strategies differing between professional inefficacy and the other two dimensions, such as their association with surface acting as demonstrated in the current study. Therefore, high stress reactivity strengthens the association of surface acting with emotional exhaustion and associations of deep acting with emotional exhaustion and depersonalization and weakens the association of the expression of naturally felt emotions with professional inefficacy as found in the present study. By contrast, low stress reactivity strengthens the association of the expression of naturally felt emotions with professional inefficacy.

Notably, although nurses with high stress reactivity showed lower personal burnout than those with low stress reactivity under low surface acting or high deep acting, there might be no marked difference between the two groups in the context of high surface acting or low deep acting under which both groups showed elevated personal burnout. These results were not consistent with the differential susceptibility model but might be consistent with the vantage sensitivity model positing that individuals with vantage sensitivity are more positively responsive to supportive environments to which they are exposed but are not vulnerable to the negative influence of adverse environments [60]. It implied that for Chinese nurses' personal burnout, high stress reactivity might be a promotive factor in the context of low job stress due to low surface acting and high deep acting while high stress reactivity might be not a risk factor or low stress reactivity might be not a protective factor in the context of high job stress due to high surface acting and low deep acting. Obviously, the interaction of stress reactivity with surface acting and deep acting showed the pattern differing in CBI personal burnout and MBI emotional exhaustion and depersonalization even though both types of syndromes are measured as burnout indices. This might be because the sensitivity to job stress differs between CBI personal burnout and MBI emotional exhaustion and depersonalization. The MBI burnout is defined as a syndrome of emotional exhaustion, depersonalization, and professional inefficacy that can occur among individuals who do the human service work [61]. The core definition remains not changed in BMI-GS where some items were slightly revised to be widely applied across a variety of occupations rather than be restricted to the human service sector [44]. This definition implies that the MBI burnout is directly and primarily caused by the characteristic stress in human service work, the high emotional labor demands. Thus, the MBI burnout has relatively high sensitivity to high emotional labor demands. In the CBI, the core of burnout remains fatigue and exhaustion. However, CBI is designed as a questionnaire with three subdimensions, personal burnout, work-related burnout, and client-related work closely associated with three specific domains in a person's life. Among them, personal burnout is defined to be "the degree of physical and psychological fatigue and exhaustion experienced by the person" [45], and its questions are formulated in a way so that all human beings can answer them. Thus, personal burnout as a truly generic syndrome is relatively insensitive to the high emotional labor demands although there are associations between them. Therefore, high stress reactivity might be a risk factor under high job stress from high surface acting and low deep acting for nurses with higher emotional exhaustion and depersonalization, but not for those with higher personal burnout.

The current study has several limitations. First, the study was a cross-sectional design, limiting the understanding of the directionality on the association between variables. Second, the study was based on a sample of Han Chinese female nurses in city hospitals, China. The generalization of the present findings to other occupations and other ethnic groups in China and non-Chinese populations in other countries with collectivistic cultures and even western countries with individualistic cultures needs to be cautious. Third, the study only utilized a single index, hair cortisol as the biomarker of stress reactivity. Multiple biomarkers of stress reactivity would be recommended in future research. Finally, the study did not consider the influence of other job demands (e.g., work load, mental load, and task complexity) and of socioeconomic status, such as family income, education degree, and nurse's rank although these variables showed strong associations with working duration as a nurse.

In summary, stress reactivity interacted with emotional labor in predicting emotional exhaustion, depersonalization, professional inefficacy, and personal burnout among Chinese hospital nurses. Their interaction patterns were varied with the nature of emotional labor strategy and job burnout. High stress reactivity might be the plasticity factor for Chinese nurses' emotional exhaustion and depersonalization in the context of surface acting and deep acting, and low stress

reactivity might be the plasticity factor for Chinese nurses' professional inefficacy in the context of the expression of naturally felt emotions, which supported the differential susceptibility model. Additionally, high stress reactivity might be a promoting factor for Chinese nurses' personal burnout in the context of low surface acting or high deep acting, which might support the vantage sensitivity model.

Data Availability

The SPSS data used to support the findings of this study are available from the corresponding author upon request.

Conflicts of Interest

The authors declare that they have no conflicts of interest.

Authors' Contributions

All authors had the substantial intellectual contributions to this study as follows: Huihua Deng: conceptualization, writing (review and editing), and funding acquisition; Hanyao Wu: methodology and writing (original draft); Xingliang Qi: conceptualization and data collection; Caixiang Jin: data collection and funding acquisition; and Jianmei Li: methodology and funding acquisition. They all approved it for publication.

Acknowledgments

This work was supported by the Humanities and Social Science Foundation of Ministry of Education (15YJAZH009), Jiangsu Provincial Social Science Foundation (15GLB017), and the Fundamental Research Funds for the Southeast University (3218006405), China. The authors appreciated Miss Shuang Ji and Jing Zhang and Mr. Shifei Li for their assistance in the collection of questionnaires and hair samples and hair cortisol analysis.

Supplementary Materials

(1) The common method bias: an exploratory factor analysis (principal components extraction) showed that the emotional labor scale and job burnout scale did not generate the unique factor with the explained variance more than 40% (28.63% for two job burnout scales, 19.31% and 31.77% for MBI and CBI). Similarly, it was true for three subscales of the emotional labor scale and six subscales of job burnout (details seen in Table S1). A confirmatory factor analysis also demonstrated that the emotional labor scale and two job burnout scales did not converge on a single factor ($\chi^2 = 7251.69$, df = 989, $\chi^2/\text{df} = 7.332$, NFI = 0.82, CFI = 0.85, GFI = 0.42, RMSEA = 0.17). Similarly, it was true for three subscales of emotional labor and six subscales of job burnout (details seen in Table S2). (2) The influences of demographic variables on the study variables. As listed in Table S3, the variables in this study were not significantly correlated with working duration as a nurse (p's > 0.128). Expression of naturally felt emotion, emotional exhaustion, depersonalization, personal burnout, work-related burnout, and client-related burnout were varied with the working department ($F_{5,223} = 2.363$, $p = 0.041$; and $F_{5,223} = 5.028$, $p = 0.001$, but it was not true for surface acting, deep acting, HCC, and professional inefficiency p's > 0.05 . Emotional exhaustion, personal burnout, and work-related burnout were varied with shift-work scheduling pattern ($F_{1,227} = 4.232$, $p = 0.041$; $F_{1,227} = 6.032$, $p = 0.015$; and $F_{1,227} = 7.628$, $p = 0.006$, but it was not true for emotional labor strategies, HCC, and the other burnouts (p's > 0.246). *(Supplementary Materials)*

References

[1] E. Demerouti, A. B. Bakker, F. Nachreiner, and W. B. Schaufeli, "The job demands-resources model of burnout," *Journal of Applied Psychology*, vol. 86, no. 3, pp. 499–512, 2001.

[2] J. R. B. Halbesleben and M. R. Buckley, "Burnout in organizational life," *Journal of Management*, vol. 30, no. 6, pp. 859–879, 2016.

[3] A. R. Hochschild, *The Managed Heart: Commercialization of Human Feeling*, University of California Press, 1983.

[4] A. A. Grandey, G. M. Fisk, and D. D. Steiner, "Must "service with a smile" be stressful? The moderating role of personal control for American and French employees," *Journal of Applied Psychology*, vol. 90, no. 5, pp. 893–904, 2005.

[5] W. T. Boyce and B. J. Ellis, "Biological sensitivity to context: I. An evolutionary-developmental theory of the origins and functions of stress reactivity," *Development and Psychopathology*, vol. 17, no. 2, pp. 271–301, 2005.

[6] S. M. Jex and T. C. Elacqua, "Self-esteem as a moderator: a comparison of global and organization-based measures," *Journal of Occupational and Organizational Psychology*, vol. 72, no. 1, pp. 71–81, 1999.

[7] A. Makikangas and U. Kinnunen, "Psychosocial work stressors and well-being: self-esteem and optimism as moderators in a one-year longitudinal sample," *Personality and Individual Differences*, vol. 35, no. 3, pp. 537–557, 2003.

[8] J. M. Diefendorff, M. H. Croyle, and R. H. Gosserand, "The dimensionality and antecedents of emotional labor strategies," *Journal of Vocational Behavior*, vol. 66, no. 2, pp. 339–357, 2005.

[9] R. H. Gosserand and J. M. Diefendorff, "Emotional display rules and emotional labor: the moderating role of commitment," *Journal of Applied Psychology*, vol. 90, no. 6, pp. 1256–1264, 2005.

[10] S. E. Hobfoll, *Stress, Culture, and Community: The Psychology and Philosophy of Stress*, Plenum Press, 1998.

[11] J. M. Diefendorff, R. J. Erickson, A. A. Grandey, and J. J. Dahling, "Emotional display rules as work unit norms: a multilevel analysis of emotional labor among nurses," *Journal of Occupational Health Psychology*, vol. 16, no. 2, pp. 170–186, 2011.

[12] Y. Gu and X. You, "Recovery experiences buffer against adverse well-being effects of workplace surface acting: a two-wave study of hospital nurses," *Journal of Advanced Nursing*, vol. 76, no. 1, pp. 209–220, 2020.

[13] U. R. Hülsheger and A. F. Schewe, "On the costs and benefits of emotional labor: a meta-analysis of three decades of research," *Journal of Occupational Health Psychology*, vol. 16, no. 3, pp. 361–389, 2011.

[14] J. S. Kim, "Emotional labor strategies, stress, and burnout among hospital nurses: a path analysis," *Journal of Nursing Scholarship*, vol. 52, no. 1, pp. 105–112, 2020.

[15] S. D. Pugh, M. Groth, and T. Hennig-Thurau, "Willing and able to fake emotions: a closer examination of the link between emotional dissonance and employee well-being," *Journal of Applied Psychology*, vol. 96, no. 2, pp. 377–390, 2011.

[16] H. Yin, S. Huang, and G. Chen, "The relationships between teachers' emotional labor and their burnout and satisfaction: a meta-analytic review," *Educational Research Review*, vol. 28, article 100283, 2019.

[17] C. M. Brotheridge and A. A. Grandey, "Emotional labor and burnout: comparing two perspectives of "people work"," *Journal of Vocational Behavior*, vol. 60, no. 1, pp. 17–39, 2002.

[18] K. Ishii and K. M. Markman, "Online customer service and emotional labor: an exploratory study," *Computers in Human Behavior*, vol. 62, pp. 658–665, 2016.

[19] T. A. Judge, E. F. Woolf, and C. Hurst, "Is emotional labor more difficult for some than for others? A multilevel, experience-sampling study," *Personnel Psychology*, vol. 62, no. 1, pp. 57–88, 2009.

[20] M. Wrobel, "Can empathy lead to emotional exhaustion in teachers? The mediating role of emotional labor," *International Journal of Occupational Medicine and Environmental Health*, vol. 26, no. 4, pp. 581–592, 2013.

[21] D. Holman, T. D. Wall, C. Clegg, P. R. Sparrow, and A. Howard, *The New Workplace: A Guide to the Human Impact of Modern Working Practices*, John Wiley & Sons, 2002.

[22] F. Spiga, J. J. Walker, J. R. Terry, and S. L. Lightman, "HPA axis-rhythms," *Comprehensive Physiology*, vol. 4, no. 3, pp. 1273–1298, 2014.

[23] J. Obradović, N. R. Bush, J. Stamperdahl, N. E. Adler, and W. T. Boyce, "Biological sensitivity to context: the interactive effects of stress reactivity and family adversity on socioemotional behavior and school readiness," *Child Development*, vol. 81, no. 1, pp. 270–289, 2010.

[24] S. S. Dickerson and M. E. Kemeny, "Acute stressors and cortisol responses: a theoretical integration and synthesis of laboratory research," *Psychological Bulletin*, vol. 130, no. 3, pp. 355–391, 2004.

[25] E. Russell, G. Koren, M. Rieder, and S. van Uum, "Hair cortisol as a biological marker of chronic stress: current status, future directions and unanswered questions," *Psychoneuroendocrinology*, vol. 37, no. 5, pp. 589–601, 2012.

[26] F. Pragst and M. A. Balikova, "State of the art in hair analysis for detection of drug and alcohol abuse," *Clinica Chimica Acta*, vol. 370, no. 1-2, pp. 17–49, 2006.

[27] Q. Zhang, Z. Chen, S. Chen et al., "Correlations of hair level with salivary level in cortisol and cortisone," *Life Sciences*, vol. 193, pp. 57–63, 2018.

[28] Z. Chen, Q. Zhang, S. Chen, W. Wang, G. Liu, and H. Deng, "Determination, intercorrelation and intraindividual stability of five steroids in hair, saliva and urine among Chinese college students," *Steroids*, vol. 149, article 108418, 2019.

[29] A. B. Bakker, E. Demerouti, and M. C. Euwema, "Job resources buffer the impact of job demands on burnout," *Journal of Occupational Health Psychology*, vol. 10, no. 2, pp. 170–180, 2005.

[30] A. B. Bakker and E. Demerouti, "The job demands-resources model: state of the art," *Journal of Managerial Psychology*, vol. 22, no. 3, pp. 309–328, 2007.

[31] D. Xanthopoulou, A. B. Bakker, E. Demerouti, and W. B. Schaufeli, "The role of personal resources in the job demands-resources model," *International Journal of Stress Management*, vol. 14, no. 2, pp. 121–141, 2007.

[32] S. E. Hobfoll, "Social and psychological resources and adaptation," *Review of General Psychology*, vol. 6, no. 4, pp. 307–324, 2002.

[33] S. E. Hobfoll, R. J. Johnson, N. Ennis, and A. P. Jackson, "Resource loss, resource gain, and emotional outcomes among inner city women," *Journal of Personality and Social Psychology*, vol. 84, no. 3, pp. 632–643, 2003.

[34] A. B. Bakker, E. Demerouti, T. W. Taris, W. B. Schaufeli, and P. J. G. Schreurs, "A multigroup analysis of the job demands-resources model in four home care organizations," *International Journal of Stress Management*, vol. 10, no. 1, pp. 16–38, 2003.

[35] M. A. Tremblay and D. Messervey, "The Job Demands-Resources model: further evidence for the buffering effect of personal resources," *SA Journal of Industrial Psychology*, vol. 37, no. 2, pp. 10–19, 2011.

[36] N. W. Van Yperen and T. A. B. Snijders, "A multilevel analysis of the demands–control model: is stress at work determined by factors at the group level or the individual level?," *Journal of Occupational Health Psychology*, vol. 5, no. 1, pp. 182–190, 2000.

[37] J. Obradović, X. A. Portilla, and P. J. Ballard, "Biological sensitivity to family income: differential effects on early executive functioning," *Child Development*, vol. 87, no. 2, pp. 374–384, 2016.

[38] S. A. Owens, S. W. Helms, K. D. Rudolph, P. D. Hastings, M. K. Nock, and M. J. Prinstein, "Interpersonal stress severity longitudinally predicts adolescent girls' depressive symptoms: the moderating role of subjective and HPA axis stress responses," *Journal of Abnormal Child Psychology*, vol. 47, no. 5, pp. 895–905, 2019.

[39] N. M. H. van de Wiel, S. H. M. van Goozen, W. Matthys, H. Snoek, and H. van Engeland, "Cortisol and treatment effect in children with disruptive behavior disorders: a preliminary study," *Journal of the American Academy of Child and Adolescent Psychiatry*, vol. 43, no. 8, pp. 1011–1018, 2004.

[40] Y. Xu, Y. Liu, Z. Chen, J. Zhang, H. Deng, and J. Gu, "Interaction effects of life events and hair cortisol on perceived stress, anxiety, and depressive symptoms among Chinese adolescents: testing the differential susceptibility and diathesis-stress models," *Frontiers in Psychology*, vol. 10, p. 297, 2019.

[41] J. Belsky, M. J. Bakermans-Kranenburg, and M. H. van Ijzendoorn, "For BetterandFor Worse," *Current Directions in Psychological Science*, vol. 16, no. 6, pp. 300–304, 2016.

[42] J. Belsky and M. Pluess, "Beyond diathesis stress: differential susceptibility to environmental influences," *Psychological Bulletin*, vol. 135, no. 6, pp. 885–908, 2009.

[43] X. Wu, J. Li, G. Liu, Y. Liu, J. Cao, and Z. Jia, "The effects of emotional labor and competency on job satisfaction in nurses of China: a nationwide cross-sectional survey," *International Journal of Nursing Sciences*, vol. 5, no. 4, pp. 383–389, 2018.

[44] W. Schaufeli, M. Leiter, C. Maslach, and S. Jackson, *Maslach Burnout Inventory – General Survey (GS)*, Consulting Psychologists Press, 1996.

[45] T. S. Kristensen, M. Borritz, E. Villadsen, and K. B. Christensen, "The Copenhagen burnout inventory: a new tool for the

assessment of burnout," *Work and Stress*, vol. 19, no. 3, pp. 192–207, 2005.

[46] A. C. Wosu, U. Valdimarsdóttir, A. E. Shields, D. R. Williams, and M. A. Williams, "Correlates of cortisol in human hair: implications for epidemiologic studies on health effects of chronic stress," *Annals of Epidemiology*, vol. 23, no. 12, pp. 797–811.e2, 2013.

[47] M. A. LeBeau, M. A. Montgomery, and J. D. Brewer, "The role of variations in growth rate and sample collection on interpreting results of segmental analyses of hair," *Forensic Science International*, vol. 210, no. 1-3, pp. 110–116, 2011.

[48] Q. Y. Bai, "The influential factors of emotional labor and the relationship between emotional labor and employees' mental health in China," Master Thesis, Zhejiang University, Hangzhou, China, 2006.

[49] F. Y. L. Cheung and C. S. K. Tang, "Quality of work life as a mediator between emotional labor and work family interference," *Journal of Business and Psychology*, vol. 24, no. 3, pp. 245–255, 2009.

[50] C. Li and K. Shi, "The influence of distributive justice and procedural justice on job burnout," *Acta Psychologica Sinica*, vol. 35, no. 5, pp. 677–684, 2003.

[51] W. Y. Yeh, Y. W. Cheng, M. J. Chen, and A. Chi, "Development and validation of an occupational burnout inventory," *Taiwan Journal of Public Health*, vol. 27, no. 5, pp. 349–364, 2008.

[52] J. L. Schafer and J. W. Graham, "Missing data: our view of the state of the art," *Psychological Methods*, vol. 7, no. 2, pp. 147–177, 2002.

[53] P. M. Podsakoff, S. B. MacKenzie, J. Y. Lee, and N. P. Podsakoff, "Common method biases in behavioral research: a critical review of the literature and recommended remedies," *Journal of Applied Psychology*, vol. 88, no. 5, pp. 879–903, 2003.

[54] L. S. Aiken, S. G. West, and R. R. Reno, *Multiple Regression: Testing and Interpreting Interactions*, Sage, 1991.

[55] J. Fox, *Regression Diagnostics: An Introduction*, SAGE, 1991.

[56] B. S. Mcewen, "mood disorders and allostatic load," *Biological Psychiatry*, vol. 54, no. 3, pp. 200–207, 2003.

[57] J. Karlén, J. Ludvigsson, A. Frostell, E. Theodorsson, and T. Faresjö, "Cortisol in hair measured in young adults - a biomarker of major life stressors?," *BMC Clinical Pathology*, vol. 11, no. 1, p. 12, 2011.

[58] X. Qi, S. Ji, J. Zhang, W. Lu, J. K. Sluiter, and H. Deng, "Correlation of emotional labor and cortisol concentration in hair among female kindergarten teachers," *International Archives of Occupational and Environmental Health*, vol. 90, no. 1, pp. 117–122, 2017.

[59] N. Schutte, S. Toppinen, R. Kalimo, and W. Schaufeli, "The factorial validity of the Maslach Burnout Inventory-General Survey (MBI-GS) across occupational groups and nations," *Journal of Occupational and Organizational Psychology*, vol. 73, no. 1, pp. 53–66, 2000.

[60] M. Pluess and J. Belsky, "Vantage sensitivity: individual differences in response to positive experiences," *Psychological Bulletin*, vol. 139, no. 4, pp. 901–916, 2013.

[61] C. Maslach, S. E. Jackson, M. P. Leiter, W. B. Schaufeli, and R. L. Schwab, *Maslach Burnout Inventory*, Consulting psychologists press, Palo Alto, CA, 1986.

Hindawi
Neural Plasticity
Volume 2020, Article ID 8841332, 12 pages
https://doi.org/10.1155/2020/8841332

Research Article

Xiaoyao Pills Attenuate Inflammation and Nerve Injury Induced by Lipopolysaccharide in Hippocampal Neurons In Vitro

Yang Fang, Boyu Shi, Xiaobo Liu, Jie Luo, Zhili Rao, Rong Liu, and Nan Zeng

Department of Pharmacology, College of Pharmacy, Chengdu University of TCM, Chengdu City, Sichuan Province 611137, China

Correspondence should be addressed to Rong Liu; 22691101@qq.com and Nan Zeng; 19932015@cdutcm.edu.cn

Received 9 July 2020; Revised 27 August 2020; Accepted 1 September 2020; Published 21 September 2020

Academic Editor: Jason H. Huang

Lipopolysaccharides (LPS) are proinflammation mediators that can induce the inflammatory model of the hippocampal neuron, and neuroinflammation participates in the pathophysiology of depression. Xiaoyao Pill is a classical Chinese medicine formula that has been used for the treatment of mental disorders such as depression in China since the Song dynasty. We established a hippocampal neuronal cell inflammation model by LPS and investigate the intervention effect and mechanism of Xiaoyao Pills. The expression levels of IL-6, TNF-α, IDO, 5-HT, brain-derived neurotrophic factor, and β-nerve growth factor were detected by enzyme-linked immunosorbent assay. mRNA levels of IL-6, TNF-α, 5-HT1A, IDO-1, brain-derived neurotrophic factor, nerve growth factor, tropomyosin receptor kinase B, tropomyosin receptor kinase A, and cAMP response element-binding protein were detected by reverse transcription-polymerase chain reaction. To further validate, protein expression was determined by western blot and immunofluorescence. Lipopolysaccharide-induced neuroinflammatory state resulted in the release of IL-6, TNF-α, and IDO and a decrease of BDNF, NGF, TrkB, TrkA, CREB, p-CREB, p-CREB/CREB, and SYP and inhibited hippocampal neurogenesis in the hippocampal neuron. Xiaoyao Pills significantly decreased the levels of IL-6, TNF-α, and IDO in cell supernatant and increased the expression of BDNF, NGF, TrkB, TrkA, CREB, p-CREB, p-CREB/CREB, and SYP as well as the average optical density of BrdU/NeuN double-labelled positive cells. Our study shows that lipopolysaccharides induce inflammation and nerve damage in hippocampal neurons, which are closely related to the pathological mechanism of depression. Xiaoyao Pills (XYW) play an important neuroprotective effect, which is related to its inhibition of neuronal inflammation and promoting the recovery of nerve injury. These results provide a pharmacologic basis for the treatment of depression of XYW in clinical application.

1. Introduction

Depression is a devastating psychiatric disease that prevails throughout the world and has profound effects on neural structure and function. It is characterized by psychophysiological changes, such as low mood, loss of self-feeling, sadness, irritability, and loss of interest in all activities [1]. The incidence of depression in every generation worldwide is increasing. Numerous studies have identified genetic factors, environmental factors, and stress as major risk factors for depression [2].

Although depression has been explained with many theories, such as the monoamine theory, hypothalamus–pituitary–adrenal (HPA) axis theory, neurotrophic hypothesis, and neuroinflammation theory, it is far more multifactorial. In a sense, inflammation is a static load involving the immune, endocrine, and nervous systems. Initially, the investigations focused mostly on the effects of systemic inflammation on the central nervous system (CNS). However, current research focuses on neuroinflammation that occurs within the CNS; these findings suggest that cytokine-mediated interventions may be valuable for treating depression in this population [3]. The process of neuroinflammation involves sentinel immune cells in the CNS, resident macrophages called microglia [4]. The activation of microglia could trigger neuroinflammation, further causing a variety of neuropsychiatric diseases, such as depression [5], Alzheimer's disease [6], and schizophrenia [7]. Neuroinflammation participates in the pathophysiology of depression by increasing proinflammatory cytokines, activating the hypothalamus–

pituitary–adrenal axis, increasing glucocorticoid resistance, and affecting serotonin synthesis and metabolism, neuronal apoptosis and neurogenesis, and neuroplasticity [8]. The current research finds that proinflammatory cytokines inhibit the negative-feedback regulation of the HPA axis and cause the depletion of serotonin [9]. It also plays a key role in neuroendocrine, neurotransmitter depletion, neural plasticity, and local brain activity. Lipopolysaccharide (LPS) challenge could stimulate the acute inflammatory response that causes depressive symptoms in humans and rodents. Therefore, based on the close relationship between neuroinflammation and depression, LPS is often used to prepare depression-like models induced by inflammatory responses [10, 11].

Hippocampal atrophy is often observed in depressed patients and is considered a biomarker of depression risk [12]. The hippocampus is susceptible to neuroinflammatory. Numerous studies have shown that the proneurogenic effect of microglia cells is related to chronic neurodegeneration, and the activation of microglia cells plays a key role in inhibiting the hippocampus neurogenesis under stress and inflammatory conditions [13, 14]. Stress could also reduce neuronal dendrite branching and plasticity in the hippocampus neurons [15]. Hippocampal plasticity in depression involves hippocampal volume, hippocampal neurogenesis, and apoptosis of hippocampal neurons. Hippocampal neurogenesis in humans may be critical to the therapy of depression.

Xiaoyao San is included in the Chinese Pharmacopoeia *[16]*, which is a classical Chinese medicine formula. It is a prescription for Xiaoyao Pills. Xiaoyao San decoction comprises eight commonly used herbs *Bupleurum chinense* DC., *Angelica sinensis* Diels., *Paeonia lactiflora* Pall., *Atractylodes macrocephala* Koidz., *Mentha haplocalyx* Briq., *Poria cocos* Wolf., *Glycyrrhiza uralensis* Fisch., and *Zingiber officinale* Rosc. And if it is used for in vitro cell experiments directly, it will interfere with the experiment. Therefore, according to the concept of "serum pharmacology" proposed by Japanese scholar Hiroko Iwama, we used drug serum as the drug for in vitro experiments; it can reduce the interference of traditional Chinese medicine preparations on experiments in vitro, and it also meets the physiological process of pharmacological effects of Chinese medicine after being digested and absorbed by the body and biological metabolism [17]. At present, there have been many reports on the ingredients that may exist in the serum of Xiaoyao San: a total of 55 blood-containing components, including 16 original components, were identified in the rat-containing serum administered by the extracts of *Bupleurum chinense* DC. and *Paeonia lactiflora* Pall. The metabolic components are derived from saponin metabolites in *Bupleurum chinense* DC. and paeoniflorin metabolites in *Paeonia lactiflora* Pall [18].. The relative content of ligustilide was found in the drug-containing serum of *Angelica sinensis* Diels. And the extract is significantly higher than that in the original drug [19]. Metabolism components of 6 parent ingredients and 5 metabolic ingredients were found in the medicated serum of male rats administered with *Poria cocos* Wolf. extract [20]. Therefore, it is reliable to use drug serum for the study of Chinese medicine in vitro. Xiaoyao San has been used for the treatment of mental disorders such as depression for about nine hundred years in China since the Song dynasty. The antidepressant potential may be closely related to its pharmacological activity for invigorating the spleen, soothing the liver, nourishing the blood, and clearing away the liver fire due to blood deficiency [21]. Xiaoyao San improved the abnormalities of the tryptophan-kynurenine metabolic pathways in depressed rats and exerted antidepressant effects, changing biological indicators in rat hippocampus [22]. The modified Xiaoyao San can improve hippocampal neurogenesis by modulating cerebral oxygen-dependent fMRI signals in the brain of mice to play an antidepressant role [23]. Clinically, Xiaoyao Pills can improve symptoms of depression and enhance the quality of life in patients. It has a good therapeutic effect on depression and is worthy of clinical application [24, 25]. Previously, we found that Xiaoyao San was a highly effective formula to prevent depression by suppressing the HPA axis signal and improving the BDNF pathway signal in CUMS rats. However, whether Xiaoyao San can attenuate the release of proinflammatory cytokines, activate the BDNF signaling pathway, and promote neurogenesis during neuroinflammatory still remains unknown.

Our previous studies found that XYW ameliorated the depression-like behavior, decreased the levels of inflammatory indicators, increased those of neurotrophic factors and synaptic proteins, and restored Nissl bodies in acute stress mice and rat, thus improving depression in vivo [26]. In this study, an inflammatory model of hippocampal neuronal cells was established by LPS to simulate the occurrence of depression which was induced by hippocampal neuronal inflammation. The model showed increased proinflammatory cytokines, abnormal tryptophan metabolism, downregulation of the BDNF pathway, and neuronal injury. So we have measured the levels of the proinflammatory cytokines TNF-α and IL-6, the expression of IDO and 5-HT, and the expression of BDNF, NGF, TrkB, TrkA, CREB, p-CREB, and SYP in the hippocampal neuronal cell. Measurement of BrdU/NeuN further confirmed the neuroprotective effects of XYW on depression in the hippocampal neuronal cell inflammation model induced by LPS.

2. Materials and Methods

2.1. Xiaoyao Pill Quality Control (QC). The analysis was performed by High-Performance Liquid Chromatography (HPLC) (Thermo, US). The column was C18 column (4.6×250 mm, 5 μm), and the chromatographic separation conditions were as follows: column temperature: 30°C; flow rate: 1.0 mL/min; mobile phase: acetonitrile+0.1% phosphoric acid (15 : 85); stock solutions of Xiaoyao Pills were prepared by dissolving 0.4 g of analyte in 25 mL dilute ethanol [21]. The content in Xiaoyao Pills was determined by quantitation paeoniflorin ($C_{23}H_{28}O_{11}$). Paeoniflorin content should not be less than 4.0 mg in 1.0 g of concentrated pills [11]. The content of paeoniflorin in 1.0 g Xiaoyao Pills is 27.5 mg.

2.2. Drugs and Reagents. Xiaoyao Pills (TaiJi, China), LPS (Escherichia coli 055:B5), fluoxetine hydrochloride (FLX),

and DAPI were provided by Sigma (St. Louis, MO). Rabbit anti-NeuN antibody (1 : 50; Cat. No. #24307S), mouse anti-BrdU antibody (1 : 1400; Cat. No. #5292S), rabbit anti-TrkB antibody (1 : 1000; Cat. No. #4603), rabbit anti-CREB antibody (1 : 1000; Cat. No. #9197S), rabbit anti-p-CREB antibody (1 : 1000; Cat. No. #9198S), and rabbit anti-β-tubulin antibody (1 : 1000; Cat. No. #2128) were all from Cell Signaling Technology. Rabbit anti-synaptophysin polyclonal antibody (1 : 1000; Cat. No. #17785-1-AP) was from Proteintech. Rabbit anti-GAPDH antibody (1 : 1000; Cat. No. #GB11002) was from Servicebio. Goat anti-mouse IgG-FITC (1 : 100; Cat. No. #10) and goat anti-rabbit IgG/Cy3 (1 : 100; Cat. No. #AG04017512) were both from Absin.

2.3. Preparation of Xiaoyao Pill Serum. Male Sprague-Dawley rats that weighed 220–240 g were purchased from Chengdu Dashuo. All animals were raised in standard cages in a room of constant temperature and humidity ($22 \pm 1^{\circ}$C; 40–60%) with a 12 : 12 dark/light cycle (lights on at 8:00 a.m.; off at 8:00 p.m.). The animals were given free access to food and water throughout the experiment. Rats in the XYW group were intragastrically administered XYW (Xiaoyao Pills, 1.86 g·kg^{-1}) daily for 14 days; meanwhile, rats in the control groups were intragastrically administered equivoluminal saline daily to ensure isocaloric intake. Rats were anesthetized after 1 h for the last lavage. Then, blood was taken from the abdominal aorta, centrifuged, in a water bath, sterilized with a filter membrane, and stored in a -80°C refrigerator, avoiding repeated freezing and thawing.

2.4. Cell Culture and Treatment. Embryonic brains were dissected, and single-cell suspensions of the hippocampus were obtained by mechanical dissociation from Sprague-Dawley rats which were purchased from Chengdu Dashuo. Primary hippocampal neurons were plated at a density of 5×10^5 cells/mL in polylysine-coated culture plates and cultured in DMEM supplemented with 10% FBS at 37°C in a humidified atmosphere of 5% CO_2/95% air using standard cell culture methods for 24 h. Then, for differentiation of neural stem cells, replace medium with Neurobasal-A medium containing 2% B-27 and 1% L-glutamine. The medium was changed every 3 days. After the 10th day, LPS was added to the medium. Then, 24 h later, hippocampal neurons were incubated with Xiaoyao Pill serum (4% and 8% concentration) in Neurobasal-A medium without 2% B-27 for 48 h. After a preliminary experiment, it was found that Xiaoyao Pill serum concentrations of 4% and 8% had no effect on cell viability.

2.5. Cell Identification. The primary hippocampal neurons were cultured in a laser confocal petri dish for 13 days according to item 2.4. After the completion of culture, abandon the culture medium and add 4% paraformaldehyde to fix for 30 min. Add 0.25% Triton X-100 to permeabilize for 15 min, then incubate with 5% BSA-PBST for 1 h. Cells were incubated overnight after adding rabbit anti-NeuN antibody diluent (1 : 50; Cell Signaling Technology; Cat. No. #24307S), then adding goat anti-rabbit IgG/Cy3 diluent (1 : 100; Absin; Cat. No. #AG04017512), and incubating for 1 h. Images were captured at 20x using a confocal microscope. NeuN is a specific marker for neurons, which can be marked red by NeuN-CY3. After the double staining of NeuN and DAPI, the distribution of red fluorescence and blue fluorescence of the cells cultured for 13 days was basically consistent, indicating that the cultured cells were neurons (Figure 1).

2.6. Mechanism Detection

2.6.1. ELISA Analysis for IL-6, TNF-α, IDO, 5-HT, BDNF, and β-NGF. The levels of IL-6, TNF-α, BDNF, and β-NGF in cell supernatant and IDO and 5-HT in cell lysate were detected by ELISA, according to the manufacturer's instructions, and the optical density was measured at 450 nm by a microplate reader.

2.6.2. Total RNA Expression in the Hippocampus and Cortex via RT-PCR. The total RNA was used to synthesize cDNA using the FastQuant RT kit (Tiangen, Beijing, China); subsequently, the amplification reactions were carried out in 96-well reaction plates with 20 μL reaction volume (Bio-Rad). The gene primer sequences of β-actin, IL-6, TNF-α, 5-HT1A, IDO1, BDNF, NGF, TrkB, TrkA, and CREB used in this study are listed in Table 1.

2.6.3. Western Blotting Analysis. RIPA lysate buffer containing 1 mM PMSF was added to each sample to collect the total protein. The total protein concentration of each sample was determined by the BCA method and adjusted all samples to the same concentration. The protein samples were mixed with a 5x loading buffer and denatured at 95°C. The proteins were separated by SDS-PAGE (8% or 15%) and electrophoretically transferred onto polyvinylidene fluoride membranes. The membranes were probed with rabbit anti-TrkB antibody (1 : 1000; Cell Signaling Technology; Cat. No. #4603), rabbit anti-CREB antibody (1 : 1000; Cell Signaling Technology; Cat. No. #9197S), rabbit anti-p-CREB antibody (1 : 1000; Cell Signaling Technology; Cat. No. #9198S), rabbit anti-β-tubulin antibody (1 : 1000; Cell Signaling Technology; Cat. No. #2128), rabbit anti-synaptophysin polyclonal antibody (1:1000; Proteintech; Cat. No. #17785-1-AP), and rabbit anti-GAPDH antibody (1 : 1000; Servicebio; Cat. No. #GB11002) overnight at 4°C and then incubated with Anti-rabbit IgG HRP-Linked Antibody (1 : 3000; Servicebio; Cat. No. #GB23303) at 37°C for 1.5 h. Detection was performed using a ChemiDoc XRS$^+$ (Bio-Rad, USA) image analysis system.

2.6.4. Immunostaining. Cultured cells were fixed in a PBS solution containing 4% paraformaldehyde for 15 min and washed 3 times with PBS. A PBS solution containing 0.25% Triton was added to the cells for 15 min at room temperature and then incubated with 5% bovine serum albumin for 1 h. After removing this blocking reagent, cells were incubated in a humidified chamber at 4°C overnight with primary antibodies: mouse anti-BrdU antibody (1 : 1400; Cell Signaling Technology; Cat. No. #5292S), rabbit anti-NeuN antibody (1 : 50; Cell Signaling Technology; Cat. No. #24307S), and rabbit anti-NeuN antibody (1 : 50; Cell Signaling Technology; Cat. No. #24307S) diluted in blocking reagent. Then, cells were washed 3 times with PBS and incubated for 1 h in the

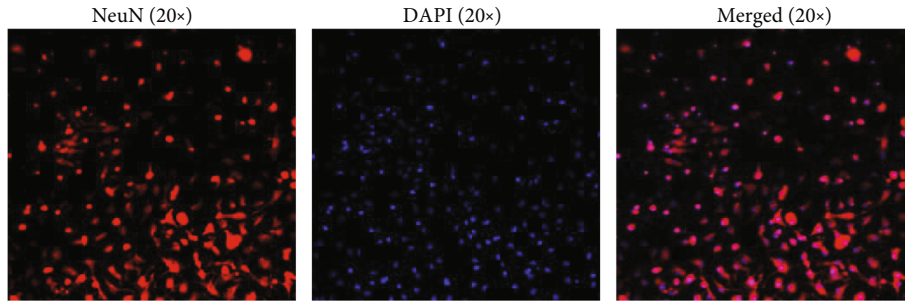

Figure 1: Identification of rat primary hippocampal neurons (20x). The hippocampal neuronal cells were incubated with anti-NeuN antibody (red) and DAPI (blue) and were observed by a laser scanning confocal microscope.

Table 1: Gene primer sequence.

Gene	Primer	Primer sequence (5′ to 3′)	Product size (bp)
β-Actin	Forward primer	CACCCGCGAGTACAACCTTC	207
	Reverse primer	CCCATACCCACCATCACACC	
IL-6	Forward primer	AGAGACTTCCAGCCAGTTGC	115
	Reverse primer	CTGGTCTGTTGTGGGTGGTA	
TNF-α	Forward primer	GATCGGTCCCAACAAGGAGG	138
	Reverse primer	GCTTGGTGGTTTGCTACGAC	
5-HT1A	Forward primer	TGATCTCGCTCACTTGGCTC	145
	Reverse primer	AAAGCGCCGAAAGTGGAGTA	
IDO1	Forward primer	GCATCAAGACCCGAAAGCAC	154
	Reverse primer	GTTGCCCTTCCAACCAGACA	
BDNF	Forward primer	TAGGCAGAATGAGCAATGTC	178
	Reverse primer	CCCAAGAGGTAAAGTGTAGAAG	
NGF	Forward primer	TGGAGATAAGACCACAGCCA	197
	Reverse primer	TGACAAAGGTGTGAGTCGTG	
TrkB	Forward primer	TGCTCAAGTTGGCGAGACAT	151
	Reverse primer	GTCCCAGGAGTTCAGCTCAC	
TrkA	Forward primer	CCCTCCTGATGTCTACGCCA	139
	Reverse primer	CTCCTAGCCCAGAACGTCCA	
CREB	Forward primer	AGCCGGGTACTACCATTC	244
	Reverse primer	GCTGCTTCCCTGTTCTTC	

dark at room temperature in the presence of the fluorescent secondary antibodies: goat anti-mouse IgG-FITC (1 : 100; Absin; Cat. No. #10) and goat anti-rabbit IgG/Cy3 (1 : 100; Absin; Cat. No. #AG04017512). Finally, the coverslips were mounted onto slides in PBS. The preparations were analysed under a fluorescent microscope (Olympus FV1200).

2.7. Statistical Analysis. All analyses were performed using SPSS. Data are presented as the mean ± SD. All analyses were performed using one-way ANOVA, t-test analysis, or Mann-Whitney test rank-sum analysis. The level of significance was set at $p \leq 0.05$.

3. Results

3.1. Xiaoyao Pills Prevent LPS-Induced Inflammation. As shown in Figures 2(a) and 2(c) and Table 1, after treatment with LPS, inflammatory cytokines, including IL-6 (Figure 1(a), $F = 2.746$, $p < 0.001$) and TNF-α (Figure 1(c), $p = 0.009$), are released from hippocampal neuronal cells. Treatment with fluoxetine hydrochloride (FLX) could reduce the IL-6 level in supernatant (Figure 2(a), $F = 3.291$, $p < 0.001$) and downregulate IL-6 mRNA expression in cells (Figure 1(b), $p = 0.009$) and TNF-α mRNA expression (Figure 2(b), $F = 8.377$, $p = 0.001$). Treatment with Xiaoyao Pill serum (8%) could decrease the levels of IL-6 (Figure 2(a), 8%: $F = 4.133$, $p = 0.010$) and TNF-α (Figure 2(c), 8%: $p = 0.009$) in supernatant, while Xiaoyao Pill serum (4%) also decreased the level of IL-6 in supernatant (Figure 2(a), $F = 1.262$, $p < 0.001$). Furthermore, in cell lysates, Xiaoyao Pill serum (4% and 8%) reduced the expression of IL-6 mRNA (Figure 2(b), 4%: $p = 0.009$; 8%: $p = 0.009$) and TNF-α mRNA (Figure 2(b), 4%: $F = 42.007$, $p < 0.001$; 8%: $F = 47.912$, $p < 0.001$). Although the serum of 4% and 8% Xiaoyao Pills could significantly reduce the IL-6 level in the supernatant, there was no obvious dose correlation, which may be related to the

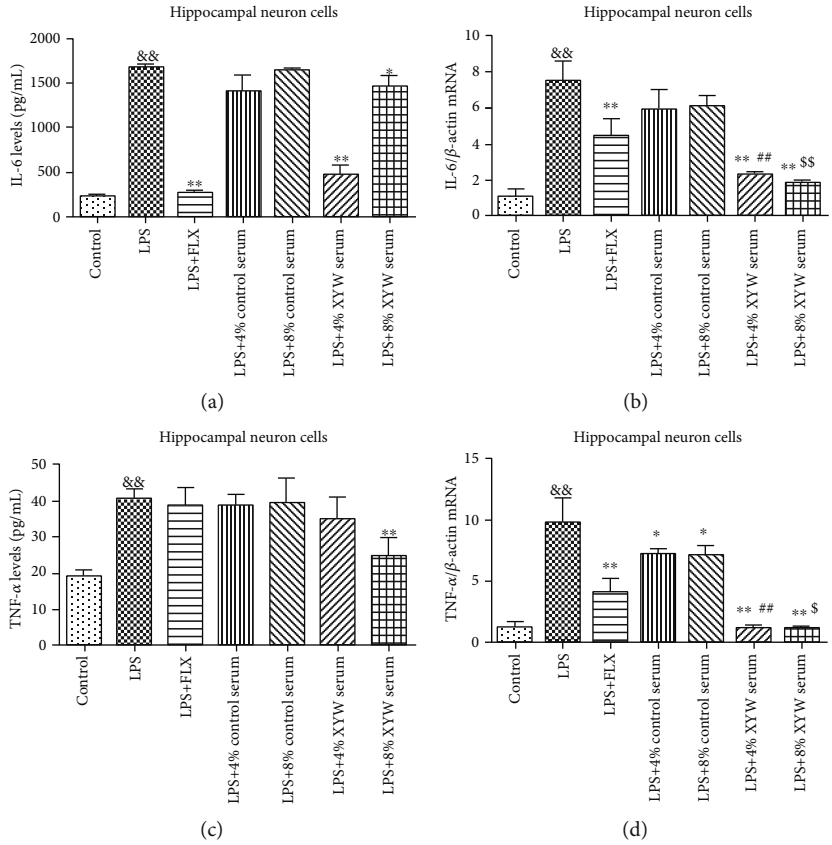

Figure 2: Xiaoyao Pill serum (final concentration of 4% and 8%) reduced the expression of IL-6 and TNF-α in hippocampal neuronal cells. The protein levels of IL-6 in supernatant (a). The relative mRNA expression of IL-6 in cell lysate (b). The protein levels of TNF-α in supernatant (c). The relative mRNA expression of TNF-α in cell lysate (d). The results were expressed as the mean ± SD (n = 4-5). $^{\&\&}p < 0.01$ compared to the control group. $^{*}p < 0.05$ and $^{**}p < 0.01$ compared to the LPS group. $^{\#\#}p < 0.01$ compared to the LPS+4% control serum group. $^{\$\$}p < 0.01$ compared to the LPS+8% control serum group.

complexity of the components of traditional Chinese medicine or the interaction between the components. In conclusion, FLX and the serum of Xiaoyao Pills could inhibit the inflammatory reaction of hippocampal neuronal cells induced by LPS.

3.2. Xiaoyao Pills Prevent LPS-Induced Limited 5-HT and IDO. We further proved that, in vitro experiments, LPS could increase the protein (Figure 3(c), $F = 0.709$, $p = 0.006$) and its mRNA expression (Figure 3(d), $p = 0.009$) of IDO in hippocampal nerve cell lysate and downregulate the 5-HT level (Figure 3(a), $F = 0.772$, $p = 0.039$) and its mRNA expression (Figure 3(b), $F = 18.479$, $p < 0.001$) compared with the control group. FLX improved the levels of 5-HT (Figure 3(a), $F = 0.368$, $p = 0.005$) and its mRNA (Figure 3(b), $F = 0.061$, $p < 0.001$) in cell lysate and decreased the levels of IDO (Figure 3(c), $F = 0.081$, $p < 0.001$) and its mRNA (Figure 3(d), $p = 0.009$) in cell lysate. Xiaoyao Pill serum (8%) also improved the levels of 5-HT (Figure 3(a), $F = 0.053$, $p = 0.007$) and its mRNA expression (Figure 3(b), $F = 7.652$, $p = 0.034$) in cell lysate, while decreasing the expression of IDO mRNA (Figure 3(d), $p = 0.009$) in cell lysate. Xiaoyao Pill serum (4%) decreased the level of IDO protein (Figure 3(c), $F = 2.793$, $p = 0.035$) and its mRNA expression (Figure 3(d), $p = 0.009$) in cell lysate. These results showed that Xiaoyao Pills could resist the abnormal upregulation of IDO induced by LPS and the abnormal downregulation of 5-HT, thus playing an inhibitory role in the inflammatory response of hippocampal nerve cells.

3.3. Xiaoyao Pills Prevent LPS-Induced Reduction of Neurotrophic Factor. In primary hippocampal neuron cells, the production of neurotrophic factors and related factors decreased after LPS treatment in hippocampal neurons, including BDNF (protein expression: Figure 4(b), $F = 8.856$, $p = 0.008$; mRNA expression: Figure 4(d), $F = 12.023$, $p = 0.024$) and NGF (protein: Figure 4(c), $F = 37.075$, $p = 0.017$; mRNA: Figure 4(e), $F = 14.076$, $p = 0.018$), as well as its high-affinity tropomyosin-related kinase, such as TrkB (protein: Figure 4(h), $F = 4.221$, $p < 0.001$; mRNA: Figure 4(f), $F = 4.157$, $p < 0.001$), TrkA (mRNA: Figure 4(g), $F = 0.010$, $p < 0.001$), and CREB (protein: Figure 4(k), $F = 2.506$, $p = 0.001$; mRNA: Figure 4(i), $F = 5.582$, $p = 0.001$), p-CREB (Figure 4(j), $F = 0.115$, $p < 0.001$), and the ratio of p-CREB/-CREB (Figure 4(l), $F = 1.118$, $p = 0.005$). Xiaoyao Pill serum (4% and 8% concentrations) and FLX could increase the levels of BDNF (Figure 4(b), FLX: $F = 4.186$, $p = 0.034$; 4% serum: $F = 8.666$, $p = 0.028$; 8% serum: $F = 5.504$, $p = 0.030$) and β-NGF (Figure 4(c), FLX: $F = 3.389$, $p < 0.001$; 4% serum: $F = 5.779$, $p = 0.034$; 8% serum: $F = 3.777$, $p = 0.003$) in the

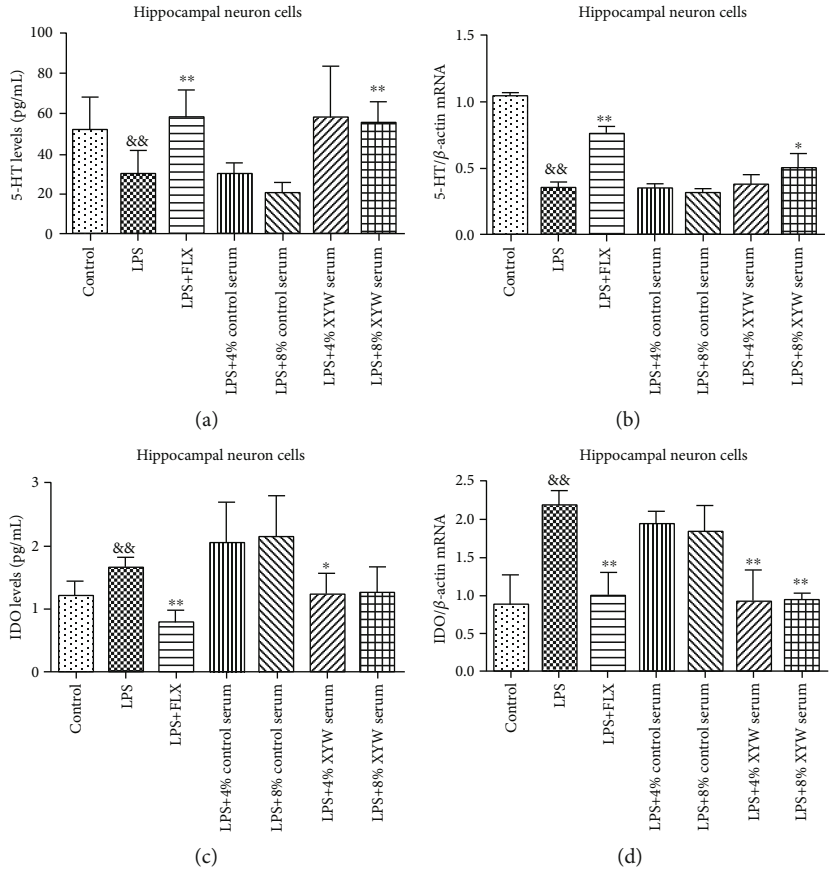

Figure 3: Xiaoyao Pill serum improved the expression of 5-HT and lowered the expression of IDO in hippocampal neuronal cells. The protein levels of 5-HT in cell lysate (a). The relative mRNA expression of 5-HT in cell lysate (b). The protein levels of IDO in cell lysate (c). The relative mRNA expression of IDO in cell lysate (d). The results were expressed as the mean ± SD ($n = 4$-6). $^{\&\&}p < 0.01$ compared to the control group. $^{*}p < 0.05$ and $^{**}p < 0.01$ compared to the LPS group.

supernatant, while increasing the transcription level of BDNF (Figure 4(d), FLX: $F = 0.890$, $p < 0.001$; 4%: $F = 0.751$, $p < 0.001$; 8%: $F = 0.116$, $p < 0.001$), NGF (Figure 4(e), FLX: $F = 33.082$, $p = 0.002$; 4% serum: $F = 0.231$, $p < 0.001$; 8% serum: $F = 1.288$, $p = 0.001$), TrkB (Figure 4(f), FLX: $F = 4.221$, $p = 0.001$; 4% serum: $F = 8.976$, $p = 0.045$; 8% serum: $F = 0.220$, $p = 0.003$), TrkA (Figure 4(g), FLX: $F = 5.901$, $p = 0.034$; 4% serum: $F = 9.288$, $p = 0.019$; 8% serum: $F = 4.224$, $p = 0.004$), and CREB (Figure 4(i), FLX: $F = 0.537$, $p = 0.004$; 4% serum: $F = 15.732$, $p = 0.024$; 8% serum: $F = 5.745$, $p = 0.006$) in the cell lysate, and the protein expression of TrkB (Figure 4(h), FLX: $F = 4.221$, $p = 0.001$; 4% serum: $F = 4.221$, $p = 0.007$; 8% serum: $F = 4.221$, $p < 0.001$), CREB (Figure 4(k), FLX: $F = 2.506$, $p = 0.021$; 4% serum: $F = 2.506$, $p = 0.049$; 8% serum: $F = 2.506$, $p = 0.033$), and p-CREB (Figure 4(j), FLX: $F = 0.024$, $p < 0.001$; 4% serum: $F = 2.741$, $p < 0.001$; 8% serum: $F = 3.851$, $p = 0.008$) in the cell lysate, as well as the ratio of p-CREB/CREB (Figure 4(l), FLX: $F = 1.291$, $p = 0.024$; 4% serum: $F = 0.079$, $p = 0.011$; 8% serum: $F = 0.053$, $p = 0.021$).

The regulation of neurogenesis and synaptic plasticity of neurons is closely related to BDNF. BDNF could self-release from neurons into the extracellular space and bind to TrkB, in turn phosphorylating CREB and playing a neuroprotective role. In this study, we mainly observed the extracellular BDNF level and the protein expression levels of intracellular TrkB, CREB, and p-CREB. The results indicated that Xiaoyao Pills prevented the reduction of neurotrophic factor induced by LPS and activated the BDNF/TrkB/CREB molecular pathway.

3.4. Xiaoyao Pills Promote LPS-Damaged Synaptic Growth. Synaptophysin (SYP) is widely regarded as scaffold proteins, involved in the regulation of synaptic function. The level of SYP in neuron cells could reflect whether neuronal synapses are damaged. In hippocampal neuron cells, LPS induced synaptic dysfunction (Figure 5(b), $F = 9.506$, $p = 0.011$). Xiaoyao Pill serum and FLX ameliorated synaptic dysfunction by promoting the expression of synaptophysin (Figure 5(b), FLX: $F = 4.430$, $p < 0.001$; 4% serum: $F = 1.106$, $p = 0.006$; 8% serum: $F = 7.353$, $p = 0.003$), suggesting Xiaoyao Pills could promote synaptic growth damaged by LPS.

3.5. Xiaoyao Pills Prevent the LPS-Induced Decrease in the Proliferation of Hippocampal Neurons. BrdU, also known as deoxyuridine bromide, is a synthetic thymidine analogue that substitutes thymine nucleosides for selective binding to cellular DNA during the S phase. Thus, cell DNA synthesis and

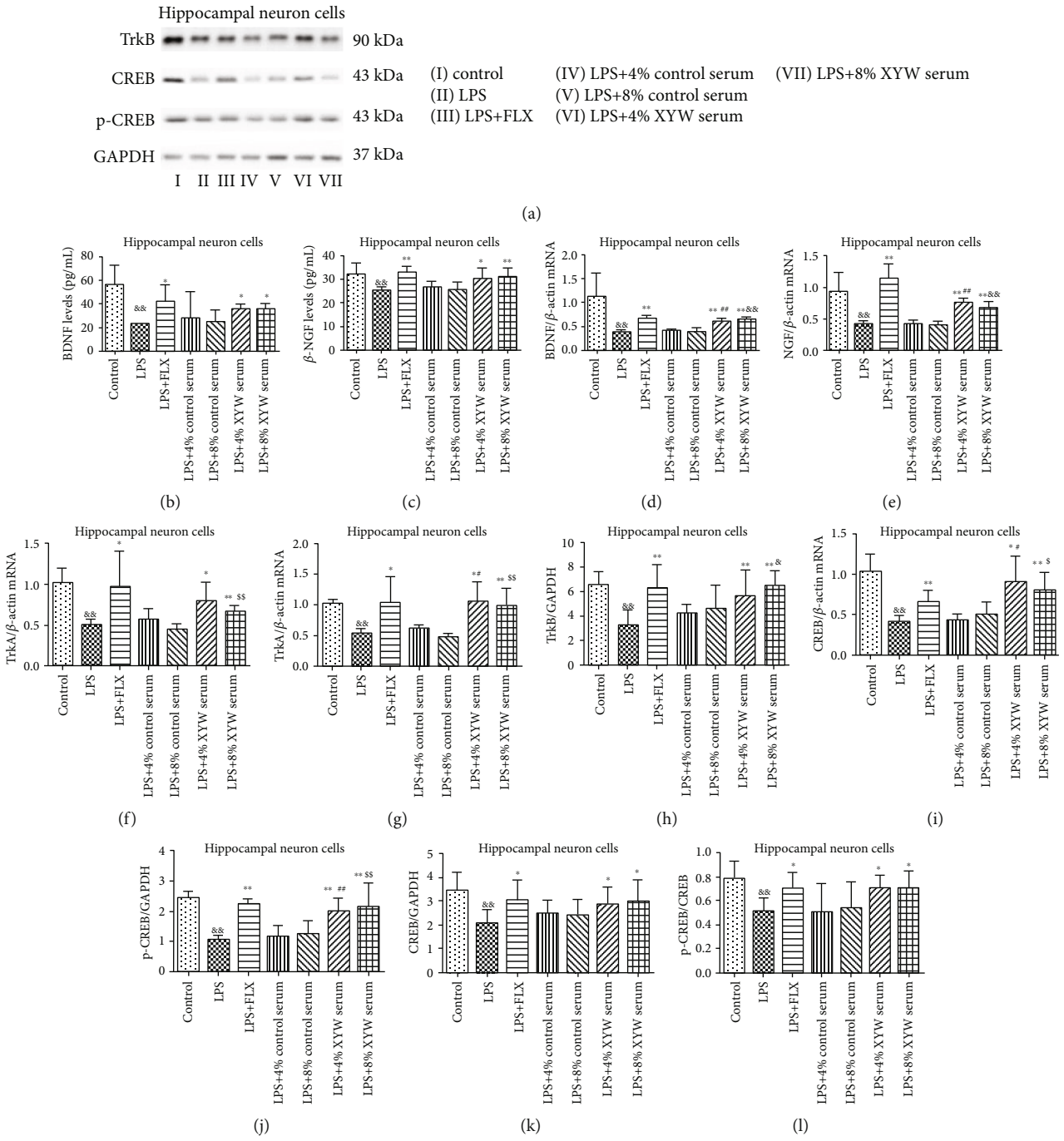

Figure 4: Xiaoyao Pills prevent LPS-induced reduction of neurotrophic factor. Representative blots of relative protein expression of TrkB, CREB, and p-CREB (a). Xiaoyao Pill serum (4% and 8%) improved the levels of BDNF (b) and β-NGF (c) in supernatant and increased the transcription level of BDNF (d), NGF (e), TrkB (f), TrkA (g), and CREB (i) and the translation levels of TrkB (h), CREB (k), and p-CREB (j) in cell lysate, as well as the ratio of p-CREB/CREB (l) higher than the LPS group. The results were expressed as the mean ± SD (n = 5-6). $^{\&\&}p < 0.01$ compared to the control group. $^{*}p < 0.05$ and $^{**}p < 0.01$ compared to the LPS group. $^{\#\#}p < 0.05$ and $^{\#\#}p < 0.01$ compared to the LPS+4% control serum group. $^{\$}p < 0.01$ and $^{\$\$}p < 0.01$ compared to the LPS+8% control serum group.

cell division and apoptosis were detected. BrdU is often used as a marker of cell proliferation. BrdU immunofluorescence chemistry has been used to study the development of the nervous system and to identify neurogenesis in the brain. The average optical density of BrdU/NeuN double-labelled positive cells in the model group was significantly lower than that in the control group (Figure 6(b), $F = 6.939$, $p = 0.013$), and the ratio of BrdU/NeuN was significantly higher in the Xiaoyao Pill serum (4%) group than that in the LPS group (Figure 6(b), $F = 7.754$, $p = 0.019$). It indicated that Xiaoyao Pills could prevent the decrease in the proliferation of hippocampal neurons induced by LPS.

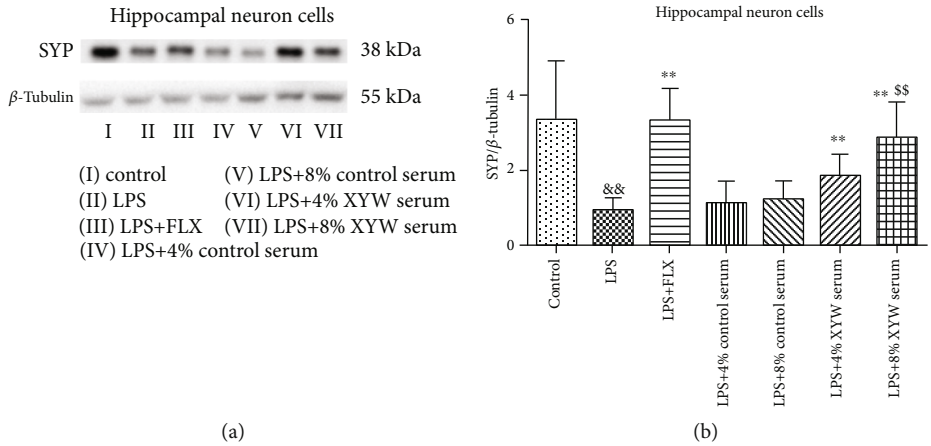

Figure 5: Xiaoyao Pill serum improved the levels of SYP in cell lysates. Representative blots and statistical graphs of relative protein expression of SYP (a, b). The results were expressed as the mean ± SD ($n = 6$). $^{\&\&}p < 0.01$ compared to the control group. $^{**}p < 0.01$ compared to the LPS group. $^{\$\$}p < 0.01$ compared to the LPS+8% control serum group.

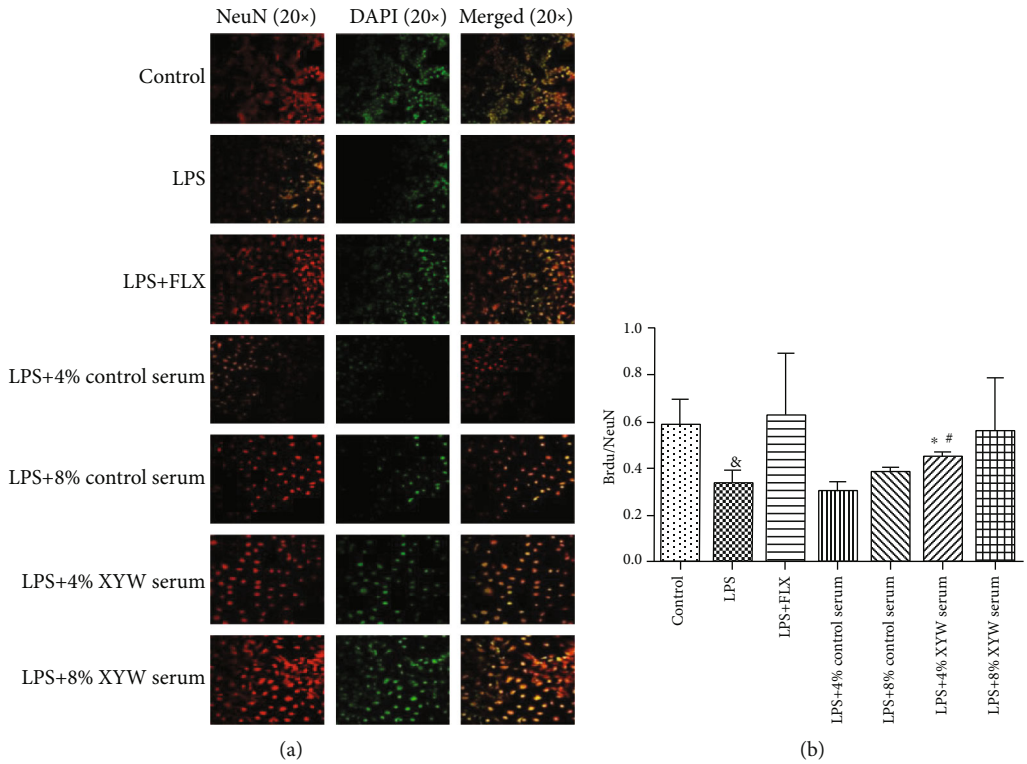

Figure 6: Xiaoyao Pills promote LPS-damaged synaptic growth. The hippocampal neuronal cells were incubated with anti-NeuN antibody (red) and anti-BrdU antibody (green) and were observed by a laser scanning confocal microscope (20x) (a). The statistical graphs of the ratio of BrdU's average optical density/NeuN's average optical density (b). Data were the mean ± SD ($n = 4$). $^{\&}p < 0.05$ compared to the control group. $^{*}p < 0.05$ compared to the LPS group. $^{\#}p < 0.05$ compared to the LPS+4% control serum group.

4. Discussion

Neurons are the basic structural and functional units of the nervous system; the role of neurons is to integrate and transmit signals. And the changes of neuronal structure and function in the brain in response to various stimuli, including stress and inflammation, cause nerve damage and eventually lead to depression. Depression is one of the most common mental illnesses. It is a multifactorial disease with both genetic and environmental factors contributing to its pathogenesis. And it affects multiple behavioral areas and presents a variety of symptoms, namely, depressed mood, anhedonia, anxiety, and cognitive impairments, leading to severe disability and impaired quality of life in patients.

Neuroinflammation is considered to be an important pathological cause of depression. It is related to the cytokine hypothesis; patients with major depression have been found to display enhancive inflammatory biomarkers, including

inflammatory cytokines. And activation of the inflammatory pathway in the brain reduces neurotrophic support and altered glutamate release/reuptake, as well as oxidative stress, leading to excitotoxicity, consistent with neuropathological findings of depression characteristics [27]. The proinflammatory cytokines can cause sickness behavior and cellular damage [28, 29]. An increase of inflammation can lead to negative emotion, which was also supported by studies that induced inflammation through the injection of LPS. Stimulated increases in proinflammatory cytokines such IL-1β, IL-6, and TNF-α were associated with depressive symptoms, and proinflammatory cytokines have been recently shown to interact with the brain, affecting neurotransmission, neuroendocrine activity, and brain structure and function, thereby changing emotion, cognition, and behavior. One of the molecular mechanisms that can contact the inflammation with emotional cognition is the proinflammatory cytokine effect on the serotonergic system. Proinflammatory cytokines activate IDO, an enzyme involved in the synthesis of kynurenine from tryptophan. Central and peripheral activation of IDO causes increased catabolism of tryptophan, leading to 5-HT deficiency and neurotoxic metabolite production. Depressive-like behaviors are associated with the reduced synthesis of 5-HT and the production of neurotoxic metabolites in the limbic-cortical-striatal-pallidal-thalamic (LCSPT) circuit [30]. Our study revealed the hippocampal neuron contents of IL-6. TNF-α and IDO in the LPS group were significantly higher than those in the control group. And the levels of 5-HT in the LPS group were significantly less than those in the control group. Xiaoyao Pills and FLX inhibited the increase of IL-6, TNF-α, and IDO levels in hippocampal neurons induced by LPS and the decrease of 5-HT levels in hippocampal neurons, showing a protective effect on the damage of model cells.

Additionally, there is abundant evidence that depressed patients are associated with the reduction of hippocampal volume, neuronal atrophy, and neuronal loss. The cause may be the lack of neurotrophic factors [31, 32]. LPS can induce neuronal death, decrease neurogenesis, and impair synaptic plasticity and memory. Studies have shown that LPS influenced neurotrophin levels in the brain; the neuroprotection mediated by neurotrophins is compromised by systemic immune activation induced by LPS [33]. BDNF belongs to the family of nerve growth factors and plays an important role in neuronal development, including growth, differentiation, and survival. Preclinical studies have shown that exposure to stress causes hippocampal atrophy and cell loss, as well as decreased neurotrophic/growth factor expression. Therefore, it supports the neurotrophic/neurogenic hypothesis of depression and antidepressant effects [34]. BDNF exerts its neurotrophic effects by activating the TrkB [35]; the phosphorylation of TrkB can activate the transcription factor CREB's gene expression and then play an antidepressant effect [36], promote neuronal survival [37], and strengthen synaptic plasticity [38]. BDNF is abundantly expressed in the brain and plays a role in maintaining the structure of adult brain cells [39]. And in rodents, direct infusion of BDNF in the hippocampus showed antidepressant-like effects by increased levels of TrkB, ERK, CREB, and phosphorylated ERK [40]. NGF is a growth factor first described as a neurite outgrowth factor [41]. And it was involved in the survival of neurons and the proliferation of neural stem cells in rats [42]. BDNF and NGF have also been shown to represent an important factor in the regulation of neurogenesis and synaptic plasticity [43]. In this study, we observed that the expression levels of NGF, BDNF, TrkA, TrkB, CREB, p-CREB, and p-CREB/CREB in hippocampal neurons of the LPS group were significantly decreased, while Xiaoyao Pills could improve the expression levels of the above indicators. The results suggest that the antidepressant effect of Xiaoyao Pills may be related to activating the NGF/BDNF-TrkA/TrkB-CREB pathway.

The BDNF signaling pathway regulates synaptic plasticity in the hippocampus, and BDNF infusion of rat hippocampus induces LTP and triggers synaptic enhancement [44]. As demonstrated by previous studies, BDNF plays a critical role in the action of antidepressants through neuronal plasticity. Synaptic plasticity represents one of the most important functions of the brain, including the ability to collect, evaluate, and store information. This function is associated with depression, including loss of neurotrophic factor support and elevation of inflammatory cytokine. Synaptophysin is now widely accepted as scaffold proteins, which are involved in the regulation of synaptic function. In our present study, LPS induces a decrease in synaptic protein expression in hippocampal neurons that the treatment of Xiaoyao Pills significantly ameliorated synaptic protein reduction.

Neurogenesis has been widely described as a key function of the hippocampus. The reduction of neurogenesis increases innate anxiety-like and approach-avoidance behavior [45]. Most animal studies have found that hippocampal neurogenesis could be achieved by directly targeting the HPA axis and related neuropeptides, thereby regulating depressive-like behaviors by promoting neurogenesis [46]. Increasing adult hippocampal neurogenesis is sufficient to reduce anxiety and depression-like behaviors [47]. In clinical research, patients with depression also exhibit decreased levels of neurogenesis [48]. Therefore, increased neurogenesis may be a potential therapeutic strategy for treating depression. To elucidate whether the impairment of hippocampal neurogenesis was related to depression, we quantified BrdU-positive cell numbers in hippocampal neuron cells and observed that infection of LPS significantly decreased survival of newborn cells and immature neurons which were consistent with previous reports. The serum of Xiaoyao Pills has a protective effect on LPS-induced damage of newborn cells and immature neurons.

Our previous studies have shown that Xiaoyao Pills administered intragastrically could reduce the levels of cytokines and mediators related to inflammation, enhance the expression of neurotrophic factors and synaptic proteins, and improve nerve injury, so as to exert the inhibitory effect on behavioral abnormalities in depression-like model rats induced by lipopolysaccharide [26]. In this study, the primary hippocampal neurons of rats were used as the experimental carrier, and the Xiaoyao Pill-containing serum of rats was used as the observation subject to further study the

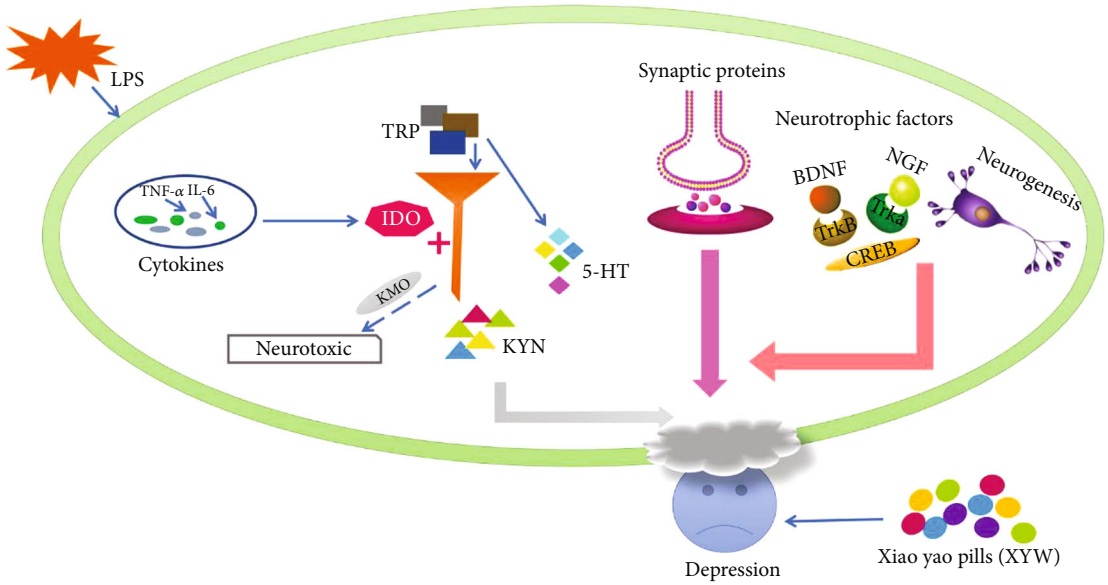

Figure 7: Graphical abstract. Xiaoyao Pills (XYW) ameliorated the depression-like behavior, decreased the levels of inflammatory indicators, increased those of neurotrophic factors and synaptic proteins, and increased hippocampal neurogenesis.

effect of Xiaoyao Pills on the inflammatory response of hippocampal neurons *in vitro*.

In this study, the serum concentrations of Xiaoyao Pills selected were 4% and 8%, and the above concentrations did not affect the cell activity and had some pharmacological effects. In the experiment, there was no significant dose-response relationship between the two concentrations, which may be related to the complexity of Chinese herbal compound components or the interaction between components [49], which needs to be further explored in combination with the research work of serum drug chemistry. In addition, traditional Chinese medicine compounds are suitable for individualized treatment plans for different body conditions, and the therapeutic effects are not judged by dosage [50, 51]. However, the efficacy of the two concentrations of the serum containing Xiaoyao Pills was similar, at least suggesting that Xiaoyao Pills may alleviate depressive symptoms by suppressing the inflammatory response or activating the NGF/BDNF-TRKA/TrkB-CREB pathway after entry into the body.

In conclusion, this study showed that LPS could increase the level of proinflammatory cytokines in neuronal cells, thereby increasing the IDO level, promoting tryptophan metabolism to kynurenine resulting in a reduction in 5-HT levels. In addition, LPS could induce the decrease of synaptic protein level in neuron cells, as well as block BDNF and NGF pathways, then inhibit the hippocampal neurogenesis. All the above pathological mechanisms are closely related to the occurrence of depression [52–54] (Figure 7). Pretreatment with Xiaoyao Pills significantly reduced the level of cytokines and mediators related to inflammation, increased the expression of neurotrophic factors and synaptic proteins, and alleviated nerve injury. These findings suggest that Xiaoyao Pills could play a neuroprotective role by inhibiting the neuroinflammatory response, promote the recovery of injured nerves, and thus reduce the symptoms of depression (Figure 7), providing possible treatment basis for its clinical application for depression.

Abbreviations

XYW: Xiaoyao Pills
FLX: Fluoxetine hydrochloride
LPS: Lipopolysaccharide
IL-6: Interleukin 6
TNF-α: Tumour necrosis factor alpha
IDO: Indoleamine 2,3-dioxygenase
5-HT: 5-Hydroxytryptamine
BDNF: Brain-derived neurotrophic factor
NGF: Nerve growth factor
TrkB: Tropomyosin receptor kinase B
TrkA: Tropomyosin receptor kinase A
CREB: cAMP response element-binding protein
PSD95: Postsynaptic density protein 95
SYP: Synaptophysin
BrdU: 5-Bromo-2-deoxyUridine
NeuN: Vertebrate neuron-specific nuclear protein.

Data Availability

The datasets generated and/or analysed during the current study are available from the corresponding author on reasonable request.

Ethical Approval

All procedures were approved by the Animal Ethics Committee, Chengdu University of TCM, China (2016-11), and complied with the National Institutes of Health Guidelines for the Care and Use of Laboratory Animals.

Conflicts of Interest

The authors declare no conflicts of interest.

Authors' Contributions

YF, BYS, XBL, JL, ZLR, RL, and NZ conceived and designed the experiments; YF, BYS, XBL, JL, ZLR, and RL performed the experiments; YF, BYS, XBL, JL, ZLR, RL, and NZ analysed the data and drafted relevant text; YF and BYS wrote the manuscript. All authors have read and approved the final version of this manuscript. Yang Fang and Boyu Shi contributed equally to this work. Yang Fang and Boyu Shi are co-first author.

Acknowledgments

This study was financed by the National Nature Science Foundation of China (81503277, 81473399), the Education Department of Sichuan (16ZB0116), and Chengdu University of Traditional Chinese Medicine (ZRQN1643).

References

[1] M. J. Knight and B. T. Baune, "Cognitive dysfunction in major depressive disorder," *Current Opinion in Psychiatry*, vol. 31, no. 1, pp. 26–31, 2018.

[2] D. S. Charney and H. K. Manji, "Life stress, genes, and depression: multiple pathways lead to increased risk and new opportunities for intervention," *Science's STKE:signal transduction knowledge environment*, vol. 2004, no. 225, p. re5, 2004.

[3] M. Li, E. Kouzmina, M. McCusker et al., "Pro- and anti-inflammatory cytokine associations with major depression in cancer patients," *Psycho-Oncology*, vol. 26, no. 12, pp. 2149–2156, 2017.

[4] A. Dey and P. A. Hankey Giblin, "Insights into macrophage heterogeneity and cytokine-induced neuroinflammation in major depressive disorder," *Pharmaceuticals*, vol. 11, no. 3, p. 64, 2018.

[5] S. L. Deng, J. G. Chen, and F. Wang, "Microglia: a central player in depression," *Current medical science*, vol. 40, no. 3, pp. 391–400, 2020.

[6] J. D. Crapser, E. E. Spangenberg, R. A. Barahona, M. A. Arreola, L. A. Hohsfield, and K. N. Green, "Microglia facilitate loss of perineuronal nets in the Alzheimer's disease brain," *eBioMedicine*, vol. 58, p. 102919, 2020.

[7] Y. Xia, Z. Zhang, W. Lin et al., "Modulating microglia activation prevents maternal immune activation induced schizophrenia-relevant behavior phenotypes via arginase 1 in the dentate gyrus," *Neuropsychopharmacology*, 2020.

[8] S. W. Jeon and Y. K. Kim, "The role of neuroinflammation and neurovascular dysfunction in major depressive disorder," *Journal of inflammation research*, vol. Volume 11, pp. 179–192, 2018.

[9] X. Wang, H. Wu, and A. H. Miller, "Interleukin 1alpha (IL-1alpha) induced activation of p38 mitogen-activated protein kinase inhibits glucocorticoid receptor function," *Molecular Psychiatry*, vol. 9, no. 1, pp. 65–75, 2004.

[10] Z. Shi, H. Ren, Z. Huang et al., "Fish oil prevents lipopolysaccharide-induced depressive-like behavior by inhibiting neuroinflammation," *Molecular Neurobiology*, vol. 54, no. 9, pp. 7327–7334, 2017.

[11] W. Jing, S. Song, H. Sun et al., "Mahuang-Fuzi-XixinDecoction reverses depression-like behavior in LPS-induced mice by regulating NLRP3 inflammasome and neurogenesis," *Neural plasticity*, vol. 2019, Article ID 1571392, 13 pages, 2019.

[12] J. Cole, S. G. Costafreda, P. McGuffin, and C. H. Y. Fu, "Hippocampal atrophy in first episode depression: a meta-analysis of magnetic resonance imaging studies," *Journal of affective disorders*, vol. 134, no. 1-3, pp. 483–487, 2011.

[13] C. De Lucia, A. Rinchon, A. Olmos-Alonso et al., "Microglia regulate hippocampal neurogenesis during chronic neurodegeneration," *Brain, behavior, and immunity*, vol. 55, pp. 179–190, 2016.

[14] A. Sierra, S. Beccari, I. Diaz-Aparicio, J. M. Encinas, S. Comeau, and M. È. Tremblay, "Surveillance, phagocytosis, and inflammation: how never-resting microglia influence adult hippocampal neurogenesis," *Neural Plasticity*, vol. 2014, 15 pages, 2014.

[15] H. Son, M. Banasr, M. Choi et al., "Neuritin produces antidepressant actions and blocks the neuronal and behavioral deficits caused by chronic stress," *Proceedings of the National Academy of Sciences of the United States of America*, vol. 109, no. 28, pp. 11378–11383, 2012.

[16] National Pharmacopoeia Committee, *Pharmacopoeia of People's Republic of China*, Part 1, China Medical Science and Technology Press, 2015.

[17] S. Cui, F. Liang, R. Zhang, and W. Huang, "Research progress on the material basis of the efficacy of traditional Chinese medicine based on serum pharmacology and serum chemistry of traditional Chinese medicine," *Health vocational education*, vol. 38, no. 1, pp. 157–159, 2020.

[18] Q. Yin, C. Chen, J. Tian et al., "Based on UPLC-QE-Orbitrap-MS technology, the chemical analysis of Bupleurum chinense and Paeonia lactiflora on serum," *Chinese Journal of Pharmacy*, vol. 54, no. 12, pp. 2296–2302, 2019.

[19] Y. Wang, Y. Liang, L. Chen, and J. Yang, "Serum medicinal chemistry research of angelica active ingredients," *Modern Chinese medicine research and practice*, no. S1, pp. 75–79, 2004.

[20] C. Shen, C. Xie, P. Liao et al., "Preliminary study on the serum medicinal chemistry of Poria cocos ethanol extract," *Journal of Wuhan University*, vol. 33, no. 4, pp. 479–482, 2012.

[21] Y. Zhang, M. Han, Z. Liu, J. Wang, Q. He, and J. Liu, "Chinese herbal formula xiao yao san for treatment of depression: a systematic review of randomized controlled trials," *Evidence-based complementary and alternative medicine : eCAM*, vol. 2012, article 931636, 13 pages, 2012.

[22] J. Wang, X. Li, S. He et al., "Regulation of the kynurenine metabolism pathway by Xiaoyao san and the underlying effect in the hippocampus of the depressed rat," *Journal of Ethnopharmacology*, vol. 214, pp. 13–21, 2018.

[23] L. Gao, P. Huang, Z. Dong et al., "Modified Xiaoyaosan (MXYS) exerts anti-depressive effects by rectifying the brain blood oxygen level-dependent fMRI signals and improving hippocampal neurogenesis in mice," *Frontiers in pharmacology*, vol. 9, p. 1098, 2018.

[24] H. G. Du, L. Ming, S. J. Chen, and C. D. Li, "Xiaoyao pill for treatment of functional dyspepsia in perimenopausal women with depression," *World journal of Gastroenterology*, vol. 20, no. 44, pp. 16739–16744, 2014.

[25] C. Man, C. Li, D. Gong, J. Xu, and Y. Fan, "Meta-analysis of Chinese herbal Xiaoyao formula as an adjuvant treatment in

relieving depression in Chinese patients," *Complementary Therapies in Medicine*, vol. 22, no. 2, pp. 362–370, 2014.

[26] B. Shi, J. Luo, Y. Fang et al., "Xiaoyao pills prevent lipopolysaccharide-induced depression by inhibiting inflammation and protecting nerves," *Frontiers in pharmacology*, vol. 10, p. 1324, 2019.

[27] A. H. Miller, V. Maletic, and C. L. Raison, "Inflammation and its discontents: the role of cytokines in the pathophysiology of major depression," *Biological Psychiatry*, vol. 65, no. 9, pp. 732–741, 2009.

[28] R. Dantzer and K. W. Kelley, "Twenty years of research on cytokine-induced sickness behavior," *Brain, behavior, and immunity*, vol. 21, no. 2, pp. 153–160, 2007.

[29] B. Zhang, P. P. Wang, K. L. Hu et al., "Antidepressant-like effect and mechanism of action of honokiol on the mouse lipopolysaccharide (LPS) depression model," *Molecules*, vol. 24, no. 11, p. 2035, 2019.

[30] L. Terroni, E. Amaro Jr., D. V. Iosifescu et al., "Stroke lesion in cortical neural circuits and post-stroke incidence of major depressive episode: a 4-month prospective study," *The world journal of biological psychiatry : the official journal of the World Federation of Societies of Biological Psychiatry*, vol. 12, no. 7, pp. 539–548, 2011.

[31] F. Duclot and M. Kabbaj, "Epigenetic mechanisms underlying the role of brain-derived neurotrophic factor in depression and response to antidepressants," *The Journal of experimental biology*, vol. 218, no. 1, pp. 21–31, 2015.

[32] T. de Azevedo Cardoso, T. C. Mondin, C. D. Wiener et al., "Neurotrophic factors, clinical features and gender differences in depression," *Neurochemical Research*, vol. 39, no. 8, pp. 1571–1578, 2014.

[33] Z. Guan and J. Fang, "Peripheral immune activation by lipopolysaccharide decreases neurotrophins in the cortex and hippocampus in rats," *Brain, behavior, and immunity*, vol. 20, no. 1, pp. 64–71, 2006.

[34] H. D. Schmidt and R. S. Duman, "The role of neurotrophic factors in adult hippocampal neurogenesis, antidepressant treatments and animal models of depressive-like behavior," *Behavioural Pharmacology*, vol. 18, no. 5-6, pp. 391–418, 2007.

[35] M. V. Chao and B. L. Hempstead, "p75 and Trk: a two-receptor system," *Trends in neurosciences*, vol. 18, no. 7, pp. 321–326, 1995.

[36] D. Liu, Z. Wang, Z. Gao et al., "Effects of curcumin on learning and memory deficits, BDNF, and ERK protein expression in rats exposed to chronic unpredictable stress," *Behavioural brain research*, vol. 271, pp. 116–121, 2014.

[37] Y. H. Chen, R. G. Zhang, F. Xue et al., "Quetiapine and repetitive transcranial magnetic stimulation ameliorate depression-like behaviors and up-regulate the proliferation of hippocampal-derived neural stem cells in a rat model of depression: the involvement of the BDNF/ERK signal pathway," *Pharmacology, biochemistry, and behavior*, vol. 136, pp. 39–46, 2015.

[38] M. Arango-Lievano, W. M. Lambert, K. G. Bath, M. J. Garabedian, M. V. Chao, and F. Jeanneteau, "Neurotrophic-priming of glucocorticoid receptor signaling is essential for neuronal plasticity to stress and antidepressant treatment," *Proceedings of the National Academy of Sciences of the United States of America*, vol. 112, no. 51, pp. 15737–15742, 2015.

[39] M. J. F. Levy, F. Boulle, H. W. Steinbusch, D. L. A. van den Hove, G. Kenis, and L. Lanfumey, "Neurotrophic factors and neuroplasticity pathways in the pathophysiology and treatment of depression," *Psychopharmacology*, vol. 235, no. 8, pp. 2195–2220, 2018.

[40] R. W. Sirianni, P. Olausson, A. S. Chiu, J. R. Taylor, and W. M. Saltzman, "The behavioral and biochemical effects of BDNF containing polymers implanted in the hippocampus of rats," *Brain Research*, vol. 1321, pp. 40–50, 2010.

[41] L. Olson, "Outgrowth of sympathetic adrenergic neurons in mice treated with a nerve-growth factor (NGF)," *Zeitschrift fur Zellforschung und mikroskopischeAnatomie*, vol. 81, no. 2, pp. 155–173, 1967.

[42] S. Cheng, M. Ma, Y. Ma, Z. Wang, G. Xu, and X. Liu, "Combination therapy with intranasal NGF and electroacupuncture enhanced cell proliferation and survival in rats after stroke," *Neurological Research*, vol. 31, no. 7, pp. 753–758, 2009.

[43] B. Lu, G. Nagappan, and Y. Lu, "BDNF and synaptic plasticity, cognitive function, and dysfunction," *Handbook of experimental pharmacology*, vol. 220, pp. 223–250, 2014.

[44] C. R. Bramham, "Control of synaptic consolidation in the dentate gyrus: mechanisms, functions, and therapeutic implications," *Progress in brain research*, vol. 163, pp. 453–471, 2007.

[45] J. M. Revest, D. Dupret, M. Koehl et al., "Adult hippocampal neurogenesis is involved in anxiety-related behaviors," *Molecular Psychiatry*, vol. 14, no. 10, pp. 959–967, 2009.

[46] A. Surget, M. Saxe, S. Leman et al., "Drug-dependent requirement of hippocampal neurogenesis in a model of depression and of antidepressant reversal," *Biological Psychiatry*, vol. 64, no. 4, pp. 293–301, 2008.

[47] A. S. Hill, A. Sahay, and R. Hen, "Increasing adult hippocampal neurogenesis is sufficient to reduce anxiety and depression-like behaviors," *Neuropsychopharmacology*, vol. 40, no. 10, pp. 2368–2378, 2015.

[48] V. A. Vaidya, K. Fernandes, and S. Jha, "Regulation of adult hippocampal neurogenesis: relevance to depression," *Expert review of neurotherapeutics*, vol. 7, no. 7, pp. 853–864, 2014.

[49] S. Q. Cai, X. Wang, M. Y. Shang, F. Xu, and G. X. Liu, ""Efficacy theory" may help to explain characteristic advantages of traditional Chinese medicines," *Zhongguo Zhong Yao Za Zhi*, vol. 40, no. 17, pp. 3435–3443, 2015.

[50] X. Ma, M. Ding, X. Shi, J. Shao, X. Li, and Z. Jin, "Modern data research on the treatment of depression with compound Chinese medicines," *World Science and Technology-Modernization of Traditional Chinese Medicine*, vol. 21, no. 7, pp. 1418–1423, 2019.

[51] H. Wang, S. Wu, and F. Geng, "Exploring the essence of "syndrome" in traditional Chinese medicine," *Journal of Chinese Medicine*, vol. 35, no. 8, pp. 1643–1645, 2020.

[52] X. Shao and G. Zhu, "Associations among monoamine neurotransmitter pathways, personality traits, and major depressive disorder," *Frontiers in Psychiatry*, vol. 11, 2020.

[53] E. Beurel, M. Toups, and C. B. Nemeroff, "The bidirectional relationship of depression and inflammation: double trouble," *Neuron*, vol. 107, no. 2, pp. 234–256, 2020.

[54] C. Li, J. Huang, Y. C. Cheng, and Y. W. Zhang, "Traditional Chinese medicine in depression treatment: from molecules to systems," *Frontiers in Pharmacology*, vol. 11, p. 586, 2020.

Hindawi
Neural Plasticity
Volume 2020, Article ID 8830670, 8 pages
https://doi.org/10.1155/2020/8830670

Research Article

In Vivo Structural and Functional Abnormalities of the Striatums Is Related to Decreased Astrocytic BDNF in *Itpr2*$^{-/-}$ Mice Exhibiting Depressive-Like Behavior

Shanmei Zeng,[1] **Kai Liu**,[1] **Jingyu Zhang**,[1] **Chunhui Chen**,[2] **Yihua Xu**,[2] **Yulan Wu**,[1] **Yanjia Deng**,[1] **Xuegang Sun**,[2] **Ge Wen**,[1] **and Linlin Jing**[3]

[1]*NanFang Hospital, Southern Medical University, Guangzhou, China*
[2]*The Second Affiliated Hospital of Guangzhou University of Chinese Medicine, Guangzhou, China*
[3]*Integrated Hospital of Traditional Chinese Medicine, Southern Medical University, Guangzhou, China*

Correspondence should be addressed to Linlin Jing; jll47379@163.com

Received 30 April 2020; Revised 7 July 2020; Accepted 17 August 2020; Published 1 September 2020

Academic Editor: Fushun Wang

Background. Previous researches indicate that *Itpr2*$^{-/-}$ mice (inositol 1,4,5-trisphosphate receptor type 2 knockout mice) show depressive-like symptoms; however, little is known regarding the *in vivo* neurobiological effect of Itpr2 as well as the specific pattern of brain abnormalities in *Itpr2*$^{-/-}$ mice. *Methods*/*Materials*. First, behavioral tests, structural magnetic resonance imaging (MRI), and resting-state functional MRI were performed on *Itpr2*$^{-/-}$ mice and matched healthy controls. Voxel-based morphometry and seed-based voxel-wise functional connectivity (FC) were, respectively, calculated to assess the gray matter volume and the functional activities of the brain in vivo. Second, the sample of relevant changed brain regions was extracted to detect the expression of BDNF. Finally, to further validate the relationship between Itpr2 deficiency and the observed brain abnormalities, we performed Western blotting to detect the expression of pro-BDNF and mBDNF in *Itpr2*$^{-/-}$ C8-D1A (a type of astrocyte). *Results*. Compared with controls, *Itpr2*$^{-/-}$ mice showed depressive-like behaviors as well as significantly lower gray matter volume in striatums mainly, periaqueductal GM, and the right frontoparietal cortices as well as lower striatal-hippocampal and striatal-right parietal cortex (mainly for the primary and secondary somatosensory cortex) FC. Moreover, decreased expression of mBDNF was found in both sample tissues of the striatum in *Itpr2*$^{-/-}$ mice and *Itpr2*$^{-/-}$ C8-D1A. *Conclusion*. By combining biochemistry and MR analyses, this study provides evidences to support that the Itpr2-related neuropathological effect is possibly mediated by the striatal abnormality associated with dysfunctional astrocytes in *Itpr2*$^{-/-}$ mice *in vivo*, thus may help us better understand underlying mechanisms of Itpr2 deficiency as well as its relation to depressive-like behavior.

1. Introduction

Inositol 1,4,5-trisphosphate receptor type 2 (IP_3R_2) is a calcium channel receptor located in the endoplasmic reticulum, which is mainly expressed in astrocytes other than other types of cell in the brain [1]. It is considered to be necessary to maintain the normal function in astrocytes especially the exocytosis by which BDNF and ATP are released to extracellular matrix [2]. In fact, a series of neuropsychological abnormal states have been found in *Itpr2*$^{-/-}$ mice [3, 4]. Notably, previous studies have found that *Itpr2*$^{-/-}$ mice exhibited depression-like behaviors which are considered to be attributed to deficiencies in astrocytic ATP release [5].

There are a lot of research that indicates structural brain abnormalities in major depressive disorder (MDD) [6, 7], while the mechanisms of these abnormalities remain unclear. *In vivo* magnetic resonance imaging (MRI) studies have exhibited that particular areas involved in emotional regulation, such as the hippocampus, amygdala, cingulate cortex, basal ganglia, and prefrontal cortex (PFC) may go through structural changes in MDD patients [8, 9]. Functional magnetic resonance imaging (fMRI) is one of the most important

tools for studying the *in vivo* brain activity and anatomy [10], and functional connectivity is one of the most common analysis ways of fMRI [11, 12]. Both the structural and functional abnormalities in depression have been found in a series of brain regions.

Astrocytes can release a variety of neurotrophins under normal conditions [13]. Previous studies indicate that the reduction of neurotrophins, especially brain-derived neurotrophic factor (BDNF), which are the most widely distributed neurotrophin in the CNS and provided by astrocytes mainly in the brain, is a mediator involved in neuronal survival and plasticity of dopaminergic, cholinergic, and serotonergic neurons[14]. BDNF are involved in the pathogenesis of depression, with decreased growth and survival of neurons, and thus possibly leads to gray matter atrophy shown on magnetic resonance imaging [15–17]. BDNF is synthesized as a precursor called proBDNF, which is proteolytically cleaved to generate mature BDNF [18]. Many previous studies have demonstrated stress could decrease the expression of brain-derived neurotrophic factor (BDNF) in limbic structures including the amygdala, hippocampus, and prefrontal cortex. Furthermore, the reduction of BDNF could contribute to the atrophy of certain limbic structures [19], and the stress-induced reduction in BDNF may result in brain tissue loss [10].

To date, little is known about the *in vivo* neurobiological effect of Itpr2 as well as the specific pattern of brain abnormalities in *Itpr2*$^{-/-}$ mice. Based on existing findings, we hypothesize that *Itpr2*$^{-/-}$ mice have the tendency of depressive-like behavior and can be observed with specific structural and functional abnormalities in the brain *in vivo*, which are possibly associated with decreased BDNF levels produced by astrocytes owing to the effect of Itpr2 deficiency. To this end, we combined animal magnetic resonance imaging techniques and biochemical experimental methods to test the hypothesis in this study.

2. Materials and Methods

2.1. Mice. *Itpr2*$^{-/-}$ mice were generated by crossing germline-heterozygous-null mutant *Itpr2*$^{+/-}$ mice, which was a gift by Prof. Tian-Ming Gao [5]. The offspring were genotyped by PCR using mouse tail DNA and wild-type (5′-GCTGTG CCCAAAATCCTAGCACTG-3′; 3′-CATGCAGAGGTCG TGTCAGTCATT-5′) and mutant allele-specific primers (neospecific primer 5′-AGTGATACAGGGCAAGTTCATA C-3′; 3′-AATGGGCTGACCGCTTCCTCGT-5′). The PCR products were visualized with ethidium bromide staining.

2.2. Cell. C8-D1A (astrocytic type I clone, GFAP positive) was cloned from mice cerebellum [20]. Cells were maintained in Dulbecco's modified Eagle medium (DMEM; Biochrome, Berlin, Germany) containing glucose, 10% heat-inactivated fetal calf serum (FCS; Sigma, St. Louis, MO), and 1% L-glutamine (Gibco, Auckland, New Zealand). *Itpr2*$^{-/-}$ C8-D1A was constructed by lentivirus transfection knocking down protein expression of IP_3R_2, and the target sequence was GCCCAGAAGCAATACTGGAAA.

2.3. Behavioral Test

2.3.1. Sucrose Consumption Test. Sucrose Consumption Test was conducted on *Itpr2*$^{-/-}$ mice ($n = 28$) and healthy controls ($n = 20$). Two bottles were placed in each cage simultaneously, both of which contained 1% sucrose water 25 ml, and the mice could drink freely for 24 h. Then, one bottle contained 1% sucrose water 25 ml with the other one containing 25 ml of tap water. Mice were given free choice for 24 h. After that, the test was conducted by providing the mice with a free choice between the two bottles (one bottle containing a 1% sucrose solution and the other bottle containing tap water) for 2 h. The consumption of sugar water and tap water was calculated simultaneously in both groups by weighing the bottles containing the liquids. The preference for sucrose was calculated according to the percentage of consumed sucrose solution with respect to the total amount of liquid consumed.

2.3.2. Tail Suspension Test (TST). TST was implemented on *Itpr2*$^{-/-}$ mice ($n = 28$) and healthy controls ($n = 20$). This experiment referred to the experimental model established by Steru et al. [21]. Briefly, the mice were acoustically and visually isolated and suspended 60 cm above the floor in an inverted position by sticking a medical adhesive cloth on roughly 2 cm of the tail of the mouse about 2 cm. The time during which the mice remained immobile was determined during a test period of 6 min. Mice were considered immobile only when the mice gave up any struggle and remained motionless.

2.3.3. Forced Swim Test (FST). FST was implemented on *Itpr2*$^{-/-}$ mice ($n = 28$) and healthy controls ($n = 20$). This test was carried out according to the method described by Porsolt et al. [22]. Each mouse was placed in a cylindrical container (diameter, 10 cm; height, 25 cm) filled with water up to 9 cm at $22 \pm 1^{\circ}$C. The immobility time was recorded during the last 4 min of the 6-min testing period. Immobility time was defined as the absence of struggle and only slight body movements keep its head afloat.

2.3.4. Open-Field Test (OFT). The OFT experiment was carried out on 16 control mice and 28 *Itpr2*$^{-/-}$ mice. The voluntary movement and behaviors of the mice were evaluated using the OFT. The OFT box is a square box with the following dimensions: height, 35 cm; length, 60 cm; and width, 60 cm, which is divided into 4 quadrants; each quadrant is divided into 36 equilateral quadrants. The experiment was conducted in a quiet laboratory room under 60 watts of light. Each mouse was gently placed at the center of the square box and observed at 5 min intervals. The apparatus used was wiped with 75% ethanol and dried before each mouse was tested. Motion detection software (EthoVision 7.0; Noldus, Wageningen, The Netherlands) was used to record the center time (CTRTIME) for each mouse.

2.4. Magnetic Resonance Scanning. All MRI scans were performed on 14 control mice and 15 *Itpr2*$^{-/-}$ mice using a 7T Bruker scanner (Pharmascan 70/16 US) equipped with a 86 mm birdcage transmit-only RF coil and a receive-only quadrature surface coil. Before scanning, the mice were

anesthetized with 3% isoflurane and then mechanically ventilated with 1-1.5% isoflurane. During the examination, the mice were placed on a plastic cradle with the head fixed with a tooth bar and plastic screws in the ear canals. A water circulation system was used to maintain the body temperature of the animals. The level of anesthesia was monitored, and the respiratory rate was kept above 60 breaths per min. For the structural MRI, a 3D T2-weighted images (3D-T2WI) were scanned using a Turbo RARE sequence with the following parameters: TR/TE = 1800/45, flip angle = 90°, matrix = 256 × 256, voxel size = 0.078 × 0.078 × 0.512 mm, 32 slices, and slice thickness/gap = 0.512/0 mm. For the resting-state fMRI, a spin-echo echo-planar imaging (SE-EPI) sequence was used with 500 time points, TR/TE = 1500/21.2 ms, flip angle = 90°, matrix = 96 × 96, voxel size = 0.156 × 0.156 × 0.7 mm, 15 slices, and slice thickness/gap = 0.7/0 mm.

2.5. MRI Preprocessing and Analysis. Prior to preprocessing, all the structural and functional MRIs were resized by a factor of 10. The 3D T2-WI images of all the mice were processed using the SPM12 software (Wellcome Department of Cognitive Neurobiology, University College of London, UK) for VBM analysis. First, the images were linearly registered (12-parameter affine) to approximate the brain space of C57Bl6, which is a previously established template specific for the brain anatomy of C57 mice [23]. Thereafter, the structural images were segmented into GM, white matter, and cerebrospinal fluid images based on the tissue probability maps provided with the C57Bl6 template. Then, based on the segmentation results, the GM images were spatially normalized to the template, and then Jacobian modulated. Finally, the resultant GM images were smoothed using an 8 mm FWHM Gaussian kernel.

For the analysis of rs-fMRI, the first 10 volumes of resting-state scans were discarded. The resulting 490 volumes were corrected for slice timing and for the head motion (a least-squares approach and a six-parameter spatial transformation). Then, the brain fMRIs were spatially normalized to the template in accordance with the transformation established by the normalization of 3D T2-WI images, with the voxel size resampled into $4 \times 4 \times 4\,\text{mm}^3$. Thereafter, an 8 mm FWHM Gaussian kernel was used to smooth the fMRIs, and voxel-wise detrending, filtering with a bandpass filter of 0.01-0.08 Hz, and regression of the white matter signal, cerebrospinal fluid signal, mean global signal, and head motion (Friston 24) was done successively.

Calculation of the seed-based FC maps was done as follows. First, the seed region of interest (ROI) was selected by referring to the VBM results as well as the previously established atlas of the mouse brain [24]. Second, the whole-brain resting-state FC map was created by calculating the Pearson correlation coefficient between the resting-state time series extracted from the seed ROI and the time series from all other brain voxels. Here, a Fisher Z-transformation was done to increase the normality of FC data, and the calculation was restricted to positive correlation.

2.6. Immunofluorescence Staining of Mouse Brain Tissues. Mouse brains were first fixed with 4% PFA at 4°C for 24 hours, and the brains were later cryoprotected in 15% and 20% sucrose in PBS for 24 hours at 4°C. Coronal sections (40 μm) were cut in a crystal. Sections were blocked with goat serum containing Triton X-100 for 2 h at room temperature and then incubated with rabbit BDNF antibodies (1:500 dilution; Abcam; ab108319) overnight at 4°C. Sections were washed and later incubated with a 1:500 dilution of Alexa 488-conjugated goat antirabbit antibodies for 1 h at room temperature.

2.7. Western Blot. The separated striatum and cells were homogenized in RIPA lysis buffer with Protease Inhibitor Cocktail at 4°C and quantified using the BCA protein assay kit (Beyotime Biotechnology). Sixty micrograms of protein was separated via sodium dodecyl sulfate polyacrylamide gel electrophoresis and was transferred to PVDF membranes (Millipore). Immunolabeling was performed using rabbit BDNF antibodies (1:1000 dilution; Abcam; ab108319), mouse IP_3R_2 antibodies (1:1000 dilution; Santacruz; sc398434), mouse monoclonal actin antibodies (1:400 dilution; BOSTER; BM0627), and rabbit monoclonal tubulin antibodies (1:1000 dilution; BOSTER; BM3885). The results were visualized by enhanced chemiluminescence (GE Healthcare Bio-Science, Uppsala, Sweden). Images were captured and documented with a charge-coupled device system (Image Station 2000MM; Kodak, Rochester, NY, USA). Quantitative analysis of the images was performed using Molecular Imaging Software (version 4.0, as part of the Kodak 2000MM System).

2.8. Statistical Analysis. The data were analyzed using the SPSS statistical software package (version 17.0; IBM Corp., Armonk, NY, USA). Mean values were compared using unpaired t-test; Welch's correction is used when variance is unequal. P values <0.05 were considered statistically significant. The voxel-wise statistical comparisons of the GM images and FC maps were done using SPM12. A two-sample t-test was adopted for the between-group comparisons with a significance threshold of $P < 0.01$ (with AlphaSim correction of $P = 0.05$).

3. Results

3.1. Itpr2$^{-/-}$ Mice Exhibit Depressive-Like Behaviors. We firstly tested whether *Itpr2*$^{-/-}$ mice exhibited depressive-like behaviors by performing behavioral tests on both the *Itpr2*$^{-/-}$ mice and controls. Results revealed that the *Itpr2*$^{-/-}$ mice exhibited less sucrose consumption ($P = 0.017$, $P < 0.05$, $t = 2.920$, df = 9, $F = 1.817$) (Figure 1(a)) and increased duration of immobility both in tail suspension test ($P = 0.0385$, $P < 0.05$, $t = 2.381$, df = 10, $F = 1.943$) (Figure 1(b)) and forced swim test ($P < 0.0001$, $t = 7.652$, df = 10, $F = 1.900$) (Figure 1(c)) compared with controls. In the open-field test, we firstly analyzed the movement speed of the two groups of mice to rule out the effect of locomotor ability on behavior performance, and there was no significant difference between the two groups (Supplementary materials Figure 1). Although there was a decreased central retention time in *Itpr2*$^{-/-}$ mice, the

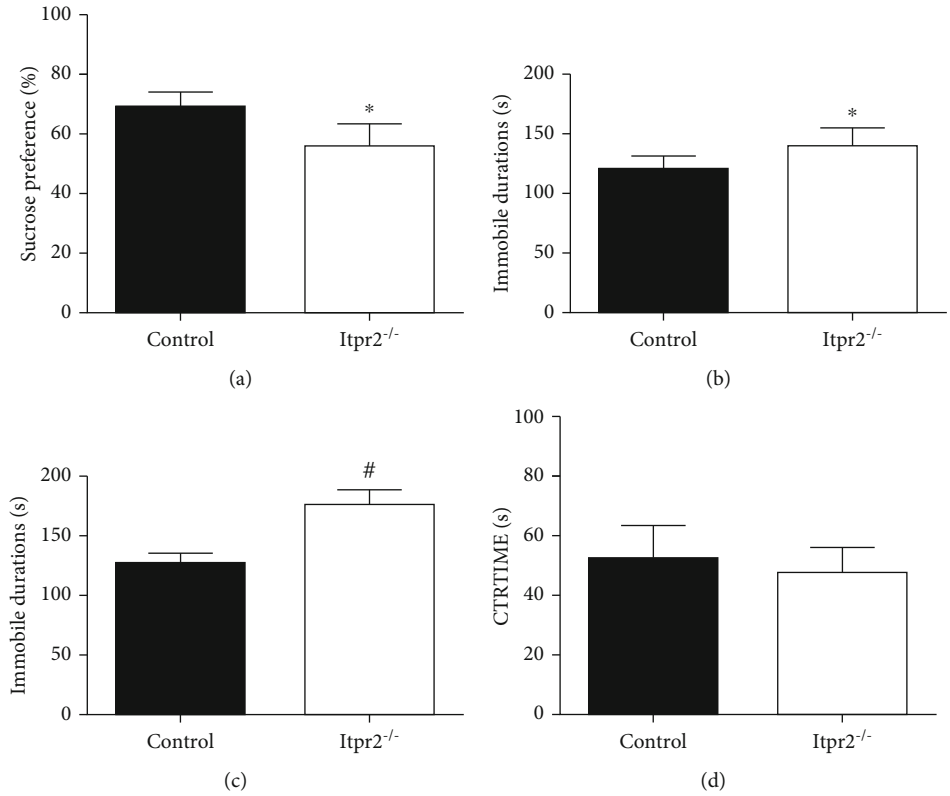

Figure 1: Behavior test of *Itpr2*$^{-/-}$ mice and controls. (a) Sucrose preference. (b) Tail suspension test immobile time. (c) Forced swim test immobile time. (d) Open-field test center time. Data are expressed as the mean ± SD. Asterisk indicates $P < 0.05$ and number sign indicates $P < 0.01$ when compared with the controls.

difference was not statistically significant ($P = 0.4602$, $t = 0.7758$, df = 8, $F = 1.643$) (Figure 1(d)).

3.2. Reduced Volume of Gray Matter in Itpr2$^{-/-}$ *Mice.* VBM analysis showed that the *Itpr2*$^{-/-}$ mice group was found to have significantly reduced gray matter volumes in bilateral striatums, the periaqueductal gray matter, and the right frontoparietal cortices compared with the control group ($P < 0.01$, AlphaSim corrected) (Figure 2), whereas no region was found with significantly increased gray matter volume in *Itpr2*$^{-/-}$ mice.

3.3. Abnormal Functional Connectivity Related to the Striatum in Itpr2$^{-/-}$ *Mice.* Based on the results in Section 3.2, the striatum was selected as seed ROI for further FC analysis (Figure 3(a)), since this region was considered highly relevant to the emotion regulation and depression in previous studies. The RSFC maps of the bilateral striatums were highly relevant to each other. Therefore, to limit the number of statistical tests and for easy interpretation of the results, the RSFC maps of the bilateral striatums were averaged for each mouse and subsequently compared between groups. Compared with controls, significantly decreased striatal FC was found in the bilateral hippocampus and right parietal cortex (mainly for the primary and secondary somatosensory cortex) in the *Itpr2*$^{-/-}$ mice ($P < 0.01$, AlphaSim corrected); however, no region was identified with increased FC (Figure 3(b)).

3.4. Decreased Expression of BDNF in the Striatums of Itpr2$^{-/-}$ *Mice and Itpr2*$^{-/-}$ *C8-D1A.* Immunofluorescence staining showed a declined level of BDNF in the striatums of *Itpr2*$^{-/-}$ mice (Figure 4(a)). And the striatums of both *Itpr2*$^{-/-}$ mice and controls (Figure 4(b)), as well as cells including *Itpr2*$^{-/-}$ *C8-D1A* and controls (Figure 4(c)), were later subjected to Western blotting using anti-BDNF antibodies. In all samples tested, we detected 14- and 28 kDa BDNF-immunoreactive bands representing pro- and mature BDNF, respectively. The intensity of the pro-BDNF band was not significantly different between *Itpr2*$^{-/-}$ samples and controls both in mice and astrocytes, while the expression of mature BDNF decreased clearly in the *Itpr2*$^{-/-}$ sample as compared with controls both in mice ($P = 0.0368$, $P < 0.05$, $t = 5.067$, df = 2, $F = 653.0$) and astrocytes ($P = 0.002$, $P < 0.01$, $t = 13.04$, df = 4, $F = 1.068$).

4. Discussion

This paper confirmed the previous finding that *Itpr2*$^{-/-}$ mice exhibit depressive-like symptoms as shown in most behavioral tests except in OFT. However, OFT is mainly used to test whether the mice perform obvious anxiety and exploratory intentions, which suggests *Itpr2*$^{-/-}$ mice did not perform these symptoms. On this basis, we further revealed *in vivo* brain abnormalities including a reduced striatum volume and relevant functional connectivity in *Itpr2*$^{-/-}$ mice. Additionally, to further study the *in vivo* MR findings, we performed

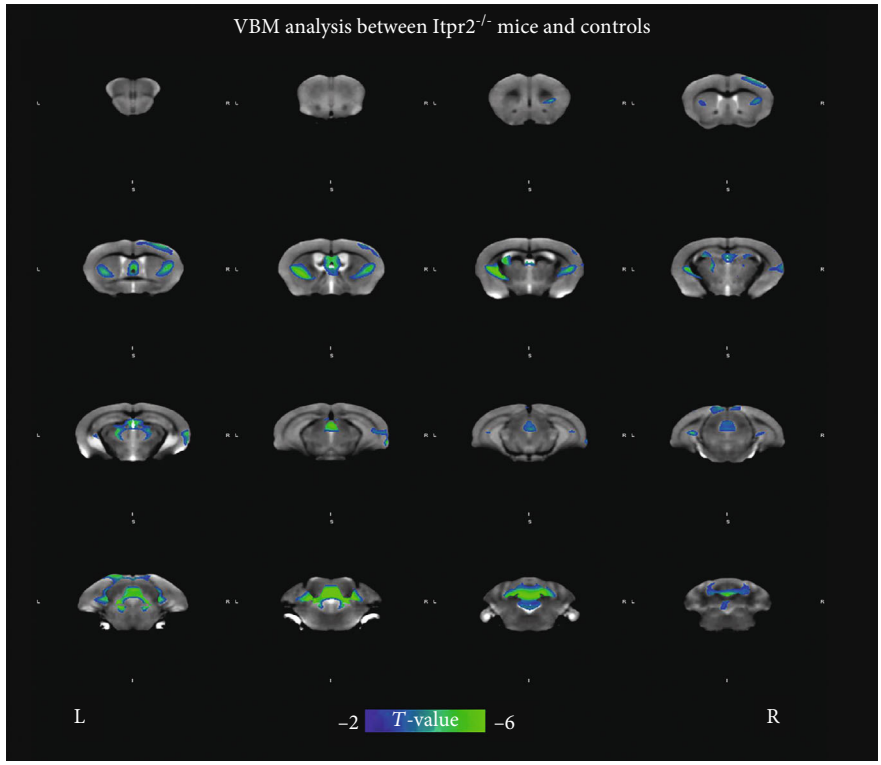

(a)

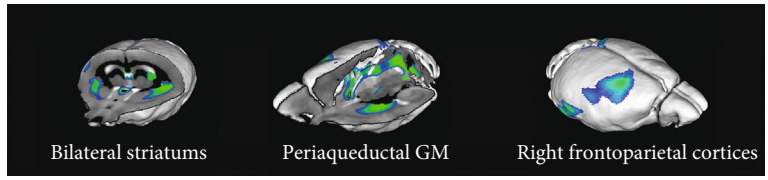

(b)

Figure 2: Abnormal volume of the gray matter in *Itpr2*$^{-/-}$ mice as compared with controls. (a) The regions of decreased volume of gray matter shown on the coronal plane. (b) The regions of decreased volume of gray matter shown on the three-dimensional images.

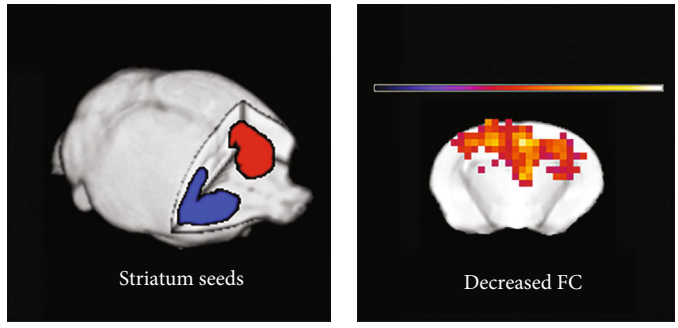

(a) (b)

Figure 3: Abnormal resting-state functional connections between other regions of the whole brain with the bilateral striatum in both groups. Whole-brain RSFC map is created based on the blood oxygen level-dependent time series from spherical seed regions of the striatum. (a) Positions of striatum seeds. (b) Decreased FC between the striatums and other brain regions in Itpr2$^{-/-}$ mice.

biochemistry analyses and found decreased BDNF expression in both the sample tissues of the striatum in the *Itpr2*$^{-/-}$ mice and *Itpr2*$^{-/-}$ C8-D1A. Thus, these findings may jointly support the relationship between the genetic deficiency of Itpr2 and the currently observed *in vivo* brain abnormalities.

As one of the crucial roles of reward and emotion regulation networks, the striatum receives cortical and dopaminergic projections; it is located at the center of functional circuits that influence motor and cognitive aspects of behavior [25–27] and has been frequently discussed in studies of emotion

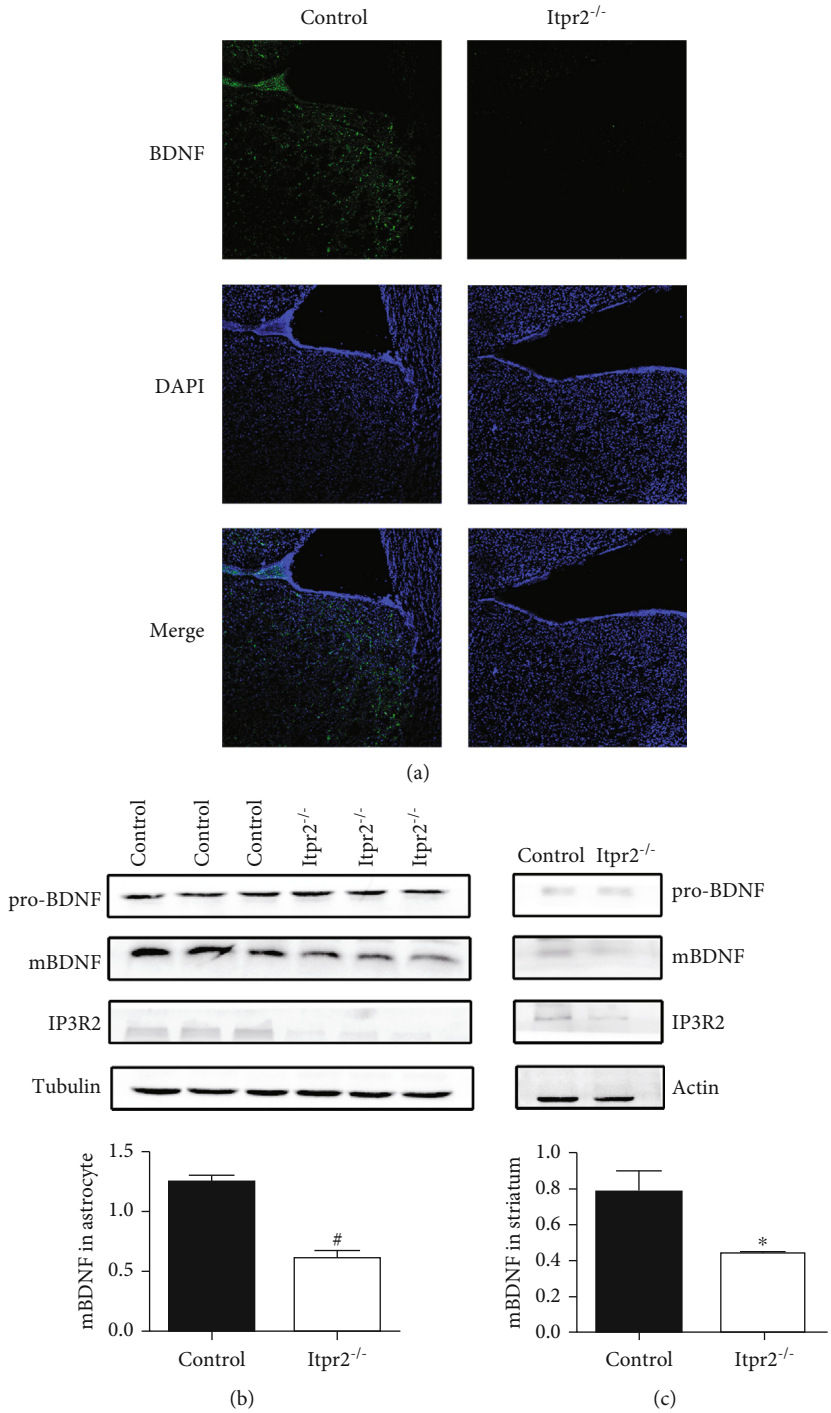

Figure 4: Detection of BDNF level in *Itpr2*$^{-/-}$ samples and controls. (a) BDNF immunofluorescence staining and expression in the striatum (×100). (b) Analysis of BDNF expression in the striatum by Western blotting. (c) Analysis of BDNF expression in C8-D1A by Western blotting. Data are expressed as the mean ± SD. Number sign indicates $P < 0.01$ when compared with the controls.

regulation strategies and was found to contribute directly to decision-making [28, 29]; the relationship between depression and the striatum is extensively studied. Previous research reported volumetric abnormalities of the striatum or part of the striatums such as the lentiform nucleus in major depression disorder (MDD) patients. Matsuo et al. have indicated that treatment-naive MDD patients have significantly smaller right striatum and right caudate (part of the striatum) volumes compared to the healthy subjects [30], suggesting that depression closely depends on the structure and functioning of the striatum [31–34].

Reduction of BDNF in the brain has been proposed as a candidate for possible involvement in depression [35]. Previous studies indicated that increased levels of BDNF in the

striatum is related to improved depressive-like behavior [36]. Moreover, this study found the decreased expression of mature BDNF in the striatum, which possibly contributes to the reduced volume of the striatum and depressive-like behaviors in *Itpr2*$^{-/-}$ mice; this is since, decreased BDNF can lead to tissue loss.

As mentioned above, IP_3R_2 is mainly expressed in astrocytes in the brain and BDNF is mainly generated and released by astrocytes. For this reason, we further detected the expression level of BDNF in astrocytes lacking Itpr2 (*Itpr2*$^{-/-}$ C8-D1A) and found it decreased. So, being consistent with our findings in tissue, this result supported that the decline of BDNF in the striatums in *Itpr2*$^{-/-}$ mice is induced by the reduced BDNF expression of astrocyte lacking Itpr2.

The strength of memory generated by the hippocampus is related to the level of FC between the hippocampus and the striatum [37]. Previous research has revealed that the FC between the hippocampus and the striatum increased significantly after a period time of memory training, promoting the changed FC is responsible for the formation of long-term memories [38]. Our results suggest the decreased FC the hippocampus and the striatum can lead to the weakened ability of memory which is a common symptom in depression. Besides, lower FC between the striatum and right parietal cortex (mainly for the primary and secondary somatosensory cortex) may participate in the painful physical symptoms which are usually present in depression.

MRI as a noninvasive tool can provide clues about *in vivo* functional connectivity and volume abnormalities, which were then combined with biochemical analyses to validate and explain the possible pathogenesis in *Itpr2*$^{-/-}$ mice from the perspective of dysfunctional astrocytes. Such kind of combined studies is of some value, especially for the psychiatric disorders like depression, since it may shed light on the neuropathological mechanism from the perspective of *in vivo* neural abnormalities, and could be a strength of this work. However, in this paper, we did not further study the specific mechanism by which the absence of Itpr2 leads to the decreased expression of BDNF in astrocyte, and we also lack research on the learning and memory abilities of mice related to decreased FC of striatums-hippocampus and painful physical symptoms related to decreased FC of striatums-right parietal cortex. So, in the future, we should go on to study the underlying mechanism in astrocytes lacking Itpr2 and supplement other experiments to complete the study.

5. Conclusion

By combining biochemistry and MR analyses, this study revealed that the Itpr2-related neuropathological effect is possibly mediated by the relevant brain especially striatum structural and functional abnormality in *Itpr2*$^{-/-}$ mice *in vivo*, which is associated with decreased BDNF in the striatum due to a decline production of BDNF from astrocyte lacking Itpr2; thus, it may help us better understand underlying mechanisms of Itpr2 deficiency as well as its relation to depressive behavior.

Data Availability

The datasets used to support the findings of this study are available from the corresponding author on reasonable request.

Conflicts of Interest

All the authors declare no conflict of interest regarding the publication of this paper.

Authors' Contributions

Shanmei Zeng and Kai Liu have contributed equally to this work.

Acknowledgments

This study was supported by the National Natural Science Foundation of China (No. 81701674), National Natural Science Foundation of China (No. 81801682), Guangdong Natural Science Foundation (No. 2018030310296), Guangdong Natural Science Foundation (2017A030313903), Guangdong Natural Science Foundation (No. 2020A1515019469), combined Science Technology Project of Guangdong Provincial Department of Science and Technology and Guangdong Provincial Academy of Traditional Chinese Medicine (2014A020221011), and Guangdong Province Bureau of Traditional Chinese Medicine Scientific Research Project (No: 20151024, 20161161, 20171284).

Supplementary Materials

Figure 1. Movement speed of the Itpr2$^{-/-}$ and control group in OF. *(Supplementary Materials)*

References

[1] A. H. Sharp, F. C. Nucifora Jr., O. Blondel et al., "Differential cellular expression of isoforms of inositol 1,4,5-triphosphate receptors in neurons and glia in brain," *Journal of Comparative Neurology*, vol. 2, no. 406, pp. 207–220, 1999.

[2] V. Parpura and R. Zorec, "Gliotransmission: exocytotic release from astrocytes," *Brain research reviews*, vol. 63, no. 1-2, pp. 83–92, 2010.

[3] M. Tanaka, X. Wang, K. Mikoshiba, H. Hirase, and Y. Shinohara, "Rearing-environment-dependent hippocampal local field potential differences in wild-type and inositol trisphosphate receptor type 2 knockout mice," *The Journal of Physiology*, vol. 595, no. 20, pp. 6557–6568, 2017.

[4] H. Monai, M. Ohkura, M. Tanaka et al., "Calcium imaging reveals glial involvement in transcranial direct current stimulation-induced plasticity in mouse brain," *Nature Communications*, vol. 7, no. 1, 2016.

[5] X. Cao, L. P. Li, Q. Wang et al., "Astrocyte-derived ATP modulates depressive-like behaviors," *Nature Medicine*, vol. 19, no. 6, pp. 773–777, 2013.

[6] W. Peng, Z. Chen, L. Yin, Z. Jia, and Q. Gong, "Essential brain structural alterations in major depressive disorder: a voxel-wise meta-analysis on first episode, medication-naive

patients," *Journal of Affective Disorders*, vol. 199, pp. 114–123, 2016.

[7] O. Ozalay, B. Aksoy, S. Tunay et al., "Cortical thickness and VBM in young women at risk for familial depression and their depressed mothers with positive family history," *Psychiatry Research: Neuroimaging*, vol. 252, pp. 1–9, 2016.

[8] V. Lorenzetti, N. B. Allen, A. Fornito, and M. Yücel, "Structural brain abnormalities in major depressive disorder: a selective review of recent MRI studies," *Journal of Affective Disorders*, vol. 117, no. 1-2, pp. 1–17, 2009.

[9] F. Amico, E. Meisenzahl, N. Koutsouleris, M. Reiser, H. J. Möller, and T. Frodl, "Structural MRI correlates for vulnerability and resilience to major depressive disorder," *Journal of Psychiatry & Neuroscience*, vol. 36, no. 1, pp. 15–22, 2011.

[10] L. Wang, D. F. Hermens, I. B. Hickie, and J. Lagopoulos, "A systematic review of resting-state functional-MRI studies in major depression," *Journal of Affective Disorders*, vol. 142, no. 1-3, pp. 6–12, 2012.

[11] E. T. Rolls, W. Cheng, J. du et al., "Functional connectivity of the right inferior frontal gyrus and orbitofrontal cortex in depression," *Social Cognitive and Affective Neuroscience*, vol. 15, no. 1, pp. 75–86, 2020.

[12] L. J. Mertens, M. B. Wall, L. Roseman, L. Demetriou, D. J. Nutt, and R. L. Carhart-Harris, "Therapeutic mechanisms of psilocybin: changes in amygdala and prefrontal functional connectivity during emotional processing after psilocybin for treatment-resistant depression," *Journal of Psychopharmacology*, vol. 34, no. 2, pp. 167–180, 2020.

[13] M. V. Sofroniew and H. V. Vinters, "Astrocytes: biology and pathology," *Acta Neuropathologica*, vol. 119, no. 1, pp. 7–35, 2010.

[14] F. Angelucci, S. Brenè, and A. A. Mathé, "BDNF in schizophrenia, depression and corresponding animal models," *Molecular Psychiatry*, vol. 10, no. 4, pp. 345–352, 2005.

[15] P. Fossati, A. Radtchenko, and P. Boyer, "Neuroplasticity: from MRI to depressive symptoms," *European Neuropsychopharmacology*, vol. 14, pp. S503–S510, 2004.

[16] C. Mirescu, J. D. Peters, and E. Gould, "Early life experience alters response of adult neurogenesis to stress," *Nature Neuroscience*, vol. 7, no. 8, pp. 841–846, 2004.

[17] H. J. Lee, J. W. Kim, S. V. Yim et al., "Fluoxetine enhances cell proliferation and prevents apoptosis in dentate gyrus of maternally separated rats," *Molecular Psychiatry*, vol. 6, no. 6, pp. 725–728, 2001.

[18] K. Hashimoto, "BDNF variant linked to anxiety-related behaviors," *Bioessays*, vol. 29, no. 2, pp. 116–119, 2007.

[19] R. S. Duman and L. M. Monteggia, "A neurotrophic model for stress-related mood disorders," *Biological Psychiatry*, vol. 59, no. 12, pp. 1116–1127, 2006.

[20] F. Alliot and B. Pessac, "Astrocytic cell clones derived from established cultures of 8-day postnatal mouse cerebella," *Brain Research*, vol. 306, no. 1-2, pp. 283–291, 1984.

[21] L. Steru, R. Chermat, B. Thierry, and P. Simon, "The tail suspension test: a new method for screening antidepressants in mice," *Psychopharmacology*, vol. 85, no. 3, pp. 367–370, 1985.

[22] R. D. Porsolt, M. le Pichon, and M. Jalfre, "Depression: a new animal model sensitive to antidepressant treatments," *Nature*, vol. 266, no. 5604, pp. 730–732, 1977.

[23] K. Hikishima, Y. Komaki, F. Seki, Y. Ohnishi, H. J. Okano, and H. Okano, "In vivo microscopic voxel-based morphometry with a brain template to characterize strain-specific structures in the mouse brain," *Scientific Reports*, vol. 7, no. 1, p. 85, 2017.

[24] A. E. Dorr, J. P. Lerch, S. Spring, N. Kabani, and R. M. Henkelman, "High resolution three-dimensional brain atlas using an average magnetic resonance image of 40 adult C57Bl/6J mice," *Neuroimage*, vol. 42, no. 1, pp. 60–69, 2008.

[25] F. A. Middleton and P. L. Strick, "New concepts about the organization of basal ganglia output," *Advances in neurology*, vol. 74, pp. 57–68, 1997.

[26] F. A. Middleton and P. L. Strick, "Basal ganglia output and cognition: evidence from anatomical, behavioral, and clinical studies," *Brain and Cognition*, vol. 42, no. 2, pp. 183–200, 2000.

[27] M. R. Delgado, "Reward-related responses in the human striatum," *Annals of the New York Academy of Sciences*, vol. 1104, no. 1, pp. 70–88, 2007.

[28] K. N. Ochsner, J. A. Silvers, and J. T. Buhle, "Functional imaging studies of emotion regulation: a synthetic review and evolving model of the cognitive control of emotion," *Annals of the New York Academy of Sciences*, vol. 1251, no. 1, pp. E1–E24, 2012.

[29] B. W. Balleine, M. R. Delgado, and O. Hikosaka, "The role of the dorsal striatum in reward and decision-making," *Journal of Neuroscience*, vol. 27, no. 31, pp. 8161–8165, 2007.

[30] K. Matsuo, et al.D. R. Rosenberg, P. C. Easter et al., "Striatal Volume Abnormalities in Treatment-Naïve Patients Diagnosed with Pediatric Major Depressive Disorder," *Journal of Child and Adolescent Psychopharmacology*, vol. 18, no. 2, pp. 121–131, 2008.

[31] A. Larry, "Magnetic-resonance morphometry in patients with major depression," *Psychiatry Research: Neuroimaging*, vol. 84, no. 1, pp. 7–15, 1998.

[32] M. J. Kim, J. P. Hamilton, and I. H. Gotlib, "Reduced caudate gray matter volume in women with major depressive disorder," *Psychiatry Research: Neuroimaging*, vol. 164, no. 2, pp. 114–122, 2008.

[33] E. Bora, B. J. Harrison, C. G. Davey, M. Yücel, and C. Pantelis, "Meta-analysis of volumetric abnormalities in cortico-striatal-pallidal-thalamic circuits in major depressive disorder," *Psychological Medicine*, vol. 42, no. 4, pp. 671–681, 2012.

[34] S. M. Grieve, M. S. Korgaonkar, S. H. Koslow, E. Gordon, and L. M. Williams, "Widespread reductions in gray matter volume in depression," *NeuroImage: Clinical*, vol. 3, pp. 332–339, 2013.

[35] H. Yu and Z. Y. Chen, "The role of BDNF in depression on the basis of its location in the neural circuitry," *Acta Pharmacologica Sinica*, vol. 32, no. 1, pp. 3–11, 2011.

[36] L. Marais, D. J. Stein, and W. M. Daniels, "Exercise increases BDNF levels in the striatum and decreases depressive-like behavior in chronically stressed rats," *Metabolic Brain Disease*, vol. 24, no. 4, pp. 587–597, 2009.

[37] I. Kahn and D. Shohamy, "Intrinsic connectivity between the hippocampus, nucleus accumbens, and ventral tegmental area in humans," *Hippocampus*, vol. 23, no. 3, pp. 187–192, 2013.

[38] D. G. Woolley, D. Mantini, J. P. Coxon, R. D'Hooge, S. P. Swinnen, and N. Wenderoth, "Virtual water maze learning in human increases functional connectivity between posterior hippocampus and dorsal caudate," *Human Brain Mapping*, vol. 36, no. 4, pp. 1265–1277, 2015.

Hindawi
Neural Plasticity
Volume 2020, Article ID 8825954, 11 pages
https://doi.org/10.1155/2020/8825954

Research Article

Inhibited CSF1R Alleviates Ischemia Injury via Inhibition of Microglia M1 Polarization and NLRP3 Pathway

Xiaoxue Du,[1,2] Yuzhen Xu,[3] Shijia Chen,[1] and Marong Fang[1]

[1]*Institute of Neuroscience, Zhejiang University School of Medicine, Hangzhou, 310006 Zhejiang, China*
[2]*Translational Medicine Center, Affiliated Hangzhou First People's Hospital, Zhejiang University School of Medicine, Hangzhou, 310006 Zhejiang, China*
[3]*Department of Neurology, Shanghai Tenth People's Hospital, Tongji University School of Medicine, Shanghai 200072, China*

Correspondence should be addressed to Marong Fang; fangmaro@zju.edu.cn

Received 17 June 2020; Revised 31 July 2020; Accepted 12 August 2020; Published 28 August 2020

Academic Editor: Fushun Wang

Ischemia cerebral stroke is one of the common neurological diseases with severe inflammatory response and neuron death. The inhibition of colony-stimulating factor 1 receptor (CSF1R) which especially expressed in microglia/macrophage exerted neuroprotection in stroke. However, the underlying neuroinflammatory regulation effects of CSF1R in ischemia stroke are not clear. In this study, cerebral ischemia stroke mice model was established. The C57/B6J mice were administered with Ki20227, a CSF1R inhibitor, by gavage for 7 consecutive days (0.002 mg/kg/day) before modeling. The Rota-Rod test and neurobehavioral score test were investigated to assess neurobehavioral functions. The area of infarction was assessed by 2, 3, 5-triphenyltetrazolium chloride (TTC) staining. The mRNA expressions of M1/M2 microglia markers were evaluated by real-time PCR. Immunofluorescence and Western blot were utilized to detect the changes of Iba1 and NLRP3 pathway proteins. Results showed that neurobehavioral function improvement was demonstrated by an increased stay time on the Rota-Rod test and a decreased neurobehavioral score in the Ki20227 treatment group. The area of infarction reduced in Ki20227 group when compared to the stroke group. Moreover, the mRNA expression of M1 microglia markers (TNF-α and iNOS) decreased while M2 microglia markers (IL-10 and Arg-1) increased. Meanwhile, compared to the stroke and stroke+PBS group, Ki20227 administration downregulated the expression of NLRP3, active caspase 1, and NF-κB protein in the ischemia penumbra of Ki20227 treatment group mice. In short, the CSF1R inhibitor, Ki20227, played vital neuroprotective roles in ischemia cerebral stroke mice, and the mechanisms may be via inhibiting microglia M1 polarization and NLRP3 inflammasome pathway activation. Our study provides a potential new target for the treatment of ischemic stroke injury.

1. Introduction

Cerebral ischemic stroke remains the leading cause of the death and disability worldwide, despite progress in reperfusion therapies. Considerable empirical evidence has demonstrated that inflammatory response of microglia/-macrophages to cerebral ischemia acts a vital part in varied phases of stroke pathobiology and outcome [1]. Excessive activation of proinflammatory cytokines, neural cell death, the blood-brain barrier, and neurogenesis disruption jointly lead to postischemic brain injury [2].

Colony-stimulating factor 1 receptor (CSF1R) is a class of tyrosine/serine kinases which especially expressed in microglia/macrophage and mainly responsible for regulating the proliferation and differentiation of microglia/macrophages [3]. Researches demonstrated the inhibition of CSF1R could regulate neurological function and exert neuroprotection in brain injury via inhibition of microglial activation [4]. Short-term elimination of microglia by CSF1R inhibitor, PLX5622, during the chronic phase of TBI disease led to long-term improvements in neurological function through decrease in NOX2 and NLRP3 inflammasome-associated neuroinflammation and improvement in the persistent neurodegenerative processes [5]. CSF1R inhibitor treatment significantly attenuates CSF1R activation and minimizes microglia cell proliferation with mRNA levels of

proinflammatory factors and then enhances motor functions [6]. In global cerebral ischemia, Ki20227 as a specific inhibitor of CSF1R effectively protect the dendritic spine density and dendritic structure of neurons from brain injury [7]. And Ki20227 could inhibit the phosphorylation of CSF1R and played an important role in microglia activation [8]. However, the underlying neuroprotective mechanism of Ki20227 in brain ischemia injury is still unclear.

NOD-like receptor 3 (NLRP3) inflammasome plays an important role in neuroimmune responses including microglial-dependent activation. Regulating NLRP3 inflammatory response may be in favor of neurofunction improvement in ischemia stroke [9]. ATP reduction and rapid ROS increase and other diverse endogenous danger signals caused by ischemic injury of brain tissue could mediate the activation of the NLRP3 inflammasome in the pathophysiological process of ischemia stroke [10]. Immune cells including microglia could be recruited by sudden increase of inflammatory cytokines released after the NLRP3 inflammasome to clear the damage-associated molecular patterns (DAMPs) and affect microglia phenotypic M1/M2 transformation by initiating the inflammatory mechanisms after ischemia stroke. For example, high level of TNF-α released from the microglia M1 phenotype activation was disadvantaged in brain tissue and neuron recovery after stroke [11], while the microglia M2 factors exerted a neuroprotective role in various stages of acute ischemia stroke [12]. Microglial M1 inhibition and microglial M2 polarization activation could protect against ischemic stroke and have the potential to improve neurogenesis [13]. Meanwhile, several researches reported the NLRP3 inflammasome overactivation could give rise to secondary brain injury following reperfusion due to sustained inflammation release and brain damage aggravation which could be improved by the inhibition of NLRP3 inflammasome [14]. Studies demonstrated RNAi-mediated NLRP3 transcript knockdown decreased microglia-related inflammatory response and neuronal injury to alleviate brain injury and improve neurological outcomes in ischemia stroke [15]. However, the regulation mechanism of CSF1R inhibitor on microglia phenotype and NLRP3 pathway in ischemia stroke is still not clear. To address this question, we probed into the neuroinflammatory regulation role of Ki20227 in postischemic brain injury mice, and we elaborated the regulation of Ki20227 to NLRP3 pathway in mice subjected to cerebral ischemic injury.

2. Material and Methods

2.1. Animals. 20–30 g weight C57BL/6 male mice were purchased from the Zhejiang Medical Academy. Before experiment, all animals were kept in pathogen-free separated clean cages with enough food and water under a constant temperature of 24°C and a 12 hours light/dark cycle. The Guide for Care and Use of Animal Center of Zhejiang University was followed, and the Ethics Committee for Use of Experimental Animals in Zhejiang University Animal treatment formally permitted animal treatment in this study.

2.2. Experimental Groups and Drug Administration. The fifth male C57BL/6 mice were stochastically split into 5 experimental groups: normal group ($n = 10$), sham group ($n = 10$), stroke group ($n = 10$), stroke+PBS group ($n = 10$), and stroke+Ki20227 group ($n = 10$). In stroke+Ki20227 group, Ki20227 (0.002 mg/kg/day dose, by gavage) was administered for 7 days [7]. After 7 days of Ki20227 administration, cerebral ischemia was established, and the Ki20227 administration was given once for the next 24 hours. Mice in stroke+PBS group underwent the same way of injection with equal volumes of PBS solution simultaneously.

2.3. Establishment of Cerebral Ischemic Mice Model. The cerebral ischemic model was established as previously described [16]. In short, Rose Bengal dye (Sigma-Aldrich, # 330000) was dissolved in 0.1 M PBS solution with a final concentration of 10 mg/mL, filtered through 0.45 m filters, and placed in the dark until use. At the beginning of the establishment of the model, Rose Bengal dye (100 mg/kg) was injected intraperitoneal. The mice were all anesthetized with inhaled isoflurane (RWD, China) when building the model. After 5 minutes, the target area (1.75 mm lateral to Bregma, +0.5 mm, left hemisphere) was exposed directly under the flexible cool light attached to a light-emitting diode cold light source (OPLENIC, M-IL-HAL 3001), and the continuous cool light irradiation was continued for 15 minutes to induce focal cerebral ischemia, and finally, the wound was sutured.

2.4. Behavioral Tests

2.4.1. Rota-Rod Test. The Rota-Rod test was employed to measure the motor coordination and antifatigue ability of mice before and after cerebral ischemia treatment. The Rota-Rod test comprises a rotating rod with a diameter of 3 cm (this rod was divided into 5 tracks with a width of 6 cm), an infrared detector, and a computer. In the test, mice were positioned on the horizontally oriented, rotating rod. The infrared sensor sensed whether mice stayed on the stick, so as to obtain the time mice stayed on the rod and the rotation speed of the rod when they fell. The total test time was set to 300 seconds, and the rotation speed of rod was expedited from 8 rpm to 40 rpm. Each group mice were trained 3 times a day with a 10-minute rest each time. The mice staying on the rotating rod track for more than 200 seconds were used to establish the stroke model. The times of each group on the rotating rod instrument two days before the model establishment and one day after stroke were recorded.

2.4.2. Neurobehavioral Score. The neurological scores were descripted previously [17]. There are 4 grades for neurobehavioral function evaluation. The higher score, the worse behavioral function. Number 4 represented unidirectional circling and consciousness reduction. Number 3 is unidirectional circling. Number 2 stands for forelimb flexion and resistance to lateral thrust reduction. Number 1 means forelimb flexion. Number 0 stands for no observable defects of mice. The above behavioral observation was performed in a blinded process. The score of each group was recorded at 24 h after stroke.

Table 1: Sequence of primer of microglia M1 and M2 type factors.

Gene name	Forward primer (5′-3′)	Reverse primer (5′-3′)
TNF-α	GATCGGTCCCCAAAGGGATG	CCACTTGGTGGTTTGTGAGTG
Arg-1	CATGGGCAACCTGTGTCCTT	TCCTGGTACATCTGGGAACTTTC
IL-10	GTCATCGATTTCTCCCCTGTG	CCTTGTAGACACCTTGGTCTTGG
iNOS	TGGTGAGGGGACTGGACTTT	CCAACTCTGCTGTTCTCCGT
β-Action	CGTGCGTGACATCAAAGAGAAG	CAAGAAGGAAGGCTGGAAAAGA

Arg: arginase-1; TNF-α: tumor necrosis factor-α; IL-10: interleukin 10.

2.5. TTC Staining. Animals in different groups were sacrificed at 24 hours after building ischemia stroke model for brain infarct formation evaluation. TTC staining purchased from Sigma-Aldrich Company was used to measure the change of infract areas. Fresh brains were removed and kept at -20°C for 30 min and then were sliced into 2 mm coronal sections rapidly. 5% TTC in physiological saline solution was used to incubate every slice at 37°C for 20 min in dark. And then 4% buffered formalin fixed the slice for 1 hour at room temperature. The infract areas were showed as the complexionless areas and presented in the figures. Infarct areas were measured using ImageJ software (NIH, Bethesda, MD, USA). The total infarction volume for each slice was calculated. The infarction volume of every mouse was calculated from the infarcted area of the ipsilateral hemisphere/total area (from both the ipsilateral and contralateral hemispheres) [17].

2.6. Immunofluorescence Staining. Brains of every group mouse were perfusion by 0.9% saline solution and fixed in 4% paraformaldehyde PBS solution at 4°C overnight. After dehydrated in 30% sucrose solution for one week, brains were sectioned coronally with embedding them with OCT. Rabbit anti-Iba1 (1 : 500; Abcam, #ab178847) and rabbit polyclonal to anti-NLRP3 (1 : 100; BOSTER, BM4490) as primary antibodies were applied. Secondary antibody including goat anti-rabbit Alexa Fluor 488 (1 : 500, EARTHOX, San Francisco, # E031220-01) was employed after primary antibodies. Before being covered with coverslips, the slides were added the antiquenching solution with DAPI dye (VECTASHIELD, USA) for observation. Images were taken in 5-vision/section stochastically to count the immunoreactive cells under Olympus BX51 fluorescence microscope [15].

2.7. Western Blot. Total proteins of ischemic brain tissue in each group were extracted by RIPA buffer containing EDTA-free protease inhibitor and phosphate inhibitor (Rocher, Switzerland). After measuring the protein concentration, 30 μg of each sample was subjected to electrophoresis on 15% SDS-PAGE gel at 200 V. The protein was transferred into the PVDF membrane at 100 V in Bio-Rad TransBlot apparatus. 5% skimmed milk diluted by TBST solution was used to block PVDF membranes containing proteins for 2.5 hours at room temperature, and then, the primary antibody, rabbit anti-GADPH (1 : 1000, Abcam, ab181602), NLRP3 (1 : 1000, Abcam, ab181602), caspase 1 (1 : 1000, Abcam, ab181602), and NF-κB (1 : 1000, Abcam, ab181602), were used to incubate PVDF membranes at 4°C overnight. And then, the second antibody HRP-conjugated goat anti-rabbit (1 : 5000; EarthOx, USA) was used to incubate membranes for 2.5 hours after washing three times per 5 mins with TBST solution. Finally, after incubating with enhanced chemiluminescence, the membranes were exposed in ChemiDoc Touch Imaging System. ImageJ software was applied to the quantification analysis of protein bands. Each experiment was performed three times [16].

2.8. Real-Time PCR. After extracting total RNA with Trizol (Invitrogen) reagent, it was reverse transcribed into complementary deoxyribonucleic acid (cDNA) according to the instructions of BestarTM qPCR RT kit (DBI-2220, Germany). Real-time PCR protocol was carried out under the guidance of BestarR SybrGreen qPCR master mix (DBI-2044, Germany). The results were interpreted in Bio-Rad CFX manager program 3.0 software. The microglia M1/M2 type factor primers are shown in Table 1.

2.9. Statistical Analysis. SPSS 22.0 software was used to perform statistical analysis. The one-way ANOVA with Tukey test evaluated the difference between the drug treatment and nondrug treatment group in stroke mouse models. For the data of multiple groups in the Rota-Rod test, the difference was analyzed by the two-way ANOVA with Bonferroni posttest. Values are presented as means ± SEM. For all of the tests, three levels of significance were determined: $^{*}P < 0.05$, $^{**}P < 0.01$, $^{***}P < 0.001$.

3. Results

3.1. Ki20227 Administration Reduced Neurological Deficits. Neurological scores and Rota-Rod test were classical methods and used to evaluate the neurobehavioral damage in each group. The increase neurological deficit score or the decrease time in Rota-Rod indicated the severe impairment of motor function of mice. Results showed animals in the stroke group and stroke+PBS group had the increased neurological score indicating more neurological deficits when compared to the sham group ($^{***}P < 0.001$) in Figure 1(a). However, Ki20227 pretreated could significantly decrease neurological score to improve neurological impairment in the stroke+Ki20227 group when compared to the stroke and stroke+PBS groups ($^{\#\#}P < 0.01$, $\wedge P < 0.05$). In the Rota-Rod test of Figure 1(b), animals in every group showed the average different time was close to 1 in pre-1 day and 2 days. After building stroke model, the average different time of animals in the stroke group and stroke+PBS group on the Rota-

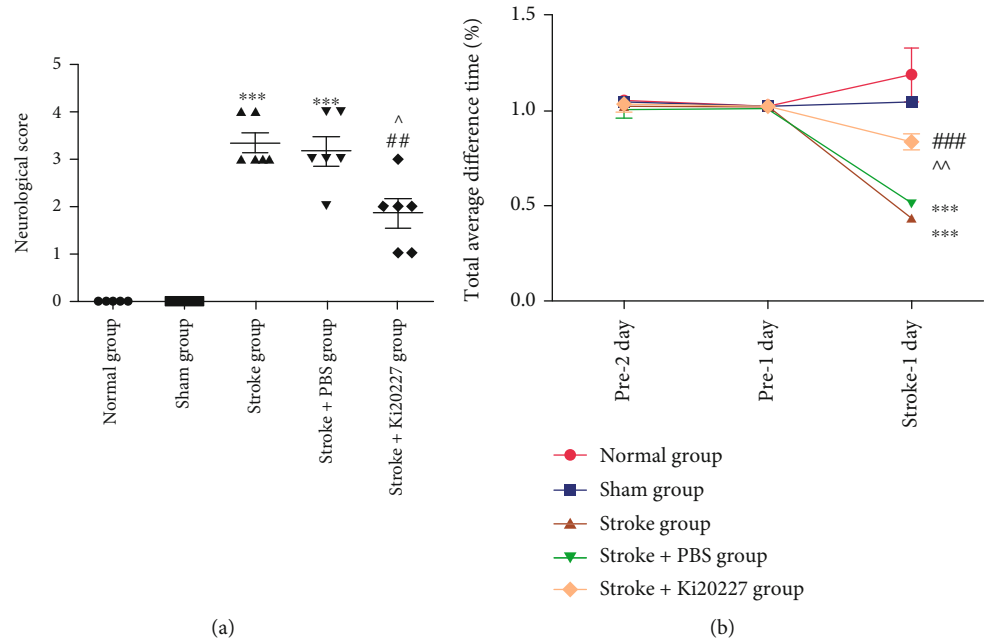

Figure 1: Ki20227 administration reduced neurological deficits. Statistical analysis of behavior tests. Statistical analysis of (a) neurobehavioral score and (b) the total average difference time in Rota-Rod test for normal, sham, stroke, stroke+PBS, and stroke+Ki20227 groups. Normal group vs. stroke group, $^{***}P < 0.001$; normal group vs. stroke+PBS group, $^{***}P < 0.001$; stroke+PBS vs. stroke+Ki20227 groups, $^{\wedge}P < 0.05$, $^{\wedge\wedge}P < 0.01$; stroke+Ki20227 group vs. stroke group, $^{\#\#}P < 0.01$, $^{\#\#\#}P < 0.001$.

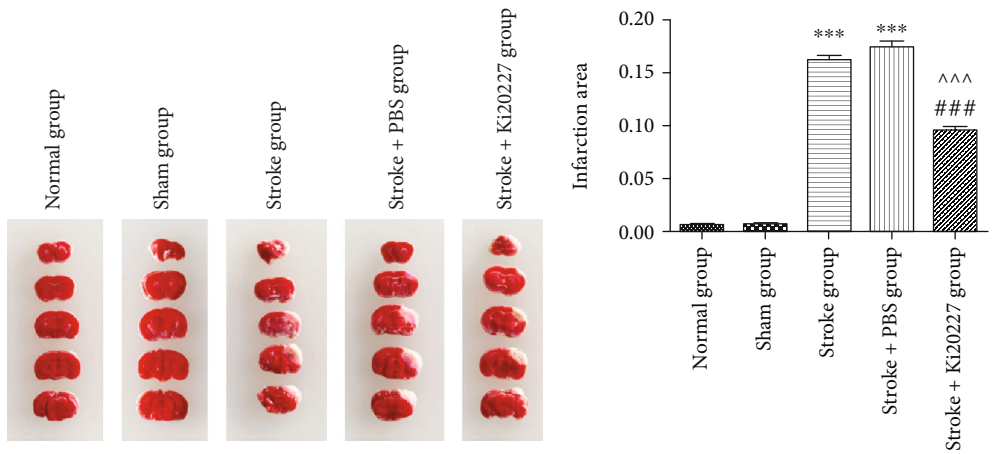

Figure 2: Ki20227 administration reduced the brain infarction volume. (a) The representative images of TTC staining in each group. (b) Statistic analysis of infarction volume in normal, sham, stroke, stroke+PBS, and stroke+Ki20227 groups. Normal group vs. stroke group, $^{***}P < 0.001$; normal group vs. stroke+PBS group, $^{***}P < 0.001$; stroke+Ki20227 group vs. stroke group, $^{\#\#\#}P < 0.001$; stroke+PBS vs. stroke+Ki20227 groups, $^{\wedge\wedge\wedge}P < 0.001$.

Rod significantly less than that of the normal and sham groups ($^{***}P < 0.001$). Meanwhile, mice in stroke+Ki20227 group had significantly more time on the Rota-Rod than that of the stroke and stroke+PBS groups ($^{\#\#\#}P < 0.001$, $^{\wedge\wedge}P < 0.01$). And there is no significant difference between stroke group and stroke+PBS group considering the results in the behavioral tests.

3.2. Ki20227 Administration Reduced the Brain Infarction Volume. The infarct volume of brain sections of every group is analyzed by TTC staining after 24 hours of the ischemic insult. In stroke and stroke+PBS groups, the infarct volume was significantly increased compared to that of normal and sham groups ($^{***}P < 0.001$). There was no significant difference in the infarction volume between the stroke and stroke+PBS groups (Figures 2(a) and 2(b)). However, compared to the stroke and stroke+PBS groups, Ki20227 treatment reduced the infarct volume of stroke+Ki20227 group mice ($^{\#\#\#}P < 0.001$, $^{\wedge\wedge\wedge}P < 0.001$).

3.3. Ki20227 Administration Reduced Iba1 Expression after Stroke. Iba1 immunofluorescent analysis was used to

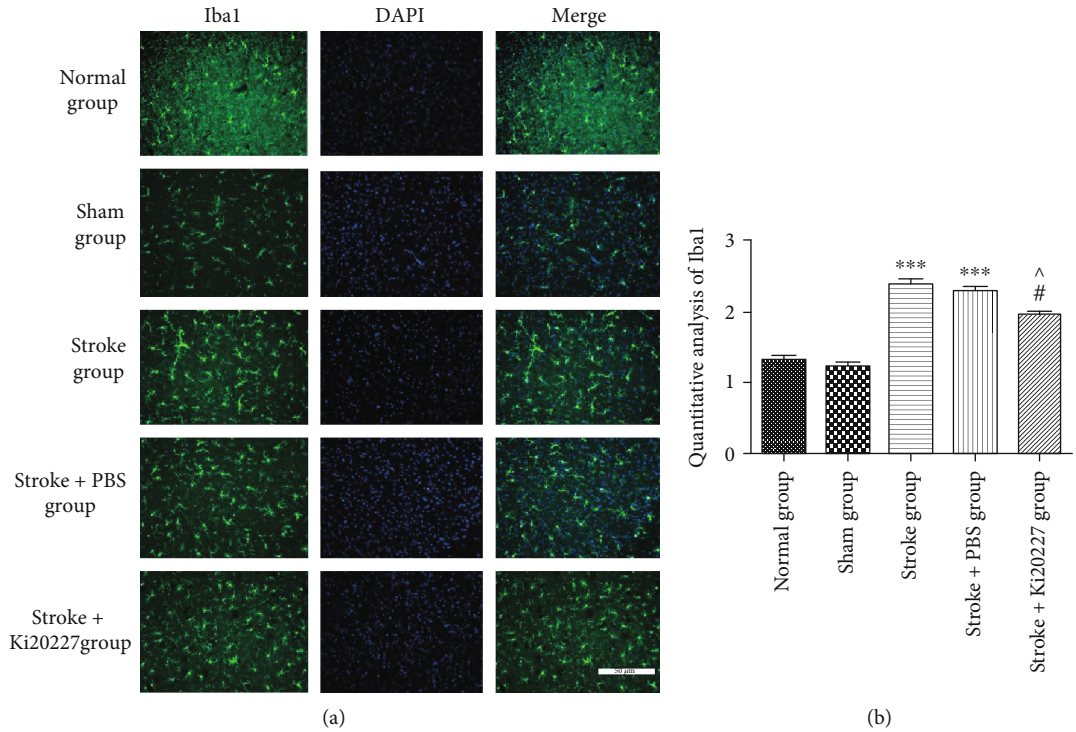

Figure 3: Ki20227 administration reduced Iba1 expression after stroke. (a) In normal, sham, stroke, stroke+PBS, and stroke+Ki20227 groups, Iba1 protein immunofluorescence staining was showed into green fluorescence. Blue fluorescence represented and was labeled as the cell nucleus. Merged pictures are showing positive cells. Bar = 50 μm. (b) Statistical analysis results of Iba1 expression in each group. The IOD/area of proteins expression assumed the comparative expression. Normal group vs. stroke group, $^{***}P < 0.001$; normal group vs. stroke+PBS group, $^{***}P < 0.001$; stroke+Ki20227 group vs. stroke group, $^{\#}P < 0.05$; stroke+PBS vs. stroke+Ki20227 groups, $\wedge P < 0.05$.

investigate the rest and activation of microglia in the penumbral area of stroke mice. As shown in Figure 3, in the stroke group and stroke+PBS group, Iba1 expression is significantly more than that of the sham group ($^{***}P < 0.05$). However, Iba1 expression significantly decreased in stroke +Ki20227 group, when compared with stroke and stroke +PBS group ($^{\#}P < 0.05$, $\wedge P < 0.05$). Results demonstrated Ki20227 could inhibit the Iba1-positive microglia in ischemia stroke model mice.

3.4. Ki20227 Administration Inhibited Microglia M1 Phenotype and Activated M2 Phenotype. To further explore the anti-inflammation effects of Ki20227, microglia M1 and M2 factors expression in the penumbra of stroke mice were illuminated by real-time PCR as shown in Figure 4. The low levels of microglia M1 phenotype (TNF-α and iNOS) were revealed in the brain of sham group mice (Figures 4(a) and 4(b)). After building stroke model, the mRNA levels of TNF-α and iNOS of penumbra of stroke and stroke+PBS groups were markedly upregulated ($^{***}P < 0.001$). In contrast, Ki20227 treatment could significantly decrease the mRNA expression of TNF-α and iNOS based on building stroke model with PBS treatment ($^{\#\#}P < 0.01$, $^{\#\#\#}P < 0.001$, $\wedge\wedge P < 0.01$, $\wedge\wedge\wedge P < 0.001$). Meanwhile, the mRNA expression of microglia M2 phenotype factors with anti-inflammatory effects was clarified to further explore the neuroprotection role of Ki20227. In Figures 4(c) and 4(d), the low mRNA expression of Arg-1 and IL-10 as microglia M2 phenotype was observed in the penumbra of sham group mice. The decrease mRNA levels of Arg-1 and IL-10 were markedly showed in stroke and stroke+PBS groups and less than that of the sham group ($^{**}P < 0.01$, $^{***}P < 0.001$). However, Ki20227 administration significantly increased Arg-1 and IL-10 mRNA expression in Ki20227+stroke group when compared to stroke and stroke+PBS groups ($^{\#}P < 0.05$, $^{\#\#\#}P < 0.001$, $\wedge P < 0.05$, $\wedge\wedge P < 0.01$).

3.5. Ki20227 Administration Inhibited NLRP3 Pathway Activation. We further investigated the expression changes of NLRP3 signaling pathway proteins caused by ischemic injury. NLRP3 inflammatory response is associated with microglia activation which maybe contributed to the neuron recovery after stroke though NF-κB and caspase 1 activation. Western blot results showed the low protein expression of NLRP3 in sham and normal groups in Figure 4. Compared with sham and normal groups, the NLRP3, NF-κB, and cleaved caspase 1 protein expression increased significantly in both stroke group and stroke+PBS group ($^{***}P < 0.001$). In contrast, Ki20227 treatment could decrease the NLRP3, NF-κB, and cleaved caspase 1 protein expression in stroke +Ki20227 group after building stroke model with PBS treatment ($^{\#\#}P < 0.01$, $^{\#\#\#}P < 0.001$, $\wedge\wedge P < 0.01$, $\wedge\wedge\wedge P < 0.001$) in Figures 5(b)–5(d).

3.6. Ki20227 Administration Inhibited NLRP3 Inflammasome Activation. Meanwhile, the NLRP3 immunofluorescent analysis was implemented to examine NLRP3 inflammasome in the penumbral area of stroke mice as displayed in Figure 6.

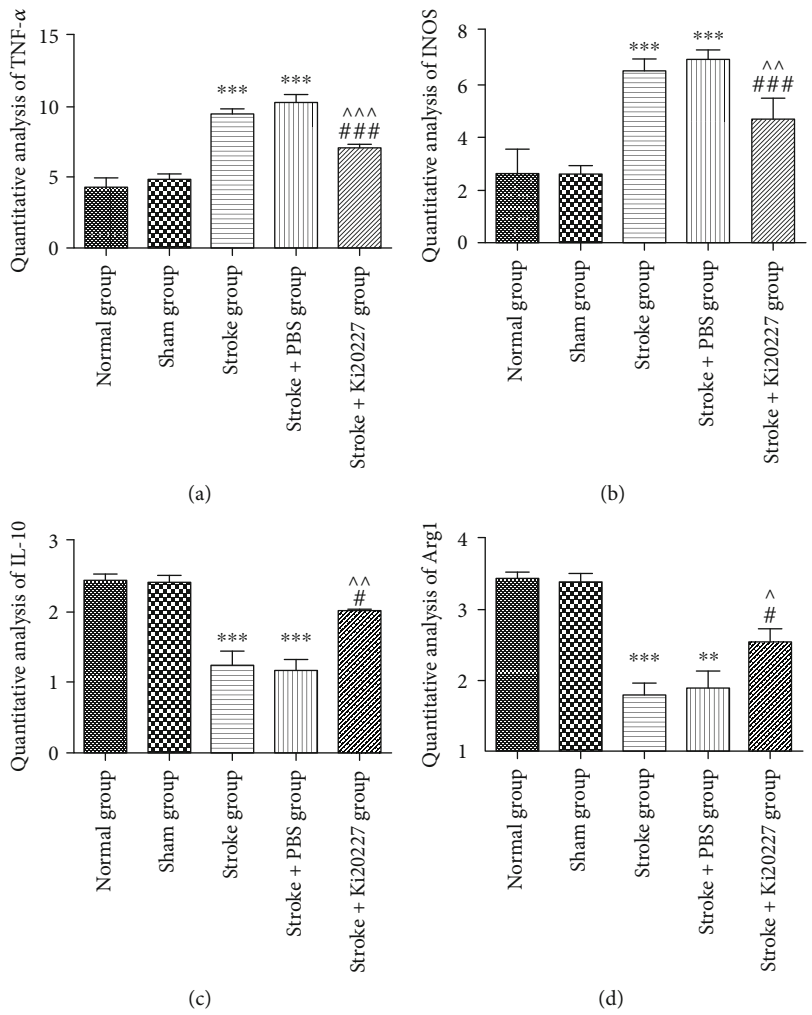

Figure 4: Ki20227 administration inhibited microglia M1 phenotype and activated M2 phenotype. Real-time PCR statistical analysis of (a) TNF-α, (b) iNOS, (c) IL-10, and (d) Arg-1 for normal, sham, stroke, stroke+PBS, and stroke+Ki20227 groups. Normal group vs. stroke group, $^{***}P < 0.001$; normal group vs. stroke+PBS group, $^{***}P < 0.001$; stroke+Ki20227 group vs. stroke group, $^{\#}P < 0.05$, $^{\#\#}P < 0.01$; stroke+PBS vs. stroke+Ki20227 groups, $^{\wedge}P < 0.05$, $^{\wedge\wedge}P < 0.01$, $^{\wedge\wedge\wedge}P < 0.001$.

Results revealed NLRP3 inflammasome was activated in the ischemic brain of stroke and stroke+PBS groups with high NLRP3 protein expression ($^{***}P < 0.001$). Ki20227 administration significantly prevented ischemia-induced NLRP3 expression when compared to stroke and stroke+PBS groups ($^{\#\#}P < 0.01$, $^{\wedge\wedge}P < 0.01$).

4. Discussion

In the present study, our results indicated that the Ki20227, as CSF1R inhibitor administration, could improve ischemia-induced behavioral deficits of mice and attenuate microglia-related inflammation, which is validated by the downregulation of mRNA expression in both microglia M1 phenotype factors and Iba1 protein expression, meanwhile, increase of microglia M2 phenotype expression shown as in Figure 7. The inhibition of NLRP3 pathway involved the neuroprotective mechanism of Ki20227 in ischemia stroke mice.

Once stroke occurs, the disruption of neural circuits including dysfunction between the different cell types could destructively affect the learning, memory, sensory, and motor abilities of mice [18]. Evaluating the behavioral performance of mice after stroke could reflect neural function injury and recovery. Meanwhile, reported data showed the upregulation of microglial-related protein is closely associated with repetitive behavior, social deficits, and synaptic dysfunction of mice. Treatment with colony-stimulating factor 1 receptor inhibitors that induced microglial depletion and repopulation could correct behavioral abnormalities by modulating neurogenic molecules in microglia [19]. Our results showed Ki20227 has no influence on the behavioral function when compared to normal group before building stroke model in Rat-Rot test. Meanwhile, animals showed significantly less time on the Rota-Rod test and higher neurological scores followed stroke. Using Ki20227 inhibitor in mice has an efficient effect to improve the behavioral function which is obviously showed through increasing the time on Rota-Rod and reducing behavioral defect score as well as decreasing Iba1 expression.

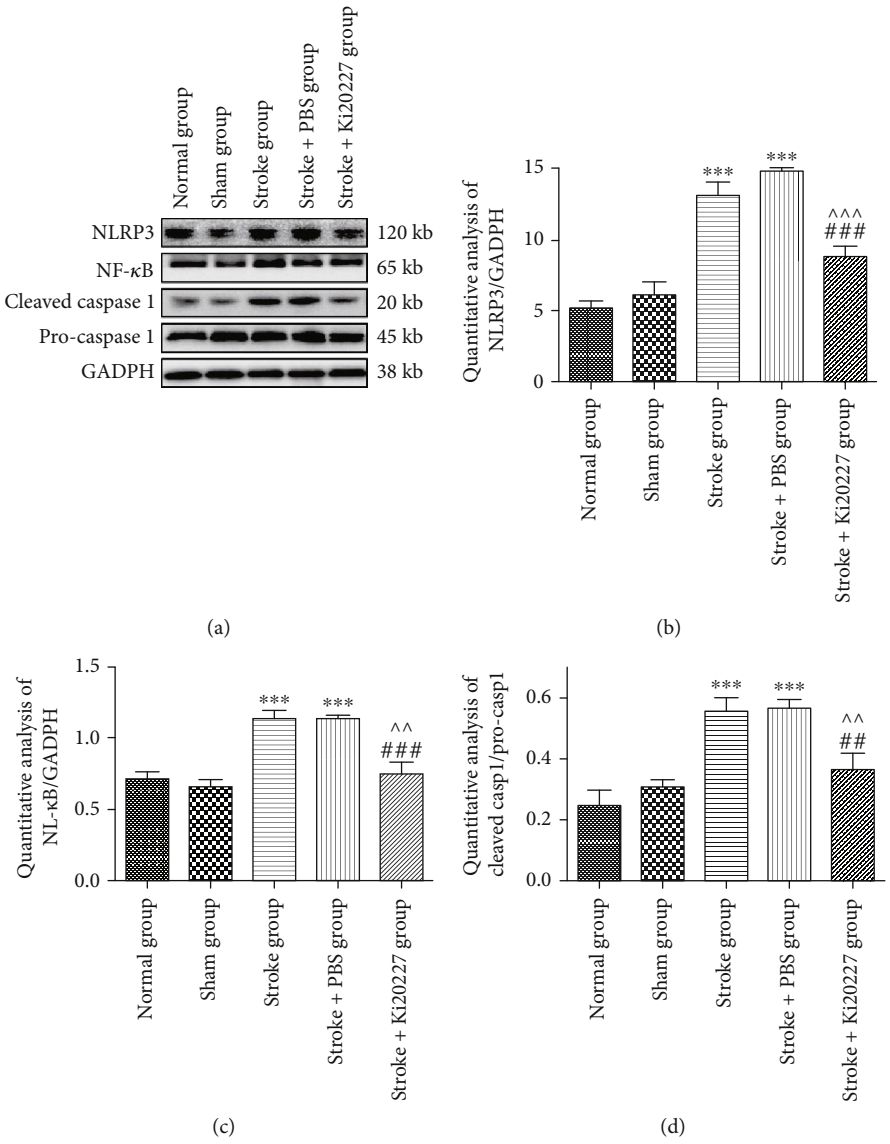

Figure 5: Ki20227 administration inhibited NLRP3 pathway activation. Western blot of (a) NLRP3, NF-κB, cleaved caspase 1, pro-caspase 1, and GADPH for normal, sham, stroke, stroke+PBS, and stroke+Ki20227 groups. Statistical analyses of (b) NLRP3, (c) NF-κB, and (d) cleaved caspase 1/pro-caspase 1. Normal group vs. stroke group, $^{***}P < 0.001$; normal group vs. stroke+PBS group, $^{***}P < 0.001$; stroke+Ki20227 group vs. stroke group, $^{\#\#}P < 0.01$, $^{\#\#\#}P < 0.001$; stroke+PBS vs. stroke+Ki20227 groups, $\wedge\wedge P < 0.01$, $\wedge\wedge\wedge P < 0.001$.

Microglial activation was initiated from hours after stroke and could develop in the next couple of days. The therapeutic intervention is presented with a much longer window for neuroprotection [20]. Some evidence demonstrated that the inflammation including microglia activation and the release of cytokines and trophic factors could reach the peak and exert significant role in the first few days after stroke [21]. In our previous studies, intracellular signal pathway including autophagy and inflammation significantly dysregulated at 24 hours after building middle cerebral artery occlusion (MCAO) model and could be revised by the drug administration. For example, triptolide exerted neuroprotection in cerebral ischemia stroke through downregulating NF-κB- and iNOS-induced inflammation and upregulating autophagy at the 24-hour timepoint after building MCAO model [17, 22]. In this study, we also did the detail experiment at the 24-hour timepoint after building stroke model. Meanwhile, microglia-related inflammatory responses take a critical part in the pathological processes of ischemia injury including microglia phenotype transformation and inflammatory factors release [1]. Numerous works indicated that activating microglia M1 phenotype response has a negative effect on the process of cerebral ischemia [23]. Inhibiting microglia M1 phenotype and activating M2 phenotype have a broad prospect in treating stroke [24]. In ischemic brain injury, the inflammatory response can prompt the massive release of microglia M1 factors such as TNF-α and iNOS [25]. Overexpression of TNF-α can aggravate brain injury, while the upregulation of iNOS expression will increase the nitric oxide (NO) synthesis and secretion, which in turn promotes the aggregation of microglia to the injury site. As a result, a toxic effect on the nervous system and an

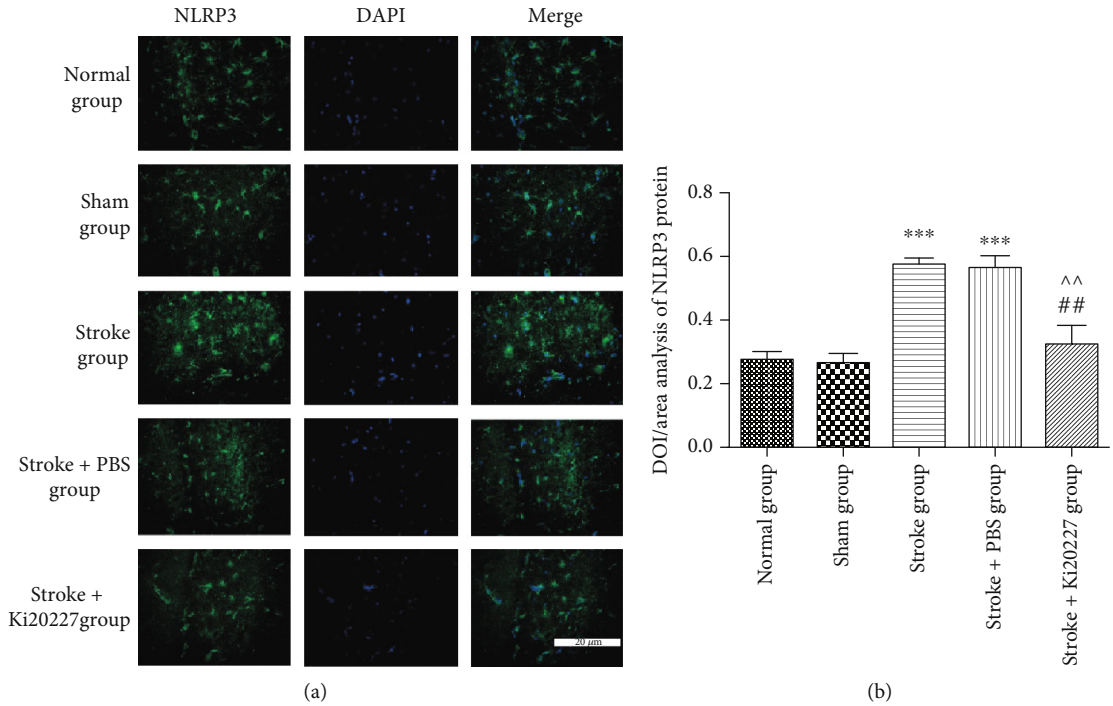

Figure 6: Ki20227 administration inhibited NLRP3 inflammasome activation. (a) NLRP3 protein in immunofluorescence staining is labeled with green fluorescence in normal, sham, stroke, stroke+PBS, and stroke+Ki20227 groups. Blue fluorescence represented and was labeled as cell nucleus. Positive cells are showed in merged pictures. Bar = 20 μm. (b) Results of Iba1 protein expression statistical analysis. Normal group vs. stroke group, $^{***}P < 0.001$; normal group vs. stroke+PBS group, $^{***}P < 0.001$; stroke+Ki20227 group vs. stroke group, $^{\#\#}P < 0.01$; stroke+PBS vs. stroke+Ki20227 groups, $\wedge\wedge P < 0.01$.

exacerbated brain injury might be occurred. Overexpression of S100B which is expressed in microglia could aggravate cerebral ischemia through activating NF-κB expression and inhibiting M2 stimuli expression to promote microglia M1 polarization [26]. Inhibited microglia M1 and activated M2 polarization by treating with curcumin and dihydrolipoic acid-gold nanoclusters prevents ischemic stroke and has the potency to ameliorate neurogenesis [27]. In this study, the expression of TNF-α and iNOS mRNA induced by focal cerebral ischemic injury was increased significantly, and the number of microglial cells at the injured site increased as well. The Ki20227 drug could effectively reduce Iba1 expression and inhibit microglia M1 factor expression (i.e., TNF-α and iNOS) expression. In the same manner, activating microglia M2 factor expression could improve the neuron connection of stroke mice along with reductions in elevated proinflammatory molecules and standardization of synaptophysin and PSD-95 expression [28, 29]. Moreover, IL-4 as cytokine anti-inflammatory factor could induce microglia M2 polarization including increasing IL-10, TGF-β, YM1, Arg-1, and IGF-1 secretion. This role might facilitate the reforming and regeneration of neurons through GSH and NGF upregulation and apoptosis inhibition [30]. Results showed a significant decrease of IL-10 and Arg-1 expression after ischemic injury of mice; meanwhile, the number of microglial cells at the injury site was increased. This implies that the Ki20227 drug can effectively increase microglia M2 factor IL-10 and Arg-1 expression.

NLRP3 inflammasome participated critical part in neuroimmune response including microglial-dependent activation [31]. This protein can be induced by various endogenous and exogenous danger signals and subsequently activate caspase 1. This action may promote the maturation and release of IL-1β and IL-18 [32]. In this regard, several previous studies have found that the activation of NLRP3 could increase the expression of inflammatory genes including NF-κB and TNF-α, which consisted with our results [33]. Recent findings demonstrated that NLRP3 inflammasome play a crucial role in regulating inflammatory responses in the pathological process of ischemic stroke. Not only that a growing number of studies have shown that the NLRP3 suppression serves as neuroprotective role in ischemia stroke through alleviating infarction volumes and neurovascular damages to improve ischemia outcomes [34]. Inhibited NLRP3 proteins using special antagonist attenuate brain injury and inflammation after hemorrhagic stroke [35]. Liu and his research team found that the NLRP3 inflammasome inhibitor provides a neuroprotection effect in stroke through TLR4/NF-κB/NLRP3 signaling pathway [36]. Genetic modulations of NLRP3 impression in the stroke animal model bring out significant protection against microglia-related inflammatory responses [37]. Moreover, gene silencing of microglia P2X7R or TMEM proteins reduced NLRP3 activation to attenuate brain edema and neurological deficits [38]. The link between microglia inflammatory signaling and NLRP3 activation was indicated by our results. CSF1R inhibitor could reduce the mRNA expression of TNF-α and

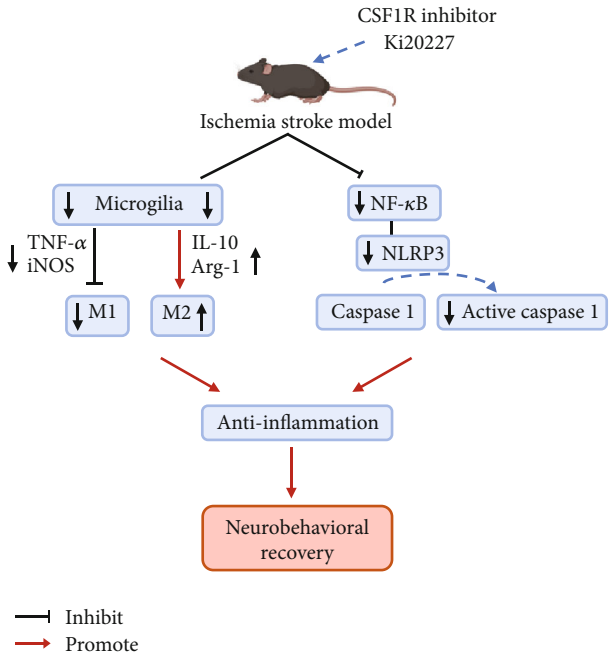

Figure 7: Illustrative mechanism for Ki20227 administration to alleviate the ischemic injury. Ki20227 treatment as CSF1R inhibitor could inhibit microglia number and improve behavioral deficits and attenuate microglia-related inflammation, which is verified by a reduction in both microglia M1 phenotype activation and Iba1 expression, meanwhile, increase of microglia M2 phenotype expression. The downregulation of the NLRP3 pathways and inflammasome activation involved the neuroprotective mechanism of CSF1R inhibitor in ischemia stroke.

protein expression of NF-κB and activate caspase 1 to inhibit the NLRP3 inflammasome activation.

The more widely held view is that the CSF1R signaling or CSF1R-dependent microglial signaling suppression would perform protective function for several diseases including cancer therapy, neurodegenerative disease, and ischemia stroke [39, 40]. A randomised phase 3 trial for tenosynovial giant cell tumour with aberrantly expressing colony-stimulating factor 1 (CSF1) showed pexidartinib as CSF1R inhibitor could improve patient symptoms and functional outcomes [41]. The underlying mechanism was indicated as the proinflammatory function activation of CSF1R signaling; however, CSF1R blockade antibody significantly minificated the inflammatory reaction and alleviated disease related symptoms [42]. In neurodegenerative disease, CSF1R signaling might activate proinflammatory processes through regulating CSF1 and IL34 signaling [43]. Inhibition of CSF1R signaling may provide an intervention approach or therapeutic due to the inhibition of the process of amyloid deposition formation at the very earliest stages of Alzheimer's disease [44]. It may be related with CSF1 participated in ameliorated memory deficits and regulated IL34 release to significantly reduce excitotoxic-induced neuronal loss [45]. In ischemia stroke, CSF1R expression upregulated with neuron death and behavioral deficit. Our results indicated Ki20227 exerted neuroprotective via improving ischemia-induced behavioral deficits and reducing the infarction volume. The inhibition of NLRP3 pathway and microglia-related factor release reduction could prove the neuroprotective role of CSF1R. The precise mechanism was also revealed that microglial density and survival were dependent on CSF1R signaling and inhibition of CSF1R in microglia contributed to the dendritic spines and neurons recovery in ischemia stroke [29].

Taken together our findings, Ki20227 takes the neuroprotective and anti-inflammatory roles via inhibiting microglia M1 phenotype and activating M2 polarization under NLRP3 inflammasome and NLRP3 signaling pathway inhibition in focal cerebral ischemia mice model. Hence, Ki20227 holds a promise as a promising drug target for clinical acute ischemia stroke patient therapy in the future.

5. Conclusion

The acute inflammatory reaction especially in microglia-mediated pathways displays an important role in regulating pathology processing after stroke. No theory has suggested a single pathway underlying stroke neuropathology to account for CSF1R inhibitor regulation on microglia. Besides, the effect of inhibited microglia in stroke is undefined. Our findings support that Ki20227 made neuroprotection through downregulating microglia M1 phenotype and NLRP3 pathways with microglia M2 phenotype activation to improving neuron behavioral recovery in stroke. Inhibited microglia CSF1R factor is indispensable in ischemic stroke to validate the evaluation of CSF1R inhibitors in clinical trials for ischemic brain diseases.

Data Availability

The data used to support the findings of this study are available from the corresponding author upon reasonable request.

Conflicts of Interest

The authors have declared no conflict of interest.

Authors' Contributions

Marong Fang and Xiaoxue Du designed the experiments. Xiaoxue Du drafted the manuscript and analyzed the data. Shijia Chen participated in the behavior test and study coordination. Xiaoxue Du and Yuzhen Xu are mainly responsible for polishing the article and manuscript editing and writing. Marong Fang is mainly responsible for obtained funding. All authors read and approved the final manuscript. Xiaoxue Du and Yuzhen Xu contributed equally to this work.

Acknowledgments

The National Natural Science Foundation of China to Marong Fang (grant numbers 81671138 and 81871063) supported this study. We extend our appreciation to Sanhua Fang and Daohui Zhang from the Core Facilities of Zhejiang University Institute of Neuroscience for their technical assistance, facilities, and support throughout this study.

References

[1] K. A. Zera and M. S. Buckwalter, "The local and peripheral immune responses to stroke: implications for therapeutic development," *Neurotherapeutics*, vol. 17, no. 2, pp. 414–435, 2020.

[2] A. Datta, D. Sarmah, L. Mounica et al., "Cell death pathways in ischemic stroke and targeted pharmacotherapy," *Translational Stroke Research*, 2020.

[3] N. Oosterhof, L. E. Kuil, H. C. van der Linde et al., "Colony-stimulating factor 1 receptor (CSF1R) regulates microglia density and distribution, but not microglia differentiation in vivo," *Cell Reports*, vol. 24, no. 5, pp. 1203–1217.e6, 2018, e6.

[4] A. Alawieh, E. F. Langley, and S. Tomlinson, "Targeted complement inhibition salvages stressed neurons and inhibits neuroinflammation after stroke in mice," *Science Translational Medicine*, vol. 10, no. 441, p. eaao6459, 2018.

[5] R. J. Henry, R. M. Ritzel, J. P. Barrett et al., "Microglial depletion with CSF1R inhibitor during chronic phase of experimental traumatic brain injury reduces neurodegeneration and neurological deficits," *The Journal of Neuroscience*, vol. 40, no. 14, pp. 2960–2974, 2020.

[6] M. L. Neal, S. M. Fleming, K. M. Budge et al., "Pharmacological inhibition of CSF1R by GW2580 reduces microglial proliferation and is protective against neuroinflammation and dopaminergic neurodegeneration," *The FASEB Journal*, vol. 34, no. 1, pp. 1679–1694, 2020.

[7] B. Hou, F. Ju, X. Guo et al., "Ki20227 influences the morphology of microglia and neurons through inhibition of CSF1R during global ischemia," *International Journal of Clinical and Experimental Pathology*, vol. 9, no. 12, pp. 12459–12469, 2016.

[8] A. Kumari, O. Silakari, and R. K. Singh, "Recent advances in colony stimulating factor-1 receptor/c-FMS as an emerging target for various therapeutic implications," *Biomedicine & Pharmacotherapy*, vol. 103, pp. 662–679, 2018.

[9] L. Freeman, H. Guo, C. N. David, W. J. Brickey, S. Jha, and J. P. Y. Ting, "NLR members NLRC4 and NLRP3 mediate sterile inflammasome activation in microglia and astrocytes," *The Journal of Experimental Medicine*, vol. 214, no. 5, pp. 1351–1370, 2017.

[10] S. J. Yang, G. F. Shao, J. L. Chen, and J. Gong, "The $NLRP_3$ inflammasome: an important driver of neuroinflammation in hemorrhagic stroke," *Cellular and Molecular Neurobiology*, vol. 38, no. 3, pp. 595–603, 2018.

[11] L. Q. Lu, J. Tian, X. J. Luo, and J. Peng, "Targeting the pathways of regulated necrosis: a potential strategy for alleviation of cardio-cerebrovascular injury," *Cellular and Molecular Life Sciences*, 2020.

[12] Q. Wang, W. Yang, J. Zhang, Y. Zhao, and Y. Xu, "TREM2 overexpression attenuates cognitive deficits in experimental models of vascular dementia," *Neural Plasticity*, vol. 2020, Article ID 8834275, 10 pages, 2020.

[13] Z. Liu, Y. Ran, S. Huang et al., "Curcumin protects against ischemic stroke by titrating microglia/macrophage polarization," *Frontiers in Aging Neuroscience*, vol. 9, p. 233, 2017.

[14] S. Wang, J. Wang, H. Wei et al., "Genistein attenuates acute cerebral ischemic damage by inhibiting the NLRP3 inflammasome in reproductively senescent mice," *Frontiers in Aging Neuroscience*, vol. 12, p. 153, 2020.

[15] Y. Hou, Y. Wang, Q. He et al., "Nrf2 inhibits NLRP3 inflammasome activation through regulating Trx1/TXNIP complex in cerebral ischemia reperfusion injury," *Behavioural Brain Research*, vol. 336, pp. 32–39, 2018.

[16] S. Demyanenko and A. Uzdensky, "Epigenetic alterations induced by photothrombotic stroke in the rat cerebral cortex: deacetylation of histone h3, upregulation of histone deacetylases and histone acetyltransferases," *International Journal of Molecular Sciences*, vol. 20, no. 12, p. 2882, 2019.

[17] Y. Yang, K. Gao, Z. Hu et al., "Autophagy upregulation and apoptosis downregulation in DAHP and triptolide treated cerebral ischemia," *Mediators of Inflammation*, vol. 2015, Article ID 120198, 2015.

[18] M. Wiesmann, N. M. Timmer, B. Zinnhardt et al., "Effect of a multinutrient intervention after ischemic stroke in female C57Bl/6 mice," *Journal of Neurochemistry*, vol. 144, no. 5, pp. 549–564, 2018.

[19] S. Ikezu, H. Yeh, J. C. Delpech et al., "Inhibition of colony stimulating factor 1 receptor corrects maternal inflammation-induced microglial and synaptic dysfunction and behavioral abnormalities," *Molecular Psychiatry*, 2020.

[20] J. H. Lee, Z. Z. Wei, W. Cao et al., "Regulation of therapeutic hypothermia on inflammatory cytokines, microglia polarization, migration and functional recovery after ischemic stroke in mice," *Neurobiology of Disease*, vol. 96, pp. 248–260, 2016.

[21] M. A. Yenari, T. M. Kauppinen, and R. A. Swanson, "Microglial activation in stroke: therapeutic targets," *Neurotherapeutics*, vol. 7, no. 4, pp. 378–391, 2010.

[22] W. Li, Y. Yang, Z. Hu, S. Ling, and M. Fang, "Neuroprotective effects of DAHP and triptolide in focal cerebral ischemia via apoptosis inhibition and PI3K/Akt/mTOR pathway activation," *Frontiers in Neuroanatomy*, vol. 9, p. 48, 2015.

[23] T. Zhang, D. Wang, X. Li et al., "Excess salt intake promotes M1 microglia polarization via a p38/MAPK/AR-dependent pathway after cerebral ischemia in mice," *International Immunopharmacology*, vol. 81, p. 106176, 2020.

[24] C. Rawlinson, S. Jenkins, L. Thei, M. L. Dallas, and R. Chen, "Post-ischaemic immunological response in the brain: targeting microglia in ischaemic stroke therapy," *Brain Sciences*, vol. 10, no. 3, p. 159, 2020.

[25] H. Wang, C. Liu, M. Han, C. Cheng, and D. Zhang, "TRAM1 promotes microglia M1 polarization," *Journal of Molecular Neuroscience*, vol. 58, no. 2, pp. 287–296, 2016.

[26] S. Zhou, W. Zhu, Y. Zhang, S. Pan, and J. Bao, "S100B promotes microglia M1 polarization and migration to aggravate cerebral ischemia," *Inflammation Research*, vol. 67, no. 11-12, pp. 937–949, 2018.

[27] L. Xiao, F. Wei, Y. Zhou et al., "Dihydrolipoic acid-gold nanoclusters regulate microglial polarization and have the potential to alter neurogenesis," *Nano Letters*, vol. 20, no. 1, pp. 478–495, 2020.

[28] Y. Tang and W. Le, "Differential roles of M1 and M2 microglia in neurodegenerative diseases," *Molecular Neurobiology*, vol. 53, no. 2, pp. 1181–1194, 2016.

[29] R. A. Rice, E. E. Spangenberg, H. Yamate-Morgan et al., "Elimination of microglia improves functional outcomes following extensive neuronal loss in the hippocampus," *The Journal of Neuroscience*, vol. 35, no. 27, pp. 9977–9989, 2015.

[30] Y. He, Y. Gao, Q. Zhang, G. Zhou, F. Cao, and S. Yao, "IL-4 switches microglia/macrophage M1/M2 polarization and alleviates neurological damage by modulating the JAK1/STAT6 pathway following ICH," *Neuroscience*, vol. 437, pp. 161–171, 2020.

[31] L. Gao, Q. Dong, Z. Song, F. Shen, J. Shi, and Y. Li, "NLRP3 inflammasome: a promising target in ischemic stroke," *Inflammation Research*, vol. 66, no. 1, pp. 17–24, 2017.

[32] P. Hong, R. N. Gu, F. X. Li et al., "NLRP3 inflammasome as a potential treatment in ischemic stroke concomitant with diabetes," *Journal of Neuroinflammation*, vol. 16, no. 1, p. 121, 2019.

[33] L. Minutoli, D. Puzzolo, M. Rinaldi et al., "ROS-mediated NLRP3 inflammasome activation in brain, heart, kidney, and testis ischemia/reperfusion injury," *Oxidative Medicine and Cellular Longevity*, vol. 2016, 2016.

[34] D. Y.-W. Fann, S.-Y. Lee, S. Manzanero et al., "Intravenous immunoglobulin suppresses NLRP1 and NLRP3 inflammasome-mediated neuronal death in ischemic stroke," *Cell Death & Disease*, vol. 4, no. 9, p. e790, 2013.

[35] H. Ren, Y. Kong, Z. Liu et al., "Selective NLRP3 (pyrin domain-containing protein 3) inflammasome inhibitor reduces brain injury after intracerebral hemorrhage," *Stroke*, vol. 49, no. 1, pp. 184–192, 2018.

[36] F. Y. Liu, J. Cai, C. Wang et al., "Fluoxetine attenuates neuroinflammation in early brain injury after subarachnoid hemorrhage: a possible role for the regulation of TLR4/MyD88/NF-κB signaling pathway," *Journal of Neuroinflammation*, vol. 15, no. 1, p. 347, 2018.

[37] T. Ishrat, I. N. Mohamed, B. Pillai et al., "Thioredoxin-interacting protein: a novel target for neuroprotection in experimental thromboembolic stroke in mice," *Molecular Neurobiology*, vol. 51, no. 2, pp. 766–778, 2015.

[38] S. Chen, Q. Ma, P. R. Krafft et al., "P2X7R/cryopyrin inflammasome axis inhibition reduces neuroinflammation after SAH," *Neurobiology of Disease*, vol. 58, pp. 296–307, 2013.

[39] M. A. Cannarile, M. Weisser, W. Jacob, A. M. Jegg, C. H. Ries, and D. Rüttinger, "Colony-stimulating factor 1 receptor (CSF1R) inhibitors in cancer therapy," *Journal for Immunotherapy of Cancer*, vol. 5, no. 1, p. 53, 2017.

[40] E. E. Spangenberg, R. J. Lee, A. R. Najafi et al., "Eliminating microglia in Alzheimer's mice prevents neuronal loss without modulating amyloid-beta pathology," *Brain*, vol. 139, no. 4, pp. 1265–1281, 2016.

[41] W. D. Tap, H. Gelderblom, E. Palmerini et al., "Pexidartinib versus placebo for advanced tenosynovial giant cell tumour (ENLIVEN): a randomised phase 3 trial," *Lancet*, vol. 394, no. 10197, pp. 478–487, 2019.

[42] S. Garcia, L. M. Hartkamp, B. Malvar-Fernandez et al., "Colony-stimulating factor (CSF) 1 receptor blockade reduces inflammation in human and murine models of rheumatoid arthritis," *Arthritis Research & Therapy*, vol. 18, no. 1, p. 75, 2016.

[43] J. Sosna, S. Philipp, R. Albay III et al., "Early long-term administration of the CSF1R inhibitor PLX3397 ablates microglia and reduces accumulation of intraneuronal amyloid, neuritic plaque deposition and pre-fibrillar oligomers in 5XFAD mouse model of Alzheimer's disease," *Molecular Neurodegeneration*, vol. 13, no. 1, p. 11, 2018.

[44] C. Domingues, "Impact of cytokines and chemokines on Alzheimer's disease neuropathological hallmarks," *Current Alzheimer Research*, vol. 14, no. 8, pp. 870–882, 2017.

[45] J. Luo, F. Elwood, M. Britschgi et al., "Colony-stimulating factor 1 receptor (CSF1R) signaling in injured neurons facilitates protection and survival," *The Journal of Experimental Medicine*, vol. 210, no. 1, pp. 157–172, 2013.

Hindawi
Neural Plasticity
Volume 2020, Article ID 8822579, 12 pages
https://doi.org/10.1155/2020/8822579

Research Article

Mesenchymal Stromal Cells Suppress Hippocampal Neuron Autophagy Stress Induced by Hypoxic-Ischemic Brain Damage: The Possible Role of Endogenous IL-6 Secretion

Miao Yang,[1,2,3,4] Wuqing Sun,[2,3,4,5] Lu Xiao,[1,2,3,4] Mulan He,[1,2,3,4] Yan Gu,[1,2,3,4] Ting Yang,[1,2,3,4] Jie Chen,[1,2,3,4] and Xiaohua Liang [1,2,3,4]

[1]*Children's Nutrition Research Center, Children's Hospital of Chongqing Medical University, Chongqing 400014, China*
[2]*Chongqing Key Laboratory of Child Nutrition and Health, Chongqing 400014, China*
[3]*Ministry of Education Key Laboratory of Child Development and Disorders, Chongqing 400014, China*
[4]*China International Science and Technology Cooperation Base of Child Development and Critical Disorders, Chongqing 400014, China*
[5]*Information Technological Service Center, Children's Hospital of Chongqing Medical University, Chongqing 400014, China*

Correspondence should be addressed to Xiaohua Liang; xiaohualiang@hospital.cqmu.edu.cn

Received 17 June 2020; Revised 17 July 2020; Accepted 28 July 2020; Published 28 August 2020

Academic Editor: Fushun Wang

Background. Increasing evidence has revealed that mesenchymal stromal cell (MSC) transplantation alleviates hypoxic-ischemic brain damage (HIBD) induced neurological impairments via immunomodulating astrocyte antiapoptosis effects. However, it remains unclear whether MSCs regulate neuron autophagy following HIBD. *Results*. In the present study, MSC transplantation effectively ameliorated learning-memory function and suppressed stress-induced hippocampal neuron autophagy in HIBD rats. Moreover, the suppressive effects of MSCs on autophagy were significantly weakened following endogenous IL-6 silencing in MSCs. Suppressing IL-6 expression also significantly increased p-AMPK protein expression and decreased p-mTOR protein expression in injured hippocampal neurons. *Conclusion*. Endogenous IL-6 in MSCs may reduce autophagy in hippocampal neurons partly through the AMPK/mTOR pathway.

1. Background

Hypoxic-ischemic brain damage (HIBD) in neonates may cause permanent brain damage, resulting in nervous system disability or even infantile mortality [1]. The hippocampus is easily damaged during the early stages of ischemia [2]. Necrosis, apoptosis, and autophagy are the main pathways of neuron death [3]. Recently, increased autophagy levels have been demonstrated following cerebral ischemia [4, 5]. It was reported that activation of autophagy after ischemia/reperfusion could be induced in neurons and astrocytes [6].

In the neuronal system, moderate autophagy is thought to be neuroprotective because it clears aggregated proteins associated with neurodegeneration, but both defective autophagy and excess autophagy may result in neuronal death [7–9]. More and more studies have demonstrated the involvement of autophagy in cerebral ischemic stroke; however, it remains unclear what effects transplanted mesenchymal stromal cells (MSCs) have on autophagy following ischemic cerebral injury.

Stem cells have potential biofunctions that induce tissue repair and regeneration. Numerous studies have demonstrated that MSC transplantation is neuroprotective in HIBD [10, 11]. MSCs could induce autolysosome formation and autophagy-dependent Aβ clearance in an Alzheimer's disease animal model to exert neuroprotective effects [12]. What is more, the results of our previous study indicated that IL-6 in the coculture medium was from MSCs, not injured neurons to play a neuroprotective role in HIBD rats [11].

Therefore, we speculated that the neuroprotective function of MSCs might partially regulate hippocampal autophagy in HIBD rats via IL-6 secretion. A series of experiments were designed to verify the above hypothesis. First, we evaluated the effects of MSCs on hippocampal neuron autophagy both *in vivo* and *in vitro*. Second, IL-6-silenced MSCs were used to verify the role of IL-6 in regulating autophagy. Finally, we tried to reveal the potential mechanisms of MSC-derived IL-6 to regulate hippocampal autophagy. This study may provide an experimental basis for the clinical application of MSCs.

2. Experimental Procedures

2.1. Animal Groups. Specific pathogen-free (SPF) grade Sprague Dawley (SD) rats (8 weeks old) were obtained from the Animal Center of Chongqing Medical University (Chongqing, China), and all animal experimental procedures followed the rules of the Animal Ethics Committee of Chongqing Medical University. The rats were fed in an SPF room at 25°C and 55-65% humidity with a 12 h light/dark cycle. At postnatal day 7, the pups were divided into a sham group ($n = 24$) and a HIBD group ($n = 76$) by the random number method. The HIBD group was subjected to HIBD injury as reported previously [13]. Briefly, the left carotid artery was ligated continuously, after two hours, the pups were then exposed to 8% oxygen at 37°C for 2.5 h. The pups in the sham group were subjected to only a cervical skin incision and subsequently sutured. The HIBD pups received intracerebroventricular transplants of 2×10^5 MSCs, siIL-6 MSCs, or GFP MSCs in 5 μl phosphate-buffered saline (PBS) (HyClone, USA) following HIBD for 30 min [14]. The intracerebroventricular injection was carried out 1.2 mm posterior to the bregma and 1.2 mm to the left of the lambdoid suture with a needle depth of 3.5 mm at a rate of 1 μl/min for 5 min. The needle was kept in place for 2 min and then withdrawn slowly. The HIBD pups were injected with the same volume of PBS as the transplant negative control group. All of the operative SD rats were anesthetized at a dose of 40 mg/kg (intraperitoneal injection), and the concentration of pentobarbital sodium was 2%. To collect fresh hippocampal tissue, the rats were deeply anesthetized with 20% urethane at a dose of 1 g/kg (intraperitoneal injection), while the rats were performed to euthanasia by inhalation of CO_2 at a 20% volume displacement per minute after the Morris water maze experiment.

2.2. Morris Water Maze. Four weeks after HIBD, the rats of the sham group ($n = 10$), the HIBD group ($n = 10$), and the HIBD+MSC group ($n = 10$) were evaluated for their spatial learning-memory functions with the Morris water maze task (MWM SLY-WMS 2.0, China) as previously described [15]. Briefly, the entire procedure was performed for six days. The first day, the rats' visual capabilities were assessed by visible platform tests, and from the 2nd to 5th days, the learning-memory function of the rats was trained with an invisible platform. On the 6th day, a probe trial was performed without the platform, and the number of times that the rats crossed the former platform location in 60 s was recorded.

2.3. Preparation of MSCs and Treatment. Primary MSCs were isolated from rats and amplified with plastic adherence methods. The rat siIL-6-transduced recombinant lentivirus was constructed by NeuronBiotech Co., Ltd. The 4 different shRNA sequences were designed (GR425, GR426, GR427, and GR428) in a vector expressing green fluorescent protein (GFP), and the control sequence (TTCTCCGAACGTGTCA CGT) served as a negative control (GFP MSCs) [16]. The siIL-6- and GFP-transduced recombinant lentiviruses were infected into the MSCs with virus titer of 3.47×10^8 and IL-6 concentration was decreased by 70-80% [11].

2.4. Primary Hippocampal Neuron Injury. Primary cultures of hippocampal neurons were prepared from SD rats at embryonic days 17-18. The hippocampal neurons were cultured for 5 days in an incubator with 5% CO_2 (Thermo, USA). For oxygen-glucose deprivation (OGD) injury, the hippocampal neurons were subjected to EBSS medium and exposed to 5% O_2/5% CO_2 for 1.5 h as described previously [17]; then, the EBSS was changed to standard neuronal culture medium. Cells cultured with standard neuronal culture medium in the presence of ambient (16%) O_2/5% CO_2 served as a control. The injured neurons were placed in Transwell inserts (Millipore, USA) for separate coculture with either (1) neural basal medium as a control or (2) MSCs subjected to the different treatments described above. After 12 h and 24 h, total protein was extracted using an extraction kit (BioTeke, China).

We found that the levels of Beclin 1 and LC3 II protein expressions were significantly increased in the rat hippocampus at 12-24 h following HIBD [18]. Meanwhile, OGD treatment upregulated autophagy-associated protein expression in primary neurons *in vitro* at 12 h.

2.5. Western Blotting. Total protein was extracted from the primary neurons and hippocampus for western blotting. The membranes were incubated in primary antibodies against Beclin 1 (1 : 1000, Abcam, USA), anti-LC3 II, anti-p62 (1 : 1000, Sigma, USA), anti-p-mTOR, anti-p-AMPK (1 : 1000, CST, USA), anti-IL-6 (1 : 500, R&D, China), and anti-β-actin (1 : 500, Santa Cruz, USA) at 4°C overnight. After incubation with HRP-conjugated secondary antibodies (Santa Cruz, USA) at room temperature for 1 h, the protein bands were developed using a chemiluminescent HRP substrate (Millipore, USA). Images were captured with a Syngene GBox Imaging System (Syngene, Europe Oxford, UK). The expression level of each protein was analyzed according to β-actin normalization.

2.6. Transmission Electron Microscopy. Primary neurons were digested with 0.1% trypsin and collected by centrifugation at 1200 rpm for 10 min. The neuron pellets were fixed in 4% glutaraldehyde and then postfixed in 1% osmium tetroxide. Following dehydration in a graded ethanol series, the samples were cut into ultrathin slices (40-60 nm thick), double stained with uranyl acetate and lead citrate, and observed by TEM (H-7500).

2.7. Statistical Analyses. Statistical analyses were performed using Statistical Product and Service Solutions 20 software.

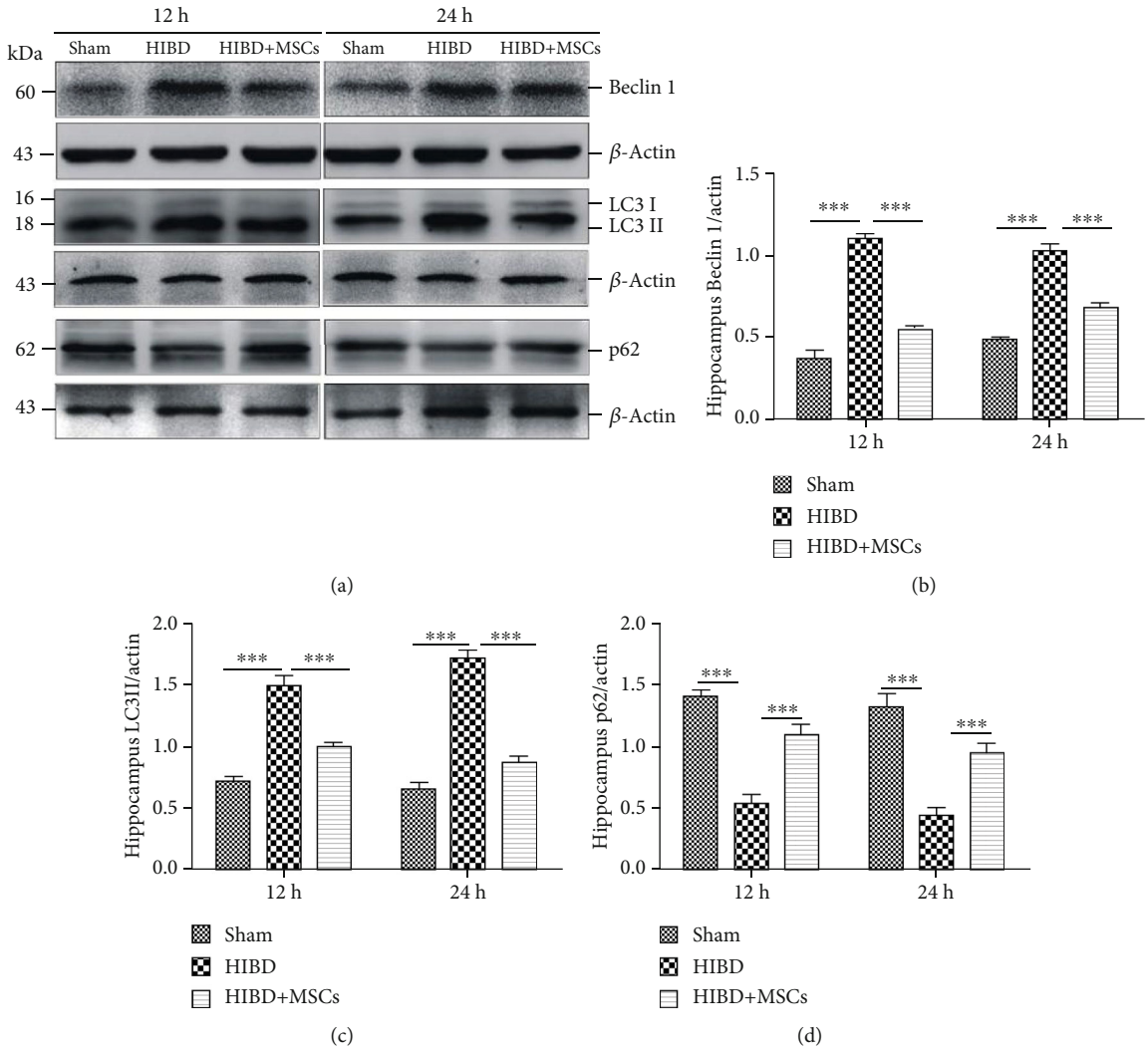

Figure 1: MSC transplantation reduced the expression levels of the autophagy-related proteins Beclin 1 and LC3 II and increased p62 expression levels in the hippocampus. (a) Representative western blots of Beclin 1, LC3 II, and p62 protein expressions in the hippocampus of the sham, HIBD, and HIBD+MSC groups following damage for 12 h and 24 h. (b–d) Quantification analysis of hippocampal protein expression levels normalized to β-actin. ($n = 7$, $^{**}P < 0.01$, $^{***}P < 0.001$).

The values are presented as the mean ± standard error of the mean (SEM). Each experiment was repeated at least three times and analyzed by Student's t-test or one-way ANOVA with the least significant difference post hoc test. The escape latencies of the rats in the three groups were determined using ANOVA for repeated measurement. The least significant difference test was used to compare the mean of two or more groups. $P < 0.05$ was considered statistically significant.

3. Results

3.1. MSC Transplantation Downregulates Hippocampal Autophagy. Beclin 1 is a positive regulator of autophagy, LC3 II can reflect autophagical activity, and p62 is one of the selective substrates for autophagy. To evaluate the effect of MSCs on autophagy in the hippocampal neurons of neonatal rats with HIBD, we measured the autophagy-related proteins Beclin 1, LC3 II, and p62 in the hippocampus 12 h and 24 h after MSC transplantation. As shown in Figures 1(a) and 1(b), MSC transplantation significantly decreased Beclin 1 expression levels in the hippocampus of HIBD rats, whereas these levels were markedly increased in HIBD rats. The changes in LC3 II expression levels were highly consistent with those of Beclin 1 (Figures 1(a) and 1(c)). However, the levels of p62 protein expression were significantly increased in the HIBD hippocampus at 12 h and 24 h after MSC transplantation (Figures 1(a) and 1(d)). The above results demonstrated that MSC transplantation may regulate the level of hippocampal autophagy.

3.2. MSC Transplantation Alleviates Cognitive Impairment in HIBD Rats. Impairment in learning-memory function is one of the major changes after HIBD. To confirm the effects of MSC transplantation on memory damage in HIBD rats, we conducted MWM tests. As shown in Figures 2(a) and 2(b), the escape latency and path length to locate the platform were

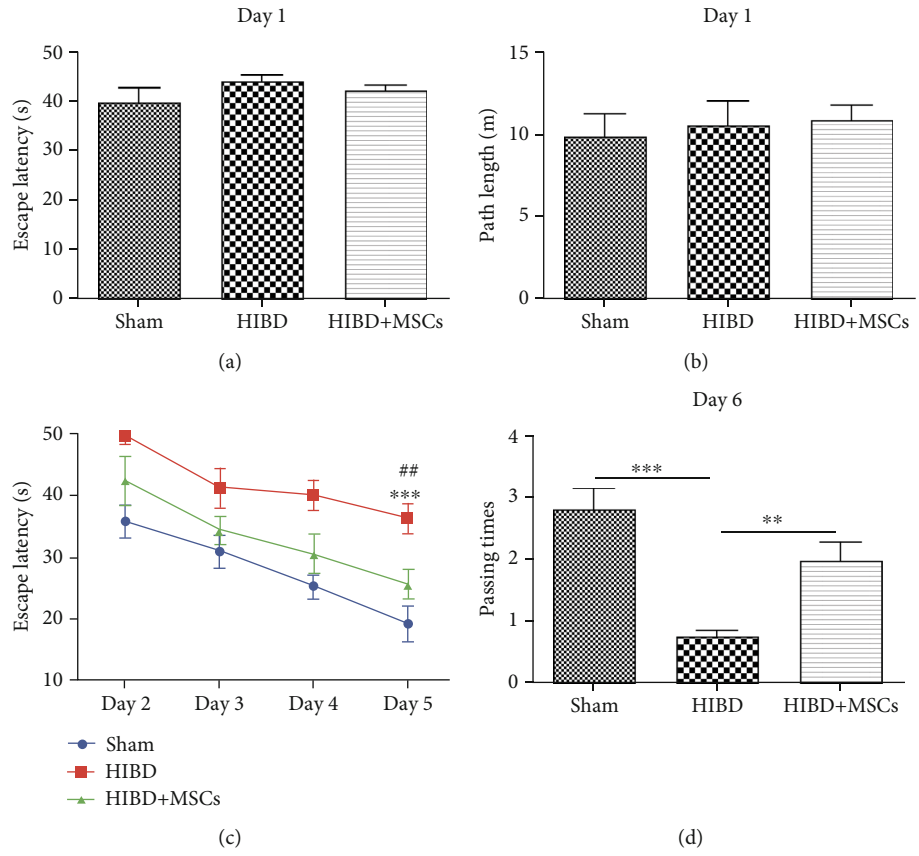

FIGURE 2: MSC transplantation improved the spatial learning-memory function of HIBD rats. (a, b) Escape latencies and path lengths to reach the visible platform for the sham, HIBD, and HIBD+MSC rats on the 1st day of the MWM test. (c) Escape latencies of each group to locate the invisible platform from the 2nd to the 5th day in the MWM test ($n = 10$, $^{***}P < 0.001$ vs. the sham group; $^{\#\#}P < 0.01$ vs. the HIBD+MSC group). (d) Number of times passing through the former platform region for each group on the 6th day of the MWM test ($n = 10$, $^{***}P < 0.001$ vs. the sham group; $^{**}P < 0.01$ vs. the HIBD+MSC group).

not significantly different among the sham, HIBD, and HIBD +MSC groups on the first day, which indicates that neither HIBD nor MSC transplantation affected the motility or vision of the rats. During the training period with the hidden platform from the 2nd to 5th day, the escape latencies decreased progressively for all groups. However, the rats in the HIBD+MSC group spent less time locating the platform than those in the HIBD group but more time than those in the sham group (Figure 2(c)). Pairwise comparisons between different treatment groups showed statistically significant differences ($^{***}P < 0.001$ vs. the sham group; $^{\#\#}P < 0.01$ vs. the HIBD+MSC group). The difference between days was significant ($^{***}P < 0.001$). There was no interaction between group and day ($P > 0.05$). In the spatial probe test on the 6th day, the number of times passed through the original platform region was higher for HIBD+MSC rats than for HIBD rats, which passed through the original platform region the least number of times among the three groups (Figure 2(d)). These results suggest that MSC transplantation may regulate the level of hippocampal autophagy to alleviate memory impairment in HIBD rats.

3.3. MSC Coculture Reduces Autophagy and Decreases the Autophagosome Number in Primary Hippocampal Neurons following OGD. To clarify the role of MSCs in regulating autophagy, we separately cocultured OGD-injured primary hippocampal neurons with MSCs. As shown in Figures 3(a)–3(d), OGD treatment obviously increased the Beclin 1 and LC3 II protein expression levels in primary neurons, while MSC-separated coculture significantly decreased Beclin 1 and LC3 II protein expression levels and induced p62 protein expression levels after OGD injury for 12 h and 24 h. These data were consistent with the changes *in vivo*. In addition, transmission electron microscopy was used to observe the numbers of autophagosomes in the OGD-damaged neurons following coculture with MSCs. The number of autophagosomes was significantly increased at 12 h and 24 h in the neurons with OGD injury. Interestingly, the increase in autophagosomes was decreased after separate MSC coculture (Figure 3(e)). The above results suggest that MSC-separated coculture could downregulate autophagy in neurons with OGD injury at the acute stage through paracrine secretion.

3.4. Silencing IL-6 Attenuated MSC Inhibition of Autophagy in OGD-Injured Neurons. Our previous study revealed that the neuroprotective function of MSCs was closely associated with IL-6 secretion and that siIL-6 lentivirus could effectively inhibit IL-6 release in MSCs [11]. To confirm the effect of endogenous IL-6 in MSCs on neuronal autophagy after

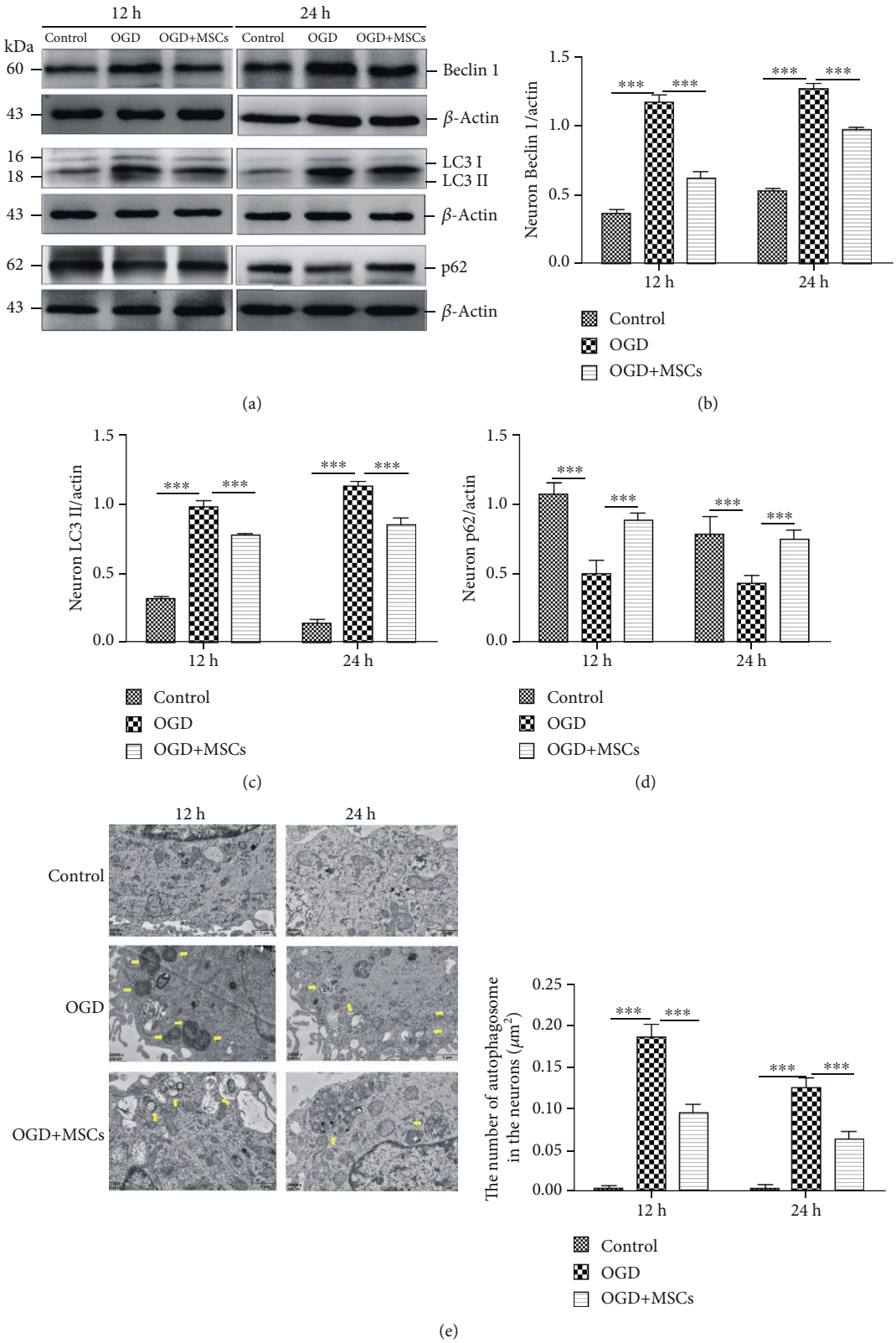

Figure 3: MSCs cocultured separately partly rescued the expression levels of the autophagy-associated proteins Beclin 1, LC3 II, and p62 and decreased the autophagosome numbers in primary hippocampal neurons with OGD injury. (a) Representative western blots of neuronal Beclin 1, LC3 II, and p62 protein expressions in the control, OGD, and OGD+MSC groups following injury for 12 h and 24 h. (b–d) Quantification analysis of the above protein expression levels normalized to β-actin in the primary neurons. (e) Number of autophagosomes in the neurons according to transmission electron microscopy (yellow arrows); quantification of the autophagosome numbers in the three groups. Scale bars = 2 μm ($n = 6$, $^{***}P < 0.001$).

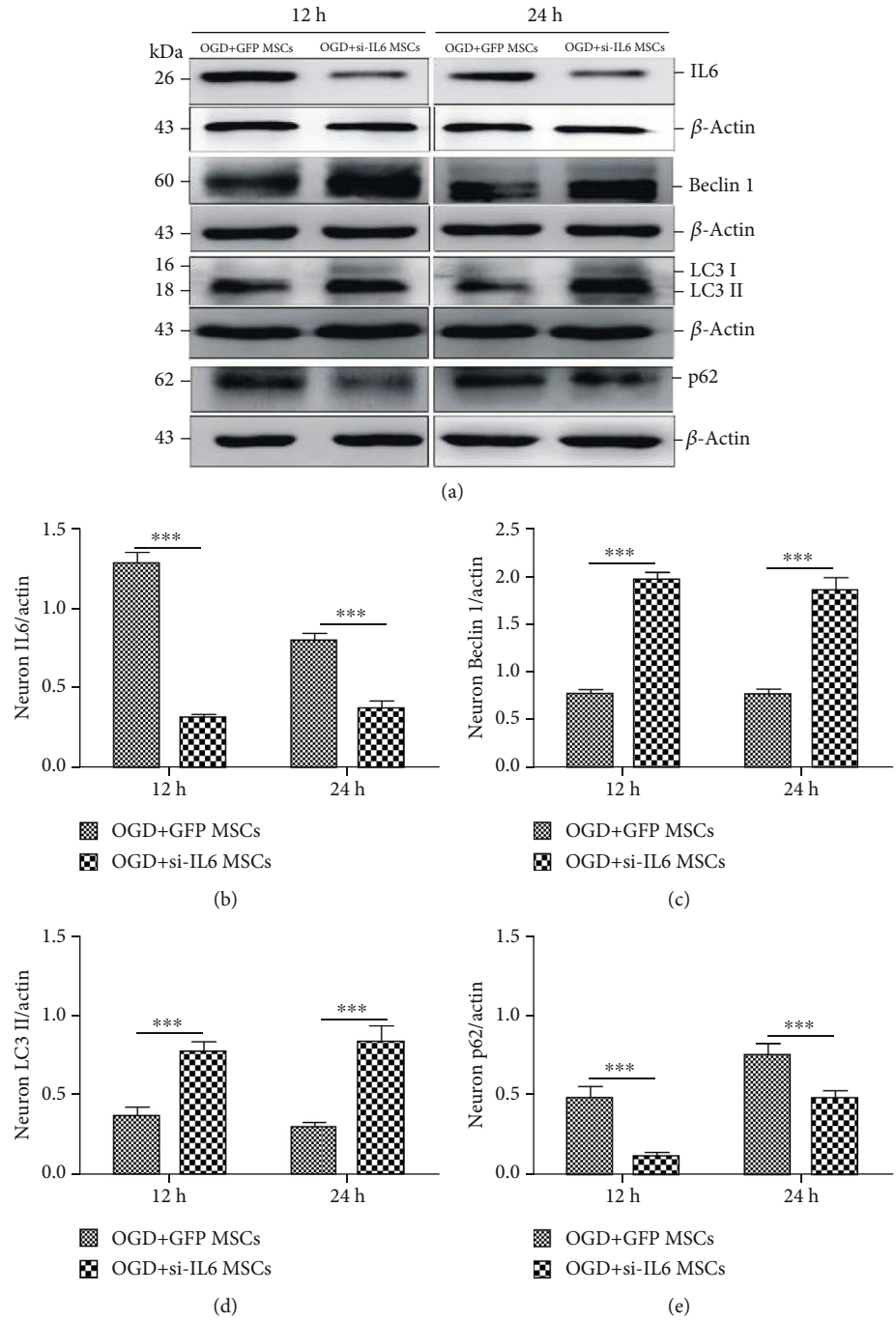

Figure 4: Continued.

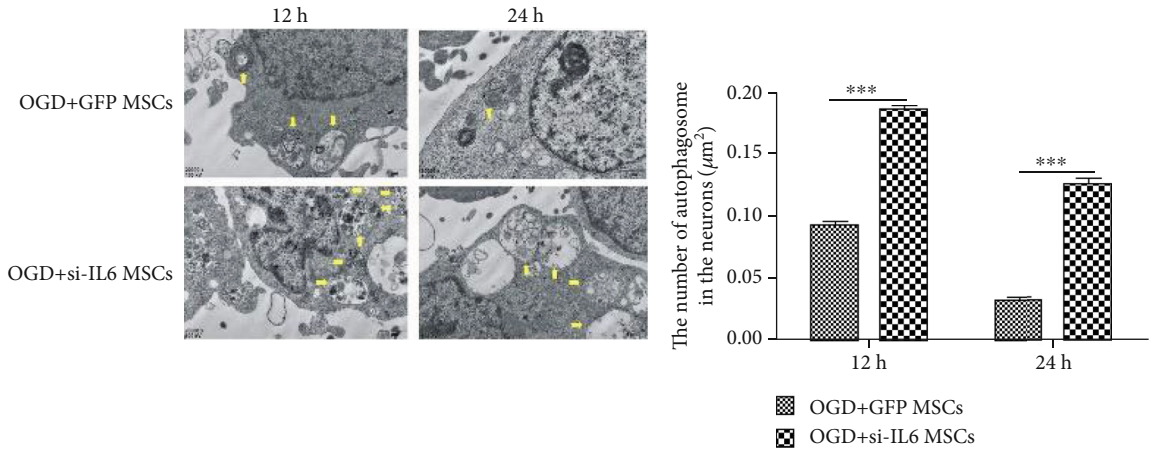

Figure 4: Separate siIL-6 MSC coculture increased Beclin 1 and LC3 II protein expression levels and reduced IL-6 and p62 protein expression levels, as well as increased the number of autophagosomes in hippocampal neurons injured by OGD, following damage for 12 h and 24 h. (a) Representative western blots of IL-6, Beclin 1, LC3 II, and p62 protein expression levels in the OGD-injured neurons cocultured with siIL-6 MSCs or GFP MSCs for 12 h and 24 h. (b–e) Quantification analysis of the neuron protein expression levels normalized to β-actin for the two groups. (f) Observation of autophagosomes in neurons from the two groups according to transmission electron microscopy (yellow arrows); quantification analysis of the autophagosome numbers in neurons from the two groups. Scale bars = 2 μm, ($n = 6$, $^{***}P < 0.001$).

injury, siIL-6 MSCs or GFP MSCs were cocultured with primary hippocampal neurons injured by OGD. As shown in Figures 4(a) and 4(b), the IL-6 levels at 12 h and 24 h after OGD were significantly lower in neurons with siIL-6 MSC-separated coculture than in those with GFP MSC coculture. Moreover, the expression levels of Beclin 1 and LC3 II were significantly higher in the OGD-damaged neurons following coculture with siIL-6 MSCs, and the p62 protein expression levels were significantly decreased (Figures 4(c)–4(e)). However, the number of autophagosomes at 12 h and 24 h was significantly increased in the siIL-6 MSC group compared with the GFP MSC group (Figure 4(f)). These results demonstrate that IL-6 secreted from MSCs could regulate autophagy in OGD-damaged neurons.

3.5. siIL-6 MSC Transplantation Weakened the Suppressive Effects of MSCs on Autophagy in the Hippocampus of HIBD Rats. When IL-6 expression levels were significantly decreased in the rat hippocampus following siIL-6 MSC transplantation (Figures 5(a) and 5(b)), the changes in Beclin 1, LC3 II, and p62 protein expressions completely mirrored the *in vitro* results (Figures 5(c)–5(e)). The results *in vivo* and *in vitro* indicate that endogenous IL-6 from MSCs can regulate autophagy in HIBD hippocampus neurons during the acute phase.

3.6. Effect of siIL-6 MSC Transplantation on AMPK/mTOR Signaling in the Rat Hippocampus after HIBD. Furthermore, to explore the possible mechanism of IL-6-mediated autophagy, we investigated the AMPK/mTOR signaling pathway, which is downstream of IL-6 and involved in autophagy. Hippocampal p-AMPK protein expression levels were significantly increased, and p-mTOR protein expression levels were significantly reduced in the HIBD+siIL-6 MSC group compared with the HIBD+GFP MSC group (Figures 6(a)–6(c)). Similarly, p-AMPK expression levels were significantly higher, and p-mTOR levels were significantly lower in the OGD+siIL-6 MSC group than in the OGD+GFP MSC group (Figures 6(d)–6(f)). The above results suggest that IL-6 secretion from MSCs may inhibit the AMPK/mTOR signaling pathway to regulate autophagy in HIBD hippocampal neurons.

4. Discussion

The present study investigated whether MSCs regulate autophagy in hippocampal neurons to alleviate the learning-memory impairment of HIBD rats through endogenous IL-6 secretion. The current study demonstrated that IL-6 from MSCs reduced neuron autophagy by suppressing the AMPK/mTOR signaling pathway. This effect consequently improved the learning-memory function in HIBD rats.

Increasing evidence indicates that MSCs have potent therapeutic benefits for functional recovery after brain damage [11, 19], which improved overall neurobehavioral in both sensorimotor and cognitive testing [20]. In the present study, we also revealed that MSC transplantation ameliorated the learning-memory deficit in HIBD rats. The potential mechanisms of the MSC-induced neuroprotective effects following brain injury include cell replacement, trophic support from MSCs, immunomodulation, and endogenous brain restoration stimulation. An increasing number of studies have indicated the immunomodulatory function of MSCs in the damaged microenvironment after HIBD [19, 21, 22]. Some studies have shown that MSCs display neurorestorative effects through enhancing autolysosome formation to induce Aβ clearance in Aβ-treated AD models [12] or modulating a-synuclein expression in neurotoxin-treated Parkinson's disease (PD) models [23]. These findings suggest that MSCs play a protective role by regulating autophagy following

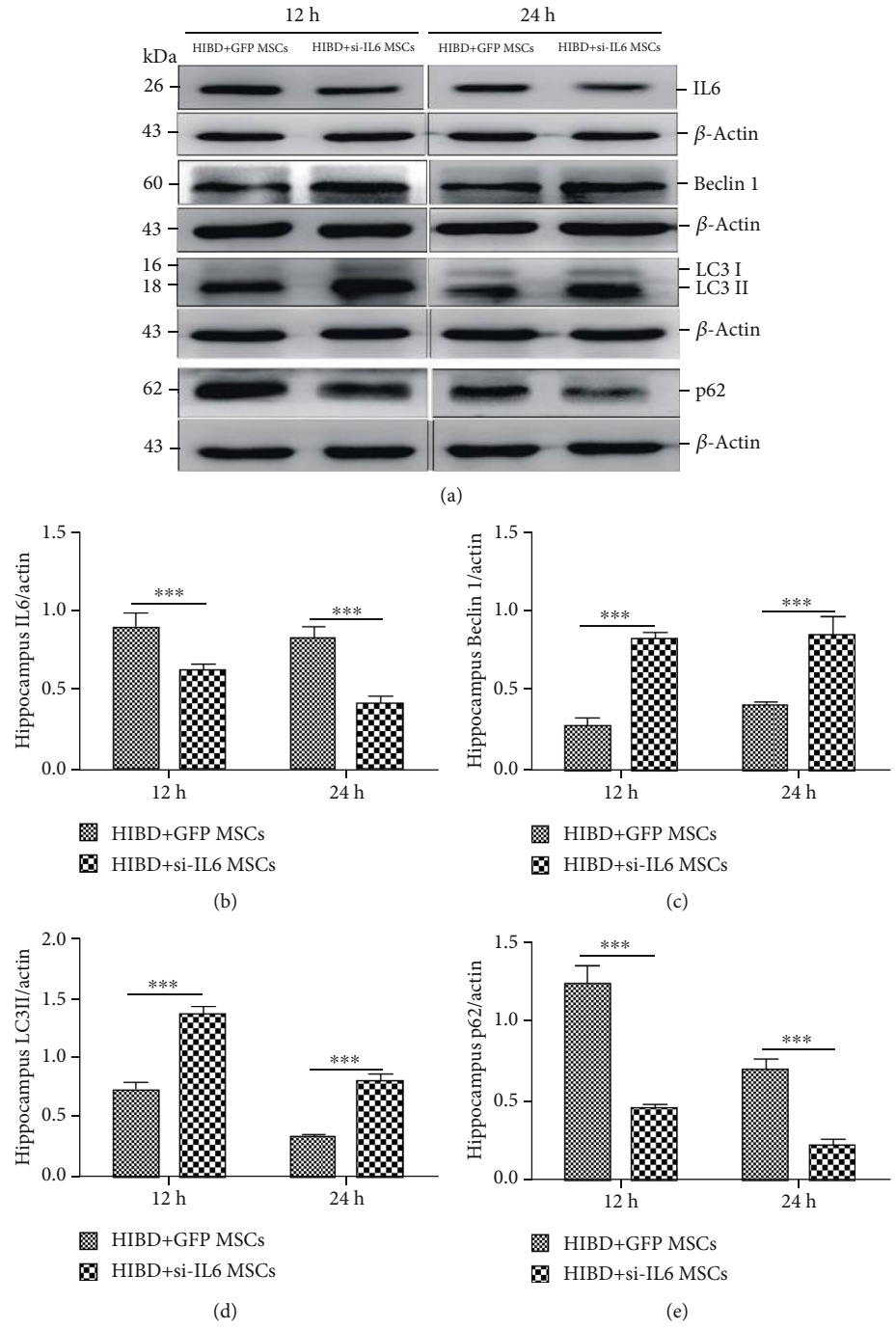

Figure 5: siIL-6 MSC transplantation impaired the effects of MSCs on Beclin 1, LC3 II, and p62 protein expression levels at 12 and 24 h after HIBD injury. (a) Representative western blots of hippocampal IL-6, Beclin 1, LC3 II, and p62 in HIBD rats following siIL-6 MSCs or GFP MSC transplantation for 12 h and 24 h. (b–e) Quantification analysis of hippocampal protein expression levels normalized to β-actin ($n = 7$, $^{***}P < 0.001$).

injury, but autophagy regulation by MSCs in the hippocampal neurons of neonatal rats with HIBD has rarely been reported. According to our results, both MSC transplantation and separate coculture ameliorated the increased Beclin 1 and LC3 II expression levels and the decreased p62 protein levels induced by HIBD or OGD damage. Additionally, the number of autophagosomes in the neurons with OGD injury was reduced at the acute stage by MSCs coculture. Our results strongly indicate that MSCs suppress hippocampal neuron autophagy in HIBD rats, in contrast to the reports by Shin et al. and Park et al. [12, 23]. This difference is due to the different disease models, experimental animal ages, insult severity, ischemia stages, and autophagy degrees. Both PD and AD are chronic diseases of the nervous system, but the model used in our study is neonatal HIBD, which is an acute brain injury disease in the neonatal period.

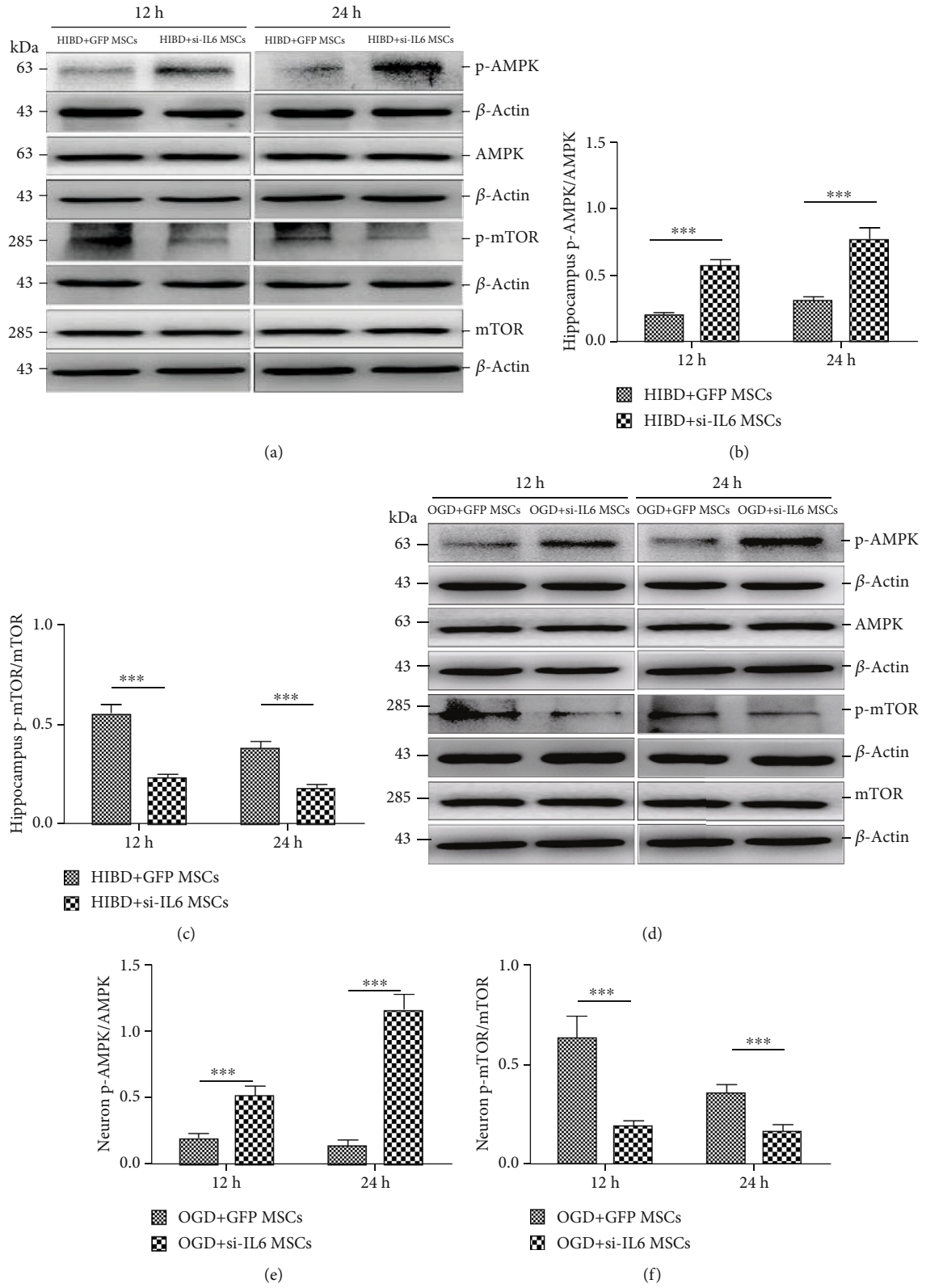

Figure 6: siIL-6 MSC transplantation increased hippocampal neuron p-AMPK protein expression levels and decreased p-mTOR levels following damage for 12 h and 24 h. (a) Representative western blots of hippocampal p-AMPK, AMPK, p-mTOR, and mTOR protein expression levels in the HIBD+siIL-6 MSC and HIBD+GFP MSC groups. (b, c) The ratio of p-AMPK/AMPK and p-mTOR/mTOR protein expression levels in the hippocampus ($n = 7$, $^{***}P < 0.001$). (d) Representative western blots of the p-AMPK, AMPK, p-mTOR, and mTOR protein expression levels in the OGD+siIL-6 MSC and OGD+GFP MSCs group. (e, f) The ratio of p-AMPK/AMPK and p-mTOR/mTOR protein expression levels in the two groups ($n = 6$, $^{***}P < 0.001$).

In our previous study, we found that both transplanting MSCs and coculture *in vitro* could facilitate IL-6 release into the injured microenvironment. It was also shown that IL-6 in the damaged hippocampal microenvironment was primarily due to MSC transplantation, even though the IL-6 concentration was slightly increased after HIBD [11]. In the central nervous system (CNS), the IL-6 secretion level is low under normal conditions but is significantly induced under disease conditions [24]. However, the role of IL-6 in the damaged brain is controversial. IL-6 upregulation might increase harmful factors and mediate inflammatory cascades to effect the vascular endothelium and exacerbate cerebral ischemic damage [25]. However, IL-6 facilitates posttraumatic healing of the CNS via enhancing angiogenesis [26]. Both *in vivo* and *in vitro* results revealed that blocking IL-6 in MSCs significantly increases the levels of the autophagy-associated proteins Beclin 1 and LC3 II in both HIBD rat hippocampi and OGD-injured neurons; IL-6 silencing also reduced p62 protein expression levels. Moreover, the number of autophagosomes was significantly increased in the OGD-injured neurons following separate coculture with siIL-6 MSCs. These results are consistent with the findings of Chang et al. and Delk and Farach-Carson [27, 28], which demonstrate that endogenous IL-6 from MSCs can regulate hippocampal neuron autophagy following HIBD.

Mammalian AMPK has been confirmed to be a downstream target of IL-6. IL-6 can suppress mTOR, which is a pivotal factor in the autophagic signaling pathway, in an AMPK-dependent and STAT3-independent manner [29]. Under physiological and disease conditions, AMPK is activated by increased AMP and/or decreased ATP in the cytoplasm [30]. In this study, we found that IL-6 suppression significantly increased p-AMPK protein expression levels after siIL-6 MSC transplantation or coculture, suggesting that IL-6 in the damaged microenvironment can negatively regulate AMPK phosphorylation levels. Therefore, we speculated that IL-6 may inhibit the nonclassical AMPK pathway via the gp130-IL-6R receptor complex [27]. However, the details of this molecular mechanism require further study. mTOR is negatively regulated by AMPK signaling and plays multiple biological functions in the CNS, particularly in autophagy [31]. A decrease in the ATP concentration during ischemia activates AMPK, which subsequently suppresses mTOR activity to induce autophagy [32]. Our *in vivo* and *in vitro* observations indicate that phospho-mTOR protein expression levels were significantly decreased by siIL-6 MSCs. These results indicate that silencing IL-6 can suppress mTOR phosphorylation levels through p-AMPK activation. Active AMPK leads to the phosphorylation and activation of TSC1/2 and the inhibition of mTORC1 activity through Rheb [33]. The above findings demonstrate that MSCs suppress autophagy in hippocampal neurons to ameliorate the functional outcomes of HIBD, and this neuroprotective effect may partly involve the biofunction of endogenous IL-6 to reduce the AMPK/mTOR signaling pathway.

In the current study, we demonstrate the biological effect of endogenous IL-6 of mesenchymal stem cell on hippocampal autophagy after HIBD injury. Combined with our previous finding of IL-6 in MSCs facilitating antiapoptosis of injured astrocytes [11], we can conclude that MSC transplantation regulates injured microenvironment to ameliorate learning-memory dysfunction through both repressing neuron autophagy and enhancing antiapoptosis of astrocytes. Of course, our study had some limitations. The experimental data was mainly displayed in western blotting, no combined with the results of IHC or IF to confirm the regional change after injury with or without MSCs treatment, because the hypothesis of the present study was whether endogenous IL-6 of mesenchymal stem cell could suppress on hippocampal neuron autophagy after HIBD injury, rather than the localization of autophagy. Therefore, at first, we measured the levels of autophagy-associated protein expressions in the hippocampus of rats following HIBD with or without MSCs transplantation, as well as in the hippocampal neurons after OGD with or without MSCs coculture. Secondly, the autophagosomes were observed in the hippocampal primary neurons injured by OGD with or without MSCs or siIL-6-MSC coculture by transmission electron microscopy. In fact, autophagy occurs in all parts of the brain during the acute stage of HIBD injury, while our study only focused on hippocampal neuronal autophagy.

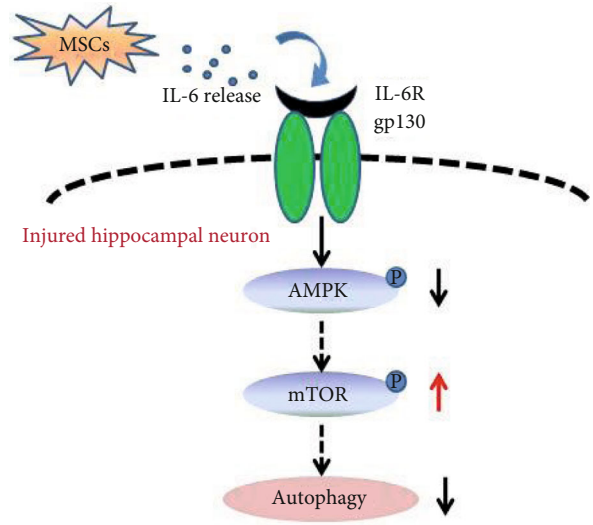

Figure 7: Summary diagram showing the role of IL-6 from MSCs in regulating hippocampal neuron autophagy in HIBD rats. In the current study, IL-6 from MSCs decreased p-AMPK protein expression levels to activate mTOR pathway phosphorylation, which in turn downregulated autophagy in the damaged hippocampal neurons.

5. Conclusion

This study revealed for the first time that endogenous IL-6 in MSCs may suppress autophagy in hippocampal neurons through inhibiting the AMPK/mTOR signaling pathway (Figure 7).

Abbreviations

HIBD: Hypoxic-ischemic brain damage
OGD: Oxygen and glucose deprivation

MSCs: Mesenchymal stromal cells
IL-6: Interleukin-6
Beclin-1: Homologue of yeast Atg6
LC3: Microtubule-associated protein 1 light chain 3
P62: Sequestosome 1, SQSTM1
p-mTOR: Phospho-mammalian target of rapamycin
p-AMPK: Phospho-mammalian AMP-activated protein kinase
SD rats: Sprague Dawley rats
SPF: Specific pathogen-free
PBS: Phosphate-buffered saline
SEM: Standard error of the mean
ANOVA: One-way analysis of variance.

Data Availability

The data used to support the findings of this study were supplied by Miao Yang and cannot be made freely available. Requests for access to these data should be made to [Miao Yang, 916844839@qq.com].

Ethical Approval

All authors have read the journal's position on issues regarding ethical publication, and all authors have approved the final version of the manuscript. Ethical approval was received for the use of animals. All procedures performed in studies involving animals were in accordance with the ethical standards of the institution (Animal Care and Use Committee of Chongqing Medical University SCXK (Yu) 2012-0015).

Conflicts of Interest

The authors declare that the research was conducted in the absence of any commercial or financial relationships that could be construed as a potential conflict of interest.

Authors' Contributions

All authors contributed substantially to the conception and design of the study and to the critical review of the manuscript. MY performed the experiments and analyzed the data. WS analyzed the data. LX, MH, and YG provided technical guidance. MY, WS, and JC wrote the manuscript. JC designed the study. JC and XL provided financial support for the study. All authors read and approved the final manuscript. Miao Yang and Wuqing Sun are the co-first authors.

Acknowledgments

We thank Professors Jie Chen and Xiaohua Liang for providing financial support, and we thank all authors for their contributions to this study. This work was supported in part by a grant to Jie Chen from the National Natural Science Foundation of China (81271385) for the treatment of rats and primary hippocampal neurons and the performance of all experiments. Publication costs are funded by a grant to Jie Chen from the Stem Cell Therapy for Special Study of the Children's Hospital of Chongqing Medical University (SCT-201203). The funder designed the experiment and provided financial support for this research.

References

[1] T. Yasuhara, N. Matsukawa, G. Yu et al., "Behavioral and histological characterization of intrahippocampal grafts of human bone marrow-derived multipotent progenitor cells in neonatal rats with hypoxic-ischemic injury," *Cell Transplantation*, vol. 15, no. 3, pp. 231–238, 2017.

[2] K. A. Allen and D. H. Brandon, "Hypoxic ischemic encephalopathy: pathophysiology and experimental treatments," *Newborn and Infant Nursing Reviews*, vol. 11, no. 3, pp. 125–133, 2011.

[3] M. A. Moskowitz, E. H. Lo, and C. Iadecola, "The science of stroke: mechanisms in search of treatments," *Neuron*, vol. 67, no. 2, pp. 181–198, 2010.

[4] F. Adhami, A. Schloemer, and C. Y. Kuan, "The roles of autophagy in cerebral ischemia," *Autophagy*, vol. 3, no. 1, pp. 42–44, 2014.

[5] M. Koike, M. Shibata, M. Tadakoshi et al., "Inhibition of autophagy prevents hippocampal pyramidal neuron death after hypoxic-ischemic injury," *The American Journal of Pathology*, vol. 172, no. 2, pp. 454–469, 2008.

[6] F. Tian, K. Deguchi, T. Yamashita et al., "In vivo imaging of autophagy in a mouse stroke model," *Autophagy*, vol. 6, no. 8, pp. 1107–1114, 2014.

[7] E. Wong and A. M. Cuervo, "Autophagy gone awry in neurodegenerative diseases," *Nature Neuroscience*, vol. 13, no. 7, pp. 805–811, 2010.

[8] R. A. Nixon, "Autophagy in neurodegenerative disease: friend, foe or turncoat," *Trends in Neurosciences*, vol. 29, no. 9, pp. 528–535, 2006.

[9] R. Banerjee, M. F. Beal, and B. Thomas, "Autophagy in neurodegenerative disorders: pathogenic roles and therapeutic implications," *Trends in Neurosciences*, vol. 33, no. 12, pp. 541–549, 2010.

[10] A. W. Phillips, M. V. Johnston, and A. Fatemi, "The potential for cell-based therapy in perinatal brain injuries," *Translational Stroke Research*, vol. 4, no. 2, pp. 137–148, 2013.

[11] Y. Gu, M. He, X. Zhou et al., "Endogenous IL-6 of mesenchymal stem cell improves behavioral outcome of hypoxic-ischemic brain damage neonatal rats by supressing apoptosis in astrocyte," *Scientific Reports*, vol. 6, no. 1, article 18587, 2016.

[12] J. Y. Shin, H. J. Park, H. N. Kim et al., "Mesenchymal stem cells enhance autophagy and increase β-amyloid clearance in Alzheimer disease models," *Autophagy*, vol. 10, no. 1, pp. 32–44, 2013.

[13] J. E. Rice, R. C. Vannucci, and J. B. Brierley, "The influence of immaturity on hypoxic-ischemic brain damage in the rat," *Annals of Neurology*, vol. 9, no. 2, pp. 131–141, 1981.

[14] Y. Bi, M. Gong, Y. He et al., "AP2α transcriptional activity is essential for retinoid-induced neuronal differentiation of mesenchymal stem cells," *The International Journal of Biochemistry & Cell Biology*, vol. 46, pp. 148–160, 2014.

[15] R. Morris, "Developments of a water-maze procedure for studying spatial learning in the rat," *Journal of Neuroscience Methods*, vol. 11, no. 1, pp. 47–60, 1984.

[16] M. L. He, J. J. Liu, Y. Gu, T. Y. Li, J. Chen et al., "Effects of inhibiting secretion of mesenchymal stromal cellss originated interleukin-6 on oxygen glucose deprivation injured PC12 cells," *Journal of Shanghai Jiao Tong University Medical Science*, vol. 34, pp. 1435–1447, 2014.

[17] J. L. M. Madrigal, C. D. Russo, V. Gavrilyuk, and D. L. Feinstein, "Effects of noradrenaline on neuronal NOS2 expression and viability," *Antioxidants & Redox Signaling*, vol. 8, no. 5-6, pp. 885–892, 2006.

[18] M. Yang, M. L. He, Y. Gu, T. Yang, T. Y. Li, J. Chen et al., "The modulation of mesenchymal stromal cells transplantation on autophagy in hippocampus of hypoxic-ischemic brain damage rats," *Journal of Shanghai Jiao Tong University Medical Science*, vol. 37, pp. 1608–1615, 2014.

[19] C. T. J. van Velthoven, A. Kavelaars, F. van Bel, and C. J. Heijnen, "Mesenchymal stem cell treatment after neonatal hypoxic-ischemic brain injury improves behavioral outcome and induces neuronal and oligodendrocyte regeneration," *Brain, Behavior, and Immunity*, vol. 24, no. 3, pp. 387–393, 2010.

[20] J. Archambault, A. Moreira, D. McDaniel, L. Winter, L. Z. Sun, and P. Hornsby, "Therapeutic potential of mesenchymal stromal cells for hypoxic ischemic encephalopathy: a systematic review and meta-analysis of preclinical studies," *PLoS One*, vol. 12, no. 12, article e0189895, 2017.

[21] C. T. J. van Velthoven, R. A. Sheldon, A. Kavelaars et al., "Mesenchymal stem cell transplantation attenuates brain injury after neonatal stroke," *Stroke*, vol. 44, no. 5, pp. 1426–1432, 2013.

[22] C. T. van Velthoven, A. Kavelaars, F. van Bel, and C. J. Heijnen, "Repeated mesenchymal stem cell treatment after neonatal hypoxia-ischemia has distinct effects on formation and maturation of new neurons and oligodendrocytes leading to restoration of damage, corticospinal motor tract activity, and sensorimotor function," *The Journal of Neuroscience*, vol. 30, no. 28, pp. 9603–9611, 2010.

[23] H. J. Park, J. Y. Shin, H. N. Kim, S. H. Oh, and P. H. Lee, "Neuroprotective effects of mesenchymal stem cells through autophagy modulation in a parkinsonian model," *Neurobiology of Aging*, vol. 35, no. 8, pp. 1920–1928, 2014.

[24] A. Spooren, K. Kolmus, G. Laureys et al., "Interleukin-6, a mental cytokine," *Brain Research Reviews*, vol. 67, no. 1-2, pp. 157–183, 2011.

[25] J. Huang, U. M. Upadhyay, and R. J. Tamargo, "Inflammation in stroke and focal cerebral ischemia," *Surgical Neurology*, vol. 66, no. 3, pp. 232–245, 2006.

[26] K. R. Swartz, F. Liu, D. Sewell et al., "Interleukin-6 promotes post-traumatic healing in the central nervous system," *Brain Research*, vol. 896, no. 1-2, pp. 86–95, 2001.

[27] P. C. Chang, T. Y. Wang, Y. T. Chang et al., "Autophagy pathway is required for IL-6 induced neuroendocrine differentiation and chemoresistance of prostate cancer LNCaP cells," *PLoS One*, vol. 9, no. 2, article e88556, 2014.

[28] N. A. Delk and M. C. Farach-Carson, "Interleukin-6: a bone marrow stromal cell paracrine signal that induces neuroendocrine differentiation and modulates autophagy in bone metastatic PCa cells," *Autophagy*, vol. 8, no. 4, pp. 650–663, 2014.

[29] J. P. White, M. J. Puppa, S. Gao, S. Sato, S. L. Welle, and J. A. Carson, "Muscle mTORC1 suppression by IL-6 during cancer cachexia: a role for AMPK," *American Journal of Physiology. Endocrinology and Metabolism*, vol. 304, no. 10, pp. E1042–E1052, 2013.

[30] Z. Yang and D. J. Klionsky, "Mammalian autophagy: core molecular machinery and signaling regulation," *Current Opinion in Cell Biology*, vol. 22, no. 2, pp. 124–131, 2010.

[31] C. H. Jung, S. H. Ro, J. Cao, N. M. Otto, and D. H. Kim, "mTOR regulation of autophagy," *FEBS Letters*, vol. 584, no. 7, pp. 1287–1295, 2010.

[32] F. Xu, J. H. Gu, and Z. H. Qin, "Neuronal autophagy in cerebral ischemia," *Neuroscience Bulletin*, vol. 28, no. 5, pp. 658–666, 2012.

[33] P. Wang, Y. F. Guan, H. du, Q. W. Zhai, D. F. Su, and C. Y. Miao, "Induction of autophagy contributes to the neuroprotection of nicotinamide phosphoribosyltransferase in cerebral ischemia," *Autophagy*, vol. 8, no. 1, pp. 77–87, 2014.

Hindawi
Neural Plasticity
Volume 2020, Article ID 2486065, 13 pages
https://doi.org/10.1155/2020/2486065

Review Article

Outcomes and Adverse Effects of Deep Brain Stimulation on the Ventral Intermediate Nucleus in Patients with Essential Tremor

Guohui Lu,[1] Linfeng Luo,[2] Maolin Liu,[2] Zijian Zheng,[2] Bohan Zhang,[2] Xiaosi Chen,[2] Xing Hua,[2] Houyou Fan,[2] Guoheng Mo,[3] Jian Duan,[1] MeiHua Li,[1] Tao Hong,[1] and Dongwei Zhou[1]

[1]*Department of Neurosurgery, The First Affiliated Hospital of Nanchang University, Nanchang, Jiangxi, China*
[2]*The First Clinical Medical College of Nanchang University, Nanchang, Jiangxi, China*
[3]*Queen Mary College of Nanchang University, Nanchang, Jiangxi, China*

Correspondence should be addressed to Dongwei Zhou; zhoudongwei123456@163.com

Received 28 March 2020; Revised 24 June 2020; Accepted 3 July 2020; Published 1 August 2020

Academic Editor: Fushun Wang

Objective. This study was aimed at identifying the potential outcome predictors, comparing the efficacy in patients with different tremor characteristics, and summarizing the adverse effect rates (AERs) of deep brain stimulation on the ventral intermediate nucleus (VIM-DBS) for essential tremor (ET). *Methods*. An extensive search of articles published to date in 2019 was conducted, and two main aspects were analyzed. Improvement was calculated as a percentage of change in any objective tremor rating scale (TRS) and analyzed by subgroup analyses of patients' tremor characteristics, laterality, and stimulation parameters. Furthermore, the AERs were analyzed as follows: the adverse effects (AEs) were classified as stimulation-related, surgical-related, or device-related effects. A simple regression analysis was used to identify the potential prognostic factors, and a two-sample mean-comparison test was used to verify the statistical significance of the subgroup analyses. *Results*. Forty-six articles involving 1714 patients were included in the meta-analysis. The pooled improvement in any objective TRS score was 61.3% (95% CI: 0.564-0.660) at the mean follow-up visit (20.0 ± 17.3 months). The midline and extremity symptoms showed consistent improvement ($P = 0.440$), and the results of the comparison of postural and kinetic tremor were the same ($P = 0.219$). In addition, the improvement in rest tremor was similar to that in action tremor (OR = 2.759, $P = 0.120$). In the simple regression analysis, the preoperative Fahn-Tolosa-Marin Tremor Rating Scale (FTM-TRS) scores and follow-up time were negatively correlated with the percentage change in any objective TRS score ($P < 0.05$). The most common adverse event was dysarthria (10.5%), which is a stimulation-related AE (23.6%), while the rates of the surgical-related and device-related AEs were 6.4% and 11.5%, respectively. *Conclusion*. VIM-DBS is an efficient and safe surgical method in ET, and the efficacy was not affected by the body distribution of tremor, age at surgery, and disease duration. Lower preoperative FTM-TRS scores likely indicate greater improvement, and the effect of VIM-DBS declines over time.

1. Introduction

Essential tremor (ET), also known as primary tremor, is defined as an isolated tremor syndrome consisting of a bilateral upper extremity action tremor for at least 3 years with or without tremor in other locations and without other neurological signs [1]. Currently, the management of this disorder focuses on controlling the symptoms, and pharmacotherapy is the primary therapy. Unfortunately, drug therapy is only effective in 50% of ET patients [2]. Surgical options include stereotactic radiofrequency thalamotomy, gamma knife thalamotomy, and deep brain stimulation [3–5] Among these options, deep brain stimulation in the ventral intermediate nucleus (VIM-DBS) is more easily reversed than thalamotomy and can effectively suppress tremors while avoiding the common complications of thalamotomies [6, 7]. The posterior subthalamic area/caudal zona incerta and subthalamic nucleus, except for the VIM, are also targets of DBS; however, thus far, studies are still limited with a short follow-up period compared to that in studies investigating VIM [8].

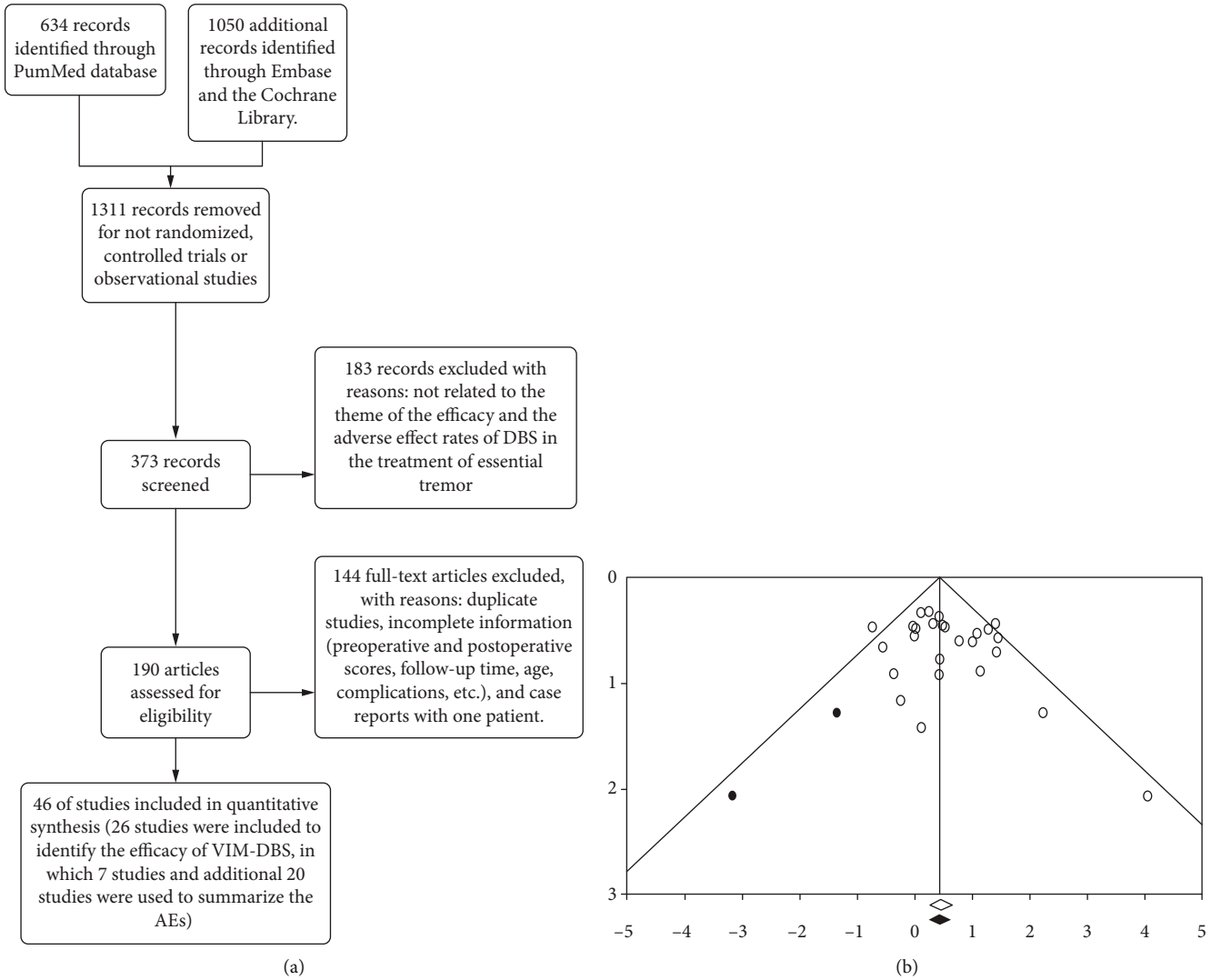

Figure 1: The PRISMA flowchart and funnel plot: (a) the PRISMA flowchart; (b) the funnel plot of the studies evaluating TRS scores. The plot shows an equal distribution of studies and has no presence of bias.

Although the effect of DBS on essential tremor is definitive, several factors influence the therapeutic effect. As reported by Putzke et al., the significant predictive factors associated with increased tremor severity at the initial clinical visit include an older age and a longer disease duration [9]. In addition, in most cases of ET, the tremor score worsens over time, and the average tremor severity increases each year [10]. Previous studies have found that the benefits of DBS are affected by laterality and stimulation parameters [11, 12]. Ondo et al. concluded that unilateral thalamic DBS is less effective than bilateral DBS in controlling appendicular and midline ET [11]. Moreover, a previous study found that to optimize tremor control, the stimulation parameters, including the voltage, frequency, and pulse width, need to be adjusted [12].

Similar to all surgical interventions, DBS may cause potential perioperative and postoperative adverse effects (AEs), such as infection, hemorrhage/hematoma, and pneumonia [13], affecting the prognosis of many patients. Therefore, further analysis of AE rates (AERs) is urgently needed. A large meta-analysis is also imperative to provide a comprehensive assessment of the prognostic factors, safety, and efficacy of VIM-DBS in the treatment of ET.

2. Methods

2.1. Search Strategy. Three electronic databases (PubMed, Embase, and the Cochrane Library) searched following the Preferred Reporting Items for Systematic Reviews and Meta-Analyses (PRISMA) guideline. We searched all articles related to DBS treatment for ET. We did not limit the age, sex, or operative time. A flow chart of the literature search is shown in Figure 1(a). We searched the literature using the keywords "essential tremor", "ventral intermediate nucleus", "deep brain stimulation", and "adverse effect". In addition, we registered the protocol of this meta-analysis in PROSPERO under the number CRD42020147313.

2.2. Inclusion Criteria and Exclusion Criteria. The inclusion criteria for eligible studies were as follows: (1) the study

subjects were ET patients treated with VIM-DBS; (2) the studies were randomized, controlled trials or observational studies published in English; (3) the studies reported any objective Tremor Rating Scale (TRS) scores at baseline and the last follow-up visit to determine the efficacy of VIM-DBS; (4) the studies specified the number of AEs in the ET patients; and (5) the studies described the tremor characteristics, such as midline (head/voice) tremor, extremity (arms/legs) tremor, rest tremor, or action (postural and kinetic) tremor. Regarding the efficacy of DBS, the studies had to meet criteria (1), (2), and (3), but the other criteria were optional. Regarding the adverse effects, the studies had to meet criteria (1), (2), and (4), but the other criteria were optional.

Conference presentations, editorials, reviews, non-English studies, and duplicate publications were excluded.

Controlled studies that included cohorts subjected to different surgical procedures were regarded as studies involving separate cohorts. For example, if a study included two cohorts that compared DBS and lesion surgery, the cohorts undergoing DBS were included in our study, and the other cohorts were excluded. Not all included studies performed follow-up evaluations or recorded the mean age, laterality, and stimulation parameters; hence, only studies that reported the same information could be combined for the data analysis. For instance, 46 original studies were included in our study, but only 13 studies reported the pulse width, and we combined these 13 studies for the statistical analysis.

2.3. Data Extraction. A data extraction template was used to build an evidence table that included the following items: author, publication year, number of patients, age, duration of disease in years, stimulation site, follow-up time, laterality (right, left, or bilateral), stimulation parameters (pulse width and voltage), any objective TRS scores (mainly including the Fahn-Tolosa-Marin Tremor Rating Scale [14], Essential Tremor Rating Assessment Scale, and Modified Unified Tremor Rating Scale) at baseline and the last follow-up visit, tremor characteristics (midline (head/voice) tremor, extremity (arms/legs) tremor, rest tremor, and action tremor (postural and kinetic)), and number of postoperative AEs.

Two authors (Luo Linfeng and Liu Maolin) independently extracted the data. If there was any disagreement or doubt, consensus was reached by consulting a third party (Lu Guohui).

2.4. Statistical Analysis. The statistical analysis was performed using Comprehensive Meta-Analysis (CMA) software (version 3.3.070) and Stata/SE 12.0. A meta-analysis of proportions was performed [15], and only 26 studies in Table 1 were included in the test of heterogeneity. The I^2 value and Q statistic were evaluated. If $I^2 \geq 50\%$, a random effects analysis using the DerSimonian-Laird model was employed to pool the data. Otherwise, a fixed effects model was used. The primary outcome was improvement, which was calculated as a percentage of change in any objective TRS scores [16], and the safety of DBS for ET was evaluated mainly based on adverse events of particular interest, such as dysarthria, paresthesia, hemiparesis/paresis, and headache.

To detect significant differences in the baseline characteristics shown in Table 2 and compare all subgroup analyses of patients' tremor characteristics, laterality, and stimulation parameters, two-sample mean-comparison tests were performed in Stata/SE 12.0, which could calculate the P values based on the mean, standard deviation, and sample size. In addition, the potential predictive factors of the percentage of change in any objective TRS score were tested using a simple regression analysis in CMA software [17], and $P \leq 0.05$ was defined as statistically significant. Publication bias was assessed using a funnel plot (Figure 1(b)) and Begg's test.

Regarding the efficacy of DBS, subgroup analyses were performed according to laterality (unilateral vs. bilateral) [18] and stimulation parameters (voltage and pulse widths) [19–21]. After we identified that the follow-up time is a predictive factor, the data from Barbe et al. [22] were excluded because the patients underwent the operation at least 3 months before their trials to optimize the efficacy of DBS, causing strong heterogeneity based on the sensitivity analysis, and we could not identify the detailed follow-up time after the first surgery.

2.5. Quality Evaluation. Two examiners independently conducted a review of the literature to eliminate bias. We used the Newcastle-Ottawa Scale [23] to assess the quality of the nonrandomized studies, including the following evaluations: adequacy of the case definition, representativeness of the cases, selection of controls, definition of controls, comparability of cases/controls, the same method of ascertainment, and nonresponse rate (Table 3). The Newcastle-Ottawa Scale is an easy-to-use, convenient tool for quality assessment, and the total score ranged from 0 (lowest quality) to 8 (highest quality), with one star representing one point. A study with 6 or more stars was classified as a high-quality study.

3. Results

3.1. Search Results. In total, 46 studies involving 1714 patients were assessed for eligibility by reviewing the full text of the articles. After excluding the articles that did not conform to the eligibility criteria, 4 randomized controlled trials (RCTs) and 42 observational studies were included (Figure 1). Moreover, the 26 studies shown in Table 1 were included to identify the efficacy of VIM-DBS; additionally, 7 of these studies and the 20 additional studies shown in Table 4 were used to summarize the AEs.

3.2. Outcome Results

3.2.1. Overall. In total, the 26 included studies involved 439 patients (Table 1). The percentage change in any objective TRS score in all included studies was 61.3% ($P < 0.001$).

3.2.2. Subgroup Analysis of Laterality. To compare the outcomes of DBS treatment with unilateral and bilateral procedures, a subgroup analysis was performed based on laterality. Nine studies involving 165 patients were included in the unilateral procedure group, while six studies involving 72 patients were included in the bilateral procedure group. The unilateral and bilateral improvement was 57.6% and

Table 1: Details of studies included in a meta-analysis of DBS in treatment of ET.

Authors & year	No. of Pts	Age in Yrs (range)	Duration of ET in Yrs (range)	Site of lesion	Follow-up in Mons	Unil/Bil	Voltage (V)	Pulse widths (μs)	Preoperative tremor scores	Postoperative tremor scores	Type of TRS	Percentage change in any TRS (%)
Koller W.C et al. 2001	25	72.3 ± 8.9	33.3 ± 15.4	VIM	40.2 ± 14.7	Unil	3.6 ± 1.3	99.6 ± 45.7	6.5 ± 1.6	1.4 ± 1.4	FTM-TRS	78.5
Ondo et al. 2001	13	71.5 ± 4.9	NS	VIM	3	Bil	NS	NS	6.7 ± 0.9	1.3 ± 1.2	MTRS	80.6
Pahwa R et al. 2001	17	73.1 (62–82)	NS	VIM	3.1	Unil	NS	NS	61.6 ± 13.2	30.5 ± 10.8	FTM-TRS	50.5
Fields J.A et al. 2003	40	71.7 ± 8.84	18.14 ± 12.88	VIM	12	Unil	L: 3.18 ± 0.53 R: 3.24 ± 0.75	L: 100.29 ± 32.49 R: 84.00 ± 25.10	19.35 ± 6.85	8.45 ± 4.13	FTM-TRS	56.3
Papavassiliou E et al. 2004	37	66.±13.6	NS	VIM	26 ± 16.2	21 Unil/16 Bil	2.7 ± 0.9	98.5 ± 27	19.3 ± 5.1	9.1 ± 6.2	FTM-TRS	52.8
Kuncel A.M et al. 2006	14	66.9 ± 17.2	NS	VIM	21.8 ± 17.9	NS	2.99 ± 0.83	87.85 ± 21.1	2.3 ± 0.7	0.04 ± 0.1	FTM-TRS	98.3
Van den Wildenberg WP et al. 2006	10	61.7 ± 11.8	13.5 ± 6.84	VIM	NS	NS	NS	NS	47.3 ± 23.42	30 ± 16.5	FTM-TRS	36.6
Pahwa R et al. 2006	22	70.6 ± 5.3	NS	VIM	60	3 Unil/20 Bil	3.6	111	23.9 ± 7.8	10 ± 4.9	FTM-TRS	58.2
Blomstedt et al. 2007	19	66 ± 11.1	NS	VIM	13	Unil	1.8 ± 0.7	68 ± 14	57.6 ± 19.2	29.2 ± 14.2	ETRS	49.3
Ellis TM et al. 2008	5	66 ± 11.1	29.6 ± 14.4	VIM	14 ± 5.33	NS	NS	NS	40.4 ± 4.41	16 ± 9.82	FTM-TRS	60.4
Zhang K et al. 2010	34	58.±12.8	22.1 ± 13.1	VIM	56.9	23 Unil/11 Bil	2.44 ± 0.89	81.9 ± 18.2	3.27 ± 0.87	0.64 ± 0.75	FTM-TRS	80.4
Morishita. et al. 2010	19	64.±12.3	26.3 ± 19.1	VIM	6	Unil	NS	ND	14.4 ± 4.43	3.63 ± 2.73	MTRS	74.8
Graft-Radford et al. 2010	31	66.4 ± 10.7	31.5 ± 20.6	VIM	6	22 Unil/9 Bil	Unil: 2.7 Bil (L): 2.7 Bil (R): 2.9	Unil: 102 Bil (L): 7 8 Bil (R): 9 3	58.2 ± 14.8	23 ± 12.6	FTM-TRS	60.5
Barbe et al. 2011	21	65 ± 14	27 ± 18	VIM	2.5	3 Unil/ 20 Bil	NS	NS	10.93 ± 7.53	7.39 ± 5.17	FTM-TRS	32.4
Vassal F et al. 2012	7	NS	NS	VIM	46.3 ± 28.7	NS	NS	NS	3.8 ± 0.3	0.37 ± 0.75	FTM-TRS	90.3
Zahos P.A. et al. 2013	7	66.6 ± 10.6	12.6 ± 6.6	VIM	10.1 ± 4.3	3 Unil/4 Bil	NS	NS	31.8 ± 13	7.7 ± 4.5	ETRS	75.8
Felicitas Ehlen et al. 2014	13	69.3 ± 9.43	15.77 ± 13.50	VIM	36.24 ± 33.69	Unil	3.13 ± 1.37	70.00 ± 14.77	16.15 ± 7.2	5.08 ± 5.12	UPDRS[a]	68.5
Rodríguez, C et al. 2016	14	61 ± 2.5	25 ± 10.5	VIM	6	3 Unil/11 Bil	90.0 ± 15.0	90.0 ± 15.0	63.3 ± 9.9	16.8 ± 11.2	FTM-TRS	73.5

Table 1: Continued.

Authors & year	No. of Pts	Age in Yrs (range)	Duration of ET in Yrs (range)	Site of lesion	Follow-up in Mons	Unil/Bil	Voltage (V)	Pulse widths (μs)	Preoperative tremor scores	Postoperative tremor scores	Type of TRS	Percentage change in any TRS (%)
Isaacs D.A et al. 2018	7	60.2 ± 11.6	NS	VIM	NS	NS	NS	NS	17.6 ± 4	6.9 ± 4	FTM-TRS	60.8
Paschen et al. 2018	21	NS	NS	VIM	NS	Bil	NS	NS	55.0 ± 3.7	20.9 ± 2.5	TRS[b]	62.0
Barbe M.T et al. 2018	13	58.9 ± 17.0	23.5 ± 17.8	VIM, PSA	12	NS	NS	NS	47.4 ± 7.9	23.8 ± 6	FTM-TRS	49.8
Akram H et al. 2018	5	63.8 ± 10.2	9.8 ± 2.0	VIM	23.6 ± 9.4	Unil	60 ± 0	60 ± 0	81.6 ± 17.6	48 ± 17.9	FTM-TRS	41.2
Fenoy, A.J et al. 2018	20	62.8 (18-81)	27.5 ± 15.4	VIM	12	2 Unil/18 Bil	2.9 ± 1.2	86 ± 33	2.1 ± 0.74	0.4 ± 0.5	ETRS	81.0
Paschen et al. 2019	20	66.6 ± 1.8	37.0 ± 3.8	VIM	13.1 ± 1.9	Bil	L: 2.44 ± 0.2 R: 2.47 ± 0.2	L: 66 ± 2.8 R: 63 ± 2.1	56.3 ± 3.7	20.9 ± 2.7	ETRS	62.9
Morishit T et al. 2019	3	70.7 ± 6.6	6 ± 4.32	VIM	16 ± 5.7	Unil	3.1 ± 0.36	110 ± 14.1	28.0 ± 2.94	15.67 ± 2.05	ETRS	44.0
Reich M et al. 2017	2	73	NS	VIM	NS	Bil	NS	NS	10.2 ± 9.5	4.8 ± 4.2	FTM-TRS	52.9
Pooled	439	—	—	—	—	—	—	—	—	—	—	61.3, $P < 0.001$

NS: not specified; Pts: patients; ET: essential tremor; Unil: Unilateral; Bil: Bilateral; TRS: Tremor Rating Scale; ETRS: Essential Tremor Rating Scale; Mons: Months. FTM: the Fahn-Tolosa-Marin; MTRS: Modified Tremor Rating Scale; UPDRS: the Unified Parkinson Disease Rating Scale. Unless otherwise stated, values are presented as the mean ± SD. [a]Tremor intensity was defined using the sum score of UPDRS subitems 20 and 21 (tremor at rest, action, and postural). [b]The detailed type of TRS was not definite in Paschen et al. 2018.

Table 2: Statistical difference of patient characteristics among laterality and stimulation parameter (pulse width and voltage) subgroups[a].

	Laterality			Voltage (V)			Pulse widths (μs)		
	Unilateral	Bilateral	*P* value	≥3.5	<3.5	*P* value	60-90	90-120	*P* value
Age at surgery (years)	69.74 ± 0.765	67.529 ± 2.201	0.115	67.868 ± 3.959	66.93 ± 1.094	0.375	65.820 ± 1.480	68.253 ± 2.617	0.782
Disease duration (years)	18.654 ± 3.488	37 ± 0.85	0.022[b]	29.053 ± 4.149	21.273 ± 5.024	0.247	26.092 ± 4.235	20.496 ± 5.405	0.205
Follow-up (months)	41.528 ± 18.174	22.787 ± 11.416	0.224	65.071 ± 26.166	42.599 ± 16.243	0.245	42.206 ± 17.054	38.828 ± 8.171	0.447

[a]The data are represented by "mean ± standard error". [b]The disease duration of bilateral procedure is almost missing, and only one data exists, so there are large biases in the significant comparison.

Table 3: Summary of critical appraisal of included studies using the Newcastle-Ottawa Scale for assessing the quality of observational studies.

Study	Selection	Comparability	Outcome
Koller W.C et al. 2001	★★	★	★
Ondo et al. 2001	★★★	★	★★
Pahwa R et al. 2001	★★★	★★	★★
Fields J.A et al. 2003	★★		★
Papavassiliou E et al. 2004	★★		★
Kuncel A.M et al. 2006	★★	★★	★★
Van den Wildenberg WP et al. 2006	★★	★	★
Pahwa et al. 2006	★		★
Blomstedt et al. 2007	★★	★	★
Ellis TM et al. 2008	★★	★	★★
Zhang K et al. 2010	★★		★
Morishita T et al. 2010	★		★
Graff-Radford J et al. 2010	★	★	★
Barbe et al. 2011	★		★★
Vassal F et al. 2012	★★	★	★★
Zahos P.A. et al. 2013	★★	★	★★
Felicitas Ehlen et al. 2014	★★	★	★
Rodríguez, C et al. 2016	★		★★
Isaacs D.A et al. 2018	★		★★
Paschen S et al. 2018	★		★
Barbe M.T et al. 2018	★★	★	★★★
Akram H et al. 2018	★★		★★
Fenoy, A.J et al. 2018	★★★	★	★★
Paschen S et al. 2019	★★		★★★
Morishita T et al. 2019	★★		★★
Reich M et al. 2017	★		★★
Hubble J.P. et al. 1996	★★	★	★
Koller W.C et al. 1999	★★	★	★
Taha J M. et al. 1999	★★	★	★★
Rehncrona S et al. 2003	★★	★	★★
Lee J Y.K. et al. 2005	★★	★	★
Törnqvist A. L et al. 2007	★★	★	★★
Lind G et al. 2008	★★	★	★★
Blomstedt P et al.2010	★★	★	★
Baizabal Carvallo JF et al. 2012	★★	★	★★
Carballal C.F. et al. 2013	★★	★	★★
Borretzen M.N. et al. 2014	★★	★	★
Baizabal Carvallo JF et al. 2014	★★	★	★
Hariz G-M et al. 2015	★★	★	★
Verla T. et al. 2015	★★	★	★
Sharma V.D et al. 2015	★★	★	★★
Silva D et al. 2016	★★	★	★★
Klein J et al. 2017	★★	★	★★
Wharen R E. et al. 2017	★★	★	★
Chen T et al. 2018	★★	★	★★
Koller W.C et al. 1999	★★★	★★	★★
Kuncel A.M et al. 2006	★★★	★★	★★
Felicitas Ehlen et al. 2014	★★★	★★	★
Barbe M.T et al. 2018	★★★	★★	★★

Each of these three categories has further subcategories and gives stars. The studies with the maximum number of stars are of higher quality than those with fewer stars. Empty cells show that no stars are available for this category.

67.8%, respectively; moreover, the efficacy did not significantly differ between the unilateral and bilateral procedure groups ($P = 0.139$). In addition, the baseline characteristics did not significantly differ between the unilateral and bilateral procedures (Table 2).

3.2.3. Subgroup Analysis of the Stimulation Parameters (Pulse Width and Voltage). The pulse width data were divided into 60-90 μs (125 patients) and 90-120 μs (142 patients). The improvement in these two subsets was 68.4% (60-90 μs) and 60.2%, respectively (90-120 μs) ($P = 0.164$). Then, the voltages were classified into the following two groups: ≥3.5 V (61 patients) and <3.5 V (236 patients). The improvement by voltages was 61.7% (<3.5 V) and 69.3% (≥3.5 V) ($P = 0.272$). The effect of VIM-DBS was not affected by the stimulation parameters ($P > 0.05$). In addition, the age at surgery and baseline characteristics did not significantly differ between the subgroups (Table 2).

3.2.4. Subgroup Analysis of the Tremor Characteristics. On the one hand, in total, 52 ET patients were included in the analysis of midline (head/voice) and extremity (arms/legs) tremor. However, the improvement in midline and extremity symptoms did not significantly differ (OR = 0.716, 95% CI: 0.307-1.670; $P = 0.440$). On the other hand, in total, 45 ET patients were included in the analysis of rest tremor and action tremor, and the improvement in rest tremor did not significantly differ from that in action tremor (OR = 2.759, 95% CI: 0.768-9.913; $P = 0.120$). Action tremor was divided into postural and kinetic tremor, and in total, 107 patients were included in this subgroup analysis (postural action: 52 patients, kinetic action: 55 patients). The improvement in the group with postural tremor (94.2%) was higher than that in the group with kinetic tremor (46.5%), but there was no statistical significance ($P = 0.219$). All detailed data are shown in Supplementary 1, 2, and 3.

3.2.5. Outcome Predictive Factors. To identify the potential outcome predictors, the clinical and demographical factors were tested separately. As shown in Figure 2, the preoperative FTM-TRS scores ($P = 0.010$) and follow-up period ($P = 0.021$) were significantly negatively correlated with the clinical outcomes. There were no significant correlations between the outcomes and other continuous clinical variables, such as age at surgery ($P = 0.802$) and disease duration ($P = 0.052$).

Table 4: Summary of all adverse effects.

Study	Adverse event		
	Stimulation	Surgical	Device
Hubble J.P. et al. 1996	Paresthesia (10), dysarthria (1), headache (2), face-arm pain (1), right-sided weakness (3), face weakness (1), decreased range of motion left shoulder(1)	0	0
Koller W.C et al. 1999	Mild paresthesia (24), mild headache (9), mild dysarthria (7), mild paresis (6), attention/cognitive deficits (2), gait disorder (2), facial weakness (2), dystonia (1), hypophonia (1), nausea (1), mild depression (1), dizziness (1)	Subdural hematoma (1), intraparenchymal hemorrhage (1), asymptomatic bleeds (3), seizures (1)	Loss of effect (8), lead replacement (2), devices explanted (2), reprogrammed (1), broken lead (1), lead extension replacements (2), IPG replacement (1)
Taha J M. et al. 1999	Disequilibrium (7), mild short-term memory loss (1), mild shock (4), dysarthria (7)	0	0
Koller W.C et al. 2001	Paresthesia (21), headache (15), paresis (6), dysarthria (4), nausea (4), disequilibrium (3), facial weakness (3), gait disorder (2), dystonia (2), mild attention/cognitive deficit (2), dizziness (2), hypophonia (1), anxiety (1), depression (1), syncope (1), vomiting (1), shocking sensation (1), drooling (1)	Asymptomatic bleeds (3), postoperative seizures (1)	Lead replacement (7), lead reposition (3), extension wire replaced (3), IPG replaced (4), entire system explanted (1)
Ondo et al. 2001	Paresthesia (3), headache (5), dysarthria (7), neck pain (2), mouth pain (1), increased saliva (1), balance and gait difficulty (10)	0	0
Pahwa R et al. 2001	Headache (9), paresthesia (10), dysarthria (1), disequilibrium (1), dizziness (2)	Seizures (1)	0
Rehncrona S et al. 2003	0	0	Lead fracture (1)
Lee J Y.K. et al. 2005	Hand tingling (3)	Temporary erythema of the incision (1)	Lead fracture (1), electrode migration (1)
Kuncel A.M et al. 2006	Dysarthria (9), posturing (7), jaw deviation (3), eye closure (2), voice affected (2)	0	0
Blomstedt et al. 2007	0	0	IPG exchange (12), lead fracture (6)
Törnqvist A. L et al. 2007	0	Infections (2)	Lead fracture (1)
Ellis TM et al. 2008	0	0	Lead fracture (1), lead migrated (1)
Lind G et al. 2008	Speech disorder (3), balance and gait difficult (2)	Infections (2)	Battery replacement (6)
Blomstedt et al. 2010	Aphasia (8), clumsy (1)	0	0
Baizabal Carvallo JF et al. 2012	0	Infections (3)	Misplacements (4), migrations (5), fractures (5)
Zahos P.A. et al. 2013	0	Wound dehiscence (2)	Lead fracture (1)
Carballal C.F. et al. 2013	Headache (9), paresthesia (6), dysarthria (17), dizziness (5), reduced balance (4)	Infections (1)	0
Borretzen M.N. et al. 2014	Dysarthria (17), headache (9), paresthesia (6), abnormal taste (8), dizziness (5), discomfort tongue (4), reduced balance or coordination (4)	0	0
Baizabal Carvallo JF et al. 2014	Incoordination (7), dysarthria (6)	0	Vasovagal reaction (1)

Table 4: Continued.

Study	Adverse event		
	Stimulation	Surgical	Device
Hariz G-M et al. 2015	Headache (1), voice affected (5), deterioration of balance (4), tiredness (1), tearful (1), felt discomfort (1)	0	0
Verla T. et al.2015	0	Hemorrhagic complication (10), infection (20), pulmonary embolism (4), pneumonia (16)	Lead revision (2), generator revision (7)
Sharma V.D et al. 2015	Incoordination (1), dysarthria (1), paresis (1), asthenia (1), reduced balance (1)	0	0
Silva D et al. 2016	Paresis (2), dysarthria (6), transient cognitive alter (1), facial numbness (1)	Hemorrhage (1), infections (1)	0
Klein J et al. 2017	0	Infections (1)	Wound revision (3), electrode dislocation (1)
Wharen R E.et al. 2017	Speech disturbances (12), gait/postural disorder (5), cognitive changes (8), dysphagia (2), tinnitus (1), shocking or jolting sensation (3), discomfort (17), headache (8), paresis (1), dystonia (2), dysarthria (1), hemiparesis (1)	Seizures (1), intracranial hemorrhage (3), wound dehiscence (4), infections (5), pocket hematoma (2)	Misplaced lead (6), IPG malfunction (4), extension malfunction (6), battery check (9)
Barbe M T et al. 2018	Right hemiparesis (1), dysarthria (11), aphasia (1), nausea (1)	Intracerebral hemorrhage (1)	0
Chen T et al. 2018	Mental status change (9), speech disturbance (7), balance or gait disturbance (6), speech & balance disturbances (5)	Hemorrhage (1), wound breakdown (1)	0

The number in brackets means the number of AE events.

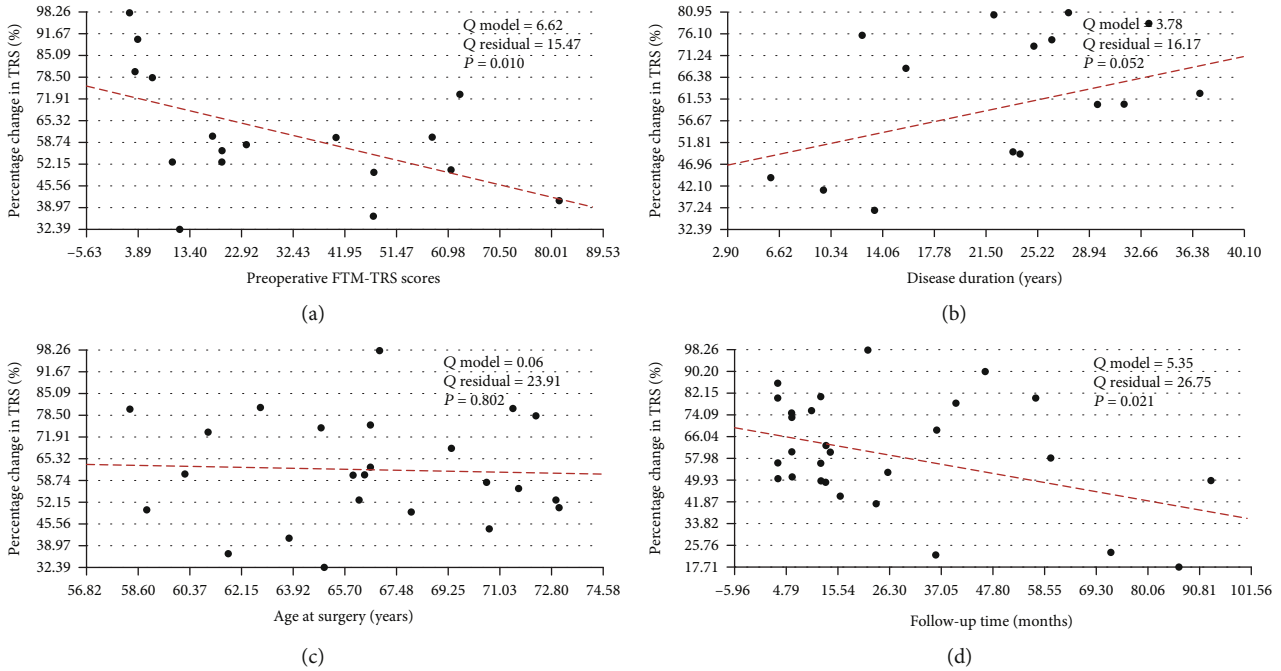

Figure 2: Potential predictive factors for percentage change in any TRS score (%). There were no significant correlations between percentage change in any TRS score (%) and (c) age at surgery ($P = 0.052$) as well as (b) disease duration ($P = 0.802$). There were significant negative correlations between percentage change in any TRS score (%) and a preoperative FTM-TRS score ($P = 0.010$) as well as (d) follow-up period ($P = 0.021$); dots: each study mean percentage change in any TRS score (%); red line of dashes: linear regression line; TRS: Tremor Rating Scale.

3.2.6. Publication Bias. A funnel plot of the comprehensive outcomes of 26 studies was drawn, and Begg's test found no significant publication bias ($P = 0.261$).

3.2.7. Common Adverse Effects. The frequent events are summarized in Supplementary 4. The incidence of stimulation-related AEs (23.6%) was higher than the incidence of device-related AEs (11.5%) and the incidence of surgical AEs (6.4%). The most common stimulation-related AEs were dysarthria (10.5%), paresthesia (6.3%), hemiparesis/paresis (6.3%), and headache (6.7%).

Rare events were classified as miscellaneous, and the specific details are shown in Supplementary 5.

4. Discussion

Our study provides the largest systematic review based on a large sample size, i.e., 46 studies involving 1714 patients, to summarize the efficacy and adverse effect rates of DBS for the treatment of essential tremor. The evidence provided in our meta-analysis shows that DBS targeting the VIM is effective in the treatment of ET, with a pooled improvement of 61.3% in any objective TRS score at 20.0 ± 17.3 months. In addition, our simple regression analysis indicated that the preoperative FTM-TRS scores and follow-up time likely predict the clinical outcomes. The most common adverse event was dysarthria, which is a stimulation-related AE. Based on the results of our study, it is possible to identify patients who are most likely to benefit from this surgical procedure and ultimately improve the quality of life of these patients.

4.1. Analysis of Subgroups. In our analysis, the efficacy in rest tremor was not more significant than that in action tremor. Two studies included in the analysis showed 100% improvement, although a ceiling effect may exist [24]. A previous publication reported that the efficacy in terms of tremor of action/intention declined and was less stable over time, while the effect on resting tremor showed limited change [25]. Moreover, Morishita et al. [26] stated that the microlesion effect did not affect resting tremor and, thus, showed a sustained improvement at 6 months after DBS, although the mechanisms leading to the significant improvement in resting tremor are unclear in advancing disease. One study stated that bilateral electrolytic lesions in the cerebellar dentate and interpositus nuclei resulted in tremor at rest [27]. The VIM, which is a target in the surgical treatment of ET, receives cerebellar afferents, and this surgery results in improvement in rest tremor in ET [28]. Hence, VIM-DBS could also be an effective strategy for ET patients with rest tremor.

In accordance with the anatomical distribution of tremor, our results revealed that similar improvements were observed in midline and extremity tremor. In a study conducted by Putzke et al., midline tremor showed significant improvement compared with baseline tremor, while head and voice tremor showed the most consistent improvement [29]. However, the effects on head tremor have been inconsistent according to an analysis conducted by Moscovich et al. [20]. Relatedly, the effect of thalamic stimulation on midline tremor tends to increase with symptom severity [29]. The significant effect of the stimulation on extremity tremor was maintained for 1 year, but the voltage had to be increased in a European trial [30]. Furthermore, it has been reported that midline tremor, including head and voice tremor, showed greater improvement after a bilateral procedure because of the bilateral innervation of neck muscles [29–31]. However, unilateral stimulation is equally effective in the treatment of contralateral hand tremor [32]. Hence, after a series of stimulation adjustments, the second implantation, and short follow-up in the included studies, the improvement in midline and extremities showed no significant difference.

4.2. Predictive Factors. Much attention has been paid to the clinical factors that may predict outcomes in patients undergoing DBS for tremor, while a few studies identified potential prognostic factors. It is important for clinicians to evaluate the variables that may influence the clinical outcomes of surgery and predict the therapeutic effects of surgery as accurately as possible [33]. In our simple regression analysis, we concluded that lower preoperative scores indicated greater improvement and that the effect of VIM-DBS declines over time based on 439 ET patients.

A published study retrospectively investigated the clinical features of tremor, including Parkinson's disease, essential tremor, cerebellar tremor, and dystonic tremor, that might predict the outcome of DBS and reported that patients with higher baseline scores had a greater DBS response [34]. Nevertheless, other recognized publications showed that a higher preoperative tremor severity predicted a worse outcome [35, 36]. According to Blomstedt et al. [37], ET patients with a more severe tremor might produce a higher level of residual tremor upon stimulation after surgery, resulting in a worse outcome. Several studies have described the loss of efficacy during a long follow-up following DBS among ET patients [12, 38, 39]. For instance, Paschen et al. concluded that the tremor severity and effect of VIM-DBS significantly deteriorate over a decade in ET patients [38]. A combination of factors has been proposed for the loss of the clinical efficacy of VIM-DBS in ET, including natural disease progression [25, 40], tolerance [25, 41], suboptimal electrode placement [42], increased impedance in brain tissue over time [7], loss of the microthalamotomy effect [7], and long-term, stimulation-induced effects [39]. However, tolerance and the natural progression of the disease are considered the most possible explanations for the gradual loss of efficacy of VIM-DBS over time [12, 25]. The need for the continuous adjustment of the stimulation parameters during the follow-up period was likely the result of tolerance. With the progression of ET, the difficulty to control tremor is associated with a severe limb action tremor in these patients with already high scores at baseline [43]; moreover, the loss of effectiveness might be corrected by modulating the synchronized oscillatory cerebellothalamocortical pathway induced by high-frequency stimulation of the VIM [12]. Some investigators have reported that applying stimulation during waking hours or alternating stimulation protocols without increasing the stimulation strength can improve tolerance [25, 40].

4.3. Adverse Effects. Among the included studies, the incidence of stimulation-related AEs, surgery-related AEs, and device-related AEs was analyzed. Among the three types of AEs, the incidence of stimulation-related AEs (23.6%) was the highest, and these types of AEs were usually mild and easily improved by adjusting the stimulation parameters. Consistent with previous reports [44, 45], dysarthria, disequilibrium, motor disturbances, and paresthesia were the most common AEs [46]. Our analysis showed that the surgical-related AEs included infections (3.4%), asymptomatic bleeding (2.9%), intraoperative intracerebral hemorrhage (2.4%), and wound dehiscence (2.6%). Moreover, postoperative infection, hemorrhagic complications, pneumonia, and death associated with DBS are rare but often serious [13, 47]. Device-related AEs were common and bothersome after DBS of the VIM. In different reports, the complication rate ranged between 6.7% and 49% and often required additional surgery [48–51]. In our study, the device-related AE rate was 6.4%, and these types of AEs mainly included lead fracture (5.3%) and lead repositioning (3.8%). The device-related AER significantly decreased after 2003 [48]. Our rates were similar to those reported in the literature, and most included studies were published after 2003. We are convinced that the key factors responsible for lowering the complication rates of VIM-DBS are technical and hardware-related improvements and surgeon experience.

5. Limitations of the Study

Our meta-analysis had some limitations. First, most included studies were observational studies, and only four studies were RCTs, which has a certain impact on the quality of the incorporated resulting report. Larger randomized trials and prospective studies are required. Second, the potential prognostic factors are predicted through a univariate regression analysis rather than a multivariate regression analysis due to incomplete information in the included studies, such as follow-up time and disease duration. Thus, to evaluate the predictive factors of DBS using a more advanced method, authors reporting clinical trials should provide comprehensive data. Third, regarding the summary of tremor characteristics, all conclusions are based on a small sample, and more studies including an analysis of tremor characteristics are needed. Finally, regarding the methodology, our review was limited to the English literature and excluded some old publications that could not be retrieved.

6. Conclusions

DBS is an effective and safe treatment for patients with ET, but we need to be aware of the AEs. The efficacy was not affected by the body distribution of tremor, age at surgery, and disease duration. Moreover, VIM-DBS could be an effective strategy for ET patients with rest tremor, and the efficacy was similar not only between midline and extremity symptoms but also between postural and kinetic tremor. Lower preoperative FTM-TRS scores likely indicate larger improvements, and the effect of VIM-DBS declines over time. The age at surgery and disease duration may be prognostic factors of DBS in ET, but this hypothesis could not be confirmed based on our data. Clinical studies involving large samples of ET patients and prospective, randomized clinical studies are warranted to predict the potential prognostic factors in the future.

Abbreviations

DBS: Deep brain stimulation
AEs: Adverse effects
ET: Essential tremor
VIM: Ventral intermediate nucleus
TRS: Tremor rating scale
AERs: Adverse effect rates
RCTs: Randomized controlled trials
OR: Odds ratio
FTM: Fahn-Tolosa-Marin.

Conflicts of Interest

The authors report no conflicts of interest concerning the materials or methods used in this study or the findings specified in this paper.

Authors' Contributions

Guohui Lu, Linfeng Luo, and Maolin Liu conceived the review and conducted the formal analysis and writing, i.e., review and editing. Zijian Zhen, Bohan Zhang, Xiaosi Chen, and Xing Hua screened the search results. Linfeng Luo and Maolin Liu extracted the data from the papers. MeiHua Li, Tao Hong, and Dongwei Zhou supervised the analysis. Linfeng Luo analyzed the data and beautified the figures. Maolin Liu assisted in screening the retrieved papers against the inclusion criteria. Houyou Fan, Guohui Lu, and Bohan Zhang appraised the quality of the studies. Houyou Fan, Guoheng Mo, and Jian Duan were responsible for reading and checking the review before submission. Moreover, Linfeng Luo, Maolin Liu, and Guohui Lu equally contributed to this paper. Linfeng Luo, Maolin Liu, and Guohui Lu are co-first authors.

Acknowledgments

We thank Doctor Zhou for language help during the writing and editing of the manuscript. We are grateful for the support of statistical experts in the data analysis. This work was funded by the General Program of National Natural Science Foundation of Jiangxi Province (grant number 20192BAB205042) and the Health and Family Planning Commission of Jiangxi Province (grant number 20195109).

Supplementary Materials

Supplementary 1: comparison of the improvement in midline and extremity symptoms following DBS among ET patients. Supplementary 2: comparison of the improvement in rest and action tremor following DBS among ET patients. Supplementary 3: comparison of the improvement in postural and kinetic tremor following DBS among ET patients.

Supplementary 4: incidence of common adverse effects. Supplementary 5: incidence of rare adverse effects. *(Supplementary Materials)*

References

[1] K. P. Bhatia, P. Bain, N. Bajaj et al., "Consensus statement on the classification of tremors. from the task force on tremor of the International Parkinson and Movement Disorder Society," *Movement Disorders*, vol. 33, no. 1, pp. 75–87, 2018.

[2] B. Thanvi, N. Lo, and T. Robinson, "Essential tremor—the most common movement disorder in older people," *Age and Ageing*, vol. 35, no. 4, pp. 344–349, 2006.

[3] F. Rincon and E. D. Louis, "Benefits and risks of pharmacological and surgical treatments for essential tremor: disease mechanisms and current management," *Expert Opinion on Drug Safety*, vol. 4, no. 5, pp. 899–913, 2005.

[4] D. Kondziolka, J. G. Ong, J. Y. K. Lee, R. Y. Moore, J. C. Flickinger, and L. D. Lunsford, "Gamma Knife thalamotomy for essential tremor," *Journal of Neurosurgery*, vol. 108, no. 1, pp. 111–117, 2008.

[5] T. A. Zesiewicz, R. Elble, E. D. Louis et al., "Practice parameter: therapies for essential tremor: report of the Quality Standards Subcommittee of the American Academy of Neurology," *Neurology*, vol. 64, no. 12, pp. 2008–2020, 2005.

[6] E. D. Flora, C. L. Perera, A. L. Cameron, and G. J. Maddern, "Deep brain stimulation for essential tremor: a systematic review," *Movement Disorders*, vol. 25, no. 11, pp. 1550–1559, 2010.

[7] A. L. Benabid, P. Pollak, D. Hoffmann et al., "Long-term suppression of tremor by chronic stimulation of the ventral intermediate thalamic nucleus," *The Lancet*, vol. 337, no. 8738, pp. 403–406, 1991.

[8] T. Xie, J. Bernard, and P. Warnke, "Post subthalamic area deep brain stimulation for tremors: a mini-review," *Translational Neurodegeneration*, vol. 1, no. 1, 2012.

[9] J. D. Putzke, N. R. Whaley, Y. Baba, Z. K. Wszolek, and R. J. Uitti, "Essential tremor: predictors of disease progression in a clinical cohort," *Journal of Neurology, Neurosurgery, and Psychiatry*, vol. 77, no. 11, pp. 1235–1237, 2006.

[10] E. D. Louis, A. Agnew, A. Gillman, M. Gerbin, and A. S. Viner, "Estimating annual rate of decline: prospective, longitudinal data on arm tremor severity in two groups of essential tremor cases," *Journal of Neurology, Neurosurgery & Psychiatry*, vol. 82, no. 7, pp. 761–765, 2011.

[11] W. Ondo, M. Almaguer, J. Jankovic, and R. K. Simpson, "Thalamic deep brain stimulation: comparison between unilateral and bilateral placement," *Archives of Neurology*, vol. 58, no. 2, pp. 218–222, 2001.

[12] P. M. Rodríguez Cruz, A. Vargas, C. Fernández-Carballal, J. Garbizu, B. de la Casa-Fages, and F. Grandas, "Long-term thalamic deep brain stimulation for essential tremor: clinical outcome and stimulation parameters," *Movement Disorders Clinical Practice*, vol. 3, no. 6, pp. 567–572, 2016.

[13] J. Voges, R. Hilker, K. Bötzel et al., "Thirty days complication rate following surgery performed for deep-brain-stimulation," *Movement Disorders*, vol. 22, no. 10, pp. 1486–1489, 2007.

[14] S. Fahn et al., "Clinical rating scale for tremor," in *Parkinson's disease and movement disorders*, J. Jankovic and E. Tolosa, Eds., pp. 271–280, Urban and Schwarzenberg, Munich, 1993.

[15] N. Mohammed, D. Patra, and A. Nanda, "A meta-analysis of outcomes and complications of magnetic resonance-guided focused ultrasound in the treatment of essential tremor," *Neurosurgical Focus*, vol. 44, no. 2, article E4, 2018.

[16] M. D. Mendonça, B. Meira, M. Fernandes, R. Barbosa, and P. Bugalho, "Deep brain stimulation for lesion-related tremors: a systematic review and meta-analysis," *Parkinsonism & Related Disorders*, vol. 47, pp. 8–14, 2018.

[17] Z. Yin, Y. Luo, Y. Jin et al., "Is awake physiological confirmation necessary for DBS treatment of Parkinson's disease today? A comparison of intraoperative imaging, physiology, and physiology imaging-guided DBS in the past decade," *Brain Stimulation*, vol. 12, no. 4, pp. 893–900, 2019.

[18] J. Becker, M. T. Barbe, M. Hartinger et al., "The effect of uni- and bilateral thalamic deep brain stimulation on speech in patients with essential tremor: acoustics and intelligibility," *Neuromodulation: Technology at the Neural Interface*, vol. 20, no. 3, pp. 223–232, 2017.

[19] C. M. McKay, H. J. McDermott, T. Perera, R. Peppard, M. Jones, and A. P. Vogel, "The influence of rate of stimulation and pulse duration on efficacy of deep brain stimulation for Essential Tremor," *Brain Stimulation*, vol. 8, no. 2, p. 331, 2015.

[20] M. Moscovich, T. Morishita, K. D. Foote, C. G. Favilla, Z. P. Chen, and M. S. Okun, "Effect of lead trajectory on the response of essential head tremor to deep brain stimulation," *Parkinsonism & Related Disorders*, vol. 19, no. 9, pp. 789–794, 2013.

[21] H. Walker, J. Faulk, A. K. M. Rahman et al., "Awake testing during deep brain stimulation surgery predicts postoperative stimulation side effect thresholds," *Brain Sciences*, vol. 9, no. 2, p. 44, 2019.

[22] M. T. Barbe, L. Liebhart, M. Runge et al., "Deep brain stimulation in the nucleus ventralis intermedius in patients with essential tremor: habituation of tremor suppression," *Journal of Neurology*, vol. 258, no. 3, pp. 434–439, 2011.

[23] G. A. Wells, B. Shea, D. O'connell et al., "The Newcastle-Ottawa Scale (NOS) for assessing the quality if nonrandomized studies in meta-analyses," 2012, October 2019, https://www.ncbi.nlm.nih.gov/pmc/articles/PMC6174461/.

[24] W. Ondo, V. Hashem, P. A. LeWitt et al., "Comparison of the Fahn-Tolosa-Marin Clinical Rating Scale and the Essential Tremor Rating Assessment Scale," *Movement Disorders Clinical Practice*, vol. 5, no. 1, pp. 60–65, 2018.

[25] P. Blomstedt, G. M. Hariz, M. I. Hariz, and L. O. D. Koskinen, "Thalamic deep brain stimulation in the treatment of essential tremor: a long-term follow-up," *British Journal of Neurosurgery*, vol. 21, no. 5, pp. 504–509, 2009.

[26] T. Morishita, K. D. Foote, S. S. Wu et al., "Brain penetration effects of microelectrodes and deep brain stimulation leads in ventral intermediate nucleus stimulation for essential tremor," *Journal of Neurosurgery*, vol. 112, no. 3, pp. 491–496, 2010.

[27] M. E. Goldberger and J. H. Growden, "Tremor at rest following cerebellar lesions in monkeys: effect of L-DOPA administration," *Brain Research*, vol. 27, no. 1, pp. 183–187, 1971.

[28] J. Graff-Radford, K. D. Foote, A. E. Mikos et al., "Mood and motor effects of thalamic deep brain stimulation surgery for essential tremor," *European Journal of Neurology*, vol. 17, no. 8, pp. 1040–1046, 2010.

[29] J. D. Putzke, R. J. Uitti, A. A. Obwegeser, Z. K. Wszolek, and R. E. Wharen, "Bilateral thalamic deep brain stimulation:

midline tremor control," *Journal of Neurology, Neurosurgery & Psychiatry*, vol. 76, no. 5, pp. 684–690, 2005.

[30] P. Limousin, J. D. Speelman, F. Gielen, M. Janssens, and study collaborators, "Multicentre European study of thalamic stimulation in parkinsonian and essential tremor," *Journal of Neurology, Neurosurgery & Psychiatry*, vol. 66, no. 3, pp. 289–296, 1999.

[31] K. T. Mitchell, P. Larson, P. A. Starr et al., "Benefits and risks of unilateral and bilateral ventral intermediate nucleus deep brain stimulation for axial essential tremor symptoms," *Parkinsonism & Related Disorders*, vol. 60, pp. 126–132, 2019.

[32] D. S. Huss, R. F. Dallapiazza, B. B. Shah, M. B. Harrison, J. Diamond, and W. J. Elias, "Functional assessment and quality of life in essential tremor with bilateral or unilateral DBS and focused ultrasound thalamotomy," *Movement Disorders*, vol. 30, no. 14, pp. 1937–1943, 2015.

[33] X. L. Su, X. G. Luo, H. Lv, J. Wang, Y. Ren, and Z. Y. He, "Factors predicting the instant effect of motor function after subthalamic nucleus deep brain stimulation in Parkinson's disease," *Translational Neurodegeneration*, vol. 6, no. 1, 2017.

[34] C. Sandoe, V. Krishna, D. Basha et al., "Predictors of deep brain stimulation outcome in tremor patients," *Brain Stimulation*, vol. 11, no. 3, pp. 592–599, 2018.

[35] G. Deuschl and P. Bain, "Deep brain stimulation for trauma: Patient selection and evaluation," *Movement Disorders*, vol. 17, no. S3, pp. S102–S111, 2002.

[36] A. Fasano, J. Herzog, and G. Deuschl, "Selecting appropriate tremor patients for DBS," in *Deep Brain Stimulation*, Oxford University Press, 2009.

[37] P. Blomstedt, U. Sandvik, M. I. Hariz et al., "Influence of age, gender and severity of tremor on outcome after thalamic and subthalamic DBS for essential tremor," *Parkinsonism & Related Disorders*, vol. 17, no. 8, pp. 617–620, 2011.

[38] S. Paschen, J. Forstenpointner, J. Becktepe et al., "Long-term efficacy of deep brain stimulation for essential tremor," *Neurology*, vol. 92, no. 12, pp. e1378–e1386, 2019.

[39] J. G. Pilitsis, L. V. Metman, J. R. Toleikis, L. E. Hughes, S. B. Sani, and R. A. E. Bakay, "Factors involved in long-term efficacy of deep brain stimulation of the thalamus for essential tremor," *Journal of Neurosurgery*, vol. 109, no. 4, pp. 640–646, 2008.

[40] C. G. Favilla, D. Ullman, A. Wagle Shukla, K. D. Foote, C. E. Jacobson, and M. S. Okun, "Worsening essential tremor following deep brain stimulation: disease progression versus tolerance," *Brain*, vol. 135, no. 5, pp. 1455–1462, 2012.

[41] L. C. Shih, K. LaFaver, C. Lim, E. Papavassiliou, and D. Tarsy, "Loss of benefit in VIM thalamic deep brain stimulation (DBS) for essential tremor (ET): how prevalent is it?," *Parkinsonism & Related Disorders*, vol. 19, no. 7, pp. 676–679, 2013.

[42] M. S. Okun, M. Tagliati, M. Pourfar et al., "Management of referred deep brain stimulation failures: a retrospective analysis from 2 movement disorders centers," *Archives of Neurology*, vol. 62, no. 8, pp. 1250–1255, 2005.

[43] O. Sydow, S. Thobois, F. Alesch, and J. D. Speelman, "Multicentre European study of thalamic stimulation in essential tremor: a six year follow up," *Journal of Neurology, Neurosurgery & Psychiatry*, vol. 74, no. 10, pp. 1387–1391, 2003.

[44] R. Pahwa, K. E. Lyons, S. B. Wilkinson et al., "Long-term evaluation of deep brain stimulation of the thalamus," *Journal of neurosurgery*, vol. 104, no. 4, pp. 506–512, 2006.

[45] N. Yousif, M. Mace, N. Pavese, R. Borisyuk, D. Nandi, and P. Bain, "A network model of local field potential activity in essential tremor and the impact of deep brain stimulation," *PLOS Computational Biology*, vol. 13, no. 1, article e1005326, 2017.

[46] J. D. Putzke, R. E. Wharen, Jr, A. A. Obwegeser et al., "Thalamic deep brain stimulation for essential tremor: recommendations for long-term outcome analysis," *Canadian Journal of Neurological Sciences / Journal Canadien des Sciences Neurologiques*, vol. 31, no. 3, pp. 333–342, 2004.

[47] A. Beric, P. J. Kelly, A. Rezai et al., "Complications of deep brain stimulation surgery," *Stereotactic and functional neurosurgery*, vol. 77, no. 1-4, pp. 73–78, 2002.

[48] S. Bhatia, M. Oh, T. Whiting, M. Quigley, and D. Whiting, "Surgical complications of deep brain stimulation," *Stereotactic and Functional Neurosurgery*, vol. 86, no. 6, pp. 367–372, 2008.

[49] D. Kondziolka, D. Whiting, A. Germanwala, and M. Oh, "Hardware-related complications after placement of thalamic deep brain stimulator systems," *Stereotactic and Functional Neurosurgery*, vol. 79, no. 3-4, pp. 228–233, 2003.

[50] K. E. Lyons, S. B. Wilkinson, J. Overman, and R. Pahwa, "Surgical and hardware complications of subthalamic stimulation: a series of 160 procedures," *Neurology*, vol. 63, no. 4, pp. 612–616, 2004.

[51] M. Y. Oh, A. Abosch, S. H. Kim, A. E. Lang, and A. M. Lozano, "Long-term hardware-related complications of deep brain stimulation," *Neurosurgery*, vol. 50, no. 6, pp. 1268–1276, 2002.

Hindawi
Neural Plasticity
Volume 2020, Article ID 8834275, 10 pages
https://doi.org/10.1155/2020/8834275

Research Article

TREM2 Overexpression Attenuates Cognitive Deficits in Experimental Models of Vascular Dementia

Qian Wang,[1,2] Weixia Yang,[3] Jingmei Zhang,[4] Yueran Zhao,[1] and Yuzhen Xu[5]

[1]*Department of Central Laboratory, Shandong Provincial Hospital Affiliated to Shandong University, Jinan, Shandong Province 250021, China*
[2]*Department of Central Laboratory, Taian City Central Hospital, Shandong First Medical University & Shandong Academy of Medical Sciences, Taian, Shandong Province 271000, China*
[3]*Department of Neurology, Qingpu Branch of Zhongshan Hospital, Fudan University, Shanghai 201700, China*
[4]*Institute of Behavioral Medicine Education, Jining Medical University, Jining, Shandong Province 272067, China*
[5]*Department of Neurology, Taian City Central Hospital, Shandong First Medical University & Shandong Academy of Medical Sciences, Taian, Shandong Province 271000, China*

Correspondence should be addressed to Yueran Zhao; yrzhao@sdu.edu.cn and Yuzhen Xu; tianyayizhe@126.com

Received 8 April 2020; Revised 9 May 2020; Accepted 28 May 2020; Published 12 June 2020

Academic Editor: Fushun Wang

Neuroinflammation plays a prominent role in the pathogenesis of vascular dementia (VD). Triggering receptor expressed on myeloid cells 2 (TREM2) is a transmembrane receptor mainly expressed on microglia and has been known for its anti-inflammatory properties during immune response. However, data evaluating the effects of TREM2 in VD are lacking. Therefore, the present study is aimed at investigating the role of TREM2 in VD. In this study, the mouse model of VD was induced by transient bilateral common carotid artery occlusion (BCCAO). We compared the hippocampal gene and protein expressions of TREM2 between the VD mice and sham-operated mice at different time points. The TREM2 mRNA and protein expression levels in the VD mice were higher than those in the sham-operated mice. The cognitive deficits of VD mice were observed in the Morris water maze test. Interestingly, overexpression of TREM2 by intracerebroventricular injection of a lentiviral vector that encoded TREM2 (LV-TREM2) significantly improved the spatial learning and memory and attenuated the hippocampal neural loss in VD mice. Further mechanistic study revealed that overexpression of TREM2 significantly inhibited microglia M1 polarization by decreasing inducible nitric oxide synthase (iNOS) and proinflammatory cytokines expression levels and conversely enhanced microglia M2 polarization by increasing Arginase-1 (Arg-1) and anti-inflammatory cytokine expression levels. These results strongly suggest that TREM2 provides a protective effect in VD via modulating the phenotype of activated microglia and may serve as a novel potential therapeutic target for VD.

1. Introduction

Vascular dementia (VD) describes a combination of the loss of cognitive functioning and memory associated with variable brain lesions of vascular origin [1]. As is well known, VD is widely considered as one of leading forms of dementia only after Alzheimer's disease (AD), accounting for 15-20% of all cases. With the advent of global aging, the incidence of VD is increasing steeply [2]. There are currently an estimated 50 million people living with dementia worldwide, and the number will rise to 82 million by 2030 and 150 million by 2050. VD poses a heavy financial burden on families and societies [3]. The global annual cost for dementia is expected to reach $2.54 trillion in 2030 and $9.12 trillion in 2050 [4]. Despite much progress on VD research over the past several decades, the exact mechanism still remains obscure. Thus, it is imperative to determine the etiology of VD and search for an effective treatment.

The triggering receptor expressed on myeloid cells 2 (TREM2) protein is a type I transmembrane innate immune receptor of the TREM family. TREM2 is expressed exclusively by myeloid cells, and in the brain, TREM2 is

predominantly expressed in microglia. TREM2 has been implicated in a wide range of functions including cell proliferation, phagocytosis, maturation, and inflammatory response [5]. Recently, several studies have also shown that TREM2 plays an important role in microglia cell activation and survival [6]. Microglia are one of the main cell types which are involved in the inflammatory responses in the central nervous system [7]. However, microglia-induced inflammation is a double-edged sword, which has both beneficial and detrimental effects on neurons according to different diseases and status.

Neuroinflammation is defined as activation of the innate immune system in response to different brain injuries. Microglial activation in the brain parenchyma is the hallmark of neuroinflammation and is thought to be a critical determinant of neuronal fate [8]. Neuroinflammation is closely related to the pathogenesis of various cerebrovascular diseases including VD [9]. Though TREM2 has been widely reported to regulate neuroinflammation, its role in VD has rarely been reported. In our previous study, we found that serum levels of soluble TREM2 are lower in VD patients than in healthy controls and TREM2 may be a potential predictive biomarker of cognitive decline in VD [10]. The purpose of our present study was to determine whether TREM2 plays a neuroprotective role by regulating inflammation in a mouse model of VD. The neuroprotective role of TREM2 in VD, if confirmed, may represent a potential therapeutic target for VD.

2. Materials and Methods

2.1. Animals. Adult male C57BL/6 mice (8-10 weeks old, purchased from Shanghai SLAC Laboratory Animal Co., Shanghai, China) were used for the experiments. All mice were accommodated in a controlled environment and free access to water and food. Animals were accommodated in steel cages under standard housing conditions in a room kept at 22 ± 1°C with a 12 h light, 12 h dark cycle. All animal experimental procedures were performed in accordance with the approved animal protocols and guidelines established by Shandong First Medical University & Shandong Academy of Medical Sciences.

2.2. Mouse Model of VD Induction. The transient bilateral common carotid artery occlusion (BCCAO) surgery was performed as previously described with minor modifications [11]. Briefly, mice were anesthetized with 2% isoflurane in 30% oxygen, then both the right and left common carotid arteries were isolated from the adjacent vagus nerve and a silk was passed below each carotid artery for closure. The bilateral carotid arteries were locked by silk strings for 15 min and then released for 15 min, and this was repeated three times. The strings were then removed and the incision was sutured. Throughout the experiment, mice were placed in an automatic temperature-controlled chamber (World Precision Instruments, Sarasota, Florida, USA) to keep their body temperature at 37°C. After surgery, the mice were then moved to their original cages after 2 h and allowed to recover for 24 h before the start of subsequent operation.

2.3. Experimental Groups. Following 24 h of recovery from surgery, mice were randomly divided into the following three groups with 10 animals in each group. (1) Sham group: mice were given the same surgical procedure without carotid artery occlusion and the control lentivirus (LV-control) was injected into the right lateral ventricle; (2) VD+LV-control group: mice were subjected to the transient BCCAO modeling surgery and the control lentivirus (LV-control) was injected into the right lateral ventricle; (3) VD+LV-TREM2 group: mice were subjected to the transient BCCAO modeling surgery and the lentivirus overexpressing TREM2 (LV-TREM2) was injected into the right lateral ventricle.

2.4. Lentiviral Vector Preparation and Administration. The lentiviral vector that encoded TREM2 and control lentiviral vector were prepared by GENECHEM Biotech. Co. Ltd. (Shanghai, China). Stereotactic intracerebral injection of lentiviral vector was conducted by technicians who were blinded to the experimental groups as previously described [12, 13]. Briefly, mice were anesthetized and fixed on a stereotactic frame, then the lentiviral vector was injected into the right lateral ventricle (stereotaxic coordinates: 1.0 mm near the midline, 0.2 mm posterior to the bregma, and 3.0 mm below the skull). The injections were performed in a volume of 2 μl for 5 min, and the infusion microsyringe (Hamilton, Reno, NV) was maintained for diffusion for an additional 5 min.

2.5. Morris Water Maze Test. Four weeks after the intracerebroventricular administration, cognitive deficits were assessed by the Morris water maze (MWM JK001 type, Beijing, China), which was performed as previously described [12, 14]. The MWM apparatus consists of a black cylindrical pool (diameter:150 cm; height:60 cm), a video camera, and a computerized system (EthoVision, Version 8.5, Noldus Information Technology, Wageningen, the Netherlands). The MWM was filled with water at 24 ± 1°C, which was divided into four quadrants and made opaque by the addition of skim milk powder. The MWM test included an acquisition training phase and a probe phase to assess memory. All the data was measured by an automated analysis system.

In the acquisition training phase, the escape platform with a diameter of 10 cm was fixed in the center of one quadrant and submerged 1 cm beneath the water surface. The acquisition training phase was repeated for four consecutive days, and a total of four trials were conducted per day. In each trial, the mice were released from the four quadrants, respectively, and given a 90 s (max) to find the submerged platform. If the mice could not find the platform in 90 s, the mice were guided onto the platform. The mice were allowed to remain on the platform for 30 s. The swim speed and the swimming time to the hidden platform (escape latency) were recorded.

In the probe phase, the platform was removed from the pool. The mice were released from the four quadrants, respectively, and allowed to swim freely for 90 s. The time spent in the target quadrant (the quadrant time) and the frequency of crossing the target quadrant (passing quadrant times) were recorded.

Table 1: Sequences of primers used in real-time PCR.

Gene name	Forward primer (5′-3′)	Reverse primer (5′-3′)	Accession number	Size (bp)
TREM2	ACAGCACCTCCAGGAATCAAG	AACTTGCTCAGGAGAACGCA	NM_031254.3	82
IL-1β	TGCCACCTTTTGACAGTGATG	TGATGTGCTGCTGCGAGATT	NM_008361.4	138
IL-6	GACAAAGCCAGAGTCCTTCAGA	TGTGACTCCAGCTTATCTCTTGG	NM_001314054.1	76
TNF-α	GATCGGTCCCCAAAGGGATG	CCACTTGGTGGTTTGTGAGTG	NM_001278601.1	92
IL-4	CCATATCCACGGATGCGACA	AAGCACCTTGGAAGCCCTAC	NM_021283.2	166
IL-10	GCTCTTGCACTACCAAAGCC	CTGCTGATCCTCATGCCAGT	NM_010548.2	112
TGFβ	AGGGCTACCATGCCAACTTC	CCACGTAGTAGACGATGGGC	NM_011577.2	168
MIP-1α	TCTGCGCTGACTCCAAAGAG	CTCAAGCCCCTGCTCTACAC	NM_011337.2	130
MCP-1	TGCCCTAAGGTCTTCAGCAC	AAGGCATCACAGTCCGAGTC	NM_011333.3	150

2.6. Real-Time PCR. Total mRNA was harvested from mouse brain tissues using TRIZOL reagent (Invitrogen, Carlsbad, CA, USA) according to the manufacturer's instructions [15]. Synthesis of cDNA was performed using a ReverTra Ace qPCR RT kit (Toyobo Co., Osaka, Japan). The sequences of the specific primers for target genes are listed in Table 1. For reverse transcriptase qPCR assays, the SYBR Green Real-Time PCR Master Mix kit was used. The real-time PCR was conducted by ABI StepOnePlus Systems (Applied Biosystems, Foster City, CA, USA). The data of real-time PCR were analyzed as $2^{-\Delta\Delta Ct}$; β-actin was used as the internal control.

2.7. Western Blotting. Western blots were performed to measure the protein expression levels of TREM2, nitric oxide synthase (iNOS), and Arginase-1 (Arg-1) as previously described [16]. Protein was collected from brain tissues using RIPA buffer (50 mM Tris (pH 7.4), 150 mM NaCl, 1% NP-40, 0.5% sodium deoxycholate, 0.1% SDS) supplemented with protease inhibitors and Halt Phosphatase Inhibitor Mixture (Beyotime Biotech, Jiangsu, China). Protein extracts were denatured and subjected to 10% sodium dodecyl sulfate-polyacrylamide electrophoresis (SDS-PAGE, Beyotime Biotech, Jiangsu, China). After electrophoresis, protein was transferred onto a polyvinylidene difluoride (PVDF) (Millipore, Billerica, MA, USA) membrane. 5% fat-free milk was used to block the membranes for 2 h at room temperature and then incubated with primary antibodies (TREM2, iNOS, and Arg-1; ABclonal Biotech, Hubei, China) overnight at 4°C. After washing with TBST, the membranes were incubated with secondary antibody (Beyotime Biotech, Jiangsu, China) for 1 h at room temperature. The images were captured using Odyssey infrared fluorescence imaging system (Odyssey, LI-COR Bioscience, Lincoln, NE, USA).

2.8. Immunohistochemistry Assays. Immunohistochemistry (IHC) staining was performed to examine iNOS and Arg-1 protein expression in the hippocampal CA1 subregion in mice as previously described [17]. The hippocampal CA1 coronal sections were incubated with primary antibodies against iNOS and Arg-1 (1 : 200, ABclonal Biotech, Hubei, China) at 4°C overnight. Then, the sections were incubated with a secondary antibody (Beyotime Biotech, Jiangsu, China), followed by nucleus counterstaining stained with DAPI (1 : 1000, Sigma, St Louis, MO, USA) for 10 min. Microscopy (Olympus, Tokyo, Japan) was performed, and images were obtained at 40x. For all IHC experiments, control sections without primary antibodies were routinely used.

2.9. Nissl Staining. Nissl staining was used to detect neuronal injury as reported previously [18]. Three hippocampal CA1 coronal sections at different depths were imaged for each mouse, and three fields of the hippocampus on each coronal section were then randomly selected for quantitative analysis. Neurons with intact morphology and dark violet nucleus were identified as Nissl staining-positive neurons, and the numbers of Nissl staining-positive neurons were counted under a microscope (Olympus, Tokyo, Japan) by observers who were blinded to the experimental groups. The data are presented as the number of Nissl staining-positive neurons in the hippocampus.

2.10. Statistical Analysis. All data are represented as mean ± SD. The MWM data were analyzed by two-way repeated-measures analysis of variance (ANOVA). And other data were analyzed by one-way ANOVA followed by Tukey post hoc test. Statistical tests were performed using statistical software package SPSS version 22.0 (SPSS Inc., Chicago, IL), and $p < 0.05$ was considered significant differences.

3. Results

3.1. TREM2 Is Upregulated in a Mouse Model of VD. In order to study the role of TREM2 during VD pathogenesis, we first detected the time course of TREM2 expression in a mouse model of VD. We examined TREM2 gene and protein levels using RT-PCR and western blot, respectively. The mRNA level of TREM2 was upregulated in the hippocampus of VD mouse model, and the peak of TREM2 mRNA occurred three days after surgery (Figure 1(a)). TREM2 protein level, consistent with the mRNA level expression, showed the similar pattern (Figure 1(b)). Together, these results suggest that TREM2 is involved in the pathogenesis of VD.

3.2. TREM2 Overexpression Attenuates Cognitive Deficits in VD Mice. To determine the therapeutic potential of TREM2, the lentiviral vector that encoded TREM2 was used in the lateral ventricle of VD mice and the MWM test was performed

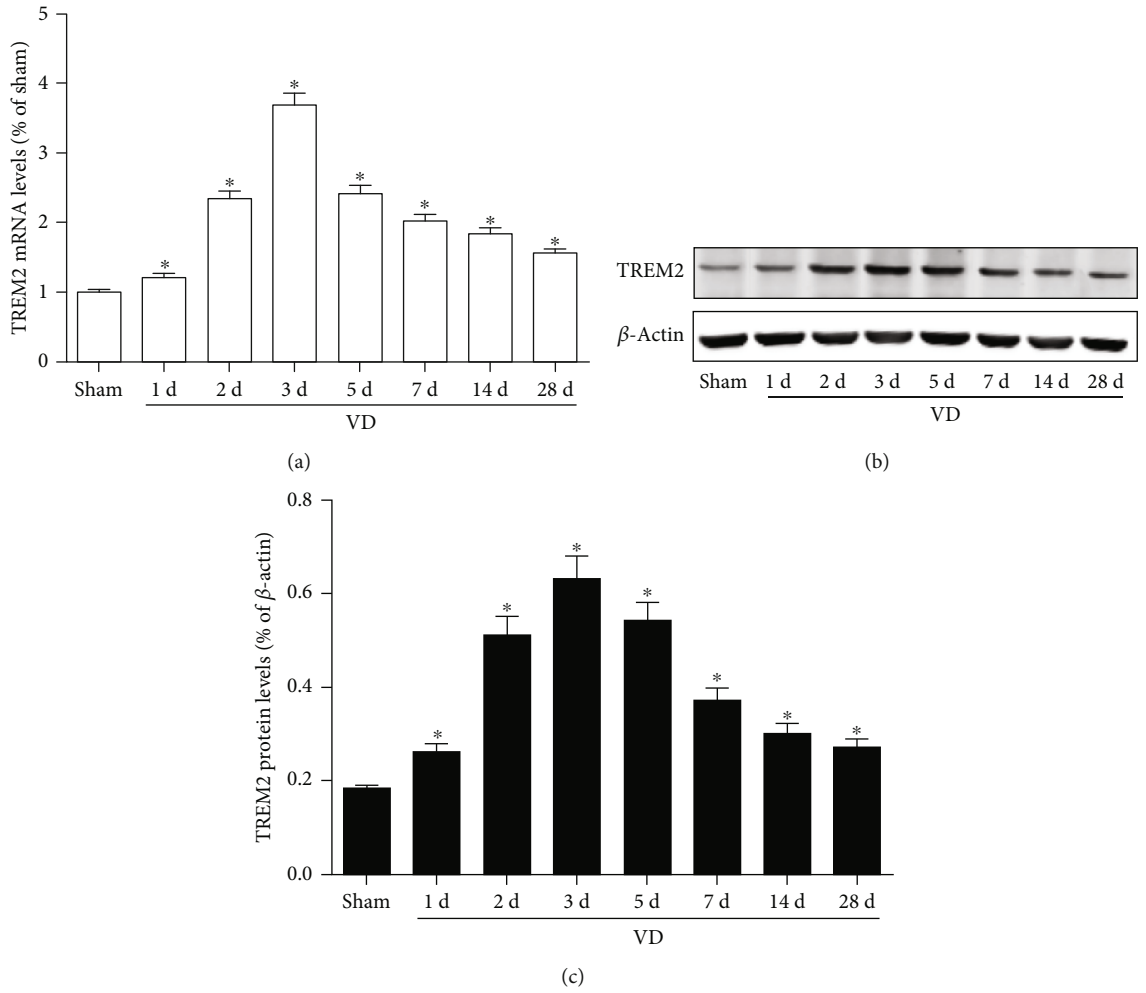

Figure 1: Expression of TREM2 in a mouse model of VD. (a) RT-PCR analysis of TREM2 mRNA level in the hippocampus at different time points of VD; (b, c) western blot analysis of TREM2 protein level in the hippocampus at different time points of VD. Compared to the sham group, $^{*}p < 0.05$.

4 weeks after the lentivirus injection. There was no statistical difference in swimming speed among the three groups ($p > 0.05$, Figure 2(a)). Compared with LV-control VD mice, LV-TREM2 VD mice showed reduced escape latency during the acquisition training phase ($p < 0.05$, Figure 2(b)). During the probe trial phase, the quadrant time ($p < 0.05$, Figure 2(c)) and passing quadrant times ($p < 0.05$, Figure 2(d)) were increased.

3.3. TREM2 Overexpression Modifies Microglia Phenotype in VD Mice. Microglia play different roles depending on its phenotype in the progression of many diseases including VD. It is generally believed that M1 phenotype microglia play a proinflammatory role, while M2 phenotype microglia play an anti-inflammatory role. In order to detect the effect of TREM2 on microglia phenotype, we used immunohistochemistry and western blotting to detect the expression of M1 microglia markers iNOS and M2microglia markers Arg-1 by TREM2 overexpression in VD mice. As indicated in Figure 3, TREM2 overexpression significantly reduced the protein levels of iNOS and increased the protein levels of Arg-1 ($p < 0.05$, Figures 3(a)–3(e)).

3.4. TREM2 Overexpression Attenuated Inflammatory Response in VD Mice. To examine the effect of TREM2 overexpressed on inflammatory response, mRNA levels of proinflammatory mediators (IL-1β, IL-6, and TNF-α), anti-inflammatory mediators (IL-4, IL-10, and TGFβ), and chemokine cytokines (MIP-1α, MCP-1) were measured by RT-PCR in VD mice. The proinflammatory mediators and anti-inflammatory mediators are considered secretions of the M1 and M2 phenotype microglia, respectively. We found that TREM2 overexpression significantly downregulated mRNA levels of proinflammatory mediators ($p < 0.05$, Figure 4(a)), while it significantly upregulated mRNA levels of anti-inflammatory mediators ($p < 0.05$, Figure 4(b)) and chemokine cytokines ($p < 0.05$, Figure 4(c)).

3.5. TREM2 Overexpression Prevents Neuronal Loss in VD Mice. Loss of neurons in the hippocampus is associated with cognitive deficits. In order to detect neuronal injury, we observed hippocampal neurons with Nissl staining. As indicated in Figure 5, TREM2 overexpression significantly attenuated neuronal loss in the hippocampus of VD mouse ($p < 0.05$, Figures 5(a) and 5(b)).

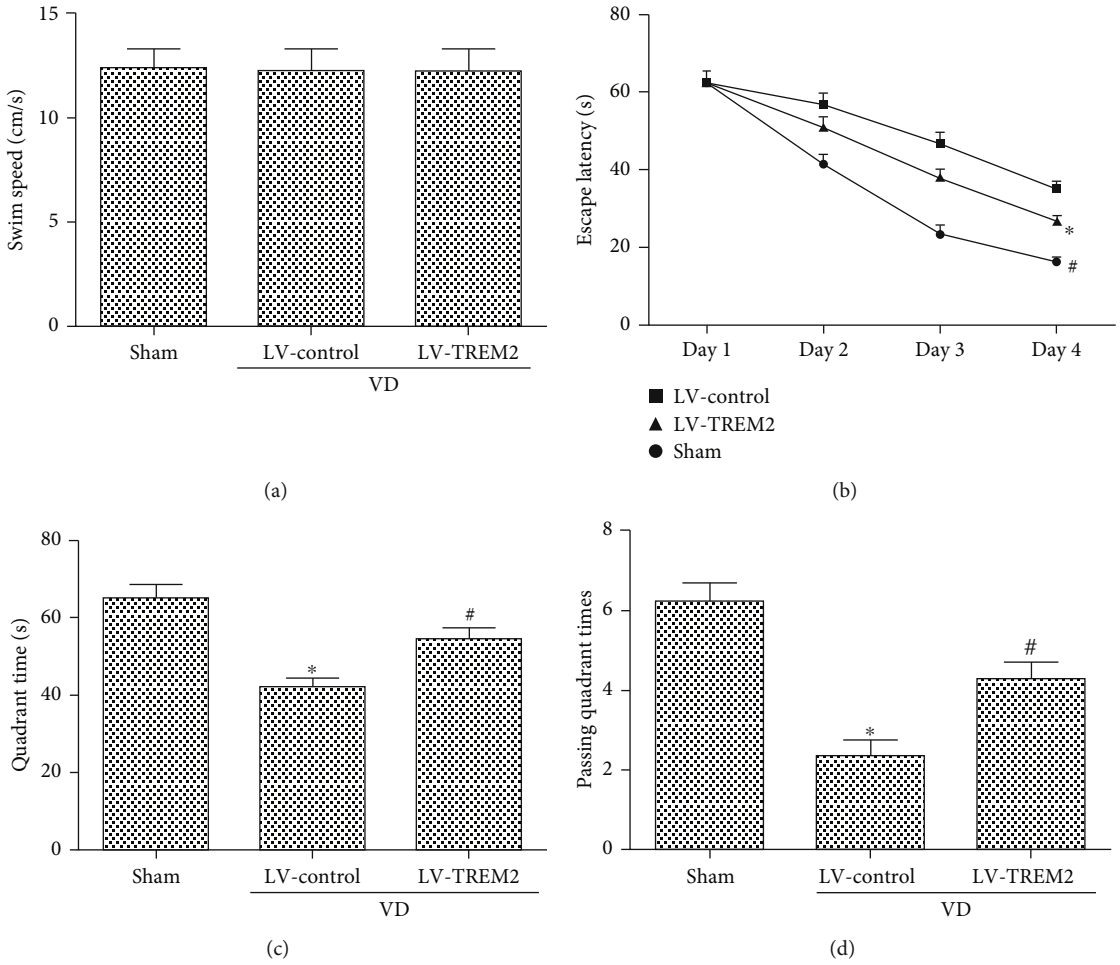

Figure 2: TREM2 overexpression attenuates cognitive deficits in VD mice: (a) swimming speed; (b) escape latency; (c) quadrant time; (d) passing quadrant times. Compared to the sham group, $^{*}p < 0.05$; compared to the LV-control group, $^{\#}p < 0.05$.

4. Discussion

In the present study, our results showed that TREM2 gene and protein levels were upregulated in the brains of VD mice compared with the sham mice, indicating that TREM2 may be involved in the pathogenesis of VD, which was consistent with our previous study [10]. Further investigation revealed that TREM2 overexpression attenuates cognitive deficits and neuronal loss. Moreover, TREM2 may regulate the release of inflammatory factors by modifying the microglia phenotype, which may partly explain the protective effects of TREM2 against cognitive deficits and neuronal loss in the mouse models of VD. To our knowledge, our present study is the first to elucidate the important role of TREM2-mediated microglial phenotypic polarization and inflammatory response in the pathogenesis of VD.

Accumulating evidence suggests that inflammation is a major contributor in the pathogenesis of many neurological diseases including VD. Neuroinflammation in VD is characterized by elevated levels of inflammatory mediators released from activated microglia [19]. In an animal study, Sun and his colleagues found that Rehmannioside A could attenuate cognitive deficits in rats with VD through reducing the release of proinflammatory cytokines, including TNF-α, IL-1β, and IL-6 [20]. Several other drugs, such as resveratrol, cannabinoid receptor agonist, and vanillic acid, have also been shown to play a neuroprotective role in different animal models of VD by reducing the inflammatory response [21–23]. Interestingly, a study suggests that acupuncture, a traditional Chinese treatment, may also improve cognitive function by reducing neuroinflammation [24]. The above animal studies suggest that inflammation is involved in the pathogenesis of vascular dementia. Apart from animal models, the important role of inflammation in the pathogenesis of VD has also been found in clinical studies. We previously found that *Helicobacter pylori* may aggravate atherosclerosis and cognitive impairment in VD patients by increasing the serum levels of inflammatory mediators [25, 26]. Although the role of inflammation in VD has been widely reported, its upstream and downstream mechanisms have not been fully elucidated.

Recently, several studies have revealed that TREM2 is involved in the inflammatory pathology of a variety of neurological disorders [27, 28]. One study showed that LPS-treated APP/PS1 transgenic mice had decreased TREM2 levels and increased TLR4 levels, indicating that TLR4/TREM2 may

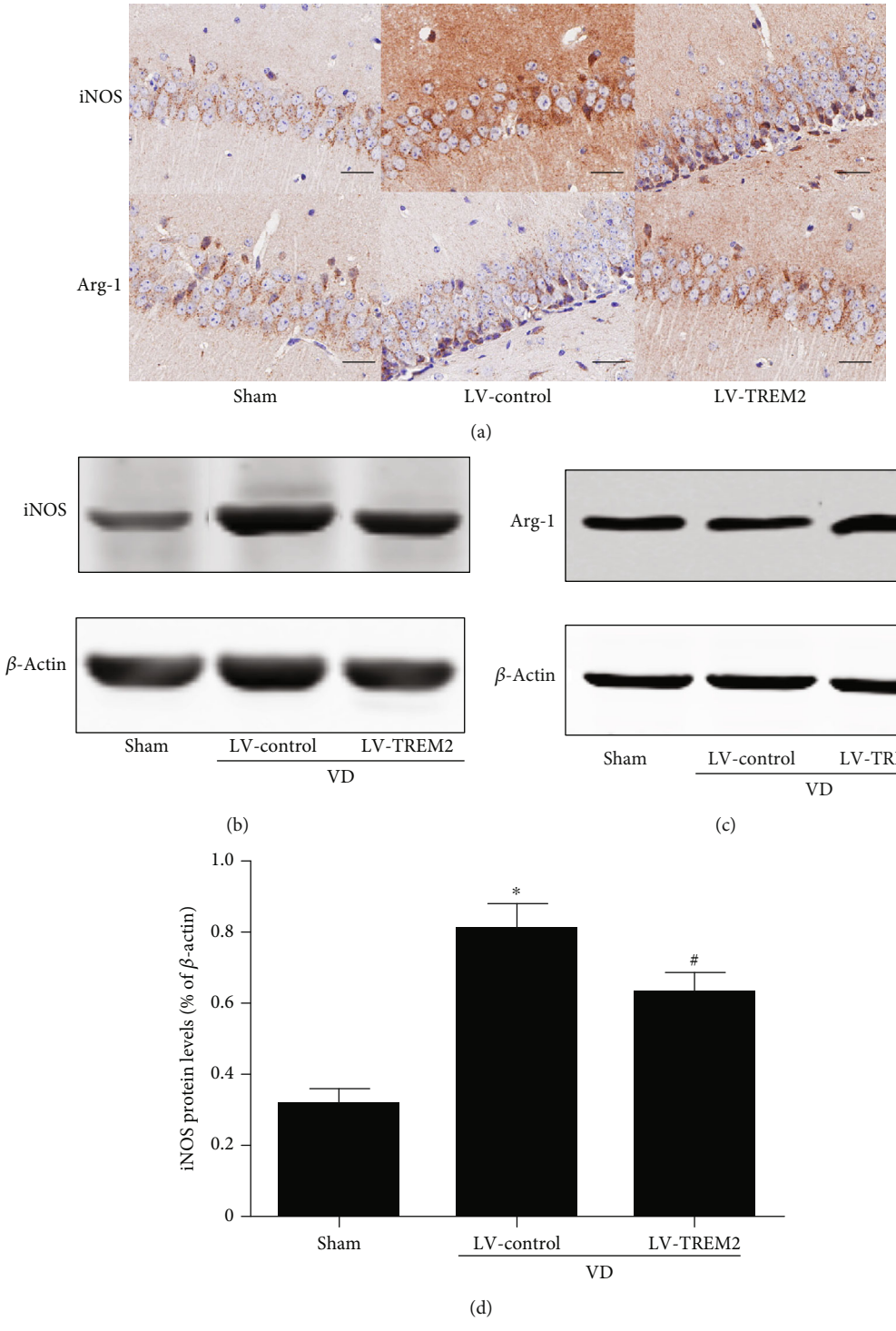

Figure 3: Continued.

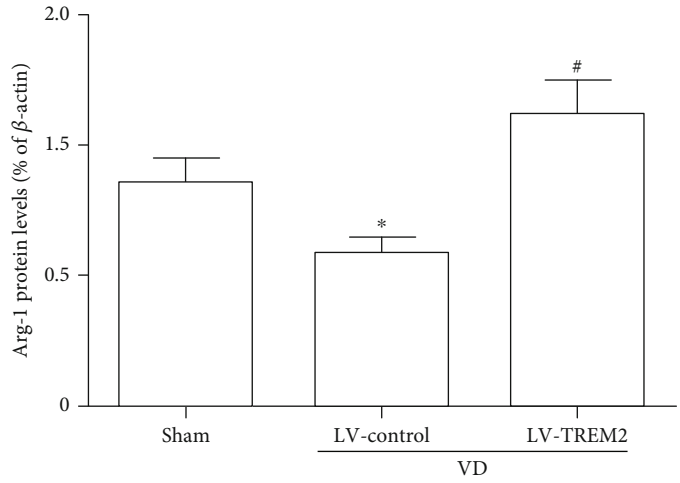

(e)

Figure 3: TREM2 overexpression modifies microglia phenotype in VD mice. (a) IHC staining of M1 microglia phenotype marker iNOS and M2 microglia phenotype marker Arg-1 in the hippocampus of VD mice. Scale bars = 50 μm. (b–e) Western blot analysis of iNOS and Arg-1 protein level in the hippocampus of VD mice. Compared to the sham group, $^{*}p < 0.05$; compared to the LV-control group, $^{\#}p < 0.05$.

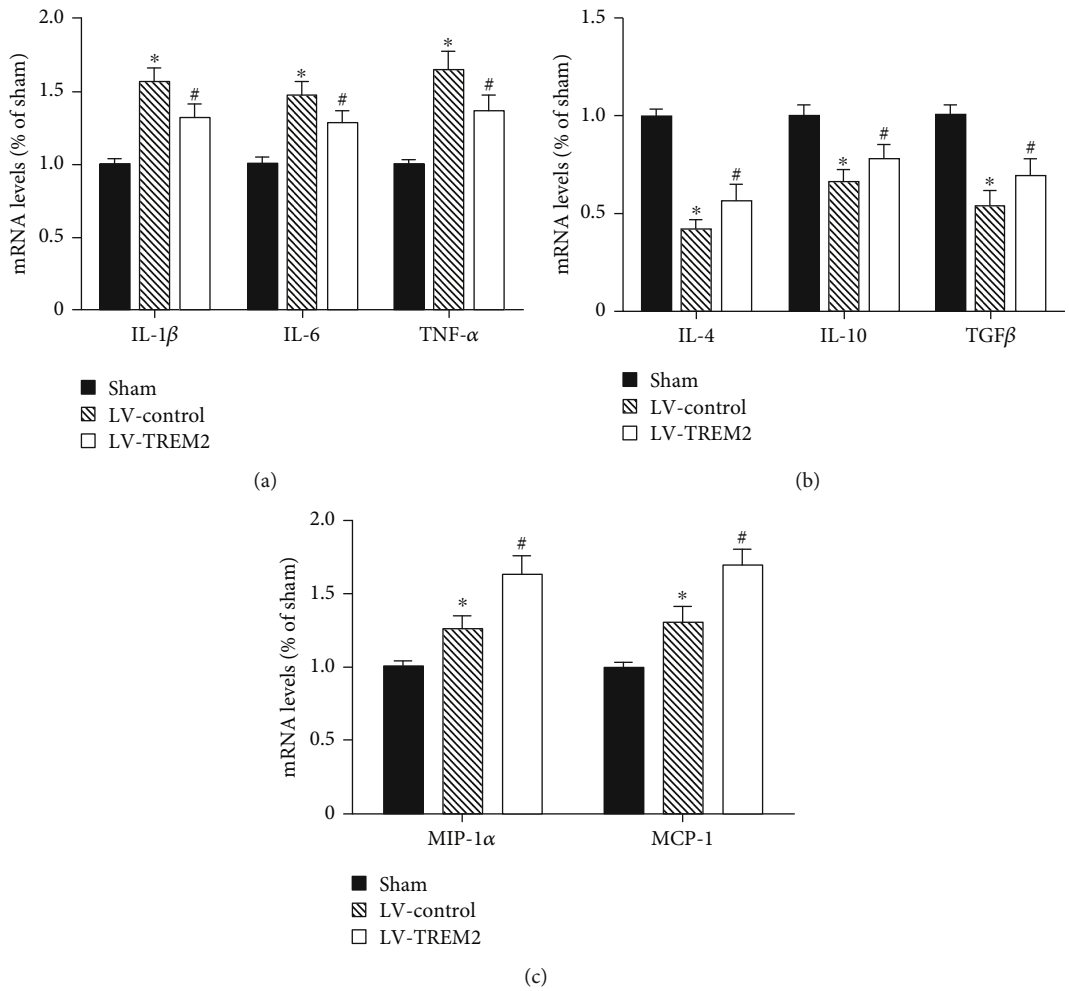

Figure 4: TREM2 overexpression attenuated inflammatory response in VD mice. (a) mRNA levels of proinflammatory mediators in the hippocampus of VD mice; (b) mRNA levels of anti-inflammatory mediators in the hippocampus of VD mice; (c) mRNA levels of chemokine cytokines in the hippocampus of VD mice. Compared to the sham group, $^{*}p < 0.05$; compared to the LV-control group, $^{\#}p < 0.05$.

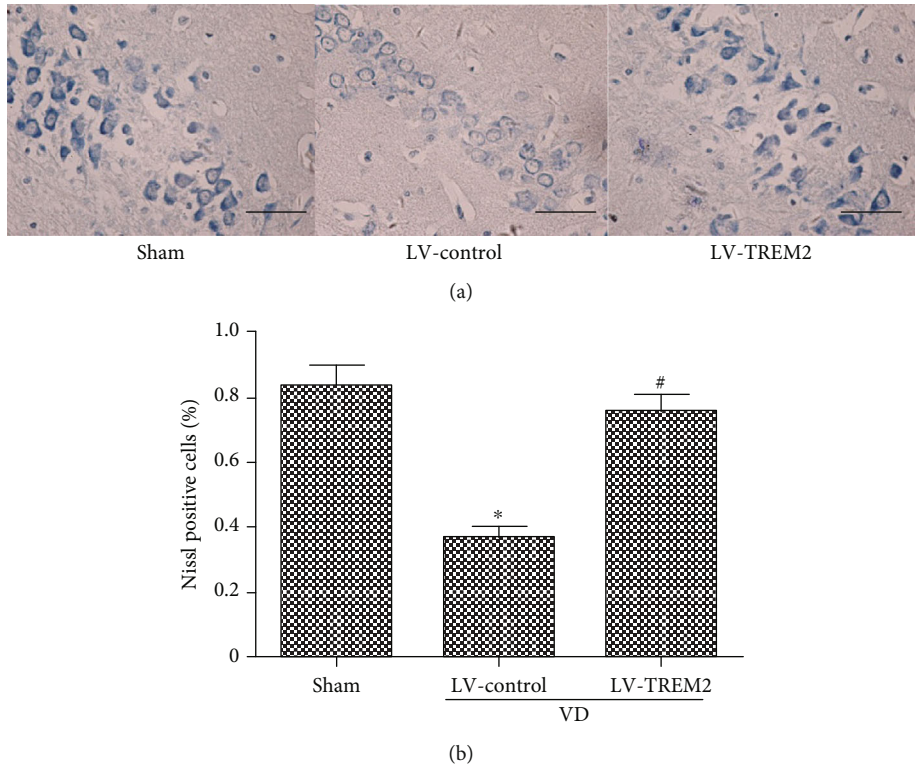

Figure 5: TREM2 overexpression prevents neuronal loss in VD mice. (a) Nissl staining was performed to detect neuronal loss in the hippocampus of VD mice. (b) The percentage of Nissl-positive neurons in the hippocampus of VD mice. Scale bars = 50 μm. Compared to the sham group, $^{*}p < 0.05$; compared to the LV-control group, $^{\#}p < 0.05$.

be a potential link between AD and systemic inflammation and TREM2 can serve as a potential therapeutic target for treating systemic inflammation in AD [29]. Another study revealed that TREM2 inhibited the activation of TNF-α-induced inflammation response in rheumatoid arthritis via the p38 pathway [30]. Moreover, the studies of Ren et al. suggested that TREM2 has a neuroprotective effect in Parkinson's disease by reducing neuroinflammation and the apoptosis of dopamine neurons [31]. Taken together, TREM2 may be an upstream regulator of inflammation in a variety of neurological disorders.

Neuroinflammation is primarily driven by microglia, which are the innate immune cells of the central nervous system and play a central role in many aspects of brain metabolism and physiology [32]. There are two main types of activated microglia: the proinflammatory M1 phenotype and the anti-inflammatory M2 phenotype. Different activated statuses of microglia secrete completely different arrays of cytokines. On the one hand, microglia cause neuronal injury via secreting proinflammatory cytokines, and on the other hand, they execute beneficial effects via releasing anti-inflammatory mediators. Thus, microglia are considered a double-edged sword. In recent years, the relationship between TREM2 and microglia has attracted much attention [33]. One study found that TREM2 modified microglial phenotype in P301S tau transgenic mice [34]. The other study demonstrated solution TREM2 against attenuated amyloid pathology and related toxicity, suggesting that TREM2 plays a neuroprotective role in the body and can be explored as a therapeutic target for AD [35]. A study found that TREM2 has the potential to maintain endothelial cell homeostasis as a microglial receptor and signaling hub, suggesting an underlying link between immune response and vascular disease [36]. However, the involvement of TREM2-mediated neuroinflammation in the pathogenesis of VD has not been previously reported.

In our previous study, we found that the expression of serum soluble TREM2 was decreased and serum soluble TREM2 levels were an independent risk factor for cognitive impairment in VD patients [10]. However, the results of our current study showed that the gene and protein levels of TREM2 were elevated in VD model mice. The two results seem conflicting. I think there are two reasons for this difference. The one is the different periods of inflammation. Acute inflammation is thought to have a protective effect on the body, while chronic inflammation is thought to be harmful [8]. The inflammation in VD patients is mostly in the chronic phase, whereas the inflammation in VD mice is in the acute phase. In the acute inflammatory phase of VD mice, higher TREM2 levels may be an organism's self-protection mechanism. The other is the different molecular structure and localization. Solution TREM2 (sTREM2) is a proteolytic product of TREM2 released to the extracellular space, which can be detected in the serum [37]. Assume that the total amount of sTREM2 and TREM2 is constant, there may exist a certain dynamic equilibrium between sTREM2 in the serum and TREM2 in the brain parenchyma. These two differences might partly explain the conflicting outcomes. In

future studies, we will detect levels of sTREM2 in the peripheral blood of VD mice and investigate the different roles of sTREM2 and TREM2 in the pathogenesis of VD.

5. Conclusion

Taken together, in our current study, we provide novel evidence that TREM2 overexpression attenuates cognitive deficits and neural loss through modulating the phenotype of activated microglia and reducing inflammatory reaction. These findings shed new light on the role of TREM2 in the pathogenesis of VD and indicate that TREM2 may represent a promising novel target for VD. The relationship between TREM2 and VD, if confirmed by future large multicenter studies, may have crucial clinical and therapeutic implications.

Data Availability

The data used to support the findings of this study are available from the corresponding author upon reasonable request.

Conflicts of Interest

The authors declare no conflict of interest.

Authors' Contributions

Qian Wang and Weixia Yang contributed equally to this work.

Acknowledgments

The authors are grateful to the Department of Central Laboratory, Taian City Central Hospital, Shandong First Medical University & Shandong Academy of Medical Sciences, for invaluable assistance. We also apologize to those colleagues whose excellent paper could not be cited due to space constraints. This work was supported by grants from the Shandong Medical and Health Technology Development Fund (2018WS147) and the Taian Science and Technology Development Fund (2018NS0162).

References

[1] J. T. O'Brien and A. Thomas, "Vascular dementia," *Lancet*, vol. 386, no. 10004, pp. 1698–1706, 2015.

[2] Y. Xu, Q. Wang, R. Cui, K. Lu, Y. Liu, and Y. Zhao, "Uric acid is associated with vascular dementia in Chinese population," *Brain and Behavior*, vol. 7, no. 2, article e00617, 2017.

[3] Y. Xu, Q. Wang, Z. Qu, J. Yang, X. Zhang, and Y. Zhao, "Protective effect of hyperbaric oxygen therapy on cognitive function in patients with vascular dementia," *Cell Transplantation*, vol. 28, no. 8, pp. 1071–1075, 2019.

[4] L. Jia, M. Quan, Y. Fu et al., "Dementia in China: epidemiology, clinical management, and research advances," *Lancet Neurology*, vol. 19, no. 1, pp. 81–92, 2020.

[5] T. K. Ulland and M. Colonna, "TREM2 – a key player in microglial biology and Alzheimer disease," *Nature Reviews. Neurology*, vol. 14, no. 11, pp. 667–675, 2018.

[6] H. Zheng, B. Cheng, Y. Li, X. Li, X. Chen, and Y. W. Zhang, "TREM2 in Alzheimer's disease: microglial survival and energy metabolism," *Frontiers in Aging Neuroscience*, vol. 10, 2018.

[7] L. Zhong, X. F. Chen, T. Wang et al., "Soluble TREM2 induces inflammatory responses and enhances microglial survival," *The Journal of Experimental Medicine*, vol. 214, no. 3, pp. 597–607, 2017.

[8] C. Cervellati, A. Trentini, A. Pecorelli, and G. Valacchi, "Inflammation in neurological disorders: the thin boundary between brain and periphery," *Antioxidants & Redox Signaling*, 2020.

[9] L. Poli, V. De Giuli, F. Piazza et al., "A challenging diagnosis of reversible "vascular" dementia: Cerebral amyloid angiopathy-related inflammation," *Journal of Neuroimmunology*, vol. 338, p. 577109, 2020.

[10] Q. Wang, Y. Xu, C. Qi, A. Liu, and Y. Zhao, "Association study of serum soluble TREM2 with vascular dementia in Chinese Han population," *The International Journal of Neuroscience*, pp. 1–5, 2020.

[11] R. Siracusa, D. Impellizzeri, M. Cordaro et al., "Anti-inflammatory and neuroprotective effects of Co-UltraPEALut in a mouse model of vascular dementia," *Frontiers in Neurology*, vol. 8, p. 233, 2017.

[12] Y. Xu, Q. Wang, Z. Wu et al., "The effect of lithium chloride on the attenuation of cognitive impairment in experimental hypoglycemic rats," *Brain Research Bulletin*, vol. 149, pp. 168–174, 2019.

[13] X. Zhu, S. Wang, L. Yu et al., "HDAC3 negatively regulates spatial memory in a mouse model of Alzheimer's disease," *Aging Cell*, vol. 16, no. 5, pp. 1073–1082, 2017.

[14] Y. Cao, H. Xu, Y. Zhu et al., "ADAMTS13 maintains cerebrovascular integrity to ameliorate Alzheimer-like pathology," *PLoS Biology*, vol. 17, no. 6, article e3000313, 2019.

[15] Y. Xu, Q. Wang, D. Li et al., "Protective effect of lithium chloride against hypoglycemia-induced apoptosis in neuronal PC12 cell," *Neuroscience*, vol. 330, pp. 100–108, 2016.

[16] L.-Y. Zhang, J. Pan, M. Mamtilahun et al., "Microglia exacerbate white matter injury via complement C3/C3aR pathway after hypoperfusion," *Theranostics*, vol. 10, no. 1, pp. 74–90, 2020.

[17] W. Wan, C. Zhang, M. Danielsen et al., "EGb761 improves cognitive function and regulates inflammatory responses in the APP/PS1 mouse," *Experimental Gerontology*, vol. 81, pp. 92–100, 2016.

[18] G.-H. Tian, S.-S. Tao, M.-T. Chen et al., "Electroacupuncture treatment alleviates central poststroke pain by inhibiting brain neuronal apoptosis and aberrant astrocyte activation," *Neural Plasticity*, vol. 2016, 14 pages, 2016.

[19] H. Ben-Ari, T. Lifschytz, G. Wolf et al., "White matter lesions, cerebral inflammation and cognitive function in a mouse model of cerebral hypoperfusion," *Brain Research*, vol. 1711, pp. 193–201, 2019.

[20] M. Sun, X. Shen, and Y. Ma, "Rehmannioside A attenuates cognitive deficits in rats with vascular dementia (VD) through suppressing oxidative stress, inflammation and apoptosis," *Biomedicine & Pharmacotherapy*, vol. 120, p. 109492, 2019.

[21] S. S. Gocmez, T. D. Şahin, Y. Yazir et al., "Resveratrol prevents cognitive deficits by attenuating oxidative damage and inflammation in rat model of streptozotocin diabetes induced

vascular dementia," *Physiology & Behavior*, vol. 201, pp. 198–207, 2019.

[22] S. E. Khoshnam, A. Sarkaki, M. Rashno, and Y. Farbood, "Memory deficits and hippocampal inflammation in cerebral hypoperfusion and reperfusion in male rats: neuroprotective role of vanillic acid," *Life Sciences*, vol. 211, pp. 126–132, 2018.

[23] D. P. Wang, H. Yin, K. Kang, Q. Lin, S. H. Su, and J. Hai, "The potential protective effects of cannabinoid receptor agonist WIN55,212-2 on cognitive dysfunction is associated with the suppression of autophagy and inflammation in an experimental model of vascular dementia," *Psychiatry Research*, vol. 267, pp. 281–288, 2018.

[24] S.-Q. Du, X.-R. Wang, W. Zhu et al., "Acupuncture inhibits TXNIP-associated oxidative stress and inflammation to attenuate cognitive impairment in vascular dementia rats," *CNS Neuroscience & Therapeutics*, vol. 24, no. 1, pp. 39–46, 2018.

[25] Y. Xu, Q. Wang, Y. Liu, R. Cui, K. Lu, and Y. Zhao, "Association between _Helicobacter pylori_ infection and carotid atherosclerosis in patients with vascular dementia," *Journal of the Neurological Sciences*, vol. 362, pp. 73–77, 2016.

[26] Y. Xu, Q. Wang, Y. Liu, R. Cui, and Y. Zhao, "Is Helicobacter pylori infection a critical risk factor for vascular dementia?," *The International Journal of Neuroscience*, vol. 126, no. 10, pp. 899–903, 2015.

[27] T. R. Jay, V. E. von Saucken, and G. E. Landreth, "TREM2 in neurodegenerative diseases," *Molecular Neurodegeneration*, vol. 12, no. 1, p. 56, 2017.

[28] T. Jiang, J. T. Yu, X. C. Zhu, and L. Tan, "TREM2 in Alzheimer's disease," *Molecular Neurobiology*, vol. 48, no. 1, pp. 180–185, 2013.

[29] J. Zhou, W. Yu, M. Zhang, X. Tian, Y. Li, and Y. Lü, "Imbalance of microglial TLR4/TREM2 in LPS-treated APP/PS1 transgenic mice: a potential link between Alzheimer's disease and systemic inflammation," *Neurochemical Research*, vol. 44, no. 5, pp. 1138–1151, 2019.

[30] S. H. Huang, G. W. Liu, J. H. Li et al., "Expression of TREM-2 and its inhibitory effects on TNF-α induced inflammation in fibroblast-like synoviocytes via inhibiting p38 pathway activation," *Clinical and Experimental Rheumatology*, vol. 36, no. 2, pp. 185–194, 2017.

[31] M. Ren, Y. Guo, X. Wei et al., "TREM2 overexpression attenuates neuroinflammation and protects dopaminergic neurons in experimental models of Parkinson's disease," *Experimental Neurology*, vol. 302, pp. 205–213, 2018.

[32] S. Xu, J. Lu, A. Shao, J. H. Zhang, and J. Zhang, "Glial cells: role of the immune response in ischemic stroke," *Frontiers in Immunology*, vol. 11, 2020.

[33] K. Yao and H.-b. Zu, "Microglial polarization: novel therapeutic mechanism against Alzheimer's disease," *Inflammopharmacology*, vol. 28, no. 1, pp. 95–110, 2020.

[34] T. Jiang, Y. D. Zhang, Q. Chen et al., "TREM2 modifies microglial phenotype and provides neuroprotection in P301S tau transgenic mice," *Neuropharmacology*, vol. 105, pp. 196–206, 2016.

[35] L. Zhong, Y. Xu, R. Zhuo et al., "Soluble TREM2 ameliorates pathological phenotypes by modulating microglial functions in an Alzheimer's disease model," *Nature Communications*, vol. 10, no. 1, p. 1365, 2019.

[36] G. Carbajosa, K. Malki, N. Lawless et al., "Loss of Trem2 in microglia leads to widespread disruption of cell coexpression networks in mouse brain," *Neurobiology of Aging*, vol. 69, pp. 151–166, 2018.

[37] L. Zhong and X.-F. Chen, "The emerging roles and therapeutic potential of soluble TREM2 in Alzheimer's disease," *Frontiers in Aging Neuroscience*, vol. 11, 2019.